

ACS SYMPOSIUM SERIES **763**

Flavor Release

Deborah D. Roberts, EDITOR
Nestlé Research Center

Andrew J. Taylor, EDITOR
University of Nottingham



American Chemical Society, Washington, DC



Library of Congress Cataloging-in-Publication Data

Flavor release / Deborah D. Roberts, Andrew J. Taylor.

p. cm.—(ACS symposium series, ISSN 0097-6156 ; 763)

Developed from a symposium held at the ACS 218th National Meeting in New Orleans, Louisiana from August 24–26, 1999.

Includes bibliographical references and index.

ISBN 0-8412-3692-5

1. Food—Sensory evaluation—Congresses. 2. Flavor—Congresses.

I. Roberts, Deborah D., 1969- II. Taylor, A. J. (Andrew John), 1951– III. American Chemical Society. Meeting (218th : 1999 : New Orleans, La.) IV. Series.

TX546 .F53 2000
664'.07—dc21

00-29285

The paper used in this publication meets the minimum requirements of American National Standard for Information Sciences—Permanence of Paper for Printed Library Materials, ANSI Z39.48–1984.

Copyright © 2000 American Chemical Society

Distributed by Oxford University Press

All Rights Reserved. Reprographic copying beyond that permitted by Sections 107 or 108 of the U.S. Copyright Act is allowed for internal use only, provided that a per-chapter fee of \$20.00 plus \$0.50 per page is paid to the Copyright Clearance Center, Inc., 222 Rosewood Drive, Danvers, MA 01923, USA. Republication or reproduction for sale of pages in this book is permitted only under license from ACS. Direct these and other permission requests to ACS Copyright Office, Publications Division, 1155 16th St., N.W., Washington, DC 20036.

The citation of trade names and/or names of manufacturers in this publication is not to be construed as an endorsement or as approval by ACS of the commercial products or services referenced herein; nor should the mere reference herein to any drawing, specification, chemical process, or other data be regarded as a license or as a conveyance of any right or permission to the holder, reader, or any other person or corporation, to manufacture, reproduce, use, or sell any patented invention or copyrighted work that may in any way be related thereto. Registered names, trademarks, etc., used in this publication, even without specific indication thereof, are not to be considered unprotected by law.

PRINTED IN THE UNITED STATES OF AMERICA

**American Chemical Society
Library**

**1155 16th St., N.W.
Washington, D.C. 20036**

In Flavor Release; Roberts, D., et al.;

ACS Symposium Series; American Chemical Society: Washington, DC, 2000.

Foreword

THE ACS SYMPOSIUM SERIES was first published in 1974 to provide a mechanism for publishing symposia quickly in book form. The purpose of the series is to publish timely, comprehensive books developed from ACS sponsored symposia based on current scientific research. Occasionally, books are developed from symposia sponsored by other organizations when the topic is of keen interest to the chemistry audience.

Before agreeing to publish a book, the proposed table of contents is reviewed for appropriate and comprehensive coverage and for interest to the audience. Some papers may be excluded in order to better focus the book; others may be added to provide comprehensiveness. When appropriate, overview or introductory chapters are added. Drafts of chapters are peer-reviewed prior to final acceptance or rejection, and manuscripts are prepared in camera-ready format.

As a rule, only original research papers and original review papers are included in the volumes. Verbatim reproductions of previously published papers are not accepted.

A C S B O O K S D E P A R T M E N T

Preface

Flavor is the study of the flavor compounds of food that reach the consumer's nose and mouth during eating. The field is important because flavor compounds in food are almost always in contact with the food matrix, where their release is influenced chemically and physically by the matrix components. When food is eaten, additional biochemical, physical, and perceptual changes occur. Flavor release is an area that has emerged in recent years with research escalating in the late 1990s. This is due to strong advances in the previous decades in other flavor chemistry fields and to the close applicability of the results to food products and flavor perception. One of the main thrusts that established flavor release research and collaborations in Europe was the 1995–1999 European Union Cost Action 96 on “Interactions of the Food Matrix with Small Ligands Influencing Flavor and Texture.” It was also the starting point for this American Chemical Society (ACS) Symposium.

The symposium, “Flavor Release: Linking Experiments, Theory, and Reality,” was held at the ACS 218th National Meeting in New Orleans, Louisiana, August 24–26, 1999. To our knowledge, it is the first cosponsored symposium between the ACS Division of Agricultural and Food Chemistry and the Royal Society of Chemistry Food Chemistry Group. The goal of the symposium was to bring together practitioners from around the world to establish the background to the field as well as the state-of-the-art situation. While bringing together scientists from many continents, the majority (70%) of speakers were indeed from Europe. As many of the results can be applied to product development, the food industry showed a strong interest in the symposium. Although greater than 50% in some sections, overall, industry represented a third of both speakers and audience participants.

This symposium-based book contains four main sections of research: (1) *in vivo* and dynamic analytical techniques, (2) modeling of flavor release, (3) interactions of flavors with food components, and (4) relating analytical results to human perception. Section 1 shows different methods and results for flavor release, with the emphasis on *in vivo* measurement during eating. This section combines physiology, anatomy, and analytical chemistry and is of particular interest to those who would like to know more about the flavor changes occurring in the mouth from real foods. Section 2 is comprised of chapters by chemists, chemical engineers, and physicists who seek to explain release results from model systems and the mouth using physical chemical principles. Such models, after experimental validation, can predict release from new food systems. Section 3 contains basic studies on binding between carbohydrates and proteins with flavor compounds as well as compound absorption by fat emulsions. In addition, several more complex food products are studied, showing also the important role of texture. Section 4 relates sensory results to analytical

measurements and modeling predictions. It shows not only the challenge of correlating multivariable areas but also some successes in doing so.

This book is a bit unusual because of its multidisciplinary nature. As a field, flavor release needs experts in physical chemistry, food science, theoretical modeling, and sensory science, who are found among the authors of this book. The book will appeal to a wide audience, not only flavor scientists, but also to the many food scientists and technologists who produce, analyze, and use flavorings in foods. It will allow flavor chemists who specialize in other areas, such as the reaction mechanisms or compound identification, to see how their work, which forms the fundamental knowledge needed to start flavor release work, is being applied. Those working to understand flavor delivery in foods may learn more about the influence of binding between flavor compounds and food, as well as the effect of the food medium on flavor release. Food product developers who use flavorings may learn how a change in product composition, structure, or texture brings about a change in the flavor perception of their products, as well as how to induce or inhibit this change. Sensory scientists may discover what is actually happening in panelists' mouths during eating and how chemistry results can help explain sensory findings.

Acknowledgments

We greatly appreciate the support received from our sponsors, which indicated their strong interest in the subject. Through this sponsorship we were able to assist keynote speakers with funding and the result was 41 speakers from more than 12 countries. Without the support of the sponsors, the broad extent of this symposium would not have been possible. The sponsors were ACS Division of Agricultural and Food Chemistry, Corporation Associates, Firmenich, Quest, Nestlé, and the Royal Society of Chemistry (Food Chemistry Group). The reviewers deserve commendation for their punctual refereeing and the authors should also be congratulated for the rapid return of their manuscripts that allowed a timely book publication.

DEBORAH D. ROBERTS
Nestlé Research Center
P.O. Box 44
Vers-Chez-les-Blanc
1000 Lausanne 26, Switzerland

ANDREW J. TAYLOR
Division of Food Sciences
University of Nottingham
Sutton Bonington Campus
Loughborough, Leicestershire LE12 5RD
United Kingdom

Chapter 1

Flavor Release: A Rationale for Its Study

Deborah D. Roberts¹ and Andrew J. Taylor²

¹Nestlé Research Center, P.O. Box 44, Vers-Chez-les-Blanc,
1000 Lausanne 26, Switzerland

²Division of Food Sciences, University of Nottingham, Sutton Bonington Campus,
Loughborough, Leicestershire LE12 5RD, United Kingdom

Release of flavor compounds from foods is an essential prerequisite for flavor perception. Although measurement of release at equilibrium has been practiced for many years, measuring the dynamics of release was a more difficult task, due to the speed of change and the low concentrations of flavor compounds. However, sensory techniques like time-intensity analysis showed there were perceptible changes in flavor during, and after, eating. More recently, instrumental methods have been developed to follow the change in concentrations of flavor compounds above foods, or in the mouth and nose, during consumption of food. The availability of these techniques has led to renewed interest in the fields of modeling of flavor release, in the link between flavor compounds and flavor perception, and in the interactions of flavor compounds with food matrices.

Flavor release is the study of the mechanisms that influence the volatilization of aroma compounds (or the release of tastants) from food during specific situations, especially release in the mouth during eating. This covers a wide range of situations that are mainly investigated by chemists but also by food scientists, sensory scientists, and theoretical modelers. At the one extreme, it can describe the partitioning between an aqueous solution of volatiles and the air above it (the headspace). Such systems are usually allowed to come to equilibrium where the ratio of the concentrations of volatile compound in the gas and water phases is the air-water partition coefficient. Such systems are often referred to as “static equilibrium”. At the other extreme, the release of flavor compounds during eating can be monitored in the mouth and/or nose where the system represents real time flavor release *in vivo*. In between, there are various systems that have been designed to measure the effect of specific parameters (e.g. binding of volatiles to proteins, effect of saliva on rate of volatile release) or under specific release situations (e.g. during processing). Historically, equilibrium systems were studied because of their simplicity but the emphasis now is on the dynamic measurement of flavor release. Most published studies have investigated the release of flavor compounds that are volatile as they are considered to impart the

flavor character to foods (non-volatiles provide the base flavor) and because they are easier to isolate from foods. There is growing interest in the interaction of volatile and non-volatile flavor (sapid) compounds at the molecular and perceptual levels and, thus, the dynamics of sapid flavor release have been investigated recently. Verification of analytical results with sensory perception is one of the final and needed steps, especially for food development.

Historical Development of Flavor Release Research

Flavor release has been reviewed by several authors over the last 10 years (1-9). In this book, the chapters by Escher, de Roos and Taylor review, respectively, progress in starch-flavor compound interactions, modeling of flavor release, and methodology for the real time analysis of flavor release to give a current view of these important fields.

The physicochemical study of volatile compounds was a subject for early scientific research and Henry's Law is an excellent example from that era and still widely used to express the partial pressure of a compound above an aqueous solution (10). In the late 1960s and early 1970s, partition coefficients for many flavor volatiles were published from the USDA Western Regional Laboratory, an institution that has contributed so much to flavor research in the last thirty years (11). A sensory approach to studying hydrocolloid-aroma interactions was demonstrated by Pangborn (12) and later further expanded by also correlating with headspace results from diverse systems (13). The 1970s also saw seminal work on the interactions of starch with aroma compounds through the work of Solms' group (14, 15). In 1977, Voilley published results to explain why the addition of solutes to an aqueous solution of volatiles could affect the concentration of volatiles in the headspace (16) and has since contributed much to our knowledge of the physical chemistry of flavor.

In the 1980's, Kinsella's group reported data on protein-flavor binding (5) and an ACS Symposium considered progress in flavor encapsulation (17). This process was originally intended to protect flavors from deterioration during storage but is now often used to deliver flavor compounds at the appropriate point during food preparation and consumption. Lee demonstrated flavor release from a simple device, which mimicked some of the processes that occur in-mouth during eating (18) and was followed by more complex mouth simulators (19-21). McNulty approached flavor release from a theoretical modeling angle and predicted flavor release from emulsion systems of varying oil/water composition (22). In the late 80's, a series of papers describing flavor release in mouth, was published by Unilever researchers. These publications contained many interesting ideas and hypotheses. For example, an Overbosch paper in 1986 (23-25), redefined Steven's Law to include the effect of adaptation on the intensity of the chemical stimulus. Although intuitively correct, no data have yet been published to support this hypothesis.

The 1990's saw progress in several areas. Models for flavor release were proposed by de Roos (26, 27). These were based on a mixture of mechanistic and empirical principles but, most importantly, they were validated with data from several different food systems. Subsequently, Harrison and Hills published a series of

mechanistic models for flavor release, which tackled difficult release mechanisms like in-mouth solubilisation and melting of thermo-reversible gels. The widespread use of GC-olfactometry to evaluate the contribution of individual flavor compounds to overall flavor and to determine odor thresholds was a result of pioneering work at Cornell by Acree (28) and in Munich by Grosch and coworkers (29). In fact, the advances in related flavor chemistry fields (e.g. determination of key odor-active compounds, reaction mechanisms, flavor generation, analytical methodology) have generated the technical platform for flavor release research.

Methods for measuring flavor release *in vivo* were also developed. Initial methods, based on trapping (30-32) to increase analyte concentration prior to analysis, were superseded by direct on-line methods (33-36). In the area of flavor matrix binding, a concerted research program in France saw inter-disciplinary teams studying binding of volatiles to β -lactoglobulin. Another French-led activity was the European Union COST96 action, a program that funded a series of meetings between 1995 and 1999 to discuss the interactions between small molecules (mainly flavor compounds) and matrices. There were four separate strands covering instrumental methods, dynamic and sensory methods, theoretical modeling, and kinetic and thermodynamic constants. These meetings brought together practitioners from all over Europe, mainly from academia but also, as word spread, from the food industry and further afield so that a world-wide picture of flavor research could be obtained. The COST action was both a forum for learning from other colleagues and a platform for the dissemination of new ideas; it was a huge success.

Current Key Areas of Published Research

Looking at the scientific literature and the contributions to this book, it is obvious that flavor-matrix interaction is a major research area. Within this category, the work ranges from understanding interactions of flavor compounds with solutes in aqueous media, to interactions with macromolecules (proteins and polysaccharides) and with food structure (e.g. micelles, gels). *In vivo* and dynamic release, modeling, and relating analytical results to human perception are the other major categories. There is no doubt that the 1990's saw a small but discernible step forward in terms of method development and these are now being applied assiduously to try to understand flavor release.

Future Areas for Research

Instrumental – Sensory Correlation

Our ability to relate sensory properties to flavor compounds is very limited. There are some mathematical relationships that link the amount of a single compound with its perceived intensity but they have only been tested under very simple conditions. Now that dynamic flavor release can be measured routinely, the validity of these relationships should be tested more rigorously. The importance of time in determining flavor intensity and quality also needs attention. However, these

Psychophysical Laws apply only to single compounds and there are few hypotheses to explain why a particular mixture of flavor chemicals is perceived as “good” whereas a slightly different formulation is not so well-received. In this area, we should draw from the experience already available from other sensor systems like vision and hearing and examine innovative ideas such as those proposed by Booth (37) and the receptor model proposed by Ennis (38).

These types of studies will need groups of people working together with different specialities. Sensory scientists and flavor chemists are seeing that the relationship between headspace GC-MS and quantitative descriptive analysis is not always evident and perhaps more basic studies will be necessary to link the two disciplines. In this aspect, statisticians and sensory psychologists may help to connect chemistry with perception.

In-Vivo Analysis

As the number of labs participating in experiments measuring flavor release from humans increases, the goal to better link chemical and sensorial data will hopefully be met. Although requiring specialized equipment, this area has high promise for resolving many questions regarding the importance of timing of volatile release and specific enzymatic or temperature-related changes that can occur in the mouth during eating. A review of this area shows which types of techniques are suitable for *in-vivo* analysis (see chapter by Taylor and Linforth in this book).

Molecular Level of Food-Flavor Interactions

Global methods for measuring interactions such as sensory evaluation or headspace analysis have demonstrated the degree of aroma compound retention by various food ingredients. More specific methods such as Hummel and Dreyer using HPLC (see chapters by Semenova et al.) can allow binding parameters to be measured, which give information about the number of binding sites and strengths of the bonds. Spectroscopic techniques such as NMR (see Jung et al chapter), Electronic Paramagnetic Spectroscopy (Goubet et al. chapter), and FT-IR (Lubke et al chapter) can be used to determine the region or specific binding site on the macromolecule. Information on interactions at the molecular level can help in the design of encapsulation agents and also in studies of how changing the structure of the macromolecule or functional groups of the compound, may change the binding parameters.

Texture-Structure Influences on Flavor Release

Liquid systems are relative simple to study and are necessary for forming a basic understanding of physical partitioning and release. When moving to viscous or solid systems, more parameters are involved such as diffusion and breakdown into

articles, as seen in the complex models for solid systems developed by Harrison and Hills (see chapter in this book). Real foods are often even more complex, composed of several different solid phases, and whose characteristics can be regarded more generally as texture or microscopically as structure. Two papers in this book looked specifically at the influence of gel texture and emulsion structure (see chapters by Gwartney and Charles). Benefits can begin to be reaped in this field when theoretical models predict the experimental and sensory release profiles.

Non-Volatile Release

Analytical research in flavor release has mainly concentrated on the volatile fraction, while only through sensory analysis is the effect of non-volatiles on flavor perception studied. Those who have chewed chewing gum past the point of sugar release where the gum seems flavorless (or liked the aroma but not the consumed flavor of bitter coffee) have well noted that the sensations of taste have strong influences on perceived flavor. The role of taste-active substances such as organic acids, bitter peptides, astringent polyphenols, salty ions, or meaty glutamic acid in modifying flavor release, more specifically on the perceptual processing level, may be a relevant area for future investigations.

Conclusions

The past, present, and future developments in flavor release all have the overall final goal of giving a value-added flavor perception to the consumer. This entails using a flavoring that has the correct amount, timing, and quality of flavor. Flavor release studies can provide this information from static or dynamic release data that emanate from specific release situations, such as in-mouth release. Optimizing flavor for products in the 2000s may rely heavily on this fundamental knowledge.

References

1. Darling, D.F.; Williams, D.; Yendle, P. In *Interactions of Food Components*; Birch, G.G.; Lindley, M.G., Eds.; Elsevier Applied Science: London, 1986; pp 165-188.
2. Haring, P.G.R. In *Flavour Science and Technology*; Bessiere, Y.; Thomas, A.F., Eds.; John Wiley: Chichester, 1990; pp 351-354.
3. Overbosch, P. In *Flavour Science and Technology*; Martens, M.; Dalen, G.A.; Russwurm, H., Eds.; John Wiley & Sons Ltd: Chichester, 1987; pp 291-300.
4. Overbosch, P.; Afterof, W.G.M.; Haring, P.G.M. *Food Rev. Int.* **1991**, *7*, 137-184.
5. Kinsella, J.E. In *Flavor chemistry of lipid foods*; Min, D.B.; Smouse, T.H., Eds.; American Oil Chemists' Society: Champaign, 1989; pp 376-403.
6. Bakker, J.; Brown, W.E.; Hills, B.P.; Boudaud, N.; Wilson, C.; Harrison, M. In *Flavour science: Recent developments*; Taylor, A.J.; Mottram, D.S., Eds.; Royal Society of Chemistry: Cambridge, 1996; pp 369-374.

7. Taylor, A.J.; Linforth, R.S.T.; Baek, I.; Brauss, M.S.; Davidson, J.M.; Gray, D.A. In *Advances in flavor chemistry and technology*; Risch, S.; Ho, C.-T., Eds.; American Chemical Society: Washington D.C., 1999; pp in press.
8. Taylor, A.J.; Linforth, R.S.T. *Trends Food Sci. Tech.* **1996**, *7*, 444-448.
9. DeKok, P.M.T.; Smorenburg, H.E. In *Flavor Chemistry: Thirty years of progress*; Teranishi, R.; Wick, E.L.; Hornstein, I., Eds.; Kluwer Academic: New York, 1999; pp 397-408.
10. Taylor, A.J. In *Current Topics in Flavours and Fragrances: Towards a new millenium of discovery*; Swift, K.A.D., Ed.; Kluwer Academic: Dordrecht, 1999; pp 123-138.
11. Teranishi, R.; Wick, E.L.; Hornstein, I. *Flavor Chemistry: Thirty years of progress*; Kluwer Academic: New York, 1999.
12. Pangborn, R.M.; Szczesniak, A.S. *Journal of Texture Studies* **1974**, *4*, 467-482.
13. Ebeler, S.E.; Pangborn, R.M.; Jennings, W.G. *J. Agric. Food Chem.* **1988**, *36*, 791-796.
14. Solms, J.; Osman-Ismail, F.; Beyeler, M. *Can. Inst. Food Sci. Tech.* **1973**, *6*, A10-A15.
15. Rutschmann, M.A.; Solms, J. *Chem. Senses* **1987**, *12*, 200.
16. Voilley, A.; Simatos, D.; Loncin, M. *Lebens. Wiss. Technol.* **1977**, *10*, 45-49.
17. Risch, S.J.; Reineccius, G.A. *Flavor encapsulation*; American Chemical Society: Washington D.C, 1988.
18. Lee, W.E.I. *J. Food Sci.* **1986**, *51*, 249-250.
19. Roberts, D.D.; Acree, T.E. *J. Agric. Food Chem.* **1995**, *43*, 2179-2186.
20. van Ruth, S.M.; Roozen, J.P.; Cozijnsen, J.L. *J. Sci. Food Agric.* **1995**, *67*, 189-196.
21. Elmore, J.S.; Langley, K.R. *J. Agric. Food Chem.* **1996**, *44*, 3560-3563.
22. McNulty, P.B. In *Food Structure and Behavior*; Blanshard, J.M.V.; Lillford, P., Eds.; Academic Press: London, 1987; pp 245-248.
23. Overbosch, P.; Soeting, W.J. In *Flavor chemistry: Trends and developments*; Teranishi, R.; Buttery, R.G.; Shahidi, F., Eds.; American Chemical Society: Washington DC, 1989; pp 138-150.
24. Overbosch, P. *Chem. Senses* **1986**, *11*, 315-329.
25. Overbosch, P.; Vandenenden, J.C.; Keur, B.M. *Chem. Senses* **1986**, *11*, 331-338.
26. DeRoos, K.B.; Wolswinkel, K. In *Trends in Flavour Research*; Maarse, H.; Van der Heij, D.G., Eds.; Elsevier Science: Amsterdam, 1994; pp 15-32.
27. DeRoos, K.B.; Graf, E. *J. Agric. Food Chem.* **1995**, *43*, 2204-2211.
28. Acree, T.E.; Barnard, J.; Cunningham, D. *Food Chem.* **1984**, *14*, 273-??
29. Ulrich, F.; Grosch, W. *Z. Lebensmitt. Untersuch. Forsch.* **1987**, *184*, 277-282.
30. Roozen, J.P.; Legger-Huysman, A. In *Aroma: Perception, formation, evaluation*; Rothe, M.; Kruse, H.-P., Eds.; Eigenverlag Universitat Potsdam: Potsdam, 1994; pp 627-632.
31. Linforth, R.S.T.; Taylor, A.J. *Food Chem.* **1993**, *48*, 115-120.
32. Delahunty, C.M.; Piggott, J.R.; Conner, J.M.; Paterson, A. In *Trends in Flavour Science*; Maarse, H.; van der Heij, D.G., Eds.; Elsevier: Amsterdam, 1994; pp 47-52.
33. Linforth, R.S.T.; Ingham, K.E.; Taylor, A.J. In *Flavour science: recent developments*; Taylor, A.J.; Mottram, D.S., Eds.; Royal Society Chemistry: Cambridge, 1996; pp 361-368.
34. Linforth, R.S.T.; Taylor, A.J. European Patent EP 0819 937 A2, 1998
35. Linforth, R.S.T.; Taylor, A.J. US Patent 5,869,344, 1999
36. Lindinger, W.; Hansel, A.; Jordan, A. *Chem. Soc. Rev.* **1998**, *27*, 347-354.
37. Booth, D.A.; Freeman, R.P.J.; Kendal-Reed, M.S. In *Aroma: perception, formation evaluation*; Rothe, M.; Kruse, H.-P., Eds.; Eigenverlag Deutsches Institut fuer Ernährungsforschung: Potsdam, 1994; pp 101-116.
38. Ennis, D.M. *Food Chem.* **1996**, *56*, 329-335.

Chapter 2

Techniques for Measuring Volatile Release *In Vivo* during Consumption of Food

Andrew J. Taylor and Rob S. T. Linforth

Samworth Flavour Laboratory, Division of Food Sciences,
University of Nottingham, Sutton Bonington Campus, Loughborough,
Leicestershire LE12 5RD, United Kingdom

This chapter provides an overview of the methodology for measuring volatile flavor release under conditions that are found when humans consume foods. Reasons for measuring flavor release *in vivo* are discussed along with the routes by which volatile flavors are sensed by humans. The physiological factors that need to be considered when designing suitable flavor release methodology are listed as well as the properties of the flavor compounds themselves which contain many different odor-active compounds at low concentrations. From these considerations, a list of requirements can be drawn up and the suitability of potential analytical techniques assessed against these criteria. Mass spectrometry is the method of choice with a range of sample introduction techniques available. These can be categorized as indirect methods involving pre-concentration (by adsorbents or membranes) or direct methods. Each system will be discussed and the relative merits presented.

Flavor release from food has been acknowledged as an important factor in determining the perceived flavor quality of many foods. While a simple combination of odoriferous chemicals can give an impression of a particular flavor, e.g., a fruit flavor, it is often difficult to make that same mixture of chemicals evoke the intense flavor experienced when a fresh fruit is eaten at a perfect stage of ripeness. One of the hypotheses to explain the differences between these two situations is that flavors are released at different rates from food, due to the breakdown of the food matrix during eating. This causes the flavor profile to change with time and the flavor sensors respond to the pattern of release, i.e., a combination of the intensity and timing of flavors, rather than just the intensities of the various components in the

flavor mixture. Sensory studies where people are asked to record the intensity of flavor perceived during eating (the so-called Time-Intensity (TI) method (1)) show clearly that individuals sense a change in overall flavor intensity from the initial sniff of a food through the eating phase and afterwards when some flavors persist. With a highly trained panel, it has been claimed that two flavor attributes can be followed simultaneously (2). Some authors have tried to link perceived flavor attributes of a food with flavor composition (see, for example, Togari (3)) but, given the changes that occur in mouth, (4) it seems more appropriate to measure the flavor profile close to the receptors to investigate the link between flavor chemicals and perceived flavor.

Flavor release is also an issue with encapsulated flavors. To prevent loss or chemical change during processing and storage of foods, flavor compounds are often added in an encapsulated form. While many of these encapsulants are very efficient, it is also essential that the flavor molecules are released when the food is consumed, otherwise the flavor, despite being in good condition, will not be sensed. Fisher provided an excellent demonstration of this with an encapsulated flavor in a biscuit that was only effectively released when the biscuit was “dunked” in hot tea (5).

For these reasons, methods to measure flavor release have been developed over the last twenty years since the early attempt by Mackay and Hussein (6). The last five years have seen several groups developing methods which show that flavor release does change with time and that flavor release can be related to perceived flavor measured by conventional sensory methods or using TI methods (7, 8).

Physiological, Compositional and Analytical Considerations

Overall flavor of a food is generally agreed to consist of taste (sensed on the tongue) odor (sensed in the nose) and pain (sensed by trigeminal receptors in both the mouth and nose). Most work has focused on volatile odor compounds but the potential interaction of non-volatiles and volatiles should not be ignored (9). Davidson has developed methods for following release of non-volatile flavor compounds (10, 11) and summarizes them elsewhere in this book. Volatile flavors enter the nose orthonasally (i.e. through the nostrils) before eating and “sniffing” of food provides our first flavor impression. This signal is derived from the volatiles in the air above a food (the headspace) and can be measured relatively easily. Once food is in the mouth, volatiles are “pumped” from the mouth into the throat either due to swallowing, or chewing, when the movement of the mouth introduces small quantities of air from the mouth into the tidal flow of air from the lungs. In this case, volatiles reach the odor receptors in the nose through the retronasal route. Each breath cycle lasts about 5 s and there is a substantial dilution of volatiles from the gas phase in-mouth to the gas phase in-nose (somewhere between 10 and 1000 times). The human nose is quite sensitive and the minimum volatile concentrations detectable are expressed as odor thresholds. Values can be found in the literature (12, 13). If flavor release is to be measured effectively, then any method must be capable of fulfilling the requirements listed in Table I.

Table I. Physiological Factors and Influence on Analyses

<i>Factor</i>	<i>Physiology</i>	<i>Limit</i>
Speed	Breathing cycle	Once every 5 s
Sensitivity	Odor threshold	ppm to ppt (mg/L to ng/L)
Water tolerant	Humid air in nose and mouth	Up to 100% RH
Human interface	Must allow normal eating and breathing patterns	

Similarly, commercial flavorings contain between 20 and 200 different compounds and, ideally, methods for monitoring flavor release should be able to detect all compounds (universal detection) at concentrations at, or below, their odor thresholds. Analysis should allow simultaneous monitoring of all odor active compounds and provide sufficient resolution for the compounds to be identified. The speed of analysis should also be sufficient so that release can be seen on a breath by breath basis. Since one breath cycle lasts 5 s, measurements need to be taken at least every 0.1 s to obtain enough data points to define volatile release on one exhalation/inhalation cycle. This ideal situation cannot be achieved by any of the methods currently available but provides a check list against which the merits of each system can be assessed.

Most published information on analysis of trace organic compounds in air comes from environmental monitoring for pollutants. These may originate from landfill sites, from chemical emergencies (e.g. identification of chemicals following a road accident) or from military applications (detection of chemical warfare agents). There are also reports of breath analysis as a diagnostic aid in medicine and for monitoring exposure in the workplace (14, 15). For many of these applications, instant detection at low sensitivity is required and these are the methods of interest for monitoring flavor release. Mass spectrometry is the analytical technique of choice due to its sensitivity and its potential to identify compounds. Interfacing breath samples from people to the mass spectrometer is the major issue and the various techniques are discussed below.

Sampling Air during Eating

As described above, volatiles from food are released at different rates and to different extents due to eating and due to dilution in the airways of the mouth and nose. Depending on the purpose of the analysis, air can be sampled from different positions in the mouth and nose. If the aim is to study the relationship between the volatiles and sensory perception, it seems sensible to take air as close as possible to the olfactory receptors. However, the practical problems of locating the sampling tube near the olfactory epithelium, which is located on the surface of the nasal turbinates, without causing damage, and in a manner that satisfies ethical considerations, means that collection of air at the nostril is the usual practice. Some research groups have

used tubes in both nostrils to sample all expired air (16, 17), others have devised a system of valves with an air reservoir (18), while, in our group (19), we have been keen to maintain normal eating and breathing patterns, so have sampled only a portion of air from one nostril.

Trapping/Pre-Concentration Methods

Since the concentrations of volatiles in expired air from the nose and mouth are low, the actual amount available for analysis may be below the detection limit of the analytical system. In this case, pre-concentration may be needed. Adsorbents like Tenax have been successfully used (16, 20-34) to follow flavor volatile release with time. Samples are collected over short time periods (e.g. from 0 to 20 s), the Tenax desorbed and analyzed using conventional GC-MS (Figure 1), and the data are taken to represent the average signal which is plotted at the midpoint (i.e. 10 s in this case). By overlapping the time periods, release curves can be constructed and temporal changes seen. Release can be expressed as a function of time or on an accumulated basis (35).

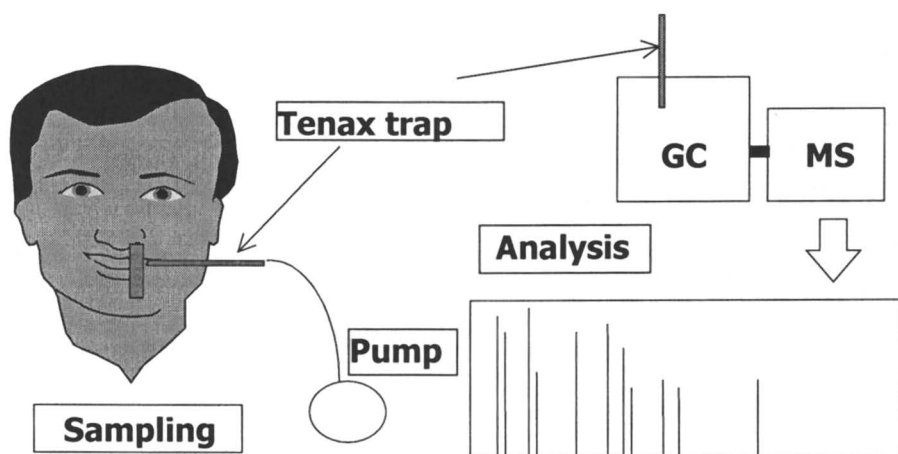


Figure 1. Collection and analysis of expired air by Tenax trapping and GC-MS.

When concentrations are very low, several samples from one time period can be collected on a single trap and then desorbed. With the advent of SPME systems, volatiles can also be trapped and analyzed relatively rapidly (36). The advantages of these methods are that the apparatus is readily available, cheap, and well-understood by flavor researchers. Through pre-concentration, there is sufficient material for GC-MS analysis, which allows unequivocal identification of most compounds. The disadvantages are that the process is very time-consuming and subject to the limitations of all adsorbents, namely their selectivity and the variations in trapping efficiencies (37). Other methods of trapping have also been reported. Kallio (38)

collected samples of headspace from onions at various times onto lengths of tubing and then analyzed them by GC. Cryotrapping onto loops of capillary tubing connected to a multiport valve has potential but needs good design to ensure efficient trapping and desorption thereafter (33, 39).

Membrane Interfaces for MS

The trapping methods described above, concentrate the volatiles from expired air to improve the signal obtained by GC-MS and also remove, to a large extent, air and water which tend to add to the noise in conventional Electron Impact (EI)-MS systems. Hence the signal to noise ratio is greatly enhanced by trapping. The same result can be obtained for selected hydrophobic compounds using a membrane interface between a gas sample and the high vacuum region of a mass spectrometer. The membrane allows certain compounds to pass from the sample gas stream (or liquid stream in some cases) into a helium stream while preventing transfer of gas. The result is a concentration of analyte molecules and a change of gas from air to helium, which puts less load on the vacuum pumps and therefore maintains high vacuum conditions without the necessity for extra pumping capacity. Cooks group at Purdue University have reported extremely low detection limits for benzene, toluene and chlorinated solvents using a membrane interface coupled with an ion trap MS (40). A detection limit of 500 parts per quadrillion (pg/kg) was claimed for toluene and other groups have reported sensitivity in the parts per trillion range for the same group of compounds (41, 42).

The technique is not so well-suited to the analysis of food flavors which contain a wide range of compounds with different hydrophobicity values and, inevitably, the membrane will not transfer all the compounds to the same extent. There is also an issue with speed as there is a finite time for the compounds to pass across the membrane and into the MS. Further, with ion traps, the dwell time (the time spent monitoring an ion) tends to be high to obtain maximum sensitivity. In the environmental systems, typical response times seem to be between 5 s (40) and 120 s (42). While this is not an issue in environmental monitoring, where changes are slow, it does limit the detail that can be seen when flavor release is followed breath by breath.

Two publications have examined the use of membrane interfaces for measuring flavor release from foods. Soeting and Heidema (17) used a solid membrane (rather than a hollow fiber) between the air flow from the nostrils and the EI source of a conventional MS. Sensitivity was in the order of ppm (mg/kg) and response time was less than 1 s giving breath by breath release curves. This paper marked the beginning of real time breath-by-breath analysis of flavor release. The same system was tested more recently (43) but with similar levels of performance. Springett (44) described a hollow fiber system with a response time of 43 s which was used to monitor diallyl sulfide release from model systems. No sensitivity data were quoted and concentrations were expressed on a relative basis.

Jet Separator Interface

Jet separators have been used to interface GC columns with high flow rates to mass spectrometers and the idea of using a jet separator to connect a dynamic headspace cell directly to a MS has been reported (45). The principle of this type of interface is that the volatiles in the headspace are enriched, thus increasing the sensitivity of the system. In practice, helium had to be used in the headspace to prevent vacuum problems and this might change the release characteristics compared to air. Chemical Ionization (CI) was used to ionize the volatiles and the authors reported several problems with “noise” from the isobutane reagent gas and short life for the electron multiplier as it was subject to air during evacuation of the sample vessel.

Atmospheric Pressure Ionization Mass Spectrometry (API-MS)

This technique is a “soft” ionization method that causes little fragmentation of the compounds and produces mainly molecular ions by addition or abstraction of a proton. Most molecules (R) are ionized by addition of a proton in positive ionization mode to give $R+H^+$. Ionization occurs through a charge transfer mechanism where water is charged initially to produce H_3O^+ ions (in the positive mode) and the charge is then transferred to analyte molecules. Conveniently, water has a proton affinity which means it will transfer its charge to flavor volatiles but will not interact with the components in air (O_2 , N_2 , CO_2), as they have lower proton affinities than water (46). Thus water is an essential component for ionization to occur, whereas, with EI and CI, it can interfere with the process. The charge transfer process tends to form cluster ions of the form $R(H_3O^+ \cdot H_2O)_n$ which can complicate the spectrum. A flow of dry nitrogen gas (curtain gas) is often used to break up (decluster) these ions so that the molecular ion $[M+H]^+$ is formed. Besides confusing the spectrum, the relative amount of charge in each ion can vary, making quantification difficult unless the sum of all ions is measured. Sensitivity also suffers as the charge is distributed across several ions, with lower signal to noise ratio, rather than concentrated into one ion with maximum signal to noise ratio.

The early literature on API-MS focused on analysis of volatiles in gases (18). Some authors used ionization from a radioactive nickel source but this has now been largely replaced by corona pin ionization giving a better dynamic range and removing some of the interference noted by Benoit (18) who attributed it to ammonia on the breath. Detection of chemical warfare agents down to the parts per trillion level were reported using a tandem MS technique (47) but these limits were achieved because the analytes had m/z values that lie outside the “chemical noise” region that is found in all atmospheric ionization techniques like API and Electrospray. Many flavor volatiles have m/z values that overlap with this chemical noise area and the limit of sensitivity is often determined by noise rather than signal. When using API, it is therefore essential to remove any potential contaminants in the nitrogen supply and to reduce the background volatiles in the environment. These may come from volatile

chemicals stored in the laboratory or from material in the fabric of the room like paint and vinyl flooring. A recirculating air purifier containing activated carbon reduces levels of these compounds significantly and can reduce background signal in the API.

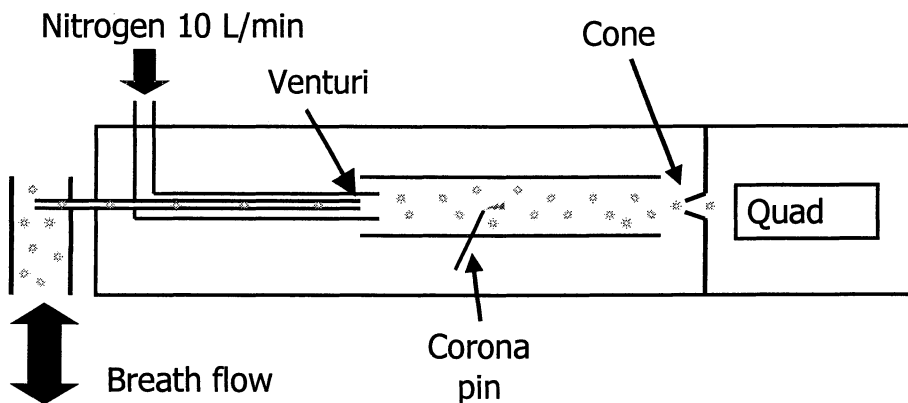


Figure 2. API-MS interface for breath by breath analysis.

In our laboratory, an interface for API-MS has been developed for the detection of volatiles in expired air from people during the consumption of food (48). The device is simple (Figure 2) and uses a venturi to sample air from the nose, mouth or the headspace above a food at flow rates of 5 to 50 mL/min. This obviates the need for pumps, which can add contaminants to the air or act as traps for volatiles, giving long lasting backgrounds. The mass spectrometer can be operated in scan mode to identify significant ions or, if the key volatile components are known, the mass spectrometer is set in the Selected Ion Recording mode which increases sensitivity considerably. For each compound, the ionization parameters (positive or negative ionization, cone voltage) are optimized so that fragmentation is either minimized or controlled. The interface is also highly effective at declustering, with the result that the spectra are relatively simple with each volatile component represented by one major ion. This avoids the need for deconvolution of the data. With a dwell time of 0.01 s for each compound and a low dead volume, the technique provides real time analysis of volatiles introduced into the interface and is now commercially available as the MS-Nose™ from Micromass, UK. Sensitivity is typically 10 ppbv (10nL/L) although some nitrogen-containing compounds with odd mass (and therefore little background noise) can be detected down to 100 pptv.

Identification of compounds depends entirely on mass resolution so neither structural isomers like 2- and 3-methylbutanal nor stereoisomers can be identified. However, the identity of some compounds with characteristic isotopic ratios can be confirmed. Allyl methyl sulfide is an example where masses of 89, 90 and 91 in a ratio of 100:5.4:4.6 would be expected for the pure compound and this has been used (49) to demonstrate that no interfering compounds were present in the analysis of

compounds following ingestion of garlic. A similar approach was reported by Spanel and Smith (50) for identification of some onion volatiles. With API-MS, the actual amount of compound in a sample can be calculated after calibration of the interface with solutions of authentic compounds in hexane. The solutions are injected from a microsyringe into the gas stream where they volatilise. From the flow rate and amount injected, the concentration of volatile in the sample can be expressed on a volume basis (ppbv; nL/L) or on a weight/volume basis (ppb; ng/L).

This version of API-MS has been used in a wide range of applications. Breath by breath release of volatile flavors from foods using API-MS from our laboratory was first reported at the Weurman Symposium in 1996 (19). Since then, the technique has proved useful to quantify the differences in flavor release profile when foods are reformulated, for example when flavoring low fat analogues (51, 52). The rapid production of volatiles through the lipid oxidation pathway in tomatoes has been measured *in vivo* for individual fruit and the fruit-to-fruit variation determined as well as the varietal differences (53). Firmenich SA (Geneva) have adopted this methodology, which they have named Analysis of Flavor and Fragrances In Real tiMe (AFFIRM) to assist in the development of flavors and fragrances. They have reported the release of mint volatiles from chewing gum containing liquid and encapsulated flavors and shown different flavor delivery profiles (54). Other applications of our version of API-MS can be found in this book in the contributions of Linforth *et al*, Marin *et al*, Parker *et al* (modeling of flavor release), Harvey *et al* (food flavor applications) and Hollowood *et al* (sensory aspects of flavor release).

Proton Transfer Reaction-Mass Spectrometry (PTR-MS)

This technique has been developed by Lindinger's group in Innsbruck, initially as a technique for studying ion chemistry at a fundamental level and then applied to the analysis of trace organic compounds in the environment and from food (46, 49, 55-59). Figure 3 shows the layout of the PTR with reagent ions (H_3O^+) being formed in the ion source after which they are mixed with the air to be analyzed through a venturi. Charge transfer and ion separation takes place in the drift tube region where the conditions are carefully controlled to minimize cluster formation. The sensitivity of the system for environmental pollutants like benzene, toluene, alkylbenzenes is high (ppt) although, like other techniques, the sensitivities for flavor compounds are lower (typically ppb, Lindinger, personal communication). The Selected Ion Flow Tube (SIFT-MS) method described by Smith and Spanel (50, 60, 61) also generates reagent ions separately but there are significant differences in the way product ions are analyzed which leads to lower sensitivity and the presence of many cluster ions. The key differences between PTR and API are that the reagent ions are formed separately and then allowed to react with analytes in the sample under reduced pressure. The result is that the background count with PTR-MS is low and this allows high sensitivity to be obtained by spending more time collecting signal for a particular ion, whereas, with API this produces no benefit.

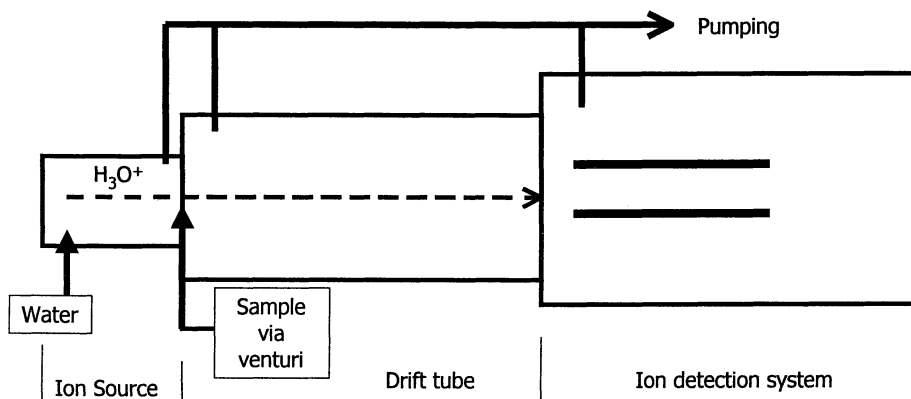
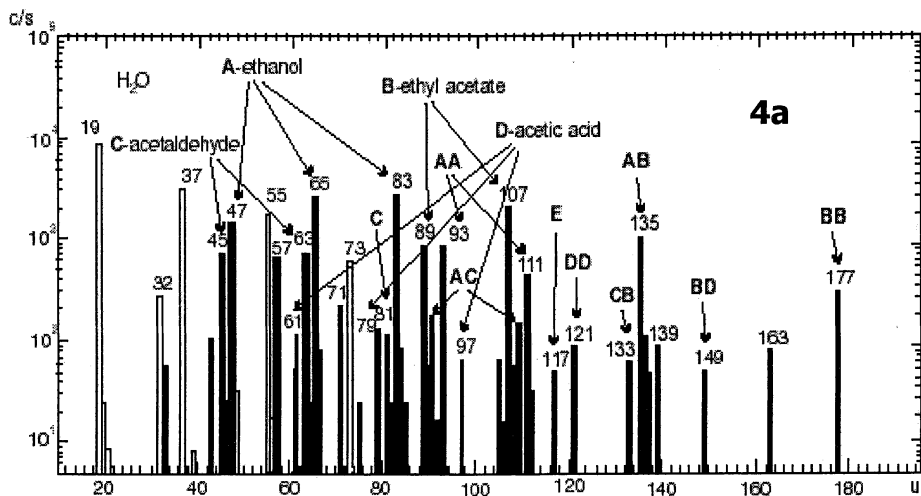


Figure 3. Key elements of Proton Transfer Reaction MS (redrawn from (46)).

The publications from Lindinger's group (49) and from Spanel and Smith (50) show some mass spectral data from headspace analysis of flavor molecules. When 2.5 ppm of allyl sulfide was analyzed with PTR-MS (Figure 2 in Taucher (49)) around thirty ions were seen in the mass range 15 to 95 due to garlic volatiles, cluster ions of water and other compounds present in air but, quantification of allyl methyl sulfide was possible in this system. The Spanel and Smith technique however, produces very complex spectra and, in the analysis of banana headspace (50), there seem to be cluster ions formed between two different compounds (Figure 4a). It is not clear what effect this has on both sensitivity and quantification. Because the charge will now be shared between several ions, the signal to noise ratio will be reduced (and therefore the sensitivity) while it is not obvious how quantification can be achieved if a compound can interact with other analytes and, presumably, the intensity of one particular ion depends on the other molecules present. An API-MS trace of banana headspace obtained using the MS-Nose interface is shown for comparison in Figure 4b. The API-MS trace shows a single, major ion for each flavor component (except for the fragment ion at 61) with little evidence of cluster ions as the ionization parameters for each compound have been optimized as described previously. It is interesting to note that Figure 4a shows ethanol and acetaldehyde as major components of banana headspace but there is no trace of isoamyl acetate ($\text{C}_7\text{H}_{10}\text{O}_2$; MW 130), the characteristic odor impact compound of banana. The tentative identities in Figure 4b are based on a separate GC-MS analysis of banana headspace. Since the volatiles from bananas are known to vary between fruit, between cultivars and with time after harvest, it is impossible to compare the PTR and API systems directly. However, the comment by Spanel and Smith (50) that, with API-MS analysis, "interpretation of the mass spectra is complicated, coupled with which the complex kinetics involved in APCI-MS makes quantification of the separate volatile organic compounds very difficult" is not borne out by Figure 4 and the fact that quantification can easily be achieved by introducing authentic compounds into the API source to calibrate it.



headspace of Chiqita banana
BBAS1 44 (1 565) Cm (30:45-1:15)

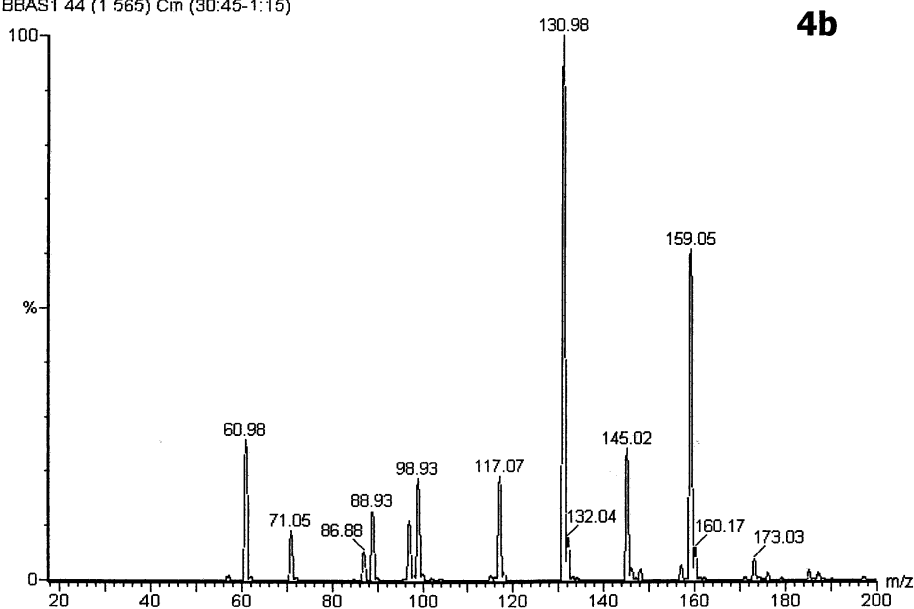


Figure 4. Headspace volatiles from banana using PTR-MS (Figure 4a; reproduced with permission from reference 50) and API-MS (Figure 4b). Tentative identifications in Figure 4b by GC-MS. All ions in Figure 4b are $[M+H]^+$ except where otherwise stated: 61 fragment from (iso)amyl acetate, 71 (iso)amyl alcohol $[M-H_2O+H]^+$; 87 diacetyl/2-pentanone; 89 ethyl acetate; 99 hexenal; 117 ethyl butyrate; 131 (iso)amyl acetate; 145 hexyl acetate; methylbutyl butyrate; 173 amyl valerate; 187 methylbutyl hexanoate.

Spanel and Smith have used cluster ions to identify compounds and have also used selective ionization (using H_3O^+ and then NO^+ reagent ions), which has allowed them to differentiate structural isomers and, in one case, stereoisomers. For instance, in the banana headspace example discussed above, the use of the two reagent ions showed that the compound B (Figure 4a) with an ion at 89 ($\text{C}_4\text{H}_8\text{O}_2$) was definitely ethyl acetate not methyl propionate. More interestingly, *trans*-2-hexenal and *cis*-3-hexenal could be differentiated by the formation of a $[\text{M-OH}]^+$ ion at 81 for the *cis* isomer (with H_3O^+ as reagent) and $[\text{M-CHO}]^+$ and $[\text{M-C}_2\text{H}_4]^+$ at 69 and 70 (with NO^+ as reagent). The challenge now is to ascertain whether these resolutions can be obtained for the isomers when they are present in complex mixtures (e.g. headspace above plant foods) or whether the ion interactions noted in the banana example will interfere and obscure these differences. However, the ability to resolve isomers using different ionization methods is a significant achievement and increases the power of direct MA analysis of volatiles considerably.

The published data on PTR-MS contains little information on flavor release *in vivo* and it is therefore difficult to evaluate this technique for breath by breath analysis. Lindinger (personal communication) has provided data on the release of volatiles from bananas during eating using a dwell time of 0.1 s that produced resolution of each breath and evidence of the pumping action of mouth movements superimposed on individual breath cycles. The concentrations of volatiles in exhaled air were between 1500ppbv (isoamyl alcohol) and 100ppbv (esters). Further work should be published soon.

Selective Ionization using Lasers

As discussed above, direct analysis of volatiles in mixtures by MS makes it difficult to identify the individual compounds present. One approach is to take a sample and analyze it off-line using conventional GC-MS. Another is the use of two reagent ions as reported for PTR-MS. An alternative approach is to use an ionization method that selectively ionizes components in the mixture. Resonance Enhanced Multiple Photon Ionization (REMPI) is one such technique. A laser is used to ionize the sample and, by selecting the wavelength of excitation, the chosen compounds will be ionized. In terms of food flavor analysis, the work by Zimmerman (62, 63) is interesting. Using a laser tuned to 266nm, the volatiles in coffee headspace were analyzed and phenolic compounds like 4-vinylguaiacol were particularly well-suited to this technique. The mass spectra obtained showed some fragmentation although it did not hinder interpretation and structures could be assigned to the majority of masses. The concentrations detected were in the order of 100 ppb and the speed of analysis was 1 Hz (one data point per second). The data show the potential of the technique but it is not clear how much selectivity can be introduced by changing the wavelength of excitation in a typical mixture of flavor chemicals. For real time analysis, a laser that is capable of rapid switching between wavelengths is required. Developments in laser technology will no doubt increase the use of this technique.

Conclusions

None of the techniques described above possesses all the attributes required for optimal breath by breath analysis. However both the techniques based on charge transfer (API- and PTR-MS) are sufficiently developed for flavor release to be followed. The published data show that there are significant changes in the volatile profile during eating and the next challenge is to try and correlate these temporal data with flavor perception, the topic of another section in this book.

Acknowledgements

The authors acknowledge financial and technical help from Firmenich SA (Geneva), Micromass (UK) and from the UK Ministry of Agriculture, Fisheries and Food and from the Biological and Biotechnological Science Research council in the development of API-MS at the University of Nottingham AJT is grateful to the University of Nottingham and to Firmenich for a sabbatical period in Geneva when this manuscript was prepared. A Blake and BA Harvey (Firmenich SA) are thanked for supplying data for Figure 4b and for helpful discussions.

References

1. Cliff, M.; Heymann, H. *Food Res. Int.* **1993**, *26*, 375-385.
2. Duizer, L.M.; Bloom, K.; Findlay, C.J. *Food Qual. Pref.* **1997**, *8*, 261-269.
3. Togari, N.; Kobayashi, A.; Aishima, T. *Food Res. Int.* **1995**, *28*, 485-493.
4. Taylor, A.J. *Crit. Rev. Food Sci. Nutr.* **1996**, *36*, 765-784.
5. Fisher, L. *Nature* **1999**, *397*, 469 only.
6. Mackay, D.A.M.; Hussein, M.M. In *Analysis of foods and beverages*; Charalambous, G., Ed.; Academic Press: New York, 1978; pp 283-357.
7. Linforth, R.S.T.; Baek, I.; Taylor, A.J. *Food Chem.* **1999**, *65*, 77-83.
8. Baek, I.; Linforth, R.S.T.; Blake, A.; Taylor, A.J. *Chem. Senses* **1999**, *24*, 155-160.
9. Noble, A.C. *Trends Food Sci. Tech.* **1996**, *7*, 439-443.
10. Davidson, J.M.; Linforth, R.S.T.; Taylor, A.J. *J. Agric. Food Chem.* **1998**, *46*, 5210-5214.
11. Davidson, J.M.; Hollowood, T.A.; Linforth, R.S.T.; Taylor, A.J. *J. Agric. Food Chem.* **1999**, *in press*.
12. Devos, M.; Patte, F.; Rouault, J.; Laffort, P.; Van Gemert, L.J. *Standardized human olfactory thresholds*; IRL Press: Oxford, 1990.
13. Van Gemert, L.J.; Nettenbreijer, A.H. *Compilation of odor threshold values in air and water*; National Institute for Water Supply: Voorburg, The Netherlands, 1977.

14. Giardino, N.J.; Gordon, S.M.; Brinkman, M.C.; Callahan, P.J.; Kenny, D.V. *Epidemiology* **1999**, *10*, 167.
15. Kenny, D.V.; Callahan, P.J.; Gordon, S.M.; Stiller, S.W. *Rapid Comm. Mass Spec.* **1993**, *7*, 1086-1089.
16. Delahunty, C.M.; Piggott, J.R.; Conner, J.M.; Paterson, A. In *Trends in Flavour Science*; Maarse, H.; van der Heij, D.G., Eds.; Elsevier: Amsterdam, 1994; pp 47-52.
17. Soeting, W.J.; Heidema, J. *Chem. Senses* **1988**, *13*, 607-617.
18. Benoit, F.M.; Davidson, W.R.; Lovett, A.M.; Nacson, S.; Ngo, A. *Anal. Chem.* **1983**, *55*, 805-807.
19. Linforth, R.S.T.; Ingham, K.E.; Taylor, A.J. In *Flavour science: recent developments*; Taylor, A.J.; Mottram, D.S., Eds.; Royal Society Chemistry: Cambridge, 1996; pp 361-368.
20. Delahunty, C.M.; Piggott, J.R.; Conner, J.M.; Paterson, A. *Ital. J. Food Sci.* **1996**, *8*, 89-98.
21. Delahunty, C.M.; Piggott, J.R.; Conner, J.M.; Paterson, A. *J. Sci. Food Agric.* **1996**, *71*, 273-281.
22. vanRuth, S.M.; Roozen, J.P.; Cozijnsen, J.L. *Food Chem.* **1995**, *53*, 15-22.
23. vanRuth, S.M.; Roozen, J.P.; Cozijnsen, J.L. *Chem. Senses* **1995**, *20*, 146.
24. vanRuth, S.M.; Roozen, J.P.; Hollmann, M.E.; Posthumus, M.A. *Z. Lebensmitt. Untersuch. Forsch.* **1996**, *203*, 7-13.
25. Odake, S.; Roozen, J.P.; Burger, J.J. *Nahrung-Food* **1998**, *42*, 385-391.
26. Ingham, K.E.; Linforth, R.S.T.; Taylor, A.J. *Food Chem.* **1995**, *54*, 283-288.
27. Ingham, K.E.; Linforth, R.S.T.; Taylor, A.J. *Lebens. Wiss. Technol.* **1995**, *28*, 105-110.
28. Ingham, K.E.; Linforth, R.S.T.; Taylor, A.J. *Flav. Frag. J.* **1995**, *10*, 15-24.
29. Ingham, K.E.; Linforth, R.S.T.; Taylor, A.J. In *Bioflavour 95*; Etievant, P.X.; Schreier, P., Eds.; INRA: Paris, 1995; pp 63-66.
30. Linforth, R.S.T.; Ingham, K.E.; Taylor, A.J. In *Bioflavour 95*; Etievant, P.X.; Schreier, P., Eds.; INRA: Paris, 1995; pp 29-34.
31. Clawson, A.R.; Linforth, R.S.T.; Ingham, K.E.; Taylor, A.J. *Lebens. Wiss. Technol.* **1996**, *29*, 158-162.
32. Ingham, K.E.; Taylor, A.J.; Chevance, F.F.V.; Farmer, L.J. In *Flavour science: recent developments*; Taylor, A.J.; Mottram, D.S., Eds.; Royal Society Chemistry: Cambridge, 1996; pp 386-391.
33. Linforth, R.S.T.; Taylor, A.J. *Food Chem.* **1993**, *48*, 115-120.
34. Linforth, R.S.T.; Savary, I.; Pattenden, B.; Taylor, A.J. *J. Sci. Food Agric.* **1994**, *65*, 241-247.
35. Delahunty, C.M.; Piggott, J.R. *Int. J. Food Sci. Tech.* **1995**, *30*, 555-570.
36. Grote, C.; Pawliszyn, J. *Anal. Chem.* **1997**, *69*, 587-596.
37. Wyllie, S.G.; Alves, S.; Filsssof, M.; Jennings, W.G. In *Analysis of foods and beverages: Headspace techniques*; Charalambous, G., Ed.; Academic Press: New York, 1978; pp 1-15.
38. Kallio, H.; Alhoniemi, P.; Tuomola, M. In *Trends in Flavour Science*; Maarse, H.; van der Heij, D.G., Eds.; Elsevier: Amsterdam, 1994; pp 463-474.

39. Taylor, A.J.; Linforth, R.S.T. *Trends Food Sci. Tech.* **1996**, *7*, 444-448.
40. Soni, M.; Bauer, S.; Amy, J.W.; Wong, P.; Cooks, R.G. *Anal.Chem.* **1995**, *67*, 1409-1412.
41. Cisper, M.E.; Gill, C.G.; Townsend, L.E.; Hemberger, P.H. *Anal.Chem.* **1995**, *67*, 1413-1417.
42. Virkki, V.T.; Ketola, R.A.; Ojala, M.; Kotiaho, T.; Komppa, V.; Grove, A.; Facchetti, S. *Anal.Chem.* **1995**, *67*, 1421-1425.
43. Reid, W.J.; Wragg, S., *Flavour release measurement by in-mouth breath mass spectrometry. 1. Development of membrane interface.* 1995, Leatherhead Food Research Association.
44. Springett, M.B.; Rozier, V.; Bakker, J. *J. Agric. Food Chem.* **1999**, *47*, 1125-1131.
45. Elmore, J.S.; Langley, K.R. *J. Agric. Food Chem.* **1996**, *44*, 3560-3563.
46. Hansel, A.; Jordan, A.; Holzinger, R.; Prazeller, P.; Vogel, W.; Lindinger, W. *Int. J. Mass Spec. Ion Proc.* **1995**, *150*, 609-619.
47. Ketkar, S.N.; Penn, S.M.; Fite, W.L. *Anal.Chem.* **1991**, *63*, 457-459.
48. Linforth, R.S.T.; Taylor, A.J. *European Patent EP 0819 937 A2* **1998**.
49. Taucher, J.; Hansel, A.; Jordan, A.; Lindinger, W. *J. Agric. Food Chem.* **1996**, *44*, 3778-3782.
50. Spanel, P.; Smith, D. *Rapid Comm. Mass Spec.* **1999**, *13*, 585-596.
51. Brauss, M.S.; Balders, B.; Linforth, R.S.T.; Avison, S.; Taylor, A.J. *Flav. Frag. J.* **1999**, *in press*.
52. Brauss, M.S.; Linforth, R.S.T.; Cayeux, I.; Harvey, B.; Taylor, A.J. *J. Agric. Food Chem.* **1999**, *47*, 2055-2059.
53. Brauss, M.S.; Linforth, R.S.T.; Taylor, A.J. *J. Agric. Food Chem.* **1998**, *46*, 2287-2292.
54. Harvey, B., *Measuring flavour release from chewing gum*, in *Kennedy's Confection.* 1997. p. 18-20.
55. Hansel, A.; Jordan, A.; Warneke, C.; Holzinger, R.; Lindinger, W. *Rapid Comm. Mass Spec.* **1998**, *12*, 871-875.
56. Jordan, A.; Hansel, A.; Holzinger, R.; Lindinger, W. *Int. J. Mass Spec. Ion Proc.* **1995**, *148*, L1-L3.
57. Lindinger, W.; Hansel, A.; Jordan, A. *Chemical Society Reviews* **1998**, *27*, 347-354.
58. Lindinger, W.; Hansel, A.; Jordan, A. *Int. J. Mass Spec.* **1998**, *173*, 191-241.
59. Taucher, J.; Hansel, A.; Jordan, A.; Fall, R.; Futrell, J.H.; Lindinger, W. *Rapid Comm. Mass Spec.* **1997**, *11*, 1230-1234.
60. Spanel, P.; Ji, Y.F.; Smith, D. *Int. J. Mass Spec.* **1997**, *165*, 25-37.
61. Spanel, P.; Smith, D. *Int. J. Mass Spec.* **1998**, *172*, 137-147.
62. Zimmerman, R.; Heger, H.J.; Dorfner, R.; Boesl, U.; Kettrup, A. *Chem Labor Biotech* **1998**, *49*, 210-214.
63. Zimmerman, R.; Heger, H.J.; Yeretian, C.; Nagel, H.; Boesl, U. *Rapid Comm. Mass Spec.* **1996**, *10*, 1975-1979.

Chapter 3

Real-Time Flavor Release from Foods during Eating

B. A. Harvey¹, M. S. Brauss², Rob S. T. Linforth², and Andrew J. Taylor²

¹Corporate R&D Division, Firmenich S. A., 1 route des Jeunes,
1211 Geneva 8, Switzerland

²Samworth Flavour Laboratory, Division of Food Sciences,
University of Nottingham, Sutton Bonington Campus, Loughborough,
Leicestershire LE12 5RD, United Kingdom

Measurement of flavor release from foods as they are eaten on a breath-by-breath basis (nosespace) has been made possible using Atmospheric Pressure Chemical Ionization (APCI) Mass Spectrometry. An overview is given of some applications of the technique, which is rapid, sensitive and quantitative. In conjunction with simultaneous sensory evaluation it may be used to assist in the design of release profiles of flavors from foods with desired perceptual characteristics; encapsulation of flavors added to chewing gum is used as an example. Change in nosespace volatile concentrations following homogenization of components of a composite food is demonstrated. The effects on flavor release of food formulation variables can be rapidly determined, illustrated by differential intensities and release rates from yogurts of varying fat content. A further example is given showing the sequential release during eating of enzymatically generated volatiles from fruit such as tomatoes.

It has long been a goal of flavor research to have an analytical procedure which could detect and discriminate odor chemicals from breath in real time with sensitivity comparable to the human nose. This has been achieved by Prof. A. Taylor and Dr. R. Linforth at the University of Nottingham in a joint project with Firmenich S.A.(1). The method used is Atmospheric Pressure Chemical Ionization (APCI) Mass Spectrometry, combined with a specially developed interface to allow continuous analysis of the breath from the nose (nosespace) of a volunteer taster. Breath is sampled at a constant rate and is diluted by a flow of nitrogen carrier gas. APCI is a soft ionization technique, typically producing an ion of a flavor molecule plus a

proton (MH⁺) without fragmentation. Many compounds may be monitored simultaneously in exhaled breath on a breath-by-breath basis and are identified by their different masses. Quantification is achieved by injection of standard solutions of volatiles in an effectively inert solvent, via a syringe pump into the carrier gas flow. Tests on a range of compounds of different functionalities have shown a linear response from the mass spectrometer over ranges of nosespace volatile concentrations commonly found during eating. APCI-MS as a technique for breath analysis has been reported elsewhere (2) although it is difficult to make a comparison of the relative performance.

The use of APCI-MS has opened up a great potential for analysis of gas phase volatiles in real time other than breath analysis. A range of such applications has been developed by Firmenich using the technique under the acronym AFFIRM[®] (Analysis of Flavors and Fragrances In Real-tiMe). Breath analysis however remains the most important application.

The main advantages of AFFIRM[®] are the capacity to measure quantitatively the kinetics of the release of flavor molecules over much shorter time periods than has previously been possible, speed of data collection and sensitivity typically down to levels of a few ppb. This paper gives an overview of some applications of AFFIRM[®] active nosespace analysis using a range of food types as examples.

Results and Discussion

Data from breath analysis using AFFIRM[®] can be used in many ways. For instance, nosespace data can be collected from trained sensory panelists as they simultaneously estimate perceived flavor intensity as a function of time. Parallel processing of the analytical and sensory data obtained in this way can lead to a better understanding of those factors which affect flavor perception (3,4). AFFIRM[®] can be used to aid flavorists in flavor creation by matching nosespace concentrations of volatiles in a flavor formula incorporated in a food to those in a target food. It can, in addition, provide rapid feedback to flavorists and scientists in the development of e.g. flavor encapsulation systems. The speed of data collection also lends itself to initial screening of products before commencing sensory testing, with substantial savings of time and resources.

Chewing gum is a good medium for demonstrating and comparing release of volatiles into the breath, since a large part of the starting material remains in the mouth for as long as required. A survey of market chewing gums has shown that the intensity and time dependence of flavor release vary greatly (5), illustrated by the release of menthol from three market sugar-free peppermint chewing gum sticks from different manufacturers (Figure 1). Release of a single flavor compound only, menthol, is presented here for clarity. Samples were chewed by the same operator for 20 minutes. Each data point represents the maximum menthol intensity from one breath. Data were collected for the first 5 minutes and for periods of one minute each after 10 and 20 minutes to compare lastingness.

While the matrix compositions of the market samples are unknown and variable, flavor bursts in the first 1-2 minutes of eating can often be associated with the presence of visible embedded granules or a hard sugar coating containing relatively high concentrations of volatiles which are released into the breath when crushed by chewing. Release profiles between individuals vary greatly owing to differences in physiological variables such as breathing rate, manner and rate of chewing, and rate of saliva production. Rates and intensities of volatile release depend also on the nature of the food matrix and physicochemical properties of the volatiles. The importance of this last factor is demonstrated in Figure 2, where the time dependence of release of a series of volatiles from gelatin/pectin gels of fixed matrix composition are compared. Each release curve is the mean of 5 replicates eaten by the same operator and normalized to the maximum intensity.

There is considerable variation between the times to maximum intensity, T_{\max} , of the different compounds. A continuous change in the relative concentrations of the different flavor compounds therefore takes place in the air passing over the olfactory receptors as the gel is eaten, which can be quantified. In conjunction with sensory evaluation, the real time capacity of AFFIRM[®] can thus lead to a better understanding of the way we appreciate the flavor of foods. In parallel with this approach, progress is being made in the development of predictive models of the release of volatiles into the breath during eating based on physicochemical properties of the volatiles (6).

Modifying Flavor Release Profiles

It is an increasingly important market requirement, that a new flavor for a particular product should make a specific perceptual impression, for instance a powerful initial impact. For a given tonality, there is limited scope to substitute flavor compounds in a liquid formula for others according to their release properties, and control of flavor release through modifications to the food matrix composition or texture is often impractical. One flexible way to achieve a required flavor impression is by encapsulation of liquid flavors in various supports such as the Flexarome[®] range of carbohydrate-based flavor delivery systems developed by Firmenich, which also provides benefits in flavor stability. The usual procedure in the development of a new flavor, involving feedback between flavorists and sensory panels, is time consuming. AFFIRM[®] can provide substantial time savings by initial product screening and, through an increasing understanding of how the kinetics of flavor release affects perception, desirable features can be identified from nosespace profiles.

Research is in progress both at the University of Nottingham and in the Corporate R & D Division of Firmenich SA to understand better those aspects of flavor release which affect perception, by simultaneous nosespace measurement and time-intensity sensory estimation by a trained panel of perceived flavor intensity. One important discovery obtained using flavored gelatin gels of varying gelatin content was a good correlation between the initial gradient of the nosespace release profile

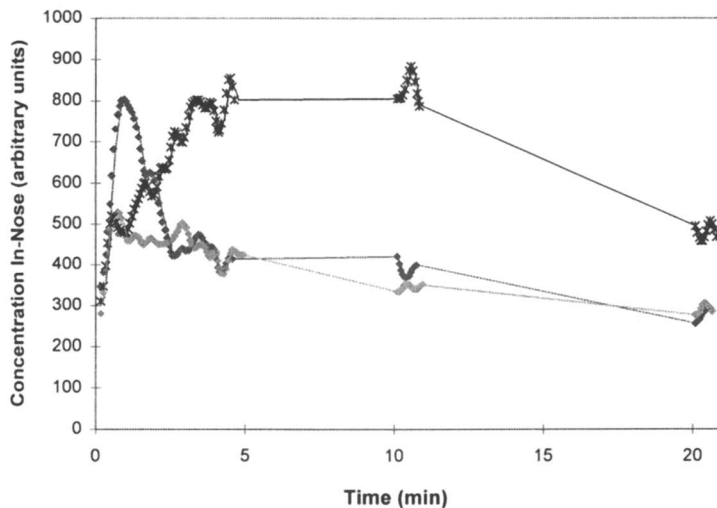


Figure 1. Menthol release from market peppermint chewing gum sticks.

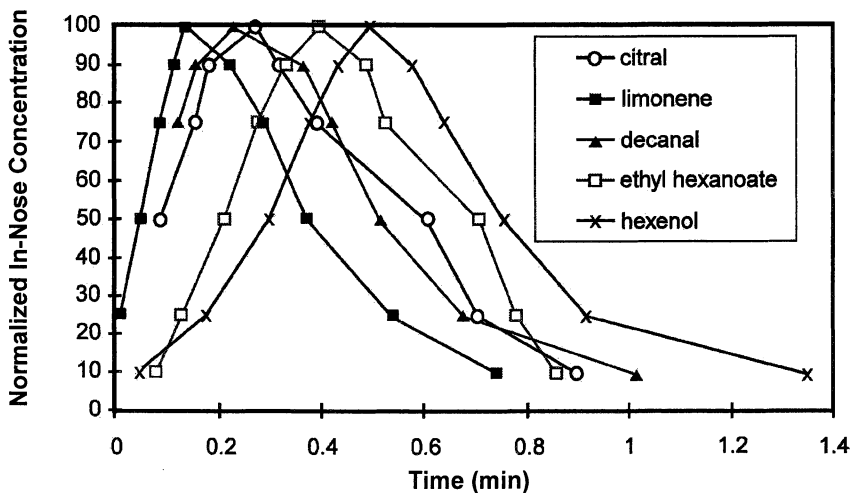


Figure 2. Release in-nose of volatiles from flavored gelatin/pectin gels normalized to maximum intensities.

and the maximum perceived flavor intensity (3). The correlation between maximum nosespace intensity and maximum perceived flavor intensity was not good. A steep

initial gradient in the nosespace profile is therefore more important than the absolute flavour dosage in achieving an intense flavor impact.

In the following example, a new Tutti Frutti flavor with a strong initial impact was required for bubble gum. A liquid flavor was encapsulated into each of three Flexarome[®] products, differing only in the composition of the Flexarome[®] matrix. The flavor level in each Flexarome[®] product was measured and batches of bubble gum were made to the same formula containing each of the Flexarome[®] products at an equivalent flavor dosage. Release profiles of amyl valerate from the different bubble gum batches are compared during the first minute of eating in Figure 3. Each curve is the mean of 3 replicates eaten by the same operator.

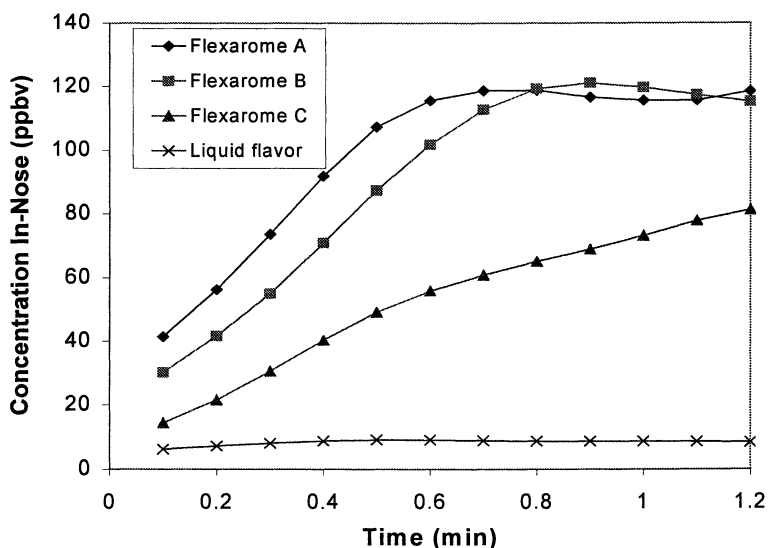


Figure 3. Effect of encapsulation in Flexarome[®] matrices on the release of amyl valerate in-nose from tutti-frutti flavored bubble gum.

The initial rate of change of amyl valerate concentration in the nosespace is many times greater from the bubble gum samples containing the Flexarome[®] products than from the sample containing the liquid flavour. This is because the carbohydrate matrices of the Flexarome[®] products provide a physical barrier restricting the rate of partitioning of amyl valerate into the gum base, a process which is thermodynamically favored by the hydrophobicity of both the gum base and amyl valerate. Other hydrophobic flavor compounds, notably limonene, showed similar differences in initial nosespace gradients between the bubble gum batches. The differences in release profiles of more hydrophilic flavor compounds between the bubble gum samples containing Flexarome[®] and that containing liquid flavor were less pronounced, as expected, but tasting confirmed the greater initial flavor impact from samples containing Flexarome[®].

The dependence of perceived flavor intensity on the rate of change of volatile concentration in the breath indicates that the optimum form for flavor release profiles over a period of time should be a series of spikes rather than a uniform level. This may be achieved using an appropriate mixture of encapsulants with different temporal flavor release characteristics. Figure 4 shows the mean of 3 replicates of menthone release from chewing gum eaten by the same operator. There are two distinct maxima, within the first minute and after about 1.7 minutes of eating, which result from formulating in a single chewing gum batch menthone encapsulated in two different matrices with clearly differentiated time release properties.

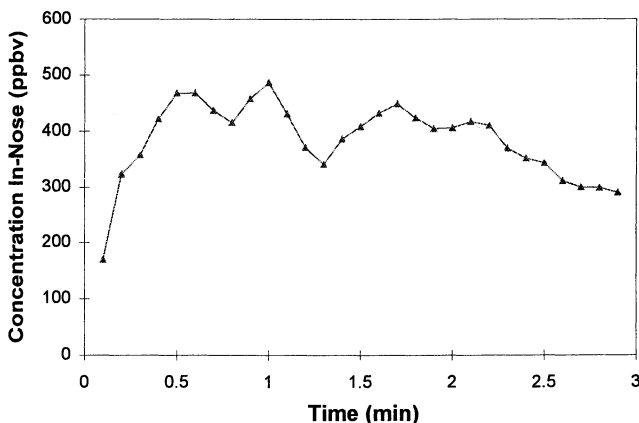


Figure 4. Release in-nose of menthone encapsulated in two different matrices from sugar free chewing gum.

When incorporated in a given food matrix, encapsulation in Flexarome[®] matrices of single flavor compounds (or groups of compounds giving rise to different notes or tonalities) with different time release characteristics can provide great flexibility in the design of temporal flavor impressions.

Integrity of Components in Composite Foods and Flavor Release

It is common experience that the flavor of foods composed of physically distinct components is adversely affected by homogenization. The components of composite foods typically differ in perceived taste, texture/mouthfeel and qualitatively in the volatiles released during eating. These are generally recognised by food scientists as the main factors contributing to flavor (7). If, for example, a plateful of freshly cooked fish, tartare sauce and French fries is mixed in a blender, few would disagree that the result was less palatable although the nutritional content was unaltered. However such a perceptual deterioration is not due solely to less desirable textural

and mouthfeel qualities; AFFIRM[®] active nosespace analysis has shown in a number of such multi-component foods that substantial quantitative changes in volatile concentrations in-nose contribute to the deterioration in perceived flavor quality following homogenization.

The approach with complex foods is firstly to obtain a mass spectrum of the headspace of each component of the food. It is then usually possible to identify one or more peaks of significant intensity at particular mass/charge ratios which are unique to that component. The chosen peaks are then monitored as the food is eaten in its usual form and when modified. It is not necessary to identify the peaks followed to observe the effect, although identification may be readily made in a preliminary step in which volatiles in the headspace of each component are trapped on Tenax, desorbed and subjected to GC-MS analysis.

Figure 5 shows an example of peanut butter and concord grape jelly sandwiches, in which the raw chromatograms of a single peak from each component are presented with a common time axis. The signal in the upper channel originates only from the grape jelly and that in the lower channel only from the peanut butter. No signal from either channel was recorded when the bread was eaten alone.

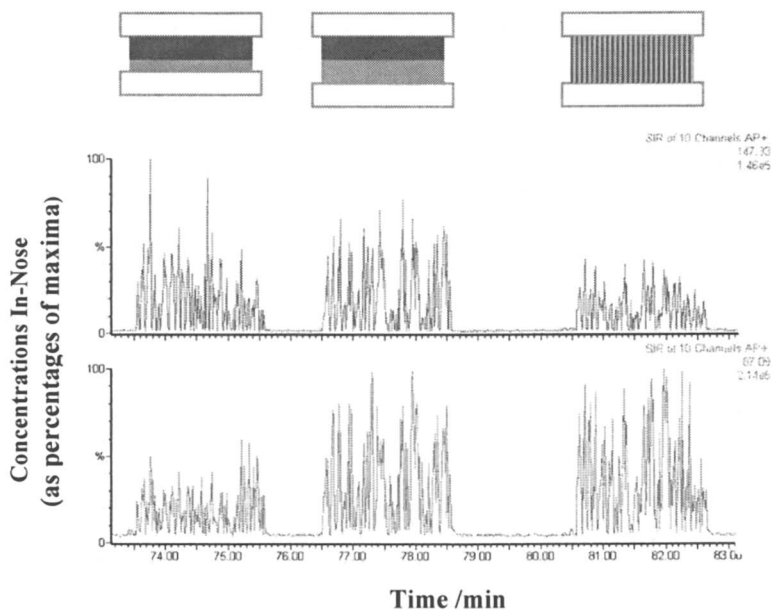


Figure 5. Release of marker volatiles in-nose from sandwiches containing peanut butter (lower channel) and grape jelly (upper channel) as discrete layers (starting at 73.5 and 76.5 minutes) and after homogenization (starting at 80.5 minutes).

At an indicated time of 73.5 minutes, an operator ate a sandwich containing a thin layer of peanut butter topped with a thicker layer of grape jelly. A second sandwich containing a thicker layer of peanut butter, of the same weight (10 g) as the grape jelly, was eaten by the same operator at 76.5 minutes, and at 80.5 minutes a further sandwich was eaten containing 10g grape jelly and 10 g peanut butter which had been previously mixed in a food blender. The intensity of the signal from the grape jelly is clearly reduced when blended with peanut butter. The same effect was seen when sandwiches of the three compositions were eaten by two other operators. Greater exposure of volatiles from grape jelly to the high fat content of the peanut butter in the sandwich with the blended filling may reduce both their mass transfer rates within the food and lower air/food partition coefficients.

Fat Levels in Yogurt and Flavor Release

The effect of fat levels on volatile release has been investigated in some detail using AFFIRM[®], particularly from cookies and from yogurt. Many physical properties of food including texture/mouthfeel and melting profile depend on fat levels. Volatile release can depend on such factors through modified mass transfer rates within the food. Fat also has an important role as a reservoir for flavor molecules, which will partition between the fat, water and air phases according to the hydrophobicity of the flavor molecules. Thus increasing the fat content in fat/water/air systems decreases the headspace concentration of hydrophobic flavor molecules which reside preferentially in the fat phase, while headspace concentrations of hydrophilic flavor compounds are affected little by fat content (8).

Quantitative instrumental data on these effects *in vivo* are sparse; compositional changes have been measured from cheeses of different fat content (9) although no comment on rates of release was possible. Sensory studies have shown clear tendencies for more intense but more transient flavor release from fat-free foods than from the full fat products (10). The dependence of both intensities and rates of volatile release on the fat content of foods can be determined rapidly using AFFIRM[®]. Rates of release of anethole, a moderately hydrophobic flavor compound, are compared in Figure 6 from set yogurts of different fat content (11).

The data are from 5 replicates eaten by the same operator. Intensities have been normalized to show more clearly the differences in release kinetics; maximum intensities were approximately four times higher from the 0% fat yogurt than from the 3.5% and 10% fat yogurts, which were of similar intensity to each other. The T_{\max} value of the 0% fat yogurt was lower than those of the 3.5% and 10% fat yogurts and there is a trend of greater persistence with increasing fat content. The difference in T_{\max} values between the 0% and 10% fat yogurts is statistically significant.

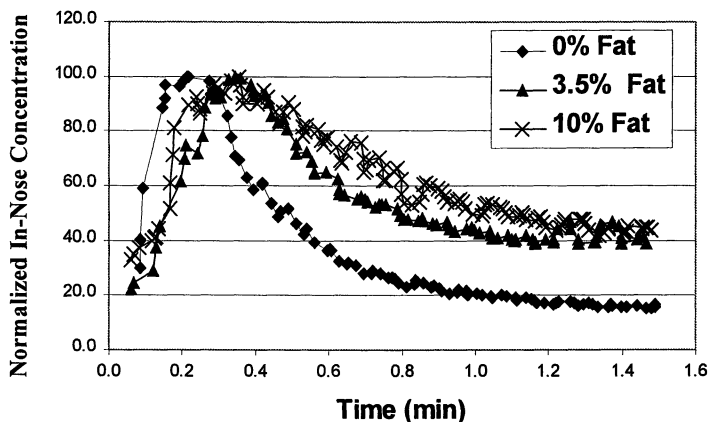


Figure 6. Volatile release in-nose of anethole from yogurts of different fat contents, normalized to maximum intensities.

(Reproduced from reference 11. Copyright 1999 American Chemical Society.)

Time Dependence of Release of Enzymatically Generated Volatiles

The short time resolution possible using AFFIRM[®] active nosespace analysis renders it particularly suitable to study the temporal aspect of flavor release from fruits such as tomatoes from which both preformed and enzymatically generated flavor molecules are liberated during eating (12). Release of the two classes of volatiles are compared in Figure 7. Intensities have been normalized to the maxima and each curve represents the mean of 5 replicates eaten by the same operator.

Isobutylthiazole is present in the intact tomato in the active form and is released first. Hexenal and hexenol are derived from linolenic acid by a sequence of enzymes in the lipid oxidation pathway. (*Z*)-3-hexenal is a product of the first enzymic step which can be followed by conversion to (*E*)-2-hexenal. As AFFIRM[®] cannot distinguish between isomers, the signal for hexenal in Figure 7 is the sum of the (*Z*)-3 and (*E*)-2 isomers. A further enzyme step from either hexenal isomer can produce the corresponding hexenol isomer. Differences in T_{\max} values between isobutylthiazole and hexenal, and between hexenal and hexenol, were statistically significant ($p < 0.05$, Student t-test). These T_{\max} values agree with the enzymic pathway and sequence responsible for production of hexenal and hexenol.

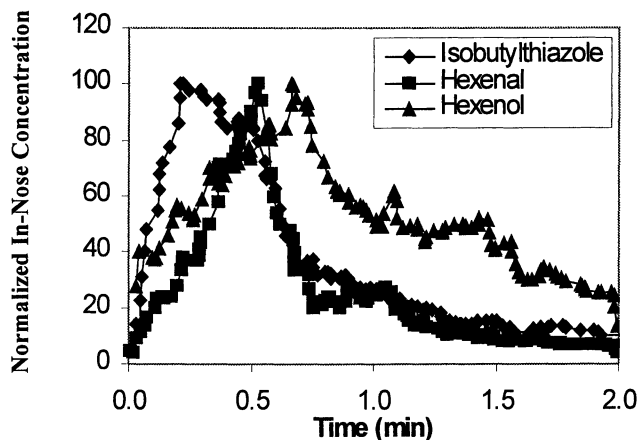


Figure 7. Release in-nose of preformed and enzymatically generated volatiles from plum tomatoes.

(Reproduced from reference 12. Copyright 1998 American Chemical Society.)

Conclusions

The examples given demonstrate how AFFIRM[®] active nosespace analysis provides a rapid method for the quantitative analysis in real time of volatiles in the breath during eating. The time resolution clearly distinguishes release rates during eating of different volatiles in a given food or of a given volatile as a function of composition variables such as fat levels in manufactured food. Combined with sensory analysis AFFIRM[®] is leading to a better understanding of those factors which affect flavor perception and is assisting in the design of flavor delivery systems. The speed of data collection and processing can offer substantial savings of resources in flavor development.

References

1. Linforth R.S.T.; Ingham K.E.; Taylor A.J. In *Flavour Science: Recent Developments*; Taylor A.J.; Mottram D.S., Eds.; Royal Society of Chemistry: London, 1996, pp 361-368.
2. De Kok P.M.T.; Smorenburg H.E. In *Flavor Chemistry, Thirty Years of Progress*; Teranishi R.; Wick E.L.; Hornstein I., Eds.; Kluwer Academic/Plenum Publishers, New York, 1999, pp 397-407.
3. Baek I.; Linforth R.S.T.; Blake A.; Taylor A.J. *Chem. Senses*. **1999**, *24*, 155-60.
4. Linforth R.S.T.; Baek I.; Taylor A.J. *Food Chem.* **1999**, *65*, 77-83.

5. Harvey B.A. *Kennedy's Confection*. May 1997, pp18-20.
6. Linforth R.S.T.; Friel E.N.; Taylor A.J. In *Flavor Release: Linking Experiments, Theory and Reality*; Roberts D.D.; Taylor A.J., Eds., American Chemical Society: Washington DC, 1999.
7. Taylor A.J. *Crit. Rev. Food Sci. Nutr.* **1996**, *36*, 765-784.
8. De Roos K.B. *Food Technol.* **1997**, *51*, 60-62.
9. Delahunty C.M.; Piggott J.R.; Conner J.M.; Paterson A. *Ital. J. Food Sci.* **1996**, *2*, 89-98.
10. Bennet C.J. *Cereal Foods World.* **1992**, *37*, 429-432.
11. Brauss M.S.; Linforth R.S.T.; Cayeux I.; Harvey B.A.; Taylor A.J. *J. Agric. Food Chem.* **1999**, *47*, 2055-2059.
12. Brauss M.S.; Linforth R.S.T.; Taylor A.J. *J. Agric. Food Chem.* **1998**, *46*, 2287-2292.

Chapter 4

Flavorspace: A Technology for the Measurement of Fast Dynamic Changes of Flavor Release during Eating

Willi Grab¹ and Hans Gfeller²

¹Givaudan Roure Flavors Ltd. and ²Givaudan Roure Research Ltd.,
CH-8600 Dübendorf, Switzerland

The FLAVORSPACE method allows the measurement of fast dynamic changes of flavor components reaching the nose during eating of food. FLAVORSPACE - measurements are performed on a commercial quadrupole mass spectrometer, equipped with an APCI (Atmospheric Pressure Chemical Ionization) ion source with a modified interface (1). Typical examples show the direct correlation of perceived and measured flavor release. The flavor of fresh strawberries changes during eating within 25 seconds from fruity to green to fatty to woody, a measurable and perceived fact that consumers are normally not aware of. The oral cavity has a discriminating effect on flavor perception: the mucous membrane interacts with polar flavor compounds and mainly influences the aftertaste. During the analysis of crackers with different extraction procedures and with the FLAVORSPACE technique, an unknown mass was noted and then identified as the labile compound 2-acetyltetrahydro-pyridine by multistage mass spectrometry (MS)ⁿ. Understanding flavor perception is only possible, when we know the key flavor molecules released in the mouth and active in the nose receptors. A multidimensional approach and a critical interpretation of the analytical results are essential for progress.

The flavor industry has a strong interest to mimic the flavor of natural foods as closely as possible. Analysis of key components and reconstitution of the natural flavor in combination with the creativity of flavorists was the basis of the flavor business in the past. The quality standard is very high. Customers are asking for more technical solutions which include flavor performance and flavor release. De

Roos (2-6) has developed a useful computer program to calculate matrix interaction factors. It allows the flavorists to adapt a flavor formula to specific applications.

Time-intensity studies show large differences between individual persons even under strictly controlled conditions. Dynamic flavor release is of interest to understand better flavor perception during eating. Several publications report experiments with an artificial mouth (7,8). Others describe traditional HS sampling to analyze flavors from the mouth (9-11).

During the Weurman symposium in Reading, 1996 Taylor and Linforth (12) presented the idea of measuring flavored gas phases with APCI-MS and progress in this field is reviewed in this book. We have developed a system to directly measure fast dynamic changes of the release of flavor components during eating (1). The dynamic composition of the expired air, exhaled from the nose, is measured directly and simultaneously during eating.

FLAVORSAPCE - measurements are performed on a commercially available quadrupole mass spectrometer, equipped with an APCI (Atmospheric Pressure Chemical Ionization) ion source (Figure 1). APCI ion sources are typically designed for the introduction of samples dissolved in water or aqueous solvent mixtures. These systems are frequently used for LC-MS experiments. In order to analyze breath samples, it was necessary to modify the APCI ion source of the mass spectrometer for the introduction of gas phase samples. APCI is a soft ionization technique. Molecules ionized by APCI preponderantly form single charged molecular ions $[M+H]^+$ with little or no fragmentation. Thus, most of the signals in a mass spectrum can be assigned to pseudomolecular ions.

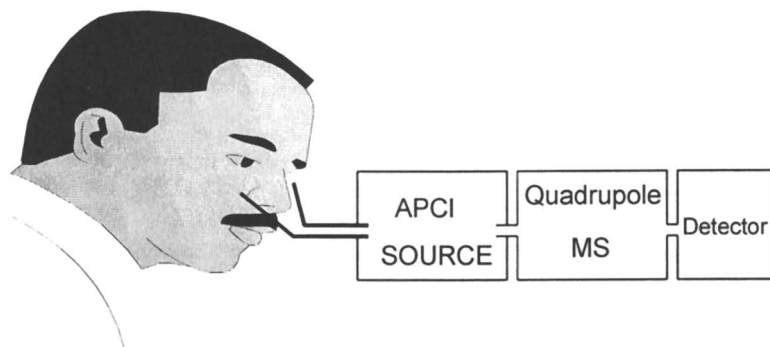


Figure 1. Schematic of APCI-MS for breath monitoring

Flavor release during eating can be measured in combination with simultaneous control of the sensory impression from breath to breath. Our real-time studies have shown a very fine structure in the release of flavor components. The fast scan rate of the mass spectrometer (two scans per second) allows not only recording the breath frequency, but also the chewing motions of the mouth. Breathing and the timing of a breath with the chewing activity influence the perception and the lasting effect of the flavor. Flavor perception is strongly affected by the way the flavor is transported

through the oral cavity and the respiratory channels. The purpose of FLAVORSPACE - measurements is to analyze rapid changes of the composition of released volatile flavor components and to correlate analytical data with the sensory perception.

Experiments with the VAS (Virtual Aroma Synthesizer, a Givaudan Roure owned instrument to deliver controlled quantities of substances into a gas phase) with different interfaces showed a linear relation between the concentration in the gas phase and the APCI signal response. Under saturation conditions we observe a discrimination and selectivity for certain molecules.

Flavor Release from Strawberry

Flavor release and flavor perceptions are subject to constant changes in quantity and quality. Drawert (13), Tressl (14, 15), Jennings (16) and Yamashita (17-20) have shown the chemical changes occurring during maturation of fruits. In 1978, we showed (21) the circadian rhythm of flavor emanation from a ripening strawberry and the fast changes of flavor release when cutting the fruit. Kaiser (22) showed, in several examples, circadian rhythms in odor emanations of flowers.

We wanted to study the fast flavor development with cell disruption *in vitro* and during eating and compare it with strawberry flavored yogurt with the new FLAVORSPACE technique. It should allow us to measure fine differences of the flavor profile during consumption of strawberries.

Headspace measurements of fresh strawberries in a vessel:

One strawberry was placed in a spice mill and the headspace allowed to equilibrate for 5 minutes prior to the start of the analysis (Figure 2). A continuous airflow from the mill through the APCI source replaced the exhausted air with ambient air (A). This led to a dilution effect of the headspace flavor. The mill was then activated for one second (B). This destroyed the fruit cells immediately, increased the surface area and flavor components were released.

Figure 2 shows mass chromatograms of components that are present in the headspace of strawberry fruit. The concentration of m/z 117 begins to drop as soon as the analysis starts and it re-equilibrates at a lower level. We observe almost the same behavior after smashing the fruit. We can conclude, that this component occurs in the fruit cells. It is released and it evaporates immediately. The signal m/z 152 shows a different behavior: it remains at a higher level than the very volatile components (hexenal and ethylbutyrate). This component also exists in the cells, but the affinity to the fruit matrix is quite strong. The signal m/z 99 (hexenal) develops with time. This component is not present in the entire fruit. It forms after the destruction of the cell walls. Lipid oxidation of cell lipids starts with cell disruption and reaches the maximum after 100 seconds.

CHRO:	I498	13-JUN-97	Elapse:	00:12:22.4	860
Samp:	Erdbeere, Wäedenswil 6		Start :	13:27:24	2128
Comm:	Capillary 190°C, Vaporizer 200°C				
Mode:	+Q1MS LMR UP TREE LR		Study :	Nase, Willi	
Oper:	g	Client: MS-Lab	Inlet :	Mixer	
Peak:	1000.00	mmu	Label w/dw:	1 > 1824	
Area:	0, 4,00	Baseline :	Masses:	20 > 300	
			Label :	0, 40,00	

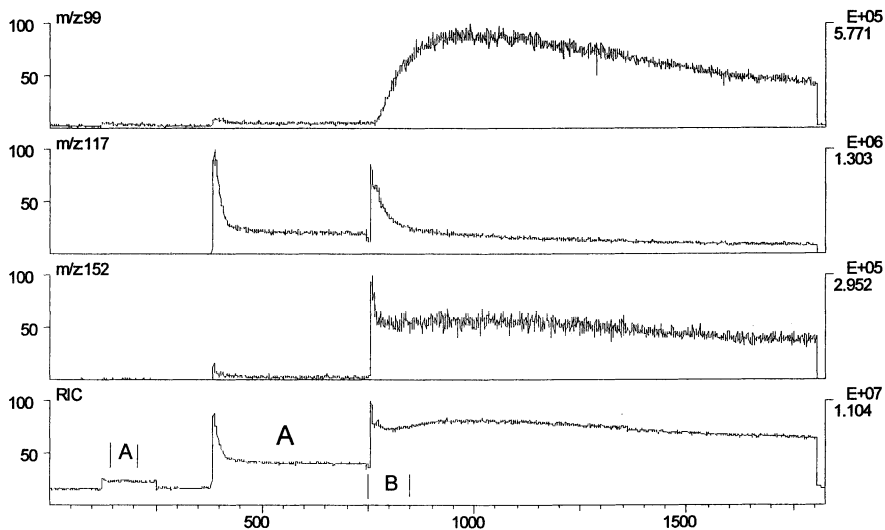


Figure 2. Release of volatiles from a strawberry. A. Headspace of intact strawberry. B. Headspace after 1 second maceration. The traces are: m/z 99 hexenal, m/z 117 ethylbutyrate, m/z 152 methylanthranilate, RIC total ion current. The x-axis scale is scan number (2 per second).

(Reproduced with permission from reference 1. Copyright 1999 Deutsche Forschungsanstalt fuer Lebensmittelchemie.)

Breath-by-breath analysis of volatile flavor release during eating

Eating a strawberry is a relatively quick process. In order to get reliable mass spectral data, the mass spectrometer has to be scanned with scantimes below one sec/scan. The response of the recorded mass chromatograms depends on the various compositions of the volatile flavor compounds. In general, we can discern compounds that are released immediately with the first bite (volatile esters like methylbutyrate m/z 103, butylacetate, ethylbutyrate etc. m/z 117), compounds that are released immediately too, but maximizing later (furanolmethylether m/z 143, methylanthranilate m/z 152) and compounds that are generated during mastication (hexenal m/z 99). The mass trace m/z 59 (acetone) monitors breath frequency. Acetone is always present in exhaled air from human beings.

The quality of the correlation of analytical data and the sensory impression improves with increasing number of analyses. The following approach, performed with one strawberry (*Senga Sengana*), points out, that real time breath-to-breath

analysis is a powerful method indeed. The flavorist described the change in sensory perception during eating from breath to breath.

The sensory perception correlates well with the analytical data: Within 25 seconds, the flavor of a strawberry changes completely. In the first breath of section 5a, just volatile fruity esters (m/z 103, m/z 117, m/z 131, m/z 145) appear. The second breath (5b) shows a small amount of furaneolmethylether (m/z 143) besides the esters. With the third breath (5c) hexenal (m/z 99) appears with the typical green note. Hexenal reaches a maximum of intensity within the fourth breath (5d) whereas the intensity of the fruity esters begins to drop. The fatty and metallic tasting substances (2,4-decadienal, 4,5-epoxy-2-decenal) are not detectable by this method. After swallowing, all components disappear with the exception of polar components like furaneolmethylether. In other experiments, we could also prove the lingering effect of furaneol and methylanthranilate.

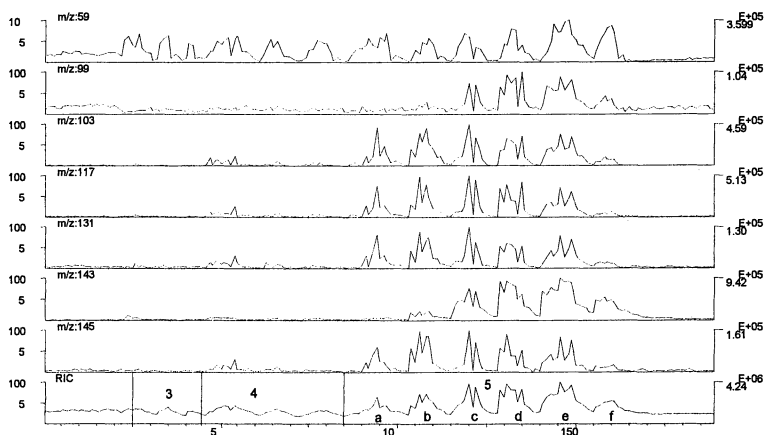


Figure 3. Breath by breath release of volatiles during eating of a strawberry.

Actions: 3.) Strawberry in mouth, regular breathing, 4.) Chewing without crunching, regular breathing, 5.) Chewing, crunching, swallowing, regular breathing. **Ions:** m/z 59: acetone; m/z 99: hexenal; m/z 103: methylbutyrate; m/z 117: ethylbutyrate, butylacetate, m/z 131 isoamylacetate, ethylvalerate, isopropylbutyrate; m/z 143 furaneolmethylether, hexenylacetate; m/z 145 butylbutyrate, ethylcaproate, hexylacetate; RIC total ion current.

Sensory impression from breath-to breath: 3) no flavor; 4) fruity; 5a) fruity; 5b) fruity, estery, fermented; 5c) estery, fermented, then green; 5d) green apple; 5e) fatty, metallic; 5f) metallic, woody. x-axis: number of spectra (2/sec)

(Reproduced with permission from reference 1. Copyright 1999 Deutsche Forschungsanstalt fuer Lebensmittelchemie.)

Flavor Release of Unstable Compounds from Crackers

The identification of key flavor ingredients is important to understand the sensory flavor characteristics of food products. Analysis of these key components is sometimes a difficult hurdle to overcome: small traces are covered by larger

components or unstable molecules with a high flavor impact are destroyed during isolation. Modern analytical tools (e.g. GC-MS), and careful isolation techniques (e.g. headspace, high vacuum distillation) combined with sensory evaluation (e.g. GC-sniffing) allow us to concentrate the analytical effort on the right molecules and to identify them. A normal analysis of the isolated flavor does not really represent the perceived flavor of a food. The selectivity of the extraction methods and instruments distort the real proportions. Careful calibration is necessary to get quantitative answers.

The modern food and flavor industry is not only interested in the composition but also in the performance and release of the food flavors to imitate the properties of natural food with manufactured food. The flavor release from food is influenced by two different principles: a static distribution of the flavor into the different phases of a product: solid matrix, hydrophilic or lipophilic liquid phase and the gas phase. This behavior is controlled by the partition coefficients of the molecules. The second principle is a dynamic factor, controlled by the mass transfer through a matrix and interfaces. Both factors influence the perception of the food. During eating the flavor release is even more complicated due to chewing, grinding, wetting / dissolving the food with saliva. Breathing and swallowing strongly influence the perception of the released flavor. Measurement of the dynamic flavor release in very short periods is necessary to understand the sensory properties of food. In this project, we had to monitor the flavor release of flavored commercial crackers based on two different production technologies. During this work, we encountered an unknown ion in the APCI - MS that could not be correlated with the results of the classical analysis.

Materials and Methods

The sample was a commercial corn cracker, flavored with spices and fried with vegetable oil (Mexican Taco Type). The sample was extracted with solvent (methyl tertiary butyl ether, MTBE), concentrated and followed by vacuum distillation. In the HEADSPACE experiment, we heated the sample (dry and wet) in a purge-and-trap system (Gerstel TDS2) and injected directly into a Hewlett Packard GCD (DBwax, 30mx0.32mm, film: 0.25 μm) with sniff port outlet). In the FLAVORSAPCE experiment, we transferred the breath air directly through an interface into the ionization chamber of APCI - MS (SSQ 710C and LCQ from Finnigan-MAT).

Results

The solvent extract (Figure 4) shows the main components from the spices and the higher boiling fatty acids. The HS from thermal desorption of dry crackers (Figure 5.) shows the low boiling volatiles, mainly fat oxidation and Maillard reaction products and the garlic volatiles used as flavoring.

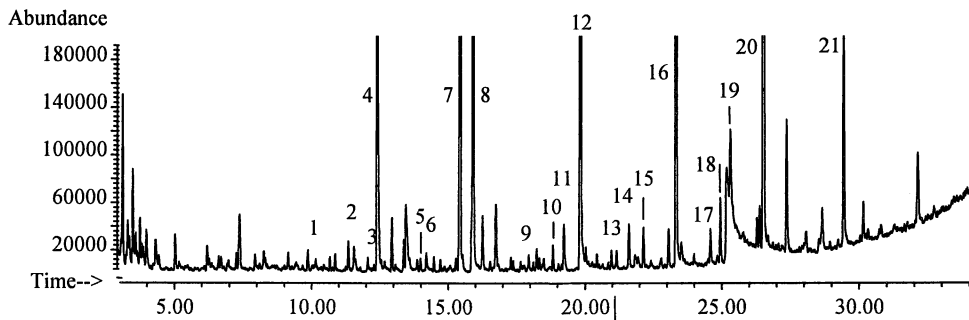


Figure 4. GC of corn cracker solvent extract.

1 dimethylpyrazine, 2 nonanal, 3 ethyloctanoate, 4 acetic acid, 5 isolongifolene, 6 (*E*)-2-nonenal, 7 caryophyllene, 8 butanoic acid, 9 pentanoic acid, 10 diallyltrisulfide, 11 (*E,E*)-2,4-decadienal, 12 hexanoic acid, 13 ethyllactylactate, 14 hexenoic acid, 15 caryophyllene epoxide, 16 octanoic acid, 17 sorbic acid, 18 nonanoic acid, 19 2-methoxy-4-vinylphenol, 20 decanoic acid, 21 dodecanoic acid

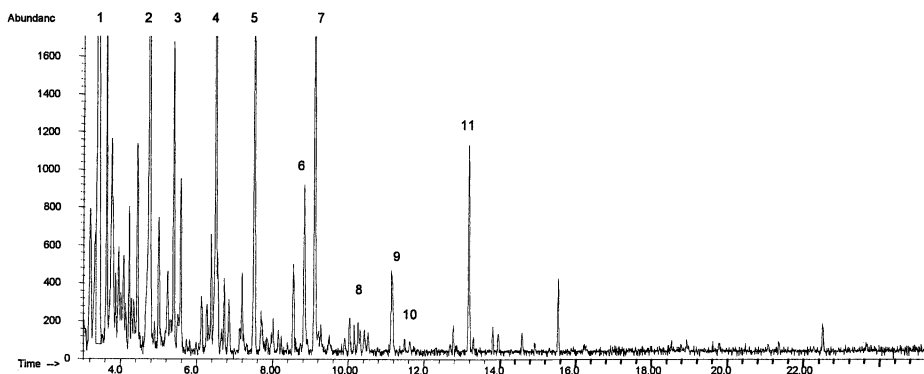


Figure 5. Headspace of dry corn crackers using direct thermal desorption of volatiles with a Gerstel TDS2 purge and trap system.

1 isovaleraldehyde, 2 toluene, 3 hexanal, 4 diallyldisulfide, 5 limonene, 6 methylpyrazine, 7 allylmethylsulfide, 8 *C*-2-pyrazine, 9 dimethyltrisulfide, 10 *C*-3-pyrazine, 11 diallyldisulfide

Additional experiments with thermal desorption of a sample treated with a small amount of water show a complete different picture than without water (Figure 6.) The total quantity of volatiles is much higher (ca. 15 times). The pattern is comparable to the solvent extract, showing mainly the volatile fatty acids from fat degradation.

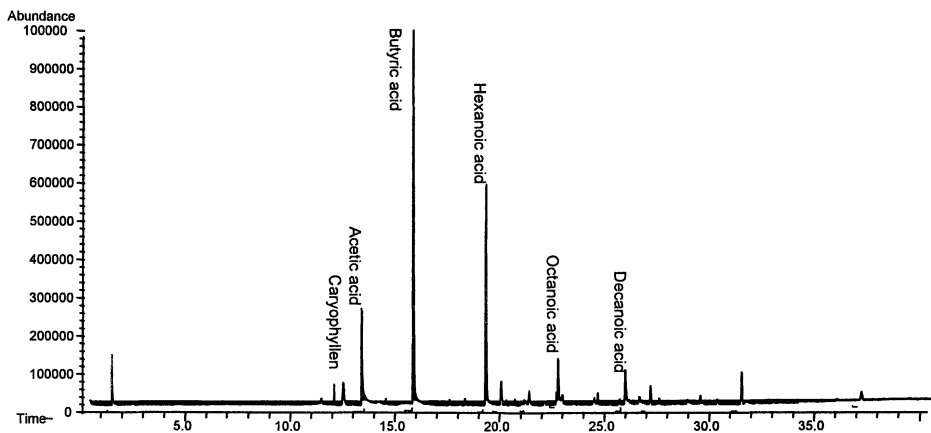


Figure 6. Headspace of corn crackers after 5% water addition using direct thermal desorption of volatiles with a Gerstel TDS2 purge and trap system

There are obviously big differences between the isolation methods, which can be explained by their selectivity in volatility and solubility.

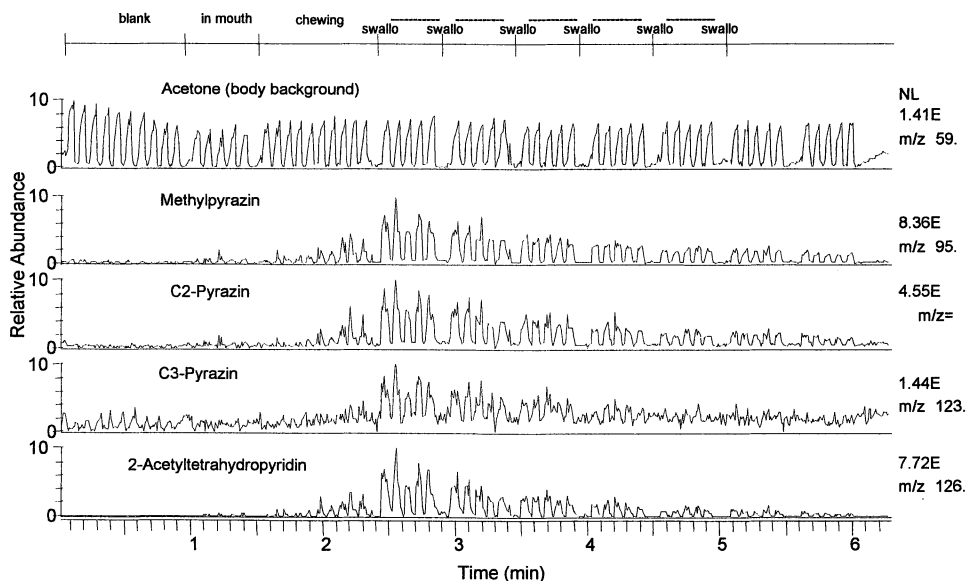


Figure 7. FLAVORSPACE of corn crackers

The measurement of breath air from the nose during eating revealed products of the Maillard reaction (pyrazines). A large signal also occurs at $m/z=126$ of an unknown molecule with a molecular weight of 125 Da not found in the solvent extract nor in the HS. The isotope distribution of the signal does not indicate a sulfur atom (Figures 7 and 8.). The use of multistage mass spectrometry (MS)ⁿ on the ion m/z 126 shows the loss of 18, 28 and 42 mass units corresponding to water, ethylene and ketene or propylene respectively (Figure 9.) The comparison with an authentic pure sample of 2-acetyltetrahydropyridin confirmed the proposed structure. We know that this molecule is extremely. The question arises, why it survives storage over months at room temperature in the crackers. There are several possibilities for an explanation: unstable extract, a precursor system or encapsulation in the matrix

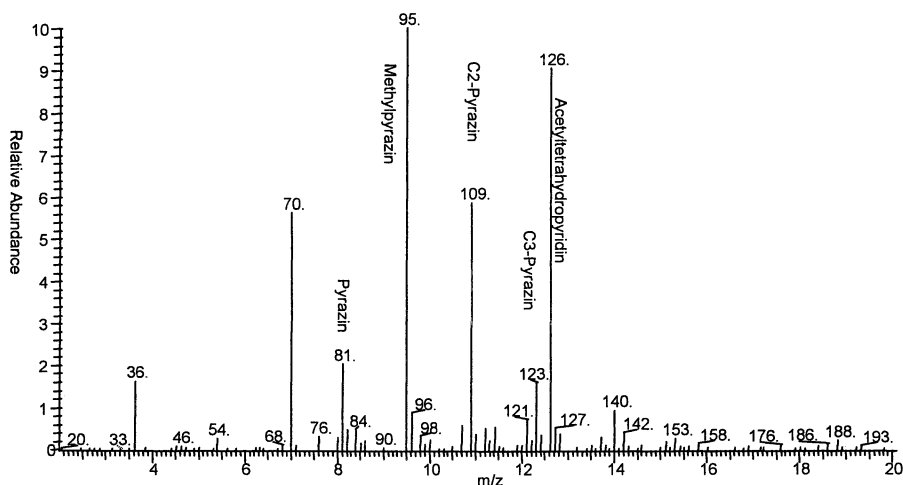


Figure 8. FLAVORSPLACE: total mass spectrum of one breath

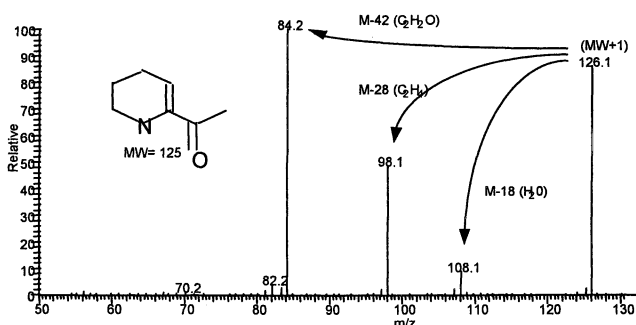


Figure 9. Mass fragmentation of m/z 126 by MSⁿ

The addition of water to crackers at room temperature immediately releases the fresh roasted note. We have measured this release using the FLAVORSPACE technology (Figure 10.)

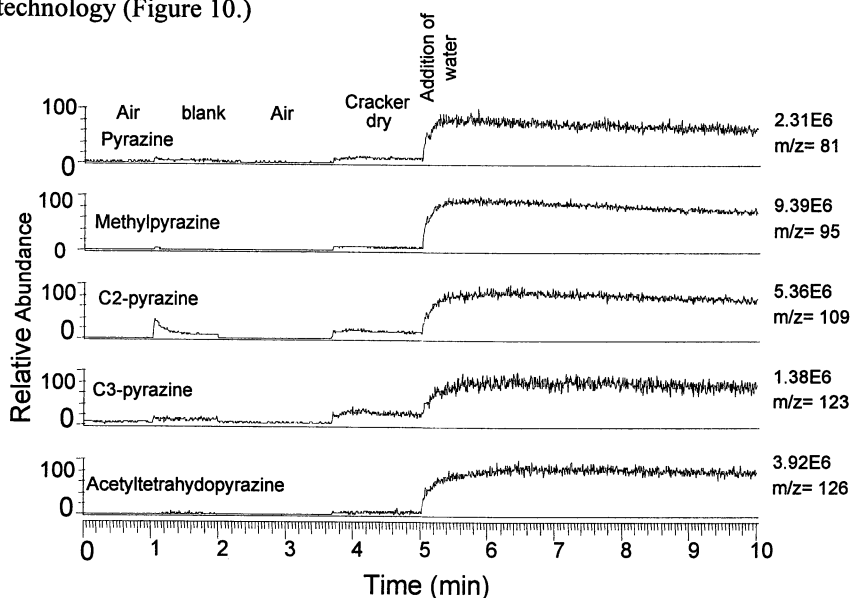


Figure 10. Flavor release from corn crackers by water addition using FLAVORSPACE measurement

We observe an instant release of all flavor components, including 2-acetyltetrahydropyridine. Although the dynamism is slightly different for the various components, we can conclude, that the modification of the rigid matrix structure releases the molecules with the addition of water. It is not yet clear, how the matrix is stabilizing the 2-acetyltetrahydropyridine.

Conclusion

The FLAVORSPACE technique is a powerful tool to measure the very fast dynamic changes of flavor release during eating (as shown by the strawberry example) and other fast dynamic processes involving volatile components (as shown by the identification of an unstable character impact chemical in crackers).

Understanding flavor perception is only possible, when we know the key flavor molecules released in the mouth and active in the nose receptors. A multidimensional approach and a critical interpretation of the analytical results are essential for progress. The FLAVORSPACE technique shows the instant release of nonpolar compounds from strawberry fruit into the oral cavity, the lingering effect of the mucous membrane to the polar compounds and the development of lipid oxidation

products after cells are broken. It helps us to understand time - intensity flavor profiles, but it also opens new questions. There is a strong influence of the oral cavity and the whole respiratory system on the flavor components from food to the receptors in the nose. Breath-by-breath sensory and instrumental analysis directly show this influence. Attentive subjects are able to distinguish the changing flavor perception, but consumers are apparently not aware of this phenomenon. The question is now focused on how we recognize a flavor? Is the image of a natural ripe strawberry in our brain a dynamic image or do we only register only the first impression. If the dynamic process is part of the flavor recognition, the flavor and food industry has a new challenge to mimic natural food flavors.

References

1. Grab, W.; Gfeller, H., In *Proceedings of the 9th Weurman Symposium Freising (Germany)* **1999** in press
2. De Roos, K.B.; Sarelse, A. In: *Flavour Science, Recent Developments* Eds.: Taylor A.J.; Mottram D.S. RSC, Cambridge **1996** pp13-16.
3. De Roos, K.B., *Food Technol.* **1997**, *51*, 60.
4. De Roos, K.B.; Graf, E., *J. Agric. Food Chem.* **1995**, *43*(8), 2204-11.
5. De Roos, K.B.; Wolswinkel, K., *Dev. Food Sci.* **1994**, *35*, 15-32.
6. De Roos, K.B., *Flavour Sci. Technol. 6th Weurman Symp.* **1990**, 355-358.
7. Roberts, D.; Acree, T., *J. Agric. Food Chem.* **1995**, *43*, 2179.
8. Nassl, K.; Kropf, F.; Klostermeyer, H., *Z. Lebensm. Unters. Forsch.* **1995**, *201*, 62.
9. Linforth, R.S.T.; Taylor, A.J., *Food Chem.* **1993**, *48*, 115.
10. Ingham, K.E.; Linforth, R.S.T.; Taylor, A.J., *Food Chem.* **1995**, *54*, 283-288.
11. Springett, M.; Rozier, V.; Bakker, J., *J. Agric Food Chem.* **1999**, *47*, 1125-1131.
12. Taylor, A.J.; Linforth, R.S.T.; Ingham, K.E., In: *Flavour Science, Recent Developments* Eds. Taylor A.J.; Mottram D.S. RSC, Cambridge **1996** pp386-391.
13. Drawert, F.; Kuenanz, H.J., *Chem. Microbiol. Technol. Lebensm.* **1975**, *3*, 185.
14. Tressl, R.; Drawert, F.; Heimann, W.; Emberger, R., *Z. Lebensm. Unters. Forsch.* **1970**, *42*, 313.
15. Tressl, R.; Drawert, F.: *J. Agric. Food Chem.* **1973**, *21*, 560.
16. Tressl, R.; Jennings, W.G.: *J. Agric. Food Chem.* **1972**, *20*, 189.
17. Yamashita, I.; Nemoto, Y.; Yosikawa, S., *J. Agric. Food Chem.* **1977**, *25*, 1165.
18. Yamashita, I.; Nemoto, Y.; Yosikawa, S., *Agric. Biol. Chem.* **1976**, *40*, 2231.
19. Yamashita, I.; Nemoto, Y.; Yosikawa, S., *Agric. Biol. Chem.* **1975**, *39*, 2303.
20. Yamashita, I.; Nemoto, Y.; Yosikawa, S., *Phytochem.* **1976**, *15*, 1633.
21. Grab, W., Veränderung des Erdbeeraromas bei Reifung, und Verarbeitung. *IFU - Symposium: Aromastoffe in Früchten und Fruchtsäften*, Bern **1978**.
22. Kaiser, R., *The Scent of Orchids*, Elsevier, Amsterdam, **1993**.

Chapter 5

Wound Response in Plants: An Orchestrated Flavor Symphony

P. Dunphy, F. Boukobza¹, S. Chengappa, A. Lanot, and J. Wilkins

Plant Science Unit, Unilever Research Laboratory,
Bedfordshire, MK44 1LQ, United Kingdom

Wound response in plants is a complex ordered collection of localised and systemic effects with a temporal span extending from seconds to hours and days. Important components of the armoury of the plant are volatile molecules emitted as part of the first line of defence. Many of the aroma signature compounds of leaves, fruits and vegetables are formed and/or released in response to wound damage. This rapid temporal subtlety can be captured by application of real time aroma analysis using atmospheric pressure chemical ionisation mass spectrometry (APCI-MS). This technique has been utilised to demonstrate the duality of tomato leaf response to mechanical damage by releasing volatiles derived principally from the terpenoid and oxylipin pathways. The wound response of the edible Genus *Allium* on the other hand employs a remarkably rapid and complex series of transformations involving unstable volatile organosulfur compounds.

The ability of plants to maintain their 'milieu interieur' in response to changing environment has evolved to a greatly developed state; this to a large extent dictated by their sessile existence. This capability has been highly refined in the area of plant wound response. Plants manage repair of tissue damage by invoking constitutive defense measures and induced responses effectively sealing off damaged tissue before opportunistic microbes invade the wounded site (1,2). This involves activation of genes for structural wound repair and may involve strategies to signal distal tissue including systemin and proteinase inhibitor gene activation (3,4). These responses also include defence initiatives that serve to minimise further ingress and even elicit in many cases the mutualistic support of natural enemies of the aggressor by release of wound induced volatiles from the plant. These compounds may have

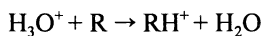
¹Current address: Division of Food Sciences, University of Nottingham, Sutton Bonington Campus, Loughborough, Leicestershire LE12 5RD, United Kingdom.

potent biological properties acting as phytoalexins, recruiting cues for predators of the invading organism or airborne warning signals for distal parts of the plant or neighboring plants (5-9). From a flavor point of view many of these components contribute significantly to the aroma signature of the particular fruits, vegetables or herbs and to their perceived quality. Classically these wound response aroma molecules fall into two functional groups, those generally stable molecules endogenously present in the plant and the *de novo* produced, generally unstable compounds derived enzymatically from non-volatile precursors (10).

The plant therefore possesses a number of distinct but overlapping armories of responses falling into the above two categories that not only nullify or minimize the assault but also counter-attack the aggressor – a good model perhaps for military strategists.

A key component in the response strategy is the ability to rapidly deploy defence initiatives over a timescale of fractions of a second through minutes to hours; aroma volatile release responses to wounding encompasses this whole timespan (11,12). The short timescale of responses are exemplified by the generic oxylipin cascade (1) and the group specific alk(en)yl cysteine sulfoxide pathway of the Genus *Allium* (13). The ability to measure the very rapid formation and transformation of trace volatiles in complex structures such as viable plant tissues has, until now, been a significant challenge to scientists.

Chemical ionisation mass spectrometry (CI-MS) is a powerful technique for the identification and quantitation of mixtures of volatile organic molecules in the vapor phase depending on ion-molecule reactions rather than electron impact processes. The CI method generally results in less fragmentation of the charged molecular species and simpler spectra. A variety of proton transfer reaction systems operating at medium pressure [e.g. proton transfer reaction-MS (PTR-MS)] and atmospheric pressure chemical ionisation-MS (APCI-MS) have been developed using protonated water (H_3O^+) as the primary reactant ion (14-16). Protonated water in this mode has several advantages including non-interaction with the natural components of air and reactivity, in the proton transfer mode, with most organic molecules as well as tolerance of water in the system; a very useful advantage for a wide range of applications. Reaction occurs as follows:-



where R = reactant gas; RH^+ = product ion

These CI-MS systems are capable of real time monitoring of complex mixtures in the gas phase over the concentration range of parts per million and in some cases as low as a few parts per trillion by volume. A number of applications of this type based on APCI-MS and PTR-MS have been documented (15,17,18). This paper describes the release of aroma compounds in response to mechanical damage in plants exemplified by:-

- constitutively derived stable volatile molecules endogenous to the plant
- induced unstable compounds derived by enzymatic transformation of stable non-volatile precursors.

The strategy for intercellular segregation of responses by cellular specialisation within the same plant tissue will be exemplified by consideration of the

photosynthetic tomato leaf surface whilst the intracellular segregation of precursors and enzymes will be demonstrated in both tomato leaf epidermal cells and cells of the garlic clove.

The volatile responses of these mechanically damaged tissues will be probed in real time using APCI-MS in conjunction with solid phase micro extraction-GC-MS (SPME-GC-EI-MS) and solvent extraction for molecular characterisation.

EXPERIMENTAL

Materials.

Mature garlic bulbs were obtained locally and single cloves carefully removed for experimental purposes. Leaves from greenhouse grown tomatoes of the processing variety BOS 3155 were picked from the second apical branch; flavor measurements were carried out from the adaxial surface. Authentic standard reference chemicals of the highest purity were purchased from Aldrich or the Fluka Chemical Company.

Real Time Headspace Analysis.

Experiments were performed using APCI-MS with gaseous sample introduction. This represents a non-standard mode of operation since APCI is generally used for solute analysis in the liquid phase, principally from HPLC eluates. The production and detection of intact protonated molecular species was encouraged by the use of a low cone (skimmer) voltage potential.

APCI-MS. Volatiles release measurements were carried using the Finnigan Navigator Mass Spectrometer fitted with a new probe design incorporating a Silcosteel® (Restek Corporation) flexible silica coated tube (id 2 mm) heated to 100°C. The instrument end of the steel tube was adjacent to the corona needle whilst the other end was connected via PTFE tubing to the reaction chamber. This provided an inert and heated transfer line directly from the sample chamber to the ionisation zone of the mass spectrometer to prevent vapour condensation and minimise unwanted chemical reactions. Nitrogen was used as the bath gas for the API region. The source temperature was 100°C; corona discharge 3kV and a cone voltage of 20V. Acquisition was in the positive ion mode and continuous from m/z 20-300. The reaction chamber was a screw threaded clear glass vial (od 29mm x 81mm length with a capacity of 40mL) with a PTFE-silicone septum kept in place via an open topped phenolic enclosure. The air inlet (length 40mm) to the reaction chamber and outlet (length 60 mm) to the APCI probe ferrule connector was via flexible PTFE tubing (id 2mm and od 4mm). The flow rate from the reaction vessel to the APCI was 1.25mL/sec under the venturi conditions employed and the tubing lengths and diameters indicated. The reaction vessel was filled to approx. 50% of its volume by adding inert #4 Ballotine beads (870-1275 μ m diameter). For the studies with garlic a single garlic clove (~3.5g) was placed on top of the glass beads. Damage to the clove was achieved via a syringe needle (65-85 μ diameter) passing through the septum and penetrating the garlic clove to a depth of ~7.5mm via two rapid repetitions without opening the vessel or interrupting gas flow. For studies with tomato leaf, the PTFE

tube connected to the probe inlet was placed ~1cm above the leaf surface which was still attached to the intact plant to be treated, and in the open atmosphere. Volatiles were drawn directly into the APCI for analysis.

APCI-MS-MS The air above the sample was drawn into the megaflow APCI interface of a Micromass Quattro I Mass Spectrometer. Nitrogen was used as bath gas for the API region. The source temperature was 100°C. The corona discharge pin was at 2.5 kV. Positive ion continuum MS data were acquired, generally from m/z 10 to 300. The cone potential was 20 V. MS/MS experiments were performed using collision energy of 30 V, with argon as the collision gas.

Extraction and Analysis of Volatiles.

Garlic and Onion.

a) SPME. A 100 µm polydimethylsiloxane sampling fibre of a Supelco SPME syringe was introduced into a headspace vial (4 mL capacity) containing approx. 1g of a freshly chopped garlic clove (cut into about 7-10 pieces) and retained in this position, at room temperature, for 2 min. The fibre was retracted and introduced into an ATAS Optic-2 PTV GC Injector fitted with a 2 mm injection liner, splitless injection, with a purge off of 0.5 min, injector temperature 150°C, for a 1 min desorption period. The helium carrier gas flow was 1.0 mL/min. (For GC-EI-MS see section c below).

b) Direct Solvent Extraction. A single garlic clove (about 3g) was submerged in 20mL HPLC grade hexane in a 50ml beaker. The clove was sectioned five times under the solvent and swirled for 20sec. A 1mL aliquot of the hexane extract was removed and 1 µl transferred to the GC injector held at 240°C. Analysis was by GC-EI-MS (see section c below).

c) GC-EI-MS Analysis. An HP5890 GC was employed using a DB624 column (30m x 0.25mm x 1.5µ film thickness); GC temperature programme, 40°C(0 min) to 250°C at 10°C/min followed by holding at the same temperature for 4 min. The GC column was coupled directly by a transfer line heated at 250°C into a Finnigan Mass Lab Trio-1000 mass spectrometer, source temperature 200°C, operating at 70eV electron ionisation (EI+) mode, acquiring full scan data from m/z 30-200 over a GC run time of 30 min.

Tomato Leaf and Stem Analysis by SPME.

Direct volatile analysis of leaf or stem trichomes was achieved by gently rubbing the plant surface with the exposed SPME fibre (100µm polydimethyl solixane [PDMS] (ex Supelco). The fibre was withdrawn back into its protective sheath until ready for injection, which was carried out by inserting the fibre holder into the GC-MS injection port where the fibre was exposed for 2 min at 200°C to allow needle absorbed components to desorb onto the GC column. GC-EI-MS employed a HP 5890 GC with an HP5-MS column (30 m x 0.25 mm x 0.25µ film thickness). The GC temperature programme was set at 50°C (1 min) to 160°C at 10°C/ min, then to 240°C at 20°C /min. The GC column was coupled directly, via a heated transfer line heated at 250°C, into an HP 5972A MSD; source temperature 250°C,

**American Chemical Society
Library**

1155 16th St., N.W.

Washington, D.C. 20036

EI (70eV source); acquisition m/z 30-300. Helium was used as the carrier gas at a constant flow of 1.0mL/min.

For peak identification mass spectra were compared with those of known standards from the NIST MS Library (1992 edition). The identification of the terpene hydrocarbons was confirmed, where possible, using authentic standards.

Scanning Electron Microscopy (SEM).

Samples of upper leaf surface from the second apical spur of greenhouse-grown tomatoes were prepared by mounting leaf tissue (20 x 10 mm) onto an SEM stub followed by quenching in liquid nitrogen and transferring to an Oxford CP2000 SEM preparation chamber. Surface frost was removed by holding at -98°C at 5×10^{-7} torr for 5min. The sample was then cooled to -110°C and the surface coated with Gold/Palladium, 6mA at 5×10^{-1} millibar Argon for 20 sec followed by recovery of the vacuum to 5×10^{-7} torr. The coated sample was finally transferred under vacuum to a Jeol JSM 6301 FESEM and images recorded at 5kV and at -165°C on a Cressington cold stage at a working distance of 48mm.

RESULTS AND DISCUSSION

Brushing and Crushing of Tomato Leaves.

Gentle handling of tomato plants produces a persistent and characteristic aroma. Visual inspection of the adaxial leaf surface and stem revealed in both cases a down-like surface appearance. Close examination of the leaf surface by SEM revealed projecting from the epidermis two types of structural outgrowth or trichomes namely hair-like and capitate. The capitate glandular hairs, which are characteristic of the *Solanaeae* family, are reported to contain a four-celled head surrounding an intercellular space containing essential oil drops (19,20). Gentle brushing of the leaf and stem trichomes was carried out by gently stroking the exposed needle of the SPME fibre across the trichome layer, parallel to the epidermal surface for a period of about 3 sec. The fibre was then heat desorbed and analysed by GC-EI-MS. Figure 1 shows the SPME-GC-TIC chromatograms for both stem and leaf trichomes. The leaf gland volatiles were dominated by monoterpene hydrocarbons (65% of the total ion current) of which β -phellandrene was the major component. Sesquiterpene hydrocarbons accounted for ca. 30% with (E)-caryophyllene the major contributor. These findings were in keeping with previous observations on tomato leaf volatile components with the exception that the C_6 aldehydes (Z)-3- and (E)-2-hexenal and hexanal were present at trace levels reflecting slight tissue bruising during sampling (21). Comparison of the volatiles from stem trichomes in Figure 1 showed a much greater predominance of monoterpene hydrocarbons (about 91% of the total ion current) and a much lower level (about 1%) of sesquiterpene hydrocarbons. The significance of these compositional differences on the same plant is not clear.

It should be noted however that the wild and cultivated potato species *Solanum berthaultii* Hawkes and *S. tuberosum* L. respectively contain two types of foliar glandular trichomes (types A and B). The type A glands contained sesquiterpenes as the major volatile constituents whilst, in type B glands, the C_{15} hydrocarbons were

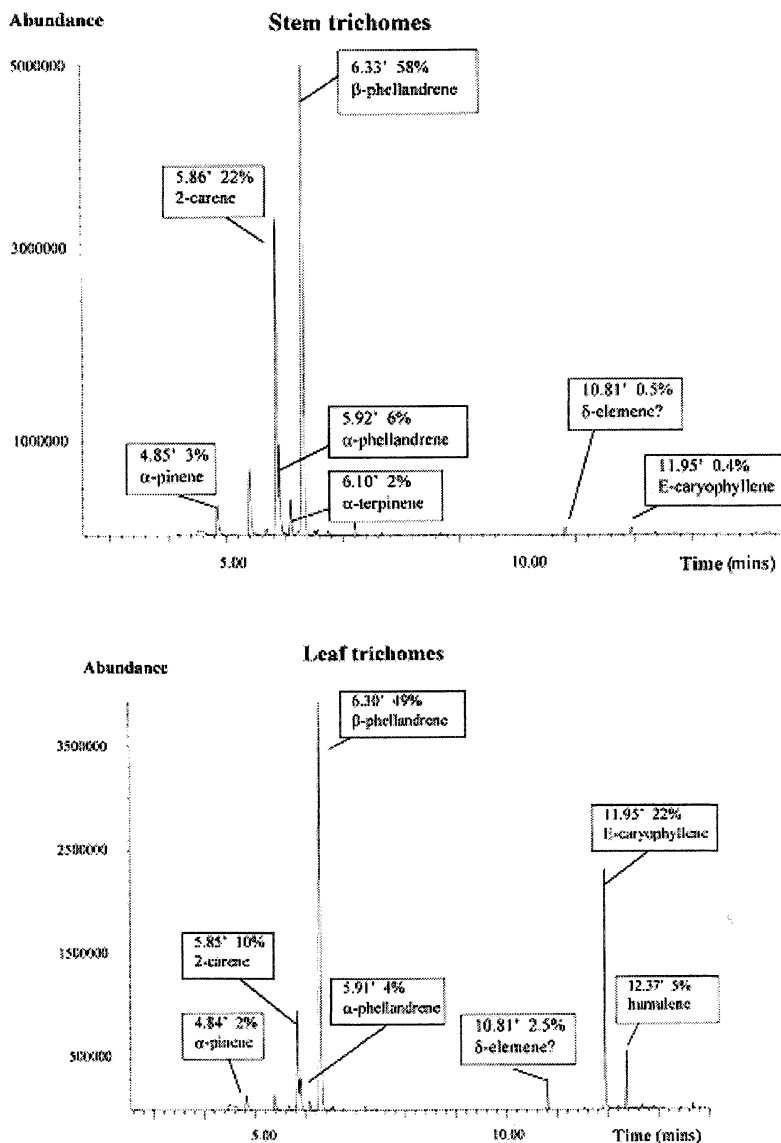


Figure 1. SPME-GC-EI-MS of aroma compounds of tomato stem and leaf trichomes. For analysis method see Experimental section.

minor components (22). Exudates from these types of glands probably help to limit infestation of the plants by arthropods such as the green peach aphid, *Myzus persicae* (23). It is noteworthy that elicitor treatment of tobacco cell suspension cultures induces sesquiterpene phytoalexin production (24).

APCI-MS analysis of volatiles released from tomato leaf was also conducted to study the time course of the reactions to different degrees of tissue mechanical damage. The brushed leaf surface shows the expected ions at m/z 137 and 205 corresponding to $C_{10}H_{17}^+$ and $C_{15}H_{25}^+$, the protonated molecular ions of the monoterpene and sesquiterpene hydrocarbons, respectively. These findings in general were in keeping with the results of the SPME-GC-MS analysis. Crushing the leaf surface with a glass rod of circular cross section (radius 5mm) resulted in a similar mass spectrum again with dominant ions at m/z 137 and 205. In addition however in the latter sample there was an additional peak at m/z 99. From previous work this ion was identified as the protonated molecular ion, $(M+H)^+$, for (E)-2-hexenal (25). This compound originates by isomerisation of (Z)-3-hexenal the first volatile product formed from the lipoxygenase/hydroperoxide lyase transformation of *cis*-9,12,15-linolenic acid (26). The sequence of leaf brushing and crushing was repeated and monitored over time, by APCI-MS, following the indicator ions at m/z 99, 137 and 205 corresponding to the C_6 unsaturated aldehydes, monoterpene- and sesquiterpene hydrocarbons respectively. Figure 2 exhibits the real time responses for these three ions.

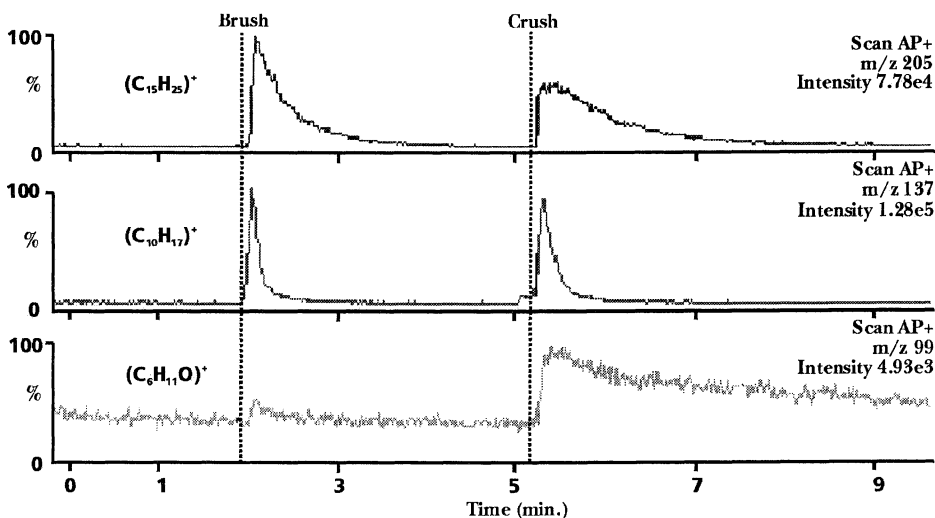


Figure 2. SIM-APCI-MS of the volatiles released from a mechanically damaged tomato leaf. For method see Real Time Headspace Analysis, under APCI-MS.

Brushing the leaf surface elicits an immediate release of mono- and sesquiterpene hydrocarbons (ions at m/z 137 and 205) whilst the ion at 99 due to (E)-2-hexenal was very weak and showed a delay in initiation compared to the other two. Post-stimulus, the decay of the m/z 137 peak was very rapid whilst the m/z 205 ion decayed more slowly. On crushing the leaf tissue, the general profiles of the m/z 137 and m/z 205 peaks were retained whilst the m/z 99 peak gave an increased response, the rate of development of which was slower than that observed for the two hydrocarbon peaks. In addition the decline of the m/z 99 peak was prolonged and decayed over a period of approx. 7 min having half of its initial maximum response level after about 3 min. The major differences observed, particularly for the monoterpene hydrocarbon and the (Z)-3-hexenal indicator peaks are probably due to the following factors. The monoterpene hydrocarbons reside within the glandular trichomes on the epidermal leaf surface. They are probably present as the free hydrocarbons within the glandular trichomes and are released when the trichomes are ruptured. Their temporal release and decay are probably reflective of a breaking of the retaining encapsulating cell structure with the rapid release and discharge of their contents. (Z)-3-hexenal is not present to any significant extent in viable undamaged tissue and is only formed enzymatically in response to tissue damage via the oxylipin lipoxygenase/hydroperoxide lyase pathway (26,27). Thus tomato leaf probably exhibits two response pathways to mechanical damage. The first is at the level of the trichome and probably involves the rapid release of hydrocarbons retained within glandular cell structures. The second front involving enzymatic formation and release of C_6 aldehydes by mechanical damage and decompartmentation of enzymes and precursors within the epidermal tissues; this latter being one component of the much more complex oxylipin plant defence reaction (1). It is interesting to speculate whether damage to trichomes activates the above general wound response reaction.

Freshly cut garlic cloves.

The characteristic aroma of garlic is associated with sulfur-containing volatiles derived by the wound initiated transformation of non-volatile alk(en)yl cysteine sulfoxide precursors typified by the 2-propenyl (2-Pe-) derivative (alliin) present in the cytoplasm being transformed by the vacuolar enzyme allinase. The first-formed enzymatic products, the sulfenic acids, are unstable and participate in a series of chemical transformations dependent on their structure and environment (13,28). In garlic the alk(en)yl residue of the amino acid precursor is dominated by the 2-Pe-group with lower levels of the 1-propenyl (1-Pe-) derivative. This major 2-Pe-component defines the structure of the first formed enzymatic product namely 2-Pe-sulfenic acid and its primary thiosulfinate transformation products.

Headspace analysis by SPME-GC-MS was carried out on fresh chopped garlic clove after a sampling time of 3 min and run under conditions described in the experimental section. The TIC chromatogram was dominated by three GC peaks with M^+ ions at m/z 146 and retention times of 11.45, 11.71 and 11.94 min which were identified as the isomeric di-(2-Pe)-, (2-Pe),(1-Pe)- and the di-(1-Pe)-disulfides respectively. Lesser amounts of peaks with M^+ at m/z 120 and retention times 8.35 and 8.79 min corresponded to (2-Pe), (methyl)- and (1-Pe), (methyl)- disulfides respectively. There

was no evidence in the spectrum for the corresponding alkenyl thiosulfinate, e.g. allicin; this among the earliest formed volatiles derived from the alk(en)yl cysteine sulfoxides. There was however, evidence for two minor peaks at Rt. 5.98 and 7.90 min with M^+ at 90. The 7.90 min peak exhibited some chromatographic tailing indicative of the relatively high polarity of the component(s) involved. The closest match to the spectra of these two peaks, on the MS database, was thiopropanal-S-oxide. RT and MS confirmed the identity of the peak at 5.89 min as thiopropanal-S-oxide via the SPME-GS-EI-MS analysis of the headspace of freshly chopped onion. This compound in onion is a major and moderately stable isomerisation product of (1-Pe)-sulfenic acid. Additional clarification of the identity of these two compounds was achieved by cutting a garlic clove under hexane and analysing the extract by GC-EI-MS. The larger of the two M^+ peaks at m/z 90 was at RT 7.90 min whilst the RT 5.98 min peak again matched by RT and MS with thiopropanal-S-oxide. By a process of elimination therefore it would seem that the RT 7.90 min peak, was in the case of garlic, the (2-Pe)-sulfenic acid.

Further definitive work would need to be carried out to confirm this identity. Of equal interest was the observation that the TIC-MS spectrum of the hexane extract of garlic was dominated by the isomeric 3-vinyl-3,4-dihydro-1,2-dithiin and 2-vinyl-2,4-dihydro-1,3-dithiin respectively. These compounds were probably derived by decomposition of diallyl thiosulfinate (allicin) via thioacrolein (13). It was of interest that the major component profile of the SPME and hexane extracts of fresh cut garlic are very different with the former dominated by disulfides whilst the latter by the isomeric dithiins. These differences probably reflect the air atmosphere of the SPME system vs the relatively inert environment provided by the hexane extract. There would appear to be some novelty in the tentative identification of (2-Pe)-sulfenic acid by these techniques though clear differences with respect to the major component profiles are observed dependent on environment. Although extraction and GC methods of analysis are known to produce artefacts due to the reactivities of the volatile sulphur species the combination of the rapidity of SPME sampling and low temperature desorption have resulted in some improvement in stability during the analysis of fresh onion volatiles (29). Even in this case however the more stable thiopropanal-S-oxide rather than the sulfenic acid or thiosulfinate was detected. The extraction environment as well as the thermal regime for analysis clearly needs further consideration.

Rapid analysis of a freshly cut garlic clove was applied using APCI-MS (Figure 3). The most prominent ion at m/z 91 corresponded to $(C_3 H_7 OS)^+$ and its $^{34}S/^{32}S$ ratio confirmed monosulfur and the likely structure as (2-Pe)-sulfenic acid. Further circumstantial evidence supporting this position was the lability of the m/z 91 ion since a spectrum run 3 mins after cutting the fresh clove did not exhibit the original m/z 91 ion. Another ion in the spectrum that showed similar but slower loss was at m/z 163, a disulfur compound, corresponding to $(C_6 H_{11} OS_2)^+$. This ion probably corresponds to the protonated molecular ion of di-(2-Pe)-thiosulfinate. Similarly the disulfur compound at m/z 147 $(C_6 H_{11} S_2)^+$ is likely to be the protonated molecular ion of di-(2-Pe)-disulfide. The temporal relationships between these three ions at m/z 91,

147 and 163 were determined in the reaction cell by puncturing a single garlic clove with a steel needle under the controlled conditions described in the experimental section

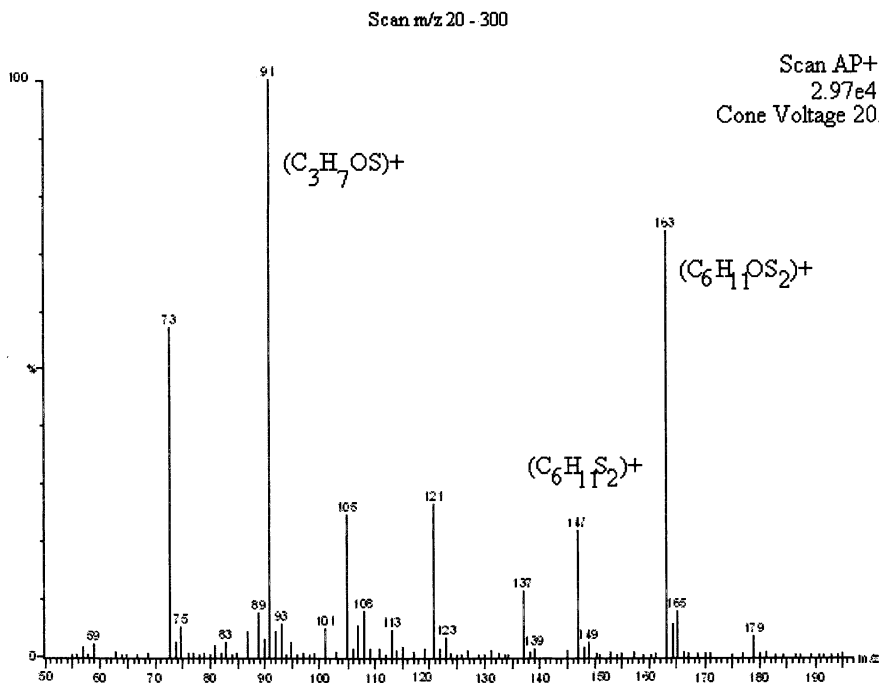


Figure 3. APCI-MS of the volatiles released from a freshly cut garlic clove. For method see Real Time Headspace Analysis, under APCI-MS.

The data displayed in Figure 4 shows a potential precursor product relationship between these three ionic species. The m/z 91 peak is the first very rapidly formed volatile compound; which also declines rapidly. The decline of this peak corresponds with a rapid build up and slower decline of the m/z 163 peak. The peak at m/z 147 forms very slowly and reaches a maximum when both m/z 91 and m/z 163 have reached baseline values.

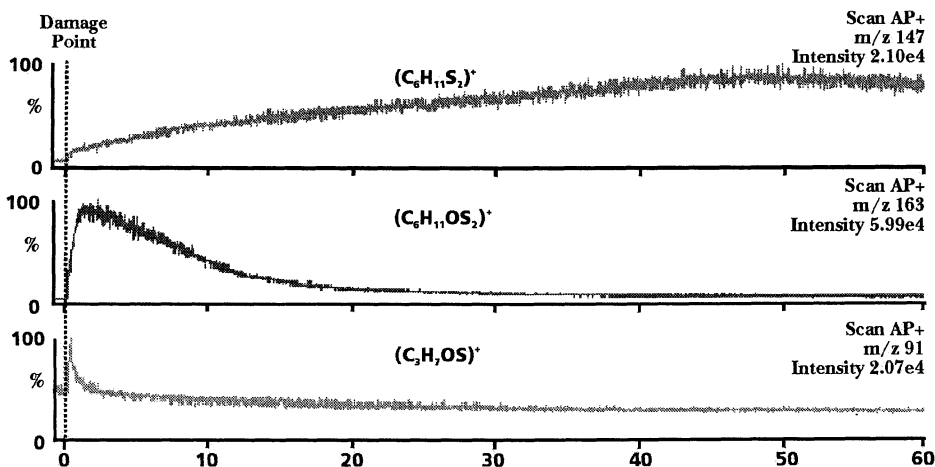


Figure 4. SIM-APCI-MS of the volatiles released from a needle damaged garlic clove. For method see Real Time Headspace Analysis, under APCI-MS.

The likely interrelationship therefore between these compounds is as follows:-

Non-volatile precursor \rightarrow m/z 91 \rightarrow m/z 163 \rightarrow m/z 147.

This pattern is consistent with the following identities of the species

m/z 91 [(2-Pe)- sulfenic acid] H^+

m/z 163 [di-(2-Pe)- thiosulfinate] H^+

m/z 147 [di-(2-Pe)- disulfide] H^+

Further support for the structures proposed was derived by MS-MS analysis of the APCI⁺ (M+H)⁺ ions at m/z 91, 147 and 163 from fresh garlic. In all cases an ion at m/z 73 was present as the dominant species from the m/z 147 and 163 parents, and as the largest ion after the m/z 91 parent. This m/z 73 fragment was probably (C₃H₅S)⁺ corresponding to the structure of protonated thioacrolein (CH₂=CH-CH=SH)⁺. This reactive compound is formed as an intermediate in the flash vacuum pyrolysis of di-(2-Pe)-sulfide and disulfide and in the thermal decomposition of di-(2-Pe)-thiosulfinate (13,30). The ions at m/z 147 and 163 also gave prominent daughter ions at m/z 105 tentatively due to the structure (CH₂=CH-CH₂SS)⁺. This fragment would be expected for both di-(2-Pe)-disulfide and the corresponding thiosulfinate. The m/z 163 parent ion gave a strong daughter ion at m/z 121 equivalent to the structure [CH₂=CH-CH₂SS(O)]⁺; this latter was absent from the spectrum of the m/z 147 ion.

This combination of the APCI-MS technique with SPME-GC-EI-MS, solvent extraction and other methodologies including cryotrapping, UV and MS-HPLC (31,32) may realise further deconvolution of these complex sulfur chemistries.

The APCI-MS technique employed readily supports this demonstrated transformation pathway for the alk(en)yl cysteinyl sulfoxide precursor in garlic (13) and permits the monitoring of the rapid reactions involved and in particular the fate of the labile alk(en)yl sulfenic acids.

SUMMARY

Flavor release from mechanically damaged plant tissues employs at least two key strategies for management of the response. For inducible flavor systems segregation of non-volatile precursors from the catalysing enzymes may be achieved by separate localisation within the cell. This method is employed for:-

- the alk(en)yl cysteine sulfoxides/C-S lyase (allinase) in the Genus *Allium* where the enzyme appears to reside in the vacuole and the precursor in the cytoplasm (33).
- the oxylipin lipoxygenase/lyase system in leaves, fruit and vegetables. In this case the plastid appears to be the organelle capable of generating the C₆ aldehyde products from polyunsaturated fatty acids with perhaps the stress signal transmission emanating from the plasma membrane (34, 35).

For constitutive flavor systems cellular specialisation usually occurs with essential oil drops resident within or between modified cells. This is the system employed in the glandular trichomes of tomato leaf. Such functional separation provides the plant with the capability to react specifically and selectively to induced stress. APCI-MS has been used successfully in this study to follow the real time release of aroma molecules from both induced and constitutively based flavor systems. In addition SPME and solvent extraction in combination with GC-EI-MS has been applied to the further characterisation and identification of the volatile species involved. Their usefulness in this context is related to the stability of the molecules involved and care must therefore be taken in its application and interpretation.

This capacity of APCI-MS to measure rapid changes in complex mixtures of very reactive species, in real time, provides a tool to develop a greater understanding of the pathways of generation and transformation of plant aroma signalling compounds.

Acknowledgements

We wish to thank Unilever Research for permission to publish this work. We gratefully acknowledge the expertise of our Unilever colleagues, Roy Dobb for carrying out the SPME-GC-EI-MS on tomato leaves, Clare Yorke for the SPME-GC-EI-MS and the GC-EI-MS analysis of the garlic and onion tissues and Mark Kirkland for producing the SEM images. We also wish to appreciate the contribution of Dr Willi Grab, Givaudan Roure Flavors Ltd., Switzerland, for discussion on the isolation and structure of (2-Pe)-sulfenic acid from garlic.

LITERATURE CITED

1. Blée, E. *Prog. Lipid Res.* **1998**, 37, 33.
2. Benhamau, N. *Trends Plant Sci.* **1996**, 1, 233.
3. Green, T.; Ryan, C.A. *Science.* **1972**, 175, 776.
4. Pearce, G.; Strydom, D.; Johnson, S.; Ryan, C.A. *Science.* **1991**, 253, 895.
5. Bate, N.J. and Rothstein, S.J. *Plant J.* **1998**, 16, 561.
6. Thaler, J.S. *Nature.* **1999**, 399, 86.
7. Baldwin, I.T. and Preston, C.A. *Planta.* **1999**, 208, 137.
8. Takabayashi, J. and Dicke, M. *Trends Plant Sci.* **1996**, 1, 109.
9. Stowe, M.K.; Turlings, T.C.J.; Loughlin J.H.; Lewis, W.J. and Tumlinson, J.H. *Proc. Natl. Acad. Sci.* **1995**, 92, 23.
10. Buttery, R.G. In *Flavor Research; Recent Advances*; Teranishi, R.; Flath, R.A.; Sugisawa, H., Eds.; Marcel Dekker, Inc.:**1971**, Chapter 6, p 175.
11. Brauss, M.S.; Linforth, R.S.T. and Taylor, A.J. *J. Agric. Food Chem.* **1998**, 46, 2287.
12. Paré, P.W. and Tumlinson, J.H. *Plant Physiol.* **1997**, 114, 1161.
13. Block, E. *Angew. Chem. Int. Edn. Engl.* **1992**, 31, 1135.
14. Hansel, A.; Jordan, A.; Holzinger, R.; Prazellar, P.; Vogel, W. and Lindinger, W. *Mass Spectrom. Ion Proc.* **1995**, 149/150, 609.
15. Lindinger, W.; Hansel, A. and Jordan, A. *Int. J. Mass Spectrom. Ion Proc.* **1998**, 173, 191.
16. Bruins, A.P. *Mass Spectrom. Rev.* **1991**, 10, 53.
17. Linforth, R.S.T.; Ingham, K.E. and Taylor, A.J. *Flavor Science:Recent Developments*. Taylor, A.J. and Mottram, D.S.,Eds.; Royal Soc. Chem. London, **1996**, p 261.
18. Smith, D. and Spanel, P. *Int. Rev. Phys. Chem.* **1996**, 15, 231.
19. Bancher, E. and Hölzl, J. *Protoplasma.* **1959**, 50, 356.
20. Fahn, A. *Secretory Tissues in Plants*. Academic Press. **1979**, p 158.
21. Buttery, R.G.; Ling, L.C. and Light, D.M. *J. Agric. Food Chem.* **1987**, 35, 1039.
22. Ave, D.A.; Gregory, P. and Tingey, W.M. *Entomol. Exper. Applic.* **1987**, 44, 131.
23. Gibson, R.W. and Pickett, J.A. *Nature.*, London. **1983**, 302, 608.
24. Chappell, J. and Nabel, R. *Plant Physiol.* **1987**, 85, 469.
25. Spanel, P.; Yufeng, J. and Smith, D. *Int. J. Mass Spectrom. Ion Proc.* **1997**, 165/166, 25.
26. Hatanaka, A. *Phytochem.* **1993**, 34, 1201.
27. Fall, R.; Karl, T.; Hansel, A.; Jordan, A. and Lindinger, W. *J. Geophys. Res. Atmos.* **1999**, 104, 15963.
28. Fischer, C. and Scott, T.R. *Food Flavors:Biological and Chemistry*. Royal Soc. Chem. **1997**, p 51.
29. Jarvenpaa, E.P.; Zhang, Z.; Houpalchti, R. and King, J.W. *Z. Lebensm. Unter Forsch A.* **1998**, 207, 39.

30. Block, E.; Iyer, R.; Grisoni, S.; Saha, C.; Belman, S. and Lossing, F. *J. Am. Chem. Soc.* **1988**, 110, 7813.
31. Ferary, S. and Auger, J. *J. Chromatog. A.* **1996**, 750, 63.
32. Ferary, S.; Thibout, E. and Augur, J. *Rapid Commun. Mass Spectrom.* **1996**, 10, 1327.
33. Lancaster, J. E. and Collin, H. A. *Plant Sci. Lett.* **1981**, 2, 169.
34. Bell, E.; Creelman, R. A. and Mullet, J. E. *Proc. Natl Acad Sci. USA.* **1995**, 92, 8675.
35. Blée, E. and Joyard, J. *Plant Physiol.* **1996**, 110, 445.

Chapter 6

Time-Resolved Headspace Analysis by Proton-Transfer-Reaction Mass-Spectrometry

C. Yeretjian¹, A. Jordan², H. Brevard¹, and W. Lindinger²

¹Nestlé Research Center, Vers-Chez-les-Blanc, 1000 Lausanne 26, Switzerland

²Institut für Ionenphysik, Leopold-Franzens-Universität,
Technikerstr. 25, 6020 Innsbruck, Austria

A recently developed technique, **Proton-Transfer-Reaction Mass-Spectrometry (PTR-MS)**, is reviewed based on applications on coffee. PTR-MS is a sensitive and fast method for on-line trace gas analysis. It consists of a specially designed chemical ionization cell, where headspace gas is continuously introduced and volatile organic compounds ionized by proton-transfer from H_3O^+ . Protonated compounds are then mass analyzed in a quadrupole mass filter. First a description of the method will be given, with emphasis on the ionization mechanism. We then discuss a series of experiments that allow mass spectral intensities to be related to chemical compounds. Finally, two applications on coffee are discussed.

Food products all along the food chain, from raw materials to final products, continuously emit volatile organic compounds (VOCs). These volatiles released from and hence surrounding the food, form the **Headspace (HS)**. While VOCs represent only a small mass-fraction of the food product, they are related to important properties of the product itself, such as flavor, age or shelf-life, geographic or genetic origin, history of processing, safety, packaging, the presence of micro-organisms or others.

Headspace-Gas of Food Products: A Rich Source of Information: Due to the substantial information that can be gained from a detailed knowledge of the chemical

composition of the HS, several analytical techniques have been developed that sample and analyze the HS of food. Nearly all of them are based on gas chromatographic separation (1-3). Yet, in spite of advances made over the last twenty years, gas-chromatography (GC) based approaches are limited when it comes to monitor, in real time, the temporal evolution of HS profiles.

The Added Value of Time-Intensity Profiles: The benefits, to the food industry, of having means to monitor fast on-line changes in volatile compositions are numerous. Here, we will mention just three: (i) Many food-processing steps involve fast transformations of foods, such as roasting, drying or cooking, with a marked trend towards ever shorter processing-times. Real-time monitoring of HS-gas can help to better control these processes. (ii) Flavor generation in thermal, enzymatic or fermentation processes is intrinsically dynamic. Time-resolved HS techniques can help to better understand the underlying chemistry and optimize process flavors. (iii) In situations of real-life sensory experiences of foods, the temporal evolution of flavor profiles within the oral or nasal cavity is believed to be a crucial attribute for the perceived quality of foods. In order to address experimentally these dynamic problems, one needs fast on-line analytical techniques. Over the last few years, several approaches have been implemented which provide temporal information on volatile compositions. Two main directions have dominated (Figure 1).

Electronic Nose: One direction headed towards the development of a great variety of gas sensors. If grouped, such sensor arrays give fingerprint type time-intensity profiles of products (4). These techniques have been colloquially termed "Electronic Noses" (EN), and are in a stage of rapid development.

Direct inlet mass spectrometry: Another group of scientists has taken the approach to directly inject HS-gas into an MS. The critical element of this approach is the ionization, and a series of ionization modes have been investigated. If volatile compounds are (close to) pure or have been separated prior to MS analysis (e.g. by GC), fragmentation can provide valuable structural information. Here the most appropriate mode of ionization is electron impact (EI) ionization. This "hard" ionization mode ionizes gases that have high ionization potentials, such as O₂, N₂ or CO₂, but reveals little chemical information if used on complex mixtures of VOCs. Such mixtures are often investigated by chemical ionization methods, using "soft" ionization via ion-molecule reactions, where little or ideally no fragmentation occurs. One CI approach, by now well known in the field of flavour release, is atmospheric pressure chemical ionization (APCI) (5). Another particularly powerful CI method is Proton-Transfer-Reaction Mass-Spectrometry (PTR-MS). Besides CI, lasers are also used for soft ionization. Depending on the photon energy, two types of ionization processes are known: either resonant multiphoton ionization with ultraviolet (UV) photons, to selectively ionize VOCs out of a complex mixture, or vacuum ultraviolet (VUV) laser ionization, to ionize with a single laser photon, again with high sensitivity but less selectivity. Application of UV ionization to coffee roasting is documented in a series of publications (6-9). In a recent paper, we have outlined the advantages and limitations of both soft ionization approaches (10). Here we will discuss PTR-MS and present applications on coffee.

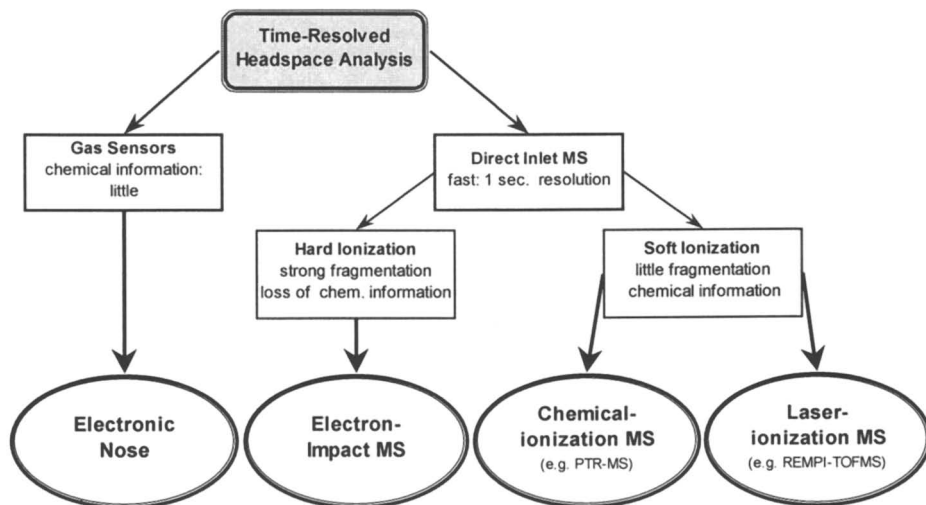


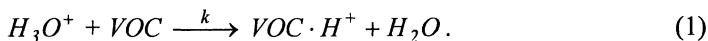
Figure 1: Analytical techniques for time-resolved HS analysis. EN can be used as a low cost process-monitoring device, where chemical information is not mandatory. EI-MS adds sensitivity, speed and some chemical information. Yet, due to the hard-ionization mode, most chemical information is lost. PTR-MS is a sensitive one-dimensional method which provides characteristic HS profiles (detailed fingerprints) and chemical information. Finally, REMPI-TOFMS combines selective ionization and mass separation and hence represents a two-dimensional method.

Proton Transfer Reaction Mass Spectrometry

PTR-MS was introduced in 1993 by Lindinger and co-workers (11). Since then it has been steadily improved and applied to a variety of subjects. Medical and nutritional applications by means of breath analysis allow monitoring of metabolic processes in the human body (12-19). Environmental applications include investigations of VOC emissions from decaying bio-matter (20,21), or diurnal variations of VOCs in the troposphere. Finally, PTR-MS has been shown to be an ideal tool to measure Henry's law constants and their dependence on temperature and matrix (22). Detailed discussions of technical aspects of PTR-MS have been published in a series of review papers (23-25). Here, only a brief description will be given. A schematic drawing of the apparatus is shown in Figure. 2.

An electrical discharge in 1.5 mbar H_2O within the ion source generates nearly exclusively H_3O^+ (>98%), and no mass filter is needed to pre-select H_3O^+ reactant ions. H_3O^+ ions are driven by a small electric field, through an orifice, into the drift tube, while HS gas is introduced coaxially to the orifice into the drift tube. The HS gas consists mainly of air or inert gas that acts as a buffer in the drift tube, and VOCs are present only in trace quantities. Using H_3O^+ as reactant ions has many advantages.

H_2O has a proton affinity (PA) of 166.5 kcal/mol. Hence, VOCs with a PA exceeding 166.5 kcal/mol become ionized by proton transfer from H_3O^+ :



These reactions are invariably fast, whenever they are exothermic, with rate coefficients, k , close to the collisional limiting values, $k_0 \approx 10^{-9} \text{ cm}^3/\text{s}$ (26,27). From Table I, we see that all natural constituents of air have PAs smaller than 166.5 kcal/mol, and are therefore not ionized in collisions with H_3O^+ . In contrast, nearly all VOCs have PAs exceeding the one of H_3O^+ , and will therefore be protonated. Consequently, H_3O^+ ions on their way through the drift tube, will perform many non-reactive collisions with the molecules of air. However, once they collide with a VOC they may undergo a reaction, provided their PA is higher than 166.5 kcal/mol. Protonated VOCs will drift downstream towards the end of the drift tube where several of them are accelerated by an electric field out of the drift tube and into a quadrupole mass spectrometer.

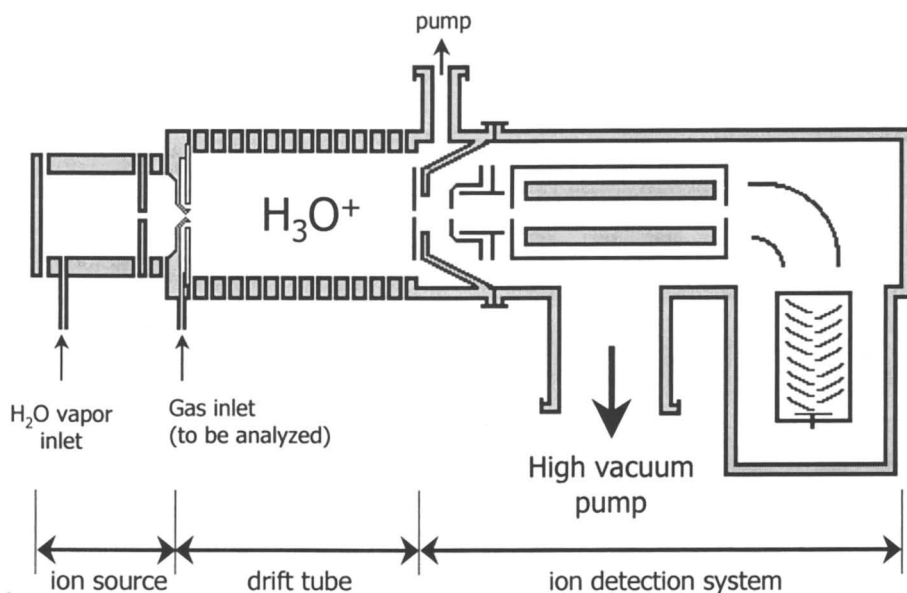


Figure 2: Schematic drawing of the PTR-MS apparatus.

What distinguishes PTR-MS from other CI-approaches is that the generation of the primary H_3O^+ and the CI of VOCs are individually controlled and spatially and temporally separated processes. One important consequence is that absolute HS concentrations can be calculated, without calibration or addition of standards (23,25).

A simple relation exists between measured PTR-MS intensities (counts per seconds, cps) and actual concentrations of the neutral compounds in the HS:

$$[VOC] = \frac{1}{k_{Rate} \cdot t_{Rtime}} \cdot \frac{cps(VOC \cdot H^+)}{cps(H_3O^+)} \quad (2)$$

The HS concentrations of VOCs, [VOC], are proportional to the ratio between measured count rates of protonated VOCs, cps(VOC·H⁺), and of protonated water, cps(H₃O⁺), and inversely proportional to the reaction rate coefficient, k_{Rate} ($\approx 10^{-9}$ cm³/s), and the reaction time, t_{Rtime} (≈ 105 μ s), for proton transfer in the drift tube.

Table I: Proton affinities (PA) of the constituents of clean air and various VOCs.

<i>Compounds</i>	<i>PA (kcal/mol)</i>	<i>Compounds</i>	<i>PA (kcal/mol)</i>
He	42.5	Methanol	181.9
Ne	48.1	Acetaldehyde	186.6
Ar	88.6	Acetonitrile	188.0
O ₂	100.9	Ethanol	188.3
N ₂	118.2	Furan	192.2
CO ₂	130.9	2,3-butanedione	194.8
CH ₄	132	Acetone	196.7
N ₂ O	136.5	2, 3-methylbutanal	ca. 195
CO	141.9	Ammonia	204.0
Water	166.5	Pyrrole	207.6
Butane	163.3	Oxazole	208.2
Hydrogensulfide	170.2	Pyrazine	209.0
Hydrogencyanide	171.4	Pyrazole	212.8
Formic acid	178.8	Dimethylamine	217.0
Propane	179.8	Pyridine	220.8
Benzene	181.9	Trimethylamine	225.1

Another important characteristic of PTR-MS is its linear response over four orders of magnitude as demonstrated in Figure 3. A gas mixture of 10 ppm benzene and toluene in N₂ was stepwise diluted with N₂ and the mass spectral intensities were measured. Using formula (2) and known apparatus constants, the concentrations of benzene and toluene were calculated and plotted along the vertical axis. For the undiluted system, the calculated concentrations, 10ppm, are as specified by the supplier. Furthermore, they are strictly linear to the mixing-ratio (HS-concentrations), over four orders of magnitude. Included in the figure are also the concentrations of the compounds appearing at one mass unit above the parents, which correspond to the

natural ^{13}C -isotopes of benzene and toluene. Calculated and measured concentrations are indistinguishable all the way down to the mixing ratio of about 200 ppt.

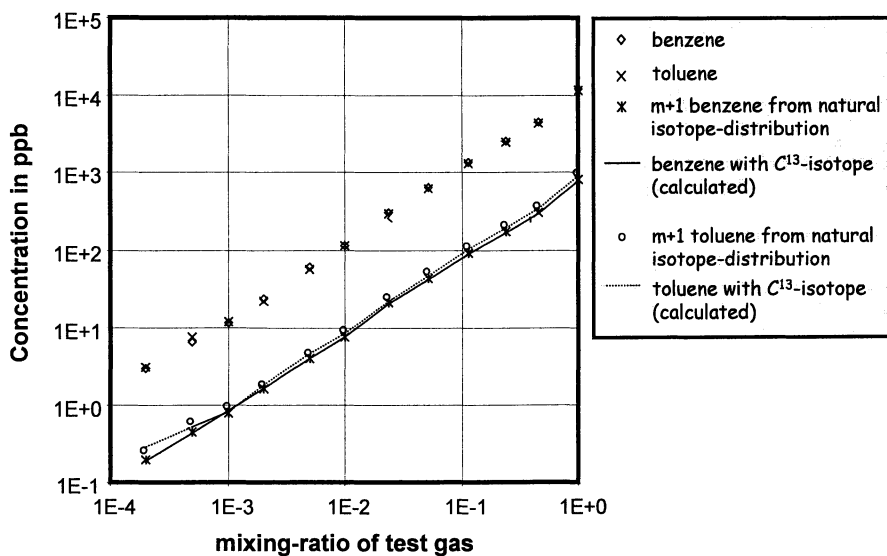


Figure 3: Using a commercial gas mixture benzene/toluene, a linear relationship between PTR-MS signal-intensity and HS concentration is shown to be valid for over four orders of magnitude.

PTR-MS has three key features that make it a very valuable complement to GC. *First*, it is fast (0.2 second resolution). *Second*, the VOCs do not experience any work-up. *Finally*, mass spectral intensities can be related to absolute HS concentrations, without calibration or use of standards. However, there are also some potential difficulties:

(1) Separation in an MS requires that the compounds be ionized. This can induce fragmentation and complicates the chemical interpretation of mixtures. In most experiments on food products, rather complex volatile mixtures have to be analyzed. Hence, to relate mass spectral intensities to the chemical composition, one absolutely needs to minimize ionization-induced fragmentation. CI by proton-transfer is a soft ionization mode. Based on PTR-MS results of 97 pure compounds, we find that about 70% of the mass spectral intensity appear at the protonated parent mass. A closer look at the fragmentation reveals that protonated compounds very often fragment selectively into one single fragment only. The prominent fragment peak then takes the role of a characteristic mass for the compounds. In fact more than 85% of the mass spectral intensity appears at either the parent or the most prominent fragment mass. Hence, ionization induced fragmentation has a limited impact on PTR-MS data,

and measured ion-distributions roughly reflect the genuine HS distributions (shifted by one mass unit due to protonation).

(2) The other potential difficulty stems from the fact that PTR-MS is a one-dimensional technique. It measures intensity as a function of mass. There are, however, a large number of potential VOCs having the same nominal mass (isobaric), particularly in coffee. Hence, mass-information alone is often insufficient for unambiguous identification. Here, PTR-MS has to be complemented with information from the literature and from a variety of additional supporting techniques available in PTR-MS (as will be outlined below) or GC experiments (22-25). These experiments provide complementary information, which assists in the identification. Ultimately, chemical assignments in complex systems, based on a PTR-MS profile alone, have to be considered as tentative, and need confirmation by additional experiments. In general, the strength of PTR-MS is not the identification of unknown compounds but rather the real-time, direct monitoring and quantification of known compounds.

In a typical experiment (Figure 4), HS gas is swept with a flow of synthetic air and introduced into the drift tube. In low energy collision with H_3O^+ , VOCs having a PA exceeding 166.5 kcal/mol are quantitatively protonated, and mass analyzed. A time resolution of 0.2 second can so be reached. In the configuration of Figure 4, two

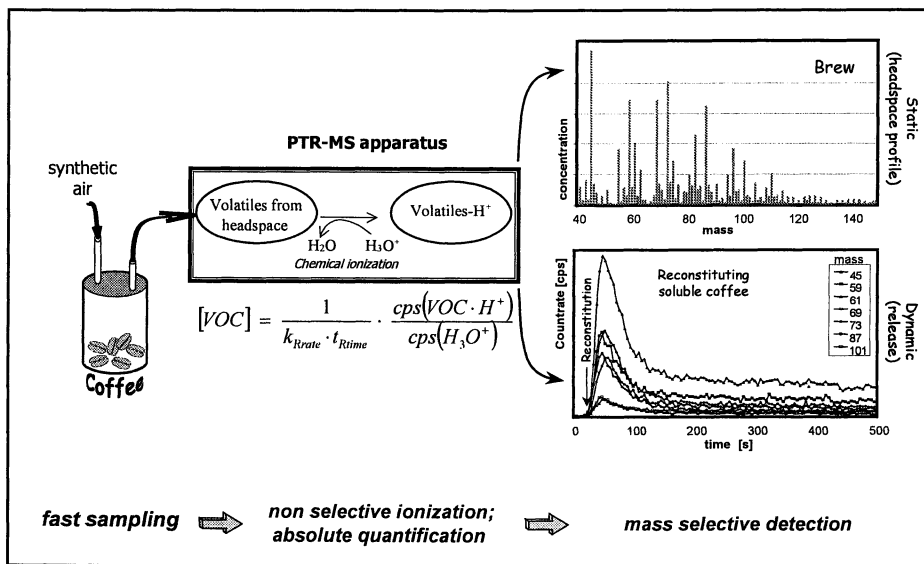


Figure 4: Two distinct types of information can be recorded by PTR-MS. HS profiles can either be averaged over a given time to yield concentration vs. mass spectra (static data), or temporal changes analyzed via ion-intensity plots (dynamic data).

qualitatively different types of experiments are illustrated. Either HS is averaged over a period of time and plotted as mass vs. concentration (static data), or the temporal evolution of a series of masses is monitored (dynamic data).

Linking Mass Peaks to Chemical Compounds

As shown above, PTR-MS provides mass-intensity spectra with a time resolution of better than one second. However, mass-information alone is insufficient, particularly when analyzing complex volatile mixtures such as from coffee. If one does not link mass peaks to the chemical compounds, then a PTR-MS spectrum is just a “fingerprint”. It can be used to assess authenticity, monitor deviations in production from a reference, or classify products and raw materials. Yet, beside these “fingerprint” applications, we clearly want to relate mass spectral intensities in PTR-MS to concentrations of identified chemical compounds in the HS.

The starting point for the chemical assignment of PTR-MS spectra of coffee is the literature on coffee volatiles. Today around 900 VOC have been reported in coffee (28). Taking the sensitivity of PTR-MS into consideration (~ 100 ppt) we can reduce the number of compounds contributing to a PTR-MS spectrum to about 100. But even then, isobaric compounds remain an issue. Here a series of additional experiments can help to clarify the situation.

Collision-Induced Break-Up Patterns: Inducing fragmentation via collisions with the background gas is achieved by applying a variable voltage between the last drift segment and the end plate of the drift tube. We see in Figure 5 that the two isobaric compounds propanal and acetone have very distinct breakup patterns. While fragmentation of protonated propanal has nearly gone to completion at 35 V, hardly any break-up occurs for acetone at 35 V. Furthermore, the appearance of a fragment at mass 31, that equals the intensity of the parent mass at a break-up voltage of 30 V, is indicative of pure propanal. Similarly, other isobaric compounds can be differentiated as well.

Bracketing Proton Affinities by Selective Chemical Ionization: Typically, H_3O^+ is used for PTR-MS experiments, since its PA is well suited to protonate essentially all VOCs of interest while discriminating against the natural constituents of air. Yet, for the purposes of chemical assignment, it can be interesting to have a more selective ionization. Exchanging the ionizing agent from H_3O^+ to NH_4^+ , which is achieved by replacing the water vapor in the ion source by NH_3 , one eliminates from a PTR-MS profile all compounds with PA between 166.5 kcal/mol and 204.0 kcal/mol. PAs are known for most compounds of interest to us (29). Such bracketing of PAs provides additional information for chemical assignments. In Figure 6, the PTR-MS of coffee brew is shown, ionized with H_3O^+ and NH_4^+ respectively. Clearly, some mass peaks disappear or strongly decrease when NH_4^+ is used as primary reactant ion, indicating that the compound(s) contributing to this mass have a PA below 204.0 kcal/mol.

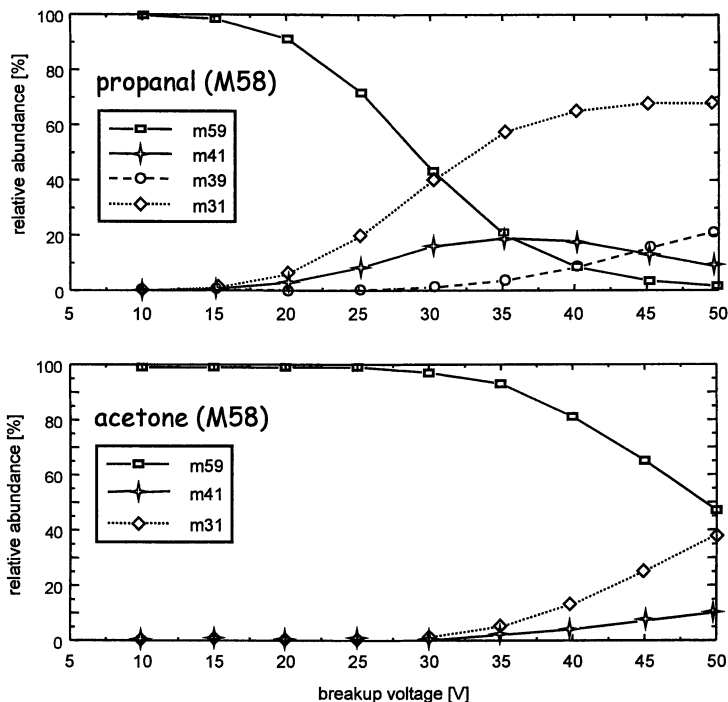


Figure 5: Propanal and acetone cannot be separated by mass, since they both have exactly the same sum-formula, C_3H_6O . Yet, they differ in their break-up patterns.

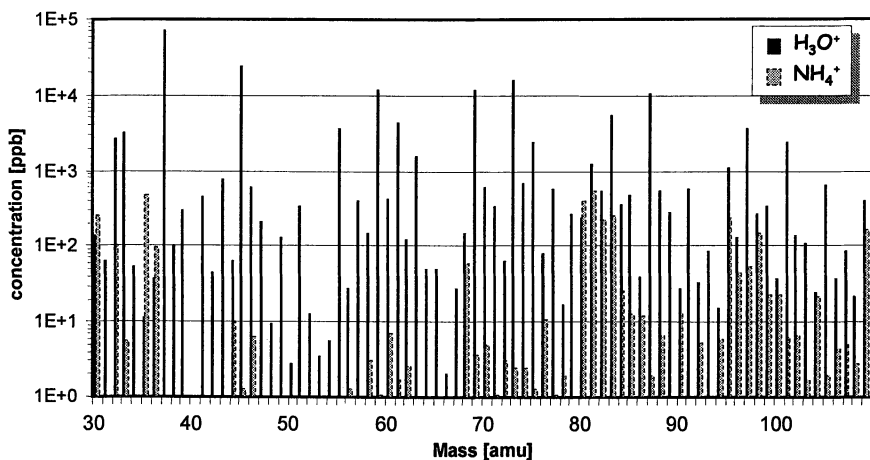


Figure 6: HS profiles of coffee analyzed with different primary reactant ions. The dark full-line spectrum was ionized with H_3O^+ (proton affinity 166.5 kcal/mol). In contrast, the dashed, gray spectrum was ionized with NH_4^+ (204 kcal/mol).

Liquid–Gas Partitioning of Volatile Compounds: The most effective way to identify and quantify compounds is derived from a method to measure liquid-gas partition coefficients. An advanced dynamic technique was introduced by Leroi (30) and Mackay (31) and was recently combined with PTR-MS (22). A flow of inert gas bubbling through a solution strips dissolved VOCs and leads to a decrease of their concentration in the liquid phase. Plotting the measured cps(t) of the VOCs vs. time, as shown in Figure 7, the partition coefficient can be calculated from the slope of Equation 3.

$$\ln(\text{cps}(t)) = - \frac{F}{H \cdot V \cdot R \cdot T} \cdot t + \ln(\text{cps}_0) \quad (3)$$

The Henry's law constants, H, can be calculated from the slope, with cps(t) being the count rate of [VOC·H⁺] at time t, and cps₀ being the initial count rate of [VOC·H⁺], at time 0. Except H, all values in the slope (F/H·V·R·T) are known constants, such that H can be calculated.

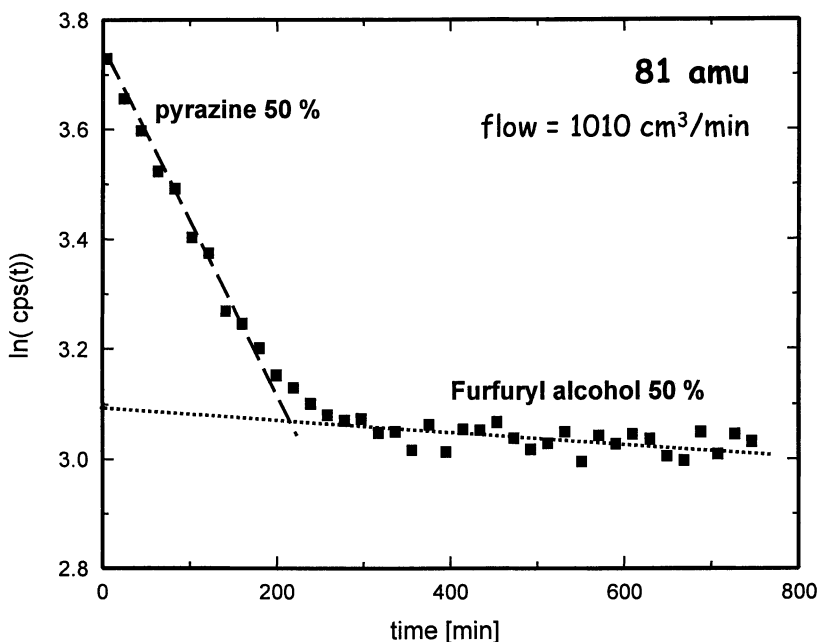


Figure 7: Plotting $\ln(\text{cps}(t))$ vs. time, one can calculate the Henry's law constant from the slopes of the linear portions, and the absolute concentrations from the intercepts with the $\ln(\text{cps}(t))$ axis.

In Figure 7, plotting $\ln(\text{cps}(t))$ vs. time at mass 81, we see that at around 220 minutes the slope abruptly changes. This break is related to a change in volatility indicating that at least two compounds contribute to mass 81. From that time on, the slope is given by the most volatile compound among those remaining. For each linear section on a $\ln(\text{cps}(t))$ vs. t plot, we can calculate the partition coefficient of the respective compound and compare these to the Henry's constants of VOCs of coffee that we would expect at this mass. In this way we determined that both pyrazine and furfuryl-alcohol are contributing to mass 81. (protonated furfuryl alcohol nearly quantitatively fragments into mass 81 by loss of H_2O).

Besides just assessing which compounds are contributing to a given mass, a $\ln(\text{cps}(t))$ vs. t plot also allows determining the absolute concentrations of compounds in the HS. For this, one extrapolates the linear portions of the slope, to time zero. From the intercept with the vertical axis, $\ln(\text{cps}_0)$, the intensity at time zero can be determined and concentrations calculated from Equation 2. This reveals that pyrazine and furfuryl alcohol contribute each by 50% to the mass peak intensity.

Integrating all the above pieces of evidence and combining with what is known from the literature, we can link a large number of measured mass peaks to the underlying chemical compounds in the HS.

Selected Applications on Coffee

Coffee has one of the most complex headspace profiles among food products. It is, therefore, a particularly challenging candidate for analytical investigations. Over the last year, we have extensively investigated the HS of coffee under a variety of conditions. Here we would like to show just two generic types of results.

As indicated by Figure 4, two qualitatively different types of experiments can be performed. Under so called "static" conditions, an averaged HS profile can be measured by integrating mass spectral intensities over a period of time and plotted as mass vs. concentration. Figure 8 shows the equilibrium HS profile of brew coffee, plotted on a linear as well as logarithmic intensity scale. Using these profiles as "fingerprints" they can help to accurately differentiate between origins, quality, products type or history of processing. Yet, using literature data and a variety of complementary informations from PTR-MS (as discussed above) and GC chromatograms, we are able to identify and roughly quantify over 50 compounds in the HS of coffee brew. This will be discussed in a separate work. Briefly, the most prominent masses have been assigned as follows; 45→acetaldehyde, 59→acetone, 61→acetic acid, 69→furan, 73→butanal, isobutanal, 2-butanone, 87→2,3-butanedione, 2-methylbutanal, 3-methylbutanal, 97→furfural, dimethylfuran, 101→2,3-pentanedione, 111→5-methylfurfural. At some masses, more than just one compound is significantly contributing to the mass intensity.

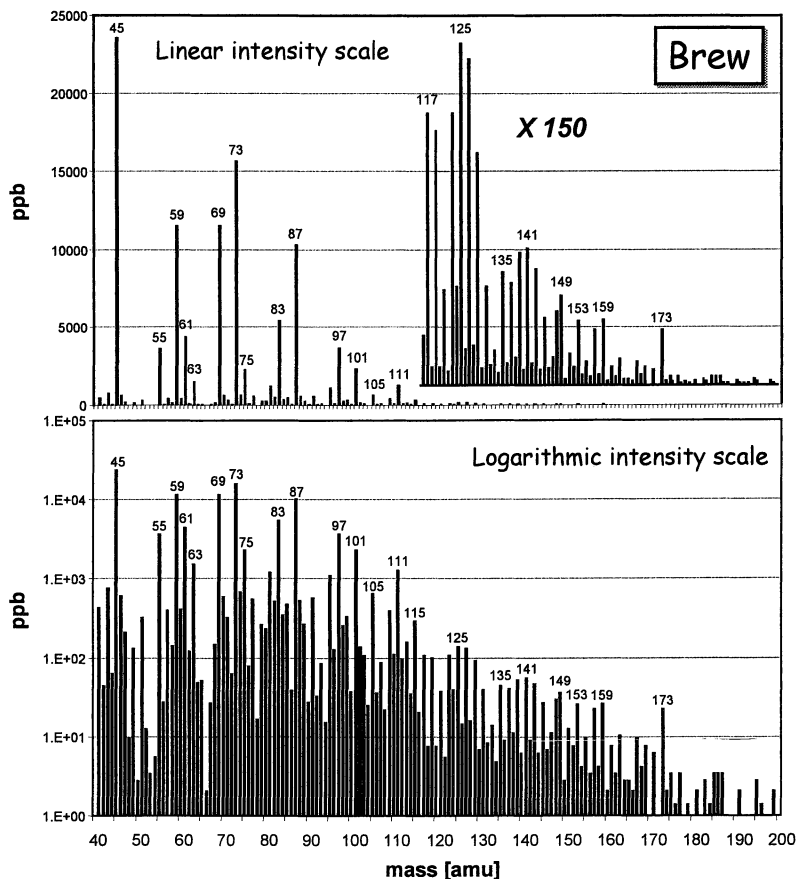


Figure 8: HS profiles of coffee brew plotted on linear (top frame) and logarithmic (bottom) intensity scales. Each type of scaling has its merits and drawbacks. Linear plots are often found in the literature on flavor release. In contrast, single logarithmic plots facilitate a comparison of intensities which are spread over a large range.

The most unique feature of PTR-MS is its capacity to monitor time-dependent variations of HS profiles on a scale of seconds (dynamic data). This is particularly important when we need to understand or even control fast processes, as they often occur in food processing. As an example of a dynamic process, we have reconstituted 2 grams of soluble coffee with 90 ml of hot water (70°C) and monitored the time-intensity evolution of 50 masses with a time resolution of about 5 seconds. For reasons of clarity we show in Figure 9 only seven masses. The assignment of these masses is analogous to those in Figure 8. For the first 40 seconds the HS profile of the dry soluble coffee powder is monitored. Then, we slowly add 90 ml of hot water,

which takes 15 seconds, and continue to monitor the HS profile of the liquid coffee. Immediately when adding water we observe a fast increase of HS intensities, reflecting largely two phenomem: (i) the increase in concentration of dissolved volatiles due to dissolution of the soluble powder and (ii) the permanent renewal of the liquid-gas interface for mass transfer due to turbulences during pouring of water. After about 15 seconds all the hot water was added and the turbulences slowly disappeared, reducing and ultimately ending the renewal of the interface. Experimentally, we observe a maximum concentration of VOCs at about 30 seconds followed by a strong decrease. This decrease reflects a depletion of volatiles at the interface and a release that was controlled by the diffusion of volatiles to the interface region. A detailed discussion of the physical processes behind the observed time-intensity evolution upon reconstituting of soluble coffee will be given elsewhere.

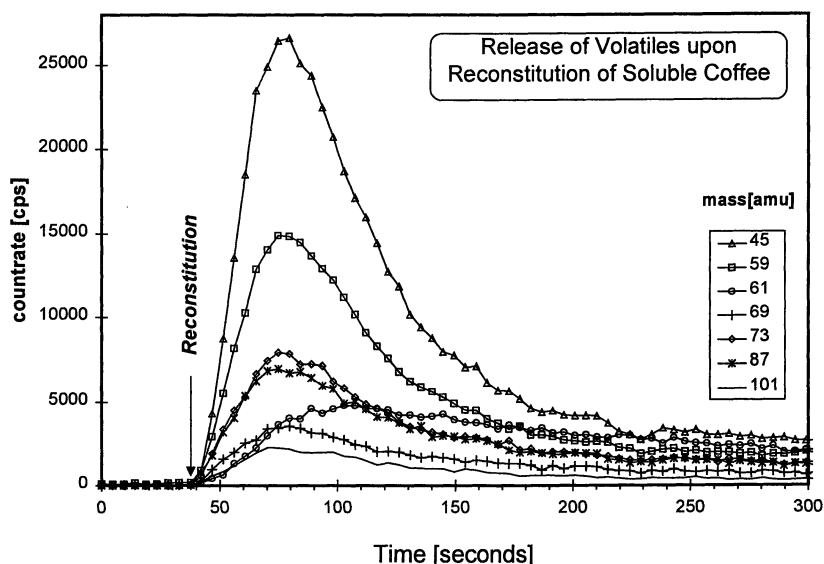


Figure 9: Ion-intensity profiles of seven selected masses upon reconstitution of 2 gram of soluble coffee with 90 ml of water at 70°C.

Conclusions

In this contribution, a detailed description of Proton-Transfer-Reaction Mass-Spectrometry (PTR-MS) was given. It has the particular feature to provide within seconds quantitative data on headspace profiles, without any workup of the sample. We then discussed a series of specific experiments which each provided important guidance towards the chemical assignment of PTR-MS mass peaks. This included

energy dependent break-up patterns of pure compounds, bracketing of proton affinities and liquid-gas partition coefficients. We have chosen to address this question on one of the most challenging systems, namely the headspace of coffee.

We would like to add that PTR-MS has many more fields of application. PTR-MS profiles, taken as fingerprints, can be used to e.g. assess authenticity, monitor deviations in production or classify raw materials and products. Ultimately, we believe that PTR-MS holds promise to become an important tool for process control.

Acknowledgements: We would like to thank A. Hansel for fruitful discussions. This project was supported by the "Fonds zur Förderung der wissenschaftlichen Forschung" under project P 12022.

References

1. Wampler, T. P. In *Techniques for Analyzing Food Aromas*; Marsili, R., Ed.; Marcel Dekker, Inc., New York, 1997; 27-58.
2. *Flavor Science: Sensible Principles and Techniques*; Acree, T. E.; Teranishi R., Eds.; ACS Professional Reference Book, III Series, American Chemical Society, Washington, DC, 1993.
3. *Techniques for Analyzing Food Aromas*; Marsili, R., Ed.; Marcel Dekker, Inc., New York, NY, 1997.
4. *Sensors and Sensory Systems for an Electronic Nose*; Gardner, J. W.; Bartlett, P. N., Eds.; Kluwer Academic Publishers: Dordrecht 1992.
5. Linforth, R. S. T.; Ingham, K. E; Taylor, A. J. In *Flavour Science: Recent Developments*; Taylor, A. J.; Mottram, D. S., Eds.; Special Publication No. 197, Royal Society of Chemistry, 1996, Thomas Graham House, Cambridge.
6. Zimmermann, R.; Dorfner, R.; Kettrup, A.; Yeretian, C. 18th International Scientific Colloquim on Coffee; Helsinki, Finland (ASIC18), August 2-6, 1999; in press.
7. Dorfner, R.; Zimmermann, R.; Yeretian, C.; Kettrup, A. Proceedings of the 9th Resonance Ionization Spectroscopy Symposium, June 1998, Manchester, UK, American Institute of Physics (AIP)-Conference Proceedings Series, AIP-Press New York, 309-312 (1998).
8. Zimmermann, R.; Heger, H. J.; Dorfner, R.; Yeretian, C.; Kettrup, A.; Boesl, U. Proceedings of the 1st International Convention on Food Ingredients: New Technologies, 15-17 September, 1997, Cuneo (Italy), 343-350.
9. Zimmermann, R.; Heger, H. J.; Yeretian, C.; Nagel, H.; Boesl, U. *Rapid Comm. Mass Spectrom.* **1996**, *10*, 1975-1979.
10. Dorfner, R.; Zimmermann, R.; Kettrup, A.; Yeretian, C.; Jordan, A.; Lindinger, W. *Lebensmittelchemie.* **1999**, *53*, 32-34.
11. Lindinger, W; Hirber, J.; Paretzke, H. *Int. J. Mass Spectrom. Ion Processes* **1993**, *129*, 79.

12. Warneke, C.; Kuczynski, J.; Hansel, A.; Jordan, A.; Vogel, W.; Lindinger, W. *Int. J. Mass Spectrom. Ion Processes* **1996**, *154*, 61.
13. Taucher, J.; Hansel, A.; Jordan, A.; Lindinger, W. *J. Agric. Food Chem.* **1996**, *44*, 3778.
14. Taucher, J.; Hansel, A.; Jordan, A.; Fall, R.; Futrell, J. H.; Lindinger, W. *Rapid Comm. Mass Spectrom.* **1997**, *11*, 1230.
15. Taucher, J.; Lagg, A.; Hansel, A.; Vogel, W.; Lindinger, W. *Alcohol Clin. Exp. Res.* **1995**, *19*, 1147.
16. Taucher, J.; Jordan, A.; Hansel, A.; Lindinger, W. *Alcohol Clin. Exp. Res.* **1997**, *21*, 939.
17. Jordan, A.; Hansel, A.; Holzinger, R.; Lindinger, W. *Int. J. Mass Spectrom. Ion Processes* **1995**, *148*, L1-L3.
18. Hansel, A.; Jordan, A.; Holzinger, R.; Paretzke, P.; Vogel, W.; Lindinger, W. *Int. J. Mass Spectrom. Ion Processes* **1995**, *149/150*, 605-619.
19. Prazeller, P.; Karl, T.; Jordan, A.; Holzinger, R.; Hansel, A.; Lindinger, W. *Int. J. Mass Spectrom. Ion Processes* **1998**, *178*, L1.
20. Warneke, C.; Karl, T.; Judmaier, H.; Hansel, A.; Jordan, A.; Lindinger, W.; Crutzen, P. J. *Global Biogeochem. Cycles* **1999**, *13*, 9-17.
21. Fall, R.; Karl, T.; Hansel, A.; Jordan, A.; Lindinger, W.; submitted.
22. Karl, T.; Yeretizian, C.; Jordan, A.; Hansel, A.; Lindinger, W. *Anal. Chem.* submitted.
23. Lindinger, W.; Hansel, A.; Jordan, A. *Int. J. Mass Spectrom. Ion Processes* **1998**, *173*, 191-241.
24. Lindinger, W.; Hansel, A.; Jordan, A. *Chem. Soc. Review* **1998**, *27*, 347-354.
25. Hansel, A.; Jordan, A.; Holzinger, R.; Prazeller, P.; Vogel, W.; Lindinger, W. *Int. J. Mass Spectrom. Ion Processes* **1995**, *149/150*, 609-619.
26. Gioumousis, G.; Stevenson, D. P. *J. Chem. Phys.* **1993**, *29*, 294.
27. Su, T.; Chesnavish, W. J. *J. Chem. Phys.* **1982**, *76*, 5182.
28. Nijssen, L. M.; Visscher, C. A.; Maarse, H.; Willemsens L. C. In *Volatile Compounds in Food*; 7th edition, 1996, TNO Nutrition and Food Research Institute.
29. *NIST Standard Reference Database Number 69 – August 1997 Release.*
30. Leroi, J.-C.; Masson, J.-C.; Renon, H.; Fabries, J.-F.; Sannier, H. *Ind. Eng. Chem., Process Des. Dev.* **1997**, *16*, 139.
31. Mackay, D.; Shui, W.; Sutherland, R. *Environ. Sci. Technol.* **1979**, *11*, 333.

Chapter 7

Released Oral Malodors Measured by Solid Phase Microextraction–Gas Chromatography Mass Spectrometry

Richard K. Payne, John N. Labows, Jr., and Xiaoyan Liu

Corporate Research and Development, Colgate Palmolive Company,
Piscataway, NJ 08855

Headspace Solid Phase Microextraction (HS-SPME) was used to investigate volatile malodors from saliva and the oral cavity. HS-SPME was found to be an effective pre-concentration technique, extracting a wide range of components in saliva headspace. Direct sampling of the oral air was not effective in extracting volatile malodor compounds.

Solid phase microextraction (SPME) has become a promising alternative to solvent extraction, purge and trap and static headspace methods (1-4). This is particularly true for the analysis of flavors, fragrances, food aromas and biological systems as is evidenced by a litany of recent publications (5-12). The SPME technique is indeed more advantageous because it maintains the benefits of the traditional methods without the inherent disadvantages (solvents, instrument cost, and sample preparation time). SPME techniques are independent of the form of the sample matrix; liquids, solids and gases all can be readily sampled (6). The focus of our study was on the suitability of SPME (static and dynamic headspace) for the analysis of salivary and oral malodors (volatile sulfur compounds -VSC). Two approaches to sampling saliva are possible; direct immersion of the fiber into the sample (13) or static (and dynamic) headspace sampling. The former approach was not appropriate for our study since we were only concerned with the malodor volatile compounds emanating from saliva.

The analysis of VSC in saliva and breath (oral malodors) has been under investigation for nearly sixty years. The study of oral malodors is particularly complicated due to the complex nature of the system (oral cavity), variability in the sample population and problems in sampling techniques. The oral cavity is a highly complex system of microorganisms, exfoliated epithelial cells, blood and proteinaceous (food) particles. Variability in the sample population can be related to the levels of certain bacteria in the oral cavity and to the oral health and extent of conditions such as, caries, gingivitis and periodontitis. Tonzetich and Rosenberg

(14,15) have described in detail the methodologies employed *in vivo* (mouth air) and *in vitro* (putrefied saliva) analyses. *In vivo* sampling is achieved by filling a calibrated loop with mouth air via a syringe coupled to a multiport valve. Carrier gas stream is switched in line with sample loop and the gases are separated (GC) and detected by either flame photometric detection (FPD) or mass spectrometry (MS) (14-16). *In vitro* sampling by headspace analysis of putrefied saliva (via indigenous microorganisms and protein substrates) correlates well with direct sampling of mouth air (17). Ghoos (18) developed an off-line closed-loop trap system coupled with GC-MS for the analysis of volatiles in biological samples. This system was adopted by Claus (19) for the analysis of malodors in saliva and tongue coatings. Kostelc (20) and Preti (21) applied purge and trap in the analysis of salivary headspace. While there are wide ranges of methods to investigate oral malodors, the use of SPME to study saliva and oral VSC has not been reported. SPME analysis of human breath was first reported by Grote (22). Ethanol, acetone and isoprene were of interest in this study of systemic air from diabetics.

Materials and Methods

Saliva Samples.

Whole saliva samples pooled from several subjects with normal oral health were used in all salivary malodor studies. A 10% (w/v) solution of fluid thioglycollate (FTG) medium (DIFCO Labs, Detroit, MI) was prepared using the whole saliva as the diluent. Three milliliters of the solution were placed into a 25 mL scintillation vial and capped with a silicone/PTFE backed septa and polyphenol cap. A stir bar (13 mm x 2 mm) was placed in the vial prior to capping. All saliva samples were incubated overnight (16 h) at 37 °C.

Headspace - Solid Phase Microextraction (HS-SPME).

Salivary and oral odors were sampled using a 75µm Carboxen™/Polydimethylsiloxane (CAR/PDMS) fiber (Supelco, Bellefonte, PA). A narrow bore (0.75mm i.d.) injector insert was used along with a Merlin Microseal septumless injector system (Varian Instruments, Walnut Creek, CA). For the septumless system, fibers with 23 gauge needles were required.

Static Headspace SPME

Incubated saliva samples were allowed to mix at 500 rpm for 15 minutes at room temperature prior to sampling. The needle depth gauge on the manual sampling device was set to 2 on the scale prior to sampling. The headspace was sampled for 15 minutes with constant mixing (500 rpm) before injection.

Determination of Equilibrium Profile

Key volatile components (MM and DMS) were monitored for the optimization of SPME extraction conditions. Several samples were prepared and extracted at room temperature for 5, 10, 15, 20 and 25 minutes using the methodology listed above. The equilibrium profile indicated that a 15 minute extraction time was optimal.

Dynamic Headspace SPME

Oral malodor release studies were conducted using a specially designed sampling tube (Crown Glass Inc., Somerville, NJ) which also acted as a mixing chamber (Figure 1). The device was silanized with a 10% solution of dimethyldichlorosilane (Supelco) in isooctane, to prevent adsorption of volatile compounds. The mouth pipe consisted of a 20 cm piece of Teflon tubing which was inserted into the tapered end of the sampling tube (5 mm i.d.) and fixed in position with tygon tubing and PTFE tape. Attached to the perpendicular glass tube, via tygon tubing, was a programmable environmental pump (Pocket Pump #210-1002, SKC Inc, Eighty Four, PA) which facilitated the removal of air from the oral cavity. The stream of air was passed over the z-axis of the SPME fiber at a constant flow rate of 20 mL/min which is equal to 1.70 cm/sec linear velocity. Before sampling, the SPME needle was inserted into the sampling tube and the needle depth gauge was set to 4 on the sampling device. The fiber was exposed in the sampling tube several seconds before the teflon tube was inserted into the subject's mouth and the sample pump actuated. Sampling time for all studies was 1 minute.

The glass sampling apparatus (Figure 1) was adapted to sample saliva in vials by inserting a 1.5 inch, 18 gauge needle (connected to the mouth pipe) into the vial septa. A second needle, attached to a charcoal filter, was also inserted into the vial septa to provide a vent for airflow. Sampling was then performed as described previously.

Gas Chromatography-Mass Spectrometry (GC-MS).

A Varian Star 3400 GC was interfaced to a Saturn 2000 GC-MS (ion trap detector) and equipped with a fused silica capillary column (Supelco; Supelcowax 10, 30 m x 0.25 mm i.d., 0.25 μ m film thickness). The GC oven was programmed from 50 °C to 200 °C at a rate of 10 °C/min, then held for 5 minutes at 200 °C. Carrier gas (Helium 99.9999%, JWS Gases, So. Plainfield, NJ) flow rate was 30.6 cm/sec at 100 °C which is equivalent to a volumetric flow of 0.9 mL/min. A split ratio of 23:1 was used and the septum purge set to 7 mL/min. The injection port temperature was 250 °C, while the injector was programmed to operate in the split mode initially, then remain splitless for 1 minute before returning to the split mode for the remainder of the analysis. SPME injections were performed manually with a fiber desorption time of 1 minute, while the needle depth gauge was set to 3 on the sampling device. The fiber was left in the injector for 12-15 minutes after the initial desorption. Electron impact mode (EI) mass spectra were obtained at an electron multiplier setting of 1550 V with a scan range of 35-275 m/z and a scan rate of 1 sec/scan. Tentative peak

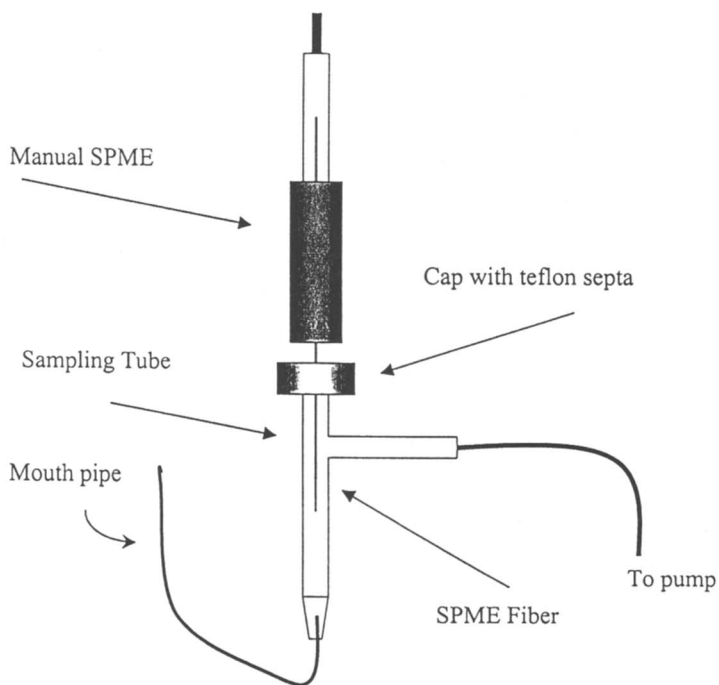


Figure 1. Dynamic Headspace Sampling Tube

identifications were made using a reverse fit algorithm comparing generated spectra with those in the NIST98 MS library (SIS, Inc., Ringoes, NJ).

Results and Discussion.

Salivary Malodors.

Tonzetich (14) established that approximately 90% of the total sulfur content in oral air was mainly hydrogen sulfide (HS), methyl mercaptan (MM) and dimethyl sulfide (DMS) and these compounds emanate an objectionable putrid malodor. It should be noted that these constituents have low odor threshold values ranging from 0.01 μ g/L (MM) to 10 μ g/L (HS) (23) and are therefore considered the most significant odor active compounds in saliva (14). Headspace analysis of saliva putrefied by incubation showed similar levels of VSC observed in oral air. Previous studies conducted by Shirey and Penton (24-26) found that porous materials such as CarboxenTM, a carbonaceous molecular sieve, physically trapped small gaseous molecules by an adsorption process. It was shown (26) that gases, particularly low molecular weight sulfur compounds, could be extracted from the headspace of beer and industrial gas streams (24,25). Based on these studies (24-26), we considered the CarboxenTM/Polydimethylsiloxane (CAR/PDMS) fiber ideally suited for the analysis of VSC present in oral malodor. An oral malodor profile was established from the analysis of incubated whole saliva sampled for five minutes using a 75 μ m CAR/PDMS fiber. Using the malodor profile data (peaks of interest), headspace sampling conditions were optimized by establishing a fiber equilibration time of 15 minutes.

The full-scale chromatographic profile of incubated saliva (Figure 2) revealed a few major peaks. By normalization of each peak to the total peak area, we determined that approximately 90% of the headspace consisted of MM, DMS, dimethyl disulfide (DMDS), dimethyl trisulfide (DMTS), phenol (PH) and indole (IN). Increasing the peak intensity scale of the chromatogram (Figure 3) revealed a large number of additional components. It should be noted that these components constitute only a fraction of the total headspace profile (approximately 10%). A list of all labeled peaks is found in Table I. The peaks labeled "F", in Figures 1 and 2, have retention times consistent with those observed when a SPME fiber background is taken (blank injection) and are from the SPME fiber coating.

Hydrogen sulfide is a key oral malodorant, however it was not observed in our chromatographic profiles using porous CarboxenTM as the adsorbent (fiber coating). In studies by Kostlec (12) and Claus (14), HS was also not detected in the headspace of saliva or tongue coatings when VSC were sampled using Tenax polymer. The responses of HS and MM in the ion trap detector was first tested by direct headspace sampling of fresh saliva samples using a gas tight syringe. The two compounds gave nearly identical responses, although the peak intensities were quite low. Since MM

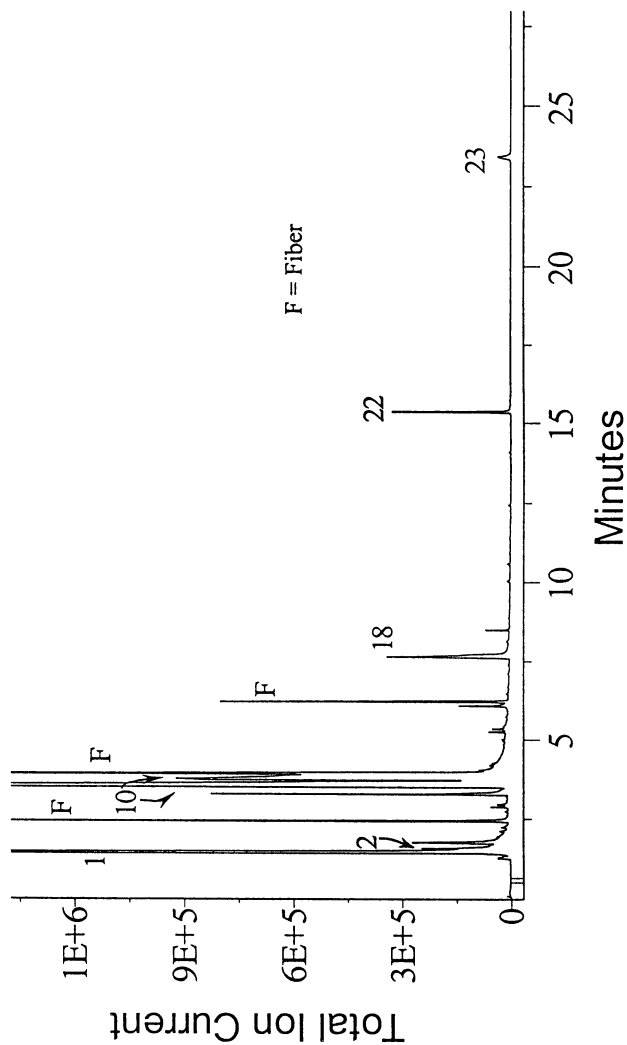


Figure 2. Static-SPME GC-MS Profile of Saliva (15 minute extraction)

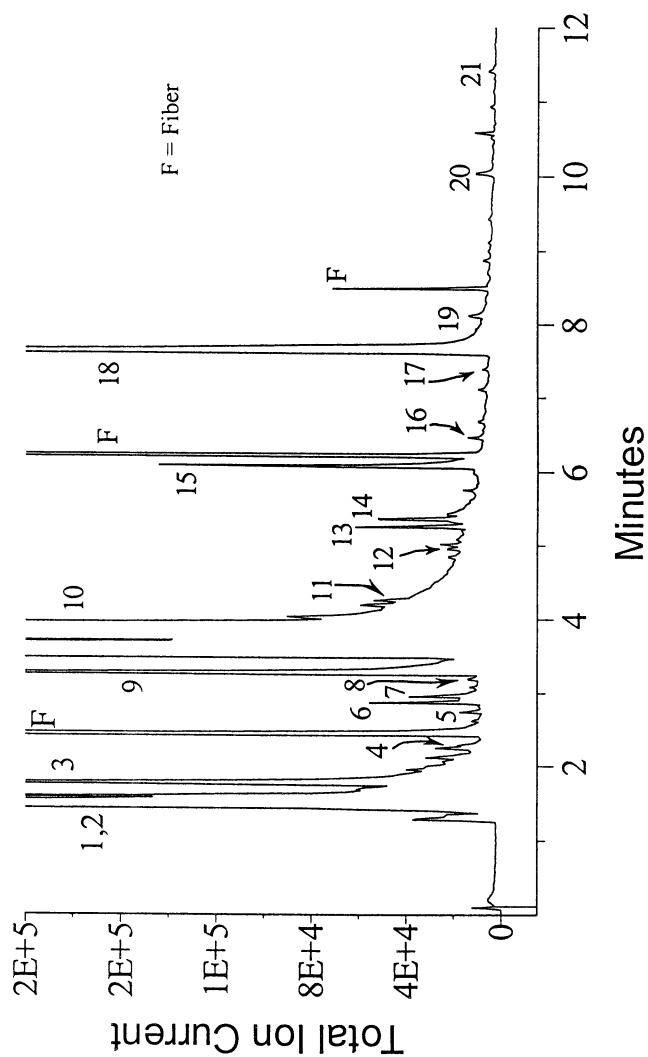


Figure 3. Static-SPME GC-MS Profile of Saliva (15 minute extraction)

was observed by SPME, adsorption of HS onto Carboxen™ fiber must be considered an issue.

Initially it was believed that HS was not adsorbed due to its small size relative to the other analytes. Modeling experiments determined that HS has a maximum length of 4.35 Å while MM and DMS were calculated to have maximum lengths of 5.25 and 6.96 Å respectively. Carboxen™ contains pores with diameters ranging from 500 to 2 Å suggesting that based on molecular size, all three molecules should be effectively trapped. Using Drieding molecular mechanics forcefield with charges from MOPAC (semi-empirical quantum mechanics), energies of adsorption were calculated by simulating adsorption onto a surface similar to Carboxen™ (an infinite graphite surface). Energies for each molecule were calculated before $E_{(\text{separate})}$ and after $E_{(\text{adsorbed})}$ adsorption; the difference is $\Delta E_{(\text{adsorption})}$ (Table II). Significant differences in $\Delta E_{(\text{adsorption})}$ were observed between HS and MM and DMS. These results suggest that adsorption properties, not size exclusion, are the driving force and as a result hydrogen sulfide cannot be effectively trapped.

Kostelc (17) and Claus (19) have established the presence of phenol and indole in the headspace of saliva. Indole is a typical bacterial fermentation compound of tryptophan, while phenol has been identified as a bacterial breakdown product of phenolic amino acids (19,27). The presence of S-methyl ethanethioate in saliva and tongue scrapings has been reported (19). In this study we have tentatively identified three S-methyl thioesters, two of which have not been reported (S-methyl 3-butanethioate and S-methyl pentanethioate). Preliminary identification was based on comparison with library spectra and through careful interpretation of the collected mass spectra.

This class of compounds has been identified in a number of materials, including numerous cheeses (e.g., Limburger (28), Saint-Nectaire (29) and Langres (30)). They have also been identified as the odor-causing compounds in urine of humans after eating asparagus (31). Recent work (32,33) describes the synthesis of a homologous series of S-methyl thioesters as well as the sensory properties of the short chain esters. Odor descriptors for the C₂ and C₅ carbon chain lengths have been described as “cabbage, rancid and cheesy”. It has been reported (34) that S-methyl thioesters have exceptionally low odor thresholds. The study by Berger (33) shows that the S-methyl ethanethioate and propanethioate are present at extremely low levels (32 and 123 µg/L) in cheese. These findings suggest that this class of compounds have significant contribution to the aroma of cheese as a result of their low odor thresholds, 5 and 100 µg/L respectively (33). Unfortunately, threshold data for S-methyl pentanethioate and S-methyl 3-methyl butanethioate have not been determined. Although it has been established that HS, MM and DMS are the major constituents of oral malodor, other minor components (S-methyl thioesters) present in saliva and oral air may contribute to the true “bouquet” of oral odor. However, before any conclusions are made regarding the odor composition of oral and salivary malodor, additional data on the olfactory contribution of individual malodor components is necessary.

Interestingly, methyl(methylthio)methyl disulfide (peak 19) was identified in saliva, whereas it had only been observed previously (19) in tongue scrapings after incubation in casein suggesting incubation media plays a role in the formation of VSC. Peaks labeled with an asterisk in Table I are of particular interest because they have not been previously reported in saliva headspace.

Table I. Compounds found in salivary headspace by static HS-SPME^a

<i>Peak No.</i>	<i>Compounds</i>	<i>Ret. Time (min)</i>	<i>ID^b</i>
1	Methyl Mercaptan	1.55	rt, ms
2	Dimethyl sulfide	1.60	rt, ms
3	Acetone	1.80	rt, ms
4	1-(methylthio)-propane	2.25	T, ms
5	Z-1-(methylthio)-1-propene*	2.77	T, ms
6	2-Methyl butanoic acid methyl ester*	2.88	T, ms
7	E-1-(methylthio)-1-propene*	2.97	T, ms
8	Toluene ^c	3.20	rt, ms
9	S-Methyl ethanethioate	3.27	T, ms
10	Dimethyl disulfide	3.62	rt, ms
11	4-Methyl pentanoic acid methyl ester*	4.27	T, ms
12	Limonene ^c	4.98	rt, ms
13	S-Methyl 3-methylbutanethioate*	5.27	T, ms
14	S-Methyl pentanethioate*	5.38	T, ms
15	Thiocyanic acid methyl ester*	6.08	T, ms
16	2,5-dimethyl pyrazine ^c	8.37	rt, ms
17	2,2-bis(methylthio)propane*	7.40	T, ms
18	Dimethyl trisulfide	7.67	rt, ms
19	Alkyl benzene ^c	8.13	T, ms
20	Dimethyl sulfoxide*	10.05	rt, ms
21	Methyl(methylthio)methyl disulfide	11.42	T, ms
22	Phenol	15.37	rt, ms
23	Indole	23.43	rt, ms

^aSamples extracted for 15 minutes.

^bIdentification was by GC retention times (rt) and mass spectrometry (ms) of authentic compounds. Tentative (T) identification by mass spectrometry only when authentic compound was not available.

^cProbable exogenous sources.

* Not previously identified in saliva

Table II. Calculated Energies of Adsorption†

<i>Molecule</i>	<i>E(separate)</i>	<i>E(adsorbed)</i>	<i>ΔE adsorption</i>
H ₂ S	0.1190	-3.3827 ± 0.0005	-3.3046
CH ₃ SH	0.3096	-5.7606 ± 0.1854	-6.1569
CH ₃ SCH ₃	-3.5993	-11.8611 ± 0.2366	-8.2627

† Calculated using a molecular dynamics simulation, averaging 20 energy minimized structures.

Oral Malodors.

To capture oral malodors, insertion of a SPME fiber directly into the mouth was first considered. However this was not feasible due to the length of time required for sampling in a static system and the potential of damaging the fiber. An indirect approach was investigated, applying dynamic HS-SPME first to incubated saliva samples to test the feasibility of the technique. Figure 4 shows the chromatogram obtained by dynamic HS-SPME and Table III lists the labeled peaks.

The objective of these experiments was to determine the capability of dynamic HS-SPME for direct measurement of oral malodors. Dynamic sampling of saliva resulted in acceptable peak intensity and a chromatographic profile similar to that obtained by static sampling, although the ratio of components extracted was quite different. This may be due to non-equilibrium conditions applied in dynamic sampling and the shorter extraction time. Qualitatively, there were a series of non-sulfur containing compounds (peaks 5, 11, 16, 17 and 23) which we consider to be exogenous, arising from food sources. Studies by Kostelc (20) also show that these constituents arise from atmospheric and water pollutants, and cosmetics.

Three subjects were evaluated for oral malodor and all were considered to be "malodor formers". Dynamic HS-SPME of the subject's oral air did not produce peaks in the chromatogram. Neither VSC nor non-sulfur containing compounds were observed. There are several possible causes for this. First, the concentration of VSC in oral air is far lower than saliva and as a result it is below the concentration necessary for dynamic sampling. Second, as analytes adsorb onto the fiber coating, they are quickly swept away, effectively reducing the partition coefficient to zero. Lastly, it is possible that air flowing past the fiber created a large boundary layer, thus preventing adsorption onto the coating surface. The boundary layer can significantly retard movement of analyte from the bulk phase into the fiber, and the degree of retardation depends strongly on the thickness of the layer (35).

To improve the efficiency of dynamic HS-SPME, the use of different fiber coatings, such as polyacrylate, PDMS and carbowax/divinylbenzene, will be investigated as an alternative to porous carbon. Conversely, a different approach to sampling oral air, for example, vacuum trapping combined with static HS-SPME, may provide a more effective sampling method.

Conclusions

The use of SPME for the evaluation of salivary malodors is extremely promising. Carboxen/PDMS fiber provides a wide range of selectivity for analytes present in saliva headspace. Based on molecular modeling experiments, hydrogen sulfide was not extracted (by Carboxen™/PDMS) due to adsorption properties. Several compounds not previously reported in saliva have been tentatively identified. To our knowledge, this is the first published application of SPME for the analysis of salivary malodors. Direct analysis of oral malodors by dynamic HS-SPME was not successful. This approach was not effective in concentrating the low level of volatiles present in the oral cavity. The evaluation of different methods to trap the oral air will

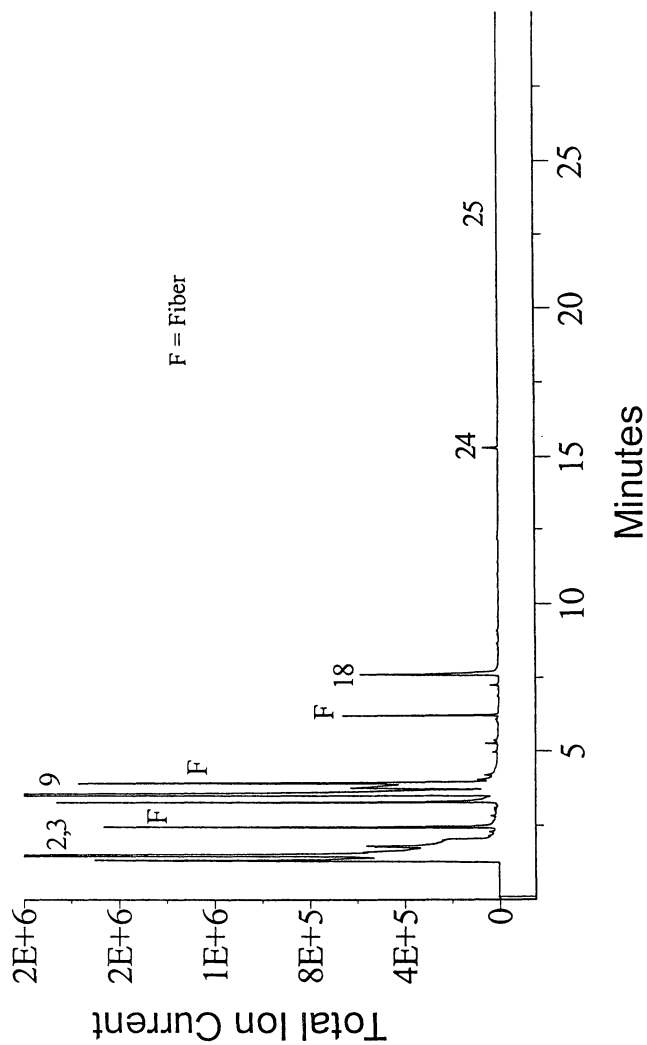


Figure 4. Dynamic -SPME GC-MS Profile of Saliva (1 minute sampling)

Table III. Compounds found in salivary headspace by dynamic HS-SPME

<i>Peak No.</i>	<i>Compounds</i>	<i>Ret. Time (min)</i>	<i>ID^a</i>
2	Methyl Mercaptan	1.55	rt,ms
3	Dimethyl Sulfide	1.63	rt,ms
4	Acetone	1.82	rt,ms
5	Butanone ^b	2.15	rt,ms
6	Z-1-(methylthio)-1-propene*	2.77	T,ms
7	E-1-(methylthio)-1-propene*	2.97	T,ms
8	S-Methyl ethanethioate	3.28	T,ms
9	Dimethyl disulfide	3.55	rt,ms
10	Limonene ^b	4.97	rt,ms
11	Amyl alcohol ^b	5.02	rt,ms
12	S-Methyl pentanethioate*	5.25	T,ms
13	S-Methyl 3-methyl butanethioate*	5.35	T,ms
14	Thiocyanic acid methyl ester*	6.08	T,ms
15	2,5-dimethyl pyrazine ^b	6.68	rt,ms
16	5-methyl-6-hepten-2-one ^b	6.88	T,ms
17	4-hydroxy-4-methyl-2-pentanone ^b	7.25	T,ms
18	Dimethyl trisulfide	7.65	rt,ms
19	Alkyl Benzene ^b	8.12	T,ms
20	Acetic acid	8.58	rt,ms
21	Dimethyl sulfoxide*	10.02	rt,ms
22	Methyl(methylthio)methyl disulfide	11.14	T,ms
23	Benzyl alcohol ^b	13.85	rt,ms
24	Phenol	15.32	rt,ms
25	Indole	23.32	rt,ms

^aIdentification was by GC retention times (rt) and mass spectrometry (ms) of authentic compounds. Tentative (T) identification by mass spectrometry only when authentic compound was not available.

^bProbable exogenous sources.

* Not previously identified in saliva

be part of future studies. In addition, olfactory analyses of oral and salivary malodors will also be included in these studies.

Acknowledgments

The authors wish to acknowledge Dr. Fiona Case for performing the molecular modeling experiments and for her insightful data analysis. Thanks also to Dr. Winston Uchiyama for his support for this research project.

References

1. Marsili, R. T.; *J. Agric. Food Chem.* **1999**, *47*, 648-654.
2. Marsili, R. T. *J. Chrom. Sci.* **1999**, *37*, 17-23.
3. Scypinski, S.; Smith, A. In *Solid Phase Microextraction: A Practical Guide*; Scheppers-Wercinski, S., Ed; Marcel Dekker: New York, 1999, pp. 111-129.
4. Almirall, J. R.; Furton, K. G. In *Solid Phase Microextraction: A Practical Guide*; Scheppers-Wercinski, S., Ed; Marcel Dekker: New York, 1999, pp. 203-216.
5. Song, J.; Fan, L.; Beaudry, R. *J. Agric. Food Chem.* **1998**, *46*, 3721-3716.
6. Harmon, A. D. In *Techniques For Analyzing Food Aroma*; Marsili, R., Ed.; Marcel Dekker: New York, 1997, pp. 81-112.
7. Krumbein, K.; Ulrich, D. In *Flavor Science: Recent Developments*; Taylor, A. J.; Mottram, D. S., Eds.; The Royal Society of Chemistry: Cambridge, UK, 1996, pp. 289-292.
8. Mookerjee, B.D.; Patel, S. M.; Trenkle, R. W.; Wilson, R. A. *Perfumer & Flavorist.* **1998**, *23*, 1-11.
9. Galipo, R.; Canhoto, A.; Walla, M.; Morgan, S. *J. Chem. Educ.* **1999**, *76*, 245-248.
10. Roberts, D.; Pollien, R. *J. Agric. Food Chem.* **1997**, *45*, 4388-4392.
11. Braggins, T. J.; Grimm, C. C.; Visser, F. R. In *Applications of Solid Phase Microextraction*; Pawliszyn, J. Ed.; The Royal Society of Chemistry: Cambridge, UK, 1999, pp. 407-422.
12. Moneti, G.; Pieraccini, G.; Sledge, M.; Turillazzi, S. In *Applications of Solid Phase Microextraction*; Pawliszyn, J. Ed.; The Royal Society of Chemistry: Cambridge, UK, 1999, pp. 448-457.
13. Hall, B. J.; Satterfield-Doerr, M.; Parikh, A. R.; Broadbelt, J. S. *Anal. Chem.* **1998**, *70*, 1788-1796.
14. Tonzetich, J. *J. Periodontol.* **1977**, *January*, 13-20.
15. Rosenberg, M.; McCulloch, C. A. G. *J. Periodontol.* **1992**, *63*, 776-782.
16. Tonzetich, J. *J. Clin Dent.* **1991**, *2*, 79-82.
17. Kostelc, J. G.; Preti, G.; Zelson, P.; Stoller, N. H.; Tonzetich, J. *J Periodontal Res.* **1980**, *15*, 185-192.
18. Ghoos, Y.; Claus, D.; Geypens, B.; Hiele, M.; Maes, B.; Rutgeerts, P. *J Chromatogr. A* **1994**, *665*, 333-345.

19. Claus, D.; Geypens, B.; Ghoos, Y.; Rutgeerts, P. *J. High Resol. Chromatogr.* **1997**, *20*, 94-98.
20. Kostlec, J. G.; Preti, G.; Zelson, P.R.; Tonzetich, J.; Huggins, G.R. *J Chromatogr.* **1981**, *226*, 315-323.
21. Preti, G.; Clark, L.; Cowart, B. J.; Feldman, R.S.; Lowry, L.D.; Weber, E.; Young, I. M. *J Periodontol* **1992**, *63*, 790-796.
22. Grote, C.; Pawliszyn, J. *Anal. Chem.* **1997**, *69*, 587-596.
23. Belitz, H. -D.; Grosch, W. *Food Chemistry*; 2nd Edition; Springer-Verlag: Berlin, 1999, pp. 337.
24. Shirey, R. E.; Mani, V. "New Trends and Applications Using Solid Phase Microextraction" Technical Report **1997**; Supelco, Bellefonte, PA.
25. Shirey, R. E.; Mani, V.; Betz, W. R. Presented at the Canadian Chemical Society Meeting, June 4, **1997**.
26. Penton, Z. Application Note No. 16, **1997**; Varian Instruments, Walnut Creek, CA.
27. Barker, H. *Ann. Rev. Biochem.* **1981**, *50*, 23.
28. Parliment, T. H.; Kolor, M. G; Rizzo, D. J. *J. Agric. Food Chem.* **1982**, *30*, 1006-1008.
29. Verdier, I.; Coulon, J. B.; Pradel, P.; Bredagué, J. L. *Lait.* **1995**, *75*, 523-533.
30. Dumont, J. P.; Roger, S.; Cerf, P.; Adda, J. *Lait.* **1974**, *54*, 31-43.
31. White, R. H. *Science.* **1975**, *189*, 810-811.
32. Khan, J. A.; Gijs, L.; Berger, C.; Martin, N.; Piraprez, G; Spinnler, H. E.; Vulfson, E. N.; Collin, S. *J. Agric. Food. Chem.* **1999**, *47*, 3269-3273.
33. Berger, C.; Martin, N.; Collin, S; Gijs, L.; Khan, J. A.; Piraprez, G.; Spinnler, H. E.; Vulfson, E. N. *J. Agric. Food. Chem.* **1999**, *47*, 3274-3279.
34. Cuer, A.; Dauphin, G.; Kergomard, A.; Roger, S.; Dumont, J. P.; Adda, J. *Lebensm.-Wiss. Technol.* **1979**, *12*, 258-261.
35. Bartelt, R. J.; Zilkowski, B. W. *Anal. Chem.* **1999**, *71*, 92-101.

Chapter 8

Changes in the Concentrations of Key Fruit Odorants Induced by Mastication

A. Buettner and P. Schieberle

Deutsche Forschungsanstalt fuer Lebensmittelchemie, Garching, Germany

Recently, the potent odorants of fresh, hand-squeezed orange juices were characterized by aroma dilution techniques. Quantification using stable isotope dilution assays (SIDA) and calculation of the odor activity values revealed ethyl butanoate, (*R*)-limonene and (*Z*)-hex-3-enal among the most potent odorants of the fresh juices. Based on these results a novel approach is proposed to observe the concentration changes of single key odorants occurring during mastication of orange juice. Changes in the concentrations of key odorants were measured by comparing their amounts before and after in-mouth "reactions". This method, designated as SOOM-concept (spit-off odorant measurement) determines the amounts of single odorants lost by certain in-mouth events such as release, adsorption, or chemical modification. Results obtained for orange juice and also model solutions indicated a strong influence of the chemical structure on substance-specific losses.

Up to now, different approaches have been applied to study the processes occurring when foods are eaten. For example, headspace techniques involving Tenax-trapping or direct MS-analysis have been used to determine the odorants being exhaled through the nose or the mouth breath-by-breath, supplying data on the degree of flavor release during consumption of food (1,2,3). Recently, the APCI-MS technique was also applied for the investigation of odorants released during consumption of orange juice and orange slices (4).

However, very little is known about certain processes in the mouth, such as the decrease of odorants in food during mastication or the amounts of odorants remaining in the mouth itself due to effects like adsorption to the mucous membrane. When considering such factors, the following physiological conditions in humans have to be regarded:

Before swallowing, the base of the tongue is in contact with the soft palate above

the tongue (5). During the mastication of food, normal respiration continues thus showing that the oral cavity is mainly closed off from the trachea by the soft palate. This prevents ingress of food material into the trachea. Up to now, the question could not be sufficiently answered to what extent odorants are transferred to the olfactory epithelium before swallowing of the food material, even before just swallowing saliva. However, it has been proposed that the main amount of odorants released during eating are transferred retronasally when the food material is swallowed. Land (1994) showed that the act of swallowing is always immediately followed by the expiration of a 5 to 15 mL volume of air mainly consisting of the gas phase above the food material in the oral cavity (6). When the tongue presses the masticated food against the soft palate above the tongue and, thereby, pushes it forward into the throat this pulse of air, enriched with odorants, is transferred to the olfactory epithelium and then perceived retronasally.

Based on these physiological prerequisites, the aim of our study was to determine the decrease of important orange odorants occurring during mastication in-mouth without swallowing. Care was also taken not to swallow saliva. Therefore, the "SOOM-concept" (spit-off odorant measurement) was developed, involving the quantification of the odorants remaining in the food material after mastication by stable isotope dilution analysis. This methodology was previously applied by Hofmann and Schieberle for the determination of concentration changes of odorants occurring during the mastication of strawberries (7). They observed significant differences in the decrease of several odorants during mastication taking into account possible enzymic degradation of the odorants investigated.

Our studies were focused on several key orange aroma compounds (8,9). The odorants and their FD factors obtained previously by AEDA are given in Table I.

Table I. FD factors of important odorants of fresh, hand-squeezed juice of Valencia late-orange (modified data from [9]).

<i>Odorant</i>	<i>FD factor ^{a)}</i>
ethyl butanoate	1024
ethyl hexanoate	32
ethyl 3-hydroxyhexanoate	64
(<i>R</i>)-limonene	64
acetaldehyde	16 ^{b)}
hexanal	32
octanal	64
decanal	16
(<i>Z</i>)-hex-3-enal	512

a) The Flavour dilution (FD) factor was determined in ethereal extracts containing the juice volatiles. Analyses were performed by two assessors in duplicates.

b) The Flavour dilution (FD) factor was determined by static headspace-olfactometry of fresh, hand-squeezed orange juice.

Experimental Procedures

Materials

Fresh oranges (*Citrus sinensis* (L.) Osbeck; cultivar Valencia late, grown in Argentina) were purchased from a local market and were used within two days. Fresh orange juice was obtained by hand-squeezing of the fruits in a kitchen juicer immediately before use for the mastication experiments.

Ethyl butanoate 99 %, ethyl hexanoate 99+ %, ethyl octanoate 99+ %, ethyl 3-hydroxyhexanoate 98+ %, acetaldehyde 99 %, hexanal 98 %, octanal 99 %, decanal 95 %, (*R*)-limonene 97 % and myrcene >90 % were obtained from Aldrich (Steinheim, Germany) and were purified prior to analysis by distillation.

Aqueous solutions of single reference aroma compounds at four different concentration levels were prepared in water. In-mouth experiments are restricted by the small amount of food that can be masticated. In these studies 25 mL of orange juice or model solution were rinsed in the mouth so the actual amount of odorants in the mouth was only 2.5 μg of odorant for the lowest concentrated model solution applied. Therefore, concentrations had to be determined by stable isotope dilution assays (10).

Quantification of Flavour Compounds

Determination of odorants in solvent extracts

Juice was masticated for a certain period of time in the mouth, then expectorated into saturated CaCl_2 solution in order to inhibit enzymic reactions, spiked with stable isotope labeled standards and stirred for equilibration. The solution was extracted with diethylether (30 mL, five times, total volume 150 mL) and the combined organic phases were dried over anhydrous Na_2SO_4 . The volatile fraction was subsequently isolated by high vacuum transfer and the obtained aroma extract concentrated by careful distillation (9). At least four replicates were performed. Quantification of the volatiles was performed by multidimensional gas chromatography (MD-HRGC) with the MS-system ITD-800 running in the CI-mode with methanol as the reagent gas as described previously (11). Myrcene was used as internal standard for the quantification of limonene (9).

Determination of odorants by static headspace analysis

For the determination of acetaldehyde, the masticated material was expectorated into saturated CaCl_2 solution, the vessel sealed immediately with a septum and spiked with known amounts of $[1,2-^{13}\text{C}_2]$ -acetaldehyde. After stirring for 30 min to reach equilibration, aliquots of the headspace were withdrawn with a gastight syringe and injected for MS-analysis using the system described previously (12). At least four replicates were performed.

Results and Discussion

Orange juice

In a first series of experiments, the SOOM-concept was applied to observe the concentration changes of seven orange odorants during mastication for 1 min of fresh, hand-squeezed orange juice in comparison to fresh juice. The results given in Figure 1 indicated that the amounts of odorants remaining in the mouth differed significantly depending on the structure of the odorant. For example, on average about 30 % more of the initial amount of ethyl hexanoate was retained in the mouth compared to ethyl butanoate. The recovery of structurally related odorants like the two aldehydes (*Z*)-hex-3-enal and hexanal differed by about 10 % after mastication. Furthermore, the recovery of the odorants varied significantly for some compounds e.g. ethyl hexanoate and hexanal, while others such as ethyl 3-hydroxyhexanoate and (*Z*)-hex-3-enal were much more consistent.

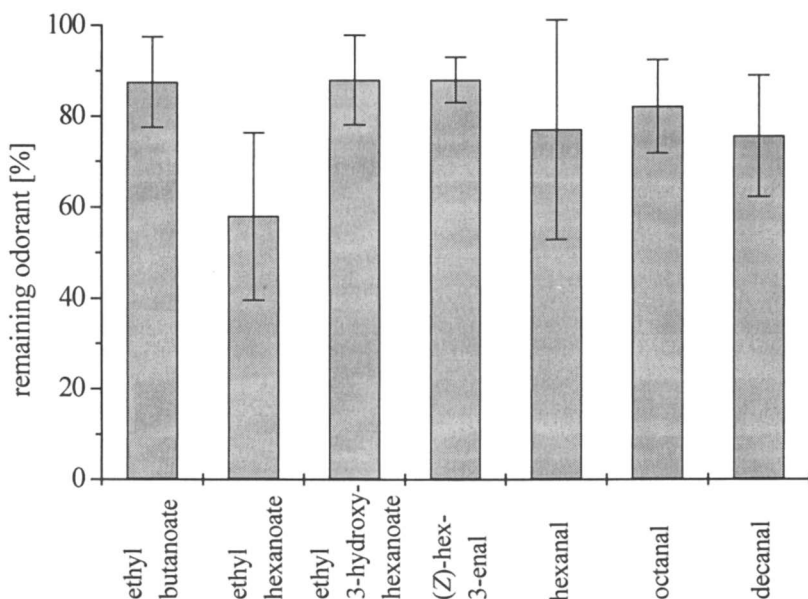


Figure 1. Remaining quantity of selected odorants (values are the means of four replicates; the error bars show the standard deviations) in spitted off orange juice after mastication for 1 min in the mouth.

Model experiments

To gain more systematic insights into the processes in mouth, the influence of the chemical structure of the odorants on their release in mouth was investigated using appropriate aqueous model solutions of reference odorants. First, the decrease of the aldehydes hexanal, octanal and decanal, during 1 min of mastication in the mouth was determined using different concentrations (100 μg , 1 mg, 10 mg to 100 mg of aldehyde per liter water). The amounts of aldehydes remaining in the solution after mastication in the mouth are displayed in Figure 2.

In all concentrations, the three aldehydes were discriminated according to their chain length, that means according to their polarity. The most polar of the three aldehydes (hexanal) was the least reduced after mastication with nearly 100 % recovery for the highest concentration. In contrast to this, for octanal a decrease of 14 % was determined in the highest concentration while the amount of decanal was even lower (29 % less than the initial concentration). Comparing the highest and the lowest concentrations for each of the aldehydes the difference in the decrease in mouth is obvious. For example, in contrast to the 100 % recovery of hexanal in the highest concentration, only 66 % of hexanal were recovered after mastication when the lowest concentration was applied. Similar results were obtained for octanal and decanal showing a decrease of 14 % and 29 %, respectively, for the highest concentration while in the lowest concentration the aldehydes were reduced to about 50 %. It is interesting to note that the difference for octanal and decanal leveled out in the lower concentration ranges.

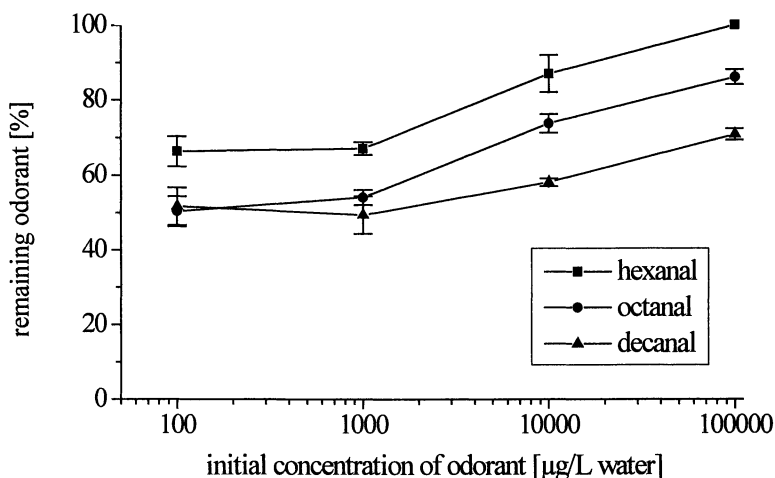


Figure 2. Remaining quantity of aldehydes (values are the means of four replicates; the error bars show the standard deviations) in spitted off aqueous solutions after mastication for 1 min in the mouth.

Similar experiments were performed using reference esters that are important in orange juice aroma. To gain additional data on the influence of the chain length, ethyl octanoate was studied as a further odorant. The data obtained for ethyl butanoate, ethyl hexanoate, ethyl octanoate and ethyl 3-hydroxyhexanoate are displayed in Figure 3. The results were very similar to the findings obtained for the aldehyde solutions. Again a discrimination for esters of different chain length was observed with the highest reduction for the least polar compound ethyl octanoate. The fact that the decrease of an odorant in mouth is directly related to its polarity is also demonstrated by comparison of the curves of ethyl 3-hydroxyhexanoate and ethyl hexanoate (top and third curve down in the diagram). The hydroxyester was significantly retained in the aqueous phase obviously due to the hydroxygroup. So, an increase in the polarity of an odorant results in a lower retardation in the mouth.

In accordance with the findings of the aldehyde experiments the reduction of all esters investigated after mastication was significantly higher when solutions containing lower concentrations were applied. So, in comparison to the highest concentrations about 10 to 20 % less of the initial concentrations of all esters were present in the lowest concentrated solutions after mastication.

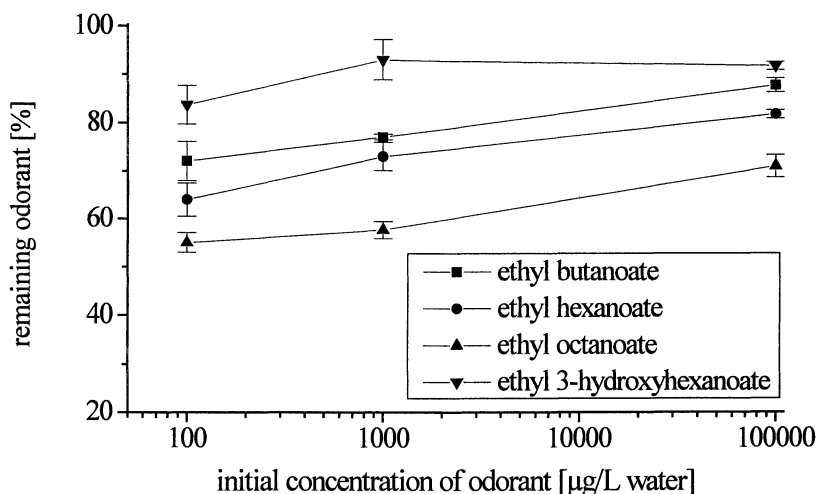


Figure 3. Remaining quantity of esters (values are the means of four replicates; the error bars show the standard deviations) in spitted off aqueous solutions after mastication for 1 min in the mouth.

Two important odorants showing very high concentrations in fresh orange juice are limonene (50 to 100 mg/kg) and acetaldehyde (5 to 10 mg/kg). The decrease of both odorants in model solutions during mastication in mouth was investigated in the concentrations naturally found in orange juice (see Figure 4). For limonene, at the higher concentration of 100 mg/L only 20 % remained in the mouth, while in the lower concentration (10 mg/L) 45 % of the odorant was retained. The difference observed for acetaldehyde was not as drastic between the highest and the lowest concentration applied. A decrease of 25 % was found for the lowest concentration and 15 % for the highest concentration after mastication. Again a difference between the more polar acetaldehyde and the less polar limonene is observed, corroborating the assumption that polar groups present in odorants lead to less significant losses during mastication compared to non-polar odorants.

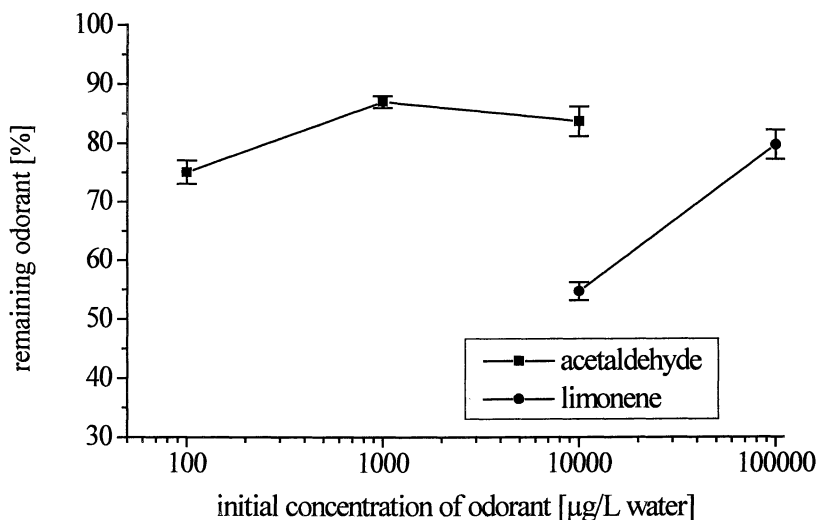


Figure 4. Remaining quantity of acetaldehyde and limonene (values are the means of four replicates; the error bars show the standard deviations) in spitted off aqueous solutions after mastication for 1 min in the mouth.

In Figure 5 the data for all esters and aldehydes in the masticated model solutions of the lowest concentration (100 $\mu\text{g/L}$ water) are compared. The discrimination according to the polarity is obvious. The increasing retardation in mouth can be clearly related to the increasing chain length in both groups of compounds.

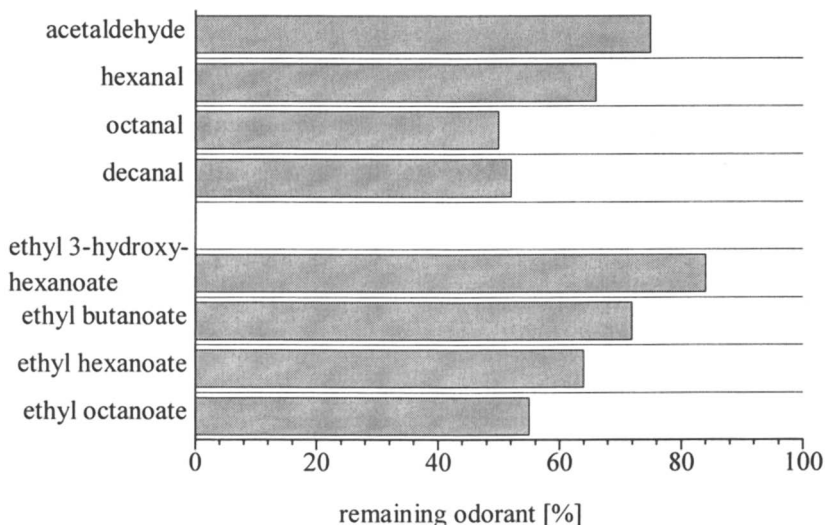


Figure 5. Remaining quantity of odorants (initial concentration 100 $\mu\text{g/L}$ water; values are the means of three replicates) in spitted off aqueous solutions after mastication for 1 min in the mouth.

Now the question arises whether the time of mastication influences the retardation of odorants in mouth. When we eat orange slices they usually remain for a while in the mouth till the fruit pieces are small enough for swallowing. However, orange juice is normally in contact with the mouth just for a few seconds prior to swallowing. So, the same experiments were performed using the model solutions but, this time, the duration of mastication was only 5 s.

The results obtained for the long-time and the short-time mastication of the aldehydes are shown in Figure 6. The mastication experiment of 5 s revealed a significantly lower decrease of the three odorants with a recovery of about 90 % of the initial concentration. Furthermore the discrimination of the aldehydes according to their chain length leveled out in comparison to the long-time mastication data, only the amount of decanal was slightly reduced.

Similar results were obtained for the short-time mastication of the esters (see Figure 7), with a significantly higher recovery for all esters of about 90 % in comparison to the long-time mastication and also no distinct discrimination between the odorants. These data indicate that the amount of odorants remaining in the mouth is significantly influenced by the duration of mastication.

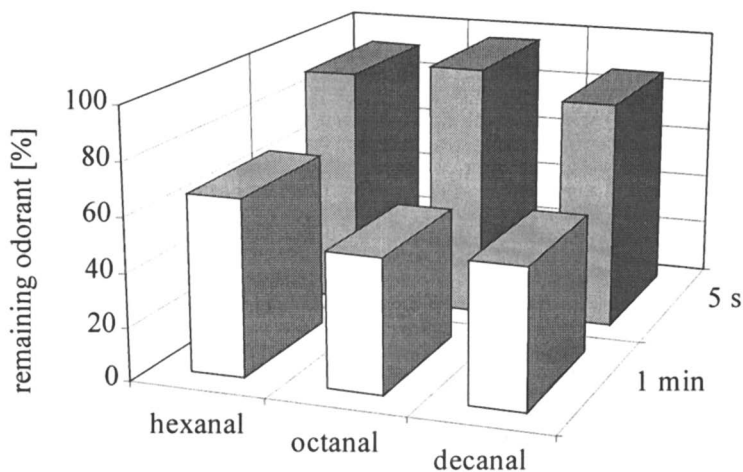


Figure 6. Influence of the duration of mastication (1 min or 5 s) on the remaining quantity of aldehydes (initial concentration 100 $\mu\text{g/L}$ water; values are the means of four replicates) in spitted off aqueous solutions.

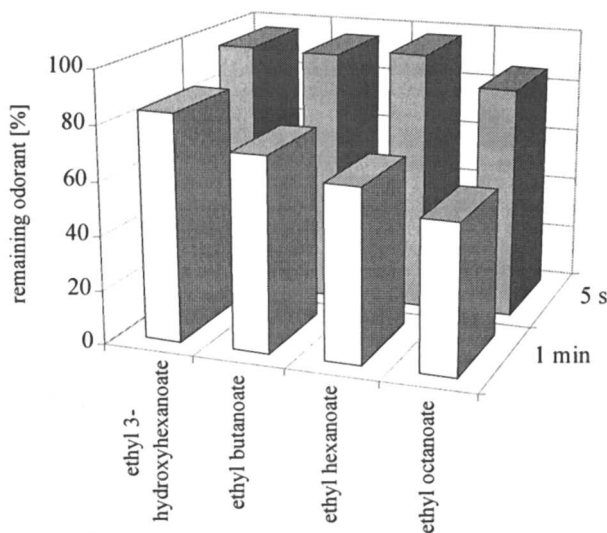


Figure 7. Influence of the duration of mastication (1 min or 5 s) on the remaining quantity of esters (initial concentration 100 $\mu\text{g/L}$ water; values are the means of four replicates) in spitted off aqueous solutions.

Application of model solutions is a first approach to study the interactions occurring between odorants and the real mouth system when no other compounds (except water) are present. However, real food systems are much more complex, containing different matrix compounds which could influence these interactions of odorants and mouth to a major extent.

A comparison of the recovery of the esters after mastication of fresh orange juice and model solutions, respectively, is given in Figure 8a. Displayed are the data of the model solutions for similar concentrations as they were determined in the fresh juice. Additionally the variance of the quantitative data is given with error bars.

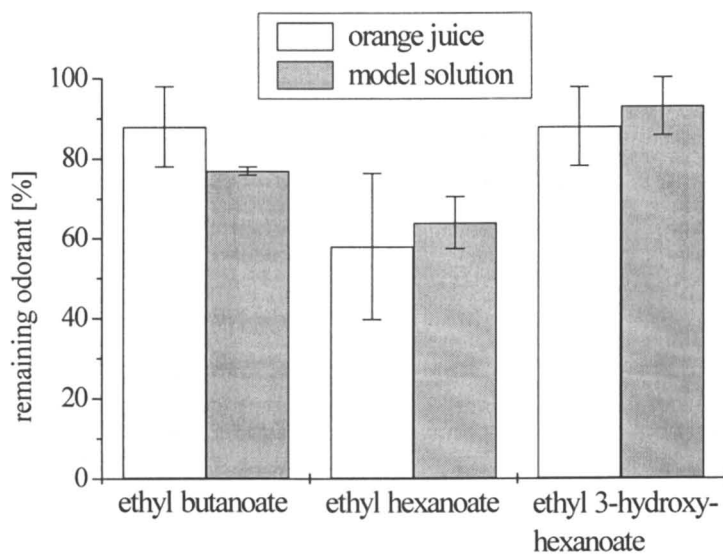
Between both systems, the fresh juice and the model solutions, the decrease of the esters did not differ to a major extent after 1 min of mastication. However, the variance between the samples of the fresh juices was a little bit higher than in the model solutions. Regarding the aldehydes (see Figure 8b) the differences between orange juice and model solution were higher, with a significantly lower decrease especially of octanal and decanal after mastication of the fresh juice. In this case interactions of the aldehydes with matrix compounds of the juice seem to take place thereby reducing the extent of flavour release in mouth in comparison to the release determined for the model solutions in water. Again a slightly higher variance in the samples of the juices were observed, especially for hexanal.

When studying real food systems one always has to keep in mind interactions occurring with matrix compounds. Furthermore the possibility of enzymic reactions has to be considered. When fruit cells are crushed, odorants can be produced or destroyed by enzymic activity. Recently we showed (in cooperation with the group of Andy Taylor in Nottingham) that the concentrations of some of the investigated odorants, e.g. hexanal and (*Z*)-3-hexenal increase two- or three-times their initial amounts due to enzymic activity one hour after the preparation of the juice (unpublished data). In contrast to this, the concentrations of ethyl butanoate and acetaldehyde did not change significantly (4).

Conclusions

The SOOM-concept is a novel approach for the exact quantification of flavour changes occurring during mastication even in relatively low concentration ranges. Our investigations showed that the structure of an odorant influences significantly its retardation in mouth being directly related to the polarity of the odorant. Furthermore it was found that the proportion of retardation in mouth increases when lowering the concentration of an odorant. This effect was observed for the first time and is especially interesting for extremely odor-active volatiles which are present in very low concentrations in food. The results indicate that the SOOM-concept can also be a useful tool for studying interactions of odorants with matrix compounds under real-mouth conditions. Combination of this methodology with other techniques like nosespace-analyses offers the possibility to balance the amounts of odorants being effective in flavour perception.

a)



b)

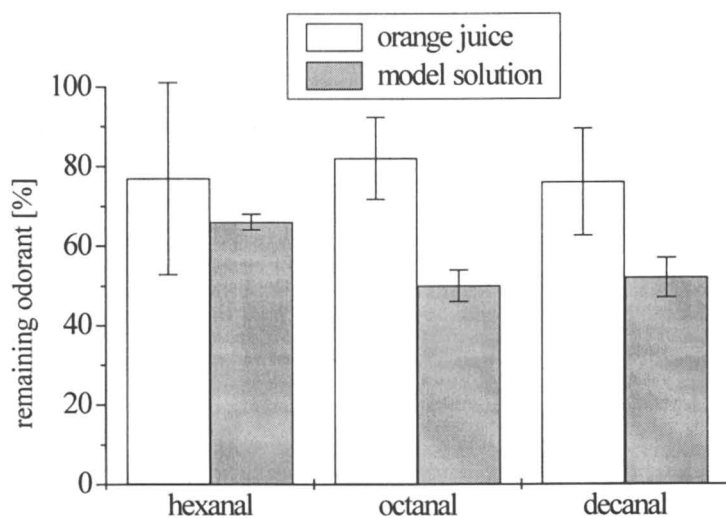


Figure 8. Remaining quantity of a) esters and b) aldehydes (values are the means of four replicates; the error bars show the standard deviations) in spitted off aqueous model solutions and in spitted off orange juice after mastication for 1 min in mouth.

References

- 1 Soeting, W.J.; Heidema, J. *Chem. Senses* **1988**, *13*, 607-617.
- 2 Linforth, R.S.T.; Taylor, A.J. *Food Chem.* **1993**, *48*, 115-120.
- 3 Ingham, K.E.; Linforth, R.S.T.; Taylor, A.J. *Food Chem.* **1995**, *54*, 283-288.
- 4 Buettner, A.; Baek, I.; Linforth, R.; Schieberle, P.; Taylor, A., in preparation.
- 5 *Taschenatlas der Anatomie: innere Organe*; Kahle, W.; Leonhardt, H.; Platzer, W., Eds.; Georg Thieme Verlag, Stuttgart, 1984, pp. 198-199.
- 6 Land, D.G. In *Flavor-Food Interactions*; McGorin, R.J., Leland, J.V., Eds.; ACS-Symp. Ser. 633, pp. 2-11.
- 7 Hofmann, T.; Schieberle, P. In *Interaction of food matrix with small ligands influencing flavour and texture*. Cost 96, Volume 3, pp. 191-194.
- 8 Hinterholzer, A.; Schieberle, P. *Flav. Fragr. J.* **1998**, *13*, 49-55.
- 9 Buettner, A.; Schieberle, P. in preparation.
- 10 Buettner, A.; Hofmann, T.; Schieberle, P.; in preparation.
- 11 Guth, H. *J. Agric. Food Chem.* **1997**, *45*, 3027-3032.
- 12 Guth, H.; Grosch, W. *J. Agric. Food Chem.* **1994**, *42*, 2862-2866.

Chapter 9

Release of Non-Volatile Flavor Compounds In Vivo

J. M. Davidson, Rob S. T. Linforth, T. A. Hollowood,
and Andrew J. Taylor

Samworth Flavour Laboratory, Division of Food Sciences,
University of Nottingham, Sutton Bonington Campus, Loughborough,
Leicestershire LE12 5RD, United Kingdom

Two methods for measuring non-volatiles in-mouth during eating have been assessed. The sucrose and menthone concentration from chewing gum were measured in-mouth and in-nose respectively, together with Time-Intensity (TI) analysis. The temporal analysis of the chemical stimuli with simultaneous TI analysis provided evidence of a perceptual interaction between non-volatile and volatile flavor compounds from chewing gum.

Swabs of saliva were taken from the tongue and analyzed using a rapid, direct liquid-mass spectrometric (L-MS) procedure. Menthone concentration in-nose was monitored on a breath-by-breath basis using direct gas phase Atmospheric Pressure Chemical Ionization-Mass Spectrometry. Simultaneously with the volatile release, trained panelists followed the change in mint flavor perception. Two types of commercial chewing gum were analyzed. Both showed that the panelists perception of mint flavor followed sucrose release rather than menthone release. Other non-volatiles were also measured from a variety of foods using a continuous sampling technique, showing that in-mouth non-volatile concentration can be measured by L-MS for a wide range of tastants.

The perceived flavor of a food is derived from signals sensed by a variety of receptors located in the mouth and nose, which are then processed in the neural system. For convenience, the sensations of taste and aroma have often been investigated separately, but the potential interaction of volatiles and non-volatiles should be considered. Besides invoking the sensation of taste, non-volatiles can also enhance the perception of aroma compounds (1, 2).

In chewing gum, volatile release increases initially but the amount in-nose remains fairly constant over long periods of time (3, 4). Flavor perception also increases initially but then decreases with time. Adaptation is one of the mechanisms that has been proposed to explain the phenomenon (4, 5, 6), but the interaction of non-volatile and volatile compounds may provide an alternative and/or additional explanation.

Duizer et al. (7) used Dual-Attribute Time-Intensity to simultaneously measure the perceived sweetness and peppermint flavor of chewing gum. They found that a gum with a faster release of sweetness enhanced the duration and intensity of sweet perception, as well as the duration of peppermint flavor. However, they did not physically measure changes in the in-mouth (taste) or in-nose (aroma) flavor compounds.

The temporal changes of volatile flavors have been monitored *in vivo* in our laboratory using Atmospheric Pressure Chemical Ionization-Mass Spectrometry (APCI-MS) (8). Changes in non-volatile concentrations in-mouth have received less attention although chew and spit methods and in-mouth sensors (9, 10) have been used with some success in food systems. Both systems have limitations, namely that chew and spit experiments may be very time consuming, while the response of sensors depends on the presence of sufficient saliva to carry the non-volatiles to the sensors. In low moisture foods especially, lack of saliva can cause a slow (or no) response (9).

This paper describes initial experiments that monitored the temporal release of sucrose and menthone from chewing gum during eating, and related the time-release curves to the sensory TI curves. Further experiments investigated the release of other non-volatile compounds from a variety of other foods.

Materials and Methods

Cotton Bud Technique

Materials

Two commercial chewing gums were tested a “stick” type gum and a “tablet” type gum (Dragees). The main sweetener used in both gums was sucrose. The cotton buds used were the standard cosmetic type. Firmenich (Geneva, Switzerland) supplied the menthone. Fisher Scientific Ltd. (Leicestershire, England) supplied the sucrose, methanol and hexane.

Saliva Sampling

Three panelists placed the gum samples in their mouths and chewed on the right side of their mouth at a rate of 80 chews/min using a metronome. They were instructed to take a swab from a specific location on the tongue using a cotton bud at pre-set time points.

Saliva was sampled from the mouth of panelists at 0, 10, 20, 30, 40, 50, 60, 120, 180, 240 and 300 s. Not all time points were obtained from a single gum sample (this would be physically difficult); instead, the time points were split into three sub-sets. Each panelist chewed a total of twelve samples of each gum, producing a minimum of four replicates of saliva samples per time point. Panelists rinsed their mouths with

water to clear their palates and 15 min breaks were taken between samples to minimize the effects of fatigue.

Each cotton bud was weighed before and after swabbing, in order to determine the weight of saliva swabbed (usually around 10 mg) and sucrose was extracted with a 3 mL solution of methanol:water (50:50; (v/v)).

Sucrose Analysis

A mass spectrometer equipped with a liquid chromatographic interface (Platform LCZ, Micromass, Manchester, England) was used for analysis of sucrose. Sucrose was monitored in negative ionization selected ion mode (m/z 340.9) using APCI-MS. A mobile phase of methanol:water (50:50; (v/v)) was continuously pumped into the interface, at a rate of 0.4 mL/min using a source block temperature of 150 °C and a desolvation temperature of 400 °C. A 10 μ L aliquot of the saliva extract or standards was injected via a Rheodyne injection loop (Rheodyne, CA, U.S.A.). Sucrose entering the source was ionized by a 3 kV corona discharge (cone voltage of 18 V). The concentration of sucrose in saliva was estimated by comparing the peak areas obtained for sample injection with those obtained for a set of seven standards (0.1 - 0.00156 g sucrose/100 mL methanol:water), and then correcting for salivary weight differences. To assess the efficiency of the extraction process, swabs were taken from standard sucrose solutions outside of the mouth. The extraction was found to be quantitative.

Measurement of breath's menthone concentration

The breath volatile analysis was conducted simultaneously with the sensory TI analysis. Previous work has shown that the menthol and menthone are released similarly in chewing gum (4). Therefore, only the release of menthone was followed in this experiment. Eleven panelists (different from those used for the sucrose analysis) trained in TI analysis placed the samples in their mouth and were told to chew at a rate of 80 chews/min using a metronome. While they ate, an open-ended plastic tube placed in one nostril guided the breath over the sampling port of the interface. The plastic tube did not interrupt the normal breathing pattern, and during exhalation, breath entered the plastic tube, allowing breath to enter the mass spectrometer.

The gas phase in the tube was sampled continuously at 30 mL/min through the heated (60 °C) interface into the APCI source of the mass spectrometer (Platform II, Micromass, Manchester, England). There, the menthone (m/z 155.0) was ionized by a 4 kV corona discharge (cone voltage 20 V) before the high vacuum region of the mass spectrometer.

A hexane solution of menthone (concentration 35 μ g/mL) was used for the calibration of the APCI-MS. The standard was introduced and volatilized, into the nitrogen make up gas entering the source (10 L/min), using a syringe pump at flow rate of 1.5 μ L/min (Harvard Apparatus, MASS, U.S.A.). This showed the signal intensity (peak height) produced when 52.5 ng/min of menthone enters the source. Comparison of the peak heights for the standard with those for the menthone in each breath, allowed an estimation of the maximum amount of menthone (ng/min) entering

the source over each exhalation. Since the breath sampling rate was known (20 mL/min), we were able to estimate the breath menthone concentration that would result in the observed rate (ng/min) entering the source. These values were determined and expressed as parts per billion in the gas phase (ppbv). Three replicates were taken for each gum, and panelists rinsed their mouths with water to clear the palate and 15 min breaks were taken between samples to minimize the effects of fatigue.

Sensory Analysis

Panelists trained in TI analysis were instructed to rate the intensity of the overall mint flavor of the gums by moving a lever with a marked scale to indicate perceived flavor intensity. Prior to the main experiment, the panelists were given samples of both gums to provide them with an example of the maximum intensity of the mint flavor they would be likely to experience. Panelists were not comparing the intensity of one chewing gum against the other, they were instructed to rate the intensity of each gum relative to the maximum for that gum. Moving the lever generated a linear change in voltage, which was fed directly into one of the analog channels of the mass spectrometer. The resulting TI curves were processed with the software provided with the mass spectrometer.

Continuous Sampling Technique

Materials

Foods used included a digestive biscuit (cookie) (Burtons), an orange (Valencia Late variety), blackcurrant gelatin gel (Sainsburys own), mild cheddar cheese (Sainsbury's own) and salted crisps (chips) (Walkers).

Saliva Sampling

The continuous technique used a motor (Parvalux 12V DC Motor) with a low voltage DC motor speed controller (RS Components 440-492) and an unregulated Power supply (RS Components 597-554) with a barrel attachment which winds a length of 1.5 mm width ribbon (Doubleface Satin; C.M. Offray & Son, Tipperary, Ireland) at a constant rate through the mouth during eating (Figure 1). The sampling rate could be changed to suit the food being measured, by varying the speed of the motor.

A single panelist placed the food samples in their mouth, then placed the ribbon across the tongue and started the motor. To help the panelist chew in the same position, a plastic tube at the side of the mouth acted as a guide for the ribbon. The panelist chewed at a rate of 70 chews/min using a metronome, and as with the swabbing technique chewed on the right side of the mouth. The ribbon was marked before and after eating in order to determine the start and end of the run. Sample size and duration of eating depended on the type of food (4 g Biscuit, duration 135 s; 12 g

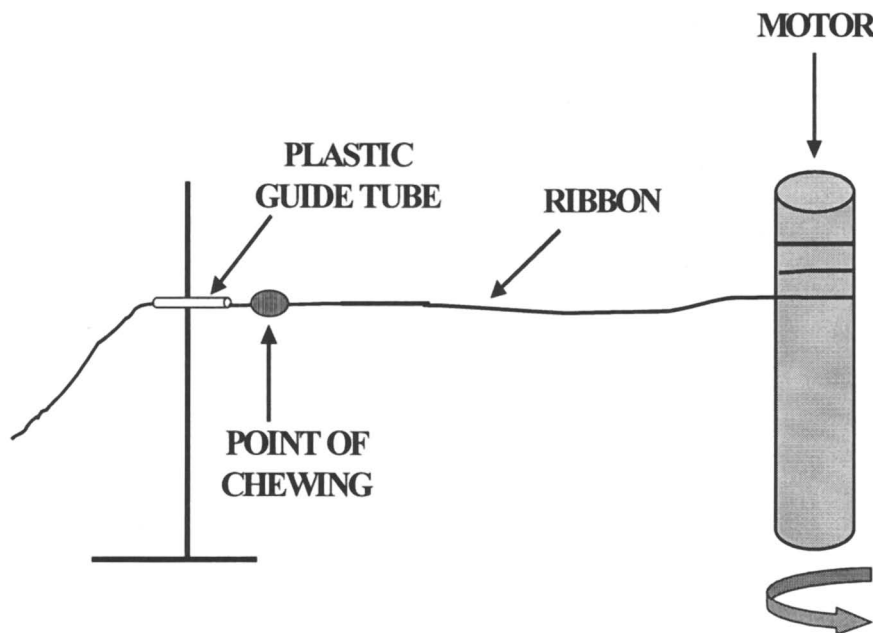


Figure 1. The setup of the ribbon technique employed to sample the liquid phase from the mouth during eating.

of Orange (a segment), duration 90 s; 11.5 g Gel, duration 120 s; 9.8g Cheese, duration 120 s and 3 g Crisps, duration 90 s). Four replicates were carried out for each food. At the end of the eating process the length of ribbon was measured and weighed. It was dried and reweighed in order to calculate the total amount of saliva gained over the whole eating process. After weighing the ribbon was cut into 5 cm lengths, where each length held approximately 10 mg saliva and represented a certain time in the eating process. As with the swabbing technique, the non-volatiles were extracted with solvent and the concentration determined by direct liquid phase API- or Electrospray (ES)-MS.

For the analysis of acids the mass spectrometer was setup in exactly the same way as it was for the sugars (see Cotton Bud Technique Method), and the ions 190.9 (citric acid) and 133.3 (malic acid) were monitored. The salts were monitored in positive ionization selected ion mode (m/z 23.7 for sodium, 39.6 for potassium and 40.6 for calcium) using API-MS. The salts entering the source were ionized by a 4.5 kV corona discharge; (cone voltage of 85 V). A series of calibrants were prepared in the concentration range 0.5 to 100 $\mu\text{g/mL}$.

For the sugars and acids each 5 cm length of ribbon was immersed in 1 mL of solvent to extract the compounds. For the salt samples 12.5 mL of solvent was used.

Results and Discussion

Cotton Bud Technique

Measuring in-mouth is a difficult task, and ideally a real time method is preferred. However, the techniques described here coupled with Liquid-Mass Spectrometry (L-MS) are the next best options. The sensitivity of L-MS was more than enough for most non-volatile compounds, the only disadvantage was that compounds of the same molecular weight could not be resolved.

Effect of swabbing location on the measured sucrose concentration

In preliminary experiments, four different locations on the tongue of one panelist were examined to investigate sucrose distribution and establish suitable locations for swabbing. Gum was chewed on the right side of the mouth and swabs were taken (at 0, 0.5, 1, 2, 3, 4, and 5 min) from each location.

Dawes and Macpherson (11) sampled saliva using small, pre-weighed filter paper strips from different tooth surfaces at specific time points during the eating of chewing gum. From the strips they determined the distribution of sucrose around the mouth, and the implications for the site specificity of caries and calculus deposition. They found an uneven distribution of sucrose in saliva on different tooth surfaces. Our results also revealed an uneven but fairly consistent distribution of sucrose on the tongue. The maximum concentration was found at the site of chewing (as might be expected) (11 g/100 g saliva) with lower concentrations at the left side of the tongue (19% of max), the back (28% of max) and the tip (50% of max). Given the distribution of the sweet taste buds (located principally on the tip of the tongue (12, 13)) this suggested that the maximum sucrose concentration experienced by the sweet taste receptors was about 5 g/100 g saliva. The pattern of sucrose concentration across the tongue seemed fairly consistent as the variation (measured over all samples during the 5 minute period) was relatively small (side of eating, 18%; left side 68%; tip 33%; and back 37%). For the subsequent experiments panelists were instructed to chew on the right side of the mouth and swab the right side of the tongue.

Relationship between sucrose and menthone concentration and perceived mint flavor

Having determined the optimum place on the tongue to sample, experiments were performed to determine how the temporal patterns of aroma and sugar release affected sensory perception (TI). Both Figures 2 and 3 clearly show that for both gums, the in-nose menthone concentration increased in the first minute and then reached a steady state (for the duration of the experiment), while the perceived mint flavor (TI mint curves) followed the in-mouth sucrose concentration very closely.

The release behavior in Figures 2 and 3 suggests that there is a relationship between the perception of mint flavor in chewing gum and the presence of sucrose in-mouth. This type of interaction has been reported previously in other systems. Noble et al. (2) showed that the perceived intensity of citral was enhanced by sucrose, citric

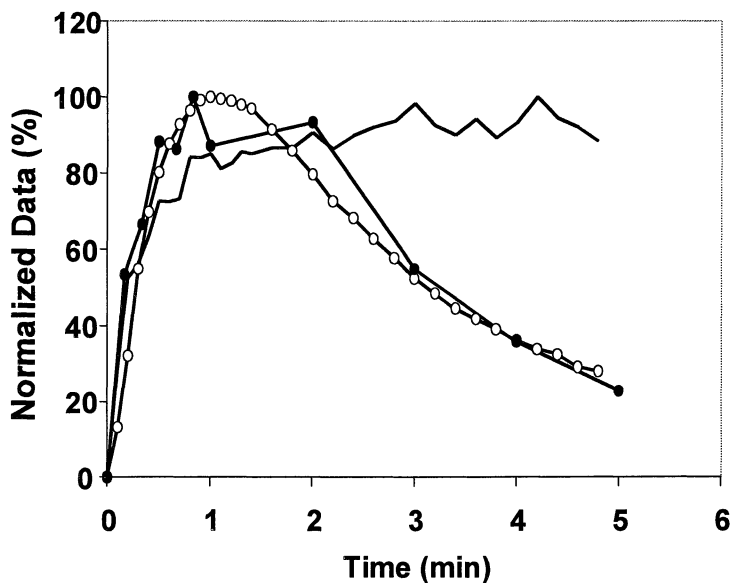


Figure 2. Sucrose release (—●—), menthone release (—) and perceived intensity of overall mint flavor (TI curve) (—○—), from a Stick type commercial chewing gum. The sucrose release data are the mean values from three panelists, whilst the menthone release and perceived intensity values are the mean of eleven panelists. Sucrose and perceived intensity values have been normalized for easy comparison (maximum mean sucrose concentration was 12.4 g/100 g saliva).

acid, or salt; and the intensity of vanillin perception was also increased by the presence of sucrose.

Sensory work carried out by Valdés et al. (14) using solutions containing sucrose, organic acids and raspberry flavoring, also found that there was a tendency for the panel to ascribe more flavor intensity to the sweeter samples. It is of course possible that the TI panelists may have confused loss of sweetness with mint flavor. However, the panel has been rigorously trained with a variety of food materials and has proved consistent in other experiments.

It is also possible that the panelists became adapted to menthone with time (see 5 for discussion) and that the adaptation period coincided with the sucrose release timings. However, for adaptation to be the sole mechanism, it must have different time courses for each type of chewing gum, which seems unlikely. The TI curves for the stick and tablet gums were clearly different. There were differences in the time to maximum intensity (T_{max}) values (Average of 0.6 min for tablet gum, 1 min for stick gum (t-test; $P < 0.001$)) and the persistence of mint flavor after the maximum intensity (I_{max}). This can be illustrated by considering the flavor intensity at 5 min, which for

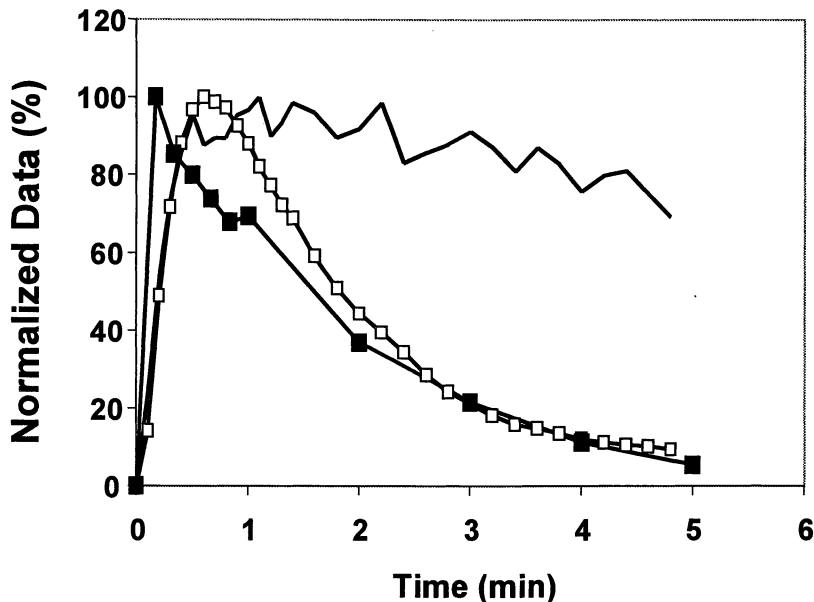


Figure 3. Sucrose release (■), menthone release (—) and perceived intensity of overall mint flavor (TI curve) (□), from a Tablet type commercial chewing gum. The sucrose release data are the mean values from three panelists, whilst the menthone release and perceived intensity values are the mean of eleven panelists. Sucrose and perceived intensity values have been normalized for easy comparison (maximum mean sucrose concentration was 21.4 g/100 g saliva).

stick gum was 28% of the maximum value, while for tablet gum the value was just 9.5% of the maximum (t-test; $P < 0.01$).

There were differences between the two gums and panelists. Both gums showed differences between panelists in the maximum concentration of sucrose in-mouth (8.5 to 17.8 g/100 g saliva for the stick gum and 15.3 to 30.5 g/100 g saliva for the tablet gum). The broad range of concentrations observed were most likely due to physiological differences between panelists, such as salivary flow rate, surface area of the teeth and tongue, and the chewing pattern adopted by each panelist. Each individual panelist seemed relatively consistent in their release of sucrose but the differences between panelists were greater. Normalizing the sucrose release data (data not shown) removed the concentration differences between panelists, and showed that the overall trends of the sucrose concentration curves were similar for all panelists. The different rates and patterns of release are due to the distribution of sugar in the two gums. Tablet gum is sugar coated allowing rapid release of sucrose,

whereas the sucrose of the stick gum is embedded in the gum matrix, which results in slower release.

The stick gum also showed differences in the time taken to achieve maximum concentration (40 – 120 s) despite attempts to standardize chewing using a metronome (80 chews/min). With the tablet gum, however, all three panelists achieved maximum concentration at 10 s. The difference in the T_{max} of the stick gum was large because the sucrose concentration remained relatively high and constant for around 1.5 min, and T_{max} could occur anywhere in this window. When the tablet gum was consumed, the in-mouth sucrose concentration rose very quickly then almost immediately declined, giving a very definite T_{max} value.

Continuous Sampling Technique

Saliva Sampling

The results from the initial technique demonstrated that saliva sampling using cotton bud swabs was effective, and sufficiently rapid to be useful. However, unlike most foods, chewing gum is very simple, as it remains a single bolus in the mouth and is chewed over long periods of time. When the same technique was applied to other foodstuffs, it became apparent that it was difficult to collect saliva samples because the increased frequency of sampling affected the chewing pattern. Therefore, there was a need to develop another method that allowed more frequent in-mouth sampling of many types of foods.

This novel technique can sample continuously with a wide range of different types of foods. However, unlike the swabbing method where each individual cotton bud could be weighed, the salivary weight gain of each individual 5 cm length of ribbon was calculated by taking an average, based on the weight gain of the entire length of the ribbon. However, the benefits of continual sampling outweigh the slight loss in accuracy.

Foods that have a low water content absorb much of the saliva in the mouth, and this has caused problems with other in-mouth measurement techniques (9). The L-MS is very sensitive and only requires that the ribbon collect a small amount of saliva in order to measure the non-volatiles. Sucrose and glucose were successfully measured from a biscuit (data not shown), and the change in sodium concentration was measured from crisps (Figure 4). The maximum concentration of sodium from the crisps occurred at just under 12 s; the in-mouth sensors used by Davidson et al. (9) had not even registered a signal at this time.

Previous work using in-mouth sensors measured the salt concentration from conductivity readings (9, 10), and the change in mouth pH gave an estimate of the change in acidity (9). However, measurements of conductivity and pH are not specific and only give an estimate of the total salt or acid concentration. This technique has the advantage that it is specific, and Figure 5 shows that release of different salts from cheese can be measured simultaneously.

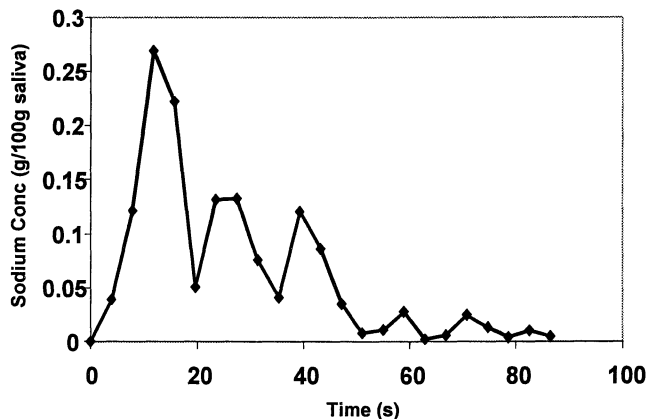


Figure 4. In-mouth sodium concentration (g/100 g saliva) from crisps when consumed by one panelist using the ribbon saliva collecting technique. Data points are the mean of four replicates.

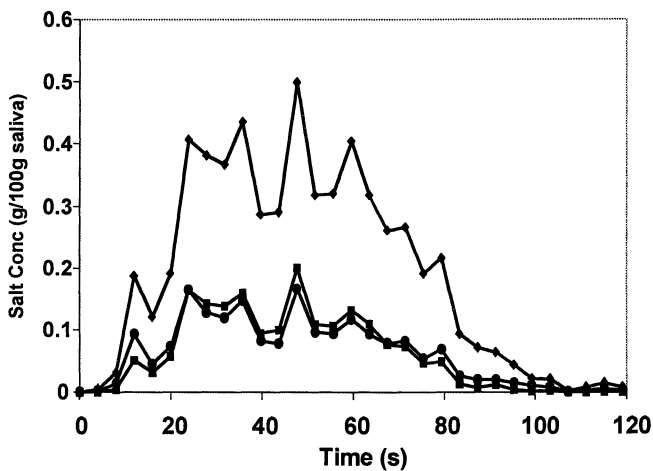


Figure 5. In-mouth sodium (\blacklozenge), calcium (\blacksquare), and potassium (\bullet) concentration (g/100 g saliva) from cheddar cheese when consumed by one panelist using the ribbon saliva collecting technique. Data points are the mean of four replicates.

The results have also shown that different types of food exhibit very different release profiles. The profiles for sucrose, glucose and fructose (glucose and fructose were both present and have the same molecular weight therefore could not be resolved), citric and malic acid from fresh orange reached the maximum intensity very quickly (Figure 6) (Average T_{max} was 6.1 – 9.5 s) then declined almost immediately. The most likely reason for this was that the majority of the non-volatile compounds were contained within the juice of the fruit, and therefore were released immediately upon chewing, and then swallowed. In contrast, the sucrose, glucose, and citric acid from the gelatin gel took longer to consume, and therefore there was an initial burst of flavor release that remained high for about 100 s (Figure 7).

The gelatin system did not show any differences in the temporal changes between glucose and citric acid, in contrast to the orange segment. The differences in the in-mouth concentration observed in Figure 6 may therefore be the result of differences in the distribution of compounds within the segment itself, rather than any differences between the molecules.

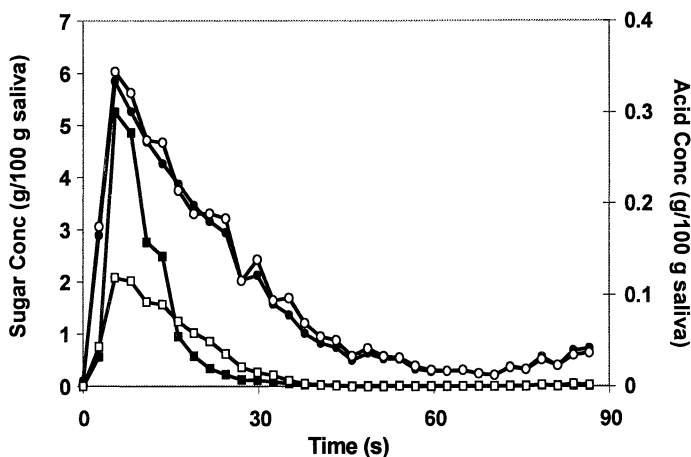


Figure 6. In-mouth sucrose (●), glucose and fructose (○), citric acid (■) and malic acid (□) concentration (g/100 g saliva) from fresh orange segments when consumed by one panelist using the ribbon saliva collecting technique. Data points are the mean of four replicates.

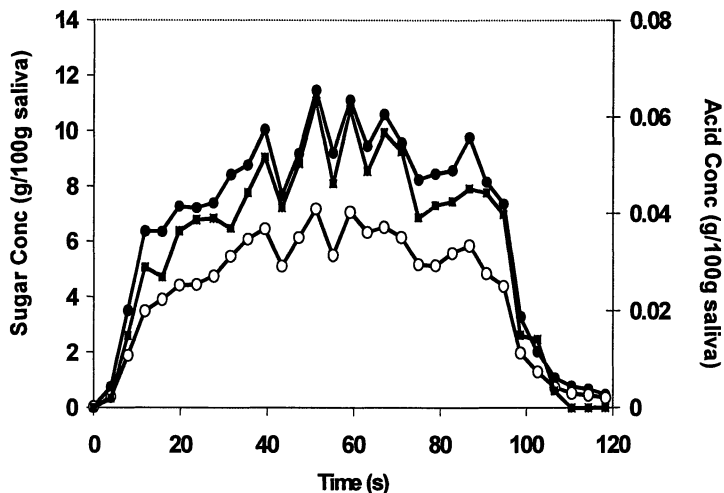


Figure 7. In-mouth sucrose (●), glucose (○), and citric acid (■) concentration (g/100 g saliva) from a gelatin gel when consumed by one panelist using the ribbon saliva collecting technique. Data points are the mean of four replicates.

Variation of I_{max} and T_{max} between the replicates was estimated by calculating the % CV value ($SD \times 100 / \text{mean}$). The % CV for the five foods ranged from 4 to 42% for I_{max} , and from 11 to 37% for T_{max} . The crisps produced the highest I_{max} % CV at 42%. However, it was unlikely that all of this error was attributed to the sampling technique, instead the lack of uniformity between the structure of different crisps was the major factor. The other foods tested were more uniform in structure.

Using ribbon as a sampling device is a very simple and yet a very efficient technique. When coupled with L-MS almost any non-volatile compound can be measured from many types of food.

Conclusions

The results have demonstrated the feasibility of sampling saliva from the mouth and analyzing non-volatiles using API- or ES-MS. The swabbing technique worked very well for foods that remain in the mouth for long periods of time, such as gum. The new technique that uses ribbon has showed that continuous sampling is now possible. Future work will attempt to further improve these techniques, and will include larger scale experiments involving more people.

J.M.Davidson is grateful to the Ministry of Agriculture Fisheries and Food for a studentship and to Firmenich (Geneva) for additional technical and financial support.

References

1. Noble, A. C. *Trends in Food Sci. & Technol.* **1996**, *7*, 439 – 444.
2. Noble, A. C.; Kuo, Y.; Pangborn, R. M. *Int. J. Food Sci. & Technol.* **1993**, *28*, 127 – 137.
3. Harvey, B. *Kennedy's Confection*. May, 1997, p18 – 20.
4. Linforth, R. S. T.; Taylor, A. J. *Perfumer & Flavorist*. **1998**, *23*, 47 – 53.
5. Overbosch, P.; Afterof, W. G. M.; Haring, P. G. M. *Flavor Rev Int.* **1991**, *7*, No.2, 137 – 183.
6. Taylor, A. J.; Linforth, R. S. T.; Baek, I.; Brauss, M.; Davidson, J.; Gray, D. A. In *Advances in Food Chem & Tech*; Risch, S. & Ho, C-T., Eds.; American Chemical Society: Washington, D.C., 1999, In Press.
7. Duizer, L.M.; Bloom, K.; Findlay, C.J. *J. Food. Sci.* **1996**, *61*, No.3, 636 – 638.
8. Linforth, R. S. T.; Ingham, K E.; Taylor, A. J. In *Flavor Science: Recent Developments*; Taylor, A. J. and Mottram, D., Eds.; The Royal Society of Chemistry: Cambridge, England, 1996, pp 361 – 368.
9. Davidson, J.M.; Linforth, R. S. T.; Taylor, A. J. *J. Agric. Food Chem.* **1998**, *46*, No.12, 5210 – 5214.
10. Jack, F. R.; Piggott, J. R.; Paterson, A. *J. Food. Sci.* **1995**, *60*, 213 – 217.
11. Dawes, C.; Macpherson, L.M.D. *J.Dent. Res.* **1993**, *72*, No.5, 852 – 857.
12. Guyton, A. C.; Hall, J. E. *Textbook of medical physiology*, 9th ed.; W. B. Saunders Company: Philadelphia, PE, 1996; pp 676 – 678.
13. Mackenna, B. R.; Callander, R. *Illustrated Physiology*, 6th ed.; Churchill Livingstone: New York, 1997; pp 266.
14. Valdés, R.M.; Hinreiner, E. H.; Simone, M.J. *Food Technol.* **1956**, *10*, No.6, 282 – 285.

Chapter 10

On-Line Monitoring of Coffee Roasting by Proton-Transfer-Reaction Mass-Spectrometry

C. Yeretzian¹, A. Jordan², H. Brevard¹, and W. Lindinger²

¹Nestlé Research Center, Vers-Chez-les-Blanc, 1000 Lausanne 26, Switzerland

²Institut für Ionenphysik, Leopold-Franzens-Universität,
Technikerstr. 25, 6020 Innsbruck, Austria

Volatiles emitted during roasting of coffee beans were monitored on-line by Proton-Transfer-Reaction Mass-Spectrometry. In a first series of experiments, roasting was performed with a large batch of beans. The dynamics of the roasting process – drying of beans in the endothermic phase, transition to the exothermic phase and emission of pyrolysis reaction products – were clearly reflected in the data. In a second experimental series, phenomena occurring at the single bean level were studied. Strong bursts of volatiles were observed that coincided with the popping sounds of beans. These experiments showed, in real-time, the complex processes that take place during roasting.

Coffee is mainly consumed for the pleasurable sensory experience it gives consumers. Its quality is assessed largely on the basis of the aroma (nose) and flavor (mouth) by expert coffee-tasters, and the highest quality beans command a considerable premium. To bring out this delicious, rich and strong flavor requires a tremendous empirical knowledge from cultivators and processors alike. The art of the cultivators consists in producing a green coffee bean, that contains all the ingredients necessary for the development of this flavor. Yet, the green bean itself does not have the characteristic look, smell or taste of a good cup of coffee and gives no clue as to final quality. To bring out this flavor, coffee has to be roasted. Roasters, all over the globe, use their eyes, nose, ears coupled with largely empirical experience to transform an unpalatable seed into a delicious coffee.

Though the art of coffee roasting is old, its chemistry is still little understood. It is a time-temperature-dependent process, whereby chemical changes are induced by

pyrolysis within the coffee beans, together with physical changes in their internal structure. During these transformations, a whole range of different volatile organic compounds (VOCs) is generated, some of which are responsible for the flavor of the coffee beverage. Out of the 900 different VOCs identified in coffee (1), about 30 are believed to be key flavor compounds (2,3,4).

The objective was to monitor on-line time-intensity profiles of VOCs emitted during roasting, and thus to relate process parameters to chemical transformations leading to the formation of the typical coffee aroma. For this, we have investigated the headspace (HS) of green (unroasted) coffee, and monitored the release of VOCs during roasting by Proton-Transfer-Reaction Mass-Spectrometry (PTR-MS). Here, we present some preliminary results from this work, and demonstrate the potential of PTR-MS for on-line process monitoring.

Experimental

Roasting is inherently a dynamic process, during which important chemical transformations take place. Over the last few years, several on-line HS techniques have been implemented (5,6,7), which are capable of capturing on-line such fast processes. One particularly interesting approach is PTR-MS, which combines soft, sensitive and efficient chemical ionization with mass analysis.

Proton-Transfer-Reaction Mass-Spectrometry (PTR-MS)

Technical aspects of PTR-MS have already been discussed in the literature (8,9,10) and elsewhere in this book (C. Yeretizian et al.). Here only a brief overview will be given. PTR-MS is in essence a chemical-ionization mass-spectrometer (Figure 1). Neutral HS-gas is swept with air, continuously injected into a chemical ionization (CI) cell, ionized by proton transfer from H_3O^+ , and mass analyzed. What distinguishes PTR-MS from other traditional CI-approaches is that the generation of the primary H_3O^+ and the chemical ionization of VOCs are individually controlled and spatially and temporally separated processes. This allows (i) maximizing signal intensity by increasing the generation of primary reactant ions, H_3O^+ , in the ion source, (ii) reducing fragmentation and clustering by optimizing the conditions for proton transfer in the drift tube, and (iii) quantifying VOCs.

The three key features of PTR-MS can be summarized as follows. *First*, it is fast. Time dependent variations of HS profiles can be monitored with a time-resolution of better than one second. *Second*, the volatile compounds do not experience any work-up or thermal stress, and measured mass spectral profiles closely reflect genuine HS distributions. *Finally*, measured mass spectral intensities can be directly related to absolute HS concentrations, without calibration or use of standards.

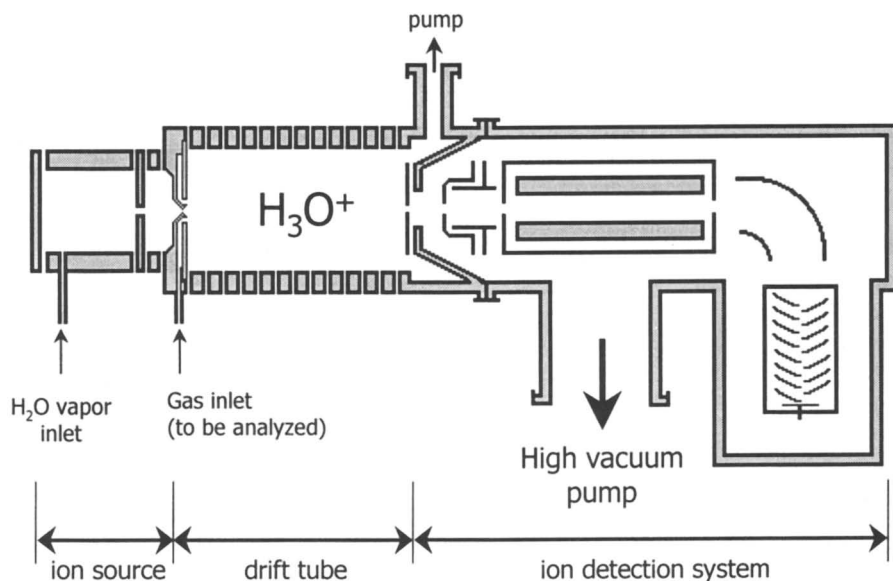


Figure 1: Schematic representation of PTR-MS. It consists of three chambers. In the first chamber, nearly pure H_3O^+ is generated by electrical discharge in H_2O vapor. A small field drives H_3O^+ ions through an orifice into the drift tube (chemical ionization chamber), while neutral VOCs are introduced coaxial to the orifice, into the drift tube. VOCs with proton affinities exceeding 166.5 kcal/mol ionize by proton transfer from H_3O^+ and are accelerated out of the drift tube into the mass filter.

Emissions from Green Coffee Beans.

The emission of volatile compounds from green coffee beans was measured for both Arabica (Bordes-Sto-Domingo) and Robusta (Indonesia). Green beans (30g) were put in a 500 ml glass vial with two openings on the top cover. Through one opening, HS-gas was sampled at a rate of 17 mL/min and replaced by air entering from the other opening. The HS-gas was directly introduced into the drift tube of the PTR-MS and the mass spectrum averaged over 30 minutes. In a separate experiment the HS profile of the empty glass vial was measured and subtracted from the green bean spectrum (background subtraction).

Emission of Volatiles during Roasting.

Two separate roasting experiments were performed. One with a larger load of green coffee beans, where beans were convectively heated by a strong flow of hot air,

and a second setup, where just 6 coffee beans were roasted within a heated vessel and the HS was probed with a moderate flow of air.

Batch Roasting: In a first setup (see Figure 2), 40 grams of Arabica (Columbia) green beans were placed on a mesh inside a roasting vessel, and convectively heated with a strong flow of hot air (more than 500 L/min). The temperature of the air was maintained at 180°C, 185°C or 190°C. First the roaster was equilibrated to the roasting temperature, with hot air flowing through the setup for about 30 minutes. The green beans were then placed inside the roaster and the exhaust air was sampled at 40 mL/min. This flow was diluted by addition of air at 171 mL/min and of this mixture, 11 mL/min were introduced into the drift tube.

Single Bean Roasting: In the second setup, a glass vial acting as a roasting vessel, with two gas-feedthroughs, was placed inside an oven chamber. The oven was heated to 185°C or 195°C, and the temperature maintained throughout the roasting process. Via the gas-feedthroughs, a flow of 1700 mL/min air, preheated to the oven temperature, swept the HS of the roasting vessel. 1% of this air was led into the PTR-MS for on-line monitoring. Once the roasting vessel was equilibrated to the oven temperature, 6 green beans (approx. 1 gram) were placed inside the glass vial. The roasting then proceeded at constant air temperature (isothermal roasting) while the HS air was monitored by PTR-MS.

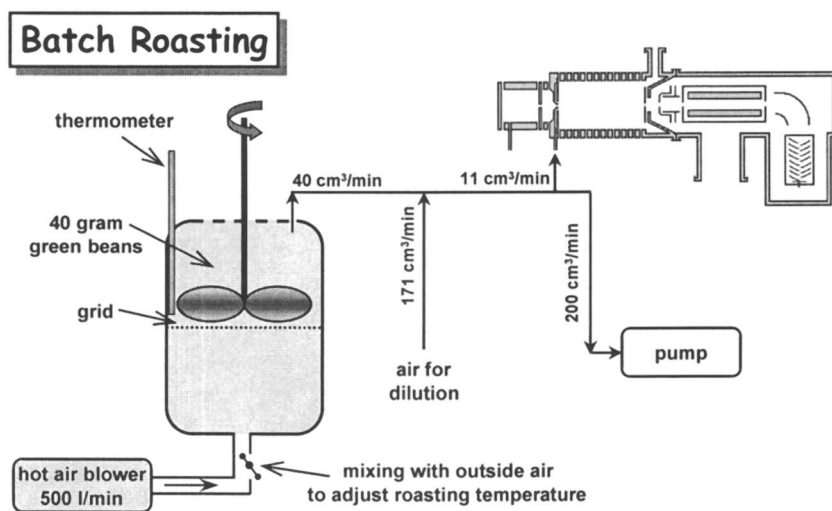


Figure 2: Setup for on-line analysis of coffee roast gas. In this configuration, 40 grams of coffee beans are roasted convectively with a strong flow of hot air.

Results and Discussion

Emissions from Green Coffee Beans.

The VOCs of green coffee beans have attracted rather limited attention so far, particularly in comparison to the large amount of published data on roasted coffee. This is due to the fact that most typical coffee aroma compounds are formed from non-volatile precursors during roasting, and only rarely could they be traced back to volatiles in the unroasted beans. Yet, in a few cases, flavor and off-flavor compounds have been characterized that appear in the green beans, survive the roasting process, and play a role for the flavor of the coffee beverage.

The first comprehensive analysis of VOCs of green coffee beans dates back to 1968 (11). Some 50 compounds were reported, but their relative sensory importance was not investigated. Vitzthum et al. were the first to explicitly combine in 1976 instrumental and sensory methods on green coffee (12). More recently (1995), Holscher and Steinhart compiled a comprehensive literature review and added new results on the HS of green coffee (13). More than 200 compounds were listed in their paper. Finally, Grosch and Czerny reported detailed studies on the potent odorants of green beans, using aroma extract dilution analysis (14,15).

An important driver for research on green coffee flavor comes from the sporadic appearance of off-flavors that affect the cup quality. A baggy off-flavor was linked to the presence of some hydrocarbons in the green beans (16). 2,4,6-Trichloroanisole was found to be responsible for a harsh, phenolic, chemical, musty off-flavor (17,18). A musty/earthy off-flavor was linked to an increase in the concentration of geosmin and 2-methylisoborneol (19), while a bell-pepper, peasy off-note was related to higher concentrations of some alkyl-methoxy-pyrazines (12,14,20).

Figure 3 shows a PTR-MS HS profile of Robusta (Indonesia) green beans. Based on a series of collateral PTR-MS experiments (see Ref. 8, and contribution by C. Yeretian et al. in this book) and published work on green coffee volatiles (13,21,22), the most intense peaks have been tentatively assigned as listed in Table I. Based on this assignment, the most abundant compounds in the HS of green coffee are alcohols (methanol, ethanol and propanol), aldehydes and alkanes. Some organic acids seem also to contribute, although to a lesser extent.

Besides Robusta, we also measured HS profiles from green Arabica (Bordes-Sto-Domingo) coffee. While both profiles show great similarities, some differences are noticed. The Arabica yields methanol and ethanol peaks an order of magnitude stronger. Whether this is related to differences in ripeness, post-harvest treatments or reflects real differences between species, remains to be answered by more systematic studies. Substantial emission of methanol was reported from leaves, and it is believed that vegetation is an important source of atmospheric methanol (23).

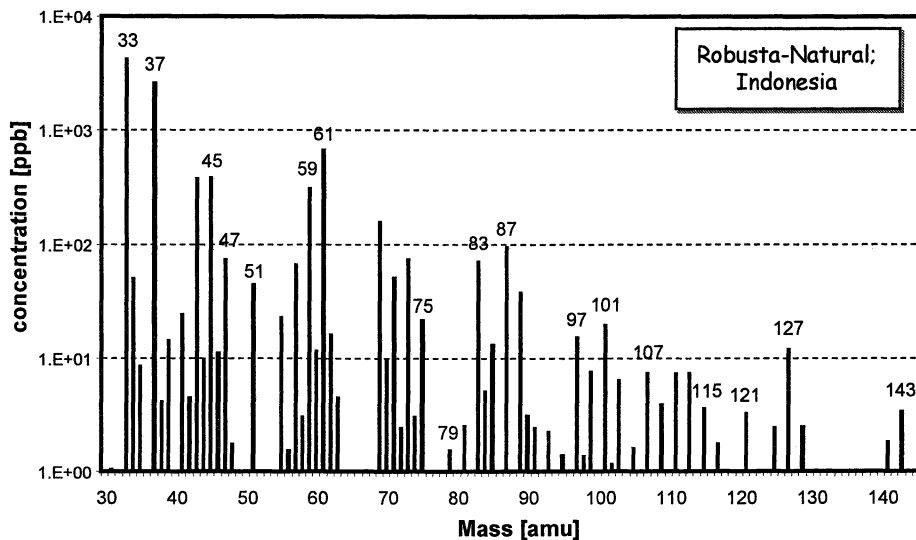


Figure 3: PTR-MS HS profile of Robusta green coffee beans.

Emissions during Roasting.

Arabica coffee (Columbia, 40g) was roasted at three different temperatures in the setup shown in Figure 2, and the roast gas was monitored on-line. Sixty masses were simultaneously monitored with a time resolution of about 40 seconds. In Figure 4, time intensity profiles are shown on a logarithmic intensity scale for roasting at 190 °C air temperature. For reasons of clarity, only 9 masses are included.

Roasting of coffee beans can roughly be divided into two phases; (i) an endothermic phase during which the water content of the beans is reduced from initially 8-12% to just a few percent, (ii) and an exothermic phase where complex pyrolysis reactions take place in the nearly dry beans, to generate among others the typical coffee flavor compounds. At the end of the roasting the moisture content of the beans is below 1%. Looking at Figure 4, we observe at 3-5 minutes a strong increase in several ion intensities. Particularly interesting is mass 37 which corresponds to a water cluster of protonated water, $(\text{H}_2\text{O}\cdot\text{H})^+(\text{H}_2\text{O})$, and reflects the drying process of the beans. Once the beans approach 100°C they start to eliminate water. After the initial sharp increase of water signal, the moisture content in the HS increases steadily but slowly, until 18 minutes. A decrease of the water signal was then observed with a concomitant strong increase at other masses, such as 61 (acetic acid), 73 (butanal, isobutanal, pentane, butanone), 75 (propanoic acid, *not shown here*), 81 (pyrazine, main fragment from furfuryl alcohol $[\text{M}+\text{H}-\text{H}_2\text{O}]^+$) and 87 (2-, & 3- methylbutanal, 2,3-butanedione). They proceed through a maximum at 19 minutes, and decrease by nearly one order of magnitude within the next two minutes.

Table I: Tentative chemical assignment of PTR-MS HS profile of Robusta green coffee beans (Figure 3), based on refs. (13,21,22). The classification of odor intensities + (weak), ++ (strong), +++ (very strong) are from GC-olfactometric evaluations of green bean extracts in ref. (13).

<i>Mass +1(*)</i>	<i>Compound</i>	<i>Odor Intensity</i>
33	Methanol	
37	(H ₃ O ⁺)(H ₂ O)	
45	Acetaldehyde	
47	Ethanol	
51	Methanol(H ₂ O)	
59	Acetone	Propanal
61	Propanol	
65	Ethanol(H ₂ O)	
73	Isobutanal	Butanal
	Butanone	
75	Propanoic acid	Butanol
	Isobutanol	
87	3-Methyl-2-buten-1-ol	2E-Butenoic acid
	3-Methyl butanal	2,3-Butanedione
89	Isobutanoic acid	Pentanol
	2-, & 3-Methylbutanol	2-Pentanol
97	2E,4E-Hexadienal	
99	2E-Hexenal	
101	Hexanal	2,3 Pentanedione +
103	3-Methyl butanoic acid	+++
107	Benzaldehyde	
113	2E-Heptenal	
115	Heptanal	
121	Phenylacetaldehyde	+++
127	1-Octen-3-one	2E-Octenal +
141	2-Nonenal	+++
143	Nonanal	++

At a few masses we observe formation of clusters between VOC-H⁺ and H₂O. Besides, (H₃O⁺)(H₂O) which has a rather high intensity, due to the strong H₃O⁺ ion signal, the other cluster peaks are quite low, showing intensities of only about 1% of the intensity of the non-clustered protonated parent peak.

(*) The indicated masses correspond to the protonated molecular masses as they are detected by PTR-MS.

From the literature it is known that the acetic acid is most abundant at medium roast level (24). Another interesting time-intensity pattern is seen at mass 33 (methanol). After reaching a maximum after about 9 minutes, the HS density of

methanol steadily decreases. Methanol is found in high concentration in the HS of green coffee (see Figure 3), and evaporates off the beans. The change in ion intensity with time shown in Figure 4 clearly documents the two phases of roasting. At the end of the experiment (33 minutes), the beans reached a very dark roast state.

To investigate the effect of the roast-gas temperature on the roast process, we roasted coffee beans at three different temperatures (180, 185, 190°C), but under otherwise identical conditions. In Figure 5, we see that an increase by only 10°C shifts the maximum (medium roast level) from 30 minutes to 19 minutes! Clearly, small differences in temperature have a major effect on the roast process. We also observe a sharpening of the ion-intensity profiles around the maximum. Considering that roast-times of 6-10 minutes are common practice in industry, we begin to understand how delicate the job of an operator is. On-line monitoring of roast gas could be critical to ensure stable and reproducible roast quality. This is particularly the case when the temperature and the moisture content of the roaster air fluctuates during a day and from day to day or the moisture level of the beans varies from batch to batch.

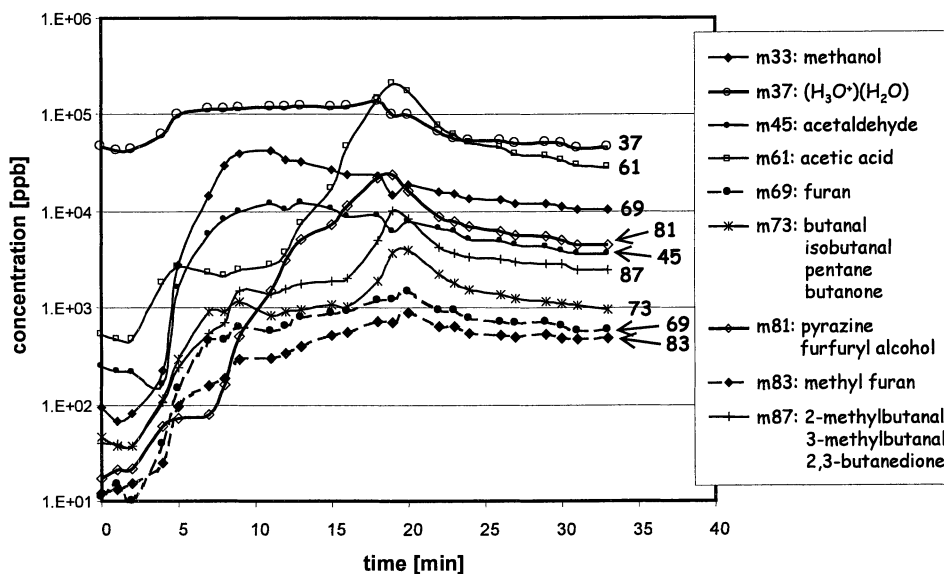


Figure 4: Ion-intensity profiles for seven masses, monitored during the roasting of 40 gram Arabica (Columbia) coffee beans at 190°C. Tentative chemical assignments are also included.

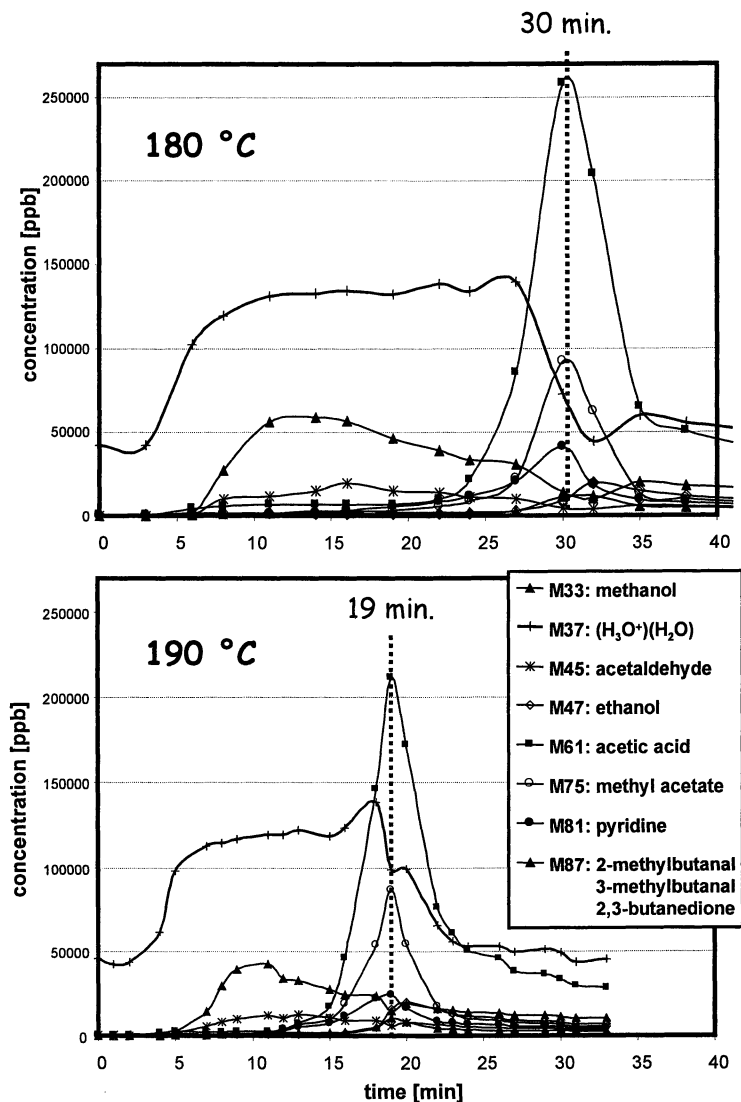


Figure 5: Ion-intensity profiles for volatile compounds during the roasting of Arabica (Columbia) coffee beans at 180°C and 190°C.

The first roasting setup was designed to monitor an averaged HS over a large number of beans (batch roasting). Yet, considering that the “elementary units” of coffee roasting are the individual beans, it is crucial to also investigate the progress at the individual bean level, rather than observing statistically averaged phenomena. For this we have designed a second setup, in which only 6 beans were roasted and a smaller stream of gas was used to sweep the HS gas (see Experimental: *Single Bean*

Roasting). Robusta and Arabica beans were roasted at 185°C and 195°C and ion-intensity profiles of 60 masses were simultaneously monitored, with a time resolution of 40 seconds. Figure 6 shows nine ion-intensity traces for the roasting of Arabica at 185°C. As in the case of the batch roasting, we observed a sharp increase of the methanol signal over more than two orders of magnitude, shortly after the beans were heated. Superimposed on this smooth curve, smaller peaks can be seen. These peaks are also seen at other masses, coincident in time with the methanol peaks. The most intense appears at mass 73. At exactly the same time these peaks appeared, we could hear popping sounds, indicating explosions of single beans due to high internal gas pressures. During the roasting process, large amounts of CO₂ are formed from a variety of reactions. Much of this CO₂ is entrapped inside the cellular structure of the beans. The internal pressure that is built up within these closed cavities can reach 25 bar before the pressure is released by cracking. The sounds of these popping can be clearly heard during the roasting process. At each of these individual popping, CO₂ is released into the HS, together with volatile compounds that have been accumulated in these cavities.

As can be seen from Figure 6, the intensities of some masses, such as 75, 80, 81 or 111 (not shown here) do not seem to be affected by these poppings. This suggests two possible explanations. Either, the physical properties of the compounds may determine whether they are released during popping or whether they remain bound to cellular structures. Or compounds are generated/released in physically distinct areas within the cell structure that are differently affected by the poppings.

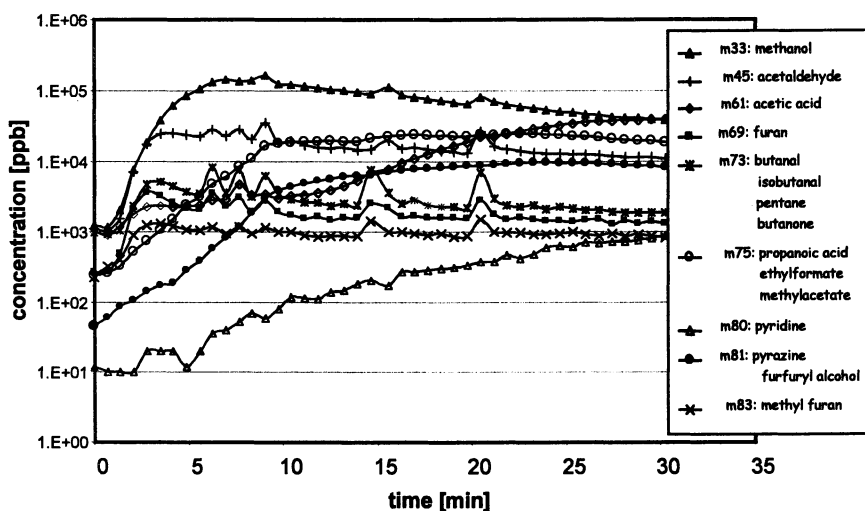


Figure 6: Ion-intensity profiles for volatile compounds during the roasting of six Arabica beans at 185°C. The experimental conditions were chosen such that emissions from single beans could be observed.

Conclusions

Volatile organic compounds, emitted during the roasting of coffee beans, were monitored on-line by Proton-Transfer-Reaction Mass-Spectrometry (PTR-MS). In a first series of experiments 40 grams of green coffee beans were roasted at 180°C, 185°C and 190°C. Monitoring the time-intensity profiles for a large number of masses, the different stages of the roasting process and their transitions could be observed in great detail. In a second series of experiments, we roasted just six beans to investigate phenomena occurring at the single bean level. We observed, in coincidence with popping sound from the beans, sharp bursts of some volatiles.

These on-line observations of the coffee roasting process, via ion-intensity profiles of volatile organic compounds, have given us a direct insight into the complex chemical transformations occurring within the beans. Furthermore, they demonstrate the potential of PTR-MS for on-line process monitoring and eventually pave the way for a rational control of fast industrial processes, via off-gas analysis.

Acknowledgements: We would like to thank A. Hansel for fruitful discussions. This project was supported by the "Fonds zur Förderung der wissenschaftlichen Forschung" under project P 12022.

References

1. Nijssen, L. M.; Visscher, C. A.; Maarse, H.; Willemsens L. C. In *Volatile Compounds in Food*; 7th edition, 1996, TNO Nutrition and Food Research Institute.
2. Semmelroch, P.; Grosch, W. *J. Agric. Food Chem.* **1996**, *44*, 537-543.
3. Semmelroch, P.; Grosch, W. *Lebensm.-Wiss. u.-Technol.* **1995**, *28*, 310.
4. Czerny, M.; Mayer, F.; Grosch W. *J. Agric. Food Chem.* **1999**, *47*, 695.
5. Linforth, R. S. T.; Ingham, K. E; Taylor, A. J. In *Flavour Science: Recent Developments*; Taylor, A. J.; Mottram, D. S., Eds.; Special Publication No. 197, Royal Society of Chemistry, **1996**, Thomas Graham House, Cambridge.
6. Zimmermann, R.; Heger, H. J.; Yeretizian, C.; Nagel, H.; Boesl, U. *Rapid Comm Mass Spectrom.* **1996**, *10*, 1975-1979.
7. Zimmermann, R.; Dorfner, R.; Kettrup, A.; Yeretizian, C. 18th International Scientific Colloquium on Coffee; Helsinki, Finland (ASIC18), August 2-6, **1999**; in press.
8. Lindinger, W.; Hansel, A.; Jordan, A. *Int. J. Mass Spectrom. Ion Processes* **1998**, *173*, 191-241.
9. Lindinger, W.; Hansel, A.; Jordan, A. *Chemical Society Review* **1998**, *27*, 347-354.

10. Hansel, A.; Jordan, A.; Holzinger, R.; Prazeller, P.; Vogel, W.; Lindinger, W. *Int. J. Mass Spectrom. Ion Processes* **1995**, *149/150*, 609-619.
11. Merrit, C.; Robertson, D. H.; McAdoo, D. J. 4th International Colloquium on the Chemistry of Coffee, Amsterdam, Netherland (ASIC4), 2-6 June **1969**, 144-148.
12. Vitzthum, O. G.; Werkhoff, P.; Ablanque, E. 7th International Colloquium on the Chemistry of Coffee, Hamburg, Germany (ASIC7), 9-14 June, **1976**, 115-123.
13. Holscher, W.; Steinhart, H. In *Food Flavors: Generation, Analysis and Process Influence*; Charalambous, C., Ed.; Elsevier Science 1995; 785-803.
14. Grosch, W. 18th International Scientific Colloquium on Coffee; Helsinki, Finland (ASIC18), August 2-6, **1999**; in press.
15. Czerny, M.; Grosch, W. *J. Agric. Food Chem.* submitted.
16. Grob, K.; Artho, A.; Biedermann, M.; Caramashi, A. *J. AOAC Intern* **1992**, *75*, 283.
17. Spadone, J. C.; Takeoka, G.; Liardon, R. *J. Agric. Food Chem.* **1990**, *38*, 226.
18. Holscher, W.; Bade-Wegner, H.; Bendig, I.; Wolkenhauser, P.; Vitzthum, O. G. 16th International Scientific Colloquium on Coffee; Kyoto, Japan (ASIC16), 9-14 April, **1995**, 174-182.
19. Cantergiani, E.; H.Brevard, H.; Amadò, R.; Krebs, Y.; Feria-Morales, A.; Yeretzian, C. 18th International Scientific Colloquium on Coffee; Helsinki, Finland (ASIC18), August 2-6, **1999**; in press.
20. Becker, R.; Döhla, B.; Nitz, S.; Vitzthum, O. G. 12th International Scientific Colloquium on Coffee; Montreux, Switzerland (ASIC12); 29 June - 3 July **1987**, 203-215.
21. Rhoades, J. W. *J. Agric. Food Chem.* **1960**, *8*, 136-141.
22. Rodriguez, D. B.; Frank, H. A.; Yamamoto, H. Y. *J. Sci. Food Agric.* **1969**, *20* 15-17.
23. MacDonald R.; Fall. R. *Atmos. Environ.* **1993**, *27A*, 1709-1713.
24. *Espresso Coffee, The Chemistry of Quality*; Illy, A.; Viani, R., Eds.; Academic Press Ltd., London, **1995**.

Chapter 11

Physicochemical Models of Flavor Release from Foods

Kris B. de Roos

Givaudan Roure Flavors, Ltd., CH-8600 Dübendorf, Switzerland

An overview is given of the physico-chemical models that have been developed to describe flavor release from foods during perception by sniff and by mouth. Three different basic models of flavor release can be distinguished which differ mainly in the way diffusion takes place. Comparison of theoretical predictions with experimental data shows that molecular diffusion is the major transport mechanism during flavor perception by sniff (release from static product phase). On the other hand, flavor release in the mouth (release from dynamic product phase) is primarily controlled by the rate of surface renewal as affected by eddy diffusion. During the last few years good progress has been made in the development of mathematical models that address specific problems that are associated with flavor release in the mouth.

A flavoring applied to different products generates often totally different odor and taste sensations. Due to the differences in sensory response to the same flavoring in different media, flavorists have to spend much time on modifying and optimizing flavorings for new target applications. In view of the large number of flavor ingredient and product types, this is a tedious and time-consuming job. Therefore, a better understanding and predictability of the changes in sensory response that result from differences in flavor release is of high practical significance. For that reason much work has been done during the last years to relate flavor compound concentrations in a product to perceived strength and character.

An overview will be given of the physico-chemical models that have been developed for predicting flavor release from foods. Special attention will be paid to the proportions released at a given time because they determine the character of the perceived flavor. To duplicate the flavor of a desirable product in another product, it is not only important to achieve the same flavor impact from the individual flavor constituents but also to achieve their impact at the right time. This means that the physico-chemical models of flavor release must be able to predict maximum flavor intensity (I_{max}), the time to reach maximum flavor intensity (t_{max}) and the duration of the flavor release.

Principal Symbols

A	Surface area of the interface (m^2)
C	Concentration (g/L)
D	Diffusion coefficient (m^2/s)
f	Volume fraction (L/L)
J	Mass flux, $\text{g/cm}^2\text{s}$
k	Mass transfer coefficient (m/s)
k_o	Overall mass transfer coefficient (m/s)
M	Mass (g)
n	Number of extraction steps in non-equilibrium model of flavor release
P	Partition coefficient
t	Time (s)
v	Air flow rate (L/s)
V	Volume (L)
V^*	Volume of one phase that is in equilibrium with volume of other phase (L)
δ	Effective thickness of the stagnant layer (m)

Subscripts

G, L, P, O and W refer to gas, liquid product, oil and water phase, respectively

Superscripts

i refers to interface

Factors Affecting Flavor Release and Perception

To be perceptible, aroma compounds must be released into the headspace in the mouth and transferred to the nose, where aroma perception takes place. In contrast with aroma compounds, taste compounds must be present in the saliva because taste compounds, such as salt and sugar, are perceived in the mouth. During consumption of solid foods, the volatile flavor compounds are generally first released into saliva before they are released into headspace and transferred to the nose. This means that interfacial mass transfer from both solid to liquid and liquid to air phase determines the flavor release from solid products. This review will focus on aroma, in particular, on aroma release during perception by sniff (smell) and by mouth (“taste”), because the release under these conditions is of highest practical significance.

The factors that affect the flavor release from foods are phase partitioning and mass transport. Flavor release from product to vapor phase will only take place if the phase equilibria are disturbed. So, non-equilibrium is the **driving force** for mass transport.

The vapor phase is in equilibrium with the product phase if there is no effective mass transport at the product-air interface. Under these conditions, the concentrations in these phases obey the following relation:

$$P_{GP} = C_G / C_P \quad (\text{eq 1})$$

where P_{GP} is the gas-product partition coefficient and C_G and C_P are the concentrations of the flavor compound in air and product, respectively.

The *rate* at which equilibrium can be achieved is determined by the mass transfer coefficient. The mass transfer coefficient k is a measure for the velocity at which the solute diffuses through the phase. Consequently, $1/k$ stands for the resistance to mass transfer.

Phase Partitioning

Vapor pressures in the product medium can be influenced by many factors, such as:

a. *Temperature*

Temperature has a strong effect on the gas-product partition coefficient. Correction for the effect of temperature on phase partitioning and flavor release has not received much attention, so far. The reason could be that the effect of temperature on phase partitioning is complex (1, 2).

b. *Composition of the Aqueous Phase*

Certain molecules, such as alcohol (3, 4), salt (2) and sugars (5, 6) influence vapor pressures of aroma compounds through their effect on the solvent properties of the aqueous phase. There is no special binding between the flavor molecules and the dissolved compounds. Depending on the nature of the change in solvent properties all flavor compounds are affected to a lower or higher extent. In practice, this means that in the physico-chemical models of flavor release, the gas-water partition coefficient P_{GW} has to be replaced by the gas-liquid partition coefficient P_{GL} .

c. *Flavor Binding / Complex Formation*

In this case there is a specific interaction between dissolved molecules and the aroma compounds. It is important to discriminate here between dissolved, bound and total flavor concentration. Only the free dissolved molecules exert a vapor pressure. In liquid foods, the exchange of flavor molecules between the bound and unbound state is often very fast compared to the transport of flavor across the water-gas interface (7). This means that the transport across the water-gas interface is the rate-determining step and that the gas-water partition coefficient in the release equations can simply be substituted by the gas-liquid partition coefficient

d. *Acid-Base Equilibria*

This is a special case of flavor binding. The ionic form of the flavor compound is here the bound form.

e. *Phase Partitioning between Aqueous and Lipid Phase*

The air-to-product partition coefficient of an emulsion can be easily calculated from the volume fractions f_o and f_w of oil and water and the oil-gas and water-gas partition coefficients P_{OG} and P_{WG} (8-10):

$$P_{GP} = C_G / C_P = \frac{C_G}{f_O C_O + f_W C_W} = \frac{1}{f_O P_{OG} + f_W P_{WG}} \quad (\text{eq } 2)$$

If the flavor compounds in the aqueous phase are also participating in the equilibria c and d mentioned above, the calculation of gas-product partition coefficients becomes more complex (11). In practice, this means that there is no longer a linear increase or decrease of the vapor pressure with carbon chain length as in water or oil (Figure 1).

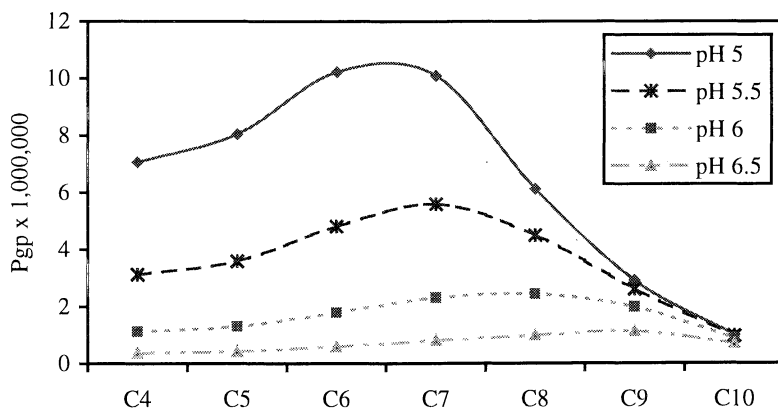


Figure 1. Effect of pH on the vapor pressure (P_{GP}) of *n*-alkanoic acids in a 5% oil-in-water emulsion at 25 °C (calculated values according to ref. 11).

f. Sorption to Suspended Particles

In suspensions the same processes can in principle take place as in solutions (flavor binding) and emulsions (flavor absorption). The main difference is in the rate of equilibration, which is often much slower in suspensions than in emulsions due to the low rate of diffusion in solids. This means that equilibration in the product phase may become rate limiting and then its effect on flavor release has to be addressed explicitly in the physico-chemical models.

g. Crystallization

If crystallization takes place in the aqueous or lipid phase, the volumes available for phase partitioning become smaller (solutes are excluded from the crystal lattice). As a consequence, equilibria will shift (12) until the solute concentrations in the fluid parts of the phases are distributed according to the partition coefficients.

Chemical reactions and adsorption to plastic beakers reduce also the free aqueous concentrations, but these processes remove the flavor compounds from the product in an irreversible way. These processes will therefore not be further discussed.

Interfacial Mass Transfer

When phase equilibria are disturbed, mass transport will take place resulting in concentration gradients in the product and vapor phases as depicted in Figure 2.

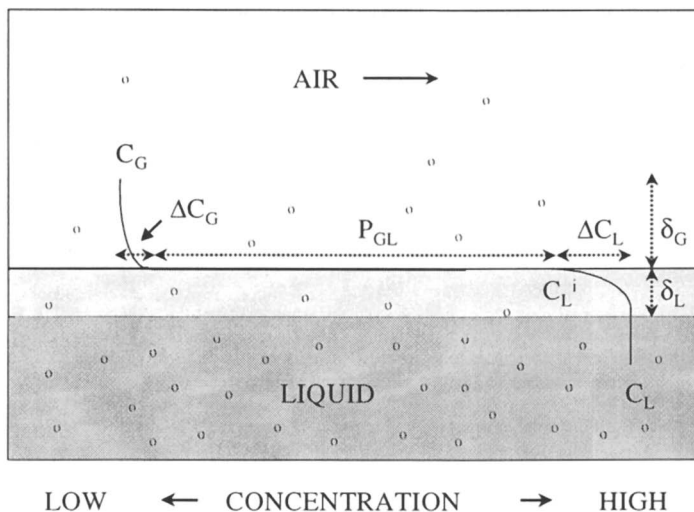


Figure 2. Schematic diagram of flavor concentrations at the liquid-gas interface during release from the liquid phase.

According to Fick's first law, the rate of the unidirectional diffusion from the product to the vapor phase is determined by the concentration gradients in each of these phases and by the respective mass transport coefficients in the product and gas phase, k_p and k_G , according to (13, 14). So, the mass flux J in either phase is given by:

$$J_p = k_p (C_p^i - C_p) \quad (\text{eq 3})$$

$$J_G = k_G (C_G - C_G^i) \quad (\text{eq 4})$$

where C and C^i are the aroma compound concentration in the bulk phase and at the interphase. In many cases one phase resistance controls flavor release and the other can be ignored.

The value of the mass transfer coefficient k is strongly influenced by the diffusion mechanism. Two distinct mechanisms of diffusion may apply. One mechanism is the molecular or static diffusion, which is caused by the random movement of the molecules in the stagnant fluid. Typical molecular diffusivities are $10^{-5} \text{ m}^2/\text{s}$ and $10^{-9} \text{ m}^2/\text{s}$ in gas and liquid aqueous phases, respectively. The rate of molecular diffusion varies only slightly with flavor type. The second mechanism is eddy or convective diffusion, which transports elements or eddies of the fluid from one location to another, carrying with them the dissolved solute. The rate of eddy diffusion is usually much higher than the rate of molecular diffusion and independent of flavor type.

In equations 3 and 4, the concentration differences $C_p^i - C_p$ (ΔC_p) and $C_G - C_G^i$ (ΔC_G) represent the driving force for mass transport. In general, ΔC_G is much smaller than ΔC_p and is neglected (9, 14, 15). The concentration C_p^i at the product surface determines then the concentration in the bulk phase of the air ($C_p^i = C_G/P_{GP}$) so that equation 3 takes the following form:

$$J_p = k_p \left(\frac{C_G}{P_{GP}} - C_p \right) \quad (\text{eq 5})$$

The concentration gradient ΔC_p in the product is determined by the volatility of the flavor compound in the medium and the resistance to mass transfer. The higher the vapor pressure of a flavor compound, the higher is the depletion of that compound at the surface. The same holds for the resistance to mass transfer: the higher it is, the more difficult it is to replenish depleted concentrations at the surface.

Figure 3 illustrates the effect of resistance to mass transfer on the flavor release from aqueous media. Differences in mass transfer were generated by varying the viscosity of the medium. During measurement under dynamic conditions a gas flow was lead over the surface of a stirred solution thus mimicking the conditions in the mouth. Although the vapor pressures of the aroma compounds (expressed as % released under equilibrium conditions in equal volume of air) in the different media are the same, the release rates under dynamic conditions differ widely. The graphs clearly show that under

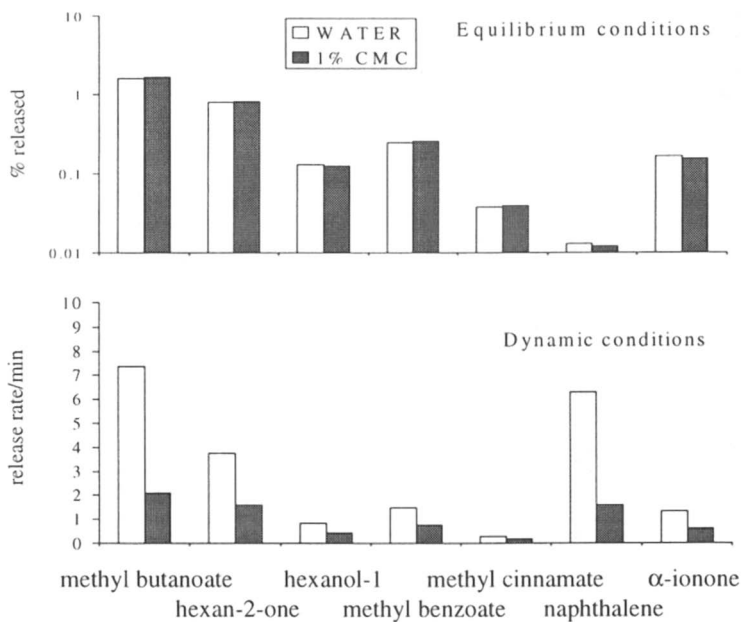


Figure 3. Flavor release under equilibrium and dynamic conditions from aqueous solutions at 37 °C (8).

dynamic conditions the release from the viscous carboxymethylcellulose (CMC) solution always slower is than from plain water, and that the highest decrease in flavor release rate is observed for the most volatile flavor compounds (8).

At very high resistance to mass transfer in the product phase flavor depletion at the surface of the product will be near to complete for all compounds ($C_p^i \approx 0$). Under these conditions, mass transport is a function of only the concentration C_p in the product bulk phase and the mass transfer coefficient k_p :

$$J_p = -k_p C_p \quad (\text{eq } 6)$$

Since k_p does not vary with flavor type (eddy diffusion) or only to a slight extent (molecular diffusion), the release under these kinetically controlled conditions is similar for all flavor compounds.

Basic Models of Interfacial Mass Transfer

Several mathematical models have been derived for predicting flavor release under dynamic conditions. The main difference between these models is in the mechanism of mass transport.

a. Stagnant-Film Model

This model assumes that the boundary layers at the interface are stagnant and that mass transport through these layers is by molecular diffusion (15, 16). According to this model, the mass transport coefficient k varies with the first power of the diffusion coefficient D and the reciprocal of the effective thickness of the stagnant layer δ . This results in the following equation for the mass flux from a product:

$$J_p = (D_p / \delta_p)(C_p^i - C_p) \quad (\text{eq } 7)$$

b. Penetration Theory

The penetration theory takes into account that the boundary layers are often not completely stagnant and that there is also mass transport by eddy diffusion. Mass transfer between the phases takes place when a volume element from the bulk phase comes into contact with a phase boundary for a short fixed time t_c . During this fixed time contact, mass transfer takes place by molecular diffusion (9, 10, 13). Subsequently, the volume element is remixed with the bulk phase and the whole process is repeated. According to this model, the mass flux from a product across the interface is given by:

$$J_p = 2(\sqrt{D / \pi t_c})(C_p^i - C_p) \quad (\text{eq } 8)$$

The penetration model predicts that k varies with the square root of the diffusion coefficient, whereas the film model predicts a first power relationship. Under dynamic conditions, the square root is often nearer to the truth.

c. *Non-Equilibrium Partition Model*

This model assumes that mass transfer takes place only by eddy diffusion. It is applicable to highly agitated systems where molecular diffusion is too slow to have a significant effect on flavor release and perception (13, 17, 18). The independence of the diffusion constant allows a simple multiple extraction model to be used, in which mass transfer takes place by eddy diffusion during a short fixed time contact between a volume element V_p^* from the product phase and a volume element V_G^* from the gas phase (8, 19). The total amount released as a function of time is given by:

$$M_p^t / M_p^0 = 1 - \{(V_p^* / V_p)\{P_{pG} / (P_{pG} + V_G^* / V_p^*)\} + (1 - V_p^* / V_p)\}^n \quad (\text{eq } 9)$$

where V_p is the total product volume, n the number of extraction steps, and superscripts t and 0 refer to time. The resistance to mass transfer is here reflected by the quotient V_G^* / V_p^* . The higher the resistance to mass transfer in the product phase, the smaller is the volume element of the product phase that is in equilibrium with a fixed volume element of the gas phase and the higher is the quotient V_G^* / V_p^* .

The model has also been successfully applied to less agitated systems such as cake dough during baking (19). This suggests that even under such pseudo-static conditions eddy diffusion is playing an important role.

With models a and b it is often assumed that the resistance in the product phase controls flavor release and that the resistance in the gas phase can be neglected (i.e. no concentration gradient in the gas phase). However, as indicated by Marin *et al.* (20), this is only true as long as the vapor pressures of the aroma compounds in the medium are relatively high. For a system consisting of a stagnant water phase and a turbulent gas this means, for example, that $P_{GW} > 10^{-3}$.

When the mass transfer coefficients in both phases are comparable, i.e., differ by a factor of less than 10, the resistances in both phases have to be taken into account. This can be done by use of the following relationship (20):

$$J = k_o(P_{GL}C_L - C_G) \quad (\text{eq } 10)$$

in which the mass flux across the interface is related to the bulk concentrations in both phases via an overall mass transfer coefficient k_o given by:

$$\frac{1}{k_o} = \frac{1}{k_G} + \frac{P_{GW}}{k_L} \quad (\text{eq } 11)$$

Since no concentrations build up in the boundary layers at the interface, the mass flux through the boundary layers must be the same at any distance from the interface. This means that the following relationships must exist:

$$J = k_L(C_L^i - C_L) = k_G(C_G^i - C_G) = k_o(C_G - P_{GL}C_L) \quad (\text{eq } 12)$$

If the resistance to mass transfer can be neglected, then $1/k_G \approx 0$ and $k_o \approx k_L/P_{GL}$. In that case equation 10 becomes identical to equation 5:

$$J_G = k_O(P_{GL}C_L - C_G) = \frac{k_L}{P_{GL}}(P_{GL}C_L - C_G) = k_L(C_L - \frac{C_G}{P_{GL}}) = -J_L \quad (\text{eq } 13)$$

All above mentioned basic physico-chemical relationships have a universal applicability to all kinds of interfacial mass transfer processes, such as extraction, steam distillation, drying and baking. For prediction of flavor release during perception by sniff and by mouth, these basic equations need to be adapted to account for the effects of the specific conditions on phase partitioning and mass transport under these conditions.

Flavor Release during Perception by Sniff

When smelling a product, the product phase is normally static and the gas phase dynamic. Under these conditions, the concentration C_p^i at the product surface will initially sharply decrease while the boundary layer thickness δ_p will slowly increase. As a consequence of both changes, the flavor release rates will initially sharply decrease and then level off (Figure 4).

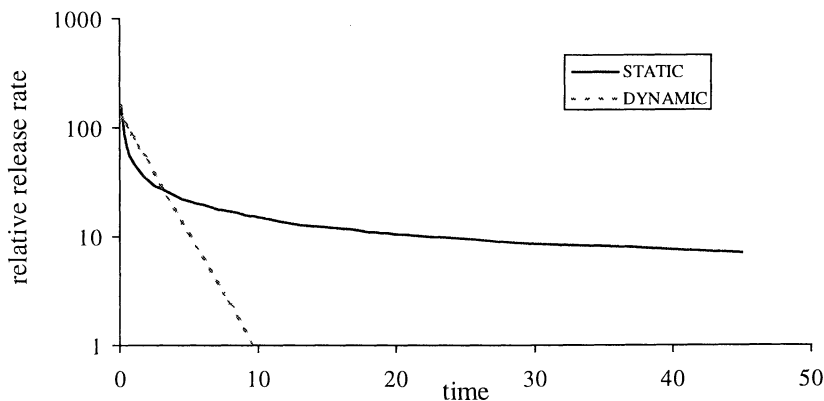


Figure 4. Schematic diagram of flavor release from a static and dynamic liquid phase at constant airflow rate over the surface.

Compared to flavor release in the mouth, the flavor release from a static product phase has received only little attention. Darling et al. (13) have used the penetration model to describe the diffusion controlled release from liquids. Assuming that the liquid phase controls flavor release and that the bulk concentration C_L remains constant, the following relationship for the mass flux from a liquid phase was derived:

$$J_L = (C_G / P_{GL} - C_L) \sqrt{D_L / \pi t} \quad (\text{eq } 14)$$

This equation is very similar to equation 7. The concentration C_L^i is replaced by the concentration, which would be in equilibrium with the bulk gas phase if this were present at the surface. Because of the assumptions made, equation 14 is suitable only for predicting long-time behavior.

Marin *et al.* (20) used the stagnant film model to describe the release from a stagnant liquid phase. For the long-term pseudo-steady-state release at time t , the following simple relationship was derived for the relative flavor concentration in the gas phase (i.e., concentration relative to the equilibrium headspace concentration at $t=0$):

$$C_G^t / C_G^0 = \frac{1}{1 + v_G / k_o A} \quad (\text{eq 15})$$

Since k_o is a function of the partition coefficient, the relative concentration in the headspace is a simple function of the partition coefficient and the gas flow rate.

Flavor Release in the Mouth – Liquid Products

In a highly agitated environment as the mouth, mass transport takes place almost exclusively by eddy diffusion (13, 17, 18). Eddy diffusion strongly reduces the concentration gradients at the interface resulting in higher concentrations at the interface and consequently also in higher release rates. At a constant rate of agitation, a steady state release will be created during which the relative surface concentration C_L^i / C_L remains constant. Figure 4 shows the differences in the time dependence between molecular and eddy diffusion controlled flavor release. At $t=0$, the release rates are the still same, but as soon as under dynamic conditions the steady state release has started, release rates become very different. The logarithmic relationship between dynamic release and time means that it is easy to calculate release rates (dM_G/dt) if the amounts released ($M_G(t)$) and t are known.

Prediction of flavor release in the mouth is complicated by the continuous change of the composition and texture of the product. Dilution with saliva and change of temperature disturbs the phase equilibria and alters the resistance to mass transport. Mass transport in the mouth is affected by the gas and saliva flow rates, the degree of agitation and the temperature. The temperature also affects mass transport through its effect on melting behavior of fat and gelatin.

Harrison and Hills developed mathematical models to describe flavor release from liquid foods in the mouth as a function of air and saliva flow rate (9, 14, 21) assuming that the penetration theory of mass transfer applies and that the resistance to mass transfer across the liquid-air interface is the rate limiting step for flavor release. These models, applied to oil-in-water emulsions and aqueous solutions containing aroma-binding macromolecules, predict that I_{max} and t_{max} are not only a function of the air and saliva flow rates but also of the flavor and product properties, such as the gas-liquid and oil-water partition coefficients and the viscosity of the liquid in the mouth. In particular, the dependence of I_{max} and t_{max} on the flavor and product properties is of high practical significance because this is the main reason behind the problems encountered in the flavor application to different products (21-24).

Practical Consequences of Differences in Flavor Release

Due to the differences in flavor release during perception by sniff and by mouth it is difficult, if possible at all, to adjust flavor compositions for same aroma perception by sniff and by mouth at the same time (8). The problem is clearly illustrated by the differences in the correction factors for same flavor perception in cream as in soft drink (Table I). The correction factor is here defined as the factor by which the concentration of a flavor compound in the cream has to be increased to obtain the same flavor intensity perception from that compound as in the soft drink. The correction factors were established by determining the concentrations at which a single flavor chemical generates the same intensity (I_{max}) during perception in different application media. The best solution to the problem of different aroma perception by sniff and by mouth is to reformulate for same aroma perception by mouth and to accept a difference in smell.

Table I. Correction Factors for Same Flavor Perception in Cream (33% Fat) as in a Soft Drink.

	Correction factors for same flavor intensity		
	Sniff		Mouth
	Static	Dynamic	Dynamic
cis-3-hexenol	1.8	2.1	1.8
Ethyl butanoate	14	6.2	5.1
tr-2-Hexenyl acetate	69	20	11
Hexyl acetate	194	35	21
Linalyl acetate	827	168	27

The differences in the time-intensity profiles of the release of flavor compounds in different application media is another problem that can result in several flavor defects such as lack of persistence, sequential release or undesirable aftertaste. The problem is not easy to solve by flavor reformulation. Probably the best solution is to change the time-intensity profile of the release by creating a microenvironment for the flavor that mimics that of the original full fat base (25-27).

Flavor Release in the Mouth - Solid Products

The release from solid foods is more complicated than that from liquid products because a third phase is involved. During consumption of solid foods, flavor is normally first released into the saliva before it is released into the mouth's headspace and transferred to the nose. It is generally assumed that the mass transport across the product-saliva interface is rate determining and that two different release mechanisms are involved in the release from solid food to saliva:

1. *Product Dissolution*

A typical example of this kind of flavor release is the release from hard candies. Characteristic for this release mechanism is that all flavor compounds are released at the same rate. This means that the release is ideal, i.e. the release is 100% and there is no change of flavor character with time. The release rate is a simple function of the rate of product dissolution and not influenced by the product-to-saliva partition coefficients. Hill and Harrison described mathematical models for the release from hard candies and gelatin jellies based on the two-film stagnant film theory (16, 28, 29). Experimental *in vitro* results with boiled sweets suggest the interfacial mass transport is reasonably well described by this theory rather than by the penetration theory (16).

2. *Product Extraction*

In principle, the basic equations for describing the interfacial mass transport from an insoluble product phase to saliva are the same as those describing mass transport from liquids to air. Characteristic for this type of flavor release is that the flavor compounds are released at different rates determined by the product-saliva partition coefficients and that the release from product to saliva is incomplete.

A major difference between the release from solid and liquid products is that molecular diffusion is playing a much more prominent part in solid than in liquid products. Release from solid products into saliva depends also strongly on chewing efficiency and surface area/ particle size. An example of the effect of chewing efficiency on flavor release is shown in Figure 5. It is clear that release from the chewing gum base is strongly kinetically controlled. This can be concluded from the differences in the release rates that are minor compared to the differences in the gum-water partition coefficients P_{Gum-W} . This holds in particular for the inefficient chewer. The efficient chewer extracts higher proportions of the water-soluble compounds, which indicates higher efficiency in decreasing the resistance to mass transfer across the gum-saliva interface.

A model for describing the flavor release from gel particles was developed by Lian (30). The model relates release rates to the composition (oil/water) and particles size and takes into account the resistance to mass transfer in both the particle and the bulk liquid phase.

In general, both release mechanisms are involved during the consumption of solid foods. The profile of the released flavor changes as soon as the water-soluble phase has been dissolved. De Roos and Wolswinkel (8) used the non-equilibrium partition model to develop a computer program for predicting flavor release from chewing gums without providing details about the mathematical relationships. Chewing gum is a two-phase system consisting of a water-soluble sugar phase and a water-insoluble gum phase. This means that the model had to cover partitioning and mass transfer between four phases, namely gum, sugar, liquid and gas phase.

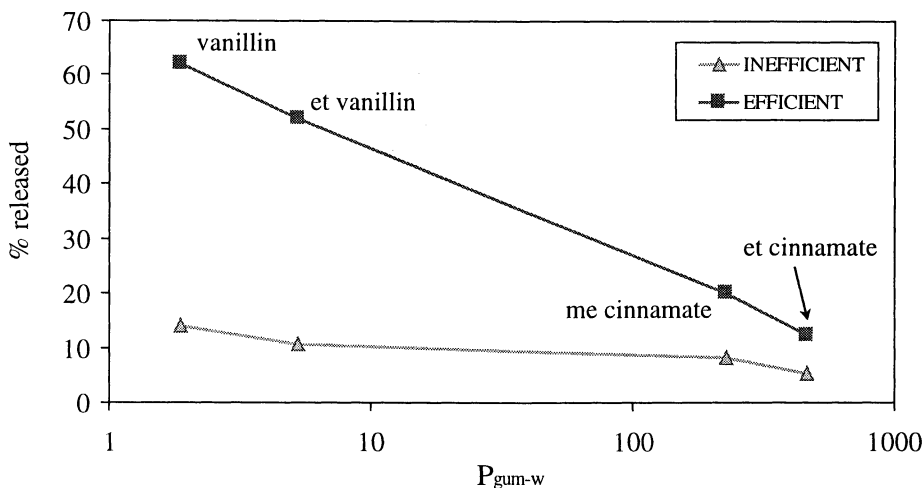


Figure 5. Effect of chewing efficiency on flavor release from chewing gum measured after 0.5 h of mastication (8).

Complicating Factors

There are several factors that complicate the development of mathematical models for describing flavor release from solid products. Examples of such complicating factors are the compartmentalization of flavor compounds and precursors (31) and the need to rehydrate the hydrophilic glassy matrix of foods in order to release the entrapped flavor (32). In both of these cases, there is no clear relationship between flavor release and product composition as with liquid products. It seems that flavor release is determined by the microenvironment in which the flavor compounds are entrapped rather than by the gross composition of the product.

The effect of compartmentalization is illustrated by the example of Figure 6 showing the flavor release from chewing gum. Chewing gum is a two-phase system consisting of about 20% of a water-insoluble gum base and 80% of a water-soluble sugar phase. Compartmentalization was here achieved by encapsulation of the flavoring in a water-soluble carbohydrate matrix, which prevents absorption of the flavor compounds by the gum base. As expected, the release of the liquid flavoring is typical for an extraction type release: it is slow and large differences in release rates are observed. On the other hand, a quick and uniform release is observed with the encapsulated flavoring due to the rapid dissolution of the water-soluble carbohydrate matrix in the saliva. The release of the encapsulated flavoring is not 100% as might have been expected. This indicates that resorption of the flavor compounds by the gum base has taken place during shelf life and/or during consumption.

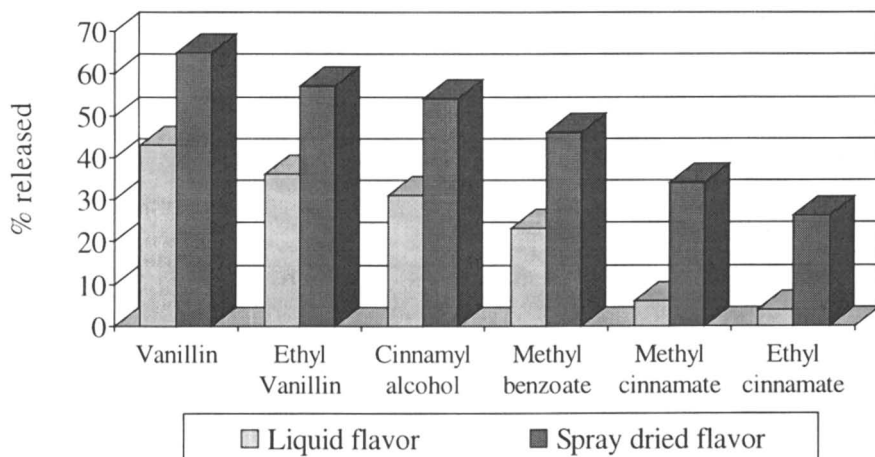


Figure 6. Effect of encapsulation on flavor release from chewing gum measured as percentage released after 5 minutes of chewing.

In principle, the same physico-chemical models could be used for predicting the flavor release of compartmentalized and un compartmentalized flavors, provided that the model takes into account that different release mechanisms are involved, each of which is rate determining at a different time. In fact, the only difference between products with liquid and encapsulated flavoring is the different distribution of the flavor compounds over the hydrophilic and hydrophobic phases.

Conclusions

Depending on product type and the conditions under which the flavor is perceived, flavor release can be properly described by three different basic physico-chemical models:

- Stagnant film model: assumes that mass transport is by molecular diffusion.
- Penetration model: which assumes that mass transport is by molecular and eddy diffusion.
- Non-equilibrium partition model: assumes that mass transport is by eddy diffusion.

By far, most work has been done on modeling of flavor release under dynamic systems that mimic flavor release in the mouth. In comparison, little attention has been paid to flavor release from static product phases, which is characteristic for flavor perception by smell.

Prediction of flavor release in the mouth is complex due to the rapidly changing conditions during consumption (liquid foods), compartmentalization of the flavor

compounds and differences in chewing efficiency (solid foods). Useful mathematical models have been developed that address some of these complicating factors. However, most of modeling is based on results from model systems. Until recently, only sporadic attempts have been made to relate the theoretical predictions to *in vivo* flavor release and perception (12, 16, 17, 23). However, with the development of sensitive methods for measurement of flavor release in the mouth (33) we are now seeing more attempts to relate theoretical predictions to *in vivo* flavor release and perception (34-36).

References

- Hall, G.; Anderson, Lebensm. Wiss. u. Technol. **1983**, *16*, 362.
- Nelson, P.E.; Hoff, J.E., *J. Food Sci.* **1968**, *33*, 479.
- Williams, A.A.; Rosser, P.R., *Chem. Senses*, **1981**, *6*, 149.
- Escalona-Buendia, H.; Piggott, J.R.; Conner, J.M.; Paterson, A., *Dev. Food Sci. (Food Flavors: Formation, Analysis and Packaging Influences)*, **1998**, *40*, p 615.
- Roberts, D.D.; Elmore, J.S.; Langley, K.R.; Bakker, J., *J. Agric. Food Chem.* **1996**, *44*, 1321.
- Nahon, D.F.; Koren, P.A.N. y; Roozen, J.P.; Posthumus, M.A., *J. Agric. Food Chem.* **1998**, *46*, 4963.
- Harrison, M.; Hills, B.P. *J. Agric. Food Chem.* **1997**, *45*, 1883.
- De Roos, K.B.; Wolswinkel, C., *Trends in Flavor Research*. Maarse, H.; Van der Heij, D.G., Eds., Elsevier Science B.V., Amsterdam, 1994, p 15.
- Harrison M.; Hills, B.P.; Bakker, J.; Clothier, T., *J. Food Sci.* **1997**, *62*, 653.
- Overbosch, P.; Afterof, W.G.M.; Haring, P.M.G., *Food Review International* **1991**, *7*, p 137.
- De Roos, K.B.; Sarelse, J.A. *Flavor Science. Recent developments*, Taylor, A.J.; Mottram, D.S., Eds.; The Royal Society of Chemistry: Cambridge, 1996, p13.
- McNulty, P.B., *Food Structure and Behaviour*, Blanshard, J.M.V.; Lillford, P., Eds., Academic Press: London, 1987, p 245.
- Darling, D.F.; Williams, D.; Yendle, P., *Interactions of Food Components*. Birch, G.G.; Lindley, M.G.; Eds., Elsevier: London, **1986**, p 165.
- Harrison, M.; Hills, B.P. *Intern J. Food Sci Technol.* **1997**, *32*, 1.
- Whitman, W.G., *Chem Eng. Metal.* **1923**, *29*, 46.
- Hills, B.P.; Harrison, M., *Int. J. Food Sci. Technol.* **1995**, *30*, 425.
- McNulty, P.B. PhD Thesis, Massachusetts Institute of Technology, Cambridge, Massachusetts, 1972.
- P.B. McNulty, P.B.; Karel, M., *J. Food Technol.* **1973**, *8*, 319.
- De Roos, K.B.; Graf, E., *J. Agric. Food Chem.* **1995**, *43*, 2204.
- Marin, M.; Baek, I.; Taylor, A.J. In *Flavor Release*; Roberts, D.D; Taylor, A.J., Eds.; ACS Symposium Series, American Chemical Society, Washington, D.C., 2000.
- Harrison, M., *J. Agric. Food Chem.* **1998**, *46*, 2727.

22. Brauss, M.S.; Linforth, R.S.T.; Cayeux, I.; Harvey, B.; Taylor, A.J., *J. Agric Food Chem.* **1999**, *47*, 2055.
23. De Roos, K.B., *Food Technol.* **1997**, *51*, 60.
24. Graf, E.; de Roos, K.B. In *Flavor-Food Interactions*. McGorin, R.J.; Leland J.V., Eds., ACS Symposium Series 633, American Chemical Society, Washington, DC, 1996, pp 24-35.
25. M.E. Malone, I.A.M. Appleqvist, T. Golf, J.E. Homan, J.P.G. Wilkins, *ACS Symposium book*
26. Graf, E; van Leersum, J.P., U.S. Patent 5,536,519, July 16, 1996.
27. Bouwmesters, J.F.G.; de Roos, K.B. WO Patent 9815192, 1998.
28. Harrison, M.; Hills, B.P., *Intern J. Food Sci Technol.* **1997**, *31*, 167.
29. Harrison M.; Campbell, S.; Hills, B.P., *J. Agric. Food Chem.* **1998**, *46*, 2736.
30. Lian, G. In *Flavor Release*; Roberts, D.D; Taylor, A.J., Eds.; ACS Symposium Series, American Chemical Society, Washington, D.C., 2000.
31. Linforth, R.S.T.; Ingham, K.E.; Taylor, A.J., *Flavor Science: Recent Developments*, Mattram, D.S.; Taylor A.J., Eds. Royal Society of Chemistry, London, U.K., 1996, p 361.
32. Clawson, A.R.; Linforth, R.S.T.; Ingham, K.E.; Taylor, A.J., *Lebensm.-Wiss. U-Technol.* **1996**, *29*, 158.
33. Taylor, A. J.; Linforth, R. S. T. In *Flavor Release*; Roberts, D.D; Taylor, A.J., Eds.; ACS Symposium Series, American Chemical Society, Washington, D.C., 2000.
34. Harrison, M. In *Flavor Release*; Roberts, D.D; Taylor, A.J., Eds.; ACS Symposium Series, American Chemical Society, Washington, D.C., 2000.
35. Harvey, B.A.; Brauss, M.S.; Linforth, R.S.T.; Taylor, A.J. In *Flavor Release*; Roberts, D.D; Taylor, A.J., Eds.; ACS Symposium Series, American Chemical Society, Washington, D.C., 2000.
36. Moore, I.P.T.; Dodds, T.M.; Turnbull, R.P.; Crawford, R.A. In *Flavor Release*; Roberts, D.D; Taylor, A.J., Eds.; ACS Symposium Series, American Chemical Society, Washington, D.C., 2000.

Chapter 12

Flavor Release from Emulsions and Complex Media

A. Voilley¹, M. A. Espinosa Diaz², C. Druaux³, and P. Landy³

¹ENSBANA, Université de Bourgogne,

1 Esplanade Erasme, F-21000 Dijon, France

²Givaudan Roure, Ueberlandstrasse 138, CH-8600 Switzerland

³Unilever Research, Olivier van Noortlaan 120,
3133 AT Vlaardingen, the Netherlands

The food matrix plays an important role in controlling flavor release at each step of food product preparation and consumption. Flavor release depends on the ability of the aroma compounds to be in the vapor phase and therefore on their affinity for the product, which participates in their rate of transfer. This is the reason why many studies of physicochemical interactions between volatiles and other constituents of the matrix have been extensively reported in simple model systems. The aim of this paper is to clarify the thermodynamic and kinetic properties of volatiles not only in relation to the composition but also with regard to the microstructure in order to explain the phenomena involved in flavor release. The results obtained recently in our group in the case of emulsions and model cheeses will be discussed; especially the modeling of mass transfer at the interface between the lipid and the aqueous phases in the matrix.

Flavor release depends on the affinity of the odorants for the food product, and therefore on their availability for the vapor phase. This is the reason why studies of the physicochemical interactions that occur between volatile and other constituents of the matrix have been so thoroughly reviewed (1-3). Past research was focused on using sensory evaluation or instrumental measurements to gain a better understanding of the mechanisms that occur between aroma compounds and non-volatile substances. The systems considered were often very simple, consisting of an aroma compound and a single constituent, usually in an aqueous solution. In general, the presence of proteins, polysaccharides, and lipids reduces the volatility of aroma compounds with respect to that in pure water, whereas the presence of salts increases their volatilities. Few studies have been reported on the volatility of aroma compounds in emulsions (4-5).

In physicochemical terms, key features influencing transfer and release are the presence of the interface between the aqueous and lipid phase, the surface area of the interface, and the nature of the surface active agent absorbed at this oil-water interface. Mathematical models describing flavor release from liquid emulsions have been developed by Mc Nulty (6) and Harrison and Hills (7). The first model is based on mass balance and partition coefficients of aroma compounds in the emulsion, whereas the second one is based on the penetration theory of interfacial mass transfer where the transfer through the emulsion-gas interface is the rate-limiting step. The penetration theory takes into account that the boundary layers are often not completely stagnant and that there is also mass transport by eddy diffusion. Mass transfer between the phases takes place when a volume element from the bulk phase comes into contact with a phase boundary for a short fixed time. During this fixed time contact, mass transfer takes place by molecular diffusion. Subsequently, the volume element is remixed with the bulk phase and the whole process is repeated. The penetration model predicts that the mass transport coefficient varies with the square root of the diffusion coefficient. Under dynamic conditions, the square root is often nearer to the truth.

The objective of this study is to show how various factors, especially composition and structure of the matrix, can influence flavor release from emulsion and complex media, and are also explained by modeling.

Materials and Methods

Six aroma compounds have been selected and their physicochemical characteristics are given in Table I. They were provided by International Flavors and Fragrances (Longvic – France) and their purity was higher than 98%.

Table I. Physicochemical Characteristics of Aroma Compounds

Aroma compound	Formula	Molecular weight	Saturated vapor pressure (Pa) 25°C		Solubility in water (g/100mL) 25°C	Log P calc**
			exp.	calc*.		
Diacetyl	C ₄ H ₆ O ₂	86	7599.2	6266	25 (15°C)	- 2.0
2-Nonanone	C ₉ H ₁₈ O	142	53.3	26.7	0.04	2.9
Ethyl acetate	C ₄ H ₈ O ₂	88	-	12265.5	8.6	0.6
Ethyl butyrate	C ₆ H ₁₂ O ₂	116	-	1599.8	0.6	1.7
Ethyl hexanoate	C ₈ H ₁₆ O ₂	144	-	133.3	0.05	2.8

* Calculated from Lee-Kesler model (8)

** Calculated from Rekker method (9)

The chemicals and food ingredients (sodium caseinate, β -lactoglobulin, triolein, n-dodecane, miglyol) used in this study were of analytical grade and purchased from suitable suppliers in France.

Processed cheese was prepared according to the technique described by Druaux (10) with essentially anhydrous milk fat, cheddar, and milk powder. Quantitative descriptive analysis on flavor attributes was performed on the cheeses, using a trained panel. The vapor-liquid partition coefficient or the volatility of aroma compounds was determined by equilibrium headspace analysis or by exponential dilution (11). This last method consists of exhausting the liquid phase of volatile compounds in equilibrium with the vapor phase. An inert gas passed through the liquid phase and carried the volatile compound into the headspace. The system was thermostated at 25°C. A sample of the vapor phase was automatically injected into a gas chromatograph at regular intervals. The variation of the chromatographic peak of the solute is an exponential function of time, provided the detector response is linear.

The diffusivity of aroma compounds was determined by using the Stokes cell (12). The cell with a porous diaphragm enables simple measurements and specifies the diffusivity within a low viscosity medium. This method is the most often used and consists of following the variation of concentration difference between solutions placed in two compartments separated by a fritted glass.

“The rotating diffusion cell” technique was used to measure the mass transfer of solutes through diffusion layers and liquid-liquid interfaces (13). The rotating diffusion cell is designed hydrodynamically in such a way that stationary diffusion layers of known thickness are created on each side of the oil layer. The thickness of the stagnant aqueous layers Z (m) present at each side of the filter filled with oil is given by the Levich equation:

$$Z = 0.643 \eta^{\frac{1}{6}} D_{aq}^{\frac{1}{3}} \omega^{-\frac{1}{2}} \quad \text{eq 1}$$

where η = viscosity of the aqueous phase (m^2/s),
 D_{aq} = solute diffusion coefficient in the aqueous phase (m^2/s),
 ω = rotation speed of filter (s^{-1}).

The total or the overall resistance $1/k$ ($\text{m}^{-1}\cdot\text{s}$), or R of a solute diffusing from one aqueous phase to another through the oil layer is expressed as follows:

$$R = \frac{1}{k} = \frac{2Z}{D_{aq}} + \frac{2}{\alpha k_i} + \frac{l}{\alpha D_{oil} P} \quad \text{eq 2}$$

where α = porosity of the filter (0.8),
 k_i = permeability coefficient (m/s),
 l = filter thickness (m),
 D_o = solute diffusion coefficient in oil (m^2/s),
 P = solute liquid-liquid partition coefficient

The significance of the three terms of eq. 2 is as follows:

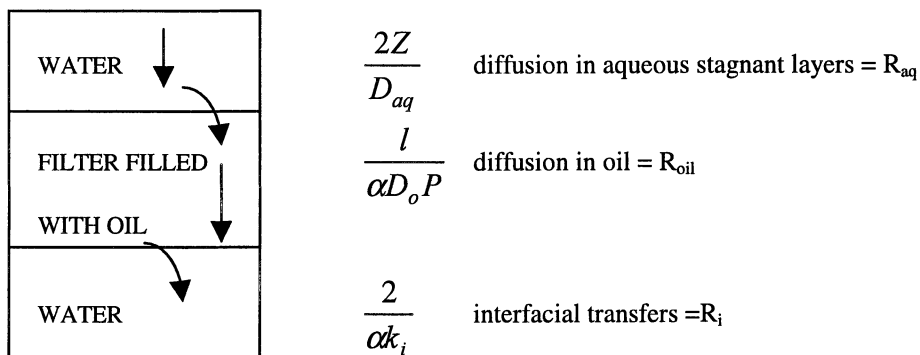
$2Z/D_{aq}$ (denoted R_{aq}) describes the resistance to diffusion through the two stagnant aqueous diffusion layers of thickness Z that are established at each side of the filter,

$2/\alpha k_i$ (denoted R_i) relates to the resistance due to the solute transfer across the two aqueous phase/oil interfaces,

$l/\alpha D_o P$ (denoted R_{oil}) is the contribution of the diffusion through the lipid in the filter. Eq.2 is then simplified:

$$\frac{1}{k} = R_{aq} + R_{oil} + R_i \quad \text{eq 3}$$

RESISTANCE OF A SOLUTE TO:



The experimental device to measure the effect of the matrix breakage on flavor release is given in Figure 1.

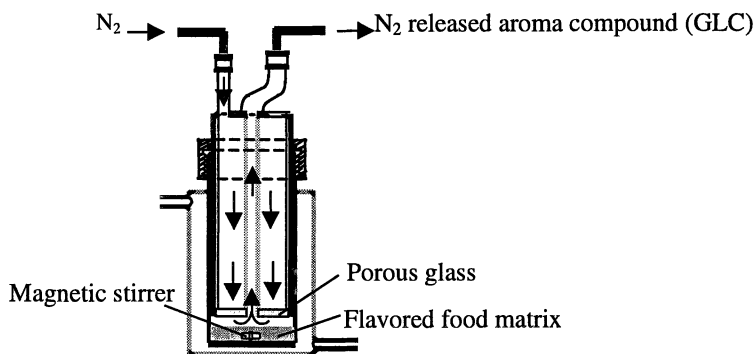


Figure 1. Experimental device used to measure flavor release from a model food matrix.

The surface of the stirred, flavored food matrix was swept by an inert gas. The aroma compounds in the gas were analyzed by gas-liquid chromatography (GLC) with a flame ionisation detector (14).

For the emulsions, which were prepared by mixing with an Ultra Turrax homogenizer, the droplet size distribution and the fat globule aggregation percentage were determined with a Malvern Mastersizer laser diffractometer (10).

Results and Discussion

The effect of food matrix composition and structure on flavor release will be presented and discussed through complementary studies carried out by thermodynamic or kinetic approaches.

Volatility of Aroma Compounds

Interactions between aroma compounds and non volatile constituents may be of two types: reversible and low energy or irreversible and high energy. In the latter case, the sensorial perception of the aroma compounds is qualitatively changed. In our study, only reversible physicochemical interactions of systems at equilibrium are considered. In this case, interactions occur at the molecular level and are expressed at a macroscopic level as changes in the equilibrium between the product and the vapor phase. The values of the vapor-liquid partition coefficients, K_i^∞ , are given in Table II, for a concentration of the volatiles of 100 ppm. The most hydrophobic aroma compounds have the highest volatility at infinite dilution in water .

Table II. Vapor-Liquid Partition Coefficients of Aroma Compounds in Water (25°C)

<i>Aroma Compound</i>	K_i^∞ in water
Diacetyl	0.6
2-Nonanone	34
Ethyl acetate	9.6
Ethyl butyrate	13.5
Ethyl hexanoate	34

Adding 5 g/L of sodium caseinate decreases the aroma compound volatility. For example, the retention by the protein in relation to water is 7.4% for ethyl butyrate and 35.3% for ethyl hexanoate. This effect is much more pronounced in triolein showing that the affinity of the aroma compounds for oil is higher than for pure water or water

with protein (15). Mixing water and lipid together also decreases the vapor-liquid partition coefficient for most aroma compounds except for very hydrophilic compounds such as diacetyl. The vapor-liquid partition coefficients (K_b) can be predicted with a simple model based on mass balance (16).

$$K_b = \frac{1}{F_{lip} \frac{1}{K_{lip}} + F_{aq} \frac{1}{K_{aq}}} \quad \text{eq 4}$$

where F_{lip} , F_{aq} are the volume fractions of the lipid and aqueous phases, respectively; K_{lip} , K_{aq} are the partition vapor-liquid coefficients of aroma compound in lipid and aqueous phases, respectively.

There is a good agreement between experimental and calculated values of K_b ; the deviation has been shown to be about 10% for the system containing only water and oil. However, this simple model shows some limits in more complex systems (Table III).

Table III. Volatility of 2-Nonanone in Different Media (25°C)

<i>Medium</i>	<i>Vapor-Liquid Partition Coefficient</i>
Water	33.6
n-Dodecane	0.04
Water + Sodium caseinate (3%) + n-Dodecane (0.05%)	7.9 22.7
0.05% n-Dodecane + 3% sodium caseinate:	
- Non emulsified	19.3
- Emulsified (droplet size 6 μ m, protein surface coverage : 25 mg.m ⁻²)	1.2
- Calculated (16)	15.8

As compared with pure water, the volatility of 2-nonanone decreased in the presence of sodium caseinate (22.7) and even more in n-dodecane (7.9). For non-emulsified biphasic systems the theoretical value calculated from the Buttery equation is very similar to the experimental one. After emulsification of the biphasic system, the air-product partition coefficient of 2-nonanone was dramatically decreased. That may be due to the high affinity of the hydrophobic 2-nonanone as the protein adsorbed at the interface of the fat droplets.

Mass Transfer of Aroma Compounds

The kinetic behavior of aroma compounds in food must also be taken into account in order to explain sensory results. One way is to determine the mass transfer in one phase.

$$J_i = -AD_i \frac{dC_i}{dx} \quad \text{eq 5}$$

where J_i , flux of aroma compound (kg/s),
 A , surface area (m²),
 dC_i , concentration gradient of solute i (kg/m³),
 dx , distance (m).

From the given conditions, the diffusivity (D_i , m²/s) can be calculated from an analytical solution given by Crank (17) or from Perkins and Geankopolis model (18).

Generally, diffusivity of aroma compounds is of the same order of magnitude for a fixed medium. However, a slight decrease in diffusivity is observed when the molar volume of aroma compounds increases within a homologous series. This effect is much more pronounced with the addition of dry matter such as sodium caseinate (Table IV). All the values were obtained by using the Stokes cell.

Table IV. Molar volume and diffusivity of aroma compounds (25°C)

Aroma Compound	Molar Volume	Diffusivity ($\times 10^{10}$) (m ² /s)		
		Water	5% sodium caseinate	
Diacetyl	96.2	8.5	5.1	-
Ethyl acetate	108.6	11.7	3.3	-
Ethyl butyrate	153.0	9.4	2.5	1.6*
Ethyl hexanoate	197.4	7.0	1.4	1.4*

* calculated from Perkins and Geankopolis model (18)

These results are in agreement with those obtained by different authors (19, 20). Generally, under these conditions, there is a reduction of the flux of the volatiles with dry matter.

The diffusivity of aroma compounds measured in the bulk solution is only a part of the phenomena involved in heterogeneous systems such as in emulsions. The rotation diffusion cell method enabled us to carry out a study on the mass transfer of solutes from aqueous phase to oil and from oil to aqueous phase (21).

Examples of results are given for ethyl esters through a layer of miglyol at 25°C in the presence and absence of sodium caseinate (Table V).

Table V. Transfer of Ethyl Esters Through a Miglyol Layer (25°C)

<i>Aroma Compound</i>	<i>Water</i>			<i>5% Sodium Caseinate</i>		
	R_{aq}	R_{oil}	R_i	R_{aq}	R_{oil}	R_i
Ethyl acetate	35	27.4	37.6	59.2	16.6	24.2
Ethyl butyrate	86.2	6.7	7.1	78.0	5.3	16.7
Ethyl hexanoate	74.4	0.4	25.2	58.8	0.3	40.9

The percentages are calculated by considering that at $\omega^{-1/2} = 0.87 \text{ s}^{-1/2}$, $1/k$ corresponds to 100 % of the resistances ($R_{aq} + R_{oil} + R_i$).

In the presence of water only, one of the important rate limiting steps in the transfer of ethyl acetate is the transfer through the oil-water interfaces; for the other solutes, the rate limiting step is the transfer through the aqueous stagnant layers.

Sodium caseinate has been observed to increase the resistance through the aqueous layer (R_{aq}) for ethyl acetate and to increase the interfacial resistance (R_i) for ethyl butyrate and ethyl hexanoate.

Effect of the Matrix Breakage on Flavor Release

2-Nonanone release from different media (water; gel with 6.9% β -lactoglobulin; emulsion with 5% miglyol and 6.9% β -lactoglobulin and gelified emulsion) was studied as a function of time. The gelation of the flavored protein solution or emulsion took place at 76°C during 10 minutes. The profiles of 2-nonanone remaining in of the medium differ depending on the presence of lipid in the medium (Figure 2).

The initial flux of 2-nonanone (expressed in ppm/min/cm²) varies with the dry matter content and the structure (Table VI).

To better understand the effect of the composition and structure of the matrix, the percentage of 2-nonanone released was determined after 200 minutes with or without gel breakage. The obtained values are 83.5% and 78.3% respectively (14). The retention depends not only on the interactions between protein and aroma compound but also on the protein network.

In more complex system, processed cheese flavored with 2-nonanone, it has been observed that some products containing the same amount of aroma compounds display different scores for flavor intensity (10). The score for a processed cheese with a 100% aggregation of the fat droplets was 50.8. However, the intensity score was 67.3 when none of the droplets were involved in fat aggregates (percentage of aggregation: 0%). This clearly points out that the composition of the product is not the only parameter to take into account when studying flavor release.

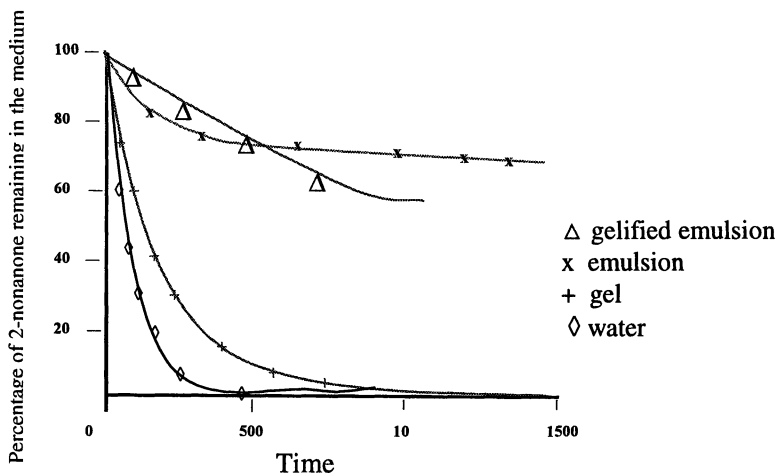


Figure 2. Flavor release from different media versus time (min) at 37°C: water (\diamond), gel (+), emulsion (x), gelified emulsion (Δ). The initial concentration of 2-nonanone is 300 ppm.

Table VI. Flavor Release From Different Media Versus Time

2-Nonanone	Flux (ppm/min/cm ²)
In water (\diamond)	1.24
In gel (+)	0.40
In emulsion (x)	0.03
In gelified emulsion (Δ)	0.02

To explain these results, the release of 2-nonanone in the vapor phase above the processed cheeses was measured using dynamic headspace with the exponential dilution device. There is no effect of structure of the processed cheese (droplet size, percentage of aggregation) in the case of a non-diluted, non-stirred product (Table VII).

When the product was diluted in water at 20 % (m/m) and stirred (200 rpm) simultaneously with the measurement of the flavor release, it appeared that both the droplet size and the percentage of aggregation affected the kinetics of release of 2-nonanone (Figure 3).

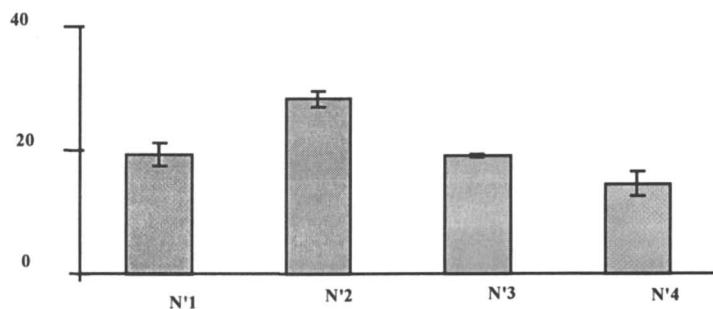
A lower droplet size and percentage of aggregation, leads to a higher effective surface area between the fat and the aqueous phase, and this faster flavor release.

These results confirm the important role of the mass transfer at the interfaces, which could be a limiting factor.

Table VII. Release of 2-Nonanone from Model Cheeses at 35°C
measured by using dynamic headspace without breakage.

<i>Model cheese</i>		<i>Surface area GLC</i>
Droplet size (μm)	Percentage of aggregation (%)	(vapor phase)
0.45	0	12500 (1.7)
0.28	100	13100 (4.5)

(), Coefficient of Variation (%)



Droplet size (μm) 0.45 0.28 0.50 0.28
 Aggregation (%) 0 0 83 100

Figure 3. Release of 2-nonanone from model cheeses – 35°C using dynamic headspace after dilution in water and with stirring during the experiment.

Conclusion

In conclusion, from a physicochemical point of view, flavor release from emulsions depends on the matrix (composition, concentration, structure but also protein conformations) and on the aroma compounds (volatility, hydrophobicity but also affinity for the matrix). In the future, studies on the relative roles of different interfaces, especially in the transfer rate of the volatiles (water and aroma compounds), and competition between volatiles in relation with the matrix, must be developed in the modeling of flavor release.

References

1. Solms, J. In *Interactions of Foods Components*; Birch, G.C.; Lindley, M.G., Eds. Elsevier Applied Science: London, U.K., 1986; pp 189-210.
2. Kinsella, J.E., *Int. News Fat Oils Relat. Matter.* **1990**, *1*, 215-226.
3. Bakker, J. In *Ingredient Interactions. Effect on Food Quality*; Gaonkar, A.G., Ed.; Marcel Dekker, Inc.: New York, U.S., 1995; pp 411-439.
4. Land, D.G. In *Progress in Flavor Research*; Land, D.G.; Nursten, H., Eds.; Applied Sciences: London, U.K., 1978; pp 53-56.
5. Dubois, C.; Sergent, M.; Voilley, A. In *Flavor-Food Interactions*; McGorin, R.J.; Leland, J.V., Eds; American Chemical Society: Washington D. C., U.S., 1996; pp 217-228.
6. McNulty, P.B.; Karel, M., *J. Food Technol.* **1973**, *8*, 309-318.
7. Harrison, M.; Hills, B., *Int. J. Food Sci. Technol.* **1997**, *32*, 1-9.
8. Lee, B.I.; Kesler, M.G., *AIChE J.* **1975**, *21*, 510-527.
9. Rekker, R.F. *Pharmacochemistry Library*; Nauta, W.; Rekker, R.F., Eds.; Elsevier Scientific: Amsterdam, N.L., 1977.
10. Druaux, C. Ph.D. thesis, Université de Bourgogne, Dijon, France, 1997.
11. Sorrentino, F.; Voilley, A.; Richon, D., *AIChE J.* **1986**, *32*, 1988-1993.
12. Voilley, A. Ph.D. thesis, Université de Bourgogne, Dijon, France, 1975.
13. Harvey, B.A.; Druaux, C.; Voilley, A. In *Food Macromolecule and Colloids*; Dickinson, E.; Lorient, D., Ed.; The Royal Society of Chemistry: Cambridge, U.K., 1995; pp 154-163.
14. Espinosa-Diaz, M.A. Ph.D. thesis, Université de Bourgogne, Dijon, France, 1999.
15. Landy, P.; Courthaudon, J.-L.; Dubois, C.; Voilley, A., *J. Agric. Food Chem.* **1996**, *44*, 526-530.
16. Buttery, R.G.; Guadagni, D.G.; Ling, L.C., *J. Agric. Food Chem.* **1973**, *21*, 198-201.
17. Crank, J. *The Mathematics of Diffusion*; Clarendon Press.: Oxford, U.K., 1975; pp 414.
18. Reid, C.R.; Prausnitz, J.M.; Poling, B.E. *The Properties of Gases and Liquids*; McGraw-Hill Book Company: New York, U.S., 1987; pp 741.
19. Chandrasekaran, S.K.; King, C.J. *AIChE J.* **1972**, *18*, 513-520.
20. Darling, D.F.; Williams, D.; Yendle, P. In *Interactions of Foods Components*; Birch, G.C.; Lindley, M.G., Ed.; Elsevier Applied Science: London, U.K., 1986; pp 165-188.
21. Landy, P.; Rogacheva, S.; Lorient, D.; Voilley, A., *Colloids and Surfaces B: Biointerfaces.* **1998**, *12*, 57-65.

Acknowledgement: M.-A Espinosa-Diaz and C. Druaux would like to thank CONACYT and Le Conseil Regional de Bourgogne, respectively, for financial support.

Chapter 13

Flavor Release as a Unit Operation: A Mass Transfer Approach Based on a Dynamic Headspace Dilution Method

Michèle Marin¹, I. Baek², and Andrew J. Taylor²

¹Food Process Engineering Department, INAPG-INRA,
78850 Thiverval-Grignon, France

²Division of Food Sciences, University of Nottingham, Loughborough,
Leicestershire LE12 5RD, United Kingdom

In physical terms, the mass transfer of flavor compounds between two (or more) phases is the main mechanism of flavor release. Flavor release between air and static aqueous solutions has been studied with the API-MS device. Using both mass transfer modeling and experimental results obtained from a dynamic dilution method, the contribution of the physical properties of the volatiles as well as the environmental conditions in the system were evaluated. Thermodynamic and kinetic properties of five volatiles were estimated for different aqueous solutions, with a variable concentration of sugar. It was also pointed out that the flavor release is at first a function of the volatility of the flavor molecule (**K**, the partition coefficient at equilibrium). Furthermore, kinetic properties (mass transfer coefficient) as well as hydrodynamic parameters (Reynolds number, flow rate, surface exchange area) were collected in an original dimensionless term and its effect on the flavor release was discussed depending on the value of **K**.

A quantitative description of flavor perception in a food product needs to take into account mechanisms that are complex and which differ, depending on the type of food studied. The consumer appreciation of flavor release includes psychosensorial aspects as well as social ones. Nevertheless, it is well known that physics and chemistry play a major role. Modeling the physical mechanism of flavor release is not new. Most of the emphasis has been placed on the volatile flavor compounds (1, 2, 3). The physical mechanism of flavor release is based on sequential transfer of volatile flavor molecules (aroma compounds) from one phase to another. Initially the volatile compounds are contained in a food product but ultimately, the volatiles have to be transported into the air phase so they can reach the olfactory receptors. For

example, when a container of food (bottle, bag, can) is opened, the volatiles are diluted by the surrounding air and transported to the olfactory receptors by the orthonasal route. In the mouth, food is coated with saliva, broken down by mastication and the flavor compounds are transported across the saliva film to the air-ways of the nose by the retronasal route. In both cases, environmental conditions like temperature, size of the food product, or velocity of the gas flow have an important effect on the release.

Using a chemical engineering approach, this paper seeks to identify the key physical parameters controlling flavor release from a product to the air phase. Flavor release was studied as a unit operation, such as distillation, stripping or extraction. Indeed, mass transfer of the flavor compounds are associated with momentum and heat transfer, and concepts like equilibrium stage, mass balance, and transfer are powerful analogies.

The theoretical approach developed was based on experimental data obtained with a technique that allowed the release of a series of molecules to be monitored simultaneously, under dynamic headspace conditions, and in different environmental systems (4). Thus, the model was developed to describe the release from a static liquid phase, and from this, the key factors controlling the physical mechanism were obtained. Although the model was developed for a simple system, the principles behind the model were capable of further extrapolation to other flavor release situations.

A Dynamic Headspace Dilution Method

Using Atmospheric Pressure Ionization Mass Spectrometry (API-MS), an interface has been developed that allows real time measurement of volatile release at low concentrations (5). Headspace sampling methods have been developed to measure static headspace as well as dynamic release of volatile compounds present in different kind of mediums (food products) and over short time periods (less than 10 minutes) (6).

The theoretical approach is based on the experimental conditions which involve a liquid phase containing several volatiles in a closed cell. After equilibrium between the liquid and air at atmospheric pressure, the gas phase was diluted by introducing fresh air at a fixed flow rate (Figure 1). The liquid phase contained five aroma compounds at low concentrations (from 10^{-3} to 10^{-4} kg/m³), and at a constant temperature (25°C). This system resembles the situation in real food products such as beverages, when a sealed container (volatile under equilibrium) is opened and the volatiles are diluted by the surrounding air over time. The volatile profile resulting from this process is perceived by consumers during their first “sniff” and can play a major role in food acceptance.

By connecting the air outlet of the cell via the interface to the API-MS equipment, the concentration of each volatile as a function of time was determined as mg/m³ after calibration with authentic standards. An example of an experimental release curve is given in Figure 2. At the start of the experiment, the system was

sealed to ensure equilibrium between the air and liquid phases. Thus, the first concentration (time equal to zero) measured through the API-MS was the equilibrium concentration in the headspace but, thereafter, the decrease in concentration of each compound was measured with time.

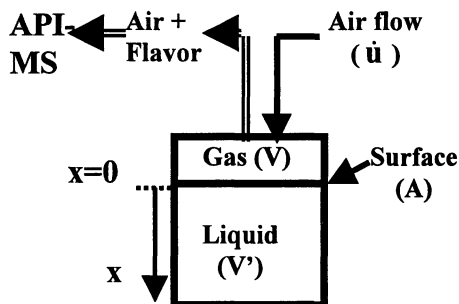


Figure 1. Schematic view of the cell.

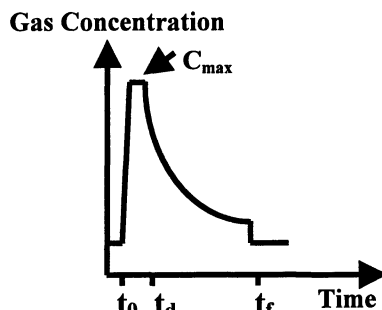


Figure 2. Curve shape as volatiles are detected as a function of time from API-MS device (t_0 =connection, t_d =dynamic headspace dilution, t_f =disconnection)

Mass Transfer of Flavor Compounds

As air flows through the headspace of the system, the concentration of the volatile in the gas phase as a function of time ($C(t)$ in kg/m^3) is the result of a mass balance between release from the sample phase and removal in the air stream crossing the system:

$$V \cdot \frac{dC(t)}{dt} = J(t) \cdot A - \dot{u} \cdot C(t) \quad \text{eq 1}$$

V is the fixed volume of the whole gas compartment (m^3), assuming a well-mixed gas phase. A is the sample-gas interface area (m^2) and \dot{u} is the gas flow rate through the system ($\text{m}^3 \cdot \text{s}^{-1}$).

The mass flux ($J(t)$) through the surface is the result of the transport from the sample to the air which was composed of three steps.

Diffusion of the Volatile from the Bulk of the Sample to the Interface

During the short experimental time frame, it was assumed that the concentration of the volatiles in the bulk liquid phase ($C'(x,t)$ in kg/m^3) remained constant and was only modified in the liquid layer near the interface. The sample was considered as a semi-infinite medium. The expression of mass transport of the volatile in the liquid

was first represented with the generalized Fick law (7). For a mono-directional transport along the x-axis (x distance from the interface), the differential equation is:

$$\frac{dC'(x, t)}{dt} = D \cdot \frac{d^2C'(x, t)}{dx^2} \quad \text{eq 2}$$

The diffusion coefficient (D) depends on the type of volatile, the medium, and the temperature.

Partition of the Molecule at the Interface

At the interface itself, a local thermodynamic equilibrium can be assumed (8). The relationship between the concentration in the sample and the gas phase is usually given by the partition coefficient (K):

$$K = \frac{C}{C'} = \left(\frac{\gamma_i \cdot P_i^0(T)}{P_T} \right) \cdot \frac{\bar{V}^l}{\bar{V}^g} \quad \text{eq 3}$$

where $P_i^0(T)$ is the vapor pressure for the pure component i (Pa), P_T , the total pressure in the gas phase (Pa) and, \bar{V}^l and \bar{V}^g are the volume for one mole of the liquid and of the gas phases respectively ($\text{m}^3 \cdot \text{mol}^{-1}$). If the volatile is highly diluted in the liquid phase, the activity coefficient γ_i can be assumed to be independent of the concentration of the volatile in the liquid, and is equal to a constant value γ_i^∞ . In this case, the product $\gamma_i^\infty \cdot P_i^0(T)$ is a constant (Henry's constant), reflecting the molecule volatility in the medium. Then, K depends only on the temperature (9).

Transport of the Molecule in the Gas Phase

Knowing that the gas phase is flowing over the sample surface, mass transport can be represented with an empirical mass transfer coefficient (kg) that is analogous to a diffusion coefficient divided by an equivalent limiting layer thickness, with:

$$J(t) = kg(C^* - C(t)) \quad \text{eq 4}$$

C^* is the concentration ($\text{kg} \cdot \text{m}^{-3}$) in the gas phase at the gas-liquid interface (wall), which is equal to $K \cdot C'(x=0)$, the product of the partition coefficient with the liquid concentration at the wall. Hence:

$$J(t) = kg(K \cdot C'(x=0, t) - C(t)) \quad \text{eq 5}$$

At the interface between liquid and gas, the mass transfer is represented by:

$$-D \left(\frac{dC'(x, t)}{dx} \right)_{x=0} = kg(K \cdot C'(x=0, t) - C(t)) \quad \text{eq 6}$$

At time zero, the initial concentration is assumed to be uniform in both phases :

$$C(t=0) = K \cdot C'(t=0) = C_{\max} \quad \text{eq 7}$$

The properties of the volatiles during the experiment were assumed to be constant. It is obvious that the thermodynamic properties (partition coefficient) are strongly linked to the kinetic ones. The system of equations (1, 2, 5, 6 and 7) were

solved numerically using Matlab software (The Matworks Inc., USA) with Simulink tool box. Concentration profiles in each phase were calculated as a function of time, also depending on the distance in the liquid medium. Based on comparison with the experimental data, the properties of the volatiles which influenced release were identified.

Results and Discussion

Thermodynamic and Kinetics of Flavor Compounds

Two kinds of factors characterized the flavor release:

- the concentration of the flavor compounds as well as its properties within the medium, which are thermodynamic (partition coefficient) and kinetic (diffusion and mass transfer coefficients);
- operating conditions like the geometry of the system (volume of the phases, surface exchange area), hydrodynamic factors (flow rate of the gas, gas stirred in the cell, non mobile liquid phase), thermal conditions (temperature).

Applying the dynamic headspace dilution method to simple solutions of volatiles, the composition of the medium and the operating conditions were fixed and it was possible to identify the thermodynamic and the kinetic properties of the molecule. Five compounds were chosen in order to cover a wide range of properties (Table I). They were highly diluted in aqueous solutions, so there was no significant effect of volatile on the activity coefficient and the probability of any interaction (or reaction) between the molecules was negligible. Different concentrations of sugar (sucrose up to 50%) were added to the aqueous solutions while maintaining the flavor at the same concentration.

Table I. List of the Molecules Studied in Aqueous Solutions

<i>Molecule</i>	<i>MW (g/mol)</i>	<i>Liquid concentration (kg/m³)</i>
Acetaldehyde	44	1.1E-3
Diacetyl	86	9.61E-4
2,5-Dimethylpyrazine	108	8.37E-3
Dimethylsulfide	62	8.46E-4
Menthone	154	8.93E-5

Partition Coefficients of Flavor Compounds Diluted in Aqueous Solutions

The partition coefficients of the flavor compounds in water were estimated with static headspace analysis as well as by using the initial concentration from the dynamic headspace measurements (C_{\max} in Figure 2), at a fixed temperature (25°C) (Table II). The experimental values of the partition coefficients obtained in aqueous solutions were in good agreement with the theoretical ones (literature or calculated data from an empirical model), which have been discussed previously (10). The molecules chosen have very different volatilities (corresponding to the partition

coefficient values K) as well as different hydrophobicities (γ_i^* increasing from acetaldehyde to menthone) (Table II). As a result, K varied from 2.5×10^{-2} for dimethylsulfide (high volatility) to 5.7×10^{-5} for 2,5-dimethylpyrazine (low volatility). Moreover, the experimental data obtained with two different concentrations of sucrose solutions (20% and 40%) showed an increase of the partition coefficient when increasing the sugar content, especially when the activity coefficient was high. The effects observed are in agreement with the literature data of activity coefficients, for other volatiles diluted in aqueous solutions with sugar which were measured in a dilutor cell at equilibrium (11).

Table II. Partition Coefficients of Flavor Compounds in Aqueous Solutions at 25°C

Molecule	γ_i^* (10)	K in water theoretical (10)	K in water experimental	K sucrose solutions experimental	
				20%	40%
Acetaldehyde	4	2.9E-3	2.7E-3	3.3E-3	3.3E-3
Diacetyl	11	5.7E-4	3.9E-4	5.7E-4	9.7E-4
2,5-Dimethylpyrazine	23	6.3E-5	5.7E-5	6E-5	10E-5
Dimethylsulfide	208	8.1E-2	2.5E-2	3E-2	6E-2
Menthone	24 870	6.9E-3	7.1E-3	7E-3	11E-3

Kinetic Properties of the Aqueous Flavored Solutions

In Figure 3, the release curves for the five flavor compounds can be seen. The curves were obtained under the standard operating conditions and are plotted as relative concentration ($C(t)$ over $C(t=0)$) as a function of time in order to compare the behavior of all compounds on the same scale. The kinetics of release seem to be directly related to the partition coefficient: the lowest change in release (highest C/C_0 value) was seen for the less volatile 2,5-dimethylpyrazine and the highest change in release (lowest C/C_0 value) was seen for the most volatile molecule, dimethylsulfide.

By fitting the solution of the system of equations (1, 2, 5, 6 and 7) with the experimental data, the mass transfer coefficient in the gas phase and the diffusion coefficient in the liquid phase for each volatile were determined. As reported in Table III, the mass transfer coefficients of volatiles in the gas phase had the same order of magnitude (around 0.03 m/s) for all molecules. The mass transfer coefficients in air were determined using the well-known power law between dimensionless parameters (Sherwood number as a function of Reynolds and Schmidt numbers) (12). The experimental mass transfer coefficient obtained confirmed that there was turbulent flow in the gas phase due to the flow rate (\dot{u}) and the geometry of the experimental cell. It has already been shown that increasing \dot{u} tends to decrease the relative concentration in the gas phase (10, 13). The diffusion coefficients in the liquid (water) phase were similar for all of the molecules studied, ranging between 2 to 6×10^{-9} m²/s. These experimental values seem to be slightly higher than literature values quoted for low molecular weight molecules in water (14). This tendency was also confirmed when the theoretical values of diffusion coefficients in water were estimated with the Wilke and Chang equation (9) (Table

III). The apparent diffusion coefficient estimated with the dynamic headspace dilution method could be overestimated due to convection in the liquid phase, which could happen in practice and which should be added to the pure diffusion mechanism.

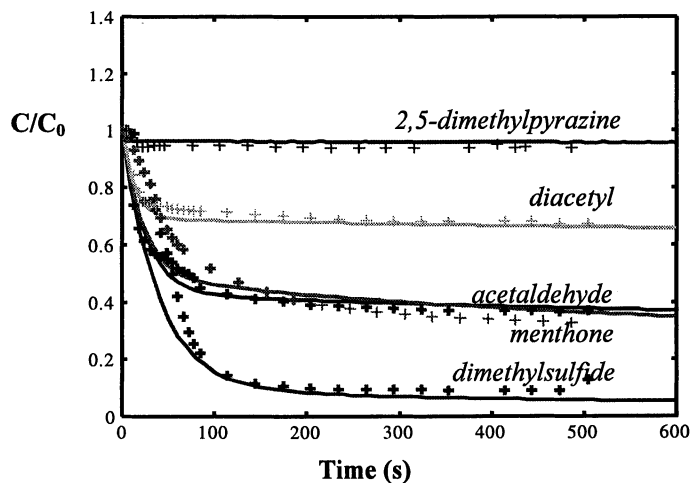


Figure 3. Release curve for the five volatiles studied. (Temperature = 25°C, $\dot{u} = 70$ mL/min, $V = 50 \cdot 10^{-6} \text{ m}^3$, Initial concentration of headspace in equilibrium with the sample). The experimental data are marks and the solution of the model is the continuous line.

Table III. Kinetic properties of the flavor compounds in water at 25°C

Molecule	D in water (m^2/s) exp.	D in water (m^2/s) theo. ^a	k_1 in water (m/s) exp. ^d	k_g in air (m/s) exp.	k_g in air (m/s) theo.	
					Re=500 ^b	Re= 25000 ^c
Acetaldehyde	3 E-9	1.4 E-9	2.5 E-6	3 E-2	0.72 E-2	4.0 E-2
Diacetyl	2.5 E-9	1.0 E-9	2.5 E-6	3 E-2	0.62 E-2	3.4 E-2
2,5-Dimethyl pyrazine	5 E-9	0.82 E-9	2 E-6	3 E-2	0.57 E-2	3.2 E-2
Dimethyl sulfide	5 E-9	1.1 E-9	3 E-6	3 E-2	0.50 E-2	2.7 E-2
Menthone	6 E-9	0.62 E-9	3 E-6	3 E-2	0.12 E-2	2.3 E-2

SOURCE : (a) Wilke and Chang equation (9); (b) Levêque equation (12); (c) Chilton and Colburn equation (12) ; (d) data obtained from eq 1, 10, 11 and 12 (10)

Nevertheless, comparing experiments and modeling, it appears that increasing the sugar content in the aqueous solution tends to decrease the diffusion coefficient of the solute in this solution. When the viscosity of the sample was measured, the experimental values for the relative diffusion coefficient of the three molecules seemed to obey the well-known Stokes-Einstein equation (9), where D is inversely

proportional to the viscosity (Figure 4). The overall effect of adding sugar on flavor release is that the relative concentration of the volatile is lowered (Figure 5), due to a higher partition coefficient (the lowest C/C_0 value was seen for the most volatile molecule) and a lower diffusion coefficient (Table 2).

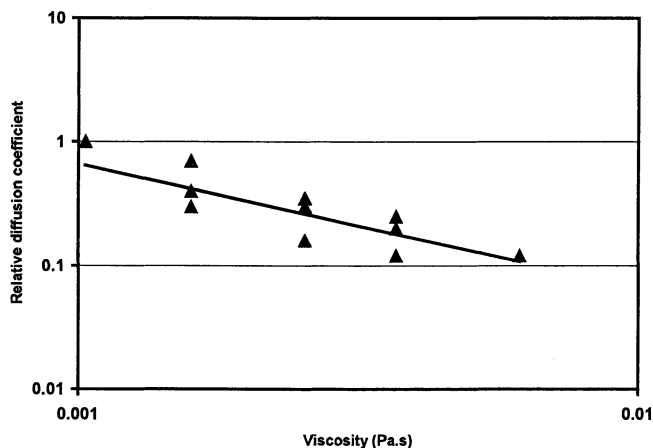


Figure 4. Relative diffusion coefficient of the volatiles (diacetyl, menthone, dimethylsulfide) in aqueous solutions with variable concentration in sucrose, as a function of the liquid viscosity (25°C).

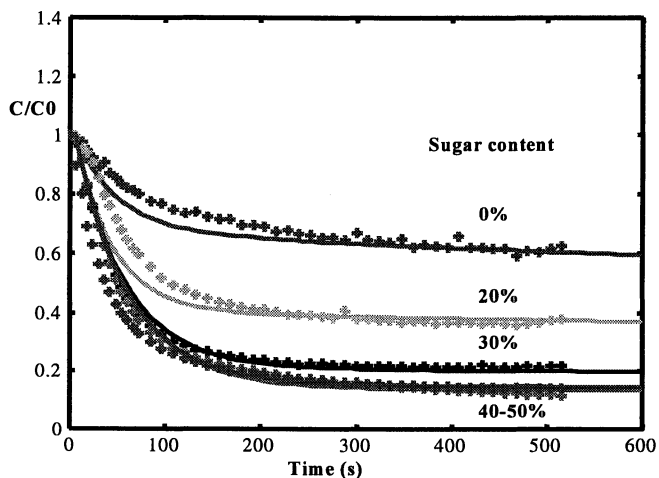


Figure 5. Release profile of diacetyl in different sugar solutions (Temperature = 25°C, $\dot{u} = 45$ mL/min, $V = 100 \cdot 10^{-6}$ m³, Initial concentration of headspace in equilibrium with the sample).

Simplification of the Model and Derivation of Dimensionless Parameters

Now that a theoretical approach was developed and validated with experimental data, it was possible to extract key parameters that had a major influence on flavor release.

Initial Release (Transient State)

The initial slope of the flavor release curves was similar for all volatiles (see Figure 3). Indeed, at time zero, assuming that the concentration in the gas phase is in equilibrium with the sample phase, the mass flux ($J(t=0)$) tends to zero and eq (1) and (7) give:

$$\left(\frac{d\left(\frac{C(t)}{C(t=0)}\right)}{dt} \right) = -\frac{\dot{u}}{V} \quad \text{eq 8}$$

The slope of the curve of the relative concentration (C/C_0), at initial time, is independent of the volatile and depends only on the operating conditions (gas flow rate and volume of the gas phase).

But, taking into account the variation of the absolute value of the concentration:

$$\frac{dC(t)}{dt} = -\frac{\dot{u}}{V} \cdot K \cdot C'(t=0) \quad \text{eq 9}$$

A high partition coefficient (highly volatile molecule) as well as a high initial concentration in the liquid would lead to a high decrease of the intensity seen during the first short period of time.

Asymptotic Value of the Concentration (Steady State)

Referring to the later part of the flavor release curves (see Figure 3), it is not so easy to extract a simple parameter from the modeling based on diffusion in the liquid phase. Assuming that pure diffusion was not completely achieved in the liquid sample, another representation for the modeling was proposed by defining an apparent mass transfer coefficient in the liquid phase (k_l), which is equivalent to the diffusion coefficient (D) divided by an equivalent limiting layer (12). This approximation introduces a simplification in the system of equations which becomes:

$$V \cdot \frac{dC(t)}{dt} = J(t) \cdot A - \dot{u} \cdot C(t) \quad \text{eq 1}$$

$$J(t) = k_O (K \cdot C'(t) - C(t)) \quad \text{eq 10}$$

$$V' \frac{dC'(t)}{dt} = -J(t) \cdot A \quad \text{eq 11}$$

$$\text{with an overall mass transfer coefficient } (k_O): \quad \frac{1}{k_O} = \frac{1}{k_g} + \frac{K}{k_l} \quad \text{eq 12.}$$

As seen in Figure 6, the model with the mass transfer coefficient in the liquid phase doesn't take into account the slight decrease characteristic of the diffusion model, but the overestimation of the relative concentration is less than 10% after 10 minutes. Consequently, the result of the simplified model was compared again systematically with the release curve of each volatile. Differences between the

release of the five flavor compounds are in good agreement (10). As seen in Table III, similar to the diffusion coefficient, the mass transfer coefficients obtained in the liquid phase do not differ significantly from one flavor compound to another, and the order of magnitude (1×10^{-6} m/s) is in accordance with literature values for a quasi-non mobile liquid (12). This simplified model was used to define criteria to characterize flavor compounds in the asymptotic part of the release curve.

In the steady state, assuming that the average concentration in the liquid phase is constant due to the short time of the experiment ($J(t) = k_O(C(t=0) - C(t))$), the variation of the concentration in the gas phase tends to zero ($J(t) \cdot A - \dot{u} \cdot C(t) \rightarrow 0$), then:

$$\frac{C(t)}{C(t=0)} = \frac{1}{\left(1 + \frac{\dot{u}}{k_O \cdot A}\right)} \quad \text{eq 13}$$

The variation of the relative concentration in the gas depends only on one dimensionless parameter $\frac{\dot{u}}{k_O \cdot A}$, which is related to the operating conditions in the system (gas flow rate, exchange surface) as well as the overall mass transfer coefficient (k_O).

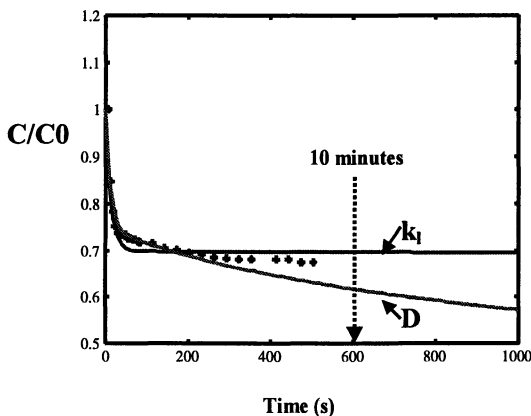


Figure 6. Comparison between experimental data (marks), and models based on diffusion coefficient (D) and on mass transfer coefficient in liquid phase (k_l). (Diacetyl, Temperature = 25°C , $\dot{u} = 70$ mL/min, $V = 50 \cdot 10^{-6}$ m³, Initial concentration of headspace in equilibrium with the sample).

It turns out that an increase in the surface (A) as well as a decrease of the flow rate (\dot{u}) leads to an increase in the relative concentration, but the effect depends on the value of the overall mass transfer coefficient (k_O), which is characteristic for each flavor compound providing other factors remain constant. The value of k_O fixes the level of each flavor concentration in a fixed system but, as seen in equation (12), when \dot{u} increases, k_O could be modified at the same time, due to the value of k_g . In Figure 7, the order of magnitude of the relative concentration (C/C_0), for the

asymptotic part of the flavor release curve, was represented as a function of the dimensionless number $\frac{\dot{u}}{k_0 \cdot A}$, for a wide range of operating conditions : \dot{u} ranged

from 1 mL/min to 1 L/min, A ranged from 1 cm² to 10 cm², K ranged from 10⁻² to 10⁻⁵, k_g from 10⁻² to 10⁻³ m/s and k_l from 10⁻⁶ to 10⁻⁸ m/s. In Figure 7, two parts corresponding to two mechanisms are identified:

- when $\frac{\dot{u}}{k_0 \cdot A}$ is less than 0.1, the partition coefficient is the only property

determining the relative concentration;

- when $\frac{\dot{u}}{k_0 \cdot A}$ is higher than 0.1, the mass transfer coefficients must be taken

into account to predict the amount of flavor released.

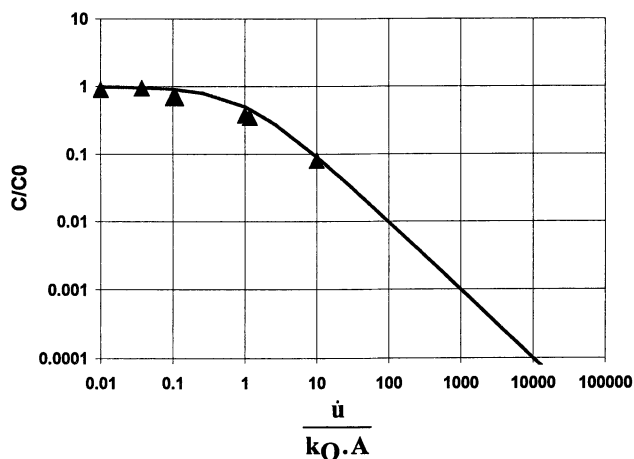


Figure 7. Relative concentration in the gas phase (C/C_0), for the asymptotic part of the flavor release curve, as a function of the dimensionless number. Operating conditions for the model (continuous line): \dot{u} ranged from 1 mL/min to 1 L/min, A ranged from 1 cm² to 10 cm², K ranged from 10⁻² to 10⁻⁵, k_g ranged from 10⁻² to 10⁻³ m/s and k_l ranged from 10⁻⁶ to 10⁻⁸ m/s. Experimental data are marks.

Three types of behavior can be defined with this approach :

- if $\frac{1}{k_g} \gg \frac{K}{k_l}$, the mass transfer in the gas phase is the limiting step. It is, for example, the case for 2,5-dimethylpyrazine (low volatility) in the non-stirred aqueous solutions in contact with air (non turbulent, Re=500). Increasing the convection inside the air phase will tend to modify its release profile.
- if $\frac{1}{k_g} \ll \frac{K}{k_l}$, the mass transfer in the liquid phase is the limiting step. It is, for example, the case for dimethylsulfide (high volatility) in the non mobile

aqueous solutions in contact with air. Modifying the viscosity of the medium would greatly influence the flavor release of this kind of molecule.

- In an intermediate range where many volatile compounds can be found, mass transfer in both phases (air and water) have an effect on the release.

Extrapolation

Initial Operating Conditions

All the experiments were carried out with equilibrium at the starting point, but other situations can also be characterized with an initial concentration in the gas phase equal to zero ($C(t = 0) = 0$). In the expression of relative concentration, C_0 now refers to the concentration in the liquid phase multiplied by the partition coefficient.

By changing the initial value of the gas phase, each molecule achieves the same plateau value (steady state) based on the relative concentration defined with equation (13).

On the other hand, in the initial transient state, it gives a new expression for the slope:

$$\frac{dC(t)}{dt} = K \cdot C'(t = 0) \frac{k_{O \cdot A}}{V} \quad \text{eq 14}$$

It is an original condition where the inert flow rate (\dot{u}) has no effect. This value has been proposed in the literature to represent the initial slope of flavor release from a liquid in the mouth (14). It is again interesting to compare the two extreme types of behavior:

- if $\frac{1}{kg} \gg \frac{K}{kl}$, (low volatility compound): $\frac{dC(t)}{dt} = K \cdot C'(t = 0) \frac{kg \cdot A}{V}$
- if $\frac{1}{kg} \ll \frac{K}{kl}$, (high volatility compound): $\frac{dC(t)}{dt} = C'(t = 0) \frac{kg \cdot A}{V}$

The influence of the partition coefficient (K) on the initial release is more important when this parameter is low (low volatility).

Complex Real Situations

This overall approach could be extrapolated to other flavor release situations. Using the example of a package of food at equilibrium opened and diluted by the surrounding atmosphere; at a low flow rate of air (\dot{u}), mixing in the gas may not be ideal. As suggested by the literature (12), it is possible to take into account this complex behavior by introducing a residence time distribution function in the final expression of the relative gas concentration. In another case, e.g. stripping of volatiles from a beverage could also be linked to the transfer of a gas (inert dissolved gas) or to the evaporation of the solvent itself which is coming from the sample (e.g.

water at high temperature). This coupling transport should be taken into account in the basic equations of mass balance as well as in mass transfer.

Conclusion

The concentration of flavor compounds released from a liquid in a gas phase and its evolution during time depend on the partition coefficient between phases (K), which are in contact, as well as on the overall mass transfer coefficient (k_o). These parameters can be estimated, in fixed operating conditions, for multi-component mixtures of very dilute aroma compounds using a headspace dynamic dilution method (API-MS). A dimensionless criteria $\frac{\dot{u}}{k_o \cdot A}$ appears as the major parameter

which drives the physical mechanism of flavor concentration evolution when a well-stirred gas is in contact with a liquid.

In attempting to define the limiting mechanisms and their relative influence during flavor release, this overall approach, based on mass balance and mass transfer equation, could be extended to other complex real situations of flavor release.

References

1. Overbosch P., Afterof W.G.M., Haring P.G.M., *Food Rev. Int.*, **1991**, 7, 137-184.
2. De Roos K.B., Wolswinkel C., in "Trends in Flavor Research", Maarse H., Van der Heij D.G. Eds, Elsevier Science B.V., Amsterdam, 1994, 15-32.
3. Hills B.P., Harrison M., *Int. J. Food Sci. Tech.*, **1995**, 30, 425-436.
4. Taylor A.J., Linforth R.S.T., Baek I., Brauss M., Davidson J.M., Gray D, In "Advances in Flavor Chemistry and Technology", Risch S.J., Ho C.T. Eds, American Chemical Society, 1999, In press.
5. Linforth R.S.T., Taylor A.J., European Patent, Number 97305409.1, 21.01.1998, Bulletin 1998/04.
6. Baek I., 1999, PhD thesis, University of Nottingham, UK.
7. Crank J., *The Mathematics of Diffusion*, 2nd Edition, 1975, Oxford University Press, New York.
8. Treybal R.E., *Mass Transfer Operations*, 1968, Mc Graw Hill, New York.
9. Reid R.C, Prausnitz J.M., Poling B.E., *Properties of Gases and Liquids*, 1987, McGraw Hill Inc., New York.
10. Marin M., Baek I., Taylor A., *J. Agric. Food Chem.*, **1999**, In press.
11. Sorrentino F., Voilley A., Richon D., *AIChE Journal*, **1986**, 32 12, 1988-1993.
12. Coulson J.M. , Richardson J.F., *Chemical Engineering*, Volumes I, II and III, 3rd Edition, 1977, Pergamon Press, Oxford, UK.
13. Harrison, M., Hills B., *Int. J. Food Sci. Tech.*, **1997**, 46, 2727-2735.
14. Cussler E.L., *Diffusion, Mass Transfer in Fluids Systems*, 2nd Edition, 1997, Cambridge University Press, UK.

Chapter 14

Modeling Aroma Release from Foods Using Physicochemical Parameters

Rob S. T. Linforth, E. N. Friel, and Andrew J. Taylor

Samworth Flavour Laboratory, Division of Food Sciences,
University of Nottingham, Sutton Bonington Campus, Loughborough,
Leicestershire LE12 5RD, United Kingdom

Models have been developed (based on physicochemical parameters) to predict the temporal changes of volatile concentration in breath from the nose when gelatin/sucrose gels were eaten. Breath volatile concentrations were determined experimentally, using the MS NoseTM and these values were correlated with physicochemical parameters of the volatiles using an empirical process contained in a chemical modeling program. The models predict both the maximum release intensity (mg/m^3) and temporal aspects such as the time to maximum intensity and persistence. The physicochemical parameters used to generate the models were Log P (the octanol water partition coefficient), Log p_L (vapor pressure), and the Hartree energy (the energy required to separate all of the electrons and nuclei of the molecule infinitely far apart), all of which can be estimated by calculation. A wide range of compounds with different functionalities were used in these experiments in order, to build a robust model capable of predicting release with good predictive power.

One of the major research areas in flavor science is the understanding of how volatile flavor compounds are released and transported to the flavor sensors during the eating process. Release behavior *in vivo* depends both on the interactions of volatile compounds with the food matrix and the interactions that occur between volatiles and the lining of the mouth, throat, and nose. Some interactions affect all volatiles equally; other interactions depend on the specific physicochemical properties of the volatile molecules.

The actual release of volatile compounds can be followed *in vivo* by monitoring the expired air from the nose of a person as they eat a food using the API-mass spectrometric interface, developed in our laboratory (1). This is now commercially available as the MS NoseTM. This system allows us to study the release of several

volatiles directly and simultaneously (2) and, from the data obtained, release curves for each volatile can be constructed. The principles of API-MS are discussed elsewhere in this book.

Rather than just measure volatile release *in vivo*, it would be desirable to predict release based on the composition of the food sample and, for this, models are needed. There are many different approaches to model production for flavor release (3). One approach is to identify the mechanisms (melting, diffusion, etc.) involved in volatile release for a particular food system and develop appropriate models to describe the release behavior. These models are complex and involve consideration of many factors, such as the air-water partition coefficient, the octanol-water partition coefficient (Log P), surface area, temperature, as well as mass transfer coefficients for the movement of compounds from the matrix into the aqueous/saliva phase (4). Mechanistic models have been produced to describe release of volatile compounds from matrices such as boiled sweets (5) or from gelatin/sucrose gels of different compositions (6). Computer simulations have been created to predict the rate of loss of aroma compounds from chewing gum during eating (7) or the overall flavor release from food into the air phase (8). Model-mouth headspace systems have also been used to study volatile release and subsequently generated models to show how the matrix affects aroma release (9). For all these models, it is necessary to establish values for key parameters like vapor pressure, mass transfer in the liquid and gas phases, and change in surface area with time in-mouth. Although some values can be found in the literature, others have to be determined experimentally. There are currently no published models, that attempt to predict the changes in intensity of aroma compounds in the nose over the eating time course.

Quantitative Structure Property Relationships (QSPR) can be used to construct models that relate the behavior of a compound (e.g. volatile release) to a range of physicochemical parameters (10) using statistical analysis. This is a different approach to the models described above, where mathematical equations are generated on the basis of defined mechanisms based on theoretical considerations (e.g. the mass transfer coefficient, sample melting point etc.). In QSPR, all of the physicochemical parameters used in the model can usually be estimated by calculation, which avoid the need for further experimentation before a prediction can be made. QSPR's have been widely used in the pharmaceutical industry to optimize drug design, as synthesis and evaluation trials are expensive. They have also been used to produce models that describe the physical behavior of compounds such as the air-water partition coefficient (11). This paper presents models derived using a QSPR approach to aroma release from gelatin gels during eating.

Materials and Methods

Gelatin gels were prepared by melting hydrated gelatin (bloom strength 250) in a water bath (60°C) before mixing it with a solution of sucrose and glucose (which had been boiled and cooled to <100°C). Citric acid and the volatile compound (dissolved

in propylene glycol) were then added to give a final composition of gelatin 6%, sucrose 30%, glucose 40%, and citric acid 1%.

The volatile compounds were added to the gels individually at 100 ppm (higher concentrations of some compounds were added to the gels if their breath concentration during eating was too low for detection). The volatile compounds were anethole, butanone, 1,4-cineole, p-cymene, α -damascenone, decanol, diethyl succinate, dimethyl pyrazine, ethanol, ethyl butyrate, ethyl hexanoate, ethyl methyl furan, ethyl undecanoate, furaneol, fufuryl acetate, hexanol, limonene, menthol, menthone, methyl acetate, methyl furan, methyl salicylate, octanone, pyrazine and undecanone. Three replicate samples of each gel were eaten by one panelist and the values (maximum intensity etc.) were averaged prior to modeling, except for the menthone and menthol gels where duplicates were prepared.

The breath volatile composition was analyzed using the MS NoseTM (Micromass, Manchester, UK) as described by Linforth and co-workers (12). Physicochemical parameters were calculated using CAChe 3.2 (Oxford Molecular, Beaverton, OR, USA). Models were produced using Design - Expert 5.0.9 (Stat - Ease Inc, Minneapolis, MN, USA).

Results and Discussion

Modeling The Breath Maximum Volatile Concentration (I_{max})

The model was developed via an iterative process. After the data for the first 12 compounds had been obtained, a preliminary correlation was attempted (using Design Expert) with Log P and Log p_L (13), which were selected on the grounds that these two parameters were associated with the processes involved in establishing maximum breath volatile concentration. This showed that these two parameters did have a significant correlation ($P < 0.05$) with the maximum breath volatile concentration (I_{max}). The model however had a low predictive power and required further development.

Compounds were then selected to broaden the model whose Log P and Log p_L values were different from the original 12 compounds. Further gels were produced, consumed, and the I_{max} data was obtained. Multiple linear regression was performed using CAChe, to determine whether any of the 60 physicochemical parameters, that had been calculated using CAChe, accounted for the variation in I_{max} . Log P, Log p_L , and an additional factor, the absolute value of the Hartree Energy (the energy required to separate all of the electrons and nuclei of the molecule infinitely far apart) were found to be significant factors ($P < 0.05$) in the estimation of the breath I_{max} . This latter parameter is broadly related to the molecular weight of a compound (Figure 1); however, when the molecular weight was used instead of the Hartree Energy, the correlations obtained were poorer.

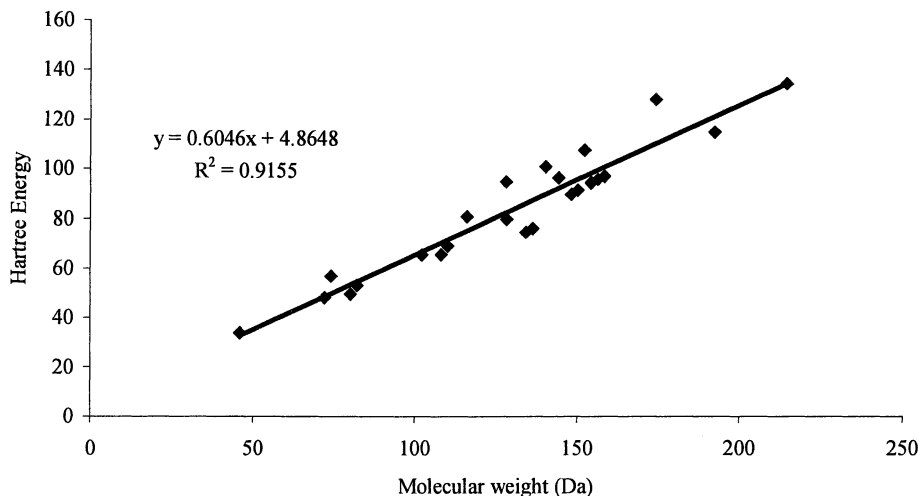


Figure 1. The relationship between the absolute value for the Hartree Energy of a compound and its molecular weight.

The equation for the final model (Eq 1) has linear and quadratic terms for all three components, and a cubic term for the Hartree Energy. The values of the three physicochemical parameters can be estimated for any compound using CAChe. The I_{max} can then be estimated by substitution of these values into Eq 1. The model has a good correlation coefficient (r^2) and predictive correlation coefficient (rCV^2), the latter being an important estimate of the predictive power of the model (values over 0.7 are considered to have a reasonable predictive power).

$$\begin{aligned} \text{Log } I_{max} = & - 1.3 + 0.9 * \text{Log } P + 0.7 * \text{Log } p_L - 0.06 * \text{Energy} \\ & - 0.15 * \text{Log } P^2 + 0.13 * \text{Log } p_L^2 + 1.4E-03 * \text{Energy}^2 \\ & - 7.3E-06 * \text{Energy}^3 \end{aligned} \quad (1)$$

$$r^2 = 0.88, rCV^2 = 0.82, n = 28, s = 0.35, F = 21.40$$

Where, n = Number of data point, s = standard deviation, F = Fisher Statistic

The model is three dimensional, and each parameter can be considered to lie on a separate axis (effectively x , y , z). A two dimensional slice through the model is shown in Figure 2, where a series of “contour lines” link regions of the plot where the breath I_{max} would be predicted to be the same. For example, a breath I_{max} value of $1\text{mg}/\text{m}^3$ (contour line labeled zero [log scale] in Figure 2) could be obtained, either when $\text{Log } P$ was 3.0 and $\text{Log } p_L$ was -1.5, or when $\text{Log } P$ was -0.9 and $\text{Log } p_L$ was 1.75. This relates to the particular “slice” shown in Figure 2 and assumes the energy values for both compounds was 93. Effectively, this means that a non-polar

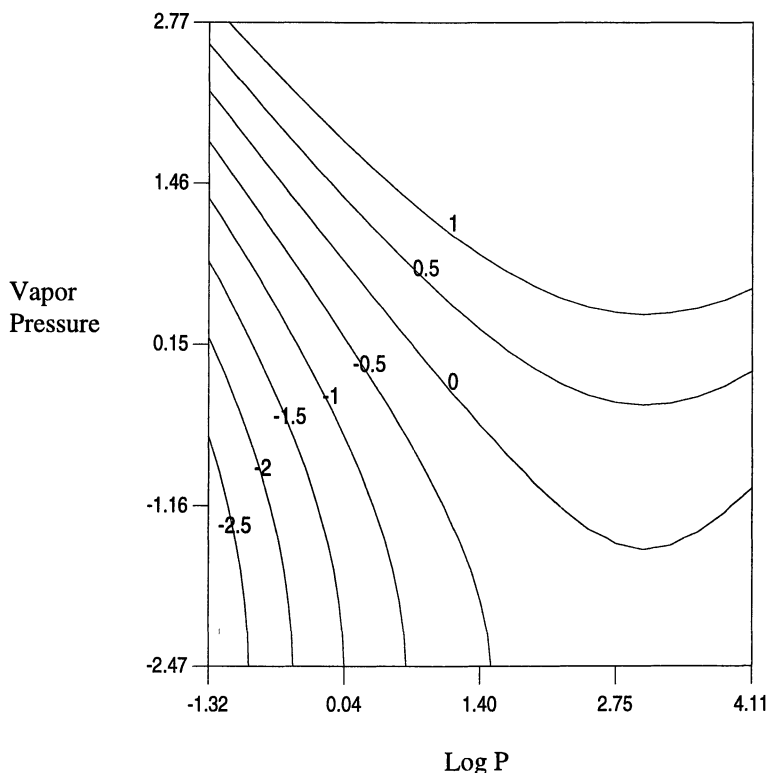


Figure 2. Contour plot of predicted I_{max} values for aroma compounds when 6% gelatin gels containing 100ppm of the volatile are eaten. Values on the contour lines are the log concentrations of volatile in the breath (i.e. 0 is equivalent to 1 ppm).

compound with a low volatility may have the same I_{max} as a polar compound with a higher volatility.

From the contour plots it was possible to show that individual physicochemical parameters did not always have significant effects on release. For compounds with a Log P value greater than 1.5, Log p_L had a far more significant effect on the breath I_{max} than Log P (Figure 2). However, for more polar compounds (Log P < 1.5) Log P and Log p_L were both important, but Log p_L exerted a greater effect for the compounds with higher vapor pressures. Consequently, if gel experiments were performed using compounds with similar vapor pressures and Log P's greater than 1.5, then only minor changes in I_{max} would be expected.

The predicted Log I_{max} (based on Eq 1) for each compound was plotted against the observed Log I_{max} measured experimentally (Figure 3). Although the data follow a clear trend, the correlation is not exact for all compounds (Table I). Log I_{max} values were in the range from -2.5 to 1.0, effectively three orders of magnitude. This was strongly dependent on the physicochemical characteristics of the compound, with polar compounds with a low vapor pressure exhibiting the lowest I_{max} values.

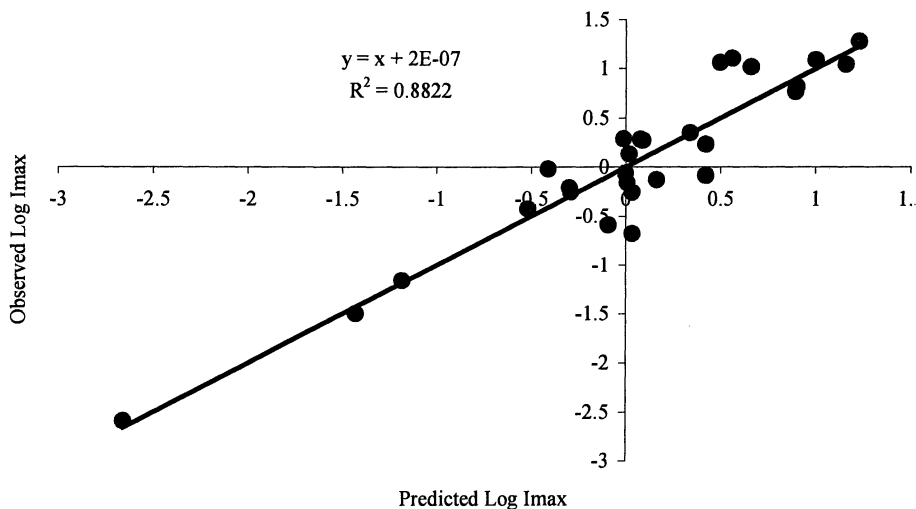


Figure 3. Correlation between predicted and observed Log Imax values.

It is difficult to visualize the effects of all three dimensions (Log P, Log p_L and Hartree energy) of the model simultaneously. However, the effect of the Hartree energy can be plotted separately (Figure 4). This shows that compounds with very low or very high Hartree energies (effectively the small and large compounds), would have a lower breath Imax relative to the compounds with intermediate Hartree energies (ca. 90 to 110). This may reflect both the greater water solubility of small compounds and the low volatility of larger compounds, thereby enhancing the model.

Model For Temporal Parameters

In addition to the maximum intensity value (Imax) there is also a temporal dimension to any volatile release curve. When volatile compounds are released from the same matrix, some are more persistent than others (14), suggesting that the physicochemical characteristics of a compound may also affect the temporal aspects of the volatile release profile. During the course of these experiments, 26 different compounds were consumed individually, but in the same gel matrix. They showed considerable variation in the temporal dimension.

Table I. Physicochemical Parameters for Compounds and Their Predicted and Observed I_{max} Values.

<i>Name^a</i>	<i>Log P</i>	<i>Log pl</i>	<i>Hartree Energy</i>	<i>Observed Log I_{max}</i>	<i>Predicted Log I_{max}</i>
Furaneol	-1.32	-0.96	95	-2.59	-2.66
Ethyl undecanoate	4.01	-1.84	135	-1.50	-1.43
Diethyl succinate	0.37	-0.08	128	-1.16	-1.18
Menthol	2.78	-1.43	96	-0.68	0.03
Dimethyl pyrazine	0.72	0.80	65	-0.59	-0.09
Pyrazine	-0.58	1.93	50	-0.43	-0.52
Menthol	2.78	-1.43	96	-0.26	0.03
Dodecanol	4.11	-2.47	105	-0.25	-0.29
α - Damascenone	3.08	-2.34	115	-0.21	-0.30
Decanol	3.32	-1.56	97	-0.16	0.01
Furfuryl acetate	0.45	0.56	101	-0.13	0.16
Menthone	3.15	-0.50	94	-0.09	0.42
Ethanol	0.08	2.06	34	-0.06	0.00
Methyl salicylate	1.49	-1.66	107	-0.02	-0.41
Hexanol	1.74	0.26	65	0.13	0.02
Menthone	3.15	-0.50	94	0.23	0.42
Undecan-2-one	3.78	-1.08	103	0.27	0.09
Cymene	3.71	-0.34	74	0.28	0.08
Anethole	2.79	-1.37	90	0.29	-0.01
Limonene	2.94	-0.07	76	0.35	0.34
Ethyl methyl furan	2.38	0.95	69	0.77	0.89
Ethyl hexanoate	2.02	0.43	96	0.82	0.90
Octanone	2.59	0.29	80	1.02	0.66
Ethyl butyrate	1.23	1.34	81	1.05	1.16
Menthofuran	2.73	-0.29	91	1.07	0.50
Butanone	1.01	2.10	48	1.09	1.00
1,4-Cineole	1.83	0.08	94	1.11	0.56
Methyl acetate	-0.14	2.77	57	1.28	1.23

^aWhere duplicate gels were prepared both values are shown for that compound.

The compounds that appeared to show the most persistence fell into one of two groups, these were the polar compounds (low Log P) and the non-polar compounds with low vapor pressures. These would lie on the top left, bottom left and bottom right of Figure 2. The compounds that were in the center of Figure 2 (medium vapor pressure and polarity) typically showed the least persistence. There were no compounds in the top right sector of the plot as compounds with high Log P values are too large to have a high vapor pressure.

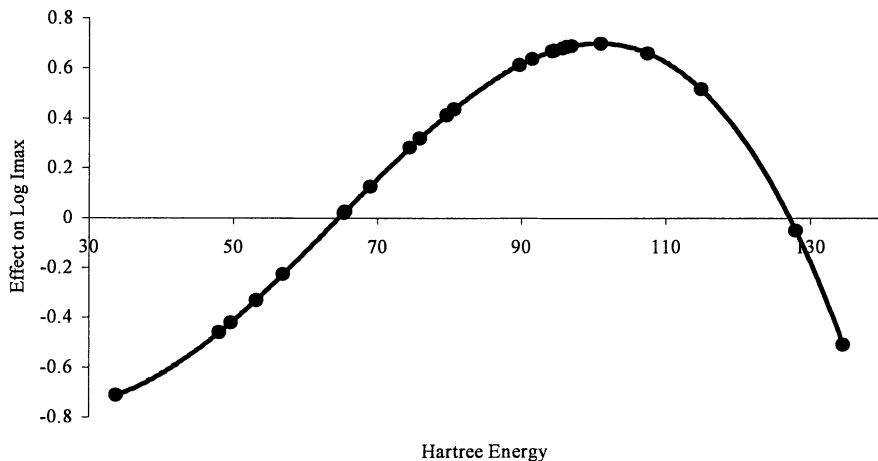


Figure 4. The effect of Hartree Energy on Log Imax

Clearly, we could identify the persistent and non-persistent compounds resolved within the two dimensional space of Log P and Log p_L . The next stage was to see if models could be produced (using Log P, Hartree energy and Log p_L) to describe the temporal aspects of aroma release such as the time to maximum intensity (Tmax), and the time for aroma to increase or decrease to 50% of maximum (T₅₀ and T_{50'} respectively).

The time for the curves to decline to 25% of maximum (T_{25'}) was modeled first because these values were likely to show the greatest differences. The equation describing T_{25'} (Eq 2) has linear components associated with each term and a quadratic component for Log P. A good correlation was found for the model, which showed that polarity, volatility, and molecular size were all correlated with the temporal aspects of aroma release. The fact that both temporal and intensity models could be constructed using the same physicochemical parameters strongly suggests that these two aspects of aroma release were related.

$$T_{25'} = 2.01 - 0.51 * \text{Log P} - 0.23 * \text{Log } p_L - 6.4 * \text{Energy} + 0.09 * \text{Log P}^2 \quad (2)$$

$$r^2 = 0.85, rCV^2 = 0.76, n = 26, s = 0.16, F = 31.08$$

The contour plot of the T_{25'} model (Figure 5) shows the range of values observed. Medium volatile and medium polar compounds had T_{25'} values of ca. 0.75 min, while the polar, low vapor pressure compounds had values greater than 2.0 min.

The persistence of the polar compounds may be associated with their ability to partition in and out of the mucous membranes of the upper airways which can then act

as a reservoir for volatile release. Decreasing the volatility of such compounds would enhance their potential to leave the gas phase and enter this reservoir. The non-polar, less-volatile compounds do not have the same affinity for the aqueous phase, and the mechanism of their persistence may be different. They could condense on the mucous membranes as a result of their low volatility creating a reservoir for further release. Alternatively they may be so hydrophobic that they are forced out of solution (into micelle like structures or, to associate with membranes) and this volatile pool could act as a reservoir. It is interesting to note in both Figure 2 and 5 that, above Log P 1.5, there was little effect of Log P on either the temporal or intensity dimensions. The major effect (in this region of the model) was dependent on Log p_L , which would be consistent with the condensation of volatiles on mucous membranes resulting in persistence.

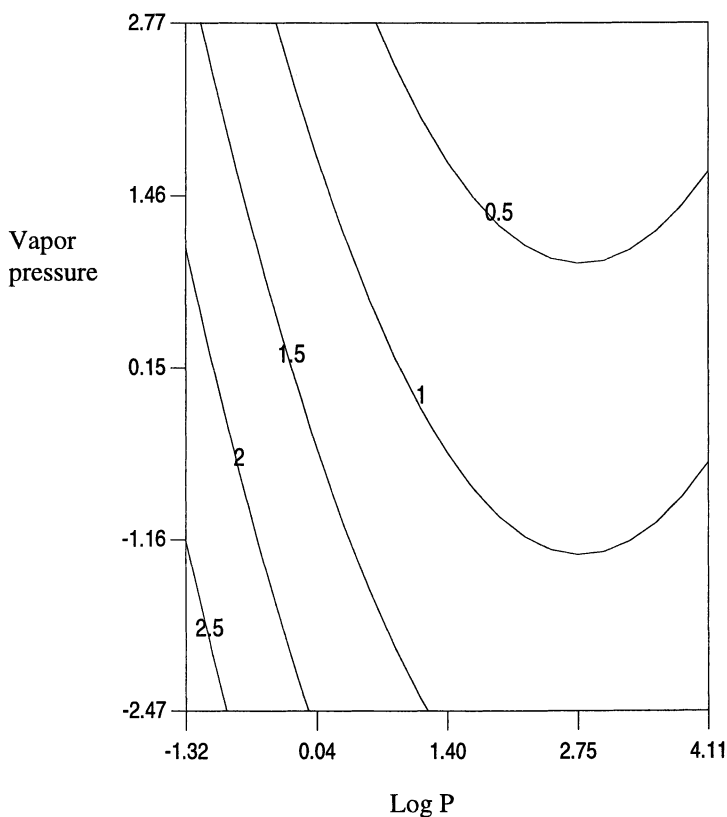


Figure 5. Contour plot of predicted $T_{25'}$ values for aroma compounds when 6% gelatin gels containing 100ppm of the volatile are eaten. The numbers on each line represent the time from the start of eating to $T_{25'}$ (min).

Modeling The Entire Release Profile

A further series of models were produced to describe different points in the temporal dimension. We were, therefore, able to predict the shape and intensity of the volatile release curve based solely on values that could be calculated using the chemical modeling program CAChe. It was not necessary to perform further experimentation.

The observed volatile release curves for ethyl butyrate (Figure 6) and pyrazine (Figure 7) were very different from each other. Ethyl butyrate had an I_{max} approximately 50 times that of pyrazine (for the same concentration in the gel), while pyrazine was much more persistent than ethyl butyrate. These actual release curves were very similar to those predicted using the models (Figure 6 and 7). This shows that these models have the capacity to predict the changes in breath aroma concentration (in both the intensity and temporal dimensions) during the consumption of gelatin gels.

Prediction Of Volatile Release For A Homologous Series.

When the release profiles of aliphatic alcohols were compared (Figure 8), few differences were observed between the I_{max} values for ethanol, hexanol and decanol. This was due to the counter-balancing effect of changes in molecular properties. As the chain length is extended from two to ten carbons, $\log P$ increases and $\log p_L$ simultaneously decreases. Therefore, the compound becomes less water soluble,

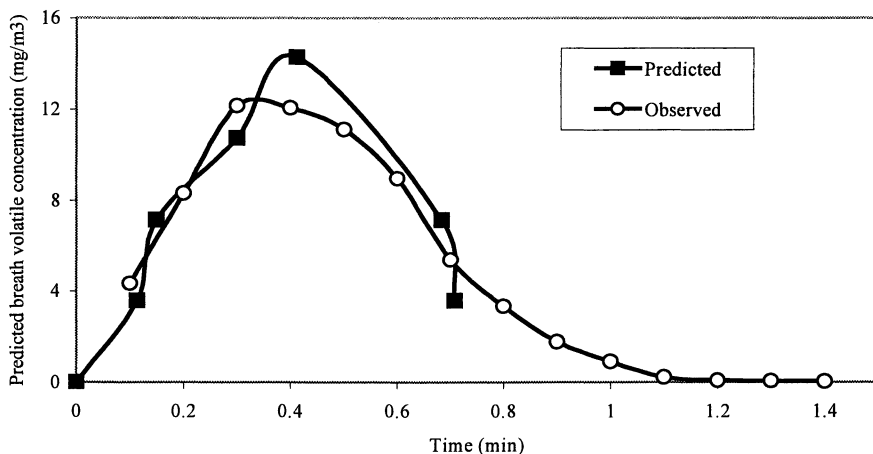


Figure 6. Observed and predicted volatile release curves for ethyl butyrate from a 6% gelatin gel (100 ppm of each volatile).

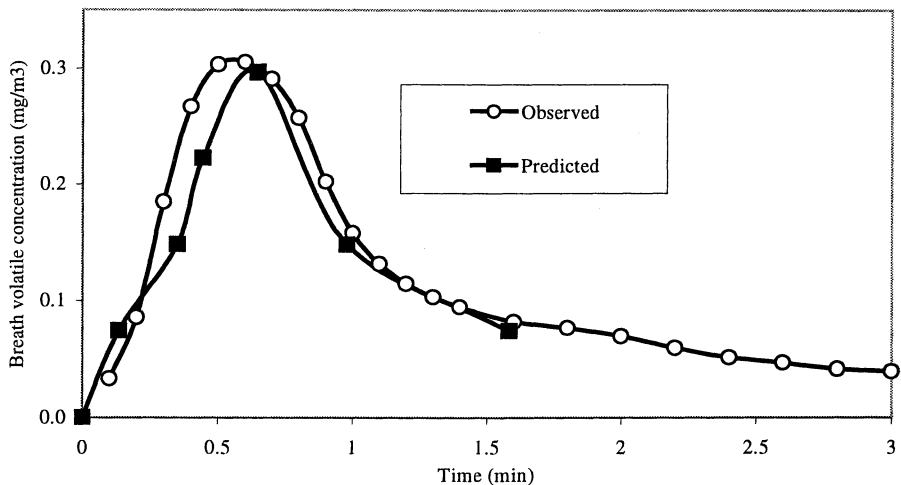


Figure 7. Observed and predicted volatile release curves for pyrazine from a 6% gelatin gel (100 ppm of each volatile).

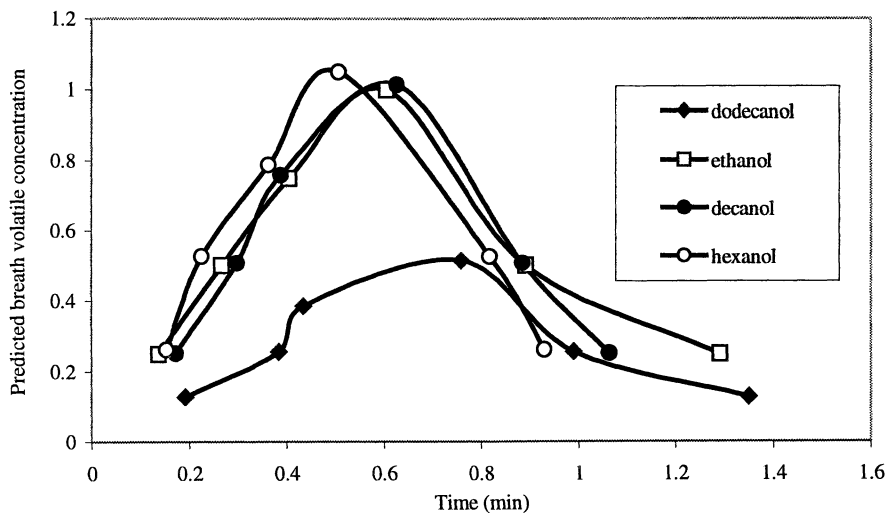


Figure 8. Predicted volatile release curves for ethanol, dodecanol, decanol and hexanol.

which should increase its tendency to move into the gas phase. However, its lower volatility restricts this. Hence, ethanol has the same I_{max} as hexanol and decanol.

All three compounds fall on the same I_{max} contour line as it moves from top left to lower right in Figure 2 (it is important to remember that there is a third dimension to these plots (Figure 4)). This balance does not however go on forever and there is a deviation from this balance in molecular properties (this can be seen by the bend in the contour plot). Consequently by the time the chain length has extended to give us dodecanol, $\log p_L$ is too low and despite the greater hydrophobicity of dodecanol its breath I_{max} decreases.

There were also temporal effects. Ethanol is a highly polar, volatile compound and decanol is non-polar and has a low volatility, these two factors again counter-balance resulting in temporal similarities (a delayed T_{max} and increased persistence). Hexanol has a volatility and polarity intermediate between these two compounds, hence it falls in the middle region of the model (Figure 5) where the “non-persistent” compounds were found. This results in the slightly earlier I_{max} and associated lack of persistence. Dodecanol again shows the largest deviation relative to the other compounds, with the latest T_{max} and greatest persistence, typical of compounds in the extreme bottom right corner of the model (Figure 5).

Conclusions

Direct measurement *in vivo* showed major differences in the release profiles of different aroma compounds during eating. Models were developed using the QSPR approach to describe these differences in the temporal and intensity dimensions of volatile release. Although the physicochemical parameters in the model were chosen by an empirical process, rather than a direct consideration of potential mechanisms, they can be used to rationalize the overall process and give an insight into the relative importance of factors like volatility and hydrophobicity. This type of “top down” modeling approach requires a minimum of experimental work, with all the physicochemical parameters being generated through software. The current model describes how compounds are released from one specific matrix. The next step is to broaden the model to incorporate changes in matrix formulation.

Acknowledgement

Dr Linforth is grateful to Firmenich SA, Geneva for their financial support.

References

1. Linforth, R. S. T. and Taylor, A. J. EU. Patent EP 0819 937 A2, **1998**.
2. Taylor, A. J. and Linforth, R. S. T. *Trends in Food Sci. Tech.* **1996**, 7, 444-448.
3. Taylor, AJ & Linforth RST, Modelling flavour release in foods. In *Modelling chemical change in food*. B Wedzicha Ed. Royal Society of Chemistry, Cambridge, 1999 in press.
4. Overbosch, P.; Afterhof, W. G. M. and Haring, P. G. M. *Food Rev. Int.* **1991**, 7, 137-184.
5. Hills, B. P; Harrison, M. *Int. J. Food Sci Tech.* **1995**, 30, 425-436.
6. Harrison, M.; Hills, B. P. *Int. J. Food Sci Tech.* **1996**, 31, 167-176.
7. De Roos, K. B. and Wolswinkel, K. In *Trends in Flavour Research*; Maarse, H. and Van Der Heij, D. G. Eds. Elsevier: Amsterdam, **1994**, pp 15-32.
8. Harrison, M., Campbell, S and Hills, B.P. *J. Agric Food Chem.* **1998**, 46, 2736-2743.
9. Roberts, D. D.; Acree, T. E. In *Flavour Science: Recent Developments*; Taylor, A. J. and Mottram, D. S., Eds. Royal Soc. Chem. Cambridge, **1996**, pp 399-404.
10. Dearden, J. C. In *Practical Applications of Quantitative Structure-Activity Relationships (QSAR) in Environmental Chemistry and Toxicology*; Karcher, W. and Devillier, J. Eds. ECSC; Brussels, **1990**, pp 25-59.
11. Katritzky, A. R.; Mu, L. and Karelson, A. R. *J. Chem. Inf. Comput. Sci.* **1996**, 36, 1162-1168.
12. Linforth, R. S T.; Baek, I. and Taylor, A. J. *Food Chem.* **1999**, 65, 77-83.
13. Liang, C. and Gallagher, D. A. *J. Chem. Inf. Comput. Sci.* **1998**, 38, 321-324.
14. Hinterholzer, A.; Baek, I.; Linforth, R.; Taylor, A and Schieberle, P. In *Interaction of food matrix with small ligands influencing flavour and texture*; Schieberle, P. Ed.; Office for Official Publications of the European Communities: Luxembourg, **1998**, Vol. 3, pp 45-50.

Chapter 15

Mathematical Models of Release and Transport of Flavors from Foods in the Mouth to the Olfactory Epithelium

Marcus Harrison

Institute of Food Research, Norwich Research Park,
Colney, Norwich NR4 7UA, United Kingdom

A computer simulation describing flavor release from chewing gum in the mouth is presented. The rate limiting step for flavor release is assumed to be the transport of flavor volatiles across the gum-saliva interface, which can be described by the stagnant-layer theory of mass transfer. Saliva-flow, mastication, swallowing and transport of the volatiles from the oral cavity through the airways to the olfactory epithelium have been incorporated into the model. In general, the results show that the rates of flavor release primarily depend on the saliva-gum partition and mass transfer coefficients. Surprisingly, release rates from the gum were found to be independent of the chewing frequency of a particular individual at all times. The simulation also predicts that the presence of mucus lining the airways further influences the time-dependent flavor concentrations arriving at the olfactory epithelium.

Flavor is one of the primary factors determining the quality and acceptance of a food product. During consumption, flavors are released from the food matrix into the oral cavity, from where they are transported to the nasal cavity through the actions of eating and breathing. The perception of a volatile depends on the concentration of the compound, threshold levels of the individual, and the duration of exposure. An individual's perception of a particular food product will therefore primarily depend on the amounts and rates of volatile release from the food matrix; however, the overall perception will also depend on cognitive factors, such as pattern recognition and mood.

Sensory panels are often trained to perceive the time-intensity (TI) characteristics of a food during eating¹. In general though, due to large variations among subjects, it is often difficult to analyse the data produced. It is easier, and more informative, to compare the differences between similar food products for one particular individual. More recently electromyography (EMG) mastication and swallowing patterns used in conjunction with sensory techniques² have revealed that the perceived flavor of a food depends greatly on how an individual interacts with it. Although flavor is generally understood to be the combined perception of both non-volatile compounds in the saliva (taste) and volatile compounds transported to the olfactory epithelium (aroma), we consider it, for our purposes, to indicate volatile aroma compounds only.

Recent technological developments now permit real-time monitoring of flavor volatiles

expired from the nose breath-by-breath during eating using Atmospheric Pressure Chemical Ionisation-Mass Spectroscopy (APCI-MS)³.

This breath-by-breath time-release profile is assumed to represent the availability of flavor volatiles free to interact with the receptors, which are situated in the olfactory bulb. A recent study comparing simultaneous TI curves and breath-by-breath concentrations for gelatine/pectin gels revealed that individuals could discriminate the qualitative aspects of the sensory release profiles, but not the quantitative aspects⁴. However, by processing the raw time-dependent concentration profiles into smooth time-release (TR) curves, these authors found a simple relationship between the changes in volatile concentration over the eating period and the perceived intensity.

Both APCI-MS and sensory TI studies have led to a greater understanding of the processes influencing flavor release from food. However, a greater depth of knowledge can be obtained by developing and validating mathematical models of flavor release from foods in the mouth. The ultimate goal of this would be to mathematically predict the effect of varying food composition, food structure, and mastication behaviour on the perceived time-intensity flavor release profile. If successful, it would then be possible to use computer simulations to formulate foods for a desired flavor profile, taking into account individual or group differences in eating behaviour.

Unfortunately, very little is understood about the mechanisms controlling flavor release from solid or semi-solid foods in the mouth. This, undoubtedly, is due to the variety and complexity of even the simplest solid foods. Despite these problems, last few years has seen rapid progress in the development of mechanistic physico-chemical models to describe flavor release from foods in the mouth⁵. The objective of this paper is to review these recent developments and, in particular, focus on a computer simulation of aroma release from chewing gum in the mouth, which includes the transportation of flavors from the oral to nasal cavities. It should be noted that this paper is concerned only with the passage of the flavor volatiles from the food matrix to the nasal cavity and ignores the psychological and physiological steps of flavor perception. However, it should be straight forward to incorporate certain aspects of perception, such as threshold concentrations and pattern recognition into future versions.

General Theoretical Model

Once a food is ingested it is rapidly coated by a thin-film of saliva. It can therefore be assumed that flavor, on release from a solid food, must first pass through the saliva phase before partitioning into the headspace of the oral cavity. Of course, for the case of semi-solid foods, such as sauces, flavor is already in the liquid phase and therefore can be released into the headspace directly. It can therefore be assumed that the passage of flavors from the food product to the headspace is a three phase problem involving the food, saliva, and gas phases. It is unlikely that simple diffusion of flavor molecules in the bulk phases of the food or saliva can determine the rates of release in the mouth as mastication removes diffusion gradients and generates fresh interfaces. Therefore, it can further be assumed that mass transfer of flavor compounds across the macroscopic interfaces is the rate limiting step for release. Based on these assumptions, Hills and Harrison proposed a general framework of flavor release in the mouth⁶. Within this framework, mathematical models were developed and validated showing that the rate-limiting step for release was the transfer of flavor mass across the solid-saliva and saliva-gas interfaces for solid^{6,7} and semi-solid^{8,9} foods.

The mechanisms governing mass transfer across the solid-saliva and liquid-gas interfaces depend greatly on the nature of the food matrix. A number of simple release

mechanisms have been established with the aid of mathematical models. By far the simplest method to consider is the dissolution of a sugar matrix, such as a boiled sweet⁶. In this case, the driving force for release across the interface is the non-equilibrium concentration difference of sucrose between the food product and saliva, which can be described by the stagnant layer theory of interfacial mass transfer. As the matrix dissolves, all flavors are simultaneously released into the surrounding saliva, from where they partition into the headspace of the oral cavity.

Another example of simultaneous release is from gelled sweets, where the surface of the gel matrix melts instead of dissolving⁷. The rate at which the phase transition proceeds depends on the bulk melting temperature of the gel, which itself is dependent on the matrix composition. For soft gels possessing melting points below the mouth temperature, the driving force for release is the rate at which heat can diffuse into the gel matrix and initiate melting. For harder gels with melting points above mouth temperature, the diffusion of sucrose from the surface of the gel into the adjacent saliva phase is the rate-limiting step for release, because this lowers the melting temperature of the surface layer. These predictions have been recently observed by time-intensity sensory studies².

A very different mechanism of release is extraction of volatiles from the food matrix during mastication. DeRoos and Wolswinkle proposed a non-equilibrium partitioning model to describe the extraction of flavor compounds from chewing gum into the surrounding saliva¹⁰. These authors found that flavor release from model systems was predicted with high precision, whereas adjustments to the basic equations had to be made in order for the theory to comply with release conditions in the mouth.

Once in the aqueous phase the concentration of flavor will be diluted by saliva flowing into the oral cavity. Partitioning of volatiles from the liquid into the gas phase is further complicated by the presence of other food ingredients in the saliva. For example, volatiles residing in the lipid phase of an emulsion will slowly partition into the aqueous phase as saliva flows into the mouth^{11,12}. Also, proteins and polysaccharides are known to bind both reversibly and irreversibly to volatiles thus reducing the free flavor available for release¹³⁻¹⁷. In addition, the presence of these macromolecules will effect the overall viscosity of the saliva further influencing the rates of release^{8,9,18-20}. Saliva viscosity will also influence the residual thickness coating the inside of the oral cavity long after the majority of the food has been swallowed, thus potentially influencing the aftertaste.

All of these models focus only on foods that either remain whole or are already liquefied. In reality, most foods breakdown via fragmentation during the mastication process. This dramatically increases the surface area of the food allowing a greater proportion of the flavor to be released from the food matrix into the surrounding saliva. For a realistic simulation of flavor release to be developed, the time-dependence of the surface area needs to be calculated as the fragmentation process proceeds. Furthermore, the effect of saliva flow into the oral cavity¹², swallowing^{2,21}, and partitioning of flavors into the gas phase all have to be incorporated into the model. Despite these difficulties, Harrison *et al.* made a first attempt at developing a computer simulation of flavor release from solids as they fragment in the mouth⁵. However, validating such a model is a challenging task, partially due to first, the complexity of the eating process and second, the difficulty in quantifying volatile concentrations in the oral cavity.

One way of validating the model is to monitor the volatiles in the breath stream with mass spectrometry. This requires that the models previously discussed be extended to include the transport of the flavors from the mouth to olfactory epithelium (figure 1). An early attempt at modelling this phenomenon was tackled by introducing a constant gas-

flow through the headspace²². However, this model is not a good representation of the physical reality as flavors are not transported to the nasal cavity at a constant rate. First, movements of the mouth, such as chewing, regularly pump flavors from the oral cavity into the breath stream; and second, absorption of flavor molecules by the mucus lining in the throat and airways influences the extent and rate at which flavors are transferred to the olfactory epithelium. In the following section, we present a new mathematical model to describe flavor release from chewing gum in the mouth and the subsequent transport of these volatiles from the oral cavity to the olfactory epithelium.

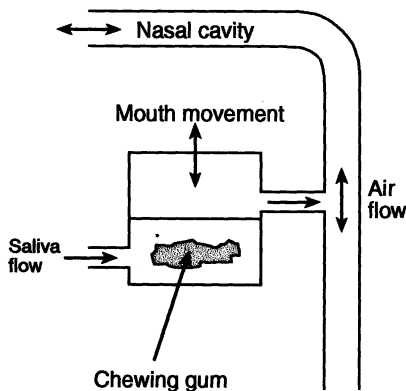


Figure 1. Schematic diagram of the oral and nasal cavities.
(Reproduced with permission from reference 25. Copyright 1998.)

Modelling Flavor Release from Chewing Gum

In comparison to most food products, chewing gum is a very simple system. The reason being that during the time-course of the eating process the volume and mass of the gum are relatively constant. For simplicity, it can be assumed that surface area of the gum remains constant and the main effect of chewing is to prevent volatile concentration gradients from being established in the surface layers of the gum. Furthermore, real-time mass spectrometry has shown that rates of flavor release from chewing gum are effectively constant and moreover, independent of an individual's chewing rate²³. All of these experimental observations aid in simplifying the model and therefore reducing the complexity of the mathematics required for the simulation.

It is unlikely that diffusion of volatiles across the surface layers of the gum is the rate-limiting step for release, otherwise the release rates would be dependent on chewing frequency. It is reasonable therefore, to assume that the mass transfer of volatiles across the macroscopic gum-saliva interface is the rate-limiting step from chewing gum. Foods possessing a well defined surface transfer of flavor volatiles across the interface can be described mathematically by the stagnant-layer theory of interfacial mass transfer⁶

$$\frac{dm}{dt} = Ah_D \left[K_{sf} c_f(t) - c_s(t) \right], \quad \text{Eq 1}$$

where m is the total mass of volatile that diffuses across the interface, h_D is the mass transfer coefficient for a particular volatile, A is the surface area of the interface and c_f and c_s are the concentrations of volatile in the bulk gum and saliva phases, respectively. The parameter K_{sf} is the equilibrium saliva-gum partition coefficient defined by

$$K_{sf} = \frac{c_s^e}{c_f^e}, \quad \text{Eq 2}$$

where c_f^e and c_s^e are the concentrations of volatile in the bulk gum and saliva phases at equilibrium.

Once in the aqueous phase, the concentration of volatiles will be diluted by saliva flow into the oral cavity. It is well known that the sight of food can stimulate the salivary glands to increase the rate of saliva flow into the oral cavity from an average of 0.5 mL/min to approximately 3-4 mL/min within 30 seconds²⁴. Thereafter the rate decreases exponentially back to the base value of 0.5 mL/min over the course of several minutes. However in this simulation, for simplicity, we assume that the saliva flow-rate, Q , is constant at 2 mL/min.

The rigorous movements of the mouth will maintain a well-mixed saliva phase devoid of concentration gradients. It can therefore be assumed that partitioning of volatiles between the saliva and headspace is extremely fast. The flavor concentration in the gas phase can then simply be calculated from the equilibrium partitioning coefficient

$$K_{gs} = \frac{c_g^e}{c_s^e}, \quad \text{Eq 3}$$

where c_g^e and c_s^e are the concentrations of flavor in the gas and saliva phases at equilibrium, respectively.

In addition to providing a well mixed environment, the chewing movements act like a bellows periodically pumping air in and out of the oral cavity²⁵. The closing motion of the mouth lasts for approximately 0.1s²⁶ during which time a proportion of flavor-enriched air is transferred into the tidal breath-stream. If the closing action occurs as an individual is inhaling, then the majority of the flavor is swept into the lungs where it is diluted and absorbed by the surrounding tissue. Conversely, if an individual is exhaling, the flavor is transported along in the breath stream to the nasal cavity. In the simulations presented in this paper, for mathematical simplicity, the velocity of the tidal breathing is assumed to be constant and either positive or negative to signify exhalation and inhalation, respectively (Figure 2).

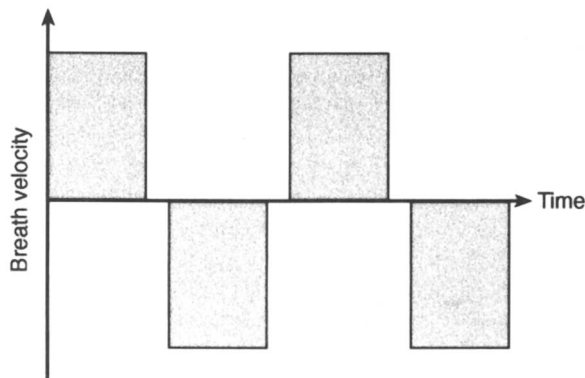


Figure 2. Mathematical representation of the breathing velocity during inhalation (maximum) and exhalation (minimum), separated by a finite pause.

(Reproduced with permission from reference 25. Copyright 1998.)

As volatiles are swept along the airway, they are free to interact with the thin mucosal lining. By ignoring the anatomy of the nasal cavity it can be assumed that the airways can be approximated by a long cylinder that acts as a continuous chromatographic column (Figure 3). Figure 3 shows, schematically, the exchange of volatiles between the air and mucus phases of such a chromatographic column. Predictions of how the airways affect flavor release can be investigated mathematically if the conditions of partition chromatography, with a linear partition isotherm, are assumed. These assumptions are:

1. thermal equilibrium exists between the air and mucus phases and the equilibrium concentrations in the two phases are proportional, i.e. linear chromatography;
2. the exchange of volatiles between the two phases is extremely fast and reversible;
3. longitudinal diffusion and other such processes having a similar effect can be ignored.

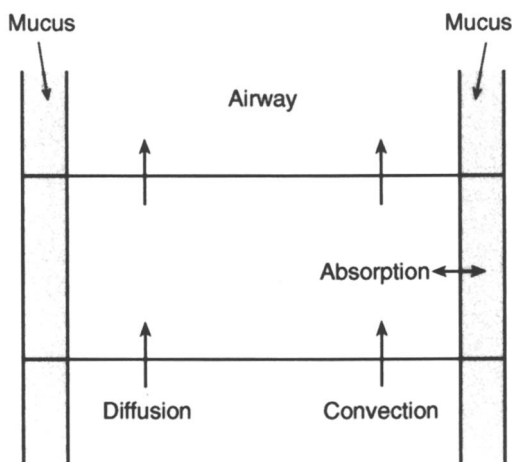


Figure 3. Schematic diagram showing diffusion, convection and absorption processes acting on the flavor volatiles in the airways.

(Reproduced with permission from reference 25. Copyright 1998.)

Once these assumptions have been made, the mass balance of flavor volatiles per unit of cross-sectional area can be written as²⁷.

$$F_a \frac{\partial c_a}{\partial t} = F_a D \frac{\partial^2 c_a}{\partial z_a^2} - F_a u \frac{\partial c_a}{\partial z} + h_m \alpha (K_{am} c_m(t) - c_a(t)) \quad \text{Eq 4}$$

and

$$F_m \frac{\partial c_m}{\partial t} = h_m \alpha (c_a(t) - K_{am} c_m(t)) \quad \text{Eq 5}$$

where α is the interfacial surface area per unit volume of airway, which is given by

$$\alpha = \frac{R_a}{(R_a + R_m)^2} \quad \text{Eq 6}$$

The parameters used in Eqs 4 and 5 are listed in Table 1.

Table I. List of symbols and corresponding descriptions.

<i>Symbol</i>	<i>Description</i>
A_{sf}	Chewing gum surface area (m ²)
$C_a(t)$	Time-dependent volatile concentration in airway (mg/cm ³)
$C_b(t)$	Time-dependent volatile concentration in breath (mg/cm ³)
$C_f(t)$	Time-dependent volatile concentration in chewing gum (mg/cm ³)
$C_g(t)$	Time-dependent volatile concentration in gas phase (mg/cm ³)
$C_m(t)$	Time-dependent volatile concentration in mucus phase (mg/cm ³)
$C_s(t)$	Time-dependent volatile concentration in saliva phase (mg/cm ³)
D	Volatile diffusion coefficient in air (m ² /s)
F_a	Fractional volume of mobile air phase in airway
F_m	Fractional volume of stationary mucus phase in airway
h_D	Gum-saliva mass transfer coefficient in air (m/s)
h_m	Air-mucus mass transfer coefficient (m/s)
K_{am}	Airway-mucus partition coefficient
K_{gs}	Gas-saliva partition coefficient
K_{sf}	Saliva-gum partition coefficient
R_a	Radius of airway (m)
R_m	Thickness of mucus lining airway (m)
t_0	Duration of flavor pulse into the airway (s)
t	Time (s)
u	Breath velocity (m/s)
z	Co-ordinate along axis of the throat (m)
α	Mucosal surface area per unit volume of airway (m ⁻¹)
τ	Time elapsed since flavor pulse introduced into airways (s)

A number of simplifying assumptions have to be introduced in order to make Eqs 4 and 5 accessible to mathematical treatment²⁷. Finally, it must be further assumed that the pulse of flavor, of concentration $c_g(t)$, introduced into the column is of a sufficiently short duration, t_0 . For the calculations presented in this paper t_0 corresponds to the time taken for the jaw to close and is taken to be 0.1 s²⁶. After taking all of these assumptions into account Eqs 4 and 5 can be solved and reduced to a Gaussian function:

$$\frac{C_b(\tau)}{C_g(t)} = \frac{\beta t_0}{\sqrt{2\pi(\sigma_1^2 + \sigma_2^2)}} \exp\left[-\frac{(z/u - \beta\tau)^2}{2(\sigma_1^2 + \sigma_2^2)}\right], \quad \text{Eq 7}$$

with

$$\frac{1}{\beta} = 1 + \frac{F_m}{F_a K_m}, \quad \text{Eq 8}$$

$$\sigma_2^1 = 2 \frac{Dz}{u^3}, \quad \text{Eq 9}$$

$$\sigma_2^1 = 2\beta^2 \frac{F_m^2 z}{\alpha h_D F_f K_{am}^2 u} \quad \text{Eq 10}$$

and where τ is the time elapsed since the flavor pulse was introduced into the airway.

Simulation Algorithm

Having mathematically described the mass transfer of flavor across the gum-saliva interface, and transport from the oral cavity to the olfactory epithelium we can now incorporate them into a computer simulation to calculate the time course of flavor concentration in the exhaled breath, $c_b(t)$.

Initialisation

First, the data files containing the chewing and swallowing times for each individual are input into the simulation and stored in arrays. Other parameters, such as mass transfer and partition coefficients, are input from separate data files and stored as constants (Table I). It is assumed that at zero time the food is placed into the mouth and immediately coated with saliva. And finally, it is assumed that the initial concentration of flavor in both the aqueous and gaseous phases is zero. The simulation commences by incrementing the time, t , by Δt .

Main Simulation Loop

After each time step, the time, t , is incremented and compared with the chew and swallow times stored in the input arrays. If t does not correspond to either a chew or swallow then the mass of flavor released into the saliva, ΔM_s , during the time interval Δt is calculated using Euler's approximation of Eq 1:

$$\Delta M_s = A_{sf} h_D \left[c_f(t) - \frac{c_s(t)}{K_{sf}} \right] \Delta t, \quad \text{Eq 11}$$

The value of ΔM_s is used to re-calculate the flavor concentration in the saliva, $c_s(t)$.

$$\text{Concentration of flavor in saliva} = \frac{\text{Mass of flavor in saliva}}{\text{Volume of saliva}}, \quad \text{Eq 12}$$

which then partitions into the gas phase to provide $c_g(t)$:

$$c_g(t) = K_{gs} c_s(t). \quad \text{Eq 13}$$

Once a new value of $c_g(t)$ has been computed, t can be incremented by and the next step can be calculated, and so on until t corresponds to a time that either corresponds to a chew or a swallow.

If t corresponds to a swallow time then a fraction of the flavor-enriched saliva is removed from the mouth. The factor by which flavor mass is lost from the mouth is given by

$$\frac{\text{Mass of flavor after swallowing}}{\text{Mass of flavor before swallowing}} = \frac{\text{Volume of saliva after swallowing}}{\text{Volume of saliva before swallowing}} \times \frac{\text{Mass of flavor before swallowing}}{\text{Mass of flavor before swallowing}}. \quad \text{Eq 14}$$

On the other hand, if t corresponds to a chew, a proportion of the gas phase is pumped into the tidal airflow. If the subject is breathing out then the time course for the flavor concentration passing through the nosespace, $c_b(t)$, is calculated using Eq 7. Otherwise, the volatiles are drawn down the trachea and absorbed by the extensive mucus covered surface of the lungs.

The simulation was developed in a Windows environment using a commercial software package (C++ Builder V4.0, Borland, US) so that multiple outputs could be viewed and compared. The simulation had a CPU time of approximately sixty seconds.

Theoretical Analysis and Discussion

There are large numbers of parameters in the model that can be varied and which result in differing flavor release profiles. These parameters can be separated into three groups: first, those that are related to the nature of the food, such as its composition, structure and flavor content; second, those that describe the eating behaviour of individuals; and third, those linked to the transport of volatiles to the olfactory epithelium. This section will illustrate the effect of varying a limited number of these parameters on the time-dependent flavor release profiles: first, we focus on the effect of partitioning on flavor release from the gum; and second, how the airways influence the rates of the flavors arriving in the nasal cavity. For a discussion on the effect of other factors that influence flavor release rates, such as saliva flow, see ref. 5.

Flavor volatiles will be released from the gum into the surrounding saliva at different rates depending on the volatiles partition and mass transfer coefficients. Figure 4 shows predictions for the time-dependent flavor concentrations in the saliva over a fifteen minute period as a function of the saliva-gum partition coefficient, K_{sf} . For low-volatility flavor compounds, the rate of release is relatively constant throughout the duration of the chewing period, which is in agreement with recent observations from APCI-MS²³. On the other hand, highly volatile flavors are rapidly released from the gum, attaining a greater maximum concentration than the low volatility flavors. Thereafter the rate of release decreases exponentially as the flavor within the gum is depleted (Figure 5).

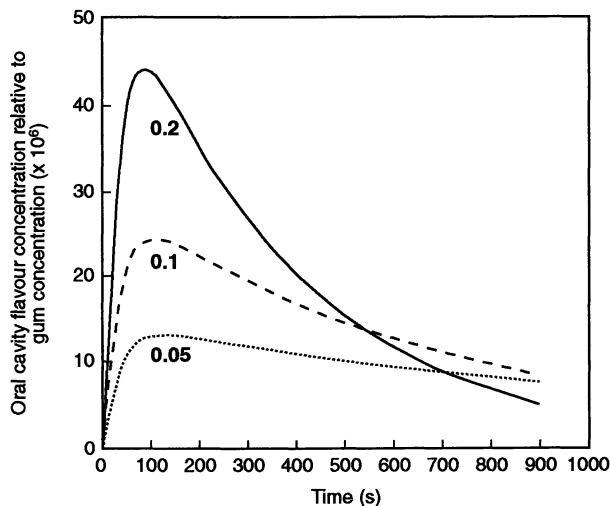


Figure 4. Time-dependent flavor concentrations in the saliva as a function of the saliva-gum partition coefficient.

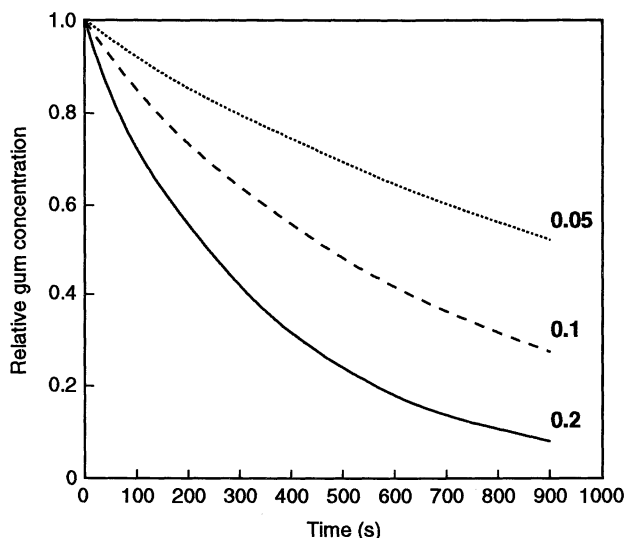


Figure 5. Time-dependent flavor concentrations in the gum as a function of the saliva-gum partition coefficient.

Surprisingly, our results predict that the rate at which flavor is released from the gum is independent of an individual's chewing frequency. Again this result agrees with recent experimental observations using APCI-MS²³. However, the force applied during a chew will influence the shape and surface area of the gum. As shown previously, the rate of flavor release is predicted to be proportional to the gum surface area. In reality it is unlikely that there are significant variations in gum surface area between individuals. This is a factor which may need to be investigated for the theory to be satisfactorily validated.

Having examined the factors that control flavor release from the gum, we can now turn our attention to the influence of the airways on the transport processes. Figure 6 shows single pulses of a series of ketones emerging from a cylindrical tube as a function of time. In this calculation it has been assumed that the cylinder length is 15 cm and air flows at a constant rate of 2 m/s along the tube. Figure 6 clearly shows that lipophilic compounds (nonanone and undecanone) quickly pass through the system, whereas the hydrophilic volatiles interact more strongly with the mucus lining resulting in a smearing out of the initial pulses. This result, therefore, predicts that flavors, although released simultaneously, arrive at the olfactory epithelium at different times. Furthermore, the strong interaction of hydrophilic volatiles with the mucus probably explains the persistence of some flavors long after the source has been removed from the oral cavity. Such a result has been observed with mints and the persistence of menthone and menthol up to 15 minutes after the food has been swallowed²⁸.

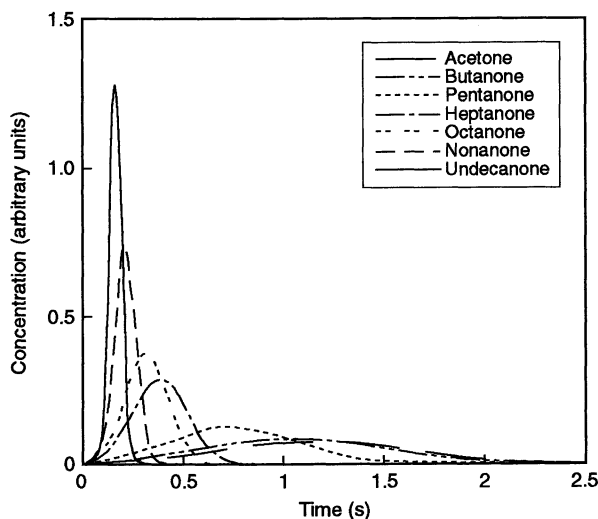


Figure 6. Ketone concentrations emerging from the nasal cavity over a period of one minute.

(Reproduced with permission from reference 25. Copyright 1998.)

The above result was obtained from a single flavor pulse injected into a stream of constant flowing gas. However, during eating there are usually a number of chews during the exhalation period and hence a number of flavor pulses are pumped into the breath stream. Figure 7 shows the time-dependent release of heptanone from chewing gum with a chewing frequency of 2.5 per second and breathing rate of 12 cycles per minute. The overall release envelope is clearly shown by the peaks of the individual pulses. These pulses are grouped into packets corresponding to the exhalation periods, separated by periods of inhalation. Re-scaling the abscissa axes of Figure 7 reveals the finer details of the release curve (Figure 8) and in particular the grouping of the pulses can be observed more clearly.

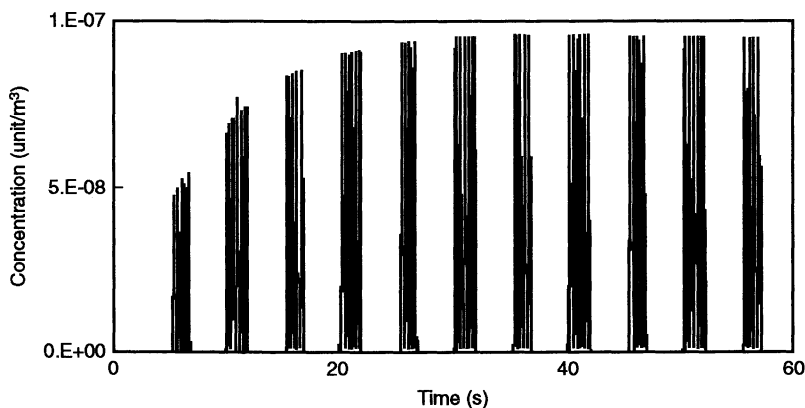


Figure 7. Time-dependent heptanone concentration in the nasal cavity over a period of one minute.

(Reproduced with permission from reference 25. Copyright 1998.)

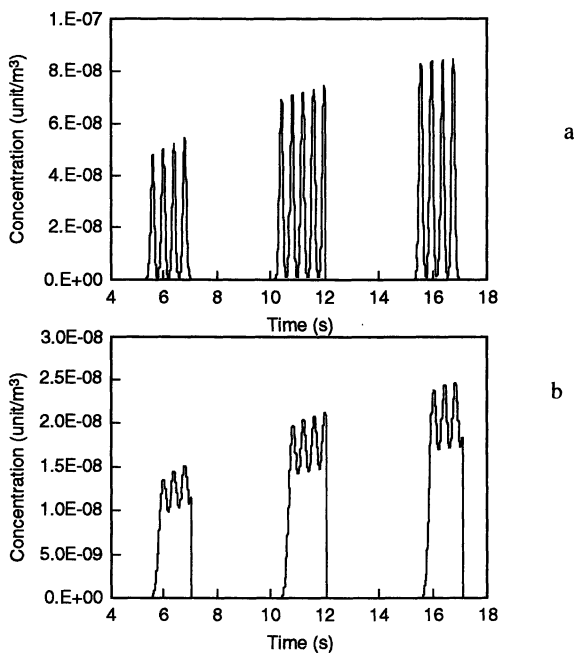


Figure 8. Influence of breathing and chewing on nose-space (a) heptanone and (b) pentanone concentrations.

(Reproduced with permission from reference 25. Copyright 1998.)

Comparison of the two release curves in Figure 8 show the effect of varying the partition coefficient on the times and rates at which volatiles arrive at the olfactory epithelium. Comparison of Figures 8a (heptanone) and 8b (pentanone) show that decreasing the air-mucous partition coefficient smears out the individual pulses due to the increased interaction of the mucus lining. This calculation was performed using identical mass transfer coefficients for the two compounds, however, it has recently been shown that values of h_D increase with increasing length of the hydrophobic chain^{17, 29}. If such values had been used for the above calculation the differences in Figure 8 would have been enhanced further.

In conclusion, therefore, the results in this paper predict that the solubility of the flavors in the mucus phase is a major factor determining the rate at which flavors are transported to the nasal cavity. Other factors influencing the rate of transport are mucus thickness, breathing velocity, and rate of volatile transfer between the air and mucus phases. In reality the flavor profile recorded by APCI-MS in the nasal cavity differs from that reaching the receptors. This is because volatiles are first selectively absorbed onto, and then diffuse across, a mucus film coating the olfactory bulb³⁰. The rate at which this process proceeds depends on the physico-chemical properties of the individual volatiles. Hence, the flavor profile interacting with the receptors may be very different to that flowing through the nasal cavity.

Obviously, the simulation presented in this paper takes a very mechanistic approach to breathing and chewing. In reality, an individual will vary their mastication pattern during the chewing process. Furthermore, differences in mastication behaviour between individuals differs further still. However, it is possible to incorporate these variations into the simulation⁵. One important aspect of the eating process that has not been considered in this paper is the effect of swallowing. This subject will be tackled in a future paper.

Acknowledgements

This work was carried out under a BBSRC (UK) LINK project with Firmenich, Nestlé and the University of Nottingham as the other Consortium partners.

References

1. Delahunty, C. M.; Piggott, J. R. *Int. J. Food Sci. Tech.* **1995**, *30*, 555-570.
2. Wilson, C. E.; Brown, W. E. *J. Sensory Studies* **1997**, *21*, 69-86.
3. Ingham, K. E.; Linforth, R. S. T.; Taylor, A. J. *Food Science and Technology-Lebensmittel-Wissenschaft & Technologie* **1995**, *28*, 105-110.
4. Linforth, R. S. T., Baek, I., Taylor, A. J. *Food Chem.*, **1999**, *6*.
5. Harrison, M.; Campbell, S.; Hills, B. P. *J. Agri. Food Chem.* **1998**, *46*, 2736-2743.
6. Hills, B. P.; Harrison, M. *Int. J. Food Sci. Tech.* **1995**, *30*, 425-436.5, 77-83.
7. Harrison, M.; Hills, B. P. *Int. J. Food Sci. Tech.* **1996**, *31*, 167-176.
8. Harrison, M.; Hills, B. P.; Bakker, J.; Clothier, T. *J. Food Sci.* **1997**, *62*, 653.
9. Bakker, J.; Boudaud, N.; Harrison, M. *J. Agri. Food Chem.* **1998**, *46*, 2714-2720.
10. deRoos, K. B.; Wolswinkel, K. In *Trends in Flavor Research*. Maarse, H.; Van Der Heij, D. G., Ed.; Elsevier: London, **1994**, Pp.15-32.
11. McNulty, P. B. In *Food Structure and Behaviour*; Blanshard, M. & Lillford, P., Ed.; Academic Press: London, **1987**, Pp 245.
12. Harrison, M. *J. Agri. Food Chem.* **1998**, *46*, 2727-2735.
13. Mills, O. E.; & Solms, J. *Lebensmittel-Wissenschaft & Technologie*, **1987**, *17*, 331-335.
14. Landy, P.; Druaux, C.; Voilley, A. *Food Chemistry* **1997**, *54*, 387-392.
15. Harrison, M.; Hills, B. P. *J. Agri. Food Chem.* **1997**, *45*, 1883-1890.
16. Goubet, I.; LeQuere, L. J.; Voilley, A. *J. Agri. Food Chem.* **1998**, *46*, 1981-1990.
17. Andriot, I.; Harrison, M.; Fournier, N.; Guichard, E. In *Interactions between ligands and the food matrix*. Proceedings of COST ACTION 96, Oslo, 20-21 May, 1999.
18. Darling, D. F.; Williams, D.; Yendle, P. In: *Interactions of food components*. Birch, G. G.; Lindley, M. G., Ed.; Elsevier: London **1986**, Pp. 165-188. London, Elsevier.
19. Roberts, D. D.; Elmore, J. S.; Langley, K. R.; Bakker, J. (1996). *J. Agri. Food Chem.* **1996**, *44*, 1321-1326.
20. Nahon, D. F.; Harrison, M.; Roozen, J. P. *J. Agri Food Chem.*, **2000** (submitted).
21. Prinz, J. F.; Lucas, P. W. *Archives of Oral Biology* **1995**, *40*, 401-403.
22. Harrison, M.; Hills, B. P. *Int. J. Food Sci. Tech.* **1997**, *32*, 1-10.
23. Linforth, R. S. T. Private communication, **1997**.
24. Dawes, C.; MacPherson, L. M. D. *Caries Research* **1992**, *26*, 176-182.
25. Harrison, M.; Pia, D. In *Interactions between ligands and the food matrix*. Proceedings of COST ACTION 96, Athens, 24-26 September, 1998.
26. Brown, W. Private communication, **1999**.
27. Van Deemter, J. J.; Zuiderweg, F. J.; Klinkenberg, A. *Chemical Engineering Sciences* **1956**, *5*, 271-289.
28. Linforth, R. S. T.; Taylor, A. J. *Perfumer and Flavorist*, **1998**, *23*, 47-53.
29. Sostmann, K.; Guichard, E. *Food Chemistry*, **1998**, *62*, 509-513.
30. Keyhani, K.; Scherer, P. W.; Mozell, M. M. *J. Theoretical Biology* **1997**, *186*, 279-301.

Chapter 16

A Gas–Liquid Interfacial Mass-Transfer Cell for Studying Flavor Release

Alan Parker¹ and Michèle Marin²

¹Corporate Research Division, Firmenich S. A.,
1, route des Jeunes, CH–1211 Geneva 8, Switzerland

²Institut National Agronomique Paris-Grignon, 78850 Thiverval-Grignon, France

Flavor release from liquids has been studied *in vitro* using an API-MS detector coupled to a novel cell allowing liquid-gas exchange. Using this setup, the release of aroma compounds can be measured in real time. The thin layer of solution can be either static or flowing. A simple equation for the mass transfer has been established. This has been compared with measurements of volatile release from solution, while varying the gas and liquid flow rates, the nature, and concentration of the sample.

Flavor release during drinking occurs on a very short time scale, as drinks are only kept in the mouth for a few seconds at most. Therefore, equilibrium measurements will not give full information about flavor release. The API-MS technique provides an opportunity to make real time measurements of flavor release from liquids on the time scale of drinking. While it is obviously essential to measure flavor release in the nose, the complexity of this process makes it very difficult to identify the limiting physical parameters. Therefore, we have measured the dynamics of flavor release *in vitro*, using a well defined geometry in which we can control all of the operating conditions. In this situation, mathematical models should be in agreement with experimental data, without the need to fit parameters in an arbitrary way.

Previous studies of flavor release can be divided into two groups. In the first are models of eating and drinking. The recent papers by Harrison and Hills (e.g. 1) are good examples. This approach is very important, as it allows comparison of theory and the real world. However, the theory inevitably contains many variables which are poorly defined and experiments (like people) are not very reproducible. Therefore, it is difficult to fully validate such models. The second group is made up of studies of flavor release *in vitro*. This usually involves bubbling gas through the sample. This is a useful experimental method to determine equilibrium data such as the Henry's constant (2). For instance, Elmore and Langley (3) measured flavor release as a

function of time while bubbling helium through a solution of volatile compound. However, the results were not very reproducible (the variance was typically 15%). They discussed the maximum concentration and time to maximum concentration in a qualitative way. No attempt was made to model the results mathematically. Experiments based on blowing air over a liquid surface have also recently been carried out (4, 5). To model the results it was assumed that the gas was well stirred.

This paper is focused on measurements of volatile release from solution, in a novel cell, where the gas and liquid are flowing in thin films. The geometry is well defined so, in principle, no arbitrary assumptions about the flow conditions are necessary. The mathematical modeling of flavor release in this geometry is developed from a chemical engineering perspective.

Experimental

Cell Design

Figure 1 shows a schematic of the new flow cell, which we call the GLIM (Gas-Liquid Interfacial Mass-transfer) cell. It has a three layer sandwich construction.

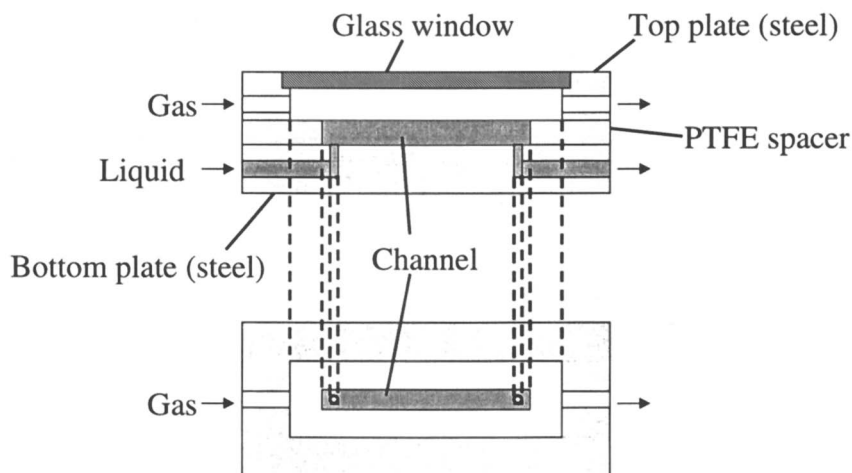


Figure 1. Schematic of the GLIM cell. Side view (above) shows the three layer construction.

Liquid flows into and out of the lower stainless steel plate through 1 mm holes. Gas-liquid contact occurs in a channel formed by a long rectangular hole in the central PTFE plate. Gas flows into and out of the upper stainless steel plate, which is fitted

with a glass window. The liquid channel is 53 mm long x 5 mm wide x 5 mm deep with a volume 1.3 cm³ and a gas-liquid contact area of 2.5 cm². The gas channel is 63 mm long x 16 mm wide x 19 mm deep with a volume of 19 cm³. Liquid is pumped through the cell using a syringe pump, which gives a more regular flow rate than a peristaltic pump. Clean air is sucked through the cell using the API interface. Liquid which has flowed through the cell goes to waste. The gas from the outlet flows directly into the API-MS for analysis. The API-MS setup has already been described by Linforth and Taylor (6).

Operating Modes

The GLIM cell can be used in three distinct ways:

1. Steady state dynamic: Liquid flowing, continuous sample injection.
 - a) Counter-current, with air and water flowing in opposite directions.
 - b) Co-current, with air and water flowing in the same direction.
2. Unsteady state dynamic: Liquid flowing, inject a slug of sample.
3. Unsteady state static: Liquid not flowing.

All the measurements discussed here were carried out under steady state dynamic conditions.

Control of the Liquid Level

The main experimental problem using the GLIM cell is maintaining the liquid level constant. On one hand, liquid must not overflow and enter the capillary leading to the API-MS. On the other hand, the cell must not become empty. Simple methods, such as sucking sample out of the cell at the same rate as pumping it in using two channels of a peristaltic pump, did not give a stable liquid level for more than short times. In addition, control was awkward when changing flow rates and samples.

For this study, a rather inelegant method, which nevertheless gave good results, was adopted: the PTFE plate was redesigned with a long (2 cm), shallow spout at the outlet end and the liquid outlet hole in the bottom plate was blocked. The flow of liquid out of the cell through the spout was controlled by moving a hydrophilic, porous plug (a pipe cleaner) up and down the spout. The entrance to the spout from the cell was always blocked by a meniscus of liquid, so that no air could flow out through it. The level of liquid in the cell was constantly checked by eye through the upper window.

At present we are implementing an automated system of level control using a feedback loop in which the volume of liquid in the channel is determined by conductivity measurements. The signal from the conductivity meter will be fed into a standalone process controller. This will adjust the flow rate of a peristaltic pump connected to the liquid outlet so that the signal from the conductivity meter, and hence

the volume of liquid in the cell, remains constant. This method proved more difficult to implement than expected, as the flat electrodes incorporated into the bottom plate give a very non-linear response as a function of liquid volume: almost all of the signal is due to the liquid causing contact. Further increases in the volume of liquid in the cell hardly affect the signal. Successful use of this method of level control requires redesign of the electrodes. They should cover the full depth of the channel.

Aroma Compounds

Octanal was used as a typical aroma compound with a high volatility (the air-water equilibrium coefficient, K_{aw} , = 1.5×10^{-2} at 25°C) and 2,5 dimethyl pyrazine (DMP) was used as an aroma compound of low volatility (K_{aw} = 6×10^{-5} at 25°C).

Theory

The air-water equilibrium constant for the aroma compound is given by:

$$K_{aw} = \frac{c_a}{c_w} = \left(\frac{\gamma \cdot P}{P_T} \right) \frac{\bar{V}_w}{\bar{V}_a} \quad (1)$$

where c_a and c_w are the concentrations (v/v) of aroma compound in air and water, respectively, γ is the aroma compound's activity coefficient in water, P is its saturated vapor pressure, and P_T is the total pressure. \bar{V}_w and \bar{V}_a are the molar volumes of air and water. Since the aroma compound is dilute, its activity coefficient can be assumed to be independent of concentration. In this case γ has its value at infinite dilution, γ^∞ . The product $\gamma^\infty P$ is the Henry's constant, which is temperature dependent.

The GLIM cell is a kind of liquid-gas contactor, a piece of equipment which is widely used in chemical engineering. Consequently, mass transfer is well understood in this geometry (7). Mass transfer is due to the difference in chemical potential between the gas and liquid phases. For a dilute compound, the rate of mass transfer through the interface is given by:

$$\frac{dm}{dt} = A \cdot k_L (c_w(t) - \frac{c_a(t)}{K_{aw}}) \quad (2)$$

where A is the interfacial area and k_L is the "overall mass transfer coefficient" referring to the liquid side, based on the "two resistance theory" (7):

$$\frac{1}{k_L} = \frac{1}{K_{aw} \cdot k_g} + \frac{1}{k_l} \quad (3)$$

The overall liquid side mass transfer coefficient, k_L , includes mass transfer through the air to the interface (k_g) and through the water to the interface (k_l), as well as the partition coefficient (K_{aw}). In interfacial mass transfer, the phase taken as reference must be clearly defined when comparing mass transfer coefficients between different studies.

The mass balance for the aroma compound is given by:

$$dm = v_a \cdot dc_a = -v_w \cdot dc_w \quad (4)$$

where v_a and v_w are the flow rates in water and air. This equation must be solved simultaneously with that for interfacial mass transfer (eq 2) to calculate the amount of aroma compound at the air outlet of the cell. The problem can be greatly simplified by making three assumptions. These will be justified experimentally below. They are:

1. A negligible fraction of the aroma compound is transferred from water to air, so the inlet and outlet concentrations in the water are equal.
2. The concentration of aroma compound in the air is much smaller than in the water so that it is a good approximation to set the driving force for mass transfer to $c_w(t)$ in eq 2.
3. The aroma compound makes a negligible contribution to the total gas flow. This is obviously true.

Integrating eqs 2 and 4 using these assumptions gives a remarkably simple expression for the mass transfer coefficient:

$$k_L = \frac{c_a \cdot v_a}{c_w \cdot A} \quad (5)$$

The interfacial area (A), the air flow rate (v_a) and the concentration of aroma compound in the water (c_w) are all known, so that measuring the concentration of aroma compound in the air at the outlet (c_a) is all that is needed to calculate the overall mass transfer coefficient.

Referring to the definition of k_L (eq 3), when the volatility is low $K_{aw} \cdot k_g \ll k_l$, so $k_L = K_{aw} \cdot k_g$, whereas when the volatility is high $K_{aw} \cdot k_g \gg k_l$, so $k_L = k_l$. In the first case, the mass transfer is *gas-phase limited*, whereas in the second, it is *liquid-phase limited*. It is important to note that all other things being equal, changing the Henry's constant will change the relative contribution of the two resistances to the overall mass transfer. Summarizing, in the two limits just described, the release of aroma compounds of low volatility will be *gas-phase limited*, whereas the release of aroma compounds of high volatility will be *liquid-phase limited*.

It is also important to note that the air-water equilibrium constant, K_{aw} , affects the interfacial flux (eq 2) in two separate ways. Firstly, it controls the driving force, which is given by the difference between a) the liquid phase concentration which would be in equilibrium with the actual gas concentration and b) the actual liquid phase concentration. Secondly, it enters into the expression for the mass transfer coefficient - eq 3. This second factor has not been taken into account explicitly in most studies in the literature. For instance, Harrison and Hills (1) use a constant overall mass transfer coefficient for all aroma compounds.

It is well known that the rate of mass transfer is much higher when the flow is turbulent than when it is laminar. The type of flow is determined by the Reynolds' number, which is the ratio of inertial to viscous forces. Above some geometry-dependent critical value, flow is no longer laminar. In the GLIM cell's rectangular tubes the critical value is several hundred, depending on the ratio of height to width. Reynolds' number is given by:

$$\text{Re} = \frac{\rho v l}{\eta} \quad (6)$$

where ρ is the fluid density, v is the fluid velocity, l is some typical dimension and η is the fluid viscosity. In a tube with a circular cross section, l is the tube diameter, whereas in a rectangular cross section tube of height a and width b , an equivalent diameter, d_{eq} is used. It is given by (8):

$$d_{eq} = \frac{2 \cdot a \cdot b}{a + b} \quad (7)$$

Equations 6 and 7 can be used to calculate the Reynolds' number for both the air and water in the GLIM cell. Inserting the cell geometry and the physical properties of water and air at 25°C gives the following relationships between Reynolds' number (Re_l and Re_g , respectively) and flow rate for the liquid and gas (q_l and q_g , respectively):

$$\begin{aligned} \text{Re}_l &= 3q_l \\ \text{Re}_g &= 0.075q_g \end{aligned} \quad (8)$$

The flow rate, q , is in mL/min. As the flow rate of water was typically 1 mL/min and that of air typically 40 mL/min, the Reynolds number was close to 3 in both phases. This value is two orders of magnitude less than the critical Reynolds number, so both liquid and gas flow were laminar. Knowing the Reynolds' number allows calculation of the mass transfer coefficient, using a relationship between dimensionless parameters (8). For instance, the Levêque correlation for laminar flow gives a mass transfer coefficient in one fluid phase which is proportional to the flow rate to the power 0.33.

Results and Discussion

In this study, only steady state dynamic measurements were considered. Figure 2 shows some typical raw data. The amount of 2,5 DMP in the air outlet was measured in five separate experiments for each of three gas flow rates. The signals did not vary with time, showing that the measurements were made at steady state. The data also show typical signal to noise ratios and run to run reproducibility. Note that the API-MS signal is not directly proportional to the aroma compound concentration. To obtain a result proportional to the concentration, the signal must be divided by the gas flow rate.

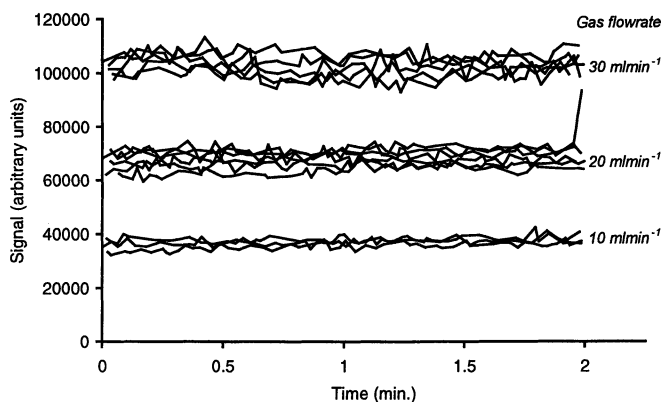


Figure 2. Raw data from API-MS. Repeat measurements of release from a 10 $\mu\text{L/L}$ solution of 2,5DMP at three different gas flow rates. Changing the water flow rate had no effect on these results.

The main observations are:

1. The coefficient of variation from run to run was typically 5%. We expect this figure to improve significantly when the control of the liquid level is automated.
2. The concentration of aroma compound in the water had no effect on the calculated mass transfer coefficient, so both mass transfer and detection by API-MS were linear over the range of operating conditions used here.
3. Table I shows that running the cell in counter-current and co-current configurations gave the same results, which implies that the concentration of aroma compound in the gas phase is always negligible relative to that in the liquid phase (eq 5). Even in this "worst case", with a volatile aroma compound, no more than 5% of the total was released.
4. The overall mass transfer coefficients for octanal (high volatility) were of the order of 10^{-6} m/s, which is typical for small molecules in liquid (9). Thus the overall mass

**Table I. Effect of co-current and counter current flow on release of octanal
0.1 mg/L octanal in water, gas flow rate = 40 mL/min**

<i>Water flow rate (mL/min)</i>	<i>Co-current: Concentration in air (nL/L) and fraction released</i>	<i>Counter current: Concentration in air (nL/L) and fraction released</i>
1	19 (5%)	20 (5%)
2	19 (2%)	19 (2%)
4	23 (1%)	26 (1%)

transfer coefficient is close to the liquid mass transfer coefficient, as expected for a volatile compound.

5. The overall mass transfer coefficients of the aroma compound with low volatility, 2,5 DMP, were of the order of 10^{-8} m/s which is lower than a liquid mass transfer coefficient. But, in this case of low volatility, the mass transfer coefficient in the gas phase (k_g) could be limiting. Taking a value of $k_g = 10^{-3}$ m/s for a molecule in a low mobile gas phase (9), the product of K_{ow} and k_g is close to the value of the overall mass transfer coefficient measured experimentally, which confirms eq 3.

Effect of Water Flow Rate

The low volatility of 2,5 DMP leads us to expect that release will be gas-phase limited, that is water flow rate will not have an effect. This is what we observed: changing the water flow rate from 1 to 2 to 4 mL/min had no effect on the API-MS signal.

Conversely, the high volatility of octanal implies that the water flow rate will influence the mass transfer, and this was in fact observed. Changing the flow rate from 2 to 4 mL/min led to an increase in the mass transfer coefficient from 3×10^{-6} to 4×10^{-6} m/s. The Levêque correlation, mentioned above, implies that doubling the flow rate should increase the mass transfer coefficient by a factor of $2^{0.33} = 1.26$ or 26%, which compares very favorably with the 33% increase observed. However, we think that this good agreement might be fortuitous. More measurements are needed to confirm the effect.

Effect of Air Flow Rate

The initial results for the effect of air flow rate were less satisfactory. For 2,5DMP, we found a linear increase with the air flow rate from 10 to 40 mL/min, greater than that predicted by the Levêque relationship. On the other hand, for octanal, the same change in air flow rates also showed a difference: for instance, the mass transfer

coefficient apparently increased from 2.4×10^{-6} to 3.2×10^{-6} m/s at a water flow rate of 2 mL/min. This is unexpected for an aroma compound of high volatility. We have two possible explanations for this result. Firstly, the range of variation of the flow rates is really too narrow to provide a good check for the theoretical relationships between dimensionless parameters. Secondly, increasing the air flow rate increases the interfacial area, by inducing surface waves (10). Even shallow waves can significantly increase the interfacial area, which increases the rate of mass transfer, without altering the mass transfer coefficient (see eq 2). The validity of this idea can be tested by adding a very small amount of surfactant to the water, as this completely damps the surface waves (10).

Conclusions

The GLIM cell coupled to the API-MS detector can be used to measure flavor release in real time from a flowing liquid. Initial tests show reasonable agreement with theory for the effects of volatility, water flow rate, and air flow rate. A larger range of operating conditions need to be studied in order to validate the theoretical relationships established for liquid-gas mass transfer. Improved control of the interfacial area and liquid level is needed if the cell's full potential is to be realized. Once these problems are resolved, the setup described here will be a useful test bed for model studies of the effects of viscosity, binding, emulsions, and so forth on flavor release.

References

1. Harrison, M.; Hills, B. P. *Int. J. Food Sci. Technol.* **1997**, *32*, 1-9.
2. Leroi, J.-C.; Masson, J.-C.; Renon, H.; Fabries J.-F.; Sannier, H. *Ind. Eng. Chem., Process Des. Dev.* **1977**, *16*, 139-144.
3. Elmore, J. S.; Langley, K. R. *J. Agric. Food Chem.* **1996**, *44*, 3560-3563.
4. Bakker, J.; Boudaud, N.; Harrison, M. *J. Agric. Food Chem.* **1998**, *46*, 2714-2720.
5. Marin, M.; Baek, I.; Taylor, A. *J. Agric. Food Chem.* **1999**, in press.55
6. Linforth, R.S.T.; Taylor, A.J. European Patent 97305409.1, 1998.
7. Treybal, R.E. *Mass transfer operations*; McGraw-Hill: New York, 1968, pp 50-53.
8. Coulson, J.M.; Richardson J.F. *Chemical Engineering*; 3rd ed.; Pergamon Press: Elmsford, NY, 1977.
9. Cussler, E.L. *Diffusion mass transfer in fluids systems*; 2nd ed.; Cambridge University Press: New York, 1997.
10. Levich, B. *Physicochemical Hydrodynamics*; Prentice-Hall: New York, 1962; pp 591-668.

Chapter 17

Modeling Flavor Release from Oil-Containing Gel Particles

Guoping Lian

Unilever Research Colworth Laboratory,
Sharnbrook, Bedford MK44 1LQ, United Kingdom

This paper presents a modelling study of flavor release from oil containing gel particles. A general equation for the diffusion of flavor molecules in gels with micro-inclusion of oil droplets has been formulated. The equation with micro-inclusion is shown in the same format of that without micro-inclusion and degenerates to the latter when the volume fraction of the micro-inclusion approaches zero. The release of a diffusive material from a spherical particle has been previously predicted either by the Crank equation or the Sherwood correlation. The Crank equation considers the diffusion in the particle and ignores the resistance by the bulk fluid. The Sherwood correlation considers the mass transfer from a particle suspended in an infinite fluid. It is proposed that the mass transfer coefficient for the release of flavor from a gel particle should take into account the both effects from the gel particle and the surrounding fluid. The effect of particle size, volume fraction of micro-inclusion and partition coefficient on flavor release rate has been investigated.

Flavor release from oil-containing gel particles involves the diffusion of flavor molecules through a heterogeneous media consisting of distinctively different phases of materials of different diffusion coefficients and partitions. Diffusion in heterogeneous media is also important in a number of areas such as drug delivery (1,5,19), food processing (14), drying and polymer processing (18). Many previous studies have considered the effective diffusion of two-phase systems where one phase is dispersed in the other continuous phase (10,13,18). The diffusive molecules were assumed to be only soluble in the continuous phase and their diffusion coefficient in the dispersed phase was considered to be sufficiently small. The diffusion equation was written as

$$(1 - \phi) \frac{dc}{dt} = D_c \nabla c \quad (1)$$

where ϕ is the volume fraction of the dispersed phase and D_e is the effective diffusion coefficient, c is concentration of flavor and ρ is the gradient operator defined as

$$\nabla = i \frac{\partial}{\partial x} + j \frac{\partial}{\partial y} + k \frac{\partial}{\partial z}$$

A number of models have been proposed for the effective diffusion. The commonly used ones include the Maxwell model (12,13,18), which is based on electric conduction theory

$$D_e = D_c \frac{1-\phi}{1+\phi} \quad (2)$$

and the Mackie-Mears model (11,18), which is based on stochastic obstruction theory

$$D_e = D_c \frac{(1-\phi)^2}{(1+\phi)^2} \quad (3)$$

where D_c is the diffusion coefficient in the continuous phase.

This paper is concerned with the more general case of effective diffusion in two-phase materials. The molecules are soluble and diffusive in both phases. The system under consideration is the release of flavor from gel particles with homogeneously distributed micro-inclusion of oil droplets. The size of the dispersed phase is assumed to be sufficiently small such that at the microscopic level the concentrations in the two phases are in instantaneous equilibrium

$$c_d = P_{dc} c_c \quad (4)$$

where P_{dc} is the partition coefficient, c_d and c_c are the concentrations of flavor in the dispersed phase and continuous phase respectively.

In the first part of the paper, the general equation of diffusion in a two-phase dispersion has been formulated. The second part of the paper considers the release of flavor from oil containing gel particles. Many previous studies used the Crank equation based on diffusion for the release of diffusive materials from a spherical particle (1,6,16,19,20). The Crank equation considers the diffusion in the particle and ignores the resistance by the bulk fluid.

Mass transfer from a solid phase to a fluid phase has been also a subject of research in fluid mechanics for many years (2,17). For a particle suspended in a fluid, the interfacial mass transfer coefficient is often predicted by Sherwood correlation (17). The Sherwood correlation considers the mass transfer to an infinite fluid from a suspended particle with a constant surface concentration. The penetration may be considered as a special case of interfacial mass transfer theory (3,7,15). The penetration theory assumes that mass transfer between phases is by a short time contact of an element of one phase with another. During the short time contact at the interface, it is assumed that non-steady-state diffusion in a semi-infinite body takes place. After the short time contact, the element is mixed thoroughly in the liquid phase and a new element come into contact. The penetration theory predicts that the mass transfer coefficient is proportional to the square root of diffusion coefficient.

Recently, a flavor release model based on two stagnant film theory has been proposed by Hills and Harrison (9). The model assumed that the mass transfer across the food-saliva interface is rate limiting. Harrison and Hills (8) have further extended their interfacial mass transfer model to gelatine-sucrose gels by considering the melting process due to heat transfer. One limitation of their model is that the mass transfer coefficient needs to be obtained by fitting with experimental data. Their model also assumed both the solid food and liquid saliva as homogeneous materials and did not consider micro-inclusions. Thus, it can not be applied to oil-containing gels.

In this study, a more general model of mass transfer across oil containing gel particle and liquid interface has been proposed. The newly proposed model includes the effects of both phases (solid and fluid) on the interfacial mass transfer coefficient. It is shown that the Crank equation and Sherwood correlation are special cases of the newly proposed equation. Application of the model has been also demonstrated by predicting the effects of particle size, volume fraction of micro-inclusion (oil) and partition coefficient on flavor release rate.

Effective Diffusion

The mass transfer rate in the continuous phase is given by Fick's first law of diffusion

$$j_c = -D_c \nabla c_c \quad (5)$$

By analogue, the mass transfer in the dispersed phase is given by

$$j_d = -D_d \nabla c_d \quad (6)$$

where D_c and D_d are the diffusion coefficients in the continuous phase and dispersed phase respectively.

Recalling eq 4, the mass transfer in the dispersed phase may be written as

$$j_d = -D_d P_d \nabla c \quad (7)$$

Thus, the mass transfer equation in the dispersed phase may be treated as the same of the continuous phase but with a different diffusion coefficient of $D_d P_{dc}$.

From eq 5 and eq 7, the overall mass transfer through a composite material may be deduced as follows

$$j = -D \nabla c \quad (8)$$

where D_e is effective diffusion coefficient, $\min(D_c, D_d P_{dc}) < D_e < \max(D_c, D_d P_{dc})$.

The effective diffusion coefficient depends on the microstructure of the dispersed phase and may be estimated by empirical correlation, e.g. the general Maxwell equation (12), by replacing D_d by $P_{dc} D_d$

$$D_e = D_c \frac{D_c (1 - \phi) \xi + P_{dc} D_d (1 + \xi \phi)}{D_c (\xi + \phi) + P_{dc} D_d (1 - \phi)} \quad (9)$$

where ξ is a shape factor ($\xi=2$ for dispersed spheres).

Particularly, if $D_c \gg D_d$, eq 9 reduces to eq 2. Introduce an effective concentration of flavor in the two-phase structured particle defined as

$$c_p = c_c(1 - \phi) + \phi c_d = c_c(1 - \phi + \phi P_{dc}) \quad (10)$$

It may be derived that the mass conservation equation of diffusion may be written as follows

$$\frac{\partial c_p}{\partial t} = \nabla(D_p \nabla c_p) \quad (11)$$

where $D_{ep} = \frac{D_e}{1 - \phi + \phi P_{dc}}$.

Note that eq 11 is in the same format of diffusion equation in homogeneous continua. At the special case $P_{dc} = 0$ and $D_d \ll D_c$, eq 11 degenerates to eq 1, a special case studied by many previous researchers. On the other hand, when the volume fraction of the dispersed phase is reduced zero, $\phi = 0$, eq 11 degenerates to the diffusion equation in homogeneous one-phase media.

Flavor Release

Crank Model

Consider flavor release from an oil-containing gel particle suspended in an aqueous phase. If the gel particle is spherical in shape, the diffusion eq 11 of flavor molecules in the particle may be written in terms of spherical polar coordinates as follows

$$\frac{\partial c_p}{\partial t} = \frac{D_p}{r^2} \frac{\partial}{\partial r} (r^2 \frac{\partial c_p}{\partial r}) \quad (12)$$

Eq 12 may be solved analytically under the boundary conditions of

$$c_p(t) = 0 \quad \text{if } r = R$$

$$\frac{\partial c_p}{\partial r} = 0 \quad \text{if } r = 0 \quad (13)$$

where R is the radius of the sphere.

From the analytical solution, the amount of diffusing substance leaving the sphere is expressed by (4)

$$\frac{M_t}{M_0} = 1 - \sum_{n=0}^{\infty} \frac{6}{\pi^2 n^2} \exp\left[-\frac{D_{ep} \pi^2}{R^2} n^2 t\right] \quad (14)$$

where M_0 is the initial total amount of the diffusive substance in the sphere and M_t is the amount of the substance diffused out of the sphere.

The underlying assumption of the boundary condition of eq 13 is that substance that diffused out of the sphere is instantaneously removed and there is no external

resistance in the surrounding aqueous phase to the mass transfer. It also implies that the surrounding aqueous phase is treated as an infinite sink.

Eq 14 contains an infinite number of terms and is very difficult to apply. In practice, the early stage of the equation can be approximated by the following equation to a good accuracy (1)

$$\frac{M_t}{M_0} = 6\sqrt{\frac{D_p t}{\pi R^2}} - 3\frac{D_p t}{R^2} \quad (15)$$

Alternatively, noticing that the leading term in eq 14 is $\exp(-D\pi^2 t/R^2)$, we may also approximate the Crank equation by the leading term. The best fit to the Crank solution using the first-term is given by

$$\frac{M_t}{M_0} = 1 - \exp\left(-1.2\frac{D_p \pi^2}{R^2}t\right) \quad (16)$$

A comparison of the above approximate expressions with the exact Crank solution is shown in Figure 1. It can be seen that the approximation of eq 15 agrees very well with the exact solution in the early stage but under-predicts the exact solution significantly as the time increases. The leading term approximation under-predicts the flavor release rate initially, but this under prediction is reduced as the time is increased.

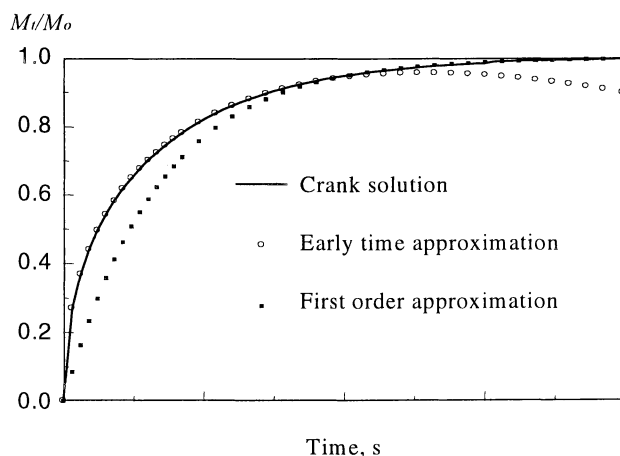


Figure 1. Dimensionless flavor release rate for a sphere predicted by Crank solution, early time approximation and first order approximation.

Sherwood Correlation

Mass transfer from particles suspended in fluid has been a subject in fluid mechanics and chemical engineering for many years (2,17). Prediction of mass transfer from a suspended particle is analogous to the prediction of heat transfer and dimensionless correlations have been applied. The Nusselt and Prandtl numbers have been substituted by the Sherwood and Schmidt numbers. For mass transfer between a fluid and solid spherical particle, the following equation has been suggested (17)

$$\frac{dM_t}{dt} = 2\pi R Sh D_f \left(\frac{c_p}{P_{pf}} - c_f \right) \quad (17)$$

where D_f is the diffusion coefficient of the fluid, P_{pf} ($=1-\phi+\phi P_{dc}$) is the effective partition coefficient between the particle and the fluid, c_f is the concentration in the bulk fluid and Sh is the Sherwood number.

The Sherwood number is a dimensionless parameter measuring the mass transfer between two phases. The following correlation has been suggested

$$Sh = 2 + 0.6 Re^{1/2} Sc^{1/3} \quad (18)$$

where Re and Sc are the Reynolds and Schmidt numbers defined as

$$Re = \frac{2\rho R u_p}{\eta}, \quad Sc = \frac{\eta}{2\rho R}$$

where u_p is the relative velocity of the particle in relation to the fluid, ρ is the density, and η is the viscosity of the fluid.

The effective concentration, c_p , is related to the amount of substance diffused out, M_t , by

$$M_t = M_0 - \frac{4\pi}{3} R^3 c_p \quad (19)$$

Under the condition of an infinite sink, $c_f = 0$. Substitution of this condition and eq 19 into eq 17 leads to the following expression

$$\frac{dM}{dt} = \frac{3ShD_f}{2R^2 P_{pf}} (M_0 - M) \quad (20)$$

Eq 20 may be integrated to give the amount of diffusing substance leaving the sphere expressed by

$$\frac{M_t}{M_0} = 1 - \exp\left(-\frac{3ShD_f}{2R^2 P_{pf}} t\right) \quad (21)$$

which is also in the same format of eq 16.

Interfacial Mass Transfer

With the Sherwood correlation, the diffusion resistance in the suspended particle is assumed to be sufficiently small and the mass transfer in the fluid phase is rate limiting. On the other hand, the Crank equation applies to the other extreme, i.e. where diffusion in the particle becomes rate limiting. While both the Crank equation and Sherwood correlation are two special cases, the interfacial mass transfer theory may be applied to the mass transfer between two phases under more general conditions. The interfacial mass transfer theory may be visualized by the two-film theory and the rate of mass transfer from a sphere to the surrounding fluid may be expressed as (15)

$$\frac{dM_t}{dt} = 4\pi R^2 k \left(\frac{c_p}{P_{pf}} - c_f \right) \quad (22)$$

where k is the mass transfer coefficient across the interface

The interfacial mass transfer coefficient is related to the mass transfer coefficients of the particle k_p and fluid k_f by

$$\frac{1}{k} = \frac{1}{P_{pf} k_p} + \frac{1}{k_f} \quad (23)$$

By analogue, with the continuous phase as an infinite sink (i.e. $c_f = 0$), eq 22 can be integrated to give the following expression

$$\frac{M_t}{M_0} = 1 - \exp \left[- \frac{3k_p k_f}{R(k_f + P_{pf} k_p)} t \right] \quad (24)$$

Again, it is a first-order kinetics equation in the same form of eq 16 and eq 21.

Specially, if the mass transfer in the particle becomes rate limiting, we have $P_{pf} k_p \ll k_f$. Comparing eq 24 with eq 16 leads to

$$k_p = 1.2 \frac{\pi^2 D_{ep}}{3R} \quad (25)$$

By analogue, the mass transfer coefficient in the fluid may be derived as

$$k_f = \frac{Sh D_f}{2R} \quad (26)$$

Thus, a more general equation for flavor release based on interfacial mass transfer theory is derived.

Results and Discussion

Eq 22 combined with eq 23, 25 and 26 forms the basic model for describing the flavor release from oil containing gel particles to liquid (e.g. saliva). The equation may be solved analytically under few special conditions. For instance, if the volume

fraction of gel particles in the fluid is ϕ_p , the finite concentration of flavor in the fluid may be expressed as

$$c_f = \frac{3\phi_p M_t}{4\pi R^3} \quad (27)$$

By substitution of eqs 19 and 27 to eq 22, the following expression is derived

$$\frac{dM_t}{dt} = \frac{3k}{RP_{pf}} [M_0 - (1 + \phi_p P_{pf}) M_t] \quad (28)$$

This equation can be integrated to give the amount of flavor released to the fluid expressed as

$$M_t = \frac{M_0}{1 + \phi_p P_{pf}} \left[1 - \exp\left(-\frac{3(1 + \phi_p P_{pf})k}{RP_{pf}} t\right) \right] \quad (29)$$

The system reaches equilibrium when the amount of flavor released is given by

$$M_t = \frac{M_0}{1 + \phi_p P_{pf}} \quad (30)$$

Analytical solutions to eq 22 can be also obtained, as shown by eq 24, if the fluid is assumed under the condition of an infinite sink. The time required to release half of the total flavor, $t_{1/2}$, may be obtained from eq 24 as follows

$$t_{1/2} = \left(\frac{3}{1.2\pi^2 D_{ep}} + \frac{2P_{pf}}{ShD_f} \right) \frac{R^2 \ln 2}{3} \quad (31)$$

Particularly, when the diffusion in the particle becomes rate limiting, the half-life is given by the following equation

$$t_{1/2} = \frac{R^2 \ln 2}{1.2\pi^2 D_e} (1 - \phi + \phi P_{dc}) \quad (32)$$

On the other hand, if the mass transfer in the surrounding fluid is rate limiting, the half-life is then obtained as

$$t_{1/2} = \frac{2R^2 \ln 2}{3ShD_f} (1 - \phi + \phi P_{dc}) \quad (33)$$

Examples of predicted half-life time of oil-containing gel particles are shown in Figures 2 and 3, using eq 32. Here, a constant effective diffusion coefficient of $1.0 \times 10^{-10} \text{ m}^2/\text{s}$ is used. In Figure 2, the half-life time is predicted as functions of partition coefficient and particle radius. The volume fraction of oil droplets is assumed to be 10%. It can be seen that as the partition coefficient from the dispersed phase of oil droplets to the continuous phase of gel is increased, the half-life time required to release half of the flavor also increased. For flavor compounds of low partition coefficients, particle size needs to be increased in order to achieve same release time of higher partition coefficients.

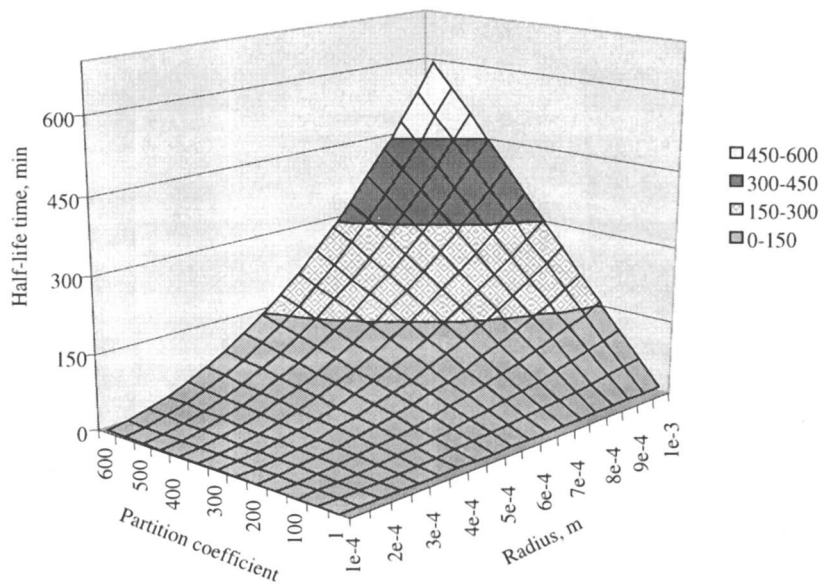


Figure 2. Predicted half-life time as a function of partition coefficient for a spherical particle containing 10% of oil.

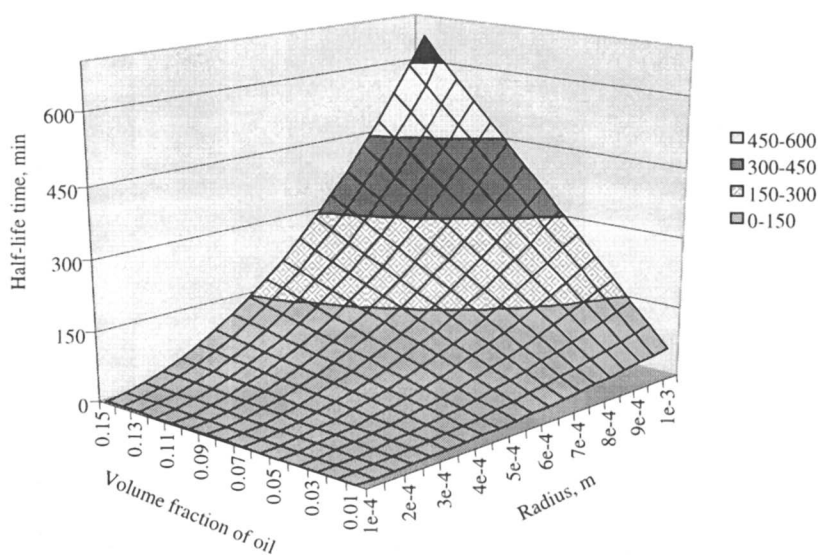


Figure 3. Predicted half-life time as a function of volume fraction of oil for a spherical particle with an oil-gel partition coefficient of 400.

Figure 3 shows the effects of the volume fraction of oil droplets and particle size on the half-life time, where the partition coefficient of dispersed oil droplets to continuous phase is set to 400. Apparently, as the volume fraction of the dispersed oil droplets is increased, the effective partition coefficient P_{pf} ($=1-\phi+\phi P_{dc}$) is also increased. As a result, the half-life time increases.

Conclusions

The diffusion of molecules in two phases of distinctively different materials has been discussed. The system under consideration is the release of flavor from gel particles with homogeneously dispersed micro-inclusion of oil droplets. Assuming that the size of the dispersed oil droplets is sufficiently small such that at the microscopic level the concentrations in the two phases are in instantaneous equilibrium, a general diffusion equation has been derived in terms of effective diffusion coefficient and effective concentration. The general diffusion equation is shown to be in the same format of the ordinary diffusion equation of one phase continuous media. When the volume fraction of the dispersed phase approaches zero, the equation degenerates to the latter.

The release of a diffusive material from a spherical particle has been previously predicted either by the Crank equation or the Sherwood correlation. The Crank equation considers the diffusion in the particle and ignores the resistance by the bulk fluid. The Sherwood correlation considers the mass transfer from a particle suspended in an infinite fluid. It is proposed that the mass transfer coefficient for the release of flavor from a gel particle should take into account of the both effects from the gel particle and the surrounding fluid. The newly proposed flavor release equation degenerates to the Crank equation if the diffusion in the particle is rate-limiting, or the Sherwood correlation when the mass transfer in the surrounding fluid becomes rate-limiting. Application of the newly proposed model has been demonstrated by examining the effect of particle size, volume fraction of micro-inclusion and partition coefficient on flavor release half-life time.

References

1. Baker, R. *Controlled Release of Biologically Active Agents*. John Wiley & Sons, New York, 1987.
2. Batchler, G. K., *J. Fluid Mech.*, **1979**, *95*, 369-400.
3. Coulson, J. M. and Richardson, J. F. *Chemical Engineering*, Pergamon Press, Oxford, 1993.
4. Crank, J. *The Mathematics of Diffusion*, Oxford University Press, London, 1956.
5. Guy, R. H., Hadgraft, J., Kellaway, I. W. and Taylor, M. J., *Int. J. Pharmaceutics*, **1982**, *11*, 199-207.
6. Kurnik, R. T., and Potts, R. O., *J Controlled Release*, **1997**, *45*, 257-264.

7. Harrison, M., Brian, P. H., Bakker, J. and Clothier, T. *J. Food Sci.*, **1997**, *62*, 653-664.
8. Harrison, M. and Hills, B. P. *Int. J. Food Sci. & Tech.*, **1996**, *31*, 167-176.
9. Hills, B. P. and Harrison, M. *Int. J. Food Sci. & Tech.*, **1995**, *30*, 425-436.
10. Jonsson, B. Wennerstrom, H. Nilsson, P. G. and Linse, P., *Colloid & Polymer Sci.*, 1986, **264**, 77-88.
11. Mackie, J. S. and Meares, P. , *Proc. R. Soc. London, A*, **1955**, *232*, 498-509.
12. Maxwell, J. C. A., *Treatise on Electricity and Magnetism*, 2nd ed.; Clarendon Press, Oxford, 1881; Vol. 1., p435.
13. Muhr, A. H., Blanshard, J. M. V., *Polymer.*, **1982**, *23*, 1012-1026.
14. Stapley, A. G. F., Fryer, P. J. and Gladden, L. F., *AIChE J.*, **1998**, *44*, 1777-1789.
15. Saravacos, G. D. In *Engineering Properties of Foods*; Rao, M. A. and Rizvi, S. S. H., Eds, Marcel Dekker, New York. 1986.
16. Schwartzberg, H. G. *J. Food Sci.*, **1975**, *40*, 211-213.
17. Sherwood, T. K., Pigford, R. L., and Wilke, C. R. *Mass Transfer*, McGraw-Hill, New York, 1975.
18. Waggoner, R. A., Blum, F. D. and MacElroy, J. M. D., *Macromolecules*, **1993**, *26*, 6841-6848
19. Washington, C. *Int. J. Pharmaceutics*, **1990**, *58*, 1-12.
20. Wedzicha, B. L. and Couet, C., *Food Chemistry*, **1996**, *55*, 1-6

Chapter 18

A Novel Approach to the Selective Control of Lipophilic Flavor Release in Low Fat Foods

Mark E. Malone, Ingrid A. M. Appelqvist, Terry C. Goff,
Jenny E. Homan, and John P. G. Wilkins

Unilever Research Colworth House, Sharnbrook, Bedford,
MK44 1LQ, United Kingdom

Measurement of real time flavor release has been performed by Atmospheric pressure chemical ionisation mass spectrometry (APCI-MS) in model emulsions and has been compared to time intensity data. This paper will cover aspects of the effect of fat on flavor release and the control of flavor release using oil containing gel particles. Results from flavor release studies as a function of fat content indicate that the release of lipophilic flavor is much more rapid as fat content is reduced and results in a significant change in the temporal release profiles. At high fat content the flavor release is gradual with a 'zeroth' order type of release whereas at lower fat content, particularly < 5% (w/w), there is an initial burst of flavor followed by a rapid fall-off in the flavor intensity. The results indicate that in order to mimic the flavor release of 'full' fat foods under low fat conditions, selective reduction in the rate of lipophilic flavor release is necessary. A novel approach, which selectively controls the release of lipophilic flavor in low fat systems is based on encapsulation of the oil within gel particles. This changes the kinetics of lipophilic flavor release, providing a lower flavor intensity, which is sustained for a longer period of time. Factors affecting the rate of release include; particle size, oil content and the partition coefficients of the flavor compounds.

Fat influences flavor attributes such as flavor character, flavor release and masking of off-flavors (2-6). Fat is a source of flavor since flavor compounds are inherent in lipid ingredients. Flavors with "fatty" sensory attributes come from a variety of different aromas and may contribute to flavor perception to give sweet, buttery, creamy and rich flavor which epitomise full fat products (3,4). Fat can also mask off-flavors because many are lipophilic in nature and have lower vapor pressures in the presence of fat. This reduces the rate at which they are released during mastication, presumably to a point below the detection threshold level.

The concentration of flavor reaching the olfactory receptors will be influenced by the rate of release from the foodstuff. Factors which affect this include flavor concentration, the microstructure and temperature of the food, the occurrence of reversible/irreversible binding, structure breakdown during mastication, mixing with saliva, and most importantly, the concentration of the fat (7-9). Lowering of fat content is known to reduce the absorption of lipophilic flavors to the food matrix thereby influencing the flavor balance (4-7,10). Reduction in the fat level not only affects the intensity of the flavor perception but also influences the temporal profile (6,7,10). In a full fat product the initial impact of the flavor is gradual giving a well balanced flavor profile which is sustained for a long period of time to give a pleasant aftertaste. In fat-free foods, the lipophilic flavor tends to be intense but transient and can manifest itself as an 'unbalanced' flavor (10).

Although sensory techniques have been used to study flavor release there is a real need to support these subjective evaluations with "hard" analytical data. Recently, a new mass spectrometry technique, atmospheric pressure chemical ionisation mass spectrometry (APCI-MS), has enabled the investigation of flavor release under real eating conditions (11). The advantage of this technique is that it is an objective measure of flavor release, providing the opportunity to investigate factors affecting flavor release and the relationship between flavor delivery and perception.

This paper reports on the effect of fat on real time flavor release and some of the issues associated with fat reduction. Furthermore a new concept, microstructured emulsions, is described whereby the release of lipophilic flavors in low fat systems can be controlled by encapsulation of oil within gel particles.

Methods and Materials

APCI MS-Breath

APCI is a mass spectroscopic technique which can be used for the real-time determination of volatiles in air, and has recently been developed in these laboratories and by others (11) as a means of flavor release analysis during mastication. In essence, exhaled air from the nose is sucked into the mass spectrometer where volatiles are generally detected as protonated $[M+H]^+$ ions and can provide a simultaneous time/intensity profile of one or more analytes. The analysis was done on a Navigator mass spectrometer (Finnigan, Manchester, UK) fitted with an APCI interface. When used with a regulated chewing and breathing pattern the MS-breath technique has been shown to have considerable potential as an analytical tool for the study of structure/flavor release phenomena. Depending on the panellist, the respiratory rate was between 6-8 breaths per minute and the rate of chewing was approximately 1 chew per second (i.e. 4 chews on inhalation and 4 chews on exhalation). Typically, the panellist ingested 2mL of sample from a syringe or a spoon and performed the analysis for 2 minutes. Each product was sampled in duplicate or triplicate. The MS-Breath "chromatograms" were integrated on MassLab software and the mean area

counts of each exhalation peak were plotted as a function of time. The products were flavored with a cocktail consisting of d6 acetone, butanone, heptan-2-one, nonan-2-one and ethyl-hexanoate each at a concentration of 5ppm. The response of the instrument was calibrated with a series of 1% xanthan solutions flavored with 1 to 20 ppm of heptan-2-one and was found to be linear in this range.

Time-Intensity Assessment of Flavor Release from Emulsion Systems

Aliquots (2 mL) of emulsion (see below) at room temperature were ingested from disposable plastic syringes. The perception of time intensity was recorded on a linear potentiometer connected via a 1.5V cell to a Servogor 220 flat bed chart recorder such that full-scale deflection (fsd) of the potentiometer gave corresponding fsd of the recorder. The flavor perception scale covers the range zero (no flavor perceived) to 100 (the maximum perceived level, either previously determined or by experience). Assessments were carried out for 60 seconds or until perception was zero.

Formation of O/W Emulsions

To investigate the effect of fat content on flavor release, two iso-viscous pourable emulsions were made consisting of 0% and 30% sunflower oil. The emulsions were made from the following ingredients using a Silverson (Silverson Machines, Watford, UK) and a Crepaco homogeniser (Alfred & Co., London, UK) which yielded oil drop sizes of 2-3 μ m. The zero fat stock was made from 0.75% Na-Caseinate (Sprayblend, DMV), 0.75% xanthan (1-7428-4, Lipton), 2.8% starch (Ultrasperse M, National Starch) and 95.7% water. The 30% emulsion comprised 30% sunflower oil, 0.75% Na-Caseinate, 0.52% Xanthan, 1.96% starch, and 66.7% water. Both emulsions were reduced to pH 3.8 using a blend of phosphoric, lactic and sorbic acid. Emulsions with oil contents between 0% and 30%, were made by mixing the two stock solutions thus ensuring that the oil drop size remained constant for all samples.

Microstructured Emulsions

Microstructured emulsions were made by spraying an o/w emulsion containing 1% Na-alginate (Manugel, ISP Alginates, Surrey, UK) into a solution of CaCl₂ to form particulate gelled emulsions. This method of bead formation by ionotropic gelation of alginate has been widely reported for the entrapment of whole cells to be used as biocatalysts (12-14). Spraying was done using a pneumatic atomising nozzle connected to a peristaltic pump, whereby particle size was primarily controlled by controlling the flow rates of the emulsion and the atomising air stream, which is concentric to the extrusion nozzle. In general the higher the air and/or emulsion flow rate the smaller the particle size. In this study particles ranging from ca. 70 μ m to 3mm were made. The stabilized Na-alginate o/w emulsions consisted of the following ingredients. 1.1% to 20% sunflower oil, 0.5% tween 60 and 1% Na-alginate. The o/w

emulsion with 2-3 μ m oil droplets was made using a Silverson and a Crepaco homogeniser. The alginate emulsion was sprayed, at room temperature, into a stirred bath of calcium chloride dihydrate solution (0.37% w/w). Gelled beadlets are rapidly formed due to the rapid ionotropic gelation of alginate in the presence of Ca⁺⁺ ions, thereby entrapping the oil droplets within a three dimensional lattice of crosslinked polymer. The suspension of beadlets was thickened with 1% w/w cold dispersion xanthan by gentle mixing at room temperature for 20 min. The samples were flavored via the aqueous phase and allowed to equilibrate at 5^oC for 48 hours.

Results and Discussion

Effect of Oil Concentration

Flavor release from a series of emulsions varying in oil content from 0% to 30% were measured by real time APCI mass spectrometry (MS-Breath). The flavor release profiles (Figure 1) demonstrate that, for lipophilic flavors, the rate of release increases as the oil level is reduced (ethyl hexanoate & heptan-2-one). At lower oil levels this manifests itself through an increase in the maximum flavor intensity (FI_{max}) and a reduction in the sustained release of flavor over longer time intervals (i.e. $t > 30$ sec). Release of the more water soluble flavor probes such as butanone do not show much change when fat is removed and their release profiles were largely unaffected by the oil concentration (Figure 1).

It is evident from Figure 1 that at times longer than t_{max} (t_{max} = time at FI_{max}) marked differences in the release profiles of the lipophilic flavors become apparent as the fat levels are reduced. At oil concentrations of $\geq 5\%$, the maximum flavor intensity is sustained for a considerable period of time whereas at oil levels of less than 5%, the flavor intensity is not sustained beyond t_{max} . Furthermore, as the oil content decreases and approaches zero, the decline in the flavor intensity beyond t_{max} becomes more pronounced and there is no sustained flavor release. There are a number of potential causes for this fall-off: (1) with decreasing fat content the flavor pool is more rapidly exhausted; (2) Dilution of the product by saliva has a greater effect at low fat levels.

Flavor release analysis at 0.5%, 5% and 20% fat was also performed over a period of 10 minutes and the total amount of each flavor released plotted as a function of time. These plots gave a reasonable fit to an expression of the form $y = a(1 - e^{-bt})$ where t = time, a reflects the total amount of flavor in the product and b is the rate constant for flavor release. This equation was fitted to the release data, and the release rates b are shown in Table 1. It can be seen that the release rate term, b , decreases with increasing fat content for the lipophilic flavors whereas the hydrophilic flavors are unaffected. Within experimental error the a term for all the flavors was independent of fat content as would be expected.

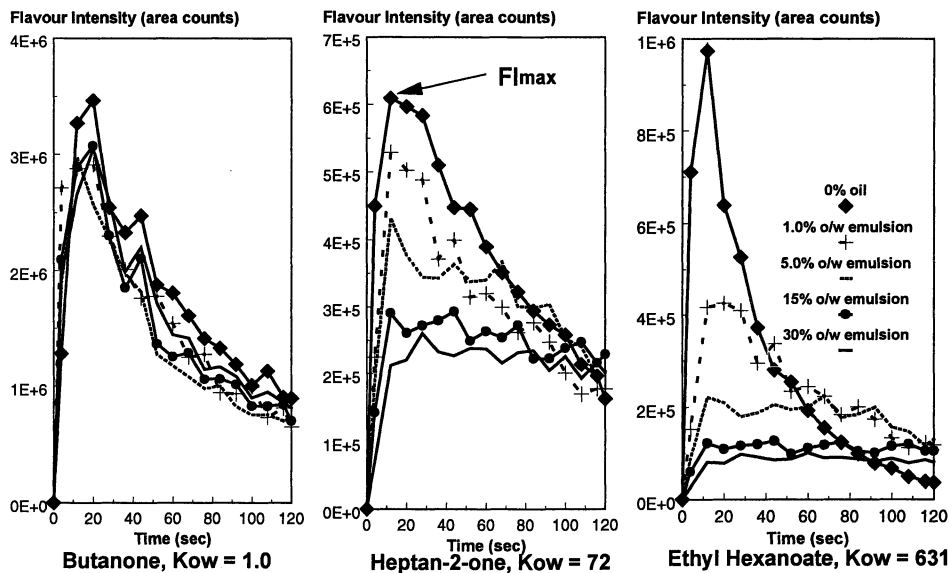


Figure 1. Flavor release profiles of butanone, heptan-2-one and ethyl hexanoate as a function of fat content.

Table I. Measured Flavor Release Rate Constants b (arbitrary scale).

Oil content	D6 acetone	Butanone	Heptan-2-one	Ethyl hexanoate	Nonan-2-one
0.5%	0.009	0.014	0.015	0.019	0.007
5%	0.009	0.013	0.009	0.007	0.0015
20%	0.009	0.013	0.005	0.003	0.0003

Air-Product Partitioning

Insight into these results can be gleaned from consideration of air/product partitioning and headspace concentrations of flavor compounds under static conditions. The effect of fat on flavor release is clearly related to partitioning phenomena and the relative amount of flavor solubilised in the oil and water phases.

Under equilibrium conditions in a closed system the partitioning of flavor compounds between the product and the gas headspace is given by the equilibrium in Eq. 1.

$$K_{gp} = \frac{C_g}{C_p} \quad \text{Eq. 1}$$

Where the equilibrium constant K_{gp} = gas/product partition coefficient, C_g = aroma concentration in the gas phase (mol dm^{-3}), and C_p = aroma concentration in the product. By mass balance it can be demonstrated that

$$C_p = C_w \cdot \phi_w + C_o \cdot \phi_o \quad \text{Eq. 2}$$

Where C_o = aroma concentration in the oil phase, C_w = aroma concentration in the aqueous phase, ϕ_o = oil phase volume, and ϕ_w = water phase volume ($\phi_o + \phi_w = 1$). By substitution of Eq. 1 into Eq. 2 and simple rearrangement it can be shown that the air/product partition coefficient is a function of the oil/water partition coefficient ($K_{ow} = C_o/C_w$), the air/water partition coefficient ($K_{gw} = C_g/C_w$) and the phase volume of the oil (ϕ_o).

$$K_{gp} = \frac{K_{gw}}{\phi_o (K_{ow} - 1) + 1} \quad \text{Eq. 3}$$

Assuming that the rate of release is proportional to K_{gp} Eq. 3 indicates that as the oil content (ϕ_o) decreases, K_{GP} for lipophilic flavors ($K_{ow} > 1$) increases, and hence the rate of flavor release increases. For hydrophilic flavors ($K_{ow} \approx 1$), K_{GP} is independent of ϕ_o and the rate of release is unaffected. Although these thermodynamic expressions account for the observed trends in the flavor intensity as a function of fat it is likely that other factors such as mixing, mass transfer, dilution with saliva and air flow, that occur during eating, also have a significant contribution, but are not easily extracted from this data. Harrison *et al.* have modelled flavor release from liquid emulsions and concluded that the rates of release are faster from low fat emulsions and that the rate limiting step was the resistance to mass transport across the emulsion-gas interface (20). However, validation of these findings are by no means complete and require further investigation.

Time-Intensity Analysis

Time intensity perception of heptan-2-one at fat levels ranging from 0% to 30% (Figure 2a) show some similar trends to the MS-Breath results in Figure 1. The sensory evaluation indicates that as the fat level is increased the heptan-2-one intensity decreases which is consistent with the MS-breath data. However, a number of differences between the time-intensity and MS-Breath profiles are noticeable. Firstly, in the time intensity plots, t_{max} appears to be fat dependent whereas this is not the case

in the MS-Breath data. This is probably due to the dead-time and resolution of the MS-Breath technique which is limited by the breathing rate of the panellist. Secondly, plots of $\text{Log}(I)$ vs $\text{Log} \phi_o$ (Figure 2b) do not follow a linear relationship as observed for the $\text{Log}(FI_{\text{MAX}})$ versus $\text{Log} \phi_o$ from the MS-Breath data (I = perceived intensity). The reasons for these differences are unclear but may be due to olfactory thresholds and the non-linear relationship between perceived intensity and strength of stimulus. Thirdly, at the lower fat levels ($\leq 5\%$) the perceived maximum flavor intensity plateaus for considerably longer than the MS-breath data suggests it should. This highlights that very little is known about the relationship between product stimuli and brain processing. Nevertheless, there is clearly a good correlation between the time intensity temporal profile in terms of flavor intensity change and that observed by MS-Breath which demonstrates the potential of this method for objective flavor release analysis.

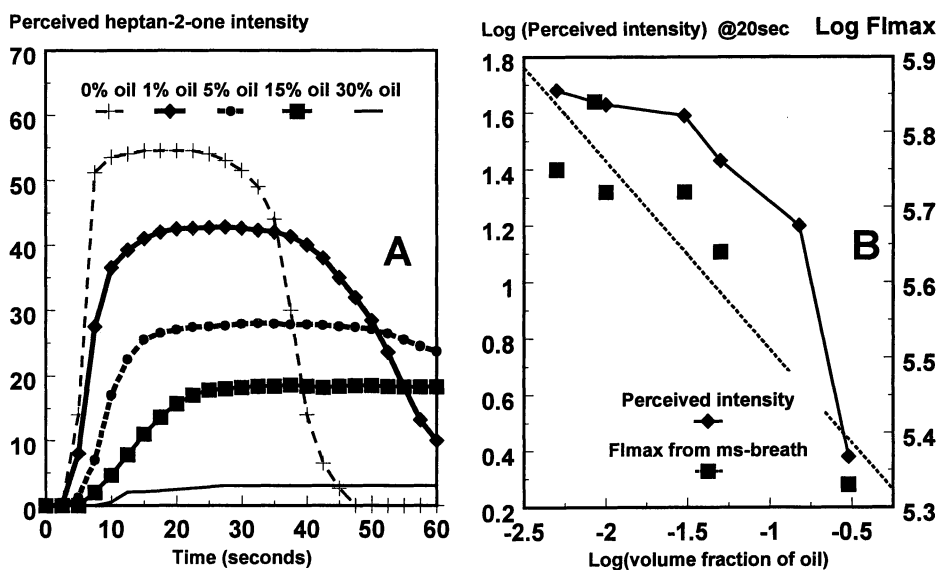


Figure 2. A) Time-Intensity flavor analysis of heptan-2-one release from model 'iso-viscous' emulsions varying in oil content from 0% to 30%. B) Plots of $\text{Log} I_{\text{max}}$ and $\text{log} FI_{\text{max}}$ versus $\text{Log} \phi_o$ comparing the sensorial and analytical responses.

Microstructured Emulsions

Microstructured emulsions are o/w emulsions in which the oil is incorporated into gelled beadlets so as to reduce the rate of lipophilic flavor release. The rationale behind this approach is that since the release of lipophilic flavors from o/w emulsions occurs in the sequence oil \rightarrow water \rightarrow air, it must be possible to control the release of these flavors by creating barriers around the oil droplets which hinder their movement into the aqueous continuous phase (Figure 3). This approach differs from conventional encapsulation techniques in that it is the oil and not the flavor that is encapsulated. The flavor is allowed to reach thermodynamic equilibrium in the product, according to their oil-water partition coefficients, and it is the concentration of lipophilic flavor in the oil phase of the gel particles which forms the basis on which the controlled release is achieved. This is an important distinction because this approach does not attempt to resist the thermodynamic distribution of flavor between the oil and water phases and therefore does not suffer from long term storage problems.

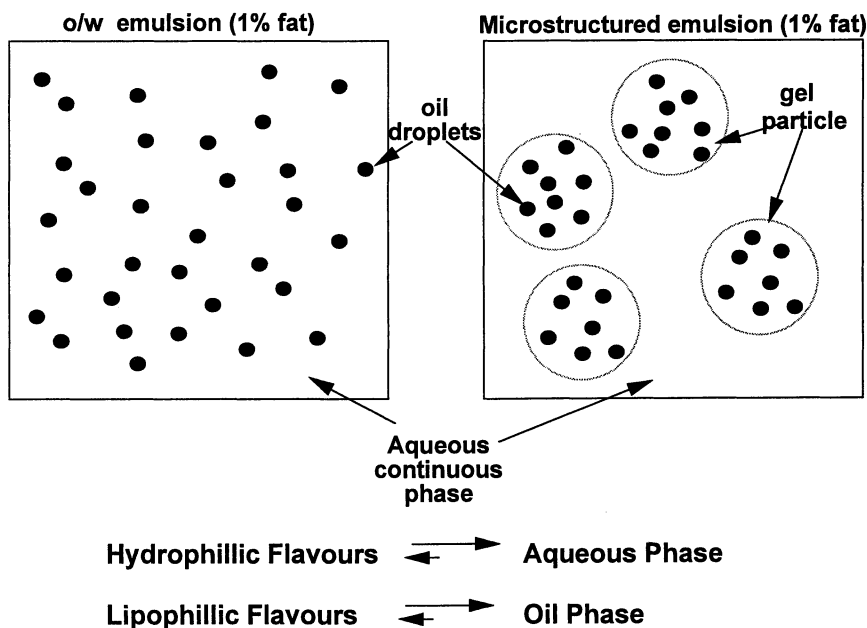


Figure 3. Schematic representation of microstructured emulsions compared to standard o/w emulsions. The gel particles increase the effective path-length for diffusion into the aqueous continuous phase.

Flavor release during mastication of a 1% oil microstructured emulsion was compared with a control comprising a standard 1% o/w emulsion (Figure 4). The results show that this approach provides a means of selectively controlling the release of lipophilic flavors, since there is a large reduction in the rate of flavor release for lipophilic flavors such as ethyl hexanoate, $K_{ow} = 631$ whereas hydrophilic flavors (e.g. acetone $K_{ow} = 0.6$) are not affected by the microstructured emulsions. When the analysis was done over 10 minutes a prolonged release of flavor similar to that of products with higher fat content was observed for the microstructured emulsions.

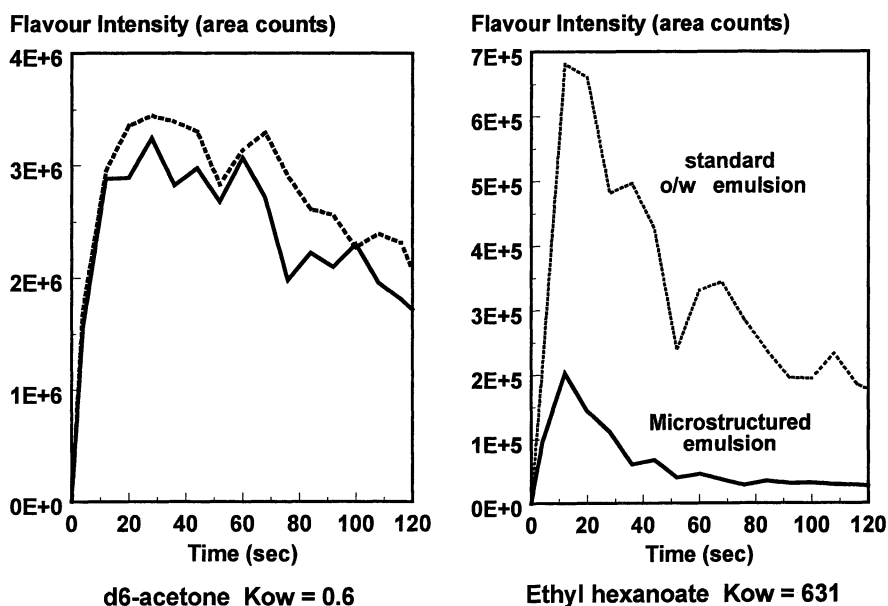


Figure 4. Flavor release from a standard and microstructured emulsion. The microstructured emulsion reduces the rate of lipophilic flavor release whilst leaving the hydrophilic flavors unaffected.

Mastication of the food is the trigger for the controlled release since it breaks the initial flavor equilibrium between the oil and water phases. As flavors are released from the continuous aqueous phase the system attempts to reestablish the o/w equilibrium by diffusion of flavor from the oil phase into the continuous phase. The additional diffusional pathway presented by the surrounding gel particle impedes the release of lipophilic flavors into the continuous aqueous phase and results in a

decrease in the rate of flavor release. Thus, unlike a standard o/w emulsion where there is mixing in the immediate vicinity of the aqueous o/w interface, there is a static (non-mixed) environment around the oil droplets, and it is the slower rate of diffusional transport relative to flow induced transport that causes the observed decrease in the flavor release.

An important question raised in these flavor release studies regards the contribution of the oil and aqueous flavor components (flav_{oil} and flav_{aq}) to the flavor release profiles of both the standard o/w and microstructured emulsions? This was investigated by comparing the flavor release from 3 systems 1) a standard 1% o/w emulsion, 2) a 1% oil microstructured emulsion and 3) The aqueous phase of a 1% oil microstructured emulsion obtained by removing the gelled emulsion beadlets by filtration (Figure 5).

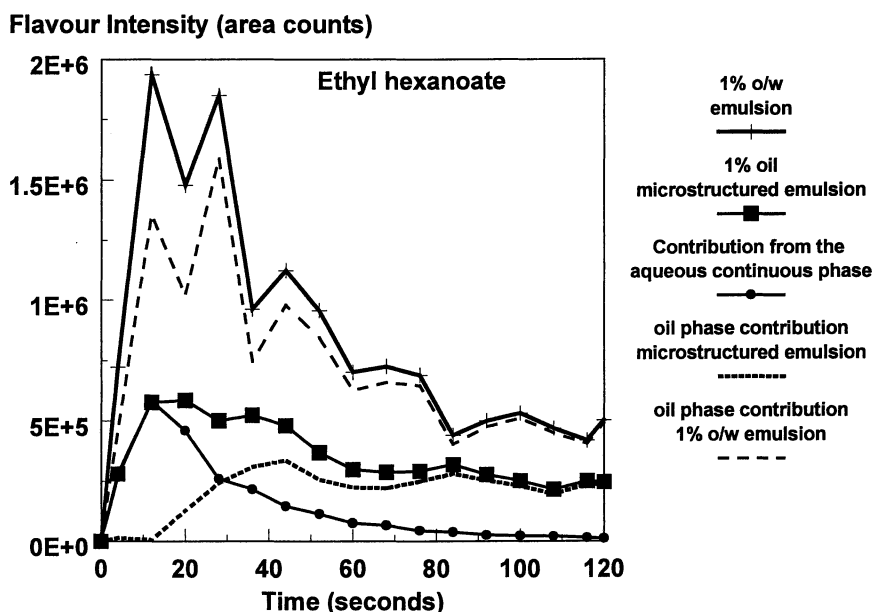


Figure 5. Ethyl hexanoate release from microstructured and standard o/w emulsions showing the contribution of the flavor from the aqueous and oil phases (flav_{oil} and flav_{aq}) to the overall release profiles. With microstructured emulsions the initial portion of the release profile ($t < 20\text{s}$) is dominated by the ethyl hexanoate from the aqueous phase. With the o/w emulsion the contribution of the oil phase dominates the entire release.

The results in Figure 5 indicate that for lipophilic flavors such as ethyl hexanoate the aqueous flavor component (flav_{aq}) is the primary contributor to the initial flavor released from the microstructured emulsion providing *ca.* 90% of the flavor in the first 20 seconds. Subtraction of flav_{aq} from the microstructured emulsion profile indicates that the contribution of flav_{oil} in the beadlets becomes significant at $t \geq 20\text{s}$ when the aqueous phase has become depleted and the re-equilibration/diffusion process is triggered. The ramification of this result is that for a given oil content there is a limit to which the initial flavor intensity can be reduced because it is the aqueous component which provides much of the initial intensity. Furthermore, for the standard o/w emulsions the aqueous flavor component provides only *ca.* 30% of the flavor intensity in the first 20 seconds. Clearly the flav_{oil} component accounts for the largest contribution of the initial flavor intensity and this supports the view that there is rapid diffusion of flavor from the oil droplets into the aqueous phase when the diameter of the droplets is small $\leq 10\mu\text{m}$. In o/w emulsions the rate of inter-phase transport of small solutes occurs on a millisecond timescale (17) due to the small droplet size, and this facilitates rapid flavor release during mastication of low fat foods.

Using the Crank approximation for diffusion from a spherical particle into an infinite sink it can be demonstrated that the half life ($t_{1/2}$) is approximated by Eq. 4 where r = radius of the particle, K_{ow} = the oil water partition coefficient of the flavor compounds, ϕ_o = the phase volume of oil in the particle and D = diffusion coefficient of the flavor compounds in the particle (21).

$$t_{1/2} = \frac{0.693r^2(1 + K_{\text{ow}}\phi_o)}{\pi^2 D} \quad \text{Eq. 4}$$

A number of assumptions are made in this equation. There is an infinite sink around the spherical particle so that any substance that diffuses out of the particle is immediately removed. The initial concentration of flavor in the sphere is uniform and an average diffusion coefficient is assumed.

The microstructured emulsions effectively increase the diffusional path (r) by entrapping the oil droplets within gel particles and are therefore regarded as diffusion controlled devices. Thus, for a spherical particle of $500\mu\text{m}$ and $D = 10^{-9} \text{m}^2\text{s}^{-1}$, the half life ($t_{1/2}$) for release into an infinite sink is greatly increased and will be in the order of approximately 12s. It is important to note that equation 4 is applicable to an infinite sink situation where there is no resistance to mass transport at the particle-continuous phase interface therefore it will underestimate $t_{1/2}$. Eq. 4 indicates that the factors that control the rate of release are: 1) K_{ow} , 2) particle size, 3) oil content of the particle, 4) the diffusion coefficient of the solute in the particle.

Oil Content and K_{ow}

The extent to which the microstructured emulsions control the release of flavor is in part determined by the proportion of flavor in the oil phase, as dictated by the K_{ow} values of the individual flavors and the oil content (Eq. 5). Where % $\text{flavor}_{\text{oil}}$ = the

percentage of flavor in the oil phase, C_p = concentration of the flavor in the product, C_o = concentration of flavor in the oil phase, ϕ_o = the oil phase volume fraction in the product, and K_{ow} = the oil water partition coefficient.

$$\% \text{flavour}_{oil} = \frac{100 \times C_o \phi_o}{C_p} = \frac{100 \times K_{ow} \phi_o}{\phi_o (K_{ow} - 1) + 1} \quad \text{Eq. 5}$$

From Eq. 5 it can be shown that for some lipophilic flavors a significant proportion of the flavor is present in the oil phase and available for controlled release even at low oil concentrations. The sizeable reduction in the rate of release exhibited by ethyl hexanoate shown in Figures 4 and 5 can be attributed to the large proportion of these flavors present in the oil phase (86% at an oil concentration of 1%).

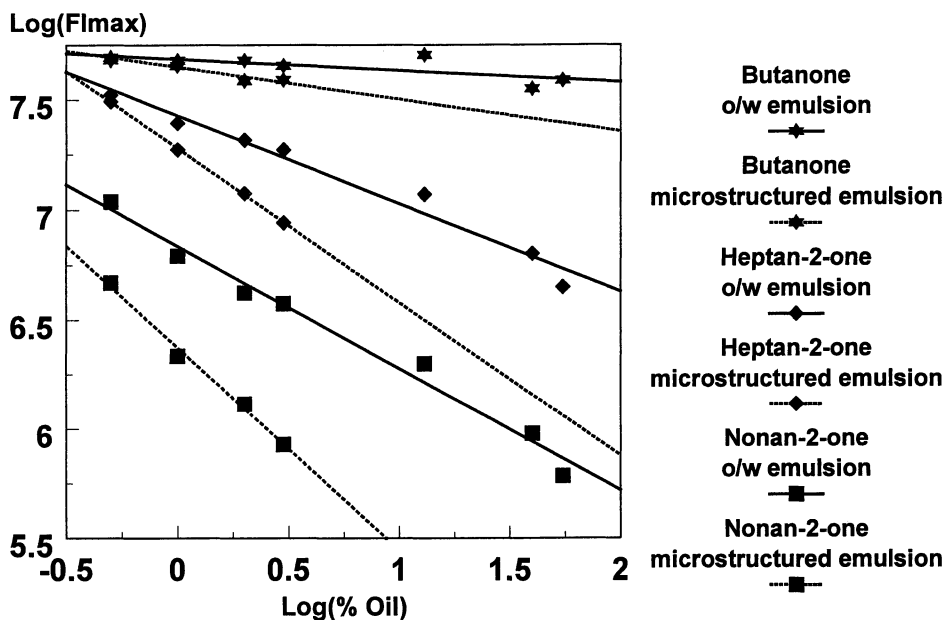


Figure 6. Log-log plot of $FI_{max}(ms-emulsion)$ and $FI_{max}(std-emulsion)$ as a function of oil content showing that high oil concentrations and large K_{ow} values facilitate the effectiveness of the microstructured emulsions the most

It is apparent from Eq. 4 that the extent to which flavor release can be controlled will be dependent on K_{ow} and the amount of oil in the product. The relationship between K_{ow} and ϕ_o is demonstrated by the log-log plot of the flavor intensity maximum (FI_{max}) as a function of oil content for both the microstructured emulsions

and the o/w emulsion controls (Figure 6). Plots of $\log FI_{\max}$ vs $\log \phi_o$ exhibit linear behaviour and the magnitude of the slope reflects the extent to which changes in the fat content affect the flavor intensity. For example, in the o/w emulsions butanone with a $K_{ow} = 1$ has a slope of -0.05 ; heptan-2-one ($K_{ow} = 72$) has a slope of -0.39 ; and nonan-2-one ($K_{ow} = 1000$) has a slope of -0.56 . In the microstructured emulsions the fat content effect is even more pronounced, as demonstrated by slopes of -0.7 and -0.93 for heptan-2-one and nonan-2-one respectively. Clearly, high oil concentrations and large K_{ow} values facilitate the effectiveness of these systems.

At a given fat content the effectiveness of the microstructured emulsions increases with larger K_{ow} values. For example, the FI_{\max} of heptan-2-one in a 3% oil microstructured emulsion is approximately equivalent to that from a 15-20% standard o/w emulsion whereas the FI_{\max} of nonan-2-one is equivalent to an emulsion with 40-50% oil. This is an important point because it means that the microstructured emulsions only affect the lipophilic flavors and have a negligible effect on hydrophilic flavors in much the same way that increasing the fat content of a standard emulsion would have.

Particle Size

For matrix systems such as the microstructured emulsions, Eq. 4 indicates that particle size is a crucial parameter for controlling the rate of release. Decreasing the particle size from 3mm to $100\mu\text{m}$ in diameter reduces the effective diffusion path-length and increases the rate of flavor release (Figure 7). Interestingly, there is little change in the flavor intensity maximum (FI_{\max}) for particles between 3mm and $500\mu\text{m}$ in diameter, but below $500\mu\text{m}$ there is a significant increase in FI_{\max} . For particles greater than 0.5mm there is no variation in FI_{\max} because it is the flavor in the continuous aqueous phase which provides most of the initial flavor release (previous section). However, at smaller particle sizes the encapsulated oil phase makes a bigger contribution to the initial release of flavor. This data indicates that in order to optimise the flavor functionality against their in-mouth detectability with the current release devices it will be necessary to use particles in the region of 200 - $1000\mu\text{m}$.

The increase in FI_{\max} which becomes apparent below particle diameters of $500\mu\text{m}$ corresponds with the pronounced increase in the surface area to volume ratio of the particles (Figure 7b), suggesting that the increase in the surface area to volume ratio is also an important factor during the early stages of release. At small particle sizes, ($< 0.5\text{mm}$) the surface-area/volume is such that greater amounts of flavor are immediately accessible over short time intervals.

Diffusion Coefficients

As indicated by Eq. 4, the effective diffusion coefficient D_{eff} in the gel particle is another factor that contributes to the rate of release. The oil content and type will also

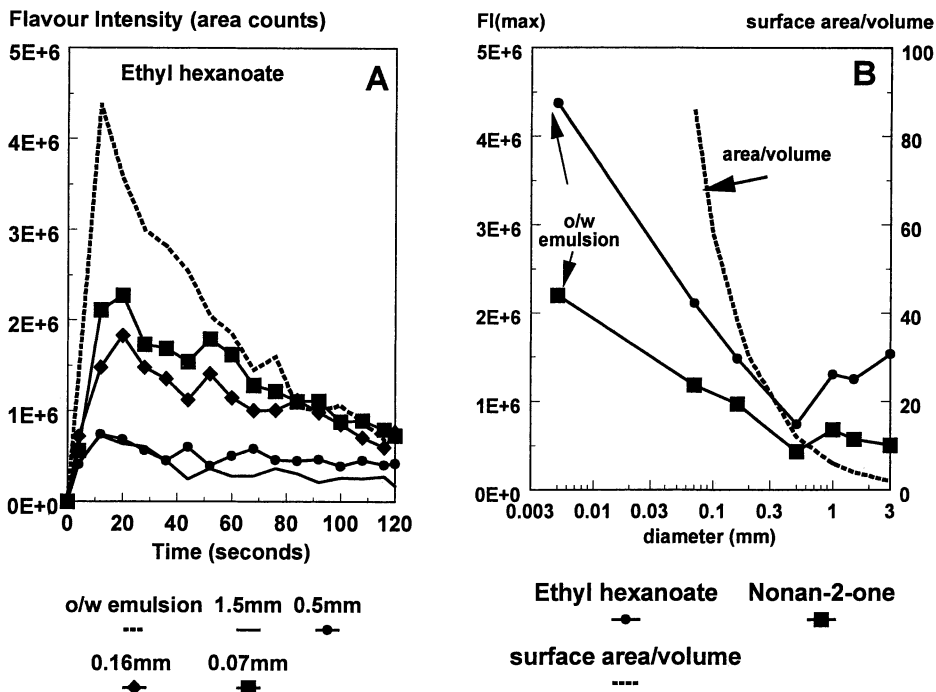


Figure 7. a) The effect of particle size on ethyl hexanoate release from microstructured emulsions. b) Plot of FI_{max} versus particle diameter.

affect the effective diffusion coefficient D_{eff} in the gel particle. This can be calculated on the basis of the Maxwell equation (equation 6) where D_g = diffusion coefficient of the aqueous gel phase, D_o = diffusion coefficient in the oil phase, ϕ_{op} = the oil phase volume in the gel particle and x is a shape factor which is equal to 2 for spheres.

$$D_{eff} = \frac{D_g \{D_o (1 + x\phi_{op}) + D_g (1 - \phi_{op})x\}}{D_g (x + \phi_{op}) + D_o (1 - \phi_{op})} \quad \text{Eq. 6}$$

The diffusion coefficients of small solutes such as flavors in the gel phase will not be very different to those in pure water. For example the decrease in the diffusion

coefficient of thiamine (mwt = 337) exhibits a decrease of ca, 35% in 6% agarose compared to water (18) indicating that the biopolymer has a small effect on diffusion. From work on the transport of low molecular weight solutes in polymer solutions it has become evident that the diffusion of these molecules is much less sensitive to the macroscopic viscosity than one may expect. The Mackie-Meares equation is one of many theoretical models (Eq. 7) for calculating the diffusion coefficient of a solvent in the presence of a polymer and can be used to estimate the reduction of a solute's diffusion coefficient as a function of polymer concentration (19).

$$\frac{D}{D_0} = \frac{(1 - \phi_p)^2}{(1 + \phi_p)^2} \quad \text{Eq. 7}$$

Where ϕ_p = volume fraction of polymer, D is the predicted diffusion coefficient of a small solute in the presence of the biopolymer, and D_0 = the diffusion coefficient of the solute in the pure solvent (water). For many gelled biopolymer systems ϕ_p is small so the fractional decrease in the diffusion coefficients relative to water will be small. At the biopolymer concentrations used in these microstructured emulsion ($\leq 1\%$) it is expected that the diffusion coefficients of the flavors would not be appreciably affected by the presence of the biopolymer. The effective diffusion coefficient (D_{eff}) will therefore be dependent on the oil phase volume in the particle, the type of oil used and the concentration of biopolymer used in the aqueous gel phase.

Conclusions

MS-Breath analysis under real eating conditions has been shown to be an extremely useful tool for studying flavor release and gaining an insight into the factors which control flavor release. The data shows that the rate and intensity of lipophilic flavor release is reduced in the presence of oil and that hydrophilic flavors are relatively unaffected by the oil content. The results suggest that thermodynamic partitioning of volatiles (K_{ow} and K_{gw}) are important factors controlling flavor intensity but that the dynamics of the eating process itself such as mixing, dilution with saliva and air flow over the product, also play a crucial role. The lipophilic flavor release profiles are significantly influenced by the fat concentration and as this is decreased the maximum flavor intensity increases. However, at oil concentrations of $\geq 5\%$ the flavor profiles (shapes not intensities) are similar whereas at oil levels of less than 5% the flavor profiles are markedly different and this becomes more pronounced as the oil concentration decreases and approaches zero. These differences arise due to the faster depletion of lipophilic flavors into the headspace and the greater effect of dilution in low fat products.

It has been demonstrated that by encapsulating oil within gel particles (microstructured emulsions) it is possible to selectively control the release of lipophilic flavors in low fat products. The microstructured emulsions do not affect the hydrophilic flavors therefore these devices are not only able to control intensity of

lipophilic flavors but also improve the flavor balance of complex flavoring mixtures, making them more like full fat products. Essentially they are partitioning and diffusion control devices and the factors which determine their effectiveness are (1) K_{ow} , increasing lipophilicity equals greater partitioning into the oil phase within the particles resulting in slower release on mastication. (2) Increasing the particle size leads to slower release due to the increase in the diffusional pathlength. It is our view that with the present matrix structures, particles in the region of 200-1000 μm will be required to provide significant control of the flavor release, whilst still maintaining an acceptable mouthfeel. (3) Increasing oil content will favor greater partitioning of the lipophilic flavors into the oil phase within the particles leading to slower release. (4) Smaller effective diffusion coefficients, which are dependent on type and phase volume of oil and biopolymer concentration, results in slower release.

References

1. O'Brien Nabors, L. *Cereal Foods World*, **1992**, *37*, 425.
2. Forss, D.A. *J. Agr. Food Chem.* **1969**, *17*, 681
3. Kinsella, J.E., *INFORM*, **1990**, *1*, 215.
4. Hatchwell, L.C., In *Flavor-Food Interactions*, McGorin, R.J. & Leland, J.V. Eds, ACS Symposium Series. Washington DC, 1996, pp 14.
5. Shamil, S.; Kilcast, D. *Nutrition and Food Science*. **1992**, *23*, 7.
6. Shamil, S.; L.J. Wyeth, L.J.; Kilcast, D., *Food Quality and Preference*. **1991**, *3*, 51.
7. Overbosch, P.; Afterof, W.G.M.; Haring, P.G.M. *Foods Rev. Int.* **1991**, *7*, 137.
8. Delahunty, C.M.; Piggott, J.R. *Int. J. Food Sci. Technol.* **1995**, *30*, 555.
9. Taylor, A.J., *Crit. Rev. Food Sc. Nutr.*, **1996**, *36*, 765.
10. Plug, H.; Haring, P. *Trends in Food Sci. Technol.* **1993**, *4*, 150.
11. Linforth, R.S.T.; Ingham, K.E; Taylor, A.J. In *Flavor Science Recent Developments*. Taylor, A.J. & Mottram, D.S. Eds. *Royal Society of Chemistry*. Cambridge. U.K., 1996; pp 361.
12. Klein, J.; Stock, J.; Vorlop, K.D.; *Eur. J. Appl. Microbiol. Biotechnol*, **1983**, *18*, 86-91.
13. Levy, M.C.; Edwards-Levy, F.; *J. Microencapsulation*, **1996**, *13*, 169.
14. Hackel, U.; Klein, J.; Mergent, R.; Wagner, F.W.; *Eur. J. Appl. Microbiol.* **1975**, *1*, 291.
15. Buttery, R.G.; Bomben, J.L.; Guadagni, D.G.; Ling, L.C., *J. Agr. Food Chem.* **1971**, *19*, 1045.
16. Buttery, R.G.; Guadagni, D.G.; Ling, L.C., *J. Agr. Food Chem.*, **1973**, *21*, 198.
17. Wedzicha, B.L.; Couet, C.; *Food Chem.*, **1995**, *55*, 1.
18. Anderson A.P. & Oste, R.E.; *J. Food Eng.*, **1994**, *23*, 631.
19. Waggoner, R.A.; Blum, F.D. & MacElroy, J.M.D.; **1993**, *26*, 6841.
20. Harrison, M.; Hills B.P; Bakker J. & Clothier T.; **1997**, *62*, 653.
21. Lian, G., In *Flavor Release*; Roberts, D.D.; Taylor, A.J., Eds.; ACS: Washington D.C., 2000.

Chapter 19

Interactions of Flavor Compounds with Starch in Food Processing

F. E. Escher, J. Nuessli¹, and B. Conde-Petit

Institute of Food Science, Swiss Federal Institute of Technology (ETH),
CH-8092 Zurich, Switzerland

Starch consists of linear amylose and branched amylopectin that are tightly packed into starch granules with intermittent amorphous and crystalline regions. In food manufacturing and preparation starch is transformed to become digestible by man and to act as a texturogen. At the same time starch interacts with flavor compounds in several ways. Non-specific sorption of volatiles to native starch granules leads to flavor retention, while diffusion controlled entrapment of volatiles is observed in thermoplastic starch. Physical entrapment is of particular importance in dehydration and in extrusion cooking. Ligand binding of some flavor molecules to amylose induces helical conformation and the reversible formation of inclusion complexes. The helical conformation and the crystallinity of the complexes depend on the type of ligand. In aqueous starch dispersions, complexation may control flavor retention, protect volatiles against oxidation, and at higher ligand concentrations change the rheological properties of starch dispersions. In real foods, the relative importance of the various mechanisms of flavor retention and release for flavor quality still needs to be determined.

Starch belongs to the major constituents of many foods of plant origin. Likewise, starch is found in food formulations and recipes as an additive to create or improve specific textural properties. While the role of starch as macronutrient and texturogen is well recognized, its contribution to flavor quality by interactions with volatile compounds in starch-containing food systems is less apparent. The present review briefly describes the molecular and supramolecular structure of starch, its

¹Present address: Laboratoire de Physicochimie des Macromolécules, Institut National de la Recherche Agronomique (INRA), F-44316 Nantes, France.

transformation during food processing, and its principle interactions with other food constituents. This information will serve as the basis for a comprehensive discussion of the various types of interactions of volatile flavor compounds with starch that control flavor retention and release phenomena in starch containing food systems.

Structure and Transformation of Starch

Native Structure

Starch presents one of the universal forms for storing energy in green plants. It consists of linear amylose and branched amylopectin, which in the native state are packed in well organized starch granules. Microscopic inspection of the granules reveals characteristic concentric zones of varying crystallinity. According to the present view (1), these zones alternately consist of crystalline, hard blocklets and semicrystalline, soft, small blocklets. In turn, all blocklets are built up of crystalline and amorphous regions. The crystalline regions are based on the double helical structure of the amylopectin side chain. The linear amylose molecules are present in the amorphous state and appear between the amylopectin crystallites. Depending on the botanic origin of the starch, small quantities of lipids are integrated into the crystalline region.

Also depending on the botanic origin, the amylopectin double helix yields a different X-ray diffraction diagram. The double helix of the A- and B-type starch polymorph, respectively, was modeled from diffraction data of amylose fiber specimens (2,3) and later of solution grown single amylose crystals (4,5) as shown in Figure 1 and 2. The crystalline part of A-starch consists of a monoclinic lattice. The unit cell contains 12 glucose residues which are located in two left-handed, parallel stranded helices. Four water molecules are present between the helices. B-type starch consists of a hexagonal unit cell in which 12 glucose residues are located in left-handed parallel stranded double helices. In contrast to A-type starch, 36 water molecules are present between the helices.

It is the tight packing of amylose and amylopectin that makes starch an ideal biological system of energy storage with the least requirement of space. In nature, the alternating crystalline, semicrystalline, and amorphous areas ensure the access of enzymes to break the biopolymers down and release monomers at the desired rate.

Transformation

In its native granular form, starch neither is digestible by man nor does it act as a texturogen to create sensory texture in foods. starch is transformed to varying degrees on the colloidal, supramolecular and molecular levels only during processing and preparing foods. This renders starch accessible to digestion and provides texturogenic properties (6). In most cases, transformation does not stop at the end of processing, but continues at least to some extent also during storage. In this respect, starch as a

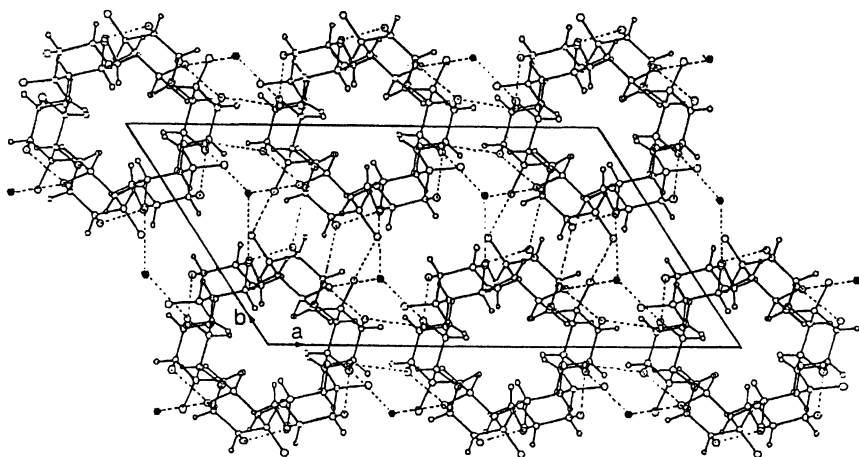


Figure 1. Model for the starch polymorph A. (Reproduced from reference 4. Copyright 1988 Academic Press Limited.)

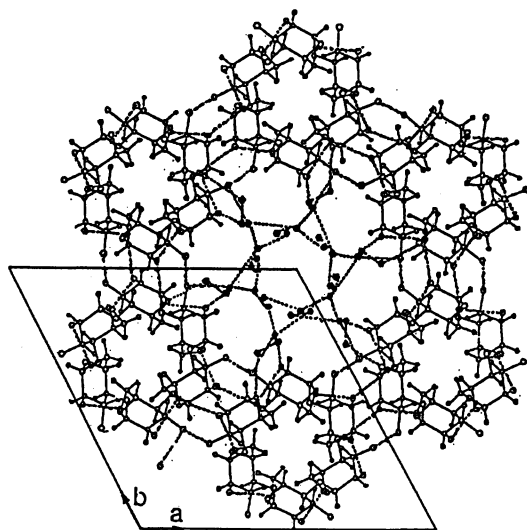


Figure 2. Model for the starch polymorph B. (Reproduced from reference 5. Copyright 1988 John Wiley & Sons.)

biopolymer does not differ in behavior from any synthetic polymer in which structural changes over time have to be considered without exception. In fact, even dry native starch is subject to structural fluctuations over extended periods of time.

The extent of transformation of native starch upon processing is influenced by extrinsic factors, that is, thermal and mechanical energy input and length of treatment. While thermal energy is responsible for glass transition, melting, retrogradation, and recrystallization of the starch biopolymers, mechanical energy acts on the microscopic scale by disrupting and dispersing the granular material (7,8).

It is important to note that in aqueous starch containing food systems, the full disintegration of granular structure and the development of a homogeneous dispersion is rather the exception than the rule. Even after the application of considerable temperature and shear forces, fragments of starch granules can still be detected. In many cases, granular organization is very important for the behavior of starch dispersions (9). Therefore, different dimensional levels have to be taken into account when studying any effect of processing on starch from the raw material to the final food product on the plate.

Starch transformation is equally influenced by intrinsic factors, that is, by the composition of the respective food system that is processed. Obviously, water content is the single most important factor. Water acts as a plasticizer in glass transition and melting, as a diluent or 'aid' in recrystallization, and as a solvent, respectively. Water is a rather poor solvent for both amylose and amylopectin. This, together with the fact that amylose and amylopectin are immiscible polymers, is the cause for demixing, aggregation, and gel formation in aqueous starch systems (10).

Interactions with other Food Components

Aside from water, a considerable variety of compounds interact with starch during processing and influence starch transformation and final product quality. These compounds are non-starch polysaccharides and proteins (11,12), lipids (13), volatile flavor molecules (14,15), and electrolytes (16). The mechanism of interaction and its consequence may be quite different. They range from non-specific effects of non-starch hydrocolloids or lipids that control the degree of swelling and disintegration of starch granules and the extent of aggregation, gel formation and precipitation of dispersed starch, to the specific inclusion of small molecules into the cavity of helicated amylose that will be discussed below in more detail. Interactions by covalent binding of selected molecules to starch leading to starch derivatives generally do not occur under conditions applied in food processing, while such reactions are exploited on a large scale in the manufacturing of modified starches.

The practical implications of interactions of starch with volatile aroma compounds are twofold. On one hand, there is the aspect of flavor retention during food processing and preparation as well as during the production of flavor ingredients. This is the area of flavor technology in which not only the highest possible retention rate of volatile is the goal during manufacturing, but also an optimal stability of these volatiles against chemical changes such as oxidation must be attained during storage.

On the other hand, there is the aspect of flavor release which creates the desired sensory property at the point of food consumption. In this area, sensory science and flavor chemistry study the mechanisms of volatile release from a starch containing food and how volatiles are perceived sensorially. As it is quite clear that retention and release basically contradict each other from a physico-chemical point of view, only a balanced use of both phenomena at the appropriate time leads to the desired sensory quality and product acceptance at the point of food consumption.

Flavor Retention by Sorption and Physical Entrapment

Sorption of Volatiles to Native Starch

Dry native starch granules exhibit enough surface porosity to enable flavor retention by physical sorption. This type of volatile retention is experienced in practice in the case of undesirable off-flavors, for example, for cereal flours that are stored under inappropriate environmental conditions.

Only little quantitative data are available so far on sorption of flavor compounds to dry starch granules (17), although dry starch might be exploited as an active flavor carrier. Instead of using individual starch granules, it has been proposed to generate spherical aggregates or agglomerates of starch granules (18). By this technique, the active surface for sorption can be increased. Experiments were carried out to produce aggregates of rice, wheat, and amaranth starch, respectively, by using a suitable non-starch hydrocolloid as binding material. After applying the flavoring, the agglomerates would then be coated with yet another hydrocolloid to protect the surface. In a similar way, native corn starch granules have been treated with a glucoamylase to increase the porosity (19). If the aroma is introduced as an oily extract, capillary effects enhance the flavor retention.

Some experimental results have been published on the sorption of water-soluble alcohols by starch granules in an aqueous suspension (20). No reference is made to the potential alteration of flavor retention in such systems.

Physical Entrapment in Starch Matrices

Physical entrapment of volatiles in starch presents one of the many techniques of flavor encapsulation. In this application, starch is transformed from its granular native state into the gelatinized state by thermal and mechanical energy input. Retention is achieved not only by sorption, but also to a large extent by minimizing diffusion rates of volatile compounds.

Mechanisms Controlling Physical Entrapment in Low Moisture Systems

Basically, barrier properties of starch are controlled by its actual physical state as described in the state diagram of the binary starch-water system. State diagrams are defined as an extension of the phase diagrams, in which only first order

thermodynamic transitions are shown, to include second order transitions, in particular the glass transition (21). The glassy state of many food components and its importance for food quality have long been recognized. More recently, the introduction of material science principles into food research has strengthened the concept of glass transition in explaining diffusion related phenomena in flavor retention (22).

When starch is present in the glassy state, that is, below the glass transition temperature T_g at low moisture content and/or low ambient temperature, it is characterized by a low free volume and an extremely high coefficient of viscosity. As diffusional transport through a medium is dependent on its free volume and viscosity, diffusion coefficients in glassy material are greatly reduced.

Free volume of amorphous starch-water systems was measured at different temperatures and moisture contents in the context of investigations of the barrier function of starch in packaging technology (23,24). As was expected, the free volume, which is the supplement of the degree of occupation to unity, is minimal at low moisture and low temperature.

Besides diffusivity of volatiles in starch, solubility of flavor compounds in starch water systems may have to be taken into account, in particular at higher moisture content (25).

Types of Starch and Processes Used for Encapsulation

In practice, native starch is replaced by partially hydrolyzed or modified starches that exhibit higher flavor compound retention and the additional advantages of better dispersibility or emulsifying capacity (26,27). Maltodextrins (DE lower than 20) and corn syrup solids (DE exceeding 20) are among the more popular carriers (28), as both have acceptable film barrier formation and dispersibility.

Many experiments were carried out with chemically modified starches in order to improve emulsifying capacity (29). Alkenylsuccinates seem to be of particular interest in this respect and have been proposed as flavor carriers with high emulsifying capacity (30). Chemically modified starches have disadvantages such as undesirable off-flavors and a low ability for protection against oxidative changes of flavors during storage. In food legislation, they cannot be considered as natural, and in Europe they have to be labeled with an E number.

Spray-drying and extrusion cooking are the two most frequently cited methods for physical entrapment in a starch carrier (27).

Starch-Flavor Interactions in Extrusion Cooking

The interest in maximizing volatile retention in extrusion cooking does not originate only from the desire to use this process for manufacturing encapsulated flavors. There is an equal need to retain as much flavor as possible in the production of extruded food products that have been flavored prior to extrusion (31).

Because extrusion cooking of starch and starch-rich raw materials is primarily a method of texturization, process parameters are usually selected to optimize the sensory texture of the extrudates. This is attained by a large rate volume expansion at

the die exit, which in turn ensures a high porosity and the desired crispness of the extrudate. Expansion is first caused by the action of normal stress upon the viscoelastic starch melt, which, however, does not yet lead to porosity. Porosity only develops when expansion takes place as the pressure drop at the die exit leads to the evaporation of the super-heated water. At the same time, the melt must have a high temperature and low viscosity to keep it expandable by the vapor pressure. As soon as the temperature drops further, the viscosity increases and the extrudate changes into the glassy state.

The flash evaporation effect due to pressure release at the die exit of the extruder presents the most obvious mechanism of loss of flavoring substances that were added prior to extrusion.

Phase Equilibria, Volatility and Diffusivity of Flavors in Starch

Data from extrusion cooking of corn flour together with n-butanol, octane, benzaldehyde, and limonene were used to develop two different models to describe volatilization/retention of flavors (31-33). The first one is a thermodynamic model based on the equilibrium between the adsorbed and vapor phases of flavor at the die exit. Calculations of the fractional loss of volatiles near liquid-vapor equilibrium are used in the analysis of flavor retention during evaporation. The model was able to predict retention of benzaldehyde and limonene within an error range of 20 to 30 %. The second model is engineering based and considers the relative volatility of flavor compounds and water. This model has also been used for describing flavor retention in evaporative and drying processes. It gave a good prediction of the retention of n-butanol and benzaldehyde, which as polar compounds escape by steam distillation.

Diffusion presents another critical factor in determining flavor volatilization/retention, in particular in connection with the expansion rate of the starch melt. Diffusion-controlled retention of volatiles is important in drying operations such as spray drying, and flash evaporation of water at the extruder exit may well be compared to the evaporation of water around the atomizer of a spray drier. In spray drying, the concept of selective diffusion and the so-called Thijssen critical ratio between the diffusion coefficients of flavor and water were introduced as a measure on how much flavor is retained (34). If the critical ratio is ≤ 0.01 , flavor retention at simultaneous dehydration is high enough to contribute to the final product quality. Because this ratio rapidly decreases with decreasing moisture content of the product to be dehydrated (34), it could be of importance for extrusion processes.

More recent investigations on extrusion of starch with several flavor compounds (35,36) indicate that initial moisture content and expansion rate indeed have an influence on the extent of flavor retention. Lower moisture of the initial blend and lower expansion lead to a small, but nevertheless significant increase in retention rates. It should be noted that experimental results for extrusion cooking are frequently difficult to explain as mere physical flavor loss is superimposed by thermal degradation of these compounds (36).

Sorbation and Formation of Staudinger Complexes

From what has been discussed so far, retention of volatile flavor compounds becomes maximal when expansion at the extruder exit is suppressed totally. In this case, flash evaporation of water does not occur and the starch melt is transformed rapidly into the glassy state, which again causes an equally rapid drop of diffusion coefficients of volatiles.

Extrusion of starch without expansion has been proposed for producing dry flavoring ingredients (37,38). It was postulated that flavors were not retained by physical entrapment but rather by 'sorbation' which was explained, for example, for vanillin, as non-stoichiometric binding of flavor molecules between the starch biopolymer. In a similar way, aroma retention was also explained in the case of freeze drying of starch (39). Sometimes, these starch ligand systems without stoichiometric binding have also been called "Staudinger complexes".

Formation of Inclusion Complexes with Amylose

Complexation of amylose with ligands in the sense as it will be further explained below also occurs during extrusion cooking. Most of the investigations on amylose complexations were carried out with emulsifiers as this phenomenon has been recognized to be relevant in extrusion processing for breakfast products and infant foods. Complexation of starch with emulsifiers and fatty acids was determined using the iodine binding value of amylose, differential scanning calorimetry (DSC) and X-ray diffractometry (40-44). Starch-lipid complexation influenced the rheological properties of the starch melt and by this the structural and mechanical properties of the final extrudate (45).

Few studies have been conducted on complexation of flavor molecules during extrusion cooking although there is little doubt that complexation with volatiles does occur. It is clear that the relevant experiments have to be based on substances that are known to form complexes in aqueous systems at steady conditions. Investigations on extrusion of starch with different amylose/amylopectin ratios together with C 6, 8 and 10 alcohols, aldehydes, and acids showed that blends which lead to complex formation in aqueous systems also result in higher volatile retention (46). However, direct evidence of complex formation is lacking in this case as neither DSC, X-ray diffractometry, nor iodine titration were carried out.

Complexation of Flavor Compounds with Amylose

Terminology

By analogy to biological systems where the non-covalent binding of one or several molecules to a single macromolecule is well known and these molecules are called ligands, flavor compounds that can interact with starch in one way or another are also defined as *ligands*.

The addition of certain ligands leads to specific interactions with amylose, the result of which is the formation of a single amylose helix due to the presence of the

small molecule. The ligand can be located in the hydrophobic cavity of the amylose helix. Alternatively, it is also conceivable that single helices are induced, but the ligand is located in the free space between the helices. Following the chemical terminology, the combination of ligand and ligand induced helicated amylose is called *inclusion complex* or *inclusion compound*.

Therefore, the term *complexation* should be restricted to the interaction of starch with ligands in such a way that single amylose helices are formed (47), although in the literature complexation often describes specific and non-specific interactions in a more general sense, that is, regardless of the formation of true inclusion compounds or the formation of a helical structure.

A very large variety of different molecules are known to form complexes with amylose. Iodine presents the most important ligand for analytical purposes, while fatty acids, emulsifiers, and flavor substances are relevant for food processing. It must be noted that no strict rule on chemical structure and conformation exists that could clearly indicate whether a molecule can act as complex forming ligand.

Complexation in Diluted Starch Solutions

Over the years, most investigations on complexation of flavor compounds with amylose have been carried out in diluted starch solutions in which starch was solubilized as much as possible. This was achieved by treatment with alkali or dimethyl sulfoxide, a method used in the classical research on starch and in particular on amylose (48). One can assume that in these diluted starch solutions with a starch concentration of up to 1 g dry starch per 100 g solution, no remnants of granules are present, and supra-molecular structures such as aggregates are absent.

Ligand binding by complexation was first investigated in binary systems with potato starch and one flavor compound (49-52) and later extended to ternary systems with two flavor compounds or a flavor compound and an emulsifier (14,15,52,53). Binding isotherms were used to determine the binding constant, the maximal amount of bound ligand and the extent of cooperativity calculated by applying the Scatchard and Hill equations. As for ternary systems, competitive binding was observed in such a way that the addition of a second ligand may change the equilibrium and replace the first ligand in the cavity of the amylose helix. It has been proposed that the selective retention or release of different flavors from starch-containing foods could be modeled and explained in this way (53).

Ligand binding of decanal, methone, and (-)-limonene was also determined in dilute solutions in which potato starch was fully solubilized by extended heat treatment with simultaneous agitation (54,55). After complexation, these solutions were freeze-dried and used for testing the oxidative stability of complexes in comparison to powders from gum arabic or maltodextrin. The flavor molecules in starch preparations were indeed much more stable. Of course, differentiation between the effect of complexation and that of different efficiency of physical entrapment by these carrier materials is not possible on the basis of these results.

Complexation in Diluted Starch Dispersions

More recently, investigations were carried out with a series of complexing flavor compounds in starch dispersions that were prepared by heat treatment of suspensions of 2 to 4 g dry starch per 100 g dispersion at 121 °C for 30 min and gentle agitation (47). The experiments were based on potato starch, which does not contain measurable amounts of lipids that could influence complex formation. According to microscopic observation (9), the system may be described as a macromolecular dispersion containing fragments of starch granules and solubilized amylose. Furthermore, the immiscibility of amylose and amylopectin resulted in a phase separation of zones rich in either one of the two biopolymers. The dispersions present a model system that is already more proximate to a real liquid starch-containing food product than the alkali solubilized starch system.

Appearance, Rheological Properties and Structure of Dispersions

Rheological studies were based on the earlier observation of complexation induced gelation of diluted starch dispersions with the addition of complexing emulsifiers (13,45,56,57). Therefore, visco-elastic properties of the dispersions were characterized by oscillatory measurement in a cone and plate rheometer, while the degree of complexation was determined by measuring the iodine binding value with amperometric iodine titration. This latter method is a classical analytical technique (58), which still proves valuable in investigating starch systems. Depending on the ligand, the visual and rheological changes as summarized in Table I were observed.

The addition of decanal, octanal, and (-)-fenchone led to a complexation induced formation of a soft gel (59). At the same time, the dispersions turned from translucent to turbid. Gel formation is attributed to the aggregation of the insoluble complexes that build a network between the granular fragments of the starch dispersion. When thymol, menthone, menthol, (+)-camphor, or α -naphthol were added, turbidity developed due to the formation of insoluble complexes. However, no change in the rheological properties was observed, regardless of whether the starch concentration was increased from 2 to 4 g dry starch/100 g dispersion. The addition of geraniol, (-)-carvone, and (+)-carvone induced the formation of a precipitate and a macroscopic phase separation. Iodine binding values confirmed complex formation of all flavor compounds with amylose. The concentrations of flavor substances for full saturation of the amylose were strongly dependent on the ligand properties (59).

It is interesting to note at this place that the complexation induced increase of viscosity was observed already many years ago when iodine was added to diluted starch dispersions (48). Probably, the complexation of iodine with amylose also yields a weak gel.

Attempts to further characterize the dispersion and the structure of the aggregates of amylose flavor complexes in situ have been unsuccessful so far. The measurements were carried out with small-angle X-ray scattering, but no difference in scattering intensity between starch dispersions with and without ligands were observed (47).

Table I. Characteristics of Potato Starch Dispersions without and with Addition of Ligands (47)

<i>Ligand</i>	<i>Critical ligand concentration (mmol/mol glucose)</i>	<i>Rheological changes</i>	<i>Melting temperature of complexes (°C)</i>	<i>Crystalline conformation</i>
Reference	--	transparent, liquid	no phase transition	amorphous halo
Decanal	50	soft gel	96	V _h amylose
Octanal	75	soft gel	88	V _h amylose
Hexanal	500	not determined	76	V _h amylose
(-)-Fenchone	125	soft gel	107	V amylose
Thymol	100	turbid and liquid	105	V amylose
Menthone	50	turbid and liquid	104	V amylose
Menthol	50	turbid and liquid	129	V amylose
(+)-Camphor	100	turbid and liquid	76	V amylose
α-Naphthol	100	turbid and liquid	109	V amylose
Geraniol	75	precipitate	91	V amylose
(+)-Carvone	100	precipitate	91	V amylose
(-)-Carvone	100	precipitate	91	V amylose

Molecular Structure of Amylose Complexes

Differential scanning calorimetry was carried out on freeze dried samples of all starch flavor preparations mentioned in the preceding paragraph (60). The amylose flavor complexes melted in a range from 76 to 109 °C, thus indicating a large variability of thermostability of the complexes (Table I). Melting temperature and enthalpy were again dependent on the ligand characteristics.

Wide-angle X-ray diffractograms of freeze-dried dispersions confirmed the formation of V amylose for all ligands investigated (60). Starch complexes with aldehydes yielded a typical pattern for V_h amylose which corresponds to a left handed single helix consisting of 6 D-glucosyl residues per turn (Figure 3). The ligand is most likely included in the hydrophobic cavity of the amylose helix. The 6 glucose residue helix was also confirmed for other linear molecules such as monoglycerides (53).

The ligands that were larger in cross section than the linear aldehydes showed X-ray diffraction diagrams from which neither the exact position of the ligands in the crystalline domain nor the configuration of the amylose helix could be fully deduced. From studies with alkali solubilized starch systems (53) the existence of a 7 glucose residue helix for menthone and (-)-limonene, and a 8 glucose residue helix for α-naphthol were proposed. These structures were derived from measurements in the 1960's on single crystals of amylose with different ligands (61-63), but are subject to discussion.

In the meantime, the crystalline structure of V_h amylose is well established and documented for single crystals not only by X-ray diffraction data, but also by electron diffraction and molecular modeling (64-66). Likewise, a helix with 8 glucose residues for the bulky α -naphthol seems to be a plausible structure (67). On the other hand, the existence of the 7 glucose residue helix is discussed controversial. Instead, it is now assumed that some ligands such as thymol may be placed between, instead of in, the 6 glucose residue helix (Figure 4). Flavor stability may well be influenced by the exact location within or between the amylose helices.

Complexation of Flavor Compounds with Amylopectin

It is conceivable that the side chains of amylopectin may also interact with ligands to form complexes. In differential scanning calorimetry, a phase transition at around 110 °C was found for a pure amylopectin emulsifier system (68). However, transitions did not occur when decanal or (-)-fenchone were added to dispersions of waxy potato starch (47). If complexation of flavor compounds with amylopectin does occur, ligand binding and complex stability would be rather weak. Therefore, it is doubtful whether flavor complexation with amylopectin would have an effect on flavor retention or release.

Flavor Retention and Release in Systems with Starch Flavor Complexes

As it has been discussed already for extrusion cooking and freeze-drying, almost no quantitative data are available on retention or release of complexed flavor compounds in starch dispersions. Therefore, although the mechanism of complexation itself has been elucidated to a considerable degree, its contribution to overall aroma quality of starch containing foods still needs to be determined, in particular also by sensory analysis.

Sensory testing of aroma quality is first determined by the direct nasal access of volatiles from headspace of a food to the nose which shows that head space concentration of the respective volatiles is important. After ingestion, volatiles are released from the food into the mouth cavity, and pass through the retronasal pathway to the nose. Mechanical breakdown of the food matrix, degradation of amylose flavor complexes, dilution of volatiles in saliva, heating of food components to 37 °C, and rate of diffusion of volatiles are key factors that control flavor release in the mouth cavity.

The effect of potato starch, corn starch, waxy corn starch, and modified waxy corn starch on the release and perception of isoamyl acetate from a dessert cream was recently investigated by chemical and sensory analysis (69). No influence of addition of starch to the recipe was observed, which is understandable in view of the fact that isoamyl acetate most probably does not form inclusion complexes.

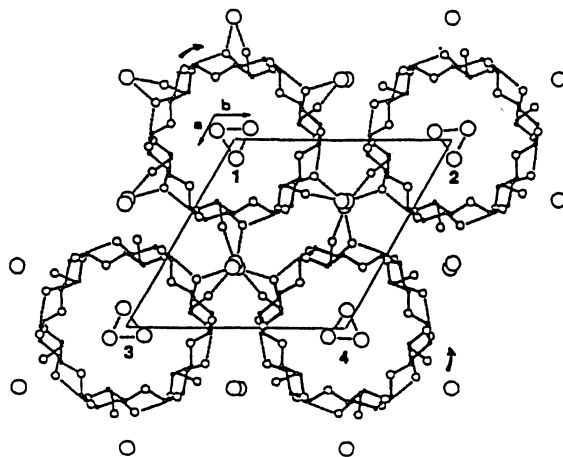


Figure 3. Representative model for the unit cell of V_h amylose (Reproduced from reference 65. Copyright 1991 Elsevier Science Limited.)

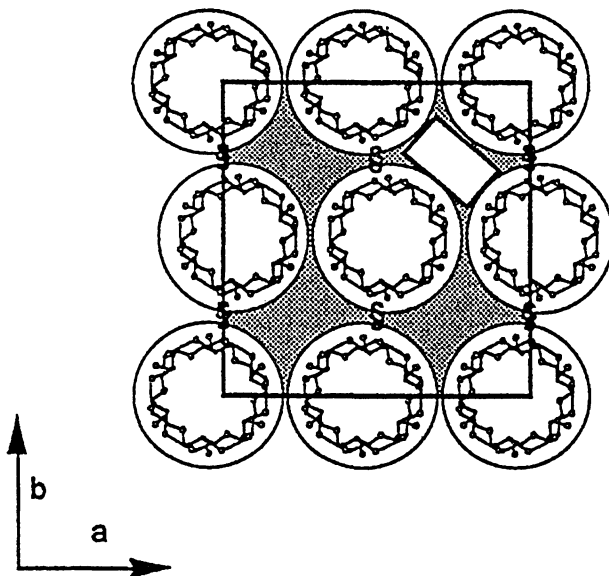


Figure 4. Schematic presentation of a possible arrangement of the helices of V amylose complexed with thymol (Reproduced from reference 67. Copyright 1994 W. Helbert.)

There is also little information on the time intensity profile of aroma compounds that are released from amylose complexes. Apparently, at least 20 s of mastication are necessary to break up the complex and release the volatiles (69).

Consequences for Real Food Systems

In real starch containing food, the various mechanisms of flavor retention and release will be superimposed on each other, depending on the flavor compounds to be considered, on the microscopic structure of food, on the proportion of major components besides starch, and on the composition and state of starch. As these mechanisms all act at different dimensional scales, investigations on starch flavor interaction in real foods should comprise

- the molecular level of flavor binding by complexation of volatiles with amylose, and potentially with amylopectin,
- the supramolecular level of crystallization of inclusion complexes,
- the colloidal level of dispersions in which aggregation, phase separation, and network forming of starch and amylose complexes occur,
- the colloidal level of semi-dry and dry products, including interfaces, in which phenomena such as glass transition, diffusional transfer, and sorption of volatiles become important.

Furthermore, one should bear in mind that starch flavor interactions may not only influence flavor quality, but also rheological properties and with this the sensory texture quality of a food.

Finally, consideration of time scale is mandatory, for example, during storage of food products. Many volatile flavor compounds undergo chemical changes due to reactions such as oxidation or condensation that, in the case of complexation, affect the concentration of individual ligands and the binding equilibrium. In contrast, starch is usually not altered chemically under regular storage conditions. However, from the point of view of material properties, starch biopolymers are almost never in a full thermodynamic equilibrium, but rather in a metastable state. Changes in physical and mechanical properties become important, in particular over longer periods of storage.

A recommendation to research the challenging area of starch-flavor interactions is to do so using interdisciplinary approaches of flavor chemistry, physical chemistry, polymer and material science, and sensory science, by introducing not only experimental techniques from these disciplines, but also their scientific views and basic concepts.

References

1. Gallant, D.J.; Bouchet, B.; Baldwin, P.M. *Carbohydr. Polym.* **1997**, *32*, 177-191.
2. Wu, H.-C.H., Sarko, A. *Carbohydr. Res.* **1978**, *61*, 7-25.
3. Wu, H.-C.H., Sarko, A. *Carbohydr. Res.* **1978**, *61*, 27-40.
4. Imberty, A.; Chanzy, H.; Buléon, A., Tran, V. *J. Mol. Biol.* **1988**, *201*, 365-378.
5. Imberty, A.; Perez, S. *Biopolym.* **1988**, *27*, 1205-1221.

6. Escher, F. In *Food Acceptance and Nutrition*; Solms, J.; Booth, A.D., Pangborn, R.M.; Raunhardt, O., Eds., Academic Press: London, 1987; pp 173-187.
7. Biliarderis, C.G. *Food Technol.* **1992**, *46* (6), 98-109.
8. Waniska, R.D.; Gomez, M.H. *Food Technol.* **1992**, *46* (6), 110-123.
9. Conde-Petit, B.; Nuessli, J.; Handschin, S.; Escher, F. *Starch/Stärke* **1998**, *50*, 184-192.
10. Aberle, T., Burchard, W. *Starch/Stärke* **1997**, *49*, 215-224.
11. Closs, C.B. Ph.D. thesis, Swiss Federal Institute of Technology (ETH), Zurich, 1998.
12. Closs, C.B., Conde-Petit, B., Roberts, I.D., Tolstoguzov, V.B., Escher, F. *Carbohydr. Polym.* **1999**, *39*, 67-77.
13. Conde-Petit, B. Ph.D. thesis, Swiss Federal Institute of Technology (ETH), Zurich, 1992.
14. Solms, J., Guggenbuehl, B. In *Flavor Science and Technology*; Bessièrè, Y., Thomas, A.F., Eds.; John Wiley and Sons: Chichester, 1990; pp 319-335.
15. Godshall, M.A., Solms, J., *Food Technol.* **1992**, *46* (6), 140-145.
16. Tomasik, P., Schilling, C.H., *Adv. Carbohydr. Chem. Biochem.* **1998**, *53*, 263-343.
17. Hau, M.Y.M., Gray, D.A., Taylor, A.J. In *Flavor-Food Interactions*; McGorin, R.J., Leland, J.V., Eds.; ACS Symposiums Series 633, Am. Chem. Soc.: Washington, DC, 1996; pp 109-117.
18. Zhao, J., Whistler, R.L., *Food Technol.* **1994**, *48* (7), 104-105.
19. Zhao, J., Madson, M.A., Whistler, R.L. *Cereal Chem.* **1996**, *73*, 379-380.
20. BeMiller, J.N., Pratt, G.W. *Cereal Chem.* **1981**, *58*, 517-520.
21. Roos, Y.H., Karel, M., Kokini, J.L. *Food Technol.* **1996**, *50* (11), 95-108.
22. Goubet, I., Le Quere, J.-L., Voilley, A.J. *J. Agric. Food Chem.* **1998**, *46*, 1981-1990.
23. Benczédi, D., Tomka, I., Escher, F. *Macromol.* **1997**, *31*, 3055-3061.
24. Benczédi, D. *Trends Food Sci. Technol.* **1999**, *10*, 21-24.
25. Hau, M.Y.M., Hibberd, S., Taylor, A.J. In *Flavor Science - Recent Developments*; Taylor, A.J., Mottram, D.S., Eds; Royal Soc. Chem.: Cambridge, 1996; pp 437-441.
26. Kenyon, M.M. In *Encapsulation and Controlled Release of Food Ingredients*; Risch, S.J., Reineccius, G.A., Eds.; ACS Symposium Series 590, Am. Chem. Soc.: Washington, DC, 1995; pp 42-50.
27. Pegg, R.B., Shahidi, R.B. In *Handbook of Food Preservation*; Rahman, M.S., Ed.; Marcel Dekker: New York, NY, 1999; pp 611-667.
28. Kenyon, M.M. In: *Flavor Encapsulation*; Risch, S.J., Reineccius, G.A., Eds.; ACS Symposiums Series 370, Am. Chem. Soc.: Washington, DC, 1988; 7-11.
29. Bangs, W.E., Reineccius, G.A. In *Flavor Encapsulation*; Risch, S.J., Reineccius, G.A., Eds. ACS Symposiums Series 370, Am. Chem. Soc.: Washington, DC, 1988; pp12-28.
30. Turbiano, P.C. In *Modified Starches: Properties and Uses*; Wurzburg, O.B., Ed.; CRC Press, Inc.: Boca Raton, FL, 1986; pp 131-147.
31. Escher, F. In *Flavour Science and Technology*; Bessièrè, Y., Thomas, A.F., Eds.; John Wiley & Sons: Chichester, 1990; pp 337-346.
32. Chen, J.Y. Ph.D. thesis, University of Minneapolis, St.Paul, MN, 1984.
33. Chen, J.Y., Reineccius, G.A., Labuza, T.P. *Internat. J. Food Technol.* **1986**, *21*, 365-
34. King, C.J. In *Preconcentration and Drying*; Bruin, S., Ed.; Elsevier Science Publ.: Amsterdam, 1988; pp 147-162.
35. Kollengode, A.N.R., Hanna, M.A., Cuppett, S. *J. Food Sci.* **1996**, *61*, 985-989, 1079.

36. Kollgengode, A.N.R., Hanna, M.A. *Cereal Chem.* **1997**, *74*, 396-399.
37. Schmidt, E. Ph.D. thesis, Technical University Carola-Wilhelmina, Braun-schweig, Germany, 1987.
38. Maier, H.G., Moritz, K., Schmidt, E. *Lebensm. Chem. Gerichtl. Chem.* **1987**, *41*, 56-60.
39. Maier, H.G., Moritz, K., Rümmler, U. *Starch/Stärke* **1987**, *39*, 126-131.
40. Stäger, G. Ph.D. thesis, Swiss Federal Institute of Technology (ETH), Zurich, Switzerland, 1988.
41. Staeger, G., Escher, F., Solms, J. In *Frontier in Flavors*; Charalambous, G., Ed.; Elsevier Science Publ.: Amsterdam, 1987; pp 639-654.
42. Staeger, G., Escher, F., Solms, J. In *Processing and Quality of Foods - COST 91bis Final Seminar*; Zeuthen, P., Cheftel, J.C., Eriksson, C., Gormley, T.R., Linko, P., Paulus, K., Eds.; Elsevier Applied Science Publ.: London, 1990; vol. 1, pp 296-301.
43. Bhatnagar, S., Ph.D. thesis, University of Nebraska, Lincoln, NE, 1993.
44. Bhatnagar, S., Hanna, M.A., *J. Food Sci.* **1996**, *61*, 778-782.
45. Conde-Petit, B., Escher, F., *J. Rheol.* **1995**, *39*, 1497-1518.
46. Maga, J.A., Kim, C.H. In *Flavor Science and Technology*; Bessière, Y., Thomas, A.F., Eds.; John Wiley & Sons: Chichester, 1990; pp 347-350.
47. Nüssli, J. Ph.D. thesis, Swiss Federal Institute of Technology (ETH), Zurich, Switzerland, 1998.
48. Banks, W., Greenwood, C.T. *Starch and Its Components*; Edinburgh University Press: Edinburgh, 1975.
49. Kuge, T., Takeo, K., *Agr. Biol. Chem.* **1968**, *32*, 1232-1238.
50. Osman-Ismail, F. Ph.D. thesis, Swiss Federal Institute of Technology (ETH), Zurich, Switzerland, 1972.
51. Osman-Ismail, F., Solms, J. *Lebensm.-Wiss. Technol.* **1973**, *6*, 147-150.
52. Rutschmann, M.A. Ph.D. thesis, Swiss Federal Institute of Technology (ETH), Zurich, Switzerland, 1987.
53. Rutschmann, M.A., Solms, J. In *Flavors and Off-Flavors*; Charalambous, G. Ed.; Elsevier Science Publ.: Amsterdam, 1989; pp 991-1010.
54. Wyler, R. Ph.D. thesis, Swiss Federal Institute of Technology (ETH), Zurich, Switzerland, 1979.
55. Wyler, R., Solms, J. *Lebensm.-Wiss. Technol.* **1982**, *15*, 93-96.
56. Conde-Petit, B., Escher, F. *Food Hydrocoll.* **1992**, *6*, 223-229.
57. Raphaelides, S.N. *Food Hydrocoll.* **1993**, *7*, 479-495.
58. Holló, J., Szejtli, J. *Starch/Stärke*, **1956**, *9*, 109-112.
59. Nuessli, J., Conde-Petit, B., Trommsdorff, U.R., Escher, F. *Carbohydr. Polym.* **1996**, *28*, 167-170.
60. Nuessli, J., Sigg, B., Conde-Petit, B., Escher, F. *Food Hydrocoll.* **1997**, *11*, 27-34.
61. Yamashita, Y. *J. Polym. Sci. Part A*, **1965**, *3*, 3251-3260.
62. Yamashita, Y., Hirai, N. *J. Polym. Sci. Part A-2*, **1966**, *4*, 161-171.
63. Yamashita, Y., Monobe, K. *J. Polym. Sci. Part A-2*, **1971**, *9*, 1471-1481.
64. Rappenecker, G., Zugenmaier, P. *Carbohydr. Res.* **1981**, *89*, 11-19.
65. Brisson, J., Chanzy, H., Winter, W.T. *Int. J. Biol. Macromol.* **1991**, *13*, 31-39.
66. Godet, M.C., Tran, V., Delage, M.M., Buléon, A. *Int. J. Biol. Macromol.* **1996**, *15*, 11-16.
67. Helbert, W. Ph.D. thesis, Université Joseph Fourier Grenoble I, Grenoble, France, 1994.
68. Gudmundsson, M., Eliasson, A.-C., *Carbohydr. Polym.* **1990**, *13*, 295-315.
69. Cayot, N., Taisant, C., Voilley, A. *J. Agric. Food Chem.* **1998**, *46*, 3201-3206.

Chapter 20

Competition between Aroma Compounds for the Binding on β -Cyclodextrins: Study of the Nature of Interactions

Isabelle Goubet¹, Jean-Luc Le Quéré², E. Sémon², A.-M. Seuvre¹,
and A. Voilley¹

¹ENSBANA—Université de Bourgogne,
1 Esplanade Erasme, 21000 Dijon, France
²INRA, 17, rue Sully, F21000, Dijon, France

Encapsulation of aroma is an efficient way to control the flavoring of food products but its main drawback is the selectivity in encapsulation and release, according to the nature of the aroma compounds. This work focuses on the behavior of volatiles when they compete for the binding on a current flavor carrier, β -cyclodextrin. The nature of interactions is studied at a molecular level, according to the characteristics of the guest molecule. The results of spectroscopic measurements are discussed in terms of affinity for β -cyclodextrin and also efficiency of retention.

Flavor is one of the most important sensory properties of foods and partly determines consumer preferences. This organoleptic quality depends both on the amount and proportions of aroma compounds retained and released by the product. In order to control flavor quality, many food products are flavored by the addition of liquid or encapsulated aroma. The use of microcapsules provides an effective way to reduce volatility of flavor compounds, to protect them against oxidation and reaction with other food components and also to control their release (1). Flavor retention and release however depend both on the nature of the carrier and of the volatile (2). This phenomenon can cause some component of the flavor to be retained whilst other are fully released, leading to perception of an unbalanced flavor. This selective retention or release constitutes the main drawback of encapsulation and is still resolved empirically.

Much research has been focused to reduce this empiricism. The effect of operating parameters during the encapsulation process has been extensively studied and is now better understood (3, 4), but relatively few publications have studied competition between aroma compounds for their binding on carriers (5, 6). Since

most aromas are complex mixture of volatiles, differing in their physico-chemical properties, the study of competitive binding of aroma compounds on a carrier could also provide further information on the observed phenomena. This article also focuses on the mechanisms involved in selective retention of volatiles by β -cyclodextrins, a polysaccharide frequently used for encapsulation of flavors. The purpose is to understand, at a molecular level, the nature of interactions that occur between volatiles and carbohydrate, in order to explain phenomena observed at a macroscopic scale.

Materials and Methods

Aroma compounds Seven aroma compounds were selected among strawberry natural flavor compounds. No homologous series of compounds was selected, since the effect of the carbon chain length of the volatile compound on its behavior in the presence of β -cyclodextrin has already been reported (7,8). This work was also focused on the effect of changes in both the chemical function and the conformation of the carbon chain of the aroma compounds. The physico-chemical characteristics of the volatile compounds are given in Table I. They were provided by International Flavors and Fragrances (Lonvic - France) (purity > 98 %).

Table I. Physico-Chemical Properties of Aroma Compounds

<i>Aroma compound</i>	<i>Molecular weight</i>	<i>Vapor pressure (Pa)</i>	<i>Solubility In water at 25°C (g/L)</i>	<i>Hydrophobicity (Log P)</i>
Ethyl propionate	102	5374	12.4	1.24
Ethyl hexanoate	144	238	0.52	2.83
Hexanal	100	1458	4.2	1.97
Hexanol	102	197	6.0	1.94
Benzyl alcohol	108	13	40.0	1.03
Hexanoic acid	116	20	7.8	1.84
2-methyl butyric acid	102	114	20.0	1.12

Log P : hydrophobic constant, calculated using Rekker's method (9).

Other materials: β -cyclodextrins, (Roquette, Lestrem, France). polymers made of seven glucose units linked by α 1 \rightarrow 4 bonds, were used as model carriers. These molecules are shaped like a hollow truncated cone, crowned at both extremities by hydroxyl groups. Paramagnetic probe 4-oxo-2,2,6,6-tetramethylpiperidine-1-oxyl (4-oxo-Tempo) was purchased from Sigma (>98 % purity). Nuclear Magnetic Resonance solvent and standard Deuterated dimethylsulfoxide (DMSO-d₆; 99.96 % purity) and tetramethylsilane (99 % purity) were used respectively as solvent and internal standard for NMR experiment (CEA, Saclay - France). Potassium Bromide

The pellets for recording Fourier transform infrared spectra were made of KBr (Aldrich, purity > 99 %).

Encapsulation of aroma Retention of single aroma compounds was studied by addition of increasing amounts of aroma to a paste composed of β -cyclodextrin and osmosed water (75% w/w). The initial amount of aroma compound in the mixture prior to dehydration ranged from 1 to 4 mole of flavor compound per mole of β -cyclodextrin. The complexes obtained after dehydration were used for the studies at molecular scale (by EPR, NMR and FT-IR spectroscopies).

To observe retention of mixtures of aroma compounds, two kinds of competition for the binding to β -cyclodextrins were performed : 1. among volatiles differing either by the conformation of their carbon chain (ethyl propionate and ethyl hexanoate) or 2. by their chemical functions (ethyl hexanoate, hexanal, hexanol and hexanoic acid). For experiment 1, two moles of ethyl propionate were first introduced into a paste made of β -cyclodextrins and osmosed water (75%, w/w) and increasing amount of ethyl hexanoate were then added. For the second experiment, an equimolar mixture of ethyl hexanoate, hexanol, hexanoic acid and hexanal was prepared and increasing amounts were added to a paste of β -cyclodextrin and water (75%, w/w).

All the mixtures were made in triplicate, in a hermetically closed flask, shaken for 24 hours at 25°C and dehydrated using a USIFROID SMJ freeze dryer. The operating conditions were as follows : samples were frozen for 2 hours at -50°C and then freeze dried. During freeze drying, the temperature of shelves was set at -25°C for 10 hours and then +30°C for 19 hours.

Retention capacity Retention of aroma, expressed as mole of aroma retained per mole of β -cyclodextrin, was measured by dilution of 0.1 wt % of dried complexes in osmosed water and injection of portions (1 μ L) of this solution on the gas chromatographic column of a 5710A Hewlett Packard chromatograph equipped with a flame ionization detector. Gas chromatographic conditions : stainless steel column (3 m x 3.15 mm) packed with 100/120 mesh Carbowax, maintained at 110°C for analysis of esters and hexanal and at 150°C for the analysis of alcohols. The injector and detector temperatures were 250 and 220°C. Nitrogen, hydrogen and air flow rates were respectively 19 mL/min, 25 mL/min and 250 mL/min.

For determination of hexanoic acid retention, a 30 min CH_2Cl_2 extraction (1/1 : v/v) was performed on the aqueous solution, prior to injection of aliquots (1 μ L) of the organic phase on a EC1000[®] capillary column (30 m X 0.32 mm, 0.25 μ m film thickness) (Alltech - France) on a GC14 Shimadzu chromatograph equipped with a flame ionization detector. Heptanoic acid was used as internal standard. Gas chromatographic conditions : capillary column temperature 130°C, injector and detector temperature : 250°C. Helium, hydrogen and air entry pressures 60 kPa, 50 kPa and 35 kPa respectively.

Determination of interaction parameters Interaction parameters were determined by the Hummel and Dreyer method. The High Performance Liquid Chromatography

conditions comprised : a Dionex pump equipped with a 50 μL Rheodyne injector, a Lichrosorb 100 Diol column (250 mm X 4.6 mm i.d., 10 μm particle size, Merck) and a SPD 6A Shimadzu UV Detector. The eluent was a solution of flavor whose concentration increased from 20 to 400 $\mu\text{L/L}$. The flow rate was 0.8 mL/min. The concentration of the bound ligand was determined by an internal calibration method. The Scatchard model was used for calculation of interaction parameters (10).

Competition between aroma and a paramagnetic probe - Electronic Paramagnetic Spectroscopy Behavior of 4-oxo-Tempo (10^{-4} M) in aqueous solution was compared to those of the same probe (10^{-4} M) in solution with β -cyclodextrin (10^{-2} M) or with complexes obtained (after dehydration) with each of the aroma compounds (10^{-2} M).

EPR spectra were recorded with a Bruker EMX spectrometer. The field modulation amplitude was 1G and the incident microwave power was 1.6 mW for the EPR measurements. The rotational correlation time of the paramagnetic probe, τ , was

calculated as following: $\tau = 6.65 \cdot 10^{-10} \Delta H_{I+1} \left(\sqrt{\frac{I_{+1}}{I_{-1}}} - 1 \right)$.

I_{+1} and I_{-1} , being respectively the height of line at high and low field and ΔH_{I+1} , being the width of the high field line of the spectrum, expressed in Gauss. It reflects the mean mobility of the probe. Measurements were done in triplicate.

Determination of spatial conformation by ^{13}C -NMR and ^1H -NMR Spatial conformation of the complexes obtained with each of the aroma compound was deduced from the comparison of the spectra of the aroma (70 g/L) and of the corresponding complexes (70 g/L) diluted in deuterated dimethylsulfoxide. In order to avoid solvent effect, tetramethylsilane (11 g/L) was used as internal standard.

NMR spectra were obtained on a Bruker FT-NMR spectrometer operating at 500 MHz for ^1H and 125.8 MHz for ^{13}C . ^1H NMR spectra were obtained by application of 90° impulses and resulted from four accumulations. ^{13}C NMR spectra were recorded in the inverse gate mode, by application of 30° impulses and were the product of 1024 accumulations. Samples were maintained at 27°C .

Fourier Transform Infrared Spectroscopy Hydrogen bonds between aroma compounds and β -cyclodextrins were examined by comparison of the spectra of aroma and β -cyclodextrins with those of the complexes. Spectra were recorded with a FTS 6000 Bio-Rad Fourier transform infrared spectrometer. A KBr beam splitter and a DTGS detector were used. The resolution limit was 2 cm^{-1} . For β -cyclodextrins and complexes, the samples were obtained by pressing 2 wt % of powder into KBr pellet. The spectra of pure aroma compounds were recorded by depositing a drop of pure aroma between two KBr pellets.

Results and Discussion

The amount of aroma compound encapsulated by β -cyclodextrin, after dehydration of mixtures in which four moles of aroma compound were initially introduced per mole of β -cyclodextrin are summarized in Table II.

Table II. Retention of Volatiles after Dehydration of Mixtures Initially Containing an Excess of Aroma (4 mole of aroma /mole of β -cyclodextrin)

<i>Aroma compound</i>	<i>Retention Mole/mole of β-cyclodextrin</i>
Ethyl propionate	0.88 \pm 0.01
Ethyl hexanoate	0.91 \pm 0.01
Hexanal	1.07 \pm 0.02
Hexanol	1.06 \pm 0.07
Benzyl alcohol	2.14 \pm 0.12
Hexanoic acid	1.13 \pm 0.04
2-methylbutyric acid	1.00 \pm 0.16

In the case of ethyl propionate, ethyl hexanoate, hexanal, hexanol, hexanoic acid and 2-methylbutyric acid, maximal retention after dehydration is close to 1 mole/mole of aroma per mole of β -cyclodextrin, even in the presence of large amounts of volatile prior to dehydration. Matsui *et al.* (11) have previously determined the spatial conformation of β -cyclodextrin complexes obtained with ethyl hexanoate. They proved that only one molecule of ethyl hexanoate can be included in each cavity. The maximal retention of 0.91 mole of aroma per mole of carrier observed in the case of ethyl hexanoate can also be explained by the fact that this aroma compound is retained in the cavity of β -cyclodextrin, whereas molecules initially present in excess are removed during freeze drying. It seems also that the only aroma compounds sufficiently strongly retained by β -cyclodextrin during dehydration, are those located in the cavity of β -cyclodextrin, interacting in a sufficient way to avoid their removal during freeze drying. Moreover, the results observed after saturation of the binding sites of β -cyclodextrin by the other aroma compounds suggest that, in the case of ethyl propionate, hexanal, hexanol as well as hexanoic or 2-methylbutyric acids, the cavity of β -cyclodextrin is also the binding site of these flavor compounds and that only one molecule of ligand can be bound per molecule of β -cyclodextrin. In contrast, two moles of benzyl alcohol were retained per mole of β -cyclodextrin. A similar result was reported by Sanemasa *et al.* (12) when comparing retention of aromatic compounds with those of aliphatic compounds. It has also been reported that, after dehydration of a mixture initially containing an excess of volatile, retention of pentane and heptane were respectively

1.1 and 0.88 mole per mole of β -cyclodextrin whereas that of aromatic compounds such as benzene and fluorobenzene reached 1.9 mole per mole of β -cyclodextrin. The difference of behavior of aromatic compounds could be explained by the difference of steric hindrance between aliphatic and aromatic compounds and also by differences in the nature of interaction between the host and its guest, the flat aromatic ring interacting in a different way with β -cyclodextrin compared to the carbon chain of aliphatic compounds. The physico-chemical properties of aroma compounds therefore have a direct influence on their retention, even for the encapsulation of single aroma compounds.

Since flavors are usually complex mixtures of aroma compounds, behavior of mixtures of volatiles was also studied. The effect of different type of volatiles and different conformations of the carbon chain in volatiles were investigated by competition studies for binding to β -cyclodextrin.

Figure 1 illustrates retention of ethyl hexanoate, hexanal, hexanol and hexanoic acid, after dehydration of a mixture in which increasing amounts of an equimolar mixture of these four compounds were initially added. There was no significant difference between retention of ethyl hexanoate, hexanoic acid and hexanal but in all cases, retention of hexanol was significantly lower than ethyl hexanoate and hexanal. Since these four compounds all have a hexyl group but differ in their other functional group, it can be deduced that there is an effect of chemical function of aroma compounds on their retention by β -cyclodextrins.

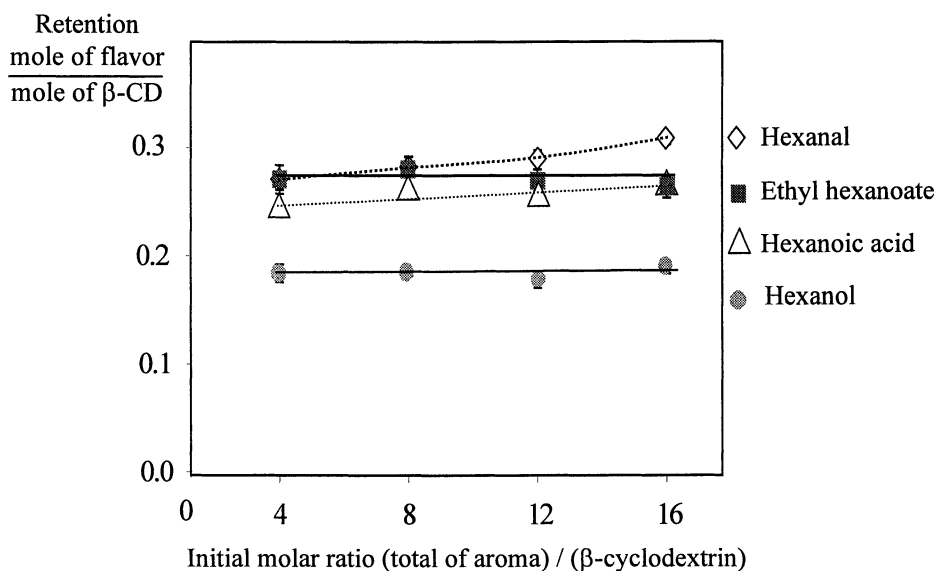


Figure 1. Retention of volatiles, after dehydration of mixtures initially composed of water, β -cyclodextrins and increasing amount of four aroma compounds

From the study of saturation of binding sites by these compounds, it has been observed that each of them can be retained at up to one mole per mole of β -cyclodextrin, and the differences in retention noticed when they are initially in a mixture are also probably explained by a difference of affinity for the binding site of β -cyclodextrin, depending on the nature of their chemical function.

Competition between ethyl propionate and ethyl hexanoate, representing two esters with different chain length, were also studied. When β -cyclodextrin was initially saturated by two moles of ethyl propionate per mole of carrier and rising amounts of ethyl hexanoate were then added, retention of the latter was strongly increased whereas retention of ethyl propionate decreased (Figure 2). When competition was done in the reverse order, retention of ethyl hexanoate decreased slowly as ethyl propionate retention increased. These results clearly show the preferential retention of ethyl hexanoate.

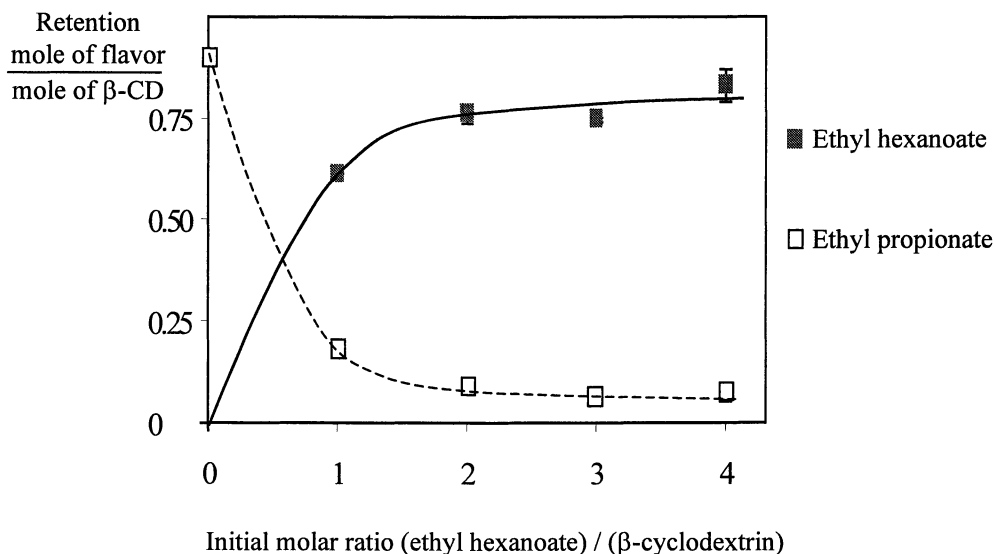


Figure 2. Retention of esters after dehydration of mixtures initially containing 2 moles of ethyl propionate per mole of β -cyclodextrin and increasing amounts of ethyl hexanoate

These two esters seem to have the same number of binding sites on β -cyclodextrin, since for both, maximal retention is close to one mole per mole of β -cyclodextrin. The difference in retention when they are in a mixture could also be explained by a difference of affinity for the cavity of β -cyclodextrin. In order to check this hypothesis, interaction parameters of these two esters with β -cyclodextrin were determined. Results are summarized in Table III.

Table III. Interaction Parameters of Ethyl Propionate and Ethyl Hexanoate with β -cyclodextrin (determined by the Hummel and Dreyer method)

<i>Aroma compound</i>	<i>Number of binding site per molecule of β-cyclodextrin (n)</i>	<i>Affinity constant (K_a) M^{-1}</i>	<i>Global affinity ($n \cdot K_a$) M^{-1}</i>
Ethyl propionate	1.08	38	41
Ethyl hexanoate	0.96	318	305

Both esters have a single binding site on β -cyclodextrin but the affinity constant of ethyl hexanoate for β -cyclodextrins is eight times greater than that of ethyl propionate. From this result it can also be deduced that the selective retention of ethyl hexanoate, when it competes with ethyl propionate for the binding on β -cyclodextrin, is at least partly explained, at a macroscopic scale, by the difference of affinity of these two esters for β -cyclodextrin. Moreover, the increasing affinity of the volatile compound for β -cyclodextrin with the increase of its carbon chain length, and also with the increase of its hydrophobicity, is in agreement with previous results (8) reported for homologous series of alcohols and ketones.

Binding of aroma compounds to β -cyclodextrin was studied at a molecular scale by competition between the volatiles and a paramagnetic probe, 4-oxo-2,2,6,6-tetramethylpiperidine-1-oxyl (4-oxo-Tempo). Prior to studying the effect of the presence of an aroma compound on the behavior of the spin probe, the interactions between 4-oxo-tempo and β -cyclodextrin were determined. In the presence of β -cyclodextrins in aqueous solution, a shoulder was noticed on the high field absorption line of the spectrum of 4-oxo-Tempo, indicating that part of probe was surrounded by a medium less polar than water (Figure 3). Moreover the mean rotational correlation time of the probe was increased by the presence of these polysaccharides. Mobility of the probe was also lowered when β -cyclodextrins were in solution. By comparison of the spectra of the same probe in solution with different carbohydrates, Florh *et al.* (13) proved that the reduction of mobility cannot be attributed to the increase of viscosity induced by the presence of β -cyclodextrin. These results also show that in the presence of β -cyclodextrin, part of the probe interacts with an apolar site of these polysaccharides. It has been shown that the inner cavity of β -cyclodextrin is rather apolar (14) and it can also be hypothesized that, when β -cyclodextrins are in solution, part of probe interacts with the apolar cavity.

When complexes are diluted in solution, the shoulder of the high field absorption line decreases compared to that observed in the presence of β -cyclodextrins and whatever the complex in solution, the mean rotational correlation time of 4-oxo-tempo is higher than that of the probe in the presence of β -cyclodextrin (Table IV). From these results it can be deduced that interactions between the probe and β -cyclodextrins are hindered by the presence of a complexed volatile and that the

aroma compounds and the probe compete for the same binding site of the carbohydrate. Moreover, the rotational correlation time of 4-oxo-Tempo is significantly lower and mobility also significantly higher in the presence of ethyl hexanoate complexes than in those of ethyl propionate, in agreement with the previous results. Indeed a higher global affinity for β -cyclodextrin was observed for ethyl hexanoate compared to ethyl propionate.

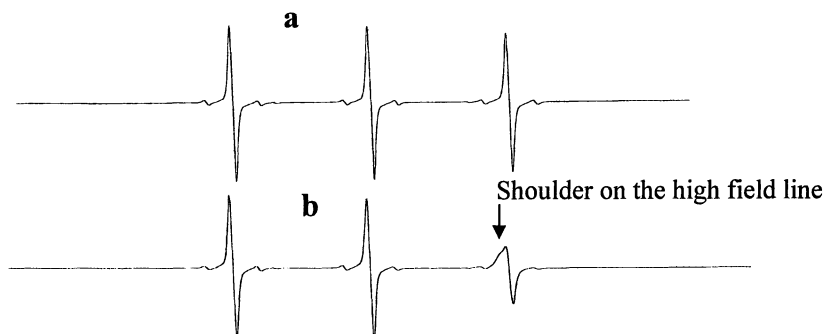


Figure 3. EPR spectrum of 4-oxo-tempo (10^{-4} M) in aqueous solution a) alone b) with β -cyclodextrin (10^{-2} M)

Table IV. Mean rotational Correlation Time of 4-oxo-Tempo(10^{-4} M) in Aqueous Solution and in Presence of β -cyclodextrin (10^{-2} M) or Complexes (10^{-2} M)

<i>Solution</i>	<i>Mean rotational correlation time (s)</i>
Water	2.7 ^A
β -cyclodextrins aqueous solution	22.7 ^F
Ethyl propionate complexes in aqueous solution	19.5 ^E
Ethyl hexanoate complexes in aqueous solution	5.4 ^B
Hexanal complexes in aqueous solution	8.5 ^C
Hexanol complexes in aqueous solution	11.8 ^D
Benzyl alcohol complexes in aqueous solution	12.0 ^D
Hexanoic acid complexes in aqueous solution	10.0 ^D
2-methyl butyric acid complexes in aqueous solution	7.0 ^{BC}

Values with the same subscript are not significantly different ($P \geq 0.05$)

As the effect of chemical function of the aroma complexed is considered, it can be noticed that mobility of the probe was significantly higher in the presence of ethyl hexanoate complexes than in the presence of hexanal complexes or hexanoic acid

complexes. When hexanol complexes were in solution, the mobility of 4-oxo-Tempo was significantly lower compared to the behavior of the probe in the presence of complexes containing ethyl hexanoate or hexanal. These results are in agreement with those obtained when encapsulating equimolar mixture of these four compounds (Figure 1). Indeed in both cases retention of aroma decreases in the order ethyl hexanoate, hexanal, hexanoic acid, hexanol. Nevertheless no significant difference could be detected between retention of carbonyl compounds after encapsulation, whereas significant differences can be noticed according to the chemical function of volatile as competitions are performed with a paramagnetic probe.

In order to explain these variations according to the aroma compound, the nature of interactions between aroma and β -cyclodextrins was then investigated at a molecular scale. It has been shown that the encapsulation of volatile in the apolar cavity of β -cyclodextrin induces a decrease of the resonance frequency of ^{13}C nuclei included in the cavity (15). Spatial conformation of the complexes has also been determined by observation of resonance frequency variations of the ^{13}C nuclei of aroma compounds after their encapsulation by β -cyclodextrin.

Table V. Variation of the Resonance Frequency (in Hz) of Ethyl Hexanoate ^{13}C Nuclei after encapsulation

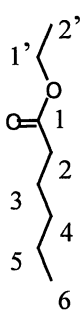
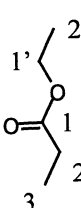
	Carbon atom	$\Delta\nu$ (Hz)
	C2'	-16.3
	C1'	-16.3
	C1	-13.4
	C2	-18.2
	C3	-21.1
	C4	-22.1
	C5	-23.0
	C6	-15.3

Table VI. Variation of the Resonance Frequency (in Hz) of Ethyl Propionate ^{13}C Nuclei after encapsulation

	Carbon atom	$\Delta\nu$ (Hz)
	C2'	-21.1
	C1'	-23.0
	C1	-16.3
	C2	-27.8
	C3	-20.2

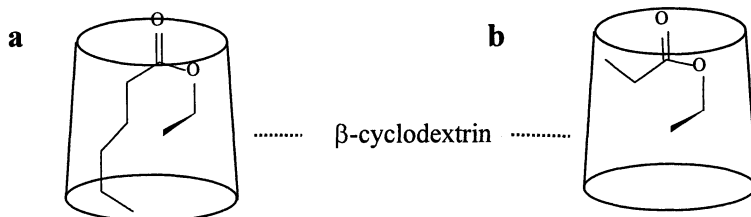


Figure 4. Possible spatial conformation for a) ethyl hexanoate complexes b) ethyl propionate complexes

Tables V and VI summarize the variations observed for ethyl propionate and ethyl hexanoate. Considering ethyl hexanoate, the resonance frequencies of its C3, C4 and C5 carbon atoms are lowered more after encapsulation whereas those of the nuclei of the methyl (C6) and of the carbonyl groups are less affected. It can also be supposed that the carbonyl and the methyl groups are in the vicinity of hydroxyl functions of β -cyclodextrin, whereas the center part of the hexyl group is deeply included in the cavity. It can also be hypothesized that the hexyl group is included along the axis of the β -cyclodextrin torus, with methyl and carbonyl groups being located near hydroxyl functions of β -cyclodextrin. After encapsulation, resonance frequencies of ^{13}C nuclei of the ethyl group are lowered. This group is also probably included in the cavity of β -cyclodextrin and involved in the binding of ethyl hexanoate to β -cyclodextrin. The spatial conformation of the complexes could also be that proposed in Figure 4, in agreement with results of Matsui *et al.* (11).

Considering complexes made with ethyl propionate, it can be stated that in this case the resonance frequency of the ^{13}C nucleus of the carbonyl groups is less affected by encapsulation. This part of ethyl propionate is also probably located near the hydroxyl groups of β -cyclodextrin. Since the decrease of resonance frequencies are greater for the other ^{13}C nuclei, they are probably more deeply included in the cavity. As resonance frequencies of the ^{13}C nuclei of the ethyl group are lowered by encapsulation, it can be deduced that this group is located in the cavity and interacts with the inner wall of β -cyclodextrin. Moreover, as resonance frequency of the C3 nucleus is less affected than those of C2, it can be supposed that the second one is less deeply inserted in the torus of β -cyclodextrin and that ethyl propionate is probably not included along the axis of the cavity but perpendicularly (Figure 4).

It also appears that the carbonyl and the ethyl groups of ethyl propionate and ethyl hexanoate interact in a similar way with β -cyclodextrins and that the differences observed in retention of these two esters are due to differences of interactions between the polymer and the propionyl or the hexyl groups of these aroma respectively. As these groups are completely included in the cavity, but the chain length of the hexyl group is greater than the propionyl group, it can be concluded that hydrophobic contribution is greater for the binding of ethyl hexanoate. Moreover, since a longer portion of carbon chain is in contact with the apolar walls of β -cyclodextrin when encapsulating ethyl hexanoate, it can be supposed that contribution of dispersion forces is more important for the binding of ethyl hexanoate than for those of ethyl propionate to β -cyclodextrins. The length of the carbon chain affects not only the amount of hydrophobic interactions but also dispersion forces between β -cyclodextrin and its ligand. Indeed, from variations of resonance frequencies of carbon nuclei of the aroma after encapsulation, it also seems that the smaller compound does not adopt the same orientation as the longer one, the hexyl group being included along the axis of the torus, whereas propionyl group could be inserted perpendicularly.

The same approach was applied to study the spatial conformation of complexes obtained with hexanal, hexanoic acid and hexanol. Variations of the resonance

frequencies of hexanoic acid and hexanal nuclei indicate that the hexyl group of these two compounds are deeply included in the cavity, whereas their methyl groups and the carboxylic group of the acid are probably located toward the rim of hydroxyl groups of β -cyclodextrins. The resonance frequency of the carbon nucleus of the carbonyl group of hexanal is the only which increases upon encapsulation. It can also be concluded that the hexyl group of hexanal, ethyl hexanoate and hexanoic acid interacts in a similar way with β -cyclodextrin but that the carbonyl group of hexanal interacts in a different way compared to ethyl hexanoate and hexanoic acid.

Table VII. Variation of the Resonance Frequency (in Hz) of Hexanal, Hexanoic Acid and Hexanol ^{13}C Nuclei after their Encapsulation by β -cyclodextrin

Carbon atom	Variation of resonance frequency (Hz)		
	Hexanal	Hexanoic acid	Hexanol
C1	+10.6	-9.	-37.4
C2	-34.6	-18.6	-44.1
C3	-33.6	-26.9	-43.2
C4	-35.5	-30.5	-45.1
C5	-33.6	-29.9	-41.3
C6	-19.2	-19.2	-25.0

Considering hexanol complexes, variation of resonance frequency led to the hypothesis that the methyl group is the only one located near the rim of hydroxyl groups of β -cyclodextrin. It seems also that this compound has a folded conformation when complexed, the hydroxyl group being included in the cavity and, as a consequence, not involved in hydrogen bonds with the hydroxyl groups of β -cyclodextrin. The hexyl group of this compound probably interacts in a different way with β -cyclodextrin compared to the hexyl group of ethyl hexanoate and hexanoic acid. The folding of the carbon chain of hexanol in the cavity should increase the contact between the carbon chain and the apolar walls of the polymer and also increase the importance of dispersion forces between this ligand and its carrier, favoring its binding. However, it has been observed that, when hexanol competes with ethyl hexanoate and hexanoic acid, it is less retained. The nature of interaction between these compounds and β -cyclodextrin has also been further studied by ^1H NMR and Fourier transform infrared spectroscopy.

Comparison of ^1H NMR spectra of pure β -cyclodextrin and those of hexanoic acid complexes clearly show the broadening of the signals attributed to protons of the hydroxyl groups of β -cyclodextrins, indicating that there are hydrogen bonds between the carboxyl group of hexanoic acid and the hydroxyl functions of β -cyclodextrins and that such interactions are also involved in the retention of hexanoic acid by β -cyclodextrin. The better retention of hexanoic acid compared to

that of hexanol is also probably due to the hydrogen bond between the carboxylic function of the acid and the hydroxyl groups of β -cyclodextrin, a kind of interaction that does not seem to be involved in retention of hexanol.

Through NMR results, hydrogen bonds have only been detected between the carrier and the acid. Since the location of the carbonyl group of the ester could allow this kind of interaction with β -cyclodextrin, hydrogen bonds were also searched between ethyl hexanoate and β -cyclodextrin by Fourier transform infrared spectroscopy. To this aim, the spectra of pure aroma and pure polymer were also compared to that of complexes.

On the spectrum of dehydrated ethyl hexanoate complexes, a shoulder can be noticed on the band attributed to the carbonyl function of the ester. This significant negative shift of absorption indicates that part of ethyl hexanoate carbonyl functions are involved in hydrogen bonds with β -cyclodextrin and that, after dehydration, such interaction are also involved in the retention of ethyl hexanoate by β -cyclodextrin. The higher retention of ethyl hexanoate compared to those of hexanal, hexanoic acid or hexanol can also be explained by the hydrophobic interactions and the dispersion forces that arise from inclusion of the ethyl group in the cavity and, after dehydration, by the hydrogen bond between the carbonyl function of this ester and the hydroxyl groups of β -cyclodextrin.

Conclusions

This study shows that at least part of preferential retention, observed between aroma compounds when they compete for binding to the same carrier, can be explained by differences in the nature of interaction that occur between volatiles and their carrier. But much remained to be done in order to fully understand the relationship between the physico-chemical properties of aromas and their behavior as they compete for the same carrier. Applying the same approach to a larger number of compounds and using computer modeling would surely help to better evaluate the effect of each factor and also decrease the role of empiricism in flavor encapsulation.

References

1. Shahidi, F.; Han, X. Q. *Crit. Rev. Food Sci. and Nut.* **1993**, *33*, 501-547.
2. *Encapsulation and Controlled Release of Food Ingredients*; Voilley A., American Chemical Society, Washington S. J. Risch. and G. A. Reineccius, Eds.; **1995**; pp 169-179.
3. Thijssen, H. A. C.; Rulkens, W. H.. *De Ingenieur* **1968**, *80*, 45-56.
4. *Spray-Drying of Food Flavors* Reineccius, G. A American Chemical Society, Washington, S. J. Risch and G. A. Reineccius, Eds.; **1988**; pp 55-64.
5. Bangs, W. E.; Reineccius, G. A. *J. Food Sci.* **1981**, *47*, 254-259.
6. Rosenberg, M.; Kopelman, I. J.; Talmon, Y. *J. Ag. and Food Chem.* **1990**, *38*, 1288-1294.
7. Matsui, Y.; Mochida, K. *Bull. Chem. Soc Jpn* **1979**, *52*, 2808-2814.

8. Tee, O. S.; Fedortchenko, A.A.; Loncke, P.G.; Gadosy, T. *J. Chem. Soc. , Perkin Trans. 2* **1996**, *2*, 1243-1249
9. *Pharmacochemistry Library*, Rekker R.F., Elsevier Scientific , Amsterdam, W. Nauta and R.F. Rekker Eds, 1977, Chapter 1.
10. Scatchard G., *Ann. NY Acad. Sci.*, **1949**, *51*, 660-672.
11. Matsui, T.; Iwasaki, H.; Matsumoto, K.; Osajima, Y. *Biosci., Biotech. and Biochem.* **1994**, *58*, 1102-1106.
12. Sanemasa, I.; Wu, Y.; Koide, Y.; Fujii, T.; Takahashi, H.; Deguchi, T *Bull. Chem. Soc. Jpn* **1994**, *67*, 2744-2750.
13. Florh, K.; Paton, R. M.; Kaiser, E. T. *J. Am. Chem. Soc.* **1974**, *97*, 1209-1218.
14. Lichtenthaler, F. W.; Immel, S. *Liebigs Ann.* **1996**, 27-37.
15. Inoue, Y.; Hoshi, H.; Sakurai, M.; Chujo, R. *J. Am. Chem. Soc.* **1985**, *107*, 2319-2323.

Chapter 21

Influence of Maltodextrins with Different Dextrose Equivalent on the Interaction between Hexyl Acetate and Legumin in an Aqueous Medium

Maria G. Semenova, Anna S. Antipova, Larisa E. Belyakova,
Yurii N. Polikarpov, Tamara A. Misharina, Margarita B. Terenina,
and Rimma V. Golovnya

Institute of Biochemical Physics of Russian Academy of Sciences,
Vavilov str. 28, 117813 Moscow, Russia

The effect of maltodextrins with different dextrose equivalent (Paselli SA-2 and SA-6) on the binding behavior of legumin relative to hexyl acetate (HxAc) has been studied by combination of ultrafiltration and gas-liquid chromatography. Both simple 1: 1 mixtures of legumin and maltodextrin as well as their heat-induced conjugates have been studied. An analysis of the binding isotherms has shown that maltodextrin with the lowest dextrose equivalent (DE 2) has a rather high binding capacity in respect to HxAc and could be a real competitor with the protein in the binding of the aroma compound. In addition, the mechanism of HxAc binding with maltodextrins is distinctly different from that of legumin. A dramatic mutual effect of maltodextrins and legumin on binding behavior (the binding isotherms, the binding mechanisms, the intrinsic binding constants, and the number of binding sites) relative to HxAc has been found. The thermodynamic basis of the effect is discussed.

Most food systems contain both proteins and polysaccharides and the nature of their interactions is of fundamental importance to their functional properties in such systems (1 - 4). One of the principal functional properties of food proteins and polysaccharides is their capacity to bind aroma compounds. Proteins, as a rule, bind aroma compounds through hydrophobic interactions, whereas polysaccharides form inclusion complexes with aroma compounds much as starch does, for example (5-8). A better understanding of the key features of the mutual effect of protein and polysaccharide on their binding capacities for an aroma compound under a variety of experimental conditions, especially when the protein and polysaccharide were alone or in a complexed form, is of great importance.

Until recently, the mutual effect of polysaccharides and proteins on their capacities for binding flavor in an aqueous medium was not well understood and the prime object of this study has been to elucidate this effect. Commercially important polysaccharides (maltodextrins with different dextrose equivalent (DE)), legumin (11S globulin of broad beans) and hexyl acetate (HxAc), being the major component of several attractive flavors, were selected as the main objects of our investigation.

Experimental

Materials

Two commercial samples of maltodextrins (Paselli SA-2 and SA-6, Avebe (the Netherlands)) were used as supplied. They are enzymatic products of the hydrolysis of a potato starch having DE values of 2 and 6, respectively. Legumin (11S globulin) was isolated from broad beans (var. "Agat") (1) and homogeneity of the isolated 11S globulin was assessed by sedimentation. A single peak of 11S globulin with a sedimentation coefficient of 12×10^{-13} S was found. Hexyl acetate (HxAc) was purchased from REACHEM (Russia) (95% purity) and distilled to reach a purity of 99%. Organic solvents (> 99% purity), namely, acetone, ethanol, diethyl ether, were obtained from REACHEM (Russia) and used without further purification. Phosphate (pH 7.2) buffer solutions were prepared using analytical grade reagents (99.9% purity) and double-distilled water.

Methods

Determination of Hexyl Acetate Concentration in Solutions

Concentration of aroma compound in solutions was determined using a Hewlett Packard 5710A gas-liquid chromatograph (integrator 3380A). Separation of extracted components was carried out using a fused silica capillary column SE-30 (JIW) (50 m \times 0.32 mm, df = 0.2 μ m and/or 60 m \times 0.32 mm, df = 0.25 μ m) at 110 °C. The operating conditions were as follows: a split ratio of the carrier gas (helium) was 1:30; rate was 1 mL/min, temperature of the injector and detector (FID) was 150 °C, injected samples ranged between 0.5 and 2 μ L. The content of HxAc was calculated based on the relation between the peak areas of HxAc and an internal standard (n-undecane).

Preparation of Maltodextrin and Mixed Legumin-Maltodextrin Solutions

Maltodextrins with different DE values were dissolved in an aqueous phosphate buffer (pH 7.2, ionic strength 0.05 mol/dm) by mechanical stirring at 85 °C for 1 hour. Thereafter the solutions were allowed to cool at room temperature. These solutions were used in all experiments and in the preparation of mixed solutions with legumin. The values of average molecular weight of maltodextrins, determined by light scattering in these solutions, were equal to 250 kDa and 102 kDa for SA-2 and SA-6, respectively (9). Concentration of maltodextrins and legumin in the solutions

were determined by evaporation at 105 °C to a constant weight. The protein or maltodextrin content in the solutions was assessed as the difference in the weight of the dry residues between a buffered solution containing biopolymer and the blank one.

Preparation of the Conjugate of Legumin with Maltodextrin

Protein-polysaccharide conjugates were prepared as described in Ref. (10). The protein-polysaccharide mixed solutions were prepared as noted above and then freeze-dried. The freeze-dried legumin - maltodextrin mixtures were kept at 60 °C in the presence of a silica gel (45% relative humidity) for a period of 3 weeks.

Preparation of Conjugate Solutions

Samples of conjugates were dissolved in an aqueous phosphate buffer (pH 7.2, ionic strength 0.05 mol/dm) by mechanical stirring at 50 °C for 1 hour. Thereafter the solutions were allowed to cool at room temperature. Conjugate concentration was determined by evaporation at 105 °C to a constant weight. The conjugate content in solution was estimated as the difference in the weight of the dry residues between a buffered solution containing conjugate and the blank one. Polysaccharide concentrations in the conjugates were measured by the phenol-sulfuric method (11). Protein concentrations in the conjugates were estimated as the difference between the total concentrations determined by drying and the polysaccharide concentrations determined by the phenol-sulfuric method.

Determination of HxAc Binding to Maltodextrins in Single Protein + Maltodextrin Mixtures and in the Protein + Maltodextrin Conjugates

Hexyl acetate was chosen as an aroma ligand for the investigation. To determine the concentration of HxAc bound to the various samples, the ultrafiltration method was used to separate HxAc bound to the macromolecules from the free ligand.

For binding experiments, concentrations of HxAc in solutions were varied from 0.5 to 2.75 mM. The calculated quantities of the aroma compound (in diethyl ether) were added into 25 mL of either maltodextrin solutions or the simple mixed solutions of maltodextrins with legumin or into the conjugate solutions as well as the same volume of an aqueous buffer being the blank solution. Concentration of the protein in the simple mixed solutions with maltodextrins was kept constant and equal to 1 % w/w. The concentration of the maltodextrins both in the binary (maltodextrin - solvent) and in the simple mixed solutions with the protein was kept constant and equal to 1 % w/w. Concentration of each biopolymer in the conjugate solutions was determined as described above.

Solutions with added HxAc were shaken for 1-2 minutes and left to stand for 30 minutes at room temperature in open flasks to allow ether to evaporate and then the closed flasks were shaken (CPLAN water bath shaker, type 357, Poland) for 1 hour to reach equilibrium. The solutions were filtered through nuclear membranes with a pore size of 0.027 μm (the membranes were made from lamsan, Russian equivalent of Darcon, and were etched with 20 wt% NaOH. There was one carboxyl group for every 200 A^2 of the membrane surface and the number of pores per cm^2 was 2×10^9 .) using a special equipment operated at 3 bar to separate free ligands from bound

ligands. Neither the protein nor the maltodextrins passed through the membrane. Aliquots of the filtered aqueous solutions (5 mL) were collected directly into test tubes containing 3 mL of diethyl ether. The two-layer mixtures were shaken and stored for 24 hours in a cool place. The organic layers were separated and used for determination of free ligand concentration in the filtrates by gas-liquid chromatography (GC). Sorption of HxAc by the biopolymers was estimated by GC from 3 - 8 experiments at each studied concentration of HxAc. About 20 experiments were carried out to estimate the sorption of HxAc by the nuclear membranes. The sorption of the aroma compound on the nuclear membrane was built into calculations to estimate the degree of bound ligand. The experimental error of a determination of the values of the aroma compound bound with macromolecules was 5 %.

Results and Discussion

Before giving an account of the effect of maltodextrins on the binding capacity of the native legumin relative to HxAc in their simple mixtures or conjugates, let us elucidate the binding ability of the maltodextrins in an aqueous medium.

Binding of Hexyl Acetate with Maltodextrins with Different Dextrose Equivalents. Comparison with Binding of Hexyl Acetate with Legumin

Figure 1a shows binding isotherms of HxAc with maltodextrins with different DE values. The binding isotherms indicate considerably more binding (ν is the number of moles of an aroma compound bound per mole of biopolymer) of HxAc by maltodextrin SA-2 than maltodextrin SA-6. This result agrees well with those obtained previously (12) and suggests an increase both in the number of binding sites and the affinity constant with increasing degree of polymerization of dextrins. It is also interesting to compare the binding isotherms of maltodextrins and legumin. Figure 1a shows this comparison. Contrary to expectations, a great binding extent ν was found for maltodextrin SA-2 as opposed to legumin at rather high concentrations of HxAc in the system. As this takes place, maltodextrin SA-6 exhibits the least binding ability. By this means maltodextrin SA-2 can play the role of a real competitor with the protein in binding of HxAc in mixed aqueous solutions. In addition, the binding data were presented in the form of a Scatchard's plot (13) in accordance with the following equation (14):

$$\frac{\nu}{[L_{free}]} = nK - \nu K .$$

Here ν is the number of moles of ligand bound per mole of bipolymer, $[L_{free}]$ is the free ligand concentration in moles per liter; n is the total number of binding sites in macromolecule; K is the intrinsic binding constant (Figure 1b). The specific shape of the curve (the magnitude of $\nu / [L_{free}]$ grows with increasing ν in the range of low values of ν) suggests the cooperative binding mechanism on the interacting binding sites for HxAc binding with both maltodextrin SA-2 and maltodextrin SA-6. This is more pronounced in the case of maltodextrin SA-2. This result is in reasonably good

agreement with the experimental data found by Rutschmann and Solms (15), which pointed to a positive cooperative effect in the formation of the complex between starch and menthone, decanal or naphthol. Moreover, the Scatchard plots clearly show the difference in the mechanism of HxAc binding to maltodextrins, compared to legumin, where binding occurred on the independent and identical binding sites on the protein globule (14).

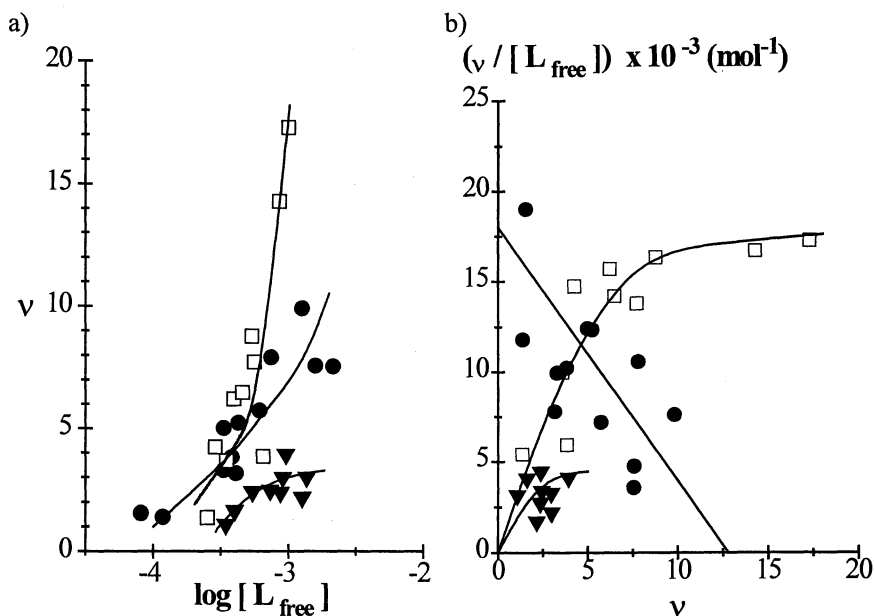


Figure 1. Binding of hexyl acetate with biopolymers in an aqueous medium (pH 7.2, ionic strength 0.05 mol/dm^3): ●, native legumin; □, maltodextrin SA-2; ▼, maltodextrin SA-6. a) Binding isotherms: binding extent v is plotted as a function of the logarithm of free ligand concentration in the system, $\log [L_{\text{free}}]$. b) Scatchard plot: the ratio of binding extent to free ligand concentration, $v / [L_{\text{free}}]$, is plotted against binding extent v .

(See more details on the HxAc binding with legumin in the relevant chapter of this book). Unfortunately, an estimation of the binding parameters by the proper extrapolation of $v / [L_{\text{free}}]$ to zero was impossible in the case of the binding according to the cooperative mechanism, because of the insolubility of HxAc in an aqueous medium at high concentration.

Based on the literature data (5,15-21) of binding aroma compounds with different polysaccharides, it is safe to assume that maltodextrins form an inclusion complex with HxAc. As this takes place, some modification of the maltodextrin conformation, (for example, some kind of maltodextrin structurization, through helix formation), occurs on binding with HxAc. According to (17) maltooligosaccharides have a ribbon-

like structure: the edges of the ribbon are occupied by polar hydroxyl groups and the flat surfaces are composed of nonpolar patches of the sugar ring faces, so that these patches could form an interior hydrophobic cavity under helix formation. Besides, according to (18) the complexes formed with dextrans should have a helical conformation between 6 and 7 D-glucose monomers per helical turn. Obviously, this process causes the cooperative mechanism of HxAc binding with maltodextrins, whereby HxAc binding with maltodextrins is facilitated with increasing HxAc molecules added to them. In line with this assumption, maltodextrin with the lowest dextrose equivalent (SA-2) exhibits the greater binding capacity regarding HxAc. This could be attributable to the larger degree of molecular polymerization, and thus to the greater readiness of the molecule to undergo structurization, that is helix formation. On the other hand, the cooperative mechanism of HxAc binding with maltodextrins, probably, may be also initiated by an increase in hydrophobicity of the maltodextrin molecules due to an addition of lipophilic HxAc molecules to them.

Effect of Maltodextrin on Binding of HxAc with Legumin in Simple Equimass Mixed Solutions: Maltodextrin + Legumin + Water

As a first approximation, let us assume that the binding capacity of maltodextrins does not change in simple mixed solutions with legumin. Bearing this in mind, to consider the effect of the maltodextrins on the legumin binding capacity, we have subtracted the number of moles of HxAc bound by maltodextrin, in accordance with the corresponding binding isotherm, from the total number of moles of HxAc bound to the mixture of legumin with maltodextrin. It is interesting to note that in so doing we have found a totally different binding behavior of legumin when it is in the mixtures with maltodextrins, depending on the DE of these latter.

Binding of HxAc with Legumin in the Simple Mixture with Maltodextrin SA-2

Figure 2a compares the binding isotherms of HxAc bound both to legumin alone and legumin in the simple equimass mixture with maltodextrin SA-2. These data suggest a considerable increase in the apparent binding extent of HxAc with legumin under the effect of maltodextrin SA-2. Thus, in the case of the simple mixtures of legumin with maltodextrin SA-2 a positive deviation from the binding behavior of legumin alone was found. The Scatchard plot (Figure 2b), points out the apparent change in the mechanism of HxAc binding with the protein under the effect of maltodextrin SA-2. That is, the binding mechanism varies from HxAc binding on the identical and independent binding sites in the protein globule to the cooperative binding on the interacting binding sites in the presence of maltodextrin SA-2.

As a first approximation, the observed effect of maltodextrin on the protein binding capacity relative to HxAc may be attributable to the weak complex formation between protein and polysaccharide in an aqueous medium (9). To gain greater insight into the validity of this assumption, we have attempted to elucidate the nature of interaction between legumin and maltodextrin in an aqueous medium by measurement both of the values of cross second virial coefficient A_{pr-pol} (that characterizes the nature and the intensity of pair biopolymer interactions in the bulk

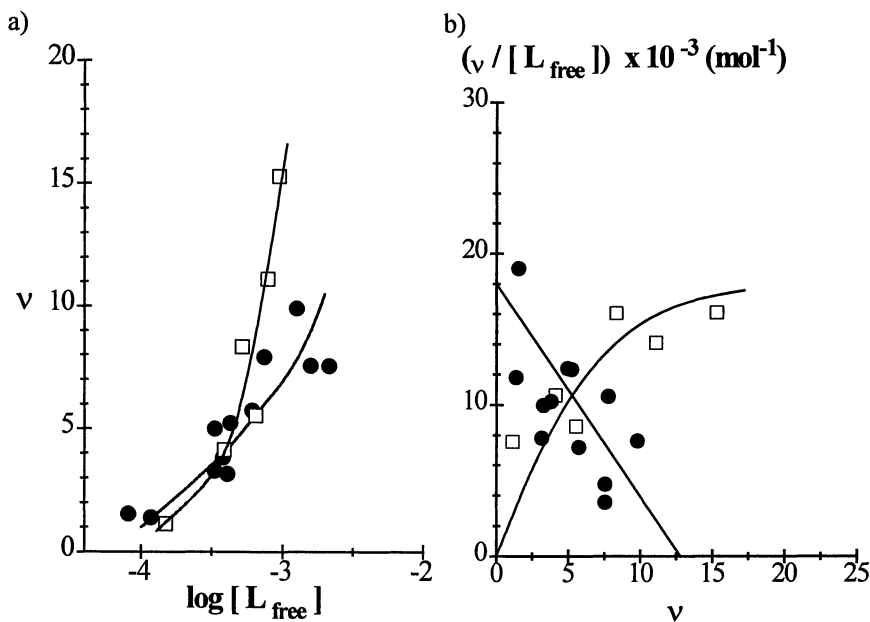


Figure 2. Binding of hexyl acetate with legumin alone and in the presence of maltodextrin SA-2 in an aqueous medium (pH 7.2, ionic strength 0.05 mol/dm^3): ●, legumin alone; □, legumin in the mixture with maltodextrin SA-2 a) Binding isotherms: binding extent v is plotted as a function of the logarithm of free ligand concentration in the system, $\log [L_{\text{free}}]$. b) Scatchard plot: the ratio of binding extent to free ligand concentration, $v / [L_{\text{free}}]$, is plotted against binding extent v .

aqueous medium (22)) by laser light scattering and the enthalpy of legumin-maltodextrin interactions by mixing calorimetry. Table I shows the values of thermodynamic parameters found. The negative values of the cross second virial coefficient were found for both legumin-maltodextrin pairs studied. Thus the net attractive (thermodynamically favorable) interactions between legumin and maltodextrins were detected in the bulk aqueous medium under the experimental conditions. What is more the values of enthalpy of interaction between legumin and maltodextrins show an exothermic effect. This experimental fact could be attributed to the formation of new bonds between protein and polysaccharide in an aqueous medium. Probably, the exothermic effect found suggests the formation of multiple hydrogen bonds between hydroxyl groups of maltodextrins and the functional groups of protein molecules in an aqueous medium (23). The lack of dextrose equivalent dependence of the thermodynamic parameters of interaction was revealed. Hence, the combined data of light scattering and mixing calorimetry suggest net attractive interactions that are most likely due to the formation of multiple hydrogen bonds between legumin and maltodextrins in the bulk aqueous medium. This weak complex formation is liable to shift the fine hydrophilic-lipophilic balance in the protein

Table I. Thermodynamic Parameters of the Interaction between Legumin and Maltodextrins in an Aqueous Medium*

<i>Biopolymer Pair</i>	$A_{pr-pol} \times 10^4$ ($m^3 \text{ mol kg}^{-2}$) ^a	ΔH ($J g^{-1}$) ^a at $C_{\Sigma} = 5 \text{ wt}\%$ in the equimass mixture
Legumin - Maltodextrin SA-2	- 0.29	- 0.46
Legumin - Maltodextrin SA-6	- 0.24	- 0.23

^a Estimated experimental error $\pm 10\%$.

* (pH 7.2, ionic strength 0.05 mol/dm^3 , 20°C)

globule in such a way that some modification of the structure of binding sites in the interior of the protein globule occurs. In response to this modification, the change of the binding mechanism occurs in the presence of maltodextrin SA-2.

On the other hand, from the binding data it is also apparent that if, in turn, we subtract the number of moles of HxAc bound by the protein, in accordance with the corresponding binding isotherm, from the total number of moles of HxAc bound to the equimass simple mixture of legumin with maltodextrin SA-2, then we can also find a positive deviation from the binding of HxAc with maltodextrin alone. This experimental fact, not to mention the probable complex formation between macromolecules, can result from an intensification of maltodextrin structurization/helix formation in the presence of legumin, but it is highly improbable. It is very difficult to imagine the mechanism by which legumin could intensify the structurization/helix formation of maltodextrin in an aqueous medium.

In summary it may be said that, from the observed data, further structural and thermodynamic elucidation at the molecular level is required to understand the binding behavior of an aroma compound with a simple mixture of legumin with maltodextrin.

Binding of HxAc with Legumin in the Simple Mixture with Maltodextrin SA-6

The binding behavior of HxAc to the simple equimass mixture of legumin and maltodextrin SA-6 was also studied. Simple subtraction of the number of moles of HxAc bound by maltodextrin SA-6, in accordance with the corresponding binding isotherm, from the total number of moles of HxAc bound to the equimass mixture showed minor or negative binding of HxAc with legumin. As this takes place, it is very difficult to imagine, on experimental grounds (see Figure 1a), that maltodextrin SA-6 could be a competitor with legumin for binding of HxAc. By contrast, legumin can be a real competitor with maltodextrin SA-6 in their equimass mixture regarding the binding of HxAc. In such a manner, legumin could, probably, exclude binding of HxAc with maltodextrin SA-6. We have tested this hypothesis using an approximation that only legumin binds HxAc in the simple equimass mixtures with

maltodextrin SA-6. Figures 3a and 3b show a comparison of the binding behavior of legumin alone and in the simple mixture with maltodextrin SA-6. Both the binding isotherms (Figure 3a) and Scatchard plots (Figure 3b) make it clear that the binding behavior of legumin is identical with both samples. (See more details on HxAc binding with the protein in the appropriate chapter of this book). Consequently, legumin is actually a real competitor for maltodextrin SA-6, that is a maltodextrin with higher dextrose equivalent, or with lower molecular weight, relative to binding of HxAc.

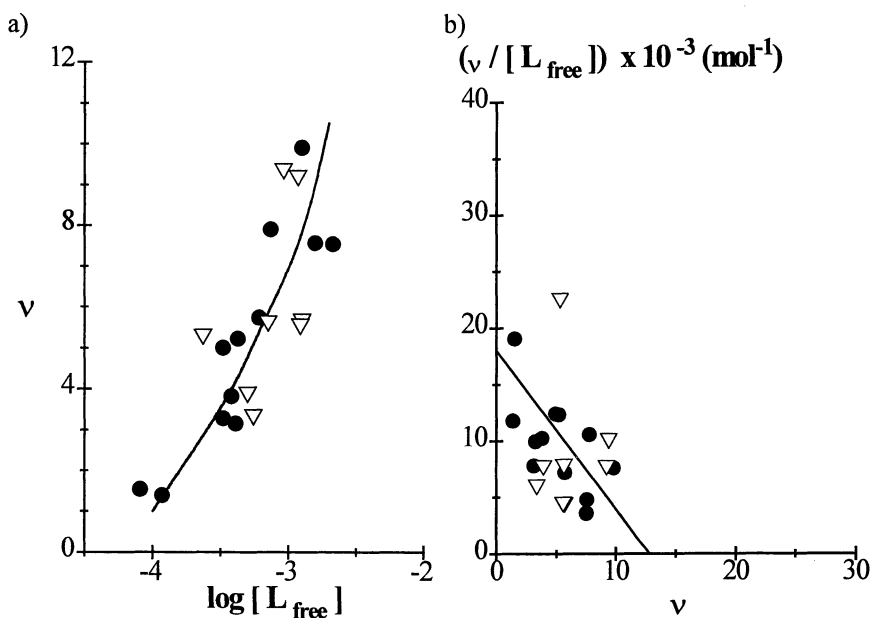


Figure 3. Binding of hexyl acetate with legumin alone and with a simple mixture of legumin and maltodextrin SA-6 in an aqueous medium (pH 7.2, ionic strength 0.05 mol/dm^3): ●, legumin alone; ▽, the mixture of legumin with maltodextrin SA-6. a) Binding isotherms: binding extent v is plotted as a function of the logarithm of free ligand concentration in the system, $\log [L_{\text{free}}]$. b) Scatchard plot: the ratio of binding extent to free ligand concentration, $v / [L_{\text{free}}]$, is plotted against binding extent v .

Effect of the Conjugate Formation between Legumin and Maltodextrin on the Binding Capacity of Legumin in Reference to HxAc

A consideration of the binding behavior of the conjugates of legumin with different maltodextrins points to the very different binding behavior of conjugates of legumin with maltodextrin SA-2 and legumin with maltodextrin SA-6.

Binding of HxAc with the Conjugate of Legumin with Maltodextrin SA-6

Just before giving an estimation of the data found we should call attention to the exact weight ratio of the protein to maltodextrin in the conjugate. By this means, in the case of the conjugate of legumin with maltodextrin SA-6 this weight ratio (protein : polysaccharide) was 1 : 2. As a first approximation, we assumed that the binding capacity of maltodextrin SA-6 did not change in the conjugate with legumin. In so doing, in studies of the effect of maltodextrin on the binding capacity of legumin in the conjugate, we have subtracted the number of moles of HxAc bound by the maltodextrin, in accordance with the corresponding binding isotherm, from the total number of moles of HxAc bound to the conjugate.

Figure 4a shows the binding isotherm of HxAc with legumin alone and then to the conjugate with maltodextrin SA-6. The binding isotherms show a drastic increase in the protein binding capacity when conjugated with maltodextrin SA-6.

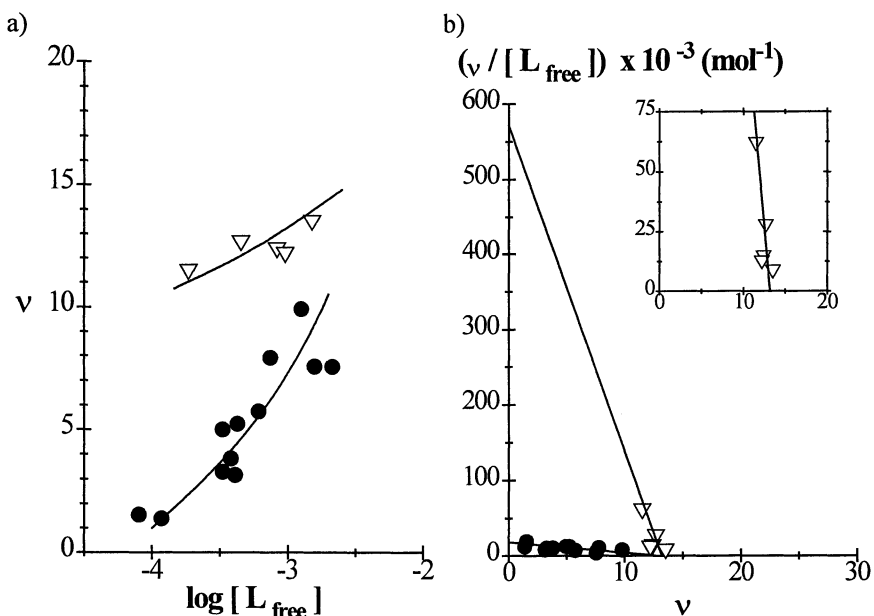


Figure 4. Binding of hexyl acetate with legumin alone and in the conjugate with maltodextrin SA-6 in an aqueous medium (pH 7.2, ionic strength 0.05 mol/dm^3): ●, legumin alone; ▽, legumin in the conjugate with maltodextrin SA-6. a) Binding isotherms: binding extent v is plotted as a function of the logarithm of free ligand concentration in the system, $\log [L_{\text{free}}]$. b) Scatchard plot: the ratio of binding extent to free ligand concentration, $v / [L_{\text{free}}]$, is plotted against binding extent v .

As this takes place, the mechanism of binding of HxAc with the protein does not change qualitatively in the conjugate as suggested by Scatchard plots (Figure 4b), namely, the binding of HxAc with legumin in the conjugate also occurs on

independent and identical binding sites. Moreover, the Scatchard plots are evidence for the existence of the same total number of binding sites both in the interior of legumin molecules alone and in the conjugate. However, the slopes of the Scatchard plots, differ markedly, pointing to a sharp distinction between the intrinsic binding constants for legumin in the conjugate and alone. Table II gives the values of the characteristic parameters of binding of HxAc both with legumin in the conjugate and alone. The total number of binding sites in the interior of protein molecule is unchanged on the conjugate formation and remains equal to 13. However, the great increase in the intrinsic binding constant suggests a wide variation of structure of binding sites and hence of the protein affinity for HxAc with the formation of conjugate. Indeed, the differential scanning calorimetry data indicate a decrease in the enthalpy of legumin denaturation in the conjugates with maltodextrins, thereby suggesting partial unfolding of the legumin globule in the conjugates (9). If we subtract the number of moles of HxAc bound by legumin (in accordance with the corresponding binding isotherm) from the total number of moles of HxAc bound to the conjugate a positive deviation from the binding of HxAc with maltodextrin SA-6 alone is found, as if an increase in the binding capacity of maltodextrin SA-6 appears in the conjugate with legumin. The binding behavior of the maltodextrin in the conjugate of this type may be attributable to either our mistaken assumptions that the binding capacity of legumin does not change under the conjugate formation or due to an intensification of the maltodextrin structurization as a result of the covalent binding with legumin. However, it is evident that an answer to this question requires further structural and thermodynamic investigations.

Table II. The Characteristic Parameters of Binding of HxAc with Legumin in the Conjugates with Maltodextrins and Alone (pH 7.2, ionic strength 0.05 mol/dm³, 20 °C)

<i>Biopolymer</i>	<i>Total number of binding sites, n</i>	<i>Intrinsic binding constant, $K \times 10^{-3} (mol^{-1})$</i>	<i>Gibbs free energy of binding, $\Delta G (kcal/mol)$</i>
Legumin	13	1.4	- 4.2
Conjugate of legumin with maltodextrin SA-6	13	6.4	- 5.1
Conjugate of legumin with maltodextrin SA-2	5	43.4	- 6.2

Binding of HxAc with the Conjugate of Legumin with Maltodextrin SA-2

Concerning the binding behavior of the conjugate of legumin with maltodextrin SA-2, it should be noted that the weight ratio of the protein to the maltodextrin in the conjugate solutions, was 1 : 6. The simple subtraction of the number of moles of HxAc bound by maltodextrin SA-2 (in accordance with the corresponding binding

isotherm) from the total number of moles of HxAc bound to the conjugate shows minor or negative binding of HxAc with legumin. This result may be attributed either to the rather high binding capacity of maltodextrin SA-2 in the conjugate or the existence of some structural restrictions on binding of HxAc with the protein coupled with an excess molecules of rather high-molecular weight maltodextrin SA-2 in the conjugate, as if maltodextrin SA-2 can prevent completely binding of HxAc with legumin in their conjugate. We have tested this supposition using an approximation that only maltodextrin SA-2 binds HxAc in the conjugate. As this takes place, we have compared the binding of HxAc with the conjugate and maltodextrin SA-2 alone. Figure 5 shows the binding data calculated. A comparison of the binding isotherms of the conjugate and maltodextrin SA-2 suggests a pronounced decrease in HxAc binding with the conjugate (Figure 5a). It follows from these results that a marked modification of the maltodextrin molecular structure occurs on the conjugate formation in this case. In line with this assumption, the

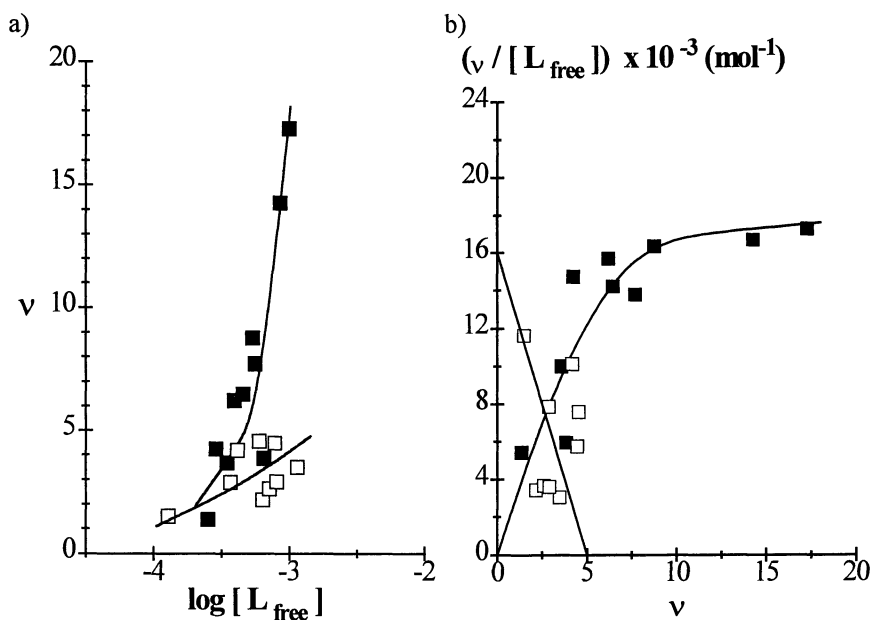


Figure 5. Data on binding of hexyl acetate with maltodextrin SA-2 alone and with the conjugate of maltodextrin SA-2 with legumin in an aqueous medium (pH 7.2, ionic strength 0.05 mol/dm^3): ■, maltodextrin SA-2 alone; □, the conjugate of maltodextrin SA-2 with legumin. a) Binding isotherms: binding extent v is plotted as a function of the logarithm of free ligand concentration in the system, $\log [L_{\text{free}}]$. b) Scatchard plot: the ratio of binding extent to free ligand concentration, $v / [L_{\text{free}}]$, is plotted against binding extent v .

mechanisms of binding of HxAc with maltodextrin SA-2 alone differs radically from that for the conjugate as shown by Scatchard plots (Figure 5b). In the case of the conjugate, binding of HxAc occurs on the independent and identical binding sites, that is similar to the case of the binding with legumin alone, but that is different from the binding behavior of maltodextrin SA-2 alone, when the cooperative binding mechanism on the interacting binding sites was found (Figure 1b).

The observed data suggest, that maltodextrin SA-2 coupled covalently with legumin loses its ability to structurization under binding of HxAc. In turn, legumin also changes dramatically its binding capacity in the conjugate as a result of the covalent binding with an excess molecules of high molecular weight maltodextrin. Table II shows a twofold decrease in the number of binding sites in the conjugate and a considerable increase in their affinity for HxAc as compared with the native legumin. This suggests the occurrence of the binding sites with the unique structure under the covalent coupling of maltodextrin SA-2 with legumin.

The revealed differences between the effects of maltodextrins with different dextrose equivalent on the protein binding capacity in the conjugate are evidently determined by the molar ratio of maltodextrin to the protein in the conjugates formed. A lower weight ratio of maltodextrin to protein and consequently the lower number of the maltodextrin molecules coupled with legumin, in the case of the conjugate of legumin with maltodextrin SA-6, entails the more fine effect of the maltodextrin on the protein binding capacity for HxAc.

Conclusions

1. In the simple equimass mixtures of legumin with maltodextrin SA-2 the observed binding data indicate a pronounced increase in the apparent binding extent of HxAc with legumin which is attended with an apparent dramatic change in the binding mechanism of HxAc with the protein
2. In the simple equimass mixtures of legumin with maltodextrin SA-6 the protein can prevent completely the HxAc binding with maltodextrin SA-6, so that, legumin is indeed a real competitor with maltodextrin SA-6 for HxAc.
3. The positive deviation from the binding of HxAc with both maltodextrin SA-6 and legumin was found for their covalent conjugates.
4. The dramatic decrease in the binding of HxAc with the conjugate of legumin with maltodextrin SA-2 was found as compared to the binding behaviors both of legumin and the maltodextrin.
5. All experimental findings suggest a profound effect of maltodextrins on the binding capacity of protein, which, evidently, requires further structural and thermodynamic systematic investigations.

Acknowledgement

The authors are most grateful to Nestle Research Centre (Switzerland) for the financial support of this research.

References

1. Tolstoguzov, V. B., *Food Hydrocoll.* **1991**, 4, 429.
2. Dickinson, E., *J. Chem. Soc. Faraday Trans.* **1992**, 88, 2973.
3. Dickinson, E.; Semenova, M. G., *J. Chem. Soc., Faraday Trans.* **1992**, 88, 849.
4. Semenova M.G., *Current Opinion in Colloid and Interface Science* **1998**, 3, 627.
5. Langourieux, S.; Crouzet, T. *Lebensmit. Wiss. Tech.* **1994**, 27, 544.
6. Nuessli, J.; Sigg, B.; Condepetit, B.; Escher, F. *Food Hydrocoll.* **1997**, 11, 27.
7. Godshall, M.A.; Solms, J. *Food Technol.* **1992**, 46, 140.
8. Cayot, N.; Taisant, C.; Voilley, A. *J. Agric. Food Chem.* **1998**, 46, 3201.
9. Semenova, M. G.; Belyakova, L. E., Antipova, A. S., Jubanova, M. A. *Colloids and Surfaces. B: Biointerfaces* **1999**, 12, 287.
10. Dickinson, E.; Galazka, V.B. *Food Hydrocoll.* **1991**, 5, 281.
11. Dubois, M.; Gilles, K.A. *Anal. Chem.* **1956**, 28, 350.
12. Guichard, E.; Etievant, P. *Nahrung Food* **1998**, 42, 376.
13. Scatchard, G., *Ann. N.Y. Acad. Sci.* **1948**, 51, 660.
14. *Biophysical Chemistry*; Cantor, Ch.R.; Schimmel, P.R., Eds. W.H. Freeman and company, San Francisco, 1980, Part III, ch. 15.
15. Rutschmann, M.A.; Solms, J. *Lebensmitt. Wiss. Tech.* **1990**, 23, 70.
16. Langourieux, S.; Crouzet, J. *Food Sci. Technol.* **1994**, 27, 544.
17. Le Thanh, M.; Thibeau, P.; Thibaut, M.A.; Voilley, A. *Food Chem.* **1992**, 43, 129.
18. Nuessli, J.; Condepetit, B.; Trommsdorff, U.R.; Escher, F. *Carboh. Polymers* **1995**, 28, 167.
19. Quioco, F.A.; Spurlino, J.C.; Robseth, L.E. *Structure* **1997**, 5, 997.
20. Rutschmann, M.A.; Solms, J. *Lebensmitt. Wiss. Tech.* **1990**, 23, 84.
21. Bredie, W. L. P., Mottram, D. S., Birch, G. *Dev. Food Sci.* **1994**, 35, 139.
22. Nagasawa, M.; Takahashi, A. *Light Scattering from Polymer Solutions*; Huglin, M. B., Ed.; Academic Press: London, 1972, p.671.
23. Jencks, W. P. *Catalysis and Chemistry in Enzymology*; McGraw-Hill: New York, 1969, p. 254.

Chapter 22

Interaction between Sulfur-Containing Flavor Compounds and Proteins in Foods

Donald S. Mottram and Ian C. C. Nobrega

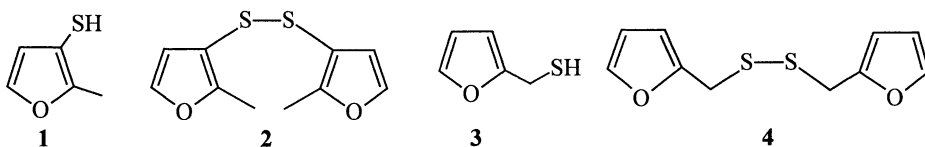
Department of Food Science and Technology, The University of Reading,
Whiteknights, Reading RG6 6AP, United Kingdom

When volatile disulfides were added to aqueous solutions containing protein, full recovery of the disulfides could not be achieved. In some protein systems the levels of disulfides recovered were almost 100 times lower than from simple aqueous solution. In addition significant quantities of the disulfides were converted to the corresponding thiols. Similar effects were shown in meat systems. Other heterocyclic sulfur compounds, such as thiophenes, were not affected by the presence of proteins. The interactions between proteins and disulfides may be explained by interchange redox reactions between the disulfides and sulfhydryl and disulfide groups of proteins. This demonstrates that chemical, as well as physical, interactions between aroma compounds and food components can be important determinants of food flavor.

Sulfur-containing volatile compounds generally have potent aromas with low odor threshold values, and many are important in determining the aroma characteristics of foods. Thiol-substituted furans, such as 2-methyl-3-furanthiol (**1**) and 2-furanmethanethiol (**3**), and the corresponding disulfides, **2** and **4**, have been shown to have meat-like or roasted, coffee-like aromas at low concentrations. During thermal processing, such compounds may be formed in the Maillard reaction (*1-3*) or from the degradation of thiamin (*4,5*). These thiols and disulfides are widely used as components of flavorings for soups, savory products and meat substitutes, where they are either added to the flavorings as nature-identical chemicals or as components of reaction-product flavorings.

Recently it has been shown that disulfides, such as bis(2-methyl-3-furyl) disulfide (**2**) and bis(2-furylmethyl) disulfide (**4**) could not be recovered completely when added to aqueous solutions containing protein. Furthermore, some of the

disulfides were converted to the corresponding thiols. This paper discusses such protein – disulfide interactions and how they may influence the aroma characteristics of heated foods containing sulfur aroma compounds. The data presented demonstrate that chemical interactions between aroma compounds and food components are important factors in the binding of flavor in food.



Recovery of Disulfides from Aqueous Solutions containing Proteins

When a commercial savory flavoring, containing thiol and disulfide flavor components, was heated at 100°C in aqueous solution with egg albumin during simultaneous steam distillation and solvent extraction (SDE), considerable changes in the relative concentration of the sulfur compounds were observed (6). The flavoring comprised a complex mixture of aroma compounds in which the major constituents were terpenes and furan disulfides. Heating egg albumin with the flavoring during SDE showed a similar recovery of the terpenes to that achieved in from an aqueous control without protein. However, there was a marked effect on some of the sulfur compounds. In particular, there was a decrease of almost 100-fold in the recovery of the major disulfide component, bis(2-furylmethyl) disulfide (4), from the egg albumin system compared with the aqueous control. Furthermore, none of disulfide 2 was recovered from the protein-containing system, although, compared with 4, it was present at much lower levels in the flavoring.

In contrast to the loss of the disulfides, a considerable increase (almost 10-fold) in the quantities of 2-furanmethanethiol was found in the egg albumin system. It was suggested that this could be due to interchange reactions between disulfide and thiol groups on the flavor compounds with sulfhydryl groups of the protein.

This was investigated further by adding disulfides 2 and 4 to a series of aqueous systems containing different proteins (casein or egg albumin) or a carbohydrate (maltodextrin). A similar effect to that shown with the commercial flavoring was observed with a marked loss of the disulfides in the presence of protein and a large increase in the level of the corresponding thiol (Table I). The recovery of the disulfide 4 from water was almost 100% and a similar recovery was obtained for a maltodextrin system, although the recovery of 2 was not complete. It appeared that all the lost disulfides were not recovered as thiols indicating that interaction had occurred with the protein. When the protein in the system was casein the disulfide losses and conversion to thiol were considerably less than in the systems containing egg albumin.

Table I. Quantities of disulfides and thiols recovered from aqueous systems containing protein or carbohydrate substrates.

<i>Compound</i>	<i>Quantity recovered (μg)</i>			
	Water alone	Egg Albumin	Casein	Malto-dextrin
bis(2-furylmethyl) disulfide	476 (1)	3 (1)	377 (63)	492 (10)
2-furanmethanethiol	1 (1) ^a	127 (14)	12 (4)	1 (1)
bis(2-methyl-3-furyl) disulfide	na	6 (2)	272 (21)	378 (24)
2-methyl-3-furanthiol	na	226 (54)	67 (8)	1 (1)

NOTE: Initial addition was 500 μg of each disulfide. Each value is the mean of triplicate determinations and standard deviations are shown in parentheses. na, not determined. ^a The disulfides contained very small amounts of the corresponding thiols as impurities.

SOURCE: Adapted from Reference 7.

Effect of Protein on Sulfur Compounds obtained from a Ribose- Cysteine Reaction System

These investigations of interactions between proteins and disulfides have now been extended to determine the effect of protein on other volatile sulfur compounds. When cysteine and pentoses, such as ribose, are heated, complex mixtures of volatiles are formed, which have meaty, savory aromas. Such mixtures are used as reaction product flavorings. Cysteine – ribose reaction mixtures have been the subject of a number of investigations in this laboratory (7-9) and over 100 compounds have been identified. These are dominated by sulfur compounds, including compounds where the sulfur is contained in a heterocyclic structure and others where the sulfur is in the form of a thiol or disulfide group. Recently we reported over 20 disulfides in the volatiles from a cysteine – ribose reaction system. These were symmetrical and unsymmetrical disulfides formed from furanthiols, thiophenethiols, and mercaptoketones (8). Heterocyclic compounds produced in the system included thiophenes, thiophenones, dithianones, and thienothiophenes. Such a system has now been used to determine the effect of protein on a range of volatile sulfur compounds.

The reaction system was prepared by heating cysteine and ribose (0.3 mmol each) in 6 mL aqueous phosphate buffer (pH 5.6) at 140 °C for 30 min (8). The mixture was then mixed with 150 mL 5% egg albumin before extracting by simultaneous distillation extraction using procedures described previously (6). A control determination was carried out using a similar system without albumin.

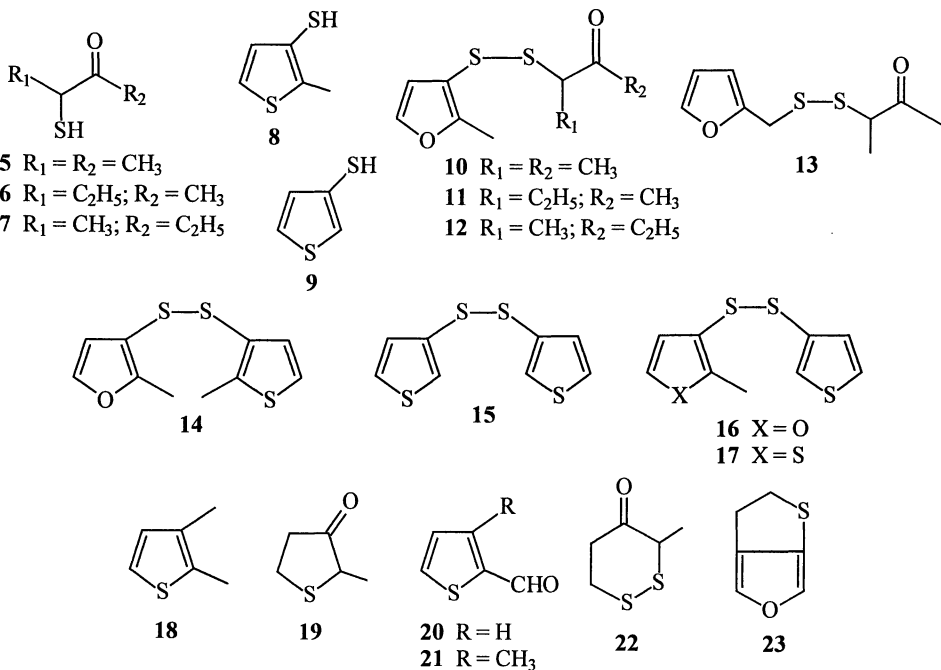
Quantities of some of the major volatiles from the systems are shown in Table II. The heterocyclic sulfur compounds were generally unaffected by the egg albumin. The mercaptoketones appeared to be present at a higher concentration in the system containing albumin although the differences were not significant ($p > 0.5$ in Student t-

Table II. Approximate quantities (ng/10 mg ribose) of selected volatile sulfur compounds recovered by SDE from cysteine and ribose model systems in the absence (blank) or presence of egg albumin.

<i>Compound</i>	<i>Blank</i>	<i>Egg albumin</i>
3-Mercapto-2-butanone 5	1390	1970
3-Mercapto-2-pentanone 6	628	725
2-Mercapto-3-pentanone 7	497	550
2-Methyl-3-furanthiol 1	1297	1014
2-Methyl-3-thiophenethiol 8	426	262
2-Furanmethanethiol 3	1643	1285
3-Thiophenethiol 9	743	471
2-Methyl-3-furyl 1-methyl-2-oxopropyl disulfide 10	63	37
2-Methyl-3-furyl 1-ethyl-2-oxopropyl disulfide 11	48	tr
2-Methyl-3-furyl 1-methyl-2-oxobutyl disulfide 12	21	tr
2-Furylmethyl 1-methyl-2-oxopropyl disulfide 13	21	14
Bis(2-methyl-3-furyl) disulfide 2	259	27
2-Methyl-3-furyl 2-methyl-3-thienyl disulfide 14	57	tr
Bis(3-thienyl) disulfide 15	43	nd
2-Methyl-3-furyl 3-thienyl disulfide 16	88	13
2-Methyl-3-thienyl 3-thienyl disulfide 17	38	nd
2,3-Dimethylthiophene 18	24	25
4,5-Dihydro-2-methyl-3(2 <i>H</i>)-thiophenone 19	1712	1675
2-Formylthiophene 20	404	302
3-Methyl-2-formylthiophene 21	463	519
3-Methyl-1,2-dithian-4-one 22	224	235
2,3-Dihydro-6-methylthieno[2,3 <i>c</i>]furan 23	715	641
a dihydrothienothiophene	1712	1604
a methyl dihydrothienothiophene	492	468

NOTE: values are means of triplicate collections (average CV = 20%); tr, trace (<1 μg); nd, not detected

test). However, significant losses of furan and thiophene thiols were observed. Much greater losses of disulfides in the presence of albumin were found, confirming the effects observed previously. An interesting, but unexplained, observation was that the smallest disulfide losses were for those derived from 3-mercapto-2-butanone (i.e. those containing the 1-methyl-2-oxopropyl moiety) and this thiol showed the greatest increase in the presence of albumin.



Recovery of Disulfides from Cooked Meat Systems

In order to determine if disulfide loss would also occur in foods, the recovery of disulfides added to cooked meat was examined. The disulfides **2** and **4** (500 μg of each) were added to lean beef muscle (100 g), which had been pressure-cooked at 140 $^\circ\text{C}$ for 30 min. The mixture was blended with 750 mL water and the volatiles were extracted using SDE (10).

In the meat systems, marked decreases in the concentration of the disulfides were observed and significant quantities of the corresponding thiols **1** and **2** were found (Table III). A quantity of the mixed disulfide **24** was also found, together with the methylthio-derivatives, 2-methyl-3-furyl methyl disulfide (**25**) and 2-furylmethyl methyl disulfide (**26**). The SDE of aqueous controls without meat confirmed the earlier observations that the furan disulfides could be recovered without significant loss and without any formation of the corresponding thiols (Table III). However, a small amount of 2-methyl-3-furyl 2-furylmethyl disulfide (**24**) was isolated from the control as well as the meat system. This indicated that some hydrolysis of the disulfides had occurred allowing the formation of this mixed disulfide. The presence

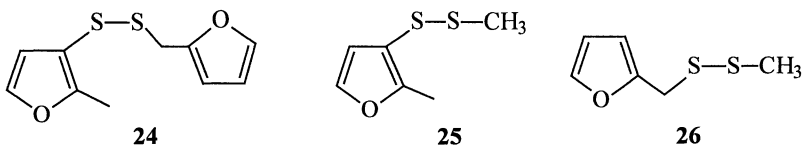


Table III. Recovery of thiols and disulfides from cooked meat systems containing added bis(2-furylmethyl) disulfide and bis(2-methyl-3-furyl) disulfide.

Compound	Quantity recovered (μg)		
	<i>Water + Disulfides</i>	<i>Cooked Beef + Disulfides</i>	<i>Cooked Beef alone</i>
bis(2-methyl-3-furyl) disulfide 3	579 (66)	126 (27)	nd
bis(2-furylmethyl) disulfide 4	516 (112)	104 (27)	nd
2-methyl-3-furanthiol 1	nd	302 (35)	1 (0)
2-furanmethanethiol 2	nd	294 (41)	13 (2)
2-methyl-3-furyl 2-furylmethyl disulfide 24	16	39 (6)	nd
2-methyl-3-methyl methyl disulfide 25	nd	7 (1)	nd
2-furylmethyl methyl disulfide 26	nd	3 (0)	nd

NOTE: Initial addition was 500 μg of each disulfide. Each value is the mean of triplicate determinations and standard deviations are shown in parentheses. nd not detected.

of the methylthio-derivatives indicates that other volatile disulfides, such as dimethyl disulfide, may participate in the interchange reactions.

Quantitatively, all of the lost disulfides were not recovered as thiols or mixed disulfides, indicating that binding to the protein may have occurred. These results are in agreement with the data for the egg albumin systems.

Interactions between Proteins and Disulfides and Thiols

It is well known that thiols are easily oxidized to the corresponding disulfides and that mixtures of different thiols readily form mixed disulfides (11,12). It has also been shown that, in boiling aqueous solution, disulfides are hydrolyzed to thiols (13). The thiols were detected using 4-vinylpyridine as a thiol trapping agent but, in the absence of such a reagent, free thiols were not detected because they re-oxidize to the disulfide. In a mixture of deuterated and unlabelled disulfides mixed disulfides were obtained (13). Thus, in the aqueous systems containing protein, a redox situation could be established that, in conjunction with disulfide hydrolysis, results in the generation of free thiols, which could then react with sulfhydryl groups on the protein or with other thiols. Reduction-oxidation (redox) reactions involving interchange of sulfhydryl and disulfide groups, within the protein or with external thiol groups, are well known in protein chemistry (14,15). An example of such interchanges is seen in bread-making where sulfhydryl-disulfide interchanges between glutathione and the flour proteins are important in relation to dough rheology (16,17).

The marked effect of the protein on the recovery of disulfides from the systems reported in this paper supports this hypothesis of redox interactions between the thiol and disulfide flavor compounds with sulfhydryl groups and disulfide bridges, from

cysteine and cystine amino acid units in the protein. This results in conversion of the disulfides to the corresponding thiols and the formation of new disulfide links between protein and thiol with the associated loss of flavor compound. This hypothesis is substantiated by the systems that used casein as the protein. Casein has a much lower proportion of sulphhydryl groups than meat or albumin and this gave rise to a much reduced influence of casein on the loss of disulfides.

The presence of the methylthio-derivatives indicates that other volatile disulfides, such as dimethyl disulfide, participated in the interchange reactions in the meat systems. Dimethyl disulfide and other methyl disulfides are found in cooked meat volatiles. The formation of small amounts of hydrogen sulfide from hydrolysis of protein sulphhydryl groups could also contribute to the redox system.

Volatile extraction using SDE involves boiling with a large excess of water for several hours and such conditions could promote the hydrolysis of the disulfides and their interaction with sulphhydryl groups on the protein. Therefore, in some recent work, dynamic headspace collections and SDE extractions from cooked meat systems with added disulfides were compared to determine whether the interactions observed in the SDE systems were an effect of the extraction method (10). The headspace analyses of the cooked meat showed large losses of the disulfides **2** and **4** compared with the aqueous blank, demonstrating that the effect was not primarily due to the analytical method. Quantities of the corresponding thiols **1** and **3** were also found plus relatively large amounts of the methylthio-compounds **25** and **26**. The latter compounds were found in greater relative concentrations in the headspace analyses than in the SDE. Although the two extraction methods both showed protein – disulfide interaction, they gave different quantitative profiles of recovered sulfur compounds. This suggests that the amount of water and the heating conditions during extraction may affect the extent of interchange reactions with the proteins, implying that the relative amounts of thiols and disulfides found in cooked meat may be influenced by cooking conditions.

The odor threshold values of the thiols may differ from those of the corresponding disulfides, e.g., the odor threshold value for the disulfide **2** is reported as 2×10^{-5} $\mu\text{g}/\text{kg}$ while that of the corresponding thiol **1** is 5×10^{-3} $\mu\text{g}/\text{kg}$. The aroma characteristics of these compounds may also change with concentration. In general, at low concentrations approaching the odor threshold values, the compounds have pleasant savory or roasted aromas but at higher concentration they become more sulfurous and unpleasant (18-20). Changes in the relative concentrations of these thiols and disulfides could result in significant changes in the sensory properties when the compounds are used in flavorings for food products. The thiol-disulfide exchanges may also contribute to the different aroma characteristics of meat cooked under different conditions. These observations demonstrate that, in the binding of flavor in food, chemical interactions between aroma compounds and food components are important in factors.

References

1. Farmer, L. J.; Mottram, D. S.; Whitfield, F. B. *J. Sci. Food Agric.* **1989**, *49*, 347-368.
2. Mottram, D. S. In *Thermally Generated Flavors. Maillard, Microwave, and Extrusion Processes*; Parliment, T. H.; Morello, M. J.; McGorin, R. J., Eds; American Chemical Society: Washington DC, 1994; pp 104-126.
3. Hofmann, T.; Schieberle, P. *J. Agric. Food Chem.* **1995**, *43*, 2187-2194.
4. van der Linde, L. M.; van Dort, J. M.; de Valois, P.; Boelens, B.; de Rijke, D. In *Progress in Flavour Research*; Land, D. G.; Nursten, H. E., Eds; Applied Science: London, 1979; pp 219-224.
5. Werkhoff, P.; Brüning, J.; Emberger, R.; Güntert, M.; Köpsel, M.; Kuhn, W.; Surburg, H. *J. Agric. Food Chem.* **1990**, *38*, 777-791.
6. Mottram, D. S.; Szauman-Szumski, C.; Dodson, A. *J. Agric. Food Chem.* **1996**, *44*, 2349-2351.
7. Mottram, D. S.; Whitfield, F. B. *J. Agric. Food Chem.* **1995**, *43*, 984-988.
8. Mottram, D. S.; Nobrega, I. C. C. In *Food Flavours: Formation, Origin, Analysis and Packaging Influences*; Contis, E. T.; Ho, C.-T.; Mussinan, C. J.; Parliment, T. H.; Shahidi, F.; Spanier, A. M., Eds; Elsevier: Amsterdam, 1998; pp 483-492.
9. Nobrega, I. C. C. PhD Thesis, The University of Reading, 1999.
10. Mottram, D. S.; Nobrega, I. C. C.; Dodson, A. T. In *Challenges in Flavor Isolation and Analysis*; Morello, M. J.; Mussinan, C. J., Eds; American Chemical Society: Washington DC, 1998; pp 78-84.
11. Hofmann, T.; Schieberle, P.; Grosch, W. *J. Agric. Food Chem.* **1996**, *44*, 251-255.
12. Mottram, D. S.; Madruga, M. S.; Whitfield, F. B. *J. Agric. Food Chem.* **1995**, *43*, 189-193.
13. Guth, H.; Hofmann, T.; Schieberle, P.; Grosch, W. *J. Agric. Food Chem.* **1995**, *43*, 2199-2203.
14. Jocelyn, P. C. *Biochemistry of the SH group*; Academic Press: London, 1972.
15. Whitesides, G. M.; Houk, J.; Patterson, M. A. K. *J. Org. Chem.* **1983**, *48*, 112-115.
16. Chen, X.; Schofield, J. D. *J. Agric. Food Chem.* **1995**, *43*, 2362-2368.
17. Grosch, W. In *Chemistry and Physics of Baking*; Blanshard, J. M. V.; Frazier, P. J.; Galliard, T., Eds; Royal Society of Chemistry: London, 1986; pp 602-604.
18. Arctander, S. *Perfume and Flavor Chemicals*; Published by the author: Monclair, NJ, 1969.
19. Tressl, R.; Silwar, R. *J. Agric. Food Chem.* **1981**, *29*, 1078-1082.
20. Fors, S. In *The Maillard Reaction in Foods and Nutrition*; Waller, G. R.; Feather, M. S., Eds; American Chemical Society: Washington DC, 1983; pp 185-286.

Chapter 23

Infrared Spectroscopic Study of β -Lactoglobulin Interactions with Flavor Compounds

Markus Lübke, Elisabeth Guichard, and Jean-Luc Le Quéré

Laboratoire de Recherche sur les Arômes,
17 rue Sully, 21034 Dijon Cedex, France

Fourier transform infrared spectroscopy of aqueous solutions of β -lactoglobulin is used to study the incidence of binding of small organic ligands on the protein conformation at pH 2.0 and 7.5. Differential spectroscopy allows the comparison of conformational changes for different ligands, while curve fitting techniques are used to determine the influence of ligand binding on the relative proportions of the protein's secondary structural elements. Results are presented which suggest that retinol, fatty acids and β -ionone bind to the central cavity of β -lactoglobulin. Binding of α -ionone to the same site is also likely, although clear differences exist compared to the β isomer. A number of other flavor compounds did not induce any conformational changes to the protein. It is therefore assumed that these compounds bind to the protein surface.

It has long been recognised that the perception of food flavors not only depends on the quantitative composition of the volatile fraction, but that matrix effects also play a very important role. One cause for this matrix dependence is the interaction between the flavor active compounds and biopolymers present in most foodstuffs. Hydrophobicity of the flavors, acting as ligands, has a strong influence on these interactions, but sterical factors or the presence or absence of certain functional groups are also known to be important. Several methods have been developed to quantitatively study interactions either in model solutions of biopolymers or in more complex systems, among which are fluorescence spectroscopy (1, 2), static headspace (3, 4), affinity chromatography on protein bonded stationary phases (5, 6) and equilibrium dialysis (7, 8). While all techniques allow the determination of association constants or at least of global affinities, usually no insight in the involved binding mechanisms can be gained. Spectroscopic techniques, on the other hand, can

be used to study a broad range of systems, and in principle quantitative data about complexes can be obtained. More importantly, information at the molecular level is available: how exactly is the ligand bound to the macromolecule, and what implications does the binding have on the protein structure?

In this study, we have focused on Fourier transform infrared spectroscopy to study complexation between the whey protein β -lactoglobulin (β -lg) and selected flavor compounds. Infrared spectroscopy is a very useful tool to study protein secondary structures (for a review, see e.g. (9)). It is in general the so called amide I band region between 1600 and 1700 cm^{-1} that reveals the most information, because it is highly conformation-sensitive. For example, the changes induced by varying the pH of aqueous solutions of β -lg can be clearly followed (10), and even the subtle structural differences between β -lg variants A and B, which differ by only two amino acids, can be detected (11). This amide I band is due mainly to C=O stretching vibrations, and is a spectroscopically unresolvable complex of a certain number of overlapping individual bands. These individual bands represent the particular molecular environments of the protein backbone in secondary structures such as α -helices, β -sheets and turns (12). By analysing this "fine structure" of the amide I band, the elements of the secondary structure can be quantified, and the obtained compositions usually correlate quite well with results computed from X-ray data. In order to avoid confusion the term "band" will be used in the following for those individual bands as opposed to the "amide I envelope" as a whole.

The protein β -lg, like other members of the lipocalin family, has a central calyx-shaped cavity that is well established by X-ray studies (13-15). However, there has been ongoing discussion on whether hydrophobic molecules bind inside that central cavity or to a putative second binding site, which has been proposed as being a groove on the protein surface (14). In the light of two very recent X-ray studies, it seems that the central cavity is indeed the favored binding site for fatty acids (16, 17). As far as retinol is concerned (a molecule which is of special interest in this context due to the close structural resemblance between β -lg and retinol binding protein), results are still contradictory (18-22), although one might conclude, in the absence of final evidence, that binding takes place in the central cavity, too. Ligand binding to β -lg is further complicated by the fact that the protein undergoes a pH-driven structural change, known as the Tanford transition, which potentially restricts the access to the central cavity at low pH. It has been shown (21) that this transition involves the displacement of a flexible loop which links the strands E and F. Part of the contradictions in the literature may be due to this phenomenon.

In principle, it is reasonable to assume that flavor compounds behave like other hydrophobic ligands such as the mentioned retinol and fatty acids. But the size and geometry of the molecule are obviously also important, and exclusion phenomena from the central cavity and weak or no binding due to an insufficient number of favorable interactions within the cavity can be expected in some cases. To our knowledge, no direct evidence has been reported for where flavor compounds bind on the β -lg molecule. Indirect clues comes from (1), who found competition between

retinol and β -ionone, thus suggesting the central cavity as the binding site. Based on competition experiments between β -ionone and other flavor compounds (6), one can further conclude that (i) lactones have some (rather weak) affinity for the central cavity, and (ii) α -ionone, β -damascenone, methyl benzoate and unsaturated aliphatic aldehydes and ketones bind elsewhere on the protein.

It is our intention here to demonstrate the feasibility of the use of infrared spectroscopy to study interactions between proteins and flavor compounds in solution, to characterize structural changes induced by the ligand binding and to correlate the findings with those obtained notably by X-ray and by ligand competition studies for a deeper understanding of where on the β -lg molecule binding takes place depending on the ligand structure. To this end, band shapes of amide I envelopes as well as the intensities of the underlying individual bands will be analyzed and discussed.

Materials and Method

Solutions were prepared by dissolving 4.6 mg of β -lg variant A (Sigma) in 50 mM phosphate buffer (pH either 2.0 or 7.5) made up to 900 μ L, then adding 100 μ L of 1:1 ethanol/buffer mixture containing the appropriate amount of ligand. Final protein concentration was 250 μ M. All ligands were from the in-house collection of volatile compounds, except all-*trans*-retinol (Sigma). For those compounds where association constants from affinity chromatography were available, the ligand concentrations were chosen such that an approximately constant fraction of 92% β -lg was in a complexed state. Solutions for ligand/solvent subtraction were prepared in exactly the same way, but without any protein. All solutions were prepared in duplicate, and left to equilibrate at ambient temperature overnight. Infrared spectra were obtained on a Bio-Rad FTS6000, equipped with a Horizon ATR flow-through accessory with an internal volume of 0.15 mL (Harrick). A total of 512 scans at a resolution of 2 cm^{-1} were co-added. Fourier transforms used Norton-Beer medium apodization and zero filling by a factor of 2. Before starting the collection of spectra, a β -lg solution (4.6 mg/mL) without ligand was introduced into the cell and left there for 15 minutes. The cell was then flushed with 4 mL of water, and dried under a stream of nitrogen. This method was adopted in order to eliminate spectral distortions arising from interactions between the ZnSe crystal and the protein. It has been shown (23) that part of these interactions are sufficiently strong to alter the protein structure and thus its infrared spectrum. Furthermore, these strongly bound protein molecules are only slowly displaced by extensive flushing. This means in practical terms that after the initial flush the crystal surface can be regarded as stable for the duration of a series of samples, which is a prerequisite for accurate ligand/solvent subtraction.

A background spectrum of the empty cell was then recorded, and the protein-free solutions were measured, followed by those containing protein. After water vapour subtraction, the spectra of ligands were subtracted from the spectra of protein plus

ligands. The subtraction factors were chosen in such a manner that a constant ratio of amide I/amide II integrals of 1.92 was obtained. This procedure makes the determination of subtraction factors (which are inevitably arbitrary to some extent) more reproducible, while the chosen ratio avoids skewing of the baseline. Spectral smoothing (Savitsky-Golay algorithm, 15 points) was then applied, followed by a baseline correction (rubber band, fixed at 1900, 1712, 1593, 1482 cm^{-1}). The spectra were then scaled to an amide I integral of 1. No spectral deconvolution was used to avoid the potential introduction of artefacts. Differential spectra were obtained as a mean of the subtraction of the spectra of both replicates (protein without ligand) from the spectra of protein plus ligand. Standard deviations were calculated from the 16 individual differential spectra obtained for a given ligand (subtraction of the 2 replicates of solvent spectra from the 2 replicates of protein spectra yields 4 solvent subtracted spectra; subtraction of the 4 spectra of protein without ligand from the 4 spectra of protein plus ligand yields 16 differential spectra). Spectral curve fitting was performed in Grams /32 software (Galactic), using Gaussian band shapes; the starting values for the optimisation of the band parameters were taken from (11). Two bands at 1605 and 1615 cm^{-1} were included in the curve fittings to account for absorbances due to amino acid side chains, which are observed in this region. Band positions and widths at half height were optimised for the totality of the obtained spectra of β -lg ligand free solutions. These parameters were then kept constant, and only intensities were allowed to vary between both pH values. Curve fitting of differential spectra was performed in essentially the same way, allowing for positive or negative intensities of the bands.

Results and Discussion

In this study, conditions of β -lg solubilization were used that led to a solution structure that was as unambiguous as possible. D_2O as a solvent, although it simplifies infrared spectroscopy of proteins (due to the absence of the intense H_2O bending vibration band around 1640 cm^{-1}), may, amongst other drawbacks (23), influence the hydrogen bonding properties due to H/D exchange and was therefore avoided. Furthermore, β -lg tends to di- or octamerize depending on pH, ionic force, temperature and variant (24-26). Two non-denaturing pH values were chosen, at which β -lg A is present in a predominantly monomeric form. At pH 2.0, the E-F loop is flipped over part of the entrance to the central cavity, whereas at pH 7.5, the cavity is completely accessible. Fig. 1 shows the obtained spectra of β -lg under these conditions and in the absence of flavor compounds. The most prominent changes in the amide I region at pH 2.0 compared to pH 7.5 are a decrease of the 1627 cm^{-1} band and an increase of the 1651 cm^{-1} band. This is illustrated by the results obtained through curve fitting (Table 1), and in accordance with earlier findings (10).

In the presence of flavor compounds acting as ligands, the spectra of β -lg are modified to a more or less pronounced extent. A total of eight ligands were included in the analysis (Table 2). Retinol and tetradecanoic acid, although odorless, were

included because of the important body of published work on β -lg complexes with retinoids and fatty acids. Differential spectra were obtained from the processed spectra of ligand-free β -lg and of β -lg in the presence of ligand, as detailed in the Materials and Method section. The method used to calculate them eliminates possible

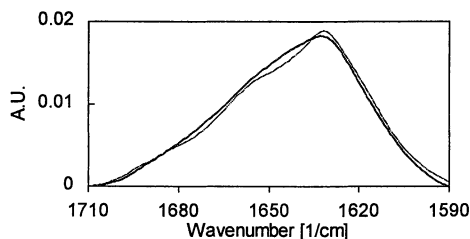


Figure 1. Amide I region of β -lg (250 μ M) in 50 mM phosphate buffer. Thin line: pH 2.0; bold line: pH 7.5.

Table I. Bands composing the amide I envelope of β -lg and their relative intensities

Band position [cm^{-1}]	Assignment ^a	Relative Intensities	
		pH 2.0	pH 7.5
1627	β -sheet	31.6	29.5
1640	β -sheet	22.7	22.9
1651	unordered	16.4	19.3
1655	α -helix	3.2	1.9
1663	turn	7.4	7.1
1673	turn	15.2	16.7
1687	turn	1.8	1.5
1693	β -sheet	1.6	1.1

^a From ref. (11)

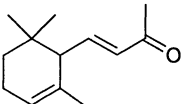
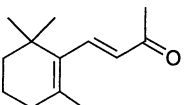
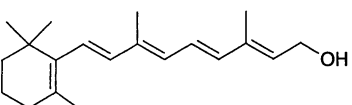
influences from bands arising from the ligands themselves. These differential spectra thus exclusively reflect changes to the β -lg spectrum inflicted in the presence of the employed ligands.

Fig. 2 shows the differential spectra obtained at pH 2.0. Tetradecanoic acid is assumed to behave like the previously studied palmitic acid (16) and 12-bromododecanoic acid (17) and thus to bind to the central cavity. A slight, but significant, deviation from zero with a maximum at 1670 cm^{-1} can be observed.

Interestingly enough, retinol shows a very similar pattern; the maximum here is also at 1670 cm^{-1} . This result supports the view that both compounds indeed occupy the same binding site.

The spectral changes induced by both ionone isomers are very similar to each other. They are characterized by an increase in intensity with two fairly sharp maxima at $1695/1697\text{ cm}^{-1}$ and $1674/1676\text{ cm}^{-1}$ and a minimum at $1641/1642\text{ cm}^{-1}$. Given the relatively small changes in structure between both isomers, this may not seem

Table II. Studied ligands and their association constants

Ligand	Concentration	Association Constant [M^{-1}]	Structure
α -ionone	1 mM	13000 ^a	
β -ionone	1 mM	19000 ^a	
retinol	250 μM	15000 ^b	
tetradecanoic acid	250 μM	-	
γ -decalactone	3.3 mM	3200 ^a	
p-cresol	23 mM	440 ^c	
eugenol	7.3 mM	1400 ^c	
2-nonanone	3.0 mM	3600 ^a	

^a by affinity chromatography at pH 3.0; from ref. (6)

^b by equilibrium dialysis at pH 7.2; from ref. (27)

^c by affinity chromatography at pH 3.0; from ref. (28)

surprising, but it is somewhat in contradiction to recent findings by affinity chromatography suggesting the absence of competition at pH 3.0 or 5.5 (6). Further ligands included were p-cresol, eugenol, γ -decalactone and 2-nonanone. Upon binding at pH 2.0, only 2-nonanone induced a small, although significant change to the amide I envelope of β -lg. The main feature of this change is a maximum at 1697 cm^{-1} . The differential spectra corresponding to the other compounds are not significantly different from zero.

Having assessed the influence of these ligands on β -Ig spectra at acidic pH, we were interested in the way this evolves when raising the pH to 7.5, at which the Tanford transition is completed. Fig. 3 presents the differential spectra obtained. Both tetradecanoic acid and retinol again show very similar differential spectra, but in

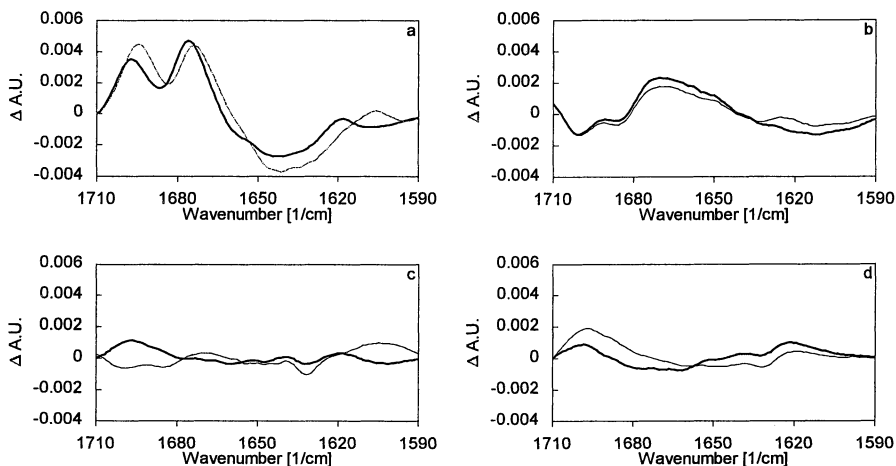


Figure 2. Differential spectra representing the changes induced to the amide I region of the β -Ig spectrum at pH 2.0 by the presence of ligands; the spectra of ligands themselves are compensated for. (a) bold line: α -ionone (1 mM), thin line: β -ionone (1 mM); (b) bold line: retinol (250 μ M), thin line: tetradecanoic acid (250 μ M); (c) bold line: *p*-cresol (23 mM), thin line: eugenol (7.3 mM); (d) bold line: γ -decalactone (3.3 mM), thin line: 2-nonanone (3.0 mM);

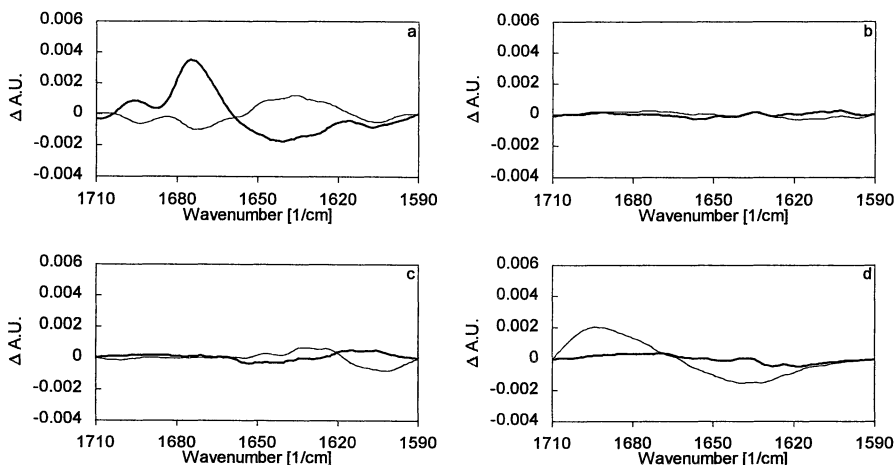


Figure 3. Same as Figure 2, but at pH 7.5.

contrast to pH 2.0, no structural change of β -lg can be detected. Despite the close resemblance of α - and β -ionone, the differential spectra are clearly different from each other at pH 7.5. The ligands p-cresol, eugenol and γ -decalactone that showed a neutral behaviour at pH 2.0 did again so at pH 7.5. Similarly, the pattern generated by 2-nonanone at pH 7.5 resembles much the one observed at pH 2.0, with a maximum at 1694 cm^{-1} .

The obtained differential spectra were then subjected to curve fitting in order to analyze the relative increase or decrease in the individual bands and thus in the underlying structural motif. In our hands, curve fitting of the differential spectra gave more reliable results as compared to curve fitting of the original spectra and subsequent calculation of differences of band intensities. The band positions from Table I and the corresponding bandwidths at half height were retained and positive or negative intensities were computed so that the sum of all bands fits the differential spectrum. Results for retinol and tetradecanoic acid (Fig. 4) and α - and β -ionone (Fig. 5) are shown. The similarity of retinol and tetradecanoic acid at both pH values is also apparent in terms of this more detailed analysis. It can be seen that the most prominent change at pH 2.0 is the increase of the 1673 cm^{-1} band, assigned to turns. The 1651 (random coil) and 1663 cm^{-1} (turns) bands also increase in intensity. When curve fitting the differential spectra for the ionone isomers in the same way, one observes again that the major change is due to an increase in the 1673 cm^{-1} band, except for β -ionone at pH 7.5, where all band areas remain essentially unchanged.

The patterns obtained for β -ionone are largely similar to those for retinol and the fatty acid. Significant differences can be found at pH 2.0, where a decrease at 1694 cm^{-1} (β -sheet) and an increase at 1651 cm^{-1} is observed, whereas for β -ionone, the tendencies are reversed. Also note that no significant changes in the intensity of the 1655 cm^{-1} band, assigned to α -helix, have been detected for any of the tested ligands, and at either pH. It appears that this part of the protein, which is at some distance from the central cavity, is not affected by ligand binding. The increase of the 1673 cm^{-1} band is about three times as big for the ionone isomers, compared to retinol. This reflects roughly the differences in the employed ligand concentrations (1 mM and 250 μM , respectively). Under the assumption that the literature affinity constants of Table I can be compared to each other (although obtained through a different method in the case of retinol), it appears that the magnitude of structural change induced by the binding event of a molecule of one of these ligands is approximately the same.

The results at pH 2.0 and 7.5, taken together, provide further evidence for the hypothesis that retinol and fatty acids bind to the same site, i.e. to the central cavity. Differences in the binding mechanism for these ligands must nevertheless exist between the acidic and the neutral pH, as some conformational rearrangement takes place upon binding at pH 2.0, contrarily to pH 7.5. One possible explanation lies in the restricted access to the central cavity at pH values below the Tanford transition. It is assumed that the flexibility of the E-F loop, which points towards the entrance of the central cavity at pH 2.0, is somewhat hindered by ligand binding. Accompanying structural changes may thus give rise to the observed marked increase in the intensity of the 1673 cm^{-1} band. It is also remarkable that β -ionone, which is structurally

speaking almost a subset of retinol, induces an overall similar pattern compared to that ligand (although, as pointed out, differences exist, e.g. for the 1694 cm^{-1} band), in contrast to the α isomer. It can therefore be assumed that this ligand also binds to the central cavity. Furthermore, it can be concluded that the presence of the cyclohexene double bond in the "retinol-like" position is essential for a binding at pH 7.5 that does not impose any significant conformational change on β -lg. This in turn suggests that (i) α -ionone is also bound in the central cavity, and (ii) the "wrong" position of the double bond leads to conformational changes upon binding at pH 7.5.

As far as the four ligands p-cresol, eugenol, 2-nonanone and γ -decalactone are

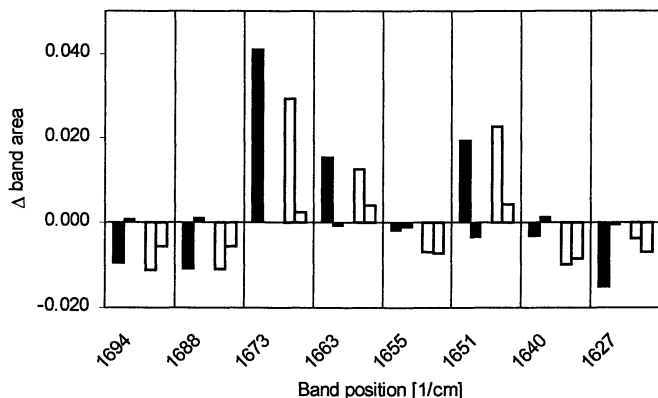


Figure 4. Changes in amide I band areas of β -lg, obtained by curve fitting of the differential spectra of retinol (black bars) and tetradecanoic acid (white bars). Within each set of two adjacent bars, the left bar is for pH 2.0, the right bar for pH 7.5.

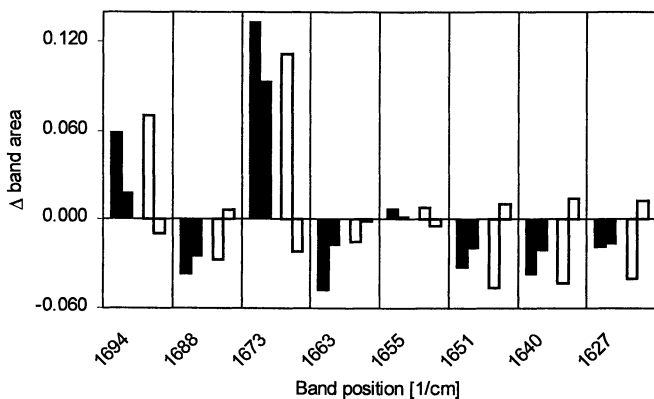


Figure 5. Changes in amide I band areas of β -lg, obtained by curve fitting of the differential spectra of α -ionone (black bars) and β -ionone (white bars). Within each set of two adjacent bars, the left bar is for pH 2.0, the right bar for pH 7.5.

concerned, it is tempting to conclude that binding takes place in the putative groove of β -lg or elsewhere outside the central cavity. If binding within this cavity occurred, one would indeed expect, at least in the case of the fairly large lactone, a differential spectrum at pH 2.0 that shows at least some similarity to that of retinol. It must nevertheless be pointed out that the present analysis can only be expected to characterize the predominant interaction, and that weak affinity of ligands to one binding site can hardly be detected in the presence of predominant binding to another site.

Conclusion

It was shown that infrared spectroscopy is an appropriate tool for the study of interactions between β -lg and small organic ligands in aqueous solution. Conformational changes of the protein induced by the presence of relatively small quantities of these ligands were detected. Building upon recently published evidence for the binding of fatty acids to the central cavity of β -lg, it was concluded that retinol, tetradecanoic acid and β -ionone also bind to this site. Differences in the binding mechanism between β -ionone and the other two ligands, and between pH 2.0 and pH 7.5 were nevertheless observed. In the case of α -ionone, binding to the central cavity is also likely, although the observed conformation upon binding at pH 7.5 was somewhat different from the β isomer. Four more ligands, p-cresol, eugenol, 2-nonanone and γ -decalactone, were studied, and little (2-nonanone) or no incidence on the protein conformation at either pH was observed. This was assumed to be due to binding of these ligands to the protein surface.

Acknowledgement

The authors are grateful to Isabelle Andriot for technical assistance. Financial support from the E.U. to M.L. (FAIR CT975011) is acknowledged.

References

1. Dufour, E.; Haertle, T. *J. Agric. Food Chem.* **1990**, *38*, 1691-1695.
2. Marin, I.; Relkin, P. *COST 96: Interaction of Food Matrix with Small Ligands Influencing Flavour and Texture*; Garching (Germany), 9-11 October 1997; European Commission; pp. 92-98.

3. Charles, M.; Bernal, B.; Guichard, E. *8th Weurman Flavour Research Symposium*; Reading (U.K.), 23-26 July 1996; Royal Society of Chemistry; pp. 433-436.
4. Jouenne, E.; Crouzet, J. *COST 96: Interaction of Food Matrix with Small Ligands Influencing Flavour and Texture*; Valencia (Spain), 14-16 November 1996; European Commission; pp. 28-31.
5. Pelletier, E.; Sostmann, K.; Guichard, E. *J. Agric. Food Chem.* **1998**, *46*, 1506-1509.
6. Sostmann, K.; Guichard, E. *Food Chem.* **1998**, *62*, 509-513.
7. Jasinski, E.; Kilara, A. *Milchwiss.* **1985**, *40*, 596-599.
8. O'Neill, T. E.; Kinsella, J. E. *J. Agric. Food Chem.* **1987**, *35*, 770-774.
9. Susi, H.; Byler, D. M. *Methods Enzymol.* **1986**, *130*, 290-311.
10. Casal, H. L.; Köhler, U.; Mantsch, H. H. *Biochim. Biophys. Acta* **1988**, *957*, 11-20.
11. Dong, A.; Matsuura, J.; Allison, S. D.; Chrisman, E.; Manning, M. C.; Carpenter, J. F. *Biochem.* **1996**, *35*, 1450-1457.
12. Bandekar, J. *Biochim. Biophys. Acta* **1992**, *1120*, 123-143.
13. Papiz, M. Z.; Sawyer, L.; Eliopoulos, E. E.; North, A. C. T.; Findlay, J. B. C.; Sivaprasadarao, R.; Jones, T. A.; Newcomer, M. F.; Kraulis, P. J. *Nature* **1986**, *324*, 383-385.
14. Monaco, H. L.; Zanotti, G.; Spadon, P.; Bolognesi, M.; Sawyer, L.; Eliopoulos, E. E. *J. Mol. Biol.* **1987**, *197*, 695-706.
15. Brownlow, S.; Morais Cabral, J. H.; Cooper, R.; Flower, D. R.; Yewdall, S. J.; Polikarpov, I.; North, A. C.; Sawyer, L. *Structure* **1997**, *5*, 481-495.
16. Wu, S. Y.; Pérez, M. D.; Puyol, P.; Sawyer, L. *J. Biol. Chem.* **1999**, *274*, 170-174.
17. Qin, B. Y.; Creamer, L. K.; Baker, E. N.; Jameson, G. B. *FEBS Lett.* **1998**, *438*, 272-8.
18. Cho, Y.; Batt, C. A.; Sawyer, L. *J. Biol. Chem.* **1994**, *269*, 1102-1107.
19. Wang, Q.; Allen, J. C.; Swaisgood, H. E. *J. Dairy Sci.* **1997**, *80*, 1047-1053.
20. Lange, D. C.; Kothari, R.; Patel, R. C.; Patel, S. C. *Biophys. Chem.* **1998**, *74*, 45-51.
21. Qin, B. Y.; Bewley, M. C.; Creamer, L. K.; Baker, H. M.; Baker, E. N.; Jameson, G. B. *Biochem.* **1998**, *37*, 14014-14023.
22. Narayan, M.; Berliner, L. *J. Protein Sci.* **1998**, *7*, 150-7.
23. Oberg, K. A.; Fink, A. L. *Anal. Biochem.* **1998**, *256*, 92-106.
24. Pessen, H.; Purcell, J. M.; Farrell, H. M. *Biochim. Biophys. Acta* **1985**, *828*, 1-12.
25. Renard, D.; Lefebvre, J.; Griffin, M. C.; Griffin, W. G. *Int. J. Biol. Macromol.* **1998**, *22*, 41-49.
26. Verheul, M.; Pedersen, J. S.; Roefs, S. P. F. M.; de Kruif, K. G. *Biopolymers* **1999**, *49*, 11-20.
27. Puyol, P.; Pérez, M. D.; Ena, J. M.; Calvo, M. *Agric. Biol. Chem.* **1991**, *55*, 2515-2520.
28. Reiners, J.; Nicklaus, S.; Guichard, E. *Le Lait* **1999**, submitted.

Chapter 24

Factors Determining Binding of Aroma Esters with Legumin in an Aqueous Medium

Maria G. Semenova, Anna S. Antipova, Tamara A. Misharina,
Margarita B. Terenina, and Rimma V. Golovnya

Institute of Biochemical Physics of Russian Academy of Sciences,
Vavilov str. 28, 117813 Moscow, Russia

The role of protein structure on the binding of hexyl acetate with legumin has been studied by a combination of ultrafiltration and gas-liquid chromatography. Molecules of native legumin possess the most binding affinity for hexyl acetate through the unique quaternary structure. Acid denaturation of the protein leads to the complete loss of its binding capacity. On heat denaturation the protein retains its capacity to bind the aroma compounds but has significantly different mechanism and binding parameters from those of the native protein. The effect of molecular structure on binding properties has been studied using a series of homologous, linear alkyl acetates and a series of branched chain esters. The implication of the length of hydrocarbon chain and polarities of molecules of the aroma esters in binding parameters and mechanisms has been shown. The peculiarities of competition and mutual influence between aroma esters, being in equimolar mixtures, in binding with the native protein have been first considered.

It is well known that a specific interaction of aroma compounds with non-volatile food ingredients, like proteins and polysaccharides, results in a disturbance of their balance in the aroma of a particular composition that may distort or even suppress this aroma (1-3). As this takes place, the structure both of biopolymers and of flavour compounds is of decisive importance in this binding. Previously, it was found that the binding capacity of a flavour compound for protein depends on the type of aroma compounds (alcohols, aldehydes, ketones), on the chain length of the compound and the position of a functional group in the chain (4-7).

In the present work, we have attempted to study binding of protein with a further class of aroma compounds, the aroma esters. These are major components of a variety of attractive flavours, and we have studied not only the binding ability of individual aroma compounds, but also their binding capacities from the mixtures. This is important because the flavour of many foods is imparted by complex mixtures of different flavour compounds and the role of competition between them in binding with protein is of fundamental importance. Legumin (11S globulin from broad beans) was selected as the protein for the investigation for several reasons. Firstly, legumin is homologous in both physico-chemical properties and biological functions to 11S globulins of the other leguminous plants (soy, pea etc.), which are promising materials for formulating new types of food products (8–10). Secondly, the content of lipids, being responsible for an unpleasant “leguminous aroma”, in broad beans is an order of magnitude lower than, for example, in soy beans (2.3% and 19.6%, respectively). For this reason alone this protein is quite a promising additive for a new food formulation and should be among the most important objects for the systematic investigation (11–14).

EXPERIMENTAL

Materials

Legumin (11S globulin) was isolated from broad beans (var. “Agat”) by the method described previously (15). Homogeneity of the isolated 11S globulin was assessed by sedimentation. It was found to be a single peak of 11S globulin with a sedimentation coefficient of 12×10^{-13} S. The aroma esters (95% of purity): alkyl acetates (butyl acetate (BuAc), amyl acetate (AmAc), hexyl acetate (HxAc), heptyl acetate (HpAc) and octyl acetate (OcAc)), butyl butyrate (BuBu), ethyl hexanoate (EtGex) and heptyl formate (HpForm) were purchased from REACHEM (Russia) and then distilled to gain a purity of 99%. Pure (> 99%) organic solvents (acetone, ethanol and diethyl ether) were obtained from REACHEM (Russia) and used without further purification. Phosphate (pH 7.2) or citric (pH 3.0) buffer solutions were prepared using analytical grade reagents (99.9% of purity) and double-distilled water.

Methods

Determination of Protein Concentration in Solutions

Concentration of the protein in solutions was determined using a spectrophotometer at a wavelength of 280 nm. The protein solutions were aged in 8 mol dm^{-3} urea for 24 hours before measurements. The extinction coefficient $A_{1\text{cm}}^{1\%} = 7.58$ was used for calculations.

Determination of Concentration of Aroma Esters in Solutions

The concentration of aroma compound in solutions was determined using gas-liquid chromatographs (Hewlett Packard 5710A; integrator 3380A).

Separation of extracted components was carried out using fused silica capillary column SE-30 (JIW) (50 m × 32 mm, $df = 0.2 \mu\text{m}$ and/or 60 m × 32 mm, $df = 0.25 \mu\text{m}$) at 110 °C. The operating conditions were as follows: split ratio of the carrier gas (helium) was 1:30 or 1:100; flow rate was 1 and/or 1.5 mL min⁻¹; temperature of the injector and detector (FID) was 150 °C and/or 200 °C; injected samples were 0.5 - 2 μL . The content of aroma compound was determined from the relation between the peak area for aroma ester and that for an internal standard (n-undecane).

Determination of Binding of Aroma Esters with the Protein

To determine the concentration of aroma compound bound by the protein, the ultrafiltration method was used to separate the protein with a bound aroma ester from free ligand.

The calculated quantities of aroma compound in diethyl ether were added to 25 mL of the protein buffered solution (1 wt%) and to the same volume of buffer (the blank solution). The mixed solutions (legumin + aroma ester) were shaken for 1-2 minutes and left to stand for 30 minutes at room temperature in opened flasks to remove traces of the ether, and then the closed flasks were shaken (CPLAN water bath shaker, type357, Poland) for 1 hour to reach equilibrium. The mixed solutions were filtered through nuclear membranes with a pore size of 0.027 μm using a special equipment operated at 3 bar to separate a free ligand from bound one. The membranes were made from lavsan (Russian equivalent of Darcon) and were etched with 20% NaOH. The number of pores per cm² was 2×10^9 . There was 1 carboxyl group for every 200 A^2 of the membrane surface. The protein did not pass through the membranes. Aliquots of the filtered aqueous solutions (5 mL) were collected into test tubes, each containing 3 mL of diethyl ether. The two-layer mixtures were shaken and aged 24 hours in a cool place. The organic layers were separated and used for determination of the free ligand concentration [L_{free}] in the filtrates by gas-liquid chromatography (GC). The values of [L_{free}] presented in this work are averaged data for 3-8 repetitions of each of the GC analyses. Using these data as the base, the concentration of bound ligands in the solutions was calculated. A sorption of the aroma compounds on the nuclear membrane was built into these calculations. The estimated experimental error was 5%.

Differential Scanning Calorimetry

Calorimetric measurements were made using a DASM-4M differential adiabatic scanning microcalorimeter (Special Design Office of Biological Instrument Making, Russian Academy of Sciences) in the temperature range from 20 to 110 °C at a scanning rate of 2 °C/min and at an excessive pressure of 2.5 atm. The concentration of protein sample was 0.005 g/mL. The accuracy of

the heat capacity measurements was about 10%. The thermodynamic parameters of legumin heat denaturation process were calculated as proposed before (16).

RESULTS AND DISCUSSION

The Role of Legumin Structure in Binding with Aroma Ester

The relationship between structure of the protein and its binding ability has been demonstrated by the example of the binding of HxAc with legumin in the different structural states in an aqueous medium. Figure 1a shows that the isotherm of binding (binding extent ν (the number of moles of ligand bound per mole of protein) versus the logarithm of free ligand concentration in the system, $\log [L_{\text{free}}]$) of HxAc with the native legumin differs dramatically from those with both heat- and acid denatured protein. For the heat-denatured protein, the binding isotherm rises with increasing concentration of HxAc more steeply than is the case for the native protein. In contrast, there is an almost complete lack of

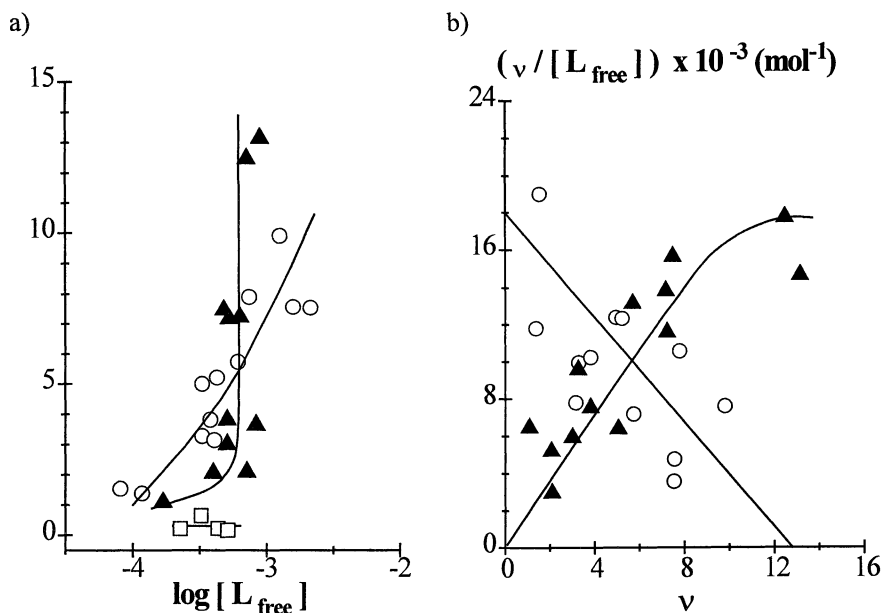


Figure 1. Data on binding of hexyl acetate with 11S globulin in an aqueous medium (ionic strength 0.05 mol/dm^3): \circ , native protein (pH 7.2); \blacktriangle , heat-treated protein (30 min at 90°C , pH 7.2); \square , acid denatured protein (pH 3.0).

a) Binding isotherms: the binding extent ν is plotted as a function of the logarithm of free ligand concentration in the system, $\log [L_{\text{free}}]$.

b) Scatchard plot: the ratio of binding extent to free ligand concentration, $(\nu/[L_{\text{free}}])$, is plotted against the binding extent ν .

binding capacity for the acid-denatured protein. Moreover, the presentation of the binding data in Scatchard graphical form in accordance with

$$\frac{\nu}{[L_{free}]} = nK - \nu K, \text{ where } \nu \text{ is the number of moles of ligand bound per mole}$$

of protein; $[L_{free}]$ is the concentration of free ligand in the system; n is the total number of binding sites in the protein molecule; K is the intrinsic binding constant (17), allows to see that the mechanism of the binding of HxAc with the native protein differs significantly from that with the heat-treated protein (Figure 1b). The reverse run of the curves indicates that whereas binding of HxAc takes place on independent and identical binding sites in the molecule of native protein, there is a cooperative binding of HxAc on the interacting binding sites in the heat-denatured protein molecule (18). Table I shows the binding parameters for the native protein, determined from the Scatchard plot, and the average binding parameters for the heat-treated protein (19), determined from the double reciprocal Scatchard plot and Hill plot in accordance with

$$\frac{1}{\nu} = \frac{1}{n} + \frac{1}{nK[L_{free}]} \quad \text{and} \quad \ln(L_{free}) = -\left(\frac{1}{\alpha_H}\right) \ln\left[\left(\frac{n}{\nu}\right) - 1\right] + \ln K,$$

respectively (18). Here L_{free} is the free ligand concentration; α_H is the Hill cooperative parameter; n is the total number of binding sites in the protein molecule; ν is the number of moles of ligand bound per mole of protein; K is the intrinsic binding constant.

Table I. Binding Parameters for HxAc with Legumin in an Aqueous Medium at pH 7.2 (ionic strength 0.05 mol/dm³)

<i>State of protein molecule</i>	<i>Total number of binding sites, n</i>	<i>Intrinsic binding constant, K (mol)</i>	<i>Gibbs free energy of binding, ΔG (kcal/mol)</i>
native	13	1406	- 4.22
heat-denatured	100	259	- 3.02

Relying on the experimental and literature data, we can suggest that the following features of protein structure define the binding mechanism in each case. The molecule of native 11S globulin is composed of disulfide-linked basic and acidic chains and can be represented either as two annular-hexagonal structures composed of 6 chains (12, 20, 21) or as two annular-trigonal structures formed by three dual-chain monomers (22), packed one on top of another so that they form a

hollow cylinder. It might be assumed that the cavity in this cylinder provides a way for HxAc molecules to bind. At pH 3.0, when 11S globulin is almost completely denatured (12) and in the form of soluble aggregates (23), it was found to be the dramatic decrease in the protein binding capacity (Figure 1a). This is in agreement with Damodaran and Kinsella (24), who reported that denaturation of 11S globulin leads to a pronounced decrease in the binding affinity of the protein for a ligand in the presence of urea. These findings add considerable support for the foregoing hypothesis that the unique quaternary structure of 11S globulin is responsible for the interaction between hexyl acetate and the protein. The heat treatment causes the irreversible denaturation of 11S globulin and formation of soluble thermoaggregates (23,25) with a rather high capacity to bind HxAc (Figure 1a). It was shown that the soluble thermoaggregates of leguminus are predominantly composed of the basic chains, which are more hydrophobic than the acidic ones, being free in the solution (12). So, it might be assumed, that the hydrophobic cavities in the interior of the protein thermoaggregates, possessing quite a high binding capacity, are formed by the unfolded basic chains. In the case of heat-denatured protein, however, the smaller intrinsic constant and the larger number of binding sites suggest a different, less specific, binding mechanism for HxAc compared to the native protein. On the basis of the data obtained, the decisive role of the structure of legumin in the interactions with aroma compounds is evident.

The Role of the Structure of Aroma Esters in Binding with Native Legumin

The Binding of Alkyl Acetates Differing in the Length of Hydrocarbon Chain (C₄ – C₈)

To understand how the structure of aroma esters influences their binding with native legumin in an aqueous medium, we initially studied binding of the protein with alkyl acetates, differing in the length of hydrocarbon chain (C₄ - C₈). Figure 2 compares the binding isotherms for alkyl acetates with the native legumin. Contrary to expectations, the highest binding extent ν was found for BuAc, whereas the least binding was for OcAc. This experimental fact suggests that the binding sites in the interior of legumin globule are more accessible for the alkyl acetate with the shortest hydrocarbon chain. It is also evident that there are some structural restrictions in the interior of the protein molecule, preventing binding with the alkyl acetate having the longest hydrocarbon chain. The shape of the binding isotherms differs dramatically, suggesting distinctions between the binding mechanisms for the alkyl acetates studied. Indeed, Scatchard plots, shown in Figure 3, point to the fact that the binding mechanisms significantly change as the length of the hydrocarbon chain of the alkyl acetates increases: from binding on identical and independent binding sites for BuAc and HxAc to cooperative binding on interacting binding sites in the case of HpAc and OcAc.

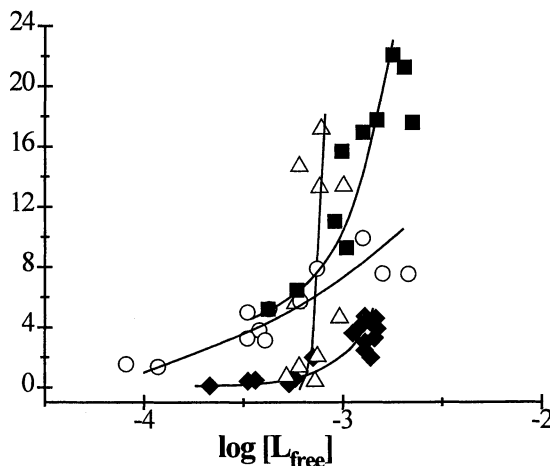


Figure 2. Binding isotherms for alkyl acetates with native legumin in an aqueous medium (pH 7.2, ionic strength 0.05 mol/dm^3). The binding extent ν is plotted as a function of the logarithm of free ligand concentration in the system, $\log [L_{\text{free}}]$: ■, BuAc; ○, HxAc; △, HpAc; ◆, OcAc.

Furthermore, from the Scatchard plots for BuAc and HxAc, it follows that the number of binding sites decreases, whereas the value of the intrinsic binding constant increases by an order of magnitude with increasing length of hydrocarbon chain (Table II).

Table II. Binding Parameters for BuAc and HxAc with Native Legumin in an Aqueous Medium at pH 7.2 (ionic strength 0.05 mol/dm^3)

<i>Aroma compound</i>	<i>Total number of binding sites, n</i>	<i>Intrinsic binding constant, K (mol)</i>	<i>Gibbs free energy of binding, ΔG (kcal/mol)</i>
BuAc	102	137	- 2.86
HxAc	13	1406	- 4.22

As is evident from Table II, HxAc possesses greater binding affinity (larger values of the intrinsic binding constant and Gibbs free energy), that correlates well with the evidence for predominantly hydrophobic nature of binding of lipophilic molecules with proteins (5-7, 26, 27). However, HxAc does not exhibit as large binding extent as BuAc shows, by virtue of the fact that some structural peculiarities in the interior of protein molecule hinder the binding. Unfortunately, the insolubility of HpAc and OcAc in an aqueous medium, constrains the

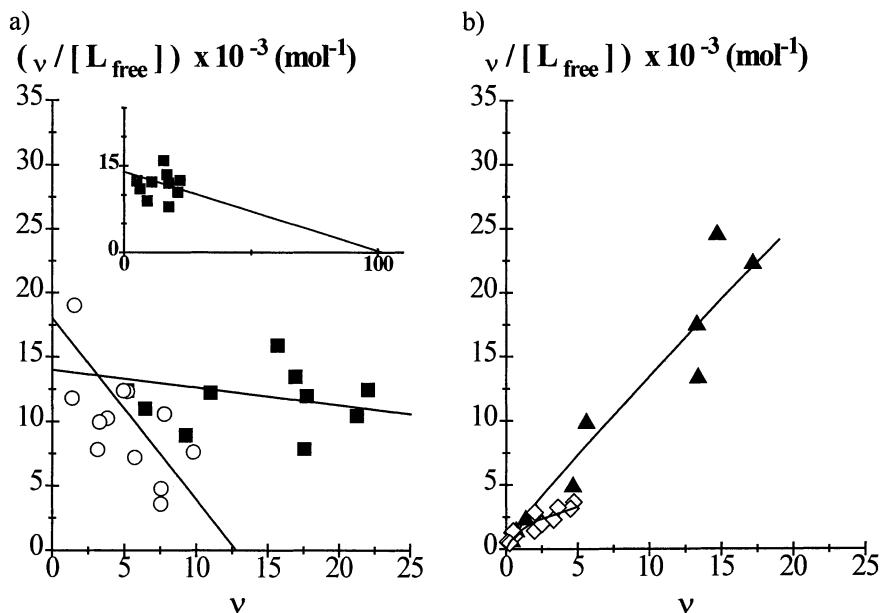


Figure 3. Scatchard plots showing binding of alkyl acetates to native legumin in an aqueous medium (pH 7.2, ionic strength 0.05 mol/dm^3). The ratio of binding extent to free ligand concentration, $(v/[L_{\text{free}}])$, is plotted against binding extent v : a) ■, BuAc; ○, HxAc; b) ▲, HpAc; ◇, OcAc.

concentration range that can be used for these aroma compounds, which is why it was impossible to extrapolate properly the binding data presented in Scatchard graphical form, and thus to estimate the binding parameters in these cases. A comparison of the shapes of the Scatchard plots for alkyl acetates studied allows us to conclude that the mechanism of binding of these aroma compounds with the native legumin depends on the length of hydrocarbon chain in the molecules of the ligands. At this take place, C_7 is the critical length of a hydrocarbon chain in this series of the alkyl acetates, at which the binding mechanism changes. In order to get a better understanding of these findings, we have carried out microcalorimetric investigations. Figure 4 shows the effect of the structure of the aroma compounds on the key thermodynamic parameters characterizing the heat denaturation process of the protein globule (the specific calorimetric enthalpy ΔH_{cal} and the difference between the specific heat capacities of the protein in the denatured and native states, $\Delta_d C_p$). The change in these parameters under

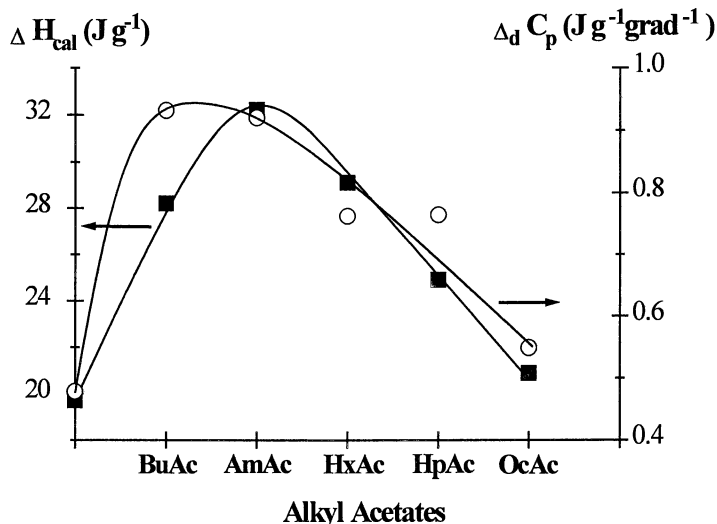


Figure 4. Effect of alkyl acetates (2.0 mmol) on the thermodynamic parameters of the legumin heat denaturation process (0.05 mol/dm³ phosphate buffer, pH 7.2):

■, ΔH_{cal} ; ○, $\Delta_d C_p$.

influence of the aroma ligands points to a modification of the conformation of native protein. The length of hydrocarbon chain dependence of ΔH_{cal} has a maximum. The increase in ΔH_{cal} may be caused by the breaking of additional bonds, formed in the interior of the protein molecule as a result of binding with alkyl acetates (28). The decrease in the values of ΔH_{cal} suggests that there is some compensating process, which is attributable to partial protein unfolding (29) due to the binding with the ligands having longer hydrocarbon chains.

The shape for the length of a hydrocarbon chain dependence of $\Delta_d C_p$ coincides closely with that for ΔH_{cal} . In this case, the increase in $\Delta_d C_p$ (up to the maximum) can be traced to two different causes: (i) an increase in the conformational stability of the protein in the native state and (ii) an increase in the hydrophobicity of the denatured protein surface contacting with water as a result of the ligand molecules attached to the protein (28,29). The following decrease in $\Delta_d C_p$ under influence of the alkyl acetates with longer hydrocarbon chains may be due to that the hydrophobicity of the native protein becomes similar to that of the denatured protein as a result of partial unfolding of the native protein molecules upon binding with these aroma compounds. It seems reasonable to say that the modification of the protein molecules resulting from the binding with alkyl acetates, is responsible for the revealed peculiarities of the binding behaviour of these ligands.

Binding of Methameric Esters Differing in the Position of Ester Group in the Hydrocarbon Chain (C₈)

Figure 5 shows that the isotherm of binding of HpForm with native legumin is very different from those of other methameric esters. Considering that HpForm is the most polar ligand in this series, it may be safely suggested that van der Waals forces, which are electromagnetic in nature, contribute to the binding of aroma esters with legumin along with hydrophobic forces.

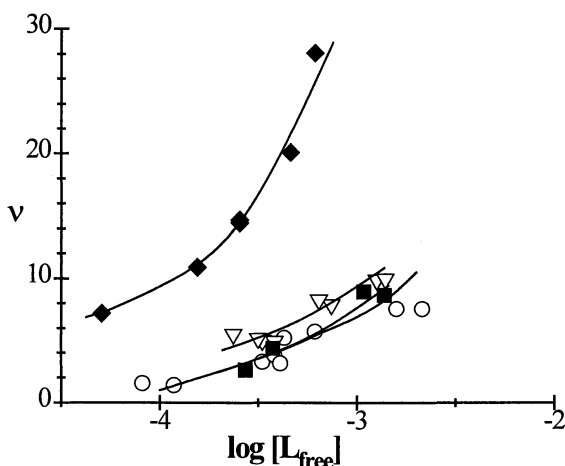


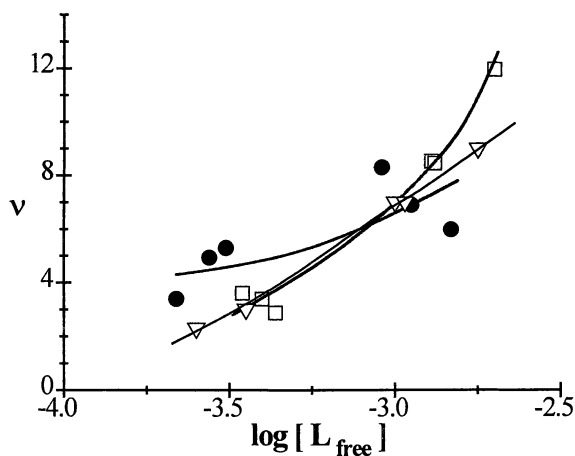
Figure 5. Binding isotherms for methameric esters, differing in the position of the ester group in the hydrocarbon chain (C₈), with native legumin in an aqueous medium (pH 7.2, ionic strength 0.05 mol/dm³). The binding extent v is plotted against the logarithm of free ligand concentration in the system $\log [L_{free}]$: \circ , HxAc; ∇ , BuBu; \blacksquare , EtGex; \blacklozenge , HpForm.

The Role of the Structure of Aroma Esters in Competitive Binding of Alkyl Acetates (C₄ – C₈) from their Equimolar Mixtures with Native Legumin

By virtue of the fact that there is the critical length of a hydrocarbon chain in alkyl acetates (C₇) at which the binding mechanism changes dramatically, we have studied two different equimolar mixtures of alkyl acetates: (BuAc+AmAc+HxAc) and (HxAc+HpAc+OcAc). In the former case, the hydrocarbon chains of the ligands were shorter than C₇. The aroma compounds, composing the second mixture, vary in the length of hydrocarbon chain as follows: HxAc < HpAc (C₇) < OcAc. As is immediately obvious from Figure 6, there is a marked difference between the shape of the binding isotherms for alkyl acetates from (BuAc+AmAc+HxAc) mixture and that from (HxAc+HpAc+OcAc). In the latter case, when the mixture is composed of the

ligands with longer hydrocarbon chains, the binding isotherms rises more steeply than is the case of (BuAc+AmAc+HxAc) mixture.

a)



b)

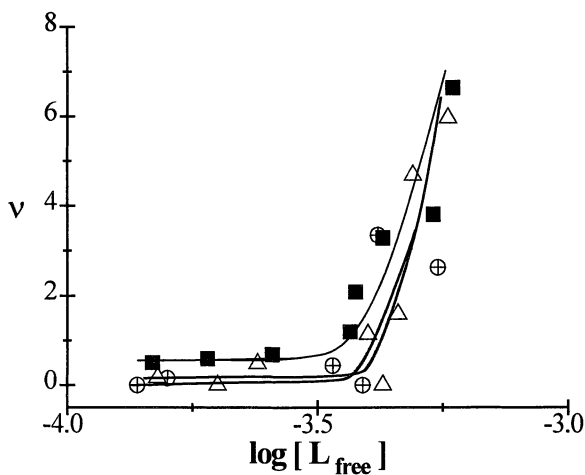


Figure 6. Binding isotherms for alkyl acetates from their equimolar mixtures, with native legumin in an aqueous medium (pH 7.2, ionic strength 0.05 mol/dm^3). The binding extent v is plotted as a function of the logarithm of free ligand concentration in the system, $\log [L_{\text{free}}]$:

a) (BuAc+AmAc+HxAc) mixture: \square , BuAc; ∇ , AmAc; \bullet , HxAc;

b) (HxAc+HpAc+ OcAc) mixture: \oplus , HxAc; Δ , HpAc; \blacksquare , OcAc.

Closer inspection of the binding isotherms for the ligands from (BuAc + AmAc + HxAc) mixture shows that for BuAc and AmAc, they coincide very closely, whereas HxAc exhibits the higher binding capacity, especially in the range of low concentrations of the aroma ligands (Figure 6a). In contrast, in the case (HxAc + HpAc + OcAc) mixture, there is no binding of HxAc with the protein over the same region of ligand concentrations (Figure 6b). For this mixture, it is easy to see that OcAc has some advantages over other compounds for binding with legumin. The fact that for either mixture, the greatest binding was observed for the ligands, containing the longest alkyl chains, is further evidence in favour of the predominantly hydrophobic nature of binding of lipophilic molecules with proteins (5-7, 26, 27). Figure 7 shows that there is an essential difference between the shape of Scatchard plots for alkyl acetates from (BuAc + AmAc + HxAc) mixture and that from (HxAc + HpAc + OcAc) mixture, which points to the fact that the binding mechanisms for the ligands are different for these two cases. Whereas for the former mixture, the binding of individual ligands takes place on the independent and identical binding sites in the protein molecule, the co-operative binding is the case for the components from the latter mixture.

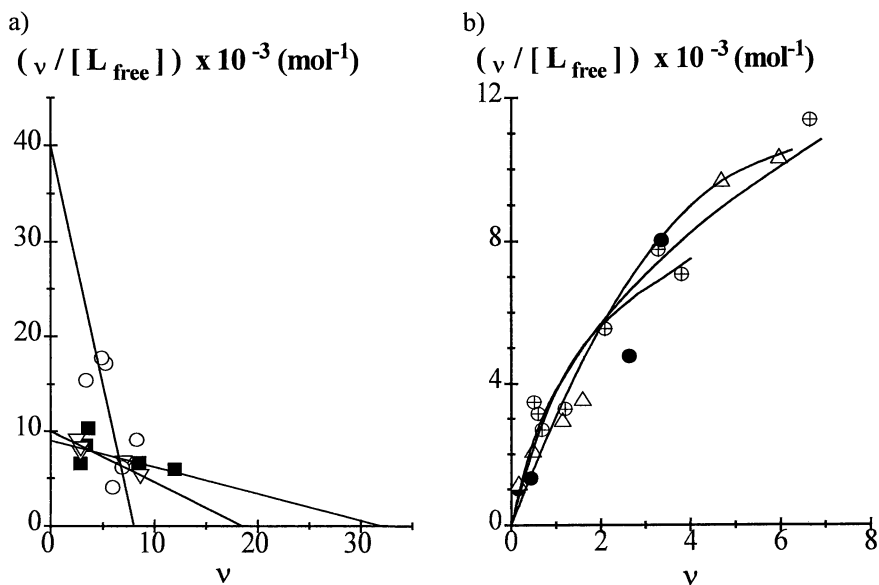


Figure 7. Scatchard plots showing binding of alkyl acetates to native legumin in an aqueous medium (pH 7.2, ionic strength 0.05 mol/dm^3). The ratio of binding extent to free ligand concentration, $(v/[L_{\text{free}}])$, is plotted against the binding extent v . a) (BuAc + AmAc + HxAc) mixture: ■, BuAc; ▽, AmAc; ○, HxAc; b) (HxAc + HpAc + OcAc) mixture: ●, HxAc; △, HpAc; ⊕, OcAc.

From the above data we can infer the distinguishing characteristics of the binding process for each of alkyl acetates from the studied mixtures. Let us consider first the case of (BuAc+AmAc+HxAc) mixture. Table III shows that, there is a decrease in the number of binding sites and an increase in the intrinsic binding constant with increasing length of hydrocarbon chain of the aroma ligands. However the values of these parameters vary several-fold in passing from BuAc to AmAc, but by an order of magnitude when one goes from AmAc to HxAc.

Table III. Binding Parameters for Alkyl Acetates with Native Legumin from Equimolar (BuAc+AmAc+HxAc) Mixture in an Aqueous Medium (pH 7.2, ionic strength 0.05 mol/dm³)

<i>Aroma compound</i>	<i>Total number of binding sites, n</i>	<i>Intrinsic binding constant, K (mol)</i>	<i>Gibbs free energy of binding, ΔG (kcal/mol)</i>
BuAc	32	281	- 3.28
AmAc	19	541	- 3.66
HxAc	8	5000	- 4.96

On the basis of the above, there is a reasonable case for assuming that the greatest binding affinity of HxAc for the native protein governs the observed preferential binding for HxAc at low concentrations of aroma compounds in the mixture (Figure 6a). In the case of BuAc, the greatest binding extent at rather high concentrations of the ligands in spite of the lowest binding affinity for the protein, can be attributed to lesser structural restrictions on the binding as compared to those for AmAc and HxAc. A comparison between binding behaviour (binding isotherms, Scatchard plots, binding parameters) of the aroma compounds alone and from their equimolar mixture, suggests that the binding for the ligands from the mixture is more ordered and takes place on the distinct binding sites of the protein molecule, which are best suited to the specific structure of particular aroma compounds, whereas when bound to the protein alone, the ligands occupy all accessible binding sites in the protein molecule and the binding appears more random. This is more noticeable for BuAc. At this takes place, the summary extent of binding for the aroma esters from their equimolar mixture can reach larger values than those for the individual aroma components at the same concentrations, as shown in Table IV.

Let us turn now to the case of the alkyl acetates with long hydrocarbon chain (HxAc, HpAc, OcAc). Referring to Table IV, an essential decrease in the binding extent for HxAc is clear, with native legumin from the equimolar mixture

(HxAc+HpAc+OcAc). The opposite is the case for HpAc and OcAc. These findings are in line with the expected hydrophobic nature of binding of these aroma compounds to the protein. On the strength of these data it is reasonable to suggest that a mutual influence of HpAc and OcAc facilitates the binding of each compound with the protein. This binding behaviour can be traced to greater hydrophobicity of the ligands, that leads to the modification of the hydrophobic cavities in the interior of the protein molecule in such a way that binding is made easier.

Table IV. Binding of Alkyl Acetates with Native Legumin. Comparison of Binding Extent for Alkyl Acetates Alone and from Equimolar Mixtures at the Same Concentration of Free Ligands in the System ($[L_{\text{free}}] = 0.55 \text{ mmol}$)

<i>Aroma compounds</i>	<i>Binding extent, ν</i>		
	<i>Alone</i>	<i>From equimolar mixture BuAc + AmAc + HxAc</i>	<i>From equimolar mixture HxAc + HpAc + OcAc</i>
BuAc	6.1	4.4	
AmAc	-	4.8	
HxAc	5.1	5.5	2.7
BuAc+AmAc+HxAc		9.0	
HpAc	0.6		6.0
OcAc	0.4		5.9
HxAc+HpAc+OcAc			1.0

Probably, this modification of the protein globule is responsible for a dramatic change in the binding mechanism for HxAc: from the binding on identical and independent binding sites in the protein molecule for HxAc alone to the cooperative binding on the interacting binding sites from the equimolar mixture (HxAc+HpAc+OcAc) (Figures 1b and 7b).

Conclusions

1. The molecules of globular native legumin possess the greatest binding affinity for hexyl acetate through the unique quaternary structure.
2. The mechanism of binding of the alkyl acetates with the protein depends on the length of the hydrocarbon chain. C_7 is the critical length of a hydrocarbon chain, at which the binding mechanism of the studied alkyl acetates changes dramatically.

3. Some structural restrictions on binding and values of the intrinsic binding constant are both responsible for competitive distributions of aroma compounds from their equimolar mixture on the binding sites of the globular protein.
4. When equimolar mixtures of esters interact with the protein there appears to be an interactive effect due to the change of hydrophobicity of the interior of native protein globule.

Acknowledgement

The authors are most grateful to Nestle Research Centre (Switzerland) for the financial support of this research.

References

1. Franzen, K.L.; Kinsella, J.E., *J. Agric. Food Chem.* **1974**, *22*, 675.
2. Malcomson, J.K.; McDaniel, M.R.; Hoehn, E., *Can. Inst. Food Sci. Technol. J.* **1987**, *20*, 229.
3. Iametti, S.; Degregori, B.; Vecchio, G.; Bonomi, F., *European Journal of Biochemistry.* **1996**, *237*, 106.
4. Fares, K.; Landy, P.; Guillard, R.; Voilley, A. *J. Dairy Sci.* **1998**, *81*, 82.
5. Landy, P.; Daraux, C.; Voilley, A., *Food Chemistry.* **1995**, *54*, 387.
6. Damodaran, S.; Kinsella, J.E., *J. Agric. Food Chem.* **1981**, *29*, 1249.
7. O'Neill, T.E.; Kinsella, J.E., *J. Agric. Food Chem.*, **1987**, *35*, 770.
8. Fauconneau, G. *Plant Proteins for Human Food*; Bodwell, C.E; Petit, L., Eds.; Martinus Nijhoff: The Hague, 1983, p.1.
9. *Food Chemistry*; Belitz, H.D.; Grosch, W., Eds.; Springer Ver-lag: Berlin, 1987, ch. 16.
10. Garcia, M.C.; Torre, M.; Marina, M.L.; Laborda, F., *Critical Reviews in Food Science and Nutrition.* **1997**, *37*, p.361.
11. Kinsella, J.E.; Damodaran, S.; German, B. *New Protein Foods. Physicochemical and functional properties of oilseed proteins with emphasis on soy proteins in new protein foods.* Altschul, A.M.; Wilcke, H.L., Eds.; Academic Press: New York, 1985, p. 107.
12. Derbyshire, E.; Wright, D.J.; Boulter, D. *Phytochemistry* **1976**, *15*, 3.
13. McDaniel, M.R.; Chan, N., *J. Food Sci.* **1988**, *53*, 93.
14. Dumont, J.P.; Land, D.G., *J.Agric. Food Chem.* **1986**, *34*, 1041.
15. Tolstoguzov, V.B., *Food Hydrocolloids* **1991**, *4*, 429.
16. Privalov, P.L.; Khechinashvili, N.N., *J.Mol.Biol.* **1974**, *86*, 665.
17. Scatchard, G., *Ann. N.Y. Acad. Sci.* **1948**, *51*, 660.
18. *Biophysical Chemistry*; Cantor, Ch.R.; Schimmel, P.R., Eds. W.H.Freeman and company, San Francisco, 1980, Part III, ch. 15.
19. Semenova, M.G.; Antipova, A. S., Misharina, T. M.; Golovnya, R. V., *unpublished*.

20. Vaintraub, I.A. *Vegetable Proteins and their biosynthesis*; Kretovich, V.L., Eds.; Nauka: Moscow, 1975, p. 142 (in Russian).
21. Plietz, P.; Damaschun, G.; Zirwer, D.; Gast, K.; Schlesier, B.; Schwenke, K.D., *Kultur-pflanzen*. **1984**, 32, 159.
22. Lawrence, M.C.; Izard, T.; Beuchat, M.; Blagrove, R.J.; Colman, P.M., *J. Mol. Biol.* **1994**, 238, 748.
23. Semenova, M.G.; Antipova, A.S.; Wasserman, L. A.; Leontiev, A. L.; Misharina, T.A.; Golovnya, R.V. *unpublished*.
24. Damodaran, S.; Kinsella, J.E., *J. Agric. Food Chem.* **1981**, 29, 1253.
25. Utsumi, Sh.; Nacamura, T.; Mori, T., *J. Agric. Food Chem.* **1983**, 31, 503.
26. Belyakova, L.E.; Semenova, M.G.; Antipova, A.S., *Colloids and Surfaces, B:Biointerfaces*. **1999**, 12, 271.
27. Dickinson, E. *J. Chem. Soc. Faraday Trans.* **1998**, 94, 1657.
28. Suurkuusk, J. *Acta Chim. Scand.* **1974**, B28, 409.
29. Pfeil, W. *Biochemical Thermodynamics.*; Tones, T.N., Ed. Elsevier: Amsterdam, 1988, ch. 2.

Chapter 25

Release of Volatile Oxidation Products from Sunflower Oil and Its Oil-in-Water Emulsion in a Model Mouth System

Saskia M. van Ruth¹ and Jacques P. Roozen²

¹Department of Food Science and Technology, Division of Nutritional Sciences,
University College Cork, Cork, Ireland

²Department of Food Technology and Nutritional Sciences, Wageningen
Agricultural University, P.O. Box 8129, 6700 EV Wageningen, the Netherlands

The amounts secondary lipid oxidation products formed in vegetable oils, which are available for perception, are determined by both lipid oxidation rates and release from the matrix. In the present work, the influence of fatty acid composition and emulsification on lipid oxidation rates and release were determined during oxidation of vegetable oils at 60 °C. Volatile compounds were released from sunflower oil, a blend of sunflower and linseed oil, and from their 40 % oil-in-water emulsions in a model mouth system and were analyzed by gas chromatography-sniffing port analysis. Higher polyunsaturated fatty acid content and emulsification of the oil resulted in more odor active compounds and greater amounts available for perception. Higher concentrations in the oil phase of these samples revealed increased lipid oxidation rates. Reference compounds added to the samples demonstrated an increase in aroma release from the oil under mouth conditions for most of these compounds. In contrary, the higher static headspace concentrations of reference compounds were higher for the emulsion than for the oil.

A major part of flavor research has dealt with analysis of volatile compounds, which is not surprising since the nose is capable of detecting hundreds of different odors. To elicit a response, an aroma compound must achieve a sufficient concentration in the vapor phase to stimulate the receptors in the nasal cavity during eating. The rate of volatilization depends upon the partition coefficient of the compound, molecular interactions between aroma compounds, the ambient temperature, the composition and viscosity of the food material, and binding to components of the food (*1*).

Analysis of volatiles in the gaseous headspace above food samples has been widely used to determine factors affecting their partitioning between the product and vapor phase (2-6). A variety of methods have been used to sample and/or isolate the trace volatiles present in such headspace. However, the term "headspace" as applied to these sampling techniques has been used to convey a number of different meanings. Headspace could be defined as the gaseous mixture surrounding a sample within a closed system at equilibrium. However, many "headspace" determinations involve the passage of a gas over the sample to sweep the volatiles into a trapping device. Under these non-equilibrium conditions, the composition of the sample as subsequently determined, i.e. the ratios of the individual volatiles, may bear little relation to the real headspace composition. As measurements in the equilibrium headspace provide information regarding factors influencing the partitioning of aroma compounds between a product and vapor phase, the dynamic headspace measurements might be useful to simulate the aroma release from products when food is sniffed prior to eating. In actual eating situations, aroma concentrations are determined kinetically rather than thermodynamically because equilibrium is not very likely (7). Only a few instrumental methods of flavor release have incorporated the crushing, mixing, dilution, and temperature conditions required to simulate aroma release in the mouth. Lee (8) reported an instrumental technique for measuring dynamic flavor release. A mass spectrometer was coupled with a dynamic headspace system, i.e. a vial with several small metal balls. The vial was shaken and the balls simulated chewing, while the headspace was flushed with helium gas in order to displace volatile compounds, one of which was analyzed directly by mass spectrometry. Roberts and Acree (7) reported a "retronasal aroma simulator", a purge-and-trap device made from a blender. It simulated mouth conditions by regulating temperature to 37 °C, adding artificial saliva, and using mechanical forces. Naßl *et al.* (9) described a "mouth imitation chamber", which consisted of a thermostated 800 mL vessel with a stirrer, while artificial saliva was added to the system. The authors of the present work presented their model mouth system for the first time in 1994 (10). The model mouth system has a similar volume as the human mouth. It is temperature controlled, and the sample is salivated and masticated. Later, it was shown that the release of volatiles from rehydrated vegetables in this model mouth did not differ significantly from release in the mouth of volunteers (11).

Both oil-in-water (e.g. milk, cream, salad dressings, and mayonnaise) and water-in-oil types (e.g. butter, margarine) emulsions are common in foods (12). Fats modify the perception of flavor compounds by influencing partitioning between the food product, saliva, and vapor phase within the oral cavity (13). The general effects of food composition and fat phase volume on flavor release have been reviewed (14), and several theoretical physicochemical models have been developed (15-16). Initially, studies were carried out to determine the partition coefficients of aroma compounds between air and water or oil (2). It soon became apparent that simple partition coefficients did not explain the release of volatiles from foods.

Volatile lipid oxidation products are important for the aroma of oils and emulsions. The perception of aroma of the latter depends on the formation of the aroma compounds as a result of lipid oxidation as well as on the release of these

compounds. The authors have shown previously the development of aroma compounds in sunflower oil and its emulsion during storage, which was related to aroma generation and aroma release (17). Fatty acid composition of the lipid phase and emulsification can both influence formation and release of compounds. In the present work, the influence of fatty acid composition and emulsification on lipid oxidation rates and release were determined during oxidation of vegetable oils.

Experimental Procedures

Experimental Samples

Sunflower oil (SFO), and a blend (VEGO) of SFO (85/100 W/W) and linseed oil (15/100 W/W) and their 40 % oil-in-water emulsion (SFO-E and VEGO-E; 40/100 W/W sunflower oil, 59/100 W/W deionized water, 1/100 W/W Tween 60) were supplied by Unilever Research Vlaardingen (Vlaardingen, the Netherlands). The C16-18 fatty acid composition determined by gas chromatography of methyl esters was for SFO: 6.0 % 16:0, 4.3 % 18:0, 23.6 % C18:1, 64.3 % C18:2, 0.12 % C18:3, and for VEGO 5.8 % C16:0, 0.01 % C16:1, 4.2 % C18:0, 23.0 % C18:1, 56.9 % C18:2, 8.5 % C18:3. SFO contained 716 mg α -, 26 mg β -, 7 mg γ -, and < 5 mg δ -tocopherol per kg oil, VEGO contained 609 mg α -, 22 mg β -, 73 mg γ -, and < 5 mg δ -tocopherol per kg oil (AOCS Official Method Ce 8-89, 1992). The emulsion was prepared using a homogenizer (APV Gaulin model LAB 40-10 RBFI, APV Gaulin GmbH, Lübeck, BRD) at 150 bar for 10 min. The average particle size in the emulsion was 1.0 μ m (Coulter Laser measurements) and stable during storage at 60 °C for 8 days. For lipid oxidation experiments, samples (65 mL) were stored in glass jars (350 mL) in the dark at 60 °C for 4 days.

For volatility and aroma release experiments, propanal, butanal, pentanal, hexanal, octanal (aldehydes: PolyScience, Niles, IL), 1-pentanol (Sigma-Aldrich, Steinheim, Germany), 3-pentanol (Aldrich, Milwaukee, WI), 1-penten-3-one (Sigma-Aldrich, Steinheim, Germany), 1-penten-3-ol and 1-octen-3-ol (both: Janssen Chimica, Geel, Belgium) were added to the fresh oils and emulsions in duplicate (0.1 % V/V). The solutions were incubated for 24 h at 4 °C in the dark before being subjected to analysis. Volatile compounds formed in the control samples, i.e. oils and emulsions without added compounds stored under the same conditions, were determined and their amounts subtracted.

Static Headspace Analysis

For static headspace gas chromatography (SHGC), 2 mL oil or emulsion, or 1 mL oil or emulsion and 1 mL artificial saliva (18) were transferred into a 10 mL vial and incubated at 60 °C for 10 min in the headspace unit of a Carlo Erba MEGA 5300 GC (Interscience bv, Breda, the Netherlands). The GC was equipped with a DB-Wax column (J&W Scientific, Folsom, CA), 30 m length, 0.53 mm i.d., film thickness 1 μ m

and a flame ionization detector (FID) at 275 °C. An initial oven temperature of 60 °C for 5 min was used, followed by a rate of 3 °C min⁻¹ to 110 °C and then by 4 °C min⁻¹ to 170 °C. Each (stored) sample was analyzed in duplicate vials. Peak areas were standardized with known concentrations in oils and emulsions. Results were calculated as mmoles per kilogram oil.

Isolation of Volatile Compounds

Volatile compounds were isolated from the oil or emulsion in a model mouth system as described previously (10). Artificial saliva (4 mL) was transferred to the sample flask (70 mL) of the model mouth system, which was kept at 37 °C, and a sample of oil and emulsion (4 mL) was added. The headspace was flushed with purified nitrogen gas (100 mL min⁻¹) for 2 min to trap the volatile compounds in 0.1 g Tenax TA (diameter 0.25-0.42 mm, Alltech Nederland bv, Zwijndrecht, the Netherlands). During isolation of the volatiles, a plunger made up and down screwing movements in order to simulate mouth movements.

Gas Chromatography/Sniffing Port Analysis (GC/SP)

In GC/SP, desorption of volatile compounds from Tenax was performed by a thermal desorption (245 °C, 5 min)/cold trap (-120 °C/260 °C) device (Carlo Erba TDAS 5000, Interscience bv, Breda, the Netherlands). Gas chromatography was carried out on a Carlo Erba MEGA 5300 (Interscience bv, Breda, the Netherlands) equipped with a Supelcowax 10 capillary column, 60 m length, 0.25 mm i.d., film thickness 0.25 µm and a FID at 275 °C. An initial oven temperature of 40 °C was used, followed by a rate of 2 °C min⁻¹ to 92 °C and then by 6 °C min⁻¹ to 272 °C. At the end of the column the effluent was split 1:2:2 for FID, sniffing port 1, and sniffing port 2, respectively. In volatility/release experiments, the sniffing ports were not occupied and the FID response was used only (20 % of the effluent). In regular GC/SP sessions two assessors were sniffing and FID response was recorded simultaneously. Ten assessors were selected based on their sensitivity, memory, ability to recognize odors, and availability. These assessors were trained on the technique of sniffing prior to sniffing the effluent of the oil and emulsion samples. Assessors used portable computers with a program in Pascal for data collection. The data were converted from the field discs into Microsoft Excel software in order to process the raw data. Aroma descriptors were generated during preliminary GC/sniffing experiments and clustered after group sessions of the panel, resulting in a list of 19 descriptors (green, mushroom, spicy, fruity, sweet, flowers, fatty, oil, rancid, rotten, musty, chemical/glue, nuts, almond, burned, caramel, chocolate, vanilla, sharp/irritating). These descriptors and "other/I do not know" had to be used for each compound detected by the assessors at the sniffing port. Tenax tubes without adsorbed volatile compounds were used as blank samples for determining the signal-to-noise level of the group of assessors. For identification

odor descriptors and the number of assessors perceiving a compound at the sniffing port were compared with those of authentic compounds at similar concentrations.

Gas Chromatography/Mass Spectrometry

Volatile compounds were isolated as described above and were identified by combined GC (Varian 3400, Varian, Walnut Creek, CA, USA) and mass spectrometry (MS; Finnigan MAT 95, Finnigan MAT, Bremen, Germany) equipped with a thermal desorption/cold trap device (TCT injector 16200, Chrompack bv, Middelburg, the Netherlands). Capillary column and oven temperature program were the same as those used in “gas chromatography of isolated volatile compounds”. Mass spectra were obtained with 70 eV electron impact ionization, while the mass spectrometer was continuously scanning from m/z 24 to 400 at a scan speed of 0.7 s/decade (cycle time 1.05 s).

Statistical Analysis

Analysis of variance (ANOVA) was used to determine significant differences between the means of quadruple analysis of aroma compounds released in the model mouth. If significant differences were found, Fisher's Least Significant Difference tests (LSD) were performed (19). The GC/SP data were subjected to Friedman two-factor ranked analysis of variance (19). Significance level is $p < 0.05$ throughout the study.

Results and Discussion

The volatile compounds of SFO, VEGO, and their emulsions were isolated in the model mouth system and analyzed by GC/SP after four days of storage at 60 °C. Figure 1 represents the chromatogram of aroma compounds of VEGO-E obtained by sniffing port detection. GC/SP revealed 14 compounds possessing detectable odors. The aroma compounds were identified by GC/MS, and by comparison of their retention times, odor descriptions, and number of assessors perceiving the compounds with those of authentic compounds. The aroma compounds were characterized by their FID peak areas and the odors described by the assessors of the sniffing panel (Table I). GC sniffing of dummy samples showed that detection of an odor at the sniffing port by one or two of ten assessors can be considered as “noise”. Odor descriptors and numbers of assessors perceiving the odor active compounds are listed for the various samples in Table I. The authors showed in a previous experiment that numbers of assessors perceiving compounds are related to the perceived intensity at the sniffing port (20). A number of odor active compounds were in common: hexanal, octanal, and 1-octen-3-one. Across all samples, pentanal, hexanal, and 1-octen-3-one were most frequently detected by the assessors. Many of the odor active compounds identified can be formed in autoxidation of linoleic acid,

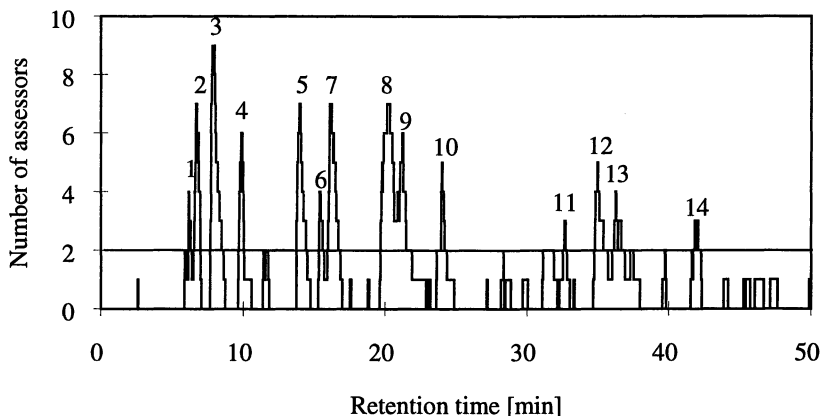


Figure 1. Sniffing chromatogram of a the 40 % oil-in-water emulsion of a blend of sunflower and linseed oil after 4 days of storage at 60 °C

which is the major fatty acid of SFO and VEGO, e.g. pentanal, hexanal, octanal, pentanol, 1-octen-3-one, and 1-octen-3-ol (21-23). Despite the common compounds, the numbers of assessors perceiving individual compounds differed significantly between the various samples (Friedman two-factor ranked analysis of variance, $p < 0.05$). Higher values were observed for the emulsions than for the oils, as well as for the oil with the higher concentration unsaturated fatty acids (VEGO). Figure 2 represents the relative FID peak areas of the formed compounds released from the different samples. The same trends are shown as for the sniffing data in Table 1, except for hexanal where SFO was not found to be less intense than SFO-E by sniffing. However, relative differences are generally greater for the FID data, which is probably due to the log linear relationship between the physical concentration of a compound in the GC effluent and the number of assessors perceiving an odor active compound (24). The differences observed between the samples, which originated from emulsification and fatty acid composition, could result from differences in formation of the compounds, as well as from differences in release from the matrix.

In order to study the formation aspect, the release of compounds formed was related to known concentrations in the oil and emulsions (calibration curve) and the amounts formed in the oil phase were calculated for those compounds with sufficient FID response (Table II). ANOVA of the amounts formed in the oil phase showed significant differences ($p < 0.05$) between the samples. As before, VEGO-E showed highest values, followed by SFO-E, VEGO and SFO, respectively (LSD, $p < 0.05$). The differences due to emulsification are in agreement with results of Frankel *et al.* (25), which showed increased formation of volatile secondary lipid oxidation products in emulsions in comparison with bulk oils. In contrary to the one phase oil matrix, in the emulsion the various molecules partition themselves between the three different regions of the emulsion system according to their polarity and surface activity. The precise molecular environment of a molecule may have a significant effect on its chemical reactivity or other properties in such a system (26). Another

Table I. Odor active compounds released from sunflower oil, a blend of sunflower and linseed oil, and their emulsions after 4 days of storage at 60 °C, odor descriptions and numbers of assessors perceiving the compounds in GC/sniffing port analysis

<i>Compound</i>	<i>Odor description</i>	<i>SFO</i> ¹	<i>SFO-E</i> ²	<i>VEGO</i> ³	<i>VEGO-E</i> ⁴
1. Pentane	Fruity, sweet, chemical	5	-	4	4
2. Heptane	Chemical, sweet, oil	-	-	-	8
3. Propanal	Chemical, fruity, fatty, sweet, oil rancid, sharp/irritating	-	-	3	10
4. Butanal	Oil, spicy, chocolate, fatty	-	7	-	9
5. Pentanal	Chemical, rancid, green, fatty, caramel	-	9	6	9
6. Unk ⁶	Chemical, oil	-	-	-	3
7. 1-Penten-3-one	Chemical, oil, musty	-	-	6	9
8. Hexanal	Green, flowers, fatty, oil, chemical	8	9	7	7
9.3-Pentanol	Chemical, rancid	-	9	4	5
10. Unk	Chemical, sweet, green	-	5	-	5
11. 1-Pentanol	Chemical, rancid	-	3	-	3
12. Octanal	Fruity, oil	3	5	3	5
13. 1-Octen-3-one	Mushroom, musty, rancid	4	9	6	4
14. 1-Octen-3-ol	Musty, oil, rancid, almond	-	4	-	4

¹SFO = sunflower oil.

²SFO-E = 40 % sunflower oil-in-water emulsion.

³VEGO = blend of vegetable oils.

⁴VEGO-E = 40 % blend of vegetable oils-in-water emulsion.

⁵At or below detection level (Q two assessors perceiving an odor).

⁶Unk = unknown, not identified.

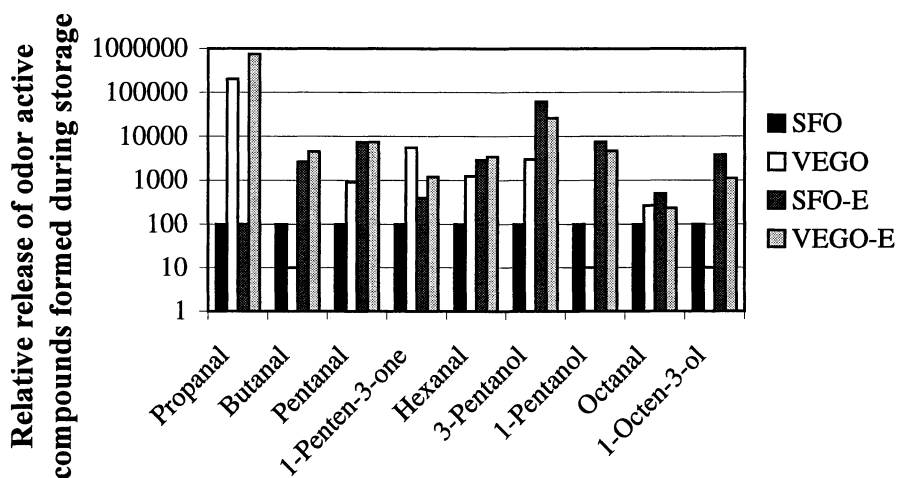


Figure 2. Relative release of odor active compounds in a model mouth system, which were formed in sunflower oil (SFO), a blend of sunflower and linseed oil (VEGO) and their 40 % oil-in-water emulsions (SFO-E and VEGO-E) during storage at 60 °C for 4 days, based on GC/FID analyses. Release of odor active compound from SFO = 100.

Table II. Amounts¹ of odor active compounds formed in oils and emulsions

Compound	SFO ²	SFO-E ³	VEGO ⁴	VEGO-E ⁵
Propanal	<0.001	<0.001	6.907	20.880
Butanal	0.007	0.255	<0.001	0.440
Pentanal	0.409	45.980	3.683	45.775
1-Penten-3-one	0.002	0.014	0.095	0.043
Hexanal	0.163	9.625	0.163	11.450
3-Pentanol	<0.001	0.395	0.007	0.166
1-Pentanol	0.002	0.638	<0.001	0.399
Octanal	0.003	0.078	0.009	0.036
1-Octen-3-ol	0.002	0.470	<0.001	0.136

¹mmol/kg oil.

²SFO = sunflower oil.

³SFO-E = 40 % sunflower oil-in-water emulsion.

⁴VEGO = blend of vegetable oil.

⁵VEGO-E = 40 % blend of vegetable oils-in-water emulsion.

factor important with regard to lipid oxidation in emulsions is the orientation of the lipid molecules in the interfacial region, because this will affect their accessibility to attack by water-soluble, reactive oxygen species (e.g. hydrogen peroxide, hydroxyl radicals and perhydroxyl radicals). Furthermore, emulsions have a highly dynamic nature as emulsion droplets are in continuous motion. Non-polar molecules may be transferred between droplets as a result of droplet-droplet collisions. These phenomena can have a significant influence on lipid oxidation in emulsified systems (27) and result in differences between emulsions and their bulk oils. Also the fatty acid composition influences the formation of aroma compounds significantly. The aroma composition reflects the fatty acid composition of the oils: highly unsaturated fatty acids are particularly susceptible to lipid oxidation (28). These fatty acids are present in increased amounts in VEGO, which is shown by the increased formation of volatile compounds in general and compounds formed specifically from linolenic acid, e.g. propanal (29).

The release aspect was studied by addition of reference compounds to the oils and emulsions. Preliminary experiments showed no effect of fatty acid composition. The effect of emulsification and the effect of artificial saliva in the model mouth system on the release of these compounds are presented in Figure 3. Under conditions as used in the lipid oxidation experiments, which included addition of artificial saliva in the model mouth system, the release of the early eluting compounds (propanal, butanal, pentanal, 1-penten-3-one, and hexanal) was increased in the emulsion, in comparison to the oil. The compounds 1- and 3-pentanol, octanal, and 1-octen-3-ol

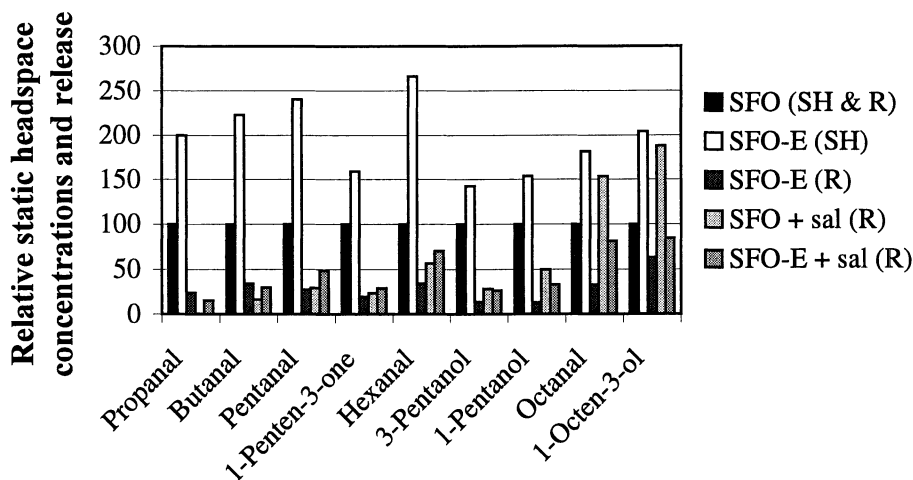


Figure 3. Relative static headspace concentrations (SH) of reference odor active compounds added to sunflower oil (SFO) and its 40 % oil-in-water emulsion (SFO-E) and their release (R) in a model mouth system with (+sal) and without addition of artificial saliva. SH and R of reference compound from SFO = 100.

showed the opposite trend and were released in higher quantities from the oil than from the emulsion. Emulsification has obviously a different effect on the release of these odor active secondary lipid oxidation products, which in turn may affect the perceived aroma of oils and emulsions. Therefore, the differences in aroma composition observed in the lipid oxidation study were not only due to differences in formation rate of these compounds. The artificial saliva is an important factor in release of volatile compounds in this model mouth system, as is shown in Figure 3 as well. Without addition of saliva, each of the compounds is released at a higher rate from the oil, which is in contrast with the static headspace concentrations of the compounds, which are higher for the emulsion than for the oil. Volatility (partitioning of compounds over product and vapor phase), as measured in static headspace analysis, is influenced by emulsification as was shown by Roozen *et al.* (30), Hatchwell (31), and Bakker and Mela (32); and certainly influenced the release of compounds. Vapor/product partition coefficients determine the potential extent of aroma release and lipids were shown to have the greatest effect on the partitioning of aroma compounds between product and vapor phase (33). However, Harrison *et al.* (34) predicted that at short times ($t < 100$ s) the partition coefficients of volatile compounds would have little effect on aroma release from emulsions/oils, which is confirmed by the present data (isolation time 120 s). Mass transfer is the other important factor in aroma release and determines the rate at which aroma compounds are released in the vapor phase. Mass transfer is determined by the texture of the product (viscosity, emulsion droplet size, etc.), the rate of surface renewal, and the surface area of the product (33). In the present work, mass transfer is considered to be an important factor, since differences in partitioning are opposite to differences in aroma release. The viscosity of the oil and emulsion could attribute to the observed differences as was demonstrated by Harrison *et al.* (34). These authors reported that the emulsion/oil viscosity was an important physical parameter affecting the mass transfer coefficient in emulsions. Moreover, it was shown that the emulsion viscosity increased with increasing oil fraction.

The present work demonstrates that emulsification and fatty acid composition influenced the formation of volatile secondary oxidation products, which contributed to the aroma. Emulsification also affected the release of the aroma compounds, which includes volatility and mass transfer factors.

Acknowledgements

The authors wish to thank Unilever Research Vlaardingen for financial support and sample materials. Furthermore, they wish to acknowledge Maarten Posthumus (Wageningen Agricultural University) for excellent GC/MS work.

References

1. Kinsella, J. E. *INFORM* **1990**, *1*, 215-226.
2. Buttery, R. G.; Ling, L. C.; Guadagni, D. G. *J. Agric. Food Chem.* **1969**, *17*, 385-389.
3. Dalla Rosa, M.; Pittia, P.; Nicoli, M. C. *Ital. J. Food Sci* **1994**, *4*, 421-432.
4. Salvador, D.; Bakker, J.; Langley, K. R.; Potjewijd, R.; Martin, A.; Elmore, J. S. *Food Quality and Preference* **1994**, *5*, 103-107.
5. Guyot, C.; Bonnafont, C.; Lesschaeve, I.; Issanchou, S.; Voilley, A.; Spinnler, H. E. *J. Agric. Food Chem.* **1996**, *44*, 2341-2348.
6. Landy, P.; Courthaudon, J. -L.; Dubois, C.; Voilley, A. *J. Agric. Food Chem.* **1996**, *44*, 526-530.
7. Roberts, D. D.; Acree, T. E. *J. Agric. Food Chem.* **1995**, *43*, 2179-2186.
8. Lee III, W. E. *J. Food Science* **1986**, *51*, 249-250.
9. Naßl, K.; Kropf, F.; Klostermeyer, H. *Z. Lebensm. Unters. Fosch.* **1995**, *201*, 62-68.
10. Van Ruth, S. M.; Roozen, J. P.; Cozijnsen, J. L. In *Trends in Flavour Research*, Maarse, H.; van der Heij, D. G., Eds; Elsevier: Amsterdam, 1994, pp. 59-64.
11. Van Ruth, S. M.; Roozen, J. P.; Cozijnsen, J. L. *Food Chem.* **1995**, *53*, 15-22.
12. Barylko-Pikielna, N.; Martin, A.; Mela, D. J. *J. Food Science* **1994**, *59*, 1318-1321.
13. Lee, W. E.; Pangborn, R. M. *Food Technol.* **1986**, *40*, 71-78, 82.
14. McNulty, P. B.; Karel, M. *J. Food Technol.* **1973**, *8*, 309-318.
15. Overbosch, P.; Achterof, W. G. M.; Haring, P. G. M. *Food Rev. Int.* **1991**, *7*, 137-184.
16. Harrison, M.; Hills, B. P. *J. Agric. Food Chem.* **1997**, *45*, 1883-1890.
17. Van Ruth, S. M.; Roozen, J.P.; Jansen, F.J.H.M. In *Proceedings of the 9th Weurman Flavour Research Symposium*, Freising, Germany 1999, in press.
18. Van Ruth, S. M.; Roozen, J. P.; Legger-Huysman, A. In *Flavour Perception. Aroma Evaluation*, Kruse, H. -P.; Rothe, M., Eds; Universität Potsdam: Potsdam, 1997, pp. 143-151.
19. O'Mahony, M. *Sensory Evaluation of Food Statistical. Methods and Procedures*, Marcel Dekker: New York, NY, **1986**.
20. Van Ruth, S. M.; Roozen, J. P., Hollmann, M. E., Posthumus, M. A. *Z. Lebensm, Unters. Forsch.* **1996**, *203*, 7-13.
21. Badings, H. T. (1970). *Ned. Melk-Zuiveltijdschr.* **1970**, *24*, 147-256.
22. Selke, E.; Rohwedder, W. K.; Dutton, J. J. *J. Am. Oil Chem. Soc.* **1980**, *57*, 25-30.
23. Ullrich, F.; Grosch, W. *Z. Lebensm. Unters. Forsch.* **1987**, *184*, 277-282.
24. Van Ruth, S. M.; Roozen, J. P.; Cozijnsen, J. L. *Food Chem.* **1996**, *56*, 343-346.
25. Frankel, E. N.; Huang, S. -W.; Kanner, J.; German, J. B. *J. Agric. Food Chem.* **1994**, *42*, 1054-1059.

26. Wedzicha, B. L. In *Advances in Food Emulsions and Foams*, Dickenson, E.; Stainsby, G., Eds; Royal Society of Chemistry, **1988**, pp. 329-371.
27. Coupland, J. N.; McClements, D. J. *Trends in Food Science and Technology* **1996**, *7*, 83-91.
28. Snyder, J. M.; Frankel, E. N.; Selke, E. *J. Am. Oil Chem. Soc.* **1985**, *62*, 1675-1679.
29. Grosch, W. In *Autoxidation of Unsaturated Lipids*, Chan H.W.S., Ed.; Academic Press: London, **1987**, pp. 95-139.
30. Roozen, J. P.; Frankel, E. N.; Kinsella, J. E. *Food Chem.* **1994**, *50*, 33-38.
31. Hatchwell, L. C. In *Flavor-Food Interactions*, McGorin, R. J.; Leland, J. V., Eds; American Chemical Society: Washington, 1996, pp. 14-23.
32. Bakker, J.; Mela, D. J. In *Flavor-Food Interactions*, McGorin, R. J.; Leland, J.V., Eds, American Chemical Society: Washington, 1996, pp. 36-47.
33. De Roos, K. *Food Techn.* **1997**, *51*, 60-62.
34. Harrison, M.; Hills, B. P.; Bakker, J.; Clothier, T. *J. Food Sci.* **1997**, *62*, 653-658, 664.

Chapter 26

Relative Influence of Milk Components on Flavor Compound Volatility

Deborah D. Roberts and Philippe Pollien

Nestlé Research Center, Vers-Chez-les-Blanc,
CP 44, 1000 Lausanne 26, Switzerland

Although specific interactions between flavor compounds and proteins or carbohydrates are often characterized in simplified model systems, the importance of these effects in more complex fat-containing food is less well-documented. This study determined the relative effects of milk components on flavor compound volatility. Within an experimental design, milk samples with different levels of milk-solids-non-fat (MSNF; milk proteins and lactose) and milk fat were compared. The relative amounts of added flavor compounds in the headspace were determined using Solid-Phase Microextraction GC-FID, using a 1 min adsorption time. Three categories of compound behavior were identified: (1) not influenced by milk component addition (diacetyl, 2,3-pentanedione, guaiacol), (2) reduced in volatility with milk fat but not with MSNF (3-methyl butanal, 2-methylpropanal, 4-ethylguaiacol), (3) reduced in volatility with MSNF and much greater reductions with fat (β -damascenone, 1-octen-3-one). This last group is the only one that showed flavor compound interactions with milk proteins or lactose. However, when fat was present in the system, the level of MSNF did not further influence flavor compound release. This shows that in complex liquid milk systems, compound absorption by fat is the primary retaining mechanism. In addition, measured lipophilicity of the compounds showed a good correlation ($R^2 = 0.9$) with retention by milk for compounds with $k_w > 0.7$.

In our eating experience, flavor compounds exist in the realm of a food product. The final flavor perception is influenced by any chemical interactions with the food components. For this reason, a certain amount of flavor research in recent years has concentrated on a better understanding of these interactions. Proteins, for example, have been shown to bind to certain flavor compounds with measurable binding

constants (1). Instances of reversible and non-reversible binding have been demonstrated (2). One protein in particular, β -lactoglobulin, has been extensively studied because its structure is very well described. Competition phenomena were observed between two compounds presumably binding at the same site. The interactions were investigated in-depth using IR spectroscopy where conformational changes by the protein were seen upon aroma addition. Modelling, headspace, and sensory analysis confirmed that the binding of β -lactoglobulin to compounds leads to lower release rates, lower perception, and a lower headspace concentration for compounds with higher affinity constants (3). Some of these binding effects have been illustrated sensorially as well as chemically. Casein and whey protein added at 0.5 % caused a perceptual decrease for some compounds such as vanillin and limonene (4-5).

Carbohydrates also have the ability to form complexes with aroma compounds, such as with α -amylose from starch (6) or specific binding with hydrocolloids (7). Additionally, hydrocolloids can markedly influence flavor release by changes in viscosity and compound diffusion: up to a 60% decrease in release has been found with 2% CMC added (8). Simple sugars can decrease or increase compound volatility as well but these effects are generally present at rather high concentrations, above 20% w/w (9). Lipids absorb and solubilize lipophilic flavor compounds, as explained by mathematical models (11-12), headspace analysis (13), and sensory analysis (9, 14). Limonene and ethyl heptanoate showed 80% decreases in volatility from water with the inclusion of only 1% vegetable oil (13).

The fact that protein - flavor interactions and oil - flavor interactions are both hydrophobic in nature brings an interesting question: In systems containing both fat and protein, are both interaction effects present or is one effect predominant? While basic model systems are necessary to show specific binding to proteins or carbohydrates, further testing on more complex systems will indicate if the binding is significant in real food products. This work seeks to take the next step in determining the relative importance of milk components (fat vs. protein/carbohydrates) in the binding and release of flavor compounds.

Experimental

Experimental Design

Two independent factors were assessed for their ability to influence flavor release: fat and milk-solids-non-fat (MSNF). Both factors were varied independently, as seen in the experimental design (Figure 1).

The extreme points of MSNF and fat content were studied as well as a middle point. The double point at the high level represents samples prepared with two different milk sources. One was a commercial UHT whole milk and the other was the in-house preparation. The zero point is water.

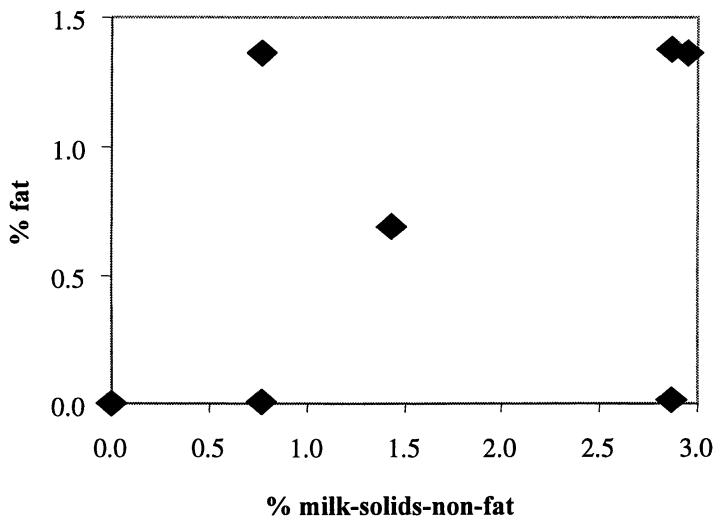


Figure 1. Experimental design for samples studies showing the choice of fat and milk-solids-non-fat levels.

Analysis of covariance was used with time between sample vial preparation and analysis as the covariant. This time showed a significant effect for 3 compounds: 2,3-pentanedione, 3-methyl-2-butanal, and 1-octen-3-one where the longer the time, the smaller the headspace peak. A multiple comparison test (Fisher's LSD, $\alpha = 0.05$) was used to determine significant differences among the samples.

Sample Preparation

The ingredients (Table I) were mixed together (except the butterfat) and heated to 60 °C. The mixture was pre-emulsified at 60 °C using a hand-held Ultraturrax for 3 min at 8000 min⁻¹ using the medium size dispersing head. During this pre-emulsification, the butterfat was added in small portions. With stirring, the mixture was then homogenised with three passes using a Buchi homogeniser at 65°C. The sample was cooled on ice and then stored in the refrigerator until use.

The fat globule size of the samples was checked microscopically and found to be of a similar size to pasteurized milk. The Malvern Mastersizer (Malvern, UK) was also used and 85% of the fat globules were found to be under 1 micron.

Table I. Recipes for Milk Preparations that Represent the Experimental Design Points in Figure 1.

<i>Skim Milk</i> ¹ (g)	<i>Butterfat</i> (g)	<i>Whole Milk</i> <i>UHT</i> (g)	<i>Water</i> (g)	<i>% MSNF</i> ²	<i>% Fat</i> ²
48	0	0	32	2.87	0.02
12.8	2.176	0	65	0.77	1.36
12.8	0	0	67.2	0.77	0
24	1.088	0	54.9	1.43	0.69
48	2.176	0	29.8	2.87	1.38
0	0	54.4	25.6	2.95	1.36
0	0	0	80	0	0

¹ Skim milk was prepared from low heat skim milk powder by adding 20 g to 180 g of water.

² % MSNF and % Fat were determined based on a proximate analysis of the skim milk powder and whole milk UHT.

Table II shows the flavor compounds chosen for this study. The compounds were analyzed in two batches of compounds that were shown to be stable together. The concentrations of aroma compounds were chosen so that they were in the linear quantification range of the SPME fiber. The aroma compounds were dissolved in water with extended vial shaking. They were prepared at double concentration as in Table II. Milk solutions (400 mg) and aqueous aroma solutions (400 mg) were added to silylated 2 mL glass vials (7 total preparations) and mixed without inverting the vial. A minimum time of 2 hours was determined for equilibration. The vials were kept at room temperature between 2 and 20 hours before analysis for batch 1 and 2 to 12 hours for batch 2.

Table II. Information about Aroma Compounds.

<i>Compound</i>	<i>Lipophilicity</i> (<i>k_w</i>)	<i>k_w</i> (<i>ref. 16</i>)	<i>Conc. used</i> (<i>ppm</i>)	<i>Batch #</i>	<i>Supplier</i>
Diacetyl	-0.3	-0.25	10	1	Fluka
2,3-Pentanedione	0.21	0.24	10	1	Fluka
3-Methylbutanal	1.24		10	1	Fluka
2-Methylpropanal	0.67		10	1	Fluka
3-Methyl-2-butenal	0.75		10	1	Aldrich
Guaiacol	0.97		10	2	St-Fons Chemie
4-Ethylguaiacol	1.87		10	2	Oxford
1-Octen-3-one	2.09		2	2	Oxford
β -Damascenone	2.79		2	2	Firmenich

Headspace Analysis by SPME GC-FID

After a 1 hour equilibration at room temperature in the SPME carousel (29°C), the headspace of the samples was sampled using a Varian 8200 autosampler. A SPME (Solid phase microextraction) fiber was inserted into the headspace and allowed to equilibrate for 1 min exactly. This time was chosen so that the extraction would be primarily from the headspace and not from the sample. The fiber used was polydimethylsiloxane with 100 μm thickness. It was placed into the injection port of the GC for 5 minutes at 250 °C containing a 0.75 mm ID liner. During the first three minutes of desorption, the purge was off and the last two minutes with purge on further cleaned the fiber. GC separation with FID detection was used for quantification of the aroma compounds (DBWAX, J&W, 30 m; 0.32 mm ID, 0.25 μm film, 10 psi helium). Milk blanks were checked and no contaminating peaks over 1 % area were found.

Aroma Compound Lipophilicity Measurement

Compound lipophilicity was determined based on its retention time on a reversed phase HPLC column (15). The conditions were the same as those used previously to measure 96 different compounds (16) so the values obtained can be directly compared. The HPLC used was a Hewlett Packard series 1100 with diode array and HP1097A refractive index detection (Avondale, PA, USA). The column used (250 mm x 4 mm) was packed with Nucleosil 50-5 C18, particle size 5 μm (Macherey-Nagel, Oensinger, Switzerland). The mobile phase was made up volumetrically from various combinations (30-70%) of methanol and a solution containing 3-morpholinopropane sulphonic acid buffer (0.01 M) plus n-decylamine (0.2% v/v). The pH of the aqueous solution was adjusted beforehand to 7.4 (4.5 for aldehydes) by addition of HCl. Retention times (t_r) were measured at room temperature with a 1.0 mL/min flow rate. The column dead time (t_0) was determined with uracil. The capacity factor was defined as $k = (t_r - t_0) / t_0$. Log k for 100 % water (low k_w) was linearly extrapolated from results obtained for different mobile phase compositions. Table II shows the lipophilicity values obtained.

Results and Discussion

Figure 2 illustrates the theory behind flavor compound interactions with milk, based on compound lipophilicity and interactions with fat and proteins. Explanations of these three categories of compounds are complemented by Figures 3-6 which show the detailed results of each compound. The headspace concentration of each compound was determined when dissolved in water and in 6 milks of different composition. The placement of the points represents the particular milk studied. The values shown are the headspace concentration relative to water (100) and the different letters correspond to statistically significant differences.

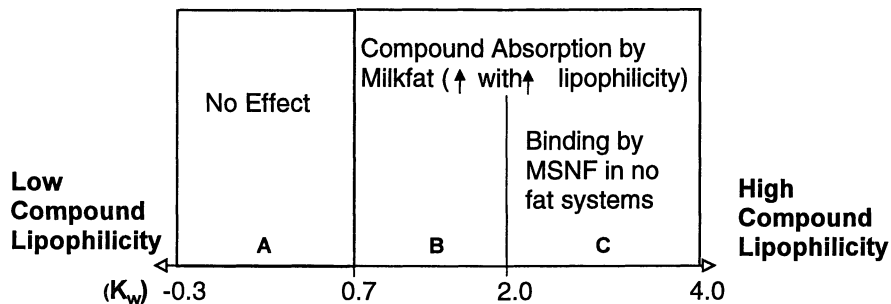


Figure 2. Three categories of compound changes in volatility from water upon milk addition, dependent on compound lipophilicity and milk composition.

(A) No Effect

Figure 3 shows results of compounds from this category. Statistically, the samples were not significantly different in their headspace concentration from water. Another study confirmed this finding: milk fat up to 12% did not influence the partition coefficient of diacetyl at 30 °C and 50 °C (17).

(B) Reduction in Volatility due to Fat but No Effect of Protein/Carbohydrates

As seen in Figure 4, increasing MSNF at a constant fat level (0 and 1.4%) did not change the headspace concentration. However, increasing fat level at a constant 2.9% MSNF level did show reductions in headspace concentration. This category contains moderately lipophilic compounds. 3-Methylbutanal and 2-methylpropanal were slightly affected by the milk fat, with up to 30% reductions in headspace concentration. 4-Ethyl guaiacol was moderately affected by milk fat, with up to 55% reductions in headspace concentration. Although 3-methyl-2-butenal (Figure 5) belongs to this category by its lipophilicity, it is the only compound that has shown low levels of specific binding to MSNF, even in the presence of 1.4% fat.

(C) Large reduction in Volatility due to Fat. Protein/Carbohydrate Effect Only at No Fat.

As seen in Figure 6, the samples that contained fat were markedly different from those fat-free samples. As interactions with proteins are also hydrophobic in nature, β -damascenone and 1-octen-3-one showed effects of MSNF, but only at zero fat content. The hydrophobic nature of fat overrides the protein effect in milks containing both ingredients. These flavor compounds had decreases of up to 94% in the headspace upon milk addition. A protein/carbohydrate binding effect was seen only in the samples without fat. Once fat is present, flavor compound absorption is the primary retaining mechanism.

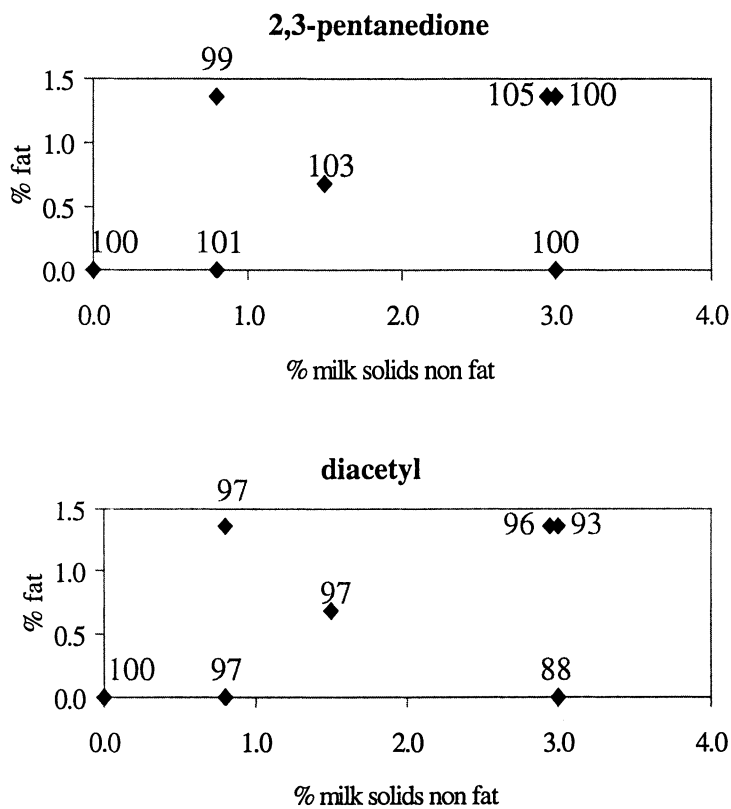


Figure 3. Relative headspace concentrations (water=100) for compounds in the presence of milk of different compositions showing no statistically significant differences from water.

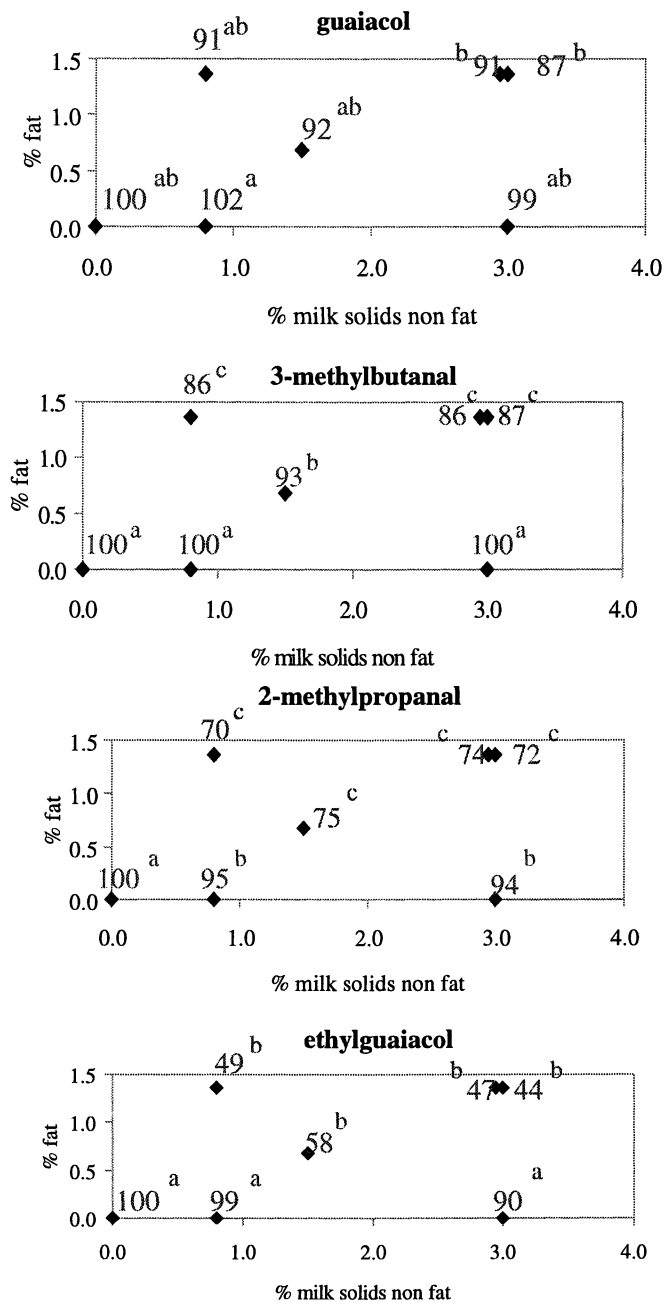


Figure 4. Relative headspace concentrations (water=100) for compounds in the presence of milk of different compositions showing statistically significant effects of fat.

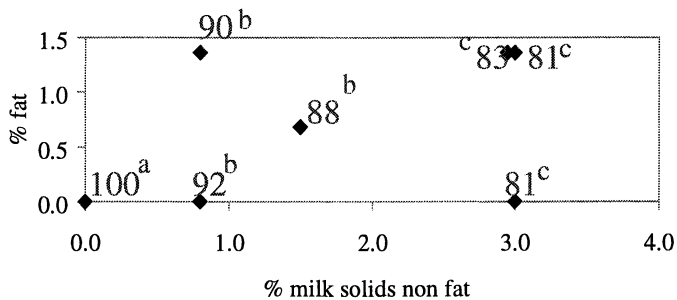


Figure 5. Relative headspace concentrations (water=100) for 3-methyl-2-butenal in the presence of milk of different compositions showing a slight effect of MSNF.

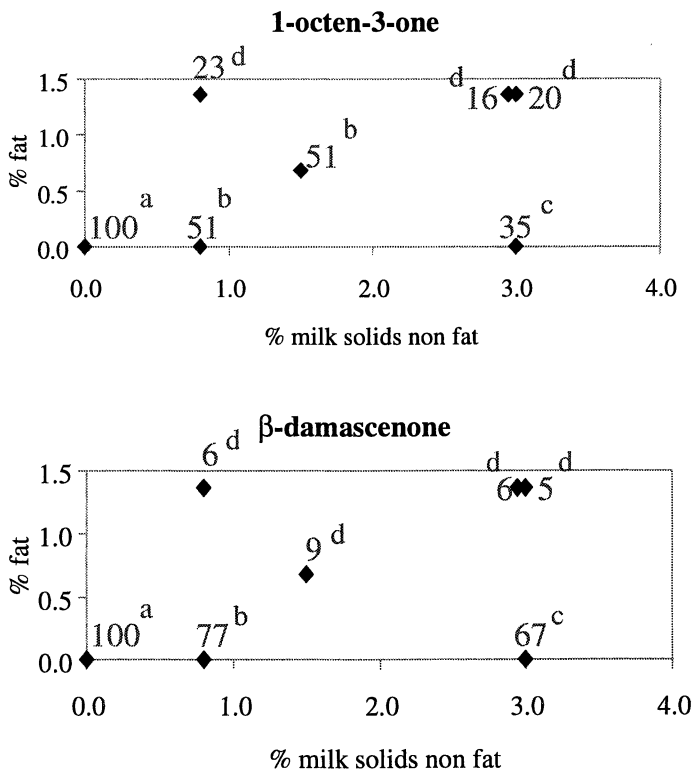


Figure 6. Relative headspace concentrations (water=100) for compounds in the presence of milk of different compositions showing statistically significant effects of fat in the presence of MSNF but not the inverse.

A general observation is, that for most compounds, the mid- and high- fat levels had similar values. The change in headspace concentration from water to a 0.7% fat milk was much larger than doubling the milk amount (to 1.4% fat milk). This indicates a non-linear relationship between fat concentration and headspace amount.

Figure 7 depicts the relationship between compounds' lipophilicity and retention by milk. There appears to be a minimum value of compound lipophilicity (k_w around 0.7) for retention by milk. For a compound with k_w over 0.7, the more the compound is lipophilic, the more it was absorbed by milk fat. A similar relationship between k_w and compound retention by triolein in fresh cheese was also found within a chemical family (18).

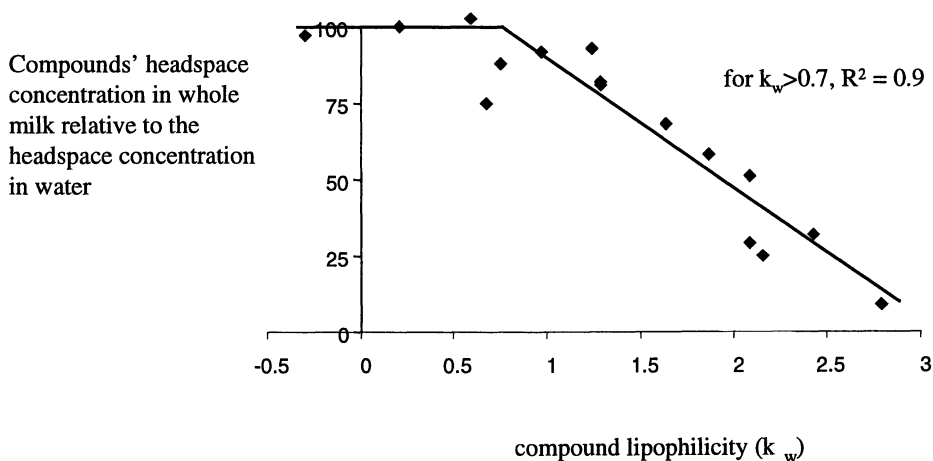


Figure 7. Relationship between compound lipophilicity and relative headspace (water=100) amount when in whole milk containing 0.7% fat and 1.4% MSNF. In addition to compounds from Table II, other compounds were also analyzed to complete the range of lipophilicity.

Figure 8 shows the difference caused by milk fat in the headspace concentrations of these 9 compounds. In the low fat sample, only the most lipophilic compounds showed a significant headspace reduction as compared to water. The higher fat sample showed greater reductions for the highly as well as the moderately lipophilic compounds.

Conclusions

As many food products contain fats, carbohydrates, and proteins, the relative flavor-binding capacity of these constituents was shown using milk as a model. In emulsion systems, milk fat had a much larger effect than binding to milk proteins or

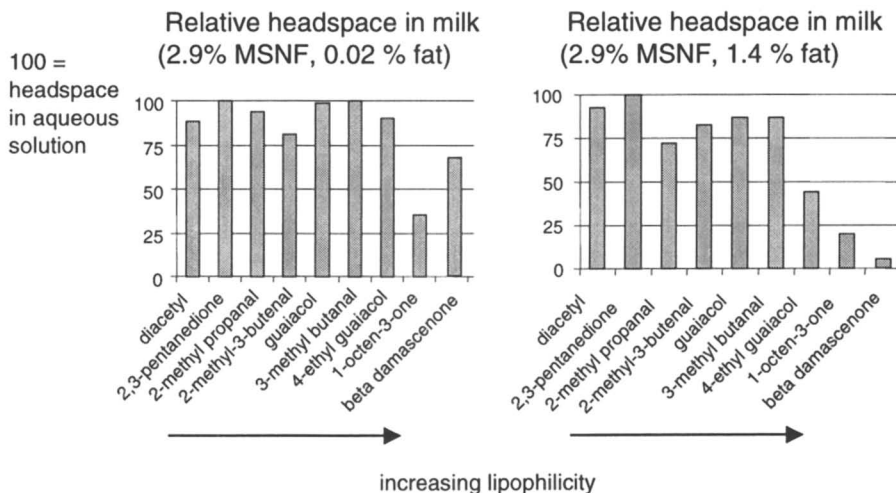


Figure 8. Comparison of flavor compound retention between whole and skim milk.

carbohydrates. Milk with a fat content of only 0.7 % showed substantial flavor absorption (up to 91%). The model based on compound lipophilicity can be used to predict which compounds will change in volatility when going from a non-fat to a fat system as well as which compounds have a potential for hydrophobic protein interactions.

Literature Cited

1. Pelletier, E.; Sostmann, K.; Guichard, E. *J. Agric. Food Chem.* **1998**, *46*, 1506-1509.
2. Overbosch, P.; Afterof, W.G.M.; Haring, P.G.M. *Food Rev. Int.* **1991**, *7*, 137-184.
3. COST 96: Interacton of food matrix with small ligands influencing flavor and texture. Volumes 1-3. 1998. European Communities. Conference Proceeding.
4. Hansen, A.P.; Heinis, J.J. *J. Dairy Sci.* **1992**, *75*, 1211-1215.
5. Hansen, A.P.; Heinis, J.J. *J. Dairy Sci.* **1991**, *74*, 2936-2940.
6. Nuessli, J.; Sigg, B.; Conde-Petit, B.; Escher, F. *Food Hydrocolloids* **1997**, *11*, 27-34.
7. Yven, C.; Guichard, E.; Giboreau, A.; Roberts, D. *J. Agric. Food Chem.* **1998**, *46*, 1510-1514.
8. Roberts, D.D.; Elmore, J.S.; Langley, K.R.; Bakker, J. *J. Agric. Food Chem.* **1996**, *44*, 1321-1326.

9. Ebeler, S.E.; Pangborn, R.M.; Jennings, W.G. *J. Agric. Food Chem.* **1988**, *36*, 791-796.
10. Nawar, W.W. *J. Agric. Food Chem.* **1971**, *19*, 1057-1059.
11. de Roos, K.B.; Wolswinkel, K. In *Trends in Flavor Research*; Maarse, H., van der Heij, D.G., Eds.; Elsevier: Amsterdam, 1994; pp 15-32.
12. Harrison, M.; Hills, B.P.; Bakker, J.; Clothier, T. *J. Food Sci.* **1997**, *62*, 653-658, 664.
13. Schirle-Keller, J.P.; Reineccius, G.A.; Hatchwell, L.C. *J. Food Sci.* **1994**, *59*, 813-815.
14. Guyot, C.; Bonnafont, C.; Lesschaeve, I.; Issanchou, S.; Voilley, A.; Spinnler, H.E. *J. Agric. Food Chem.* **1996**, *44*, 2348
15. El Tayar, N.; Van de Waterbeemd, H.; Testa, B. *J. Chromatogr.* **1985**, *320*, 305-312.
16. Piraprez, G.; Herent, M.-F.; Collin, S. *Flavor Fragr.J.* **1998**, *13*, 400-408.
17. Lee, K.D.; Lo, C.G.; Richter, R.L.; Dill, C.W. *J. Dairy Sci.* **1995**, *78*, 2666-2674.
18. Piraprez, G.; Herent, M.-F.; Collin, S. *Food Chem.* **1998**, *61*, 119-125.

Chapter 27

Effect of Beverage Base Conditions on Flavor Release

K. D. Deibler and T. E. Acree

Department of Food Science and Technology,
Cornell University, Geneva, NY 14456

Flavor released from model beverage systems in a Retronasal Aroma Simulator (RAS) was measured using solid phase microextraction (SPME) and gas chromatography mass spectrometry (GC-MS). Treatments, including temperature, air flow, percent acidity, pH, in addition to odorant, sweetener and solvent concentrations, were varied over values commonly used in commercial products. To account for interactive effects of factors, a one fourth replicate of a 2^9 full factorial experimental design was used to determine main effects of the beverage treatments on each odorant. Concentration, airflow, and the interaction of these two factors, affected most compounds consistently. The remaining factors affected the odorants differently. The changes in the ratio of odorants associated with specific ingredient and environmental factors are discussed in terms of their potential to modulate flavor.

A beverage is a complicated mixture with several ingredients that could influence the volatility of odorants. Whenever the composition of a beverage is changed, a new standard state of maximum entropy is established where new interactions result in a different enthalpy state. The high potency sweeteners commonly used in beverages such as sucralose, aspartame, and acesulfame potassium can interact directly with odorant compounds. The sweeteners and acids can affect the ionic environment of the solution modulating volatility indirectly. Solvents and other ingredients can also influence the volatility of odorant compounds both directly and indirectly.

Sensory analyses have shown that the flavor of a beverage was perceptibly different when base ingredients (non-volatile components) of a beverage are changed and the same odorant ingredients used (1, 2). This is evident in many commercial products where there was an attempt to have the same flavor in two beverages with different base solutions such as diet and regular beverages. The goal of this study was to evaluate some of the ingredient and physical factors which may affect the volatility of odorants.

Headspace sampling from a simulated mouth system for aroma analysis is intended to capture volatiles at the concentrations that would come in contact with the olfactory epithelium (3). Due to the very low levels that the odorants are present in a beverage and subsequently in the headspace, direct headspace sampling does not produce enough analyte to be detected with most chromatographic methods, therefore, the headspace is usually concentrated on an absorbant such as with solid phase microextraction (SPME) (4-10). Under static conditions, SPME changes the headspace concentration while it approaches equilibrium; in a dynamic situation, such as in a simulated mouth, the fiber comes to equilibrium without depleting the headspace. However, the use of an appropriately controlled standardization method to account for selectivity of SPME coating materials is required (11).

Experimental Procedures

Stock Solution

The compounds for the ethanol based stock solutions (Table I) were selected based on purity, having odor activity, existence in a beverage (e.g. coffee, citrus), and having no overlapping retention times under the chromatographic conditions used. Since so many compounds had overlapping retention times, two solutions were used to increase the number of compounds that could be evaluated. Compounds were used at levels to produce a model beverage with the odorants at concentrations commonly found in beverages (4.0 – 0.02 parts per million (ppm)).

Table I. Odorants used in stock solutions.

<i>Stock A</i>	<i>CAS #</i>	<i>ppm in Stock</i>	<i>Stock B</i>	<i>CAS #</i>	<i>ppm in Stock</i>
3-methylbutyl acetate	123-92-2	1600	Ethyl valerate	539-82-2	200
Heptanal	111-71-7	800	α -pinene	80-56-8	600
Ethyl valerate	539-82-2	800	Myrcene	123-35-3	600
Benzaldehyde	100-52-7	1600	1,4-cineole	470-67-7	800
Octanal	124-13-0	600	1,8-cineole	470-82-6	800
p-cymene	99-87-6	2000	linalool	78-70-6	600
E-ocimene	13877-91-3	800	isoborneol	124-76-5	100
γ -terpinene	99-85-4	2000	decanal	112-31-2	100
Nonanal	124-19-6	800	neral	5392-40-5	500
Fenchol	1632-73-1	1200	E-cinnamic aldehyde	104-55-2	1000
Camphor	464-49-3	400	geranial	141-27-5	500
Ethyl octanoate	106-32-1	800	undecanal	112-44-7	200
Perilla aldehyde	2111-75-3	1600	geranyl acetate	105-87-3	200
Citronellyl acetate	150-84-5	800	dodecanal	112-54-9	300
Ethyl decanoate	110-38-3	800	ethyl dodecanoate	106-33-2	500
Cinnamyl acetate	103-54-8	1200			

Justification for Sampling from RAS

A solution of stock solution B in 500 mL water was prepared. 50 mL of this solution was allowed to equilibrate for 2 hours in a 75 mL glass bottle with an i.d. of 3 cm and a teflon septum cap. The headspace was extracted for 5 minutes with a SPME with 95 μm thick polydimethylsiloxane (PDMS) coating (Supelco, Bellefonte, PA). The remainder of the solution was placed in a retronasal aroma simulator (RAS) with the humidified air flowing over the solution (3). The "breath" leaving the RAS was sampled by SPME exposed to the flow for 5 minutes and evaluated by gas chromatography mass spectrometry (GC-MS) multiple ion monitoring.

Test Conditions

Nine factors were evaluated within the range used for beverages at minimum, maximum and midpoint values as indicated in Table II. Design-Expert® (Stat-ease, Inc., Minneapolis, MN) was used to design an experiment that accounted for interactive effects of factors by using a one fourth replicate of a 2^9 full factorial experimental design consisting of 133 combinations of the factors. Flavor solution concentration was included to verify that differences could be measured under these test conditions.

Table II. Factors Varied in Experiment

<i>FACTOR</i>	<i>Minimum</i>	<i>Maximum</i>
Temperature (°F)	35	100
Air Flow Rate (mL/s)	50	150
Concentration (relative)	1	10
% Acid	5	10
pH (phosphoric/citric acid)	2.5	3.5
Aspartame (ppm)	100	700
Acesulfame K (ppm)	40	250
Sucralose (ppm)	50	250
Ethanol (ppm)	1	10,000

Model Beverage

A model beverage was prepared to a total volume of 500 mL in a volumetric flask and the stock solution was added just before beginning shearing and extracting air flow. The shearing of the RAS insured complete mixing of the stock solution in the beverage. A single unit concentration refers to a 0.1 mL of the stock solution added, while a 10 units concentration refers to a 10 fold concentration, thus 1 mL of stock solution was added to the beverage. Percent acidity and pH were controlled with phosphoric acid, citric acid and potassium citrate. All ingredients were food grade. The model beverage was placed in the retronasal aroma simulator (RAS) with the

humidified air flowing over the solution (3). The air flow leaving the RAS was sampled by SPME exposed to the flow for 5 minutes and evaluated by gas chromatography mass spectrometry (GC-MS) multiple ion monitoring. The SPME exposure time of 5 min was determined based on the minimum time to reach 90% absorption of the stock solution in 500 mL of water at 15 mL/s air flow rate in the RAS. When using SPME to sample from the RAS, analyte concentration in the flow remained essentially constant due to the large sample size, continual stirring, and the short extraction time. Initially (PDMS) and carbowax/divinylbenzene coated SPME's were used; however, no additional selectivity was gained using the two coatings, so PDMS 95 μm thickness was used for the entire experiment.

SPME fibers were conditioned as recommended by Supelco before use. Before each sampling, the fiber was cleaned at 225 $^{\circ}\text{C}$ for 5 minute in a GC injection port. Periodically RAS flow over 1 mL of stock in 500 mL water was extracted to monitor for coating depletion. SPME blanks were measured to verify no artifacts were interfering with sampling. The fiber was desorbed in a GC-MS for two min at 240 $^{\circ}\text{C}$ with the injection valve closed for the initial one min. GC-MS parameters were: 0.32 mm x 50 m OV101 column in an HP5890 gas chromatograph, constant flow, initial temperature 35 $^{\circ}\text{C}$ for 3 min, increased 4 $^{\circ}\text{C}/\text{min}$ to 150 $^{\circ}\text{C}$, injector temperature 240 $^{\circ}\text{C}$, detector temperature 260 $^{\circ}\text{C}$.

Results and Discussion

In order to measure the volatiles from a beverage which could potentially affect perception, volatiles liberated from a sample in a simulated mouth, a RAS, were evaluated (3). The RAS allowed for control of temperature, flow rate of air over the beverage, and stirring. The stainless steel container provided an inert environment with a relatively large sample size. Figure 1 shows a gas chromatogram of a beverage headspace sampled under static near equilibrium conditions (representing the odorants resulting from opening a bottle of beverage; Figure 1b) compared to a chromatogram of the headspace from the same beverage in the dynamic conditions of a simulated mouth (RAS, representing the actual vapor phase stimulus array of aroma chemicals available when drinking the beverage; Figure 1a). It is noteworthy that some of the major odorants, such as decanal and geranial, became much less prominent in the RAS headspace, while other odorants like ethyl undecanoate almost vanished from the relative array of compounds. Dodecanal, which had the fifth most prominent peak among odorants from the simulated mouth sample, became the predominant volatilized chemical in the static system. On the other hand, ionone was almost non-existent in the static headspace sample, but prominent from the RAS. The different ratio of the volatiles in Figure 1a to 1b demonstrates the importance of sampling headspaces which represent the headspace composition in the mouth.

PDMS-SPME provided sufficient selectivity and concentration power for extraction of the beverage odorants under the controlled situation of this model (11). The replicated midpoints showed a reproducibility of the sampling method and model production with a standard error range of 0.1-3%. Many statistically significant ($p < 0.05$) differences were measured from the robust experimental design.

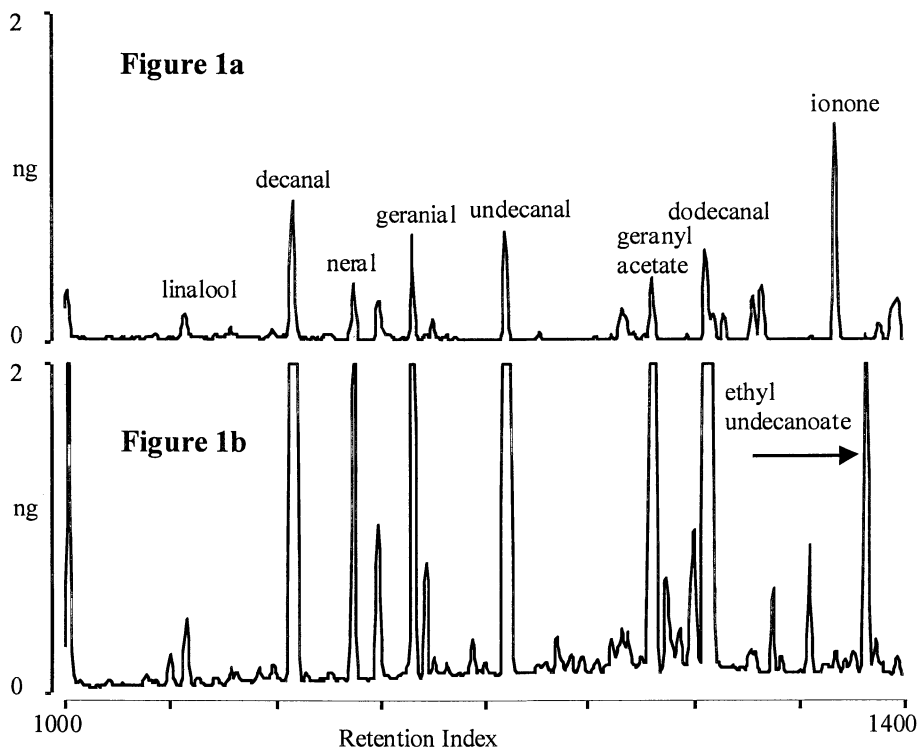


Figure 1. a.) Gas chromatogram of a beverage headspace sampled in the dynamic conditions of a simulate mouth (RAS) b.) Gas chromatogram of the headspace from the same beverage under static near equilibrium conditions.

To select for effects which produced differences of sensory significance, the data was converted using a ratio based on the observation of Weber (12). The human ability for detection of difference, described by the Weber ratio, is linear with concentration, while Steven's law, a power function, describes potency perception (13, 14). The Weber ratio describes the relationship between the perceived intensity of a sensation and the physical amount of the stimulus that produced it and is expressed as: Weber ratio = JND/concentration; where JND is the just noticeable difference (13, 14). For olfaction the Weber ratio has been found to range between 25 to 33% (15). Therefore, this data was converted to the ratio of the change in concentration resulting from varying one factor while holding the other factors constant divided by the average concentration. Since a change of 30% would likely be necessary for a perceivable difference, only changes greater than 30% with a p-value greater than 5% were included. In Tables III-V, data is expressed in multiples of 30%.

Table III. Aspartame Effects

<i>Odorant</i>	<i>Weber-based Ratio</i>
Octanal	4
Perilla aldehyde	-2
α -pinene	-2
Dodecanal	-2
Decanal	-1
Undecanal	-1
Ethyl valerate	-1
Myrcene	-1
Geranyl acetate	+/-1
Geranial	1
Cinnamyl aldehyde	1
γ -terpinene	1
E-ocimene	1

Table IV. Sucralose Effects

<i>Odorant</i>	<i>Weber-based Ratio</i>
Citronellyl acetate	3
Octanal	3
Ethyl valerate	-2
Neral	-2
Isoborneol	+/-2
Camphor	2
Fenchol	2
Nonanal	-1
Undecanal	-1
Dodecanal	-1
Geranial	-1
Ethyl Decanoate	-1
Linalool	+/-1
Perilla aldehyde	1

Table V. Acesulfame potassium Effects

<i>Odorant</i>	<i>Weber-based Ratio</i>
α -pinene	3
Fenchol	2
Myrcene	+/-2
Isoborneol	-1
E-ocimene	1

NOTE: For Tables III-V: Weber based ratio is calculated with all other factors held constant (at their minimum value) while only varying the selected factor at its minimum and maximum values. The ratio equals (odorant concentration at maximum factor value – odorant concentration at minimum factor value)/(average between the odorant concentration at maximum and minimum factor value X 30).

Ranges are used when directional changes due to factor interactions occurred between holding all other factors constant at the minimum versus maximum values.

All of the factors affected some of the odorants to varying magnitudes and directions. For example, geranial increases in volatility with increased concentration of aspartame, but decreases in volatility with increased concentration of sucralose. Sucralose boosted the volatilization of citronellyl acetate, while it suppressed neral. Increasing volatility of some compounds by increasing any of the ingredient concentrations may result in “salting out” due to competition for water; however, this does not explain the selectivity of the effects observed or the suppression of some compounds with increased ingredient concentration.

Many interactions between factors were found, indicating that the amount of an odorant volatilized was dependent on the values of more than one factor. A large

interaction was noted when they would produce an increase or decrease in volatile concentration. For example, as shown in Table III, increasing the aspartame concentration would boost or suppress geranyl acetate volatilization in an interactive function with ethanol concentration and percent acidity. The primary significance of interactions between factors is that they create complicated influences from factors. Thus the effects from an individual factor cannot be evaluated in isolation. Due to the complexity of the interactions, further evaluations are necessary to make meaningful conclusions about the nature of interactions.

As expected, a 10 fold increase in concentration "caused" a consistent 10 fold increase for all odorants. Table VI shows the independent effects of the three physical factors (concentration, air flow rate, and temperature) and the remaining largest effects including interactions. The effects of the physical factors were mostly independent of interactions and predictable. Increasing the air flow rate over the sample would have a dilution like effect on the gas phase unless the compound has a high volatilization rate, in which case the concentration in the headspace would remain constant or increase. Thus the effect of air flow rate on a compound is dependent on the kinetics of volatilization specific to each compound. Since the odorants are present in solution at low concentrations, the ideal gas law can be used to predict the effect that temperature would have on volatility. All of the compounds except the terpenes exhibited a behavior consistent with this prediction. The remaining effects indicate a complexity governed by chemical interactions, kinetics, surface characteristics, etc.

Conclusions

When an ingredient in the base of a beverage is changed, but the same odorant mixture used, the volatility of the odorants are affected in different ways and at different magnitudes producing a different flavor profile. Using the concept inherent in the Weber ratio, it was estimated that many of these effects will modulate flavor. Solution interactions in a beverage are more complicated than independent effects of factors on odorants. The competition of binding and various effects on the solution environment creates interactions between many factors which influence the volatility of odorants. A single dimensional model would neglect these interactions which were shown to have large influences. Knowing what direction and approximate magnitude that a factor may affect volatility can be helpful when optimizing a flavor formulation.

Literature Cited

1. Nahon, D. F.; Roozen, J. P.; Graaf, C. D. *Food Chemistry* **1996**, *56*, 283-289.
2. Pokorny, J.; Kalinova, L. *Czech Journal of Food Science* **1997**, *15*, 111-117.
3. Roberts, D. D.; Acree, T. E. *J. Agric. Food Chem.* **1995**, *43*, 2179-2186.
4. Belardi, R. P.; Pawliszyn, J. B. *Water Pollut. Res. J. Can.* **1989**, *24*, 179-191.
5. Zhang, Z.; Pawliszyn, J. *Anal. Chem.* **1993**, *85*, 1843-1852.
6. Coleman III, W. M.; Lawrence, B. M. *Flavour and Fragrance J.* **1997**, *12*, 1-8.
7. Druaux, C.; Thanh, M. L.; Seuvre, A.-M.; Voilley, A. *JAOCS* **1998**, *75*, 127-130.

Table VI. Major Factors and Interactions Affecting Volatility

<i>Compound</i>	<u>Independent Physical Effects</u>			<u>Other Main Effects</u>
	<i>Conc.</i>	<i>Flow</i>	<i>Temp.</i>	
Heptanal	+			AD; AF; BD; E
Octanal	+	+		AC; ACE; ABFG; ACEH; DH; E
Nonanal	+	-		ACE; ABFG; BH; DH
Decanal	+	-		AB; AC; ACF; BEF; CE
Undecanal	+	-	+	AB; AC; AH; BH; BFG; C; CE; E; EH; FG
Dodecanal	+		+	AB; AC; AH; BH; C; E; FG
Perilla aldehyde	+	-	+	ABFG; AEGH; BH; FH
E-cinnamic aldehyde	+		+	BH; BDG; CE; E; F
Neral	+	-	+	ADF; BH; BFG; CE
Geranial	+		+	ADF; BD; BH; BFG; CE
Benzaldehyde	+		+	ACD; E
3-methylbutyl acetate	+	+		ACD; ACE; ABFG; D
Citronellyl acetate	+		+	ABFG; AEGH; CDF
Cinnamyl acetate	+		+	ABD; BD; CD; DE; EG
Geranyl acetate	+		+	AC; AH; BH; E; DEF; FG
Ethyl valerate	+	+		AB; AC; ACF; BFG; C; CD; CE
Ethyl octanoate	+	-		ACE; ABFG; BH; BD; FG
Ethyl decanoate	+	-	+	ABFG; AEGH; AH; BH
Ethyl dodecanoate	+		+	AC; BH; C; E
p-cymene	+	-	-	ABFG; BH; FH
E-ocimene	+	-	-	AB; CD; DE; G
γ -terpinene	+	-	-	CD; DE; EG
α -pinene	+	-	-	BD; BE; BFG; C; CE; G
Myrcene	+	-	-	BFG; CE; C
1,4-cineole	+	+		AC; ACF; BFG; C; CE
1,8-cineole	+	-	+	AB; AC; BFG; C; CE
Linalool	+		-	ABE; BE; BFG; C; CE; G
Isoborneol	+	-	+	AC; BFG; BH; CE; D
Fenchol	+	-	+	BH; D; FH
Camphor	+		+	ABFG; ACE; AEGH; BH; C; D; E

NOTE: Criteria for inclusion was p-value < 0.05. Independent "Physical Effects" do not include interactions. + indicates an increase in volatility corresponding with an increase of the factor; - indicates a decrease in volatility with an increase of the factor. A=Temperature; B=Air Flow Rate; C=pH; D=% Acidity; E=Ethanol; F=Aspartame; G=Acesulfame Potassium; H=Sucralose.

8. Lee III, W. E. *J. Food Sci.* **1986**, *51*, 249-250.
9. Taylor, A. J.; Linforth, R. S. T. In *Trends in Flavour Research*; Maarse, H., Heij, D. G. v. d., Eds.; Elsevier: Amsterdam, 1994, pp 3-14.
10. Deibler, K. D.; Acree, T. E. In *Advances in Flavor Chemistry and Technology*; R. Teranishi, E.L. Wick, and I. Hornstein, Eds.; Kluwer Academic/Plenum: New York, NY, 1999, pp 387-395.
11. Deibler, K. D.; Acree, T. E. *J. Agric. Food Chem.* **1999**, *in press*.
12. Weber, E. H. *The Sense of Touch*; Academic Press: London, 1978.
13. Lawless, H. T. In *Tasting and Smelling, 2nd edition*; Beauchamp, G. K., Bartoshuk, L., Eds.; Academic Press: San Diego, 1997, pp 125-174.
14. Boring, E. G. *A History of Experimental Psychology*; Appleton, NY, 1950.
15. Cain, W. S. *Science* **1977**, *195*, 796-798.

Chapter 28

Influence of Formulation and Structure of an Oil-in-Water Emulsion on Flavor Release

Marielle Charles¹, Sandrine Lambert¹, Philippe Brondeur¹,
Jean-Luc Courthaudon², and Elisabeth Guichard¹

¹INRA-LRSA, 17 rue Sully, 21034 Dijon Cedex, France

²ENSBANA, 1 Esplanade Erasme, 21000 Dijon, France

The influence of proteins, polysaccharides, and droplet size on flavor release of an oil-in-water emulsion was determined using aroma compounds with different hydrophobic characteristics and static headspace analysis. Flavor release of lipophilic compounds (ethyl hexanoate and allyl isothiocyanate) was influenced by the three factors. Using protein as an emulsifier induces a decrease of flavor release of aroma compounds which interact with the protein. Emulsions with small fat droplets lead to a better release. The influence of polysaccharides depends on the fat droplet size: salting-out effect with large droplets and retention with small droplets. For hydrophilic compounds, no effect of the nature of the protein was noticed and the influence of the droplet size and polysaccharides was a function of the aroma compounds.

The food industry must constantly adapt its products to the consumer's demand. In order to minimize the number of experiments needed to study the effects of formulation or process, it is necessary to better understand the different phenomena responsible for flavor release. Salad dressings are a good example of a complex food in which flavor release is governed by several factors.

Salad dressings are oil-in-water emulsions stabilized by both surface active agents and thickeners. In this type of product, flavor release should depend on:

(1.) the oil content which affects the partition of aroma compounds between the different emulsion phases (lipid, aqueous and vapor) (1), (2.) the surface active agent which interacts with aroma compounds at the interface or in the bulk phase when present in excess (2, 3), or limits the transfer of aroma compounds between the oil and the aqueous phases (4), (3.) the polysaccharides which interact with aroma compounds (5), entrap or reduce their mass transport in the bulk phase (6, 7), (4.) the structure of emulsion (8) or emulsion type (9).

Previous results on salad dressings (50% oil) homogenized with whey protein showed that sensory perception and flavor release were affected by the modification of the droplet size: some hydrophobic compounds were better released from the finest emulsion whereas hydrophilic compounds were less released (10). But decrease of droplet size was associated with an increase of viscosity and a decrease of protein concentration at the interface. It was thus difficult to explain the differences in flavor release only by the droplet size.

This chapter deals with a fundamental study performed on model emulsions in order to determine the respective influence of proteins, polysaccharides, and fat droplet size on flavor release in dressings. Effect of proteins and polysaccharides were also determined in aqueous solutions.

Materials and Methods

Aroma Compounds

Five aroma compounds present in dressings and with different hydrophobicity constants were chosen (Table I). They were kindly supplied by International Flavours and Fragrances (I.F.F., Longvic, France).

Table I. Physico-chemical and Sensory Characteristics of Aromas

<i>Aroma compounds</i>	<i>Formula</i>	<i>Mr</i>	<i>Solubility in water (g/L)</i>	<i>Log P^a</i>	<i>Odor</i>
Diacetyl	C ₄ H ₆ O ₂	86	250 (15°C)	-2.0	Buttery
Butan-1-ol	C ₄ H ₁₀ O	74	111 (25°C)	0.8	Fusel oil
2-Methylbutan-1-ol	C ₅ H ₁₂ O	88		1.2	Fusel oil
Allyl isothiocyanate	C ₄ H ₅ NS	99	1.90 (25°C)	1.7	Pungent
Ethyl hexanoate	C ₈ H ₁₆ O ₂	114	0.597 (25°C)	2.8	Fruity

^a Hydrophobicity constant calculated according to Rekker's method (11)

Model Emulsions

Model emulsions were prepared to test the effect of proteins, polysaccharides and droplet size. The fat content (30%) was the same for all the emulsions.

Proteins

Three protein concentrates were tested as emulsifiers: α -lactalbumin (PSDI 4200, MD-Food, Videbaek, Danemark), β -lactoglobulin (Besnier Bridel Aliments, Chateaulin, France), and a mixture of β -lactoglobulin and α -lactalbumin (73:23, w:w). Proteins were solubilized in a citric acid / sodium citrate buffer (0.1 M; NaCl 25 mM, pH 3) at a concentration determined in order to have 0.5% of protein in the

final emulsions. Flavor compounds (40 mg), protein solution (31.5 g) and sunflower oil (13.5 g) were equilibrated during 1h before homogenization with an Ultra-Turax at 8000 rpm for 3 min at 5°C.

Polysaccharides

Two polysaccharides were used as thickeners : xanthan (Kelco International) and a modified starch (waxy corn chemically modified, National Starch, France). Four emulsions (two emulsification rates and with or without polysaccharides) were prepared. α -Lactalbumin was used as an emulsifier at 0.5% (w:w) and emulsions with polysaccharides contained 0.2% xanthan and 0.7% modified starch. Aqueous solutions were prepared in NaCl 25mM, pH 6 and heated at 85° for 30 min. Two emulsification rates were applied (10000 rpm or 20000 rpm) for 1 min with a Polytron at 5°C. Emulsions were flavored with a mixture of three aroma compounds. Ethyl hexanoate was solubilized in the lipid phase before emulsification and 2-methylbutan-1-ol and diacetyl were added to the emulsions with a syringe, in order to obtain concentrations in the final emulsion of respectively 500 ppm, 500 ppm, and 200 ppm. Emulsions were gently stirred 1h before analysis.

Droplet Size

Two emulsions differing by their droplet size (volume surface average diameter) and their α -lactalbumin content were made: 7 μ m and 0.4% protein; 15 μ m and 0.2% protein. Solubilization of the protein was done in citrate buffer prior to emulsification. After emulsification with a Polytron, emulsions were diluted by a factor of 1.2 with the buffer for the fine emulsion and with a 1% α -lactalbumin solution for the coarse emulsion. The final emulsions have thus a same total protein content of 0.3%. Aroma compounds alone were added to the final emulsions to obtain a final concentration of 200 to 500 ppm. Emulsions were gently stirred for 1 h, (2 h for allyl isothiocyanate) before headspace analysis.

Polysaccharide Solutions

Polysaccharide solutions (xanthan 0.2%, modified starch 0.7%, and a mixture of xanthan-modified starch 0.2%-0.7%) were prepared by solubilization in citric acid / sodium citrate buffer (0.1 M, NaCl 25 mM, pH3) and heating at 85°C for 30 min.

Emulsion Characterization

Particle size distribution was determined with a Malvern Mastersizer laser diffractometer (Model S2-01; Malvern Instruments, Orsay, France) both before and after headspace measurement to verify the stability of the emulsions. The volume surface average diameter d_{32} and the specific surface area were measured.

Protein Content Determination

Protein concentration of the aqueous phase was measured using the Kjeldahl

method (12). The amount of protein adsorbed at the interface was calculated from the difference of protein concentration between that in the solution used for making the emulsion and the one measured in the aqueous phase after emulsion centrifugation.

Measurement of Interactions between Proteins and Aroma by Affinity Chromatography

The procedure used for the immobilization of the proteins was adapted from that described by Sostmann and Guichard (13): α -lactalbumin, β -lactoglobulin or the mixture of the two proteins were immobilized onto a silica-diol support in PEEK (PolyEtherEtherKetone) columns (4.3 mm x 5 cm). One column without protein was prepared in the same conditions. The HPLC system used was a Varian 9010 pump and a Shimadzu SPD-6AV UV-vis spectrometric detector. The system was equilibrated with eluent (water, NaCl 25 mM, pH 3) at a flow rate of 1 mL.min⁻¹. Flavor compounds were dispersed in the same aqueous solution, injected and detected at their maximum of absorption. Global affinity was calculated as follows (14):

$K_b = (t_R - t) / C_p t_o$ where K_b is the global affinity (M⁻¹), t_R the retention time of compound on column with protein (min), t the retention time of compound on column without protein (min), C_p the protein concentration (mol.L⁻¹) and t_o the void time (min).

Headspace Analysis

Amber flasks (40 mL) were filled with 10 ml solutions (emulsions, or 5 mL polysaccharide solutions + 5 mL aroma solution) closed with a mininert™ valve (Supelco, St Quentin Fallavier, France) and placed in a 30°C water-bath with stirring. Vapor-liquid equilibrium analysis was used to measure the influence of proteins (24 h) and polysaccharides (2 h). To test the influence of the droplet size, flavor release was determined as a function of time. For each study, 1 mL of vapor phase above the emulsion was injected into a chromatograph Carlo Erba GC8000 series (Fisons Instruments) equipped with a DB-Wax fused capillary column (30 m x 0.32 mm i.d., film thickness 5 μ m) (J&W Scientific Inc., Folsom, USA). The operating conditions were as follows: hydrogen carrier gas velocity, 50 cm.s⁻¹; H₂ flow rate, 23 mL.min⁻¹; air flow rate, 318 mL.min⁻¹; FID injector temperature, 240°C; detector temperature, 250°C; oven temperature 120°C, 140°C or 160°C depending on the volatile compounds.

Statistical Analysis

The statistical analyses were realized with the Statistical Analysis Systems software (SAS Institute, Inc., Cary, NC). A one-way analysis of variance (proc GLM) followed by comparison of means by duncan test was applied except for results on effect of polysaccharides in aqueous solutions (t-test).

Results

Influence of the Proteins

Whey proteins are often used to emulsify dressings. Flavor release from emulsions prepared with two whey proteins, α -lactalbumin and β -lactoglobulin were compared. A mixture of these two proteins in proportions found in a commercial emulsifier was also tested (Figure 1). Average diameters (d_{32}) of emulsions were 15.3 μm for α -lactalbumin emulsions, 10.5 μm for β -lactoglobulin emulsions and 13.2 μm for mixture emulsions. Flavor release of ethyl hexanoate and allyl isothiocyanate from emulsions with β -lactoglobulin was significantly smaller ($p < 0.05$) compared with that of emulsions with α -lactalbumin or with the mixture. There was no difference between emulsions with α -lactalbumin and emulsions with the mixture. For 1-butanol, no significant difference ($p < 0.05$) was observed between the three emulsions.

To explain these observations, global affinity of proteins for the aroma compounds were determined by affinity chromatography (Figure 2). For all proteins, global affinity was the greatest for ethyl hexanoate and the weakest for butan-1-ol. β -Lactoglobulin presented more affinity for the three compounds than α -lactalbumin and the global affinity of aroma compounds for the mixture was similar to that obtained with β -lactoglobulin.

Influence of the Polysaccharides

As viscosity increases when droplet size decreases, the influence of polysaccharides in emulsion was tested for two droplet sizes. α -Lactalbumin was chosen because of its lower affinity for the aroma compounds and aqueous solutions were made at pH 6 because of the incompatibility between α -lactalbumin and polysaccharides at pH 3. Emulsions without polysaccharides presented one population of droplet size whereas emulsions with polysaccharides were constituted of two populations (Table II).

Table II. Structural Characteristic of Emulsions with or without Polysaccharides

<i>Emulsion</i>	<i>D₃₂ (μm)</i>
Fine without polysaccharides	3.81
Fine with polysaccharides	1.41
Coarse without polysaccharides	5.76
Coarse with polysaccharides	1.21

The influence of polysaccharides on flavor release depended on the aroma compounds and the droplet size (Figure 3). For ethyl hexanoate, we noticed an increase in flavor release with polysaccharides from emulsions homogenized at 10000

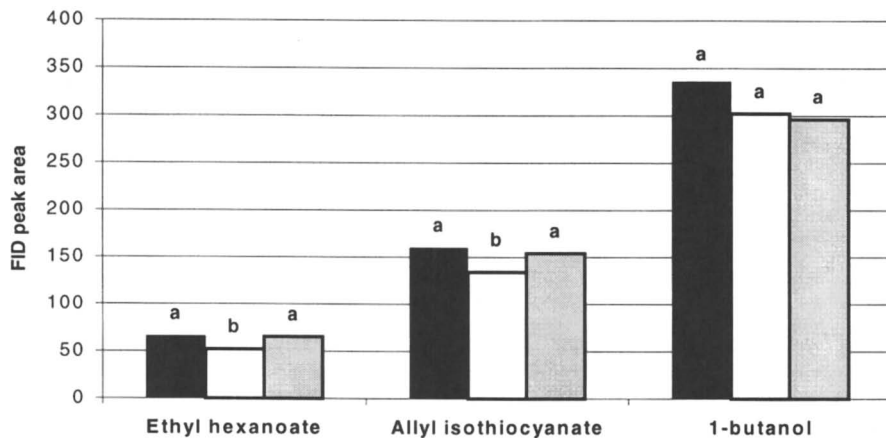


Figure 1. Effect of the nature of the proteins used as emulsifier on flavor release from an oil-in-water emulsions ($\phi = 0.3$, 0.5% protein in citric acid/sodium citrate buffer 0.1 M, NaCl 25 mM, pH 3). Bars: black for α -lactalbumin, white for β -lactoglobulin and gray for mixture of β -lactoglobulin and α -lactalbumin (73:23, w:w). a, b: areas with the same letters are not significantly different at a 5% level.

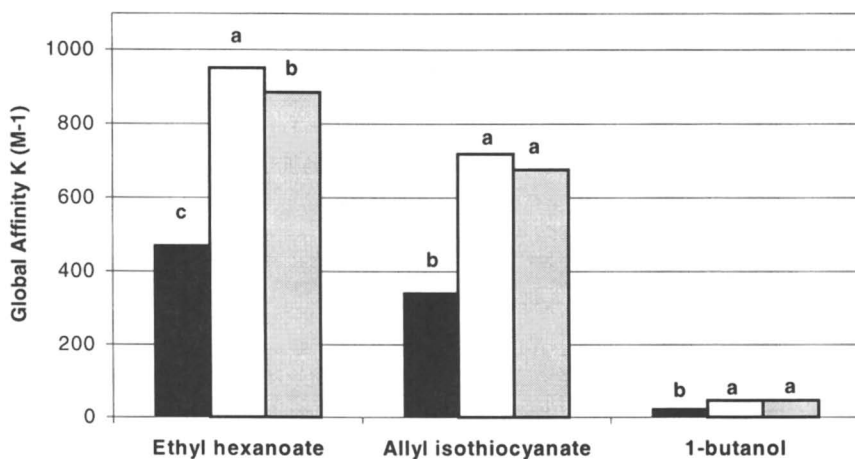


Figure 2. Global affinity of aroma compounds with the proteins (citric acid / sodium citrate buffer, 0.1 M, NaCl 25 mM, pH 3); bars: black for α -lactalbumin, white for β -lactoglobulin and gray for mixture of β -lactoglobulin and α -lactalbumin (73:23, w:w). a, b: areas with the same letters are not significantly different at a 5% level.

rpm but a decrease when homogenized at 20000 rpm. Flavor release of 2-methylbutan-1-ol increased with polysaccharides only for the finest emulsions and no effect was observed for diacetyl.

Comparison of flavor release from emulsions with two droplet sizes showed that ethyl hexanoate was better released from the finest emulsions, without (significant at a 5% level) or with polysaccharides (no significant). 2-Methylbutan-1-ol was also better released from the finest emulsion but only from emulsions with polysaccharides and flavor release of diacetyl was not influenced by the droplet size.

Flavor release from aqueous solutions containing the polysaccharides alone or in mixture were compared with flavor release from water. Several concentrations were tested for the three compounds and results for one concentration are presented on Figure 4. Peak area was expressed in relative percentage of the area obtained without polysaccharides (100%). Xanthan induced a "salting-out" effect for 2-methylbutan-1-ol and ethyl hexanoate but no effect for diacetyl. Modified starch did not lead to a modification of the volatility of the three compounds. Addition of the mixture of polysaccharides increased the flavor release of 2-methylbutan-1-ol ($p < 0,001$) and diacetyl ($p < 0,5$) but decreased that of ethyl hexanoate.

Influence of the Fat Droplet Size

Both final emulsions ($d_{32} = 7 \mu\text{m}$ and $15 \mu\text{m}$) were constituted of 25% oil and 0.3% α -lactalbumin with an interfacial protein concentration of 1.25 mg.m^2 interface. Flavor release from these emulsions are presented on Figure 5 and 6. Flavor release of ethyl hexanoate and allyl isothiocyanate was higher from the finest emulsions. For diacetyl, flavor release was also greater from the finest emulsions but in a lesser extent. No effect was noticed for butan-1-ol.

Discussion

Influence of Proteins

Varying the nature of the protein used as emulsifier induced a difference in the release of flavor compounds which have different affinity constants for these proteins. Release of ethyl hexanoate and allyl isothiocyanate from emulsions with β -lactoglobulin is lower than from emulsions made with α -lactalbumin or with the mixture. In emulsions, proteins are located at the interface and in the bulk phase. Espinoza-Diaz (15) suggested that adsorption of β -lactoglobulin at the oil-water interface could modify the binding sites for aroma compounds and that protein in the bulk phase could also interact with aroma compounds. As the global affinities of ethyl hexanoate and allyl isothiocyanate are greater for β -lactoglobulin, than for α -lactoglobulin, the differences in the release should be due to interactions with protein. Protein at the interface may also limit the transfer of volatile compounds between the lipid and the aqueous phase (4). A pH 3, Das and Kinsella (16) determined that the

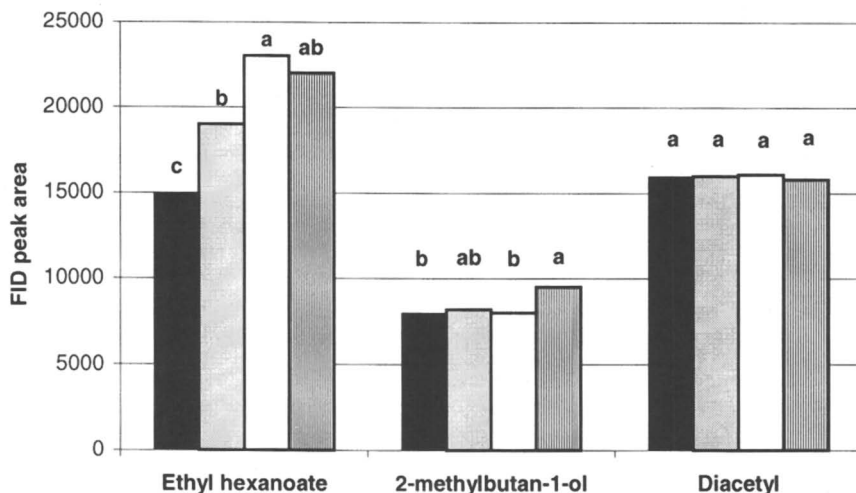


Figure 3. Effect of the polysaccharides (xanthan + modified starch) on flavor release from oil-in-water emulsions with different droplet sizes ($\phi = 0.3$, 0.5% α -lactalbumin in 25 mM NaCl solution, pH 6). Bars: black for coarse emulsions without polysaccharides, gray for coarse emulsions with polysaccharides, white for fine emulsions without polysaccharides and vertical lines for fine emulsions with polysaccharides. a, b, c: areas with the same letters are not significantly different at a 5% level.

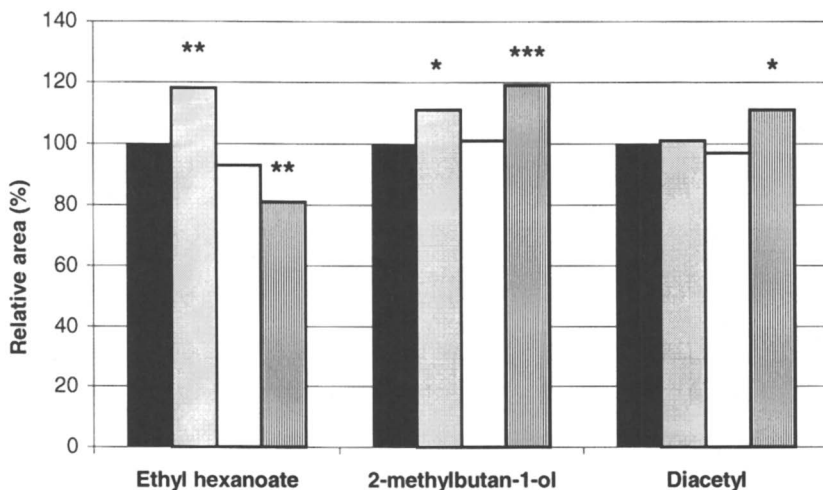


Figure 4. Effect of the polysaccharides on flavor release in aqueous solution (25 mM NaCl, pH 3). Bars: black for water, gray for xanthan (0.2%), white for modified starch (0.7%) and vertical lines for the mixture of polysaccharides. Areas significantly different from that in water at * 5%, ** 1% and *** 0.1% level.

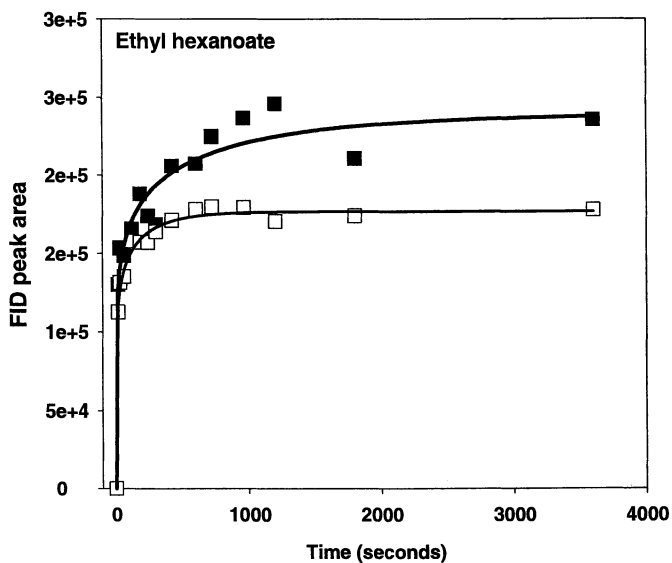
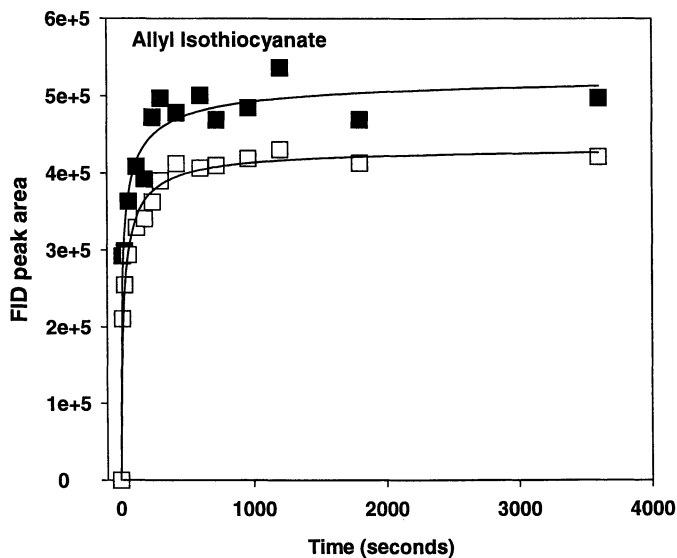


Figure 5. Effect of the droplet size on flavor release of allyl isothiocyanate (500 ppm) and ethyl hexanoate (500 ppm) from oil-in-water emulsions ($\phi = 0.25$, α -lactalbumin 0.5% in citric acid/citrate sodium buffer 0.1 mM, NaCl 25 mM, pH 3). Filled symbol for $d_{32} = 7 \mu\text{m}$ and open symbol for $d_{32} = 15 \mu\text{m}$.

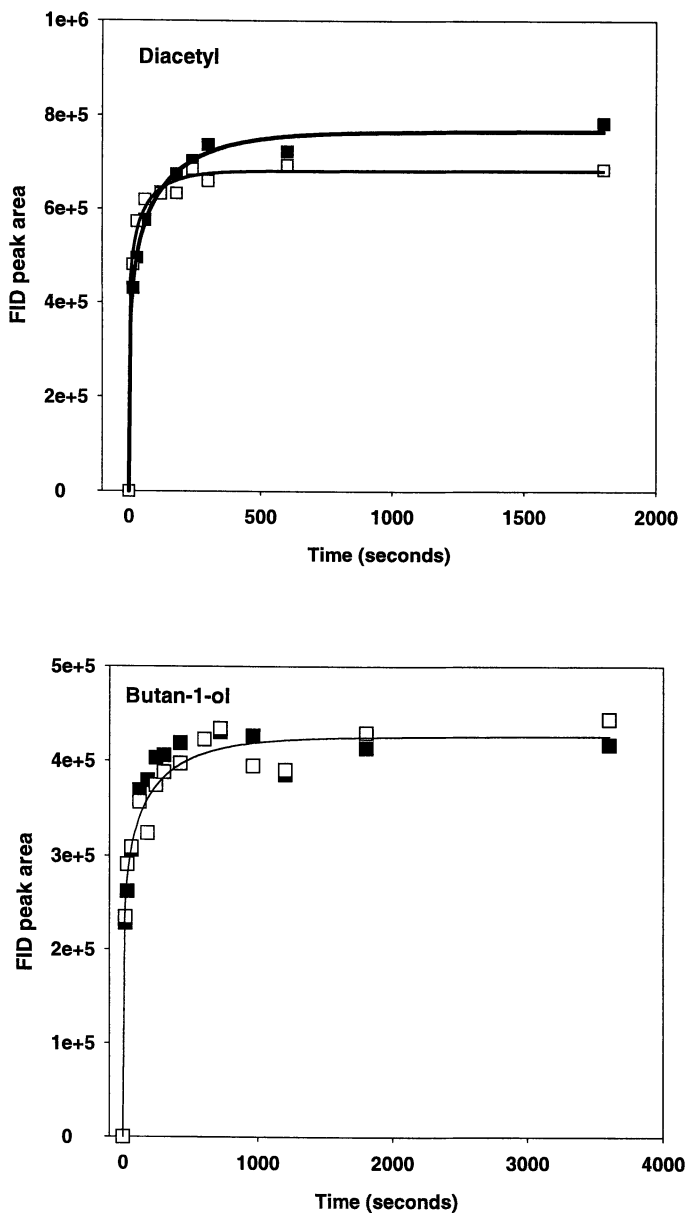


Figure 6. Effect of the droplet size on flavor release of diacetyl (500 ppm) and butan-1-ol (200 ppm) from oil-in-water emulsions ($\phi = 0.25$, α -lactalbumin 0.5% in citric acid / citrate sodium buffer 0.1 mM, NaCl 25 mM, pH 3). Filled symbol for $d_{32} = 7 \mu\text{m}$ and open symbol for $d_{32} = 15 \mu\text{m}$.

interfacial concentration of β -lactoglobulin is 7.3 mg.m^2 . Our result indicate that the protein load of α -lactalbumin is about $1,3 \text{ mg.m}^2$. In the mixture, α -lactalbumin is better adsorbed at the interface than β -lactoglobulin (17). This was confirmed by semi-quantitative determination of the proteins present in the aqueous phase after centrifugation of the emulsion, which showed a slight decrease of the peak corresponding to α -lactalbumin in comparison with the initial protein solution. Thus, the decrease observed in emulsion with β -lactoglobulin for the two volatile compounds should also be due to a limitation of their transfer at the oil-water interface when β -lactoglobulin is used. Then, fat globule size of emulsions with β -lactoglobulin is smaller than that with α -lactalbumin or the mixture and could affect the release of hydrophobic compounds.

Influence of the Polysaccharides

Polysaccharides are used to stabilize and thicken the dressings by increasing the viscosity of the continuous phase. Our assumption is that the release of hydrophobic compounds, such as diacetyl, alcohols or acids may change in the presence of the polysaccharides (10). Addition of thickening agents to emulsions affects flavor release differently as a function of aroma compounds and droplet size of emulsion.

For diacetyl, no effect of polysaccharides was noticed whatever the droplet size of emulsion. The enhancing effect observed on the flavor release of diacetyl with the mixture of polysaccharide in aqueous phase did not occurred with model emulsion (Figure 4). These result are however in agreement with those reported by Odake *et al.* (18) who observed opposite results of diacetyl release from aqueous solutions and from cream type dressings prepared with the same thickening agents.

Polysaccharides increase release of 2-methylbutan-1-ol only from the finest emulsion. In this case, the result can be explained by the salting-out effect observed in aqueous solution. As modified starch doesn't modify the volatility of alcohol, we suggest that xanthan could be responsible for the enhancement observed with the mixture. This result is in agreement with the salting-out effect of xanthan on alcohol observed by Chung and Villalota (19).

In the case of ethyl hexanoate, the effect of polysaccharides differs with droplet size. The slight but not significant decrease observed from the finest emulsion may be related to the retention observed in aqueous solution with the mixture. The combination of modified starch and xanthan leads to a decrease of the volatility of the ester whereas xanthan alone enhances and modified starch doesn't modify the volatility respectively. The association of the two polysaccharides in a network may limit the diffusivity or entrap the ester. In the coarse emulsion, the presence of polysaccharides increases the flavor release.

Our results obtained with diacetyl and ethyl ester in the finest emulsion are in agreement with those found by Wendin *et al.* (20) in sourmilk. They show that addition of xanthan in sourmilk led to a decrease of smell and aroma intensity of a non-polar compound ethyl-2-methylbutyrate, but had no effect on the intensity of a polar compound, maltol.

Influence of the Fat Droplet Size

Changing the droplet size of an oil-in-water emulsion has an effect on the flavor release of liposoluble compounds. In our first experiment with the same initial protein content (Figure 3), ethyl hexanoate was better released from fine emulsions. Protein concentration at the interface is greater when the droplet size is smaller and thus may limit the oil/water transfer of hydrophobic compounds. Druaux *et al.* (21) noticed no effect of increasing interfacial protein concentration on the release of 2-heptanone. However, ethyl hexanoate has a greater affinity for the protein than 2-heptanone ($K_b = 465 \text{ M}^{-1}$ (22) and $= 950 \text{ M}^{-1}$ (13) with β -lactoglobulin respectively). In order to suppress the interfacial protein effect, a second experiment was performed on emulsions with the same interfacial protein concentration ($\approx 1.25 \text{ mg.m}^2$ interface) and the same protein content. The results confirmed that the liposoluble compounds are better released when the fat droplets are the smallest. The results are opposite to those predicted by mathematical models (23, 24). One explanation may be that an increase in the interfacial surface area increases the mass transfer of volatile compounds from oil to water phase or to vapor phase.

These results confirm that the effect observed with hydrophobic compounds in emulsions with different proteins is not due to the difference in the droplet size but really to the different affinities of the proteins for the aroma compounds.

Conclusion

Both formulation and structure have to be taken into account when flavoring an emulsion. Flavor release of liposoluble compounds (ethyl hexanoate) but not hydrophilic compounds (diacetyl) was shown to depend on the structure of the emulsion, the nature of the protein used as emulsifier, and the presence of polysaccharides. These results on model emulsions could not explain the release of hydrophilic compounds from salad dressings (10). Formulation of model emulsions was not exactly identical to that of salad dressings. Oil volume fraction of salad dressing was 0.5 and our emulsions comprised only constituted of 30% oil for analytical purposes. As mentioned by Ford (25), the droplet size has an impact on viscosity when the oil volume fraction is above 0.2-0.4. Moreover, the process differs in the preparation of the aqueous phase and the order of incorporation of the ingredients. Therefore, flavoring dressings is still a challenge and further experiments are needed to better understand the effect of processing on flavor release.

Acknowledgement

This work was financially supported by the AMORA-MAILLE company and the Regional Council of Bourgogne.

References

1. de Roos, K.; *Food Technol.* **1997**, *51*, 60-62.
2. Land, D.; In *Progress in Flavour Research*; Land, D.G. and Nursteb H.E., Eds.; Applied Science publishers LTD: London, UK, 1978; pp. 53-66.
3. Landy, P.; Courthaudon, J.L.; Dubois, C.; Voilley, A. *J. Agric. Food Chem.* **1996**, *44*, 526-530.
4. Rogacheva, S.; Espinoza-Diaz, M.; Voilley, A. *J. Agric. Food Chem.* **1999**, *47*, 259-263.
5. Guichard, E.; Etiévant P. *Nahrung* **1998**, *42*, 376-379.
6. Darling, D.F.; Williams, D.; Yendle, P. In *Interactions of Food Components*; Birch G.G. and Lindley M.G., Eds.; Elsevier Applied Science Publishers: London, UK, 1986; pp 167-187.
7. Roberts, D.; Elmore, J.; Langley, K.; Bakker, J. *J. Agric. Food Chem.* **1996**, *44*, 1321-1326.
8. Dubois, C.; Sergent, M.; Voilley, A. In *Flavor-Food Interactions*; McGorin R. and Leland, J., Eds; American Chemical Society: Washington, US, 1996; pp 217-226.
9. Bakker, J.; Mela, D. In *Flavor-Food Interactions*; McGorin R. and Leland, J., Eds; American Chemical Society: Washington, US, 1996; pp. 36-47.
10. Charles, M.; Rosselin, V.; Sauvageot, F.; Guichard, E. *Proc. Weurman Flavour Research Symposium*, Warburg, 1999 Submitted.
11. Rekker, R.F. In *Pharmacochemistry Library*; Naute, W. and Rekker, F., Eds; Elsevier Scientific: Amsterdam, 1977.
12. Kjeldahl; *AR. 8.1.70 J.O. de la République française du 25.01.70* 1970.
13. Sostmann, K.; Guichard, E. *Food Chem.* **1998**, *62*, 509-513.
14. Nilsson, K.; Larsson, P.O. *Anal Biochem.* **1983**, *134*, 60-72.
15. Espinoza-Diaz, M.A. Ph.D. thesis, ENSBANA, Université de Bourgogne, Dijon, France, 1999.
16. Das, K.P. and Kinsella, J. *J. Dispersion Science and Food Technology* **1989**, *10*, 77-102
16. Klemaszewski, J.L.; Das, K.P.; Kinsella, J.E. *J. Food Sci.* **1992**, *57*.
17. Odake, S.; Roozen, J.P.; Burger, J.J. *Nahrung* **1998**, *42*, 385-391.
18. Chung, S.; Villota R. *J. Food Proc. Eng.* **1990**, *13*, 169-189.
19. Wendin, K.; Solheim, R.; Alimere, T.; Johansson, L. *Food Qual. Pref.* **1997**, *8*, 281-291.
20. Druaux, C.; Courthaudon, J.L.; Voilley, A. In *AGORAL 96*, 1996, 255-260.
21. Pelletier, E.; Sostmann, K.. Guichard, E. *J. Food Agric. Chem.* **1998**, *46*, 1506-1509
22. Overboosch, P.; Afteof, W.; Haring, P. *Food Reviews International* **1991**, *7*, 137-184.
23. Harrison, M.; Hills, B.; Bakker, J.; Clothier, T. *J. Food Sci.* **1997**, *62*, 653-657, 664.
24. Ford, L.; Borwankar, R.; Martin, R.; Holcomb, D. In *Food Emulsions*; Friberg, S. and Larsson, K. Eds; Marcel Dekker INC.: New York, US. 1997; pp. 361-412.

Chapter 29

The Role of Texture and Fat on Flavor Release from Whey Protein Isolate Gels

Elizabeth A. Gwartney¹, E. Allen Foegeding², and Duane K. Larick²

¹Coors Brewing Company, Golden, CO 80401-6834

²Department of Food Science, North Carolina State University, Raleigh, NC 27695-7624

The objective of this work was to investigate the role of texture and fat on the release of flavor from solid food matrices. Six different whey protein isolate gels (WPI-gels), varying in rheological and water-holding properties, were created at a constant protein concentration by varying ionic conditions. Release of 2,4-dimethylbenzaldehyde (cherry) or ethyl butyrate (grape) was measured using time-intensity methodology. Perceived maximum intensity and release rate were greater for gels with particulate structure and low water-holding properties, and lowest for stranded gels, which hold water well. The influence of lipid on flavor release was evaluated in particulate and stranded WPI-gels flavored with diacetyl (butter) or δ -decalactone (coconut). At low concentrations of lipid, flavor release was dependent on gel structure. Particulate gels released large amounts of water and broke down quickly into small, spherical particles. In contrast, stranded gels were characterized by high water-holding and a more geometric breakdown into larger and irregularly shaped particles. When the amount of lipid in WPI-gels was high, the rate and intensity of flavor release decreased and was independent of gel texture.

The market for lower fat foods is significant. A national survey conducted for the Calorie Control Council revealed that nearly three-fourths of the adult U.S. population now consume low- or reduced-fat foods (1). When fat is removed or reduced in food systems, the intensity and release rate of flavor is increased (2-5). With the growing range of reduced fat foods available to the consumer it has become increasingly important to understand the factors that affect the perception of flavor, specifically how flavor is released from food matrices.

The process of flavor release is highly dynamic. As food is chewed, it is continuously modified by the body's temperature, salivation, shearing and mixing.

Volatile flavor components are perceived by receptors in the olfactory epithelium after being released from a food matrix via a layer of saliva to the air phase. Therefore, the partitioning of flavor molecules between different food components and the air phase will change as a function of time. Further, small changes in both food structure (texture) and composition (lipid, protein, carbohydrate, salt) can have a considerable effect on the partitioning and mass transfer of flavor compounds within and out of a food matrix.

The influence of food texture on flavor release has been examined extensively in liquid systems (6,7). In general, these studies show that viscosity has a strong effect on flavor properties in that when viscosity is increased, intensity of flavor is decreased. More recently, the effects of texture on flavor release in solid matrices has been considered (8-11). These studies have shown that overall flavor intensity and release are reduced when the strength of a gel matrix is increased. In each of these studies, increasing hydrocolloid concentration was used to change gel firmness. The change in polymer concentration resulted in an increased gel firmness and decreased flavor release rate and intensity. This could be caused by physical binding of the flavor compounds to the hydrocolloid or by texture specific interactions.

The relationships among textural properties and flavor release profiles can be related to how the surface of a food changes during mastication, in terms of both surface area and structure. Surface area may be modified by the fragmentation or dissolution of the sample into smaller and smaller pieces and/or by melting. The surface structures created will depend on the food matrix composition. Fracture surfaces that are rough will create larger surface areas than those that are smooth. Therefore, differences in the way a food is broken down during mastication will be reflected in flavor release. The effect of oral breakdown on flavor release has been investigated in model gelatin systems (11). Gelatin gels that were weak in structure were broken down quickly by melting, creating rapid and intense flavor release. In contrast, stronger gels broke down slowly by fragmentation, thus producing a slow and less intense profile of flavor release.

Flavor release profiles can be measured directly using sensory and/or instrumental techniques. Sensory time-intensity (TI) methods provide quantitative information regarding the dynamic aspects of flavor perception. The methodology allows for the time progression of flavor perception to be measured from the time the product is placed in the mouth through expectoration or swallowing, until extinction. TI has been used to successfully characterize the flavor release properties of reduced- and full-fat cheeses and salad creams (3) and model gels (10,11).

The overall goal of this research was to further elucidate the role of texture and fat on flavor release. First, the relationship between the physical properties of whey protein gel matrices (microstructure, fracture, and water-holding properties) and sensory flavor release was investigated in a non-fat system. Previously, it has been shown that the microstructural, rheological, and water-holding properties of whey protein isolate gels can be varied by adjusting salt type and ionic strength (12). We developed a series of whey protein gels varying in network properties at a fixed protein concentration. Using this approach, the relationship between texture and flavor release was further investigated while eliminating flavor binding effects.

Further, the influence of fat on flavor release was evaluated in a series of whey protein gels varying in physical and flavor release properties.

Materials and Methods

Protein Gel Preparation

Protein suspensions were prepared by hydrating 12% (w/v) whey protein isolate (WPI) (Davisco International Inc., Le Sueur, MN) in solutions of 5% w/v sucrose and differing amounts of NaCl and/or CaCl₂ (ranging in ionic strength: $0.015 < \mu < 0.045$) under constant stirring for 30 min. 2,4-Dimethylbenzaldehyde(cherry flavor)(Aldrich Chemical Co., Milwaukee, WI) or ethyl butyrate (grape flavor) (Aldrich Chemical Co., Milwaukee, WI) was added to each protein suspension at a fixed concentration of 54 ppm or 28 ppm, respectively. To induce gelation, solutions were heated in stoppered glass tubes (19 mm in diameter) for 30 min in an 80°C water bath. Further, gels were cooled in an ice bath for 1 hour and stored overnight at 4°C. All analyses and sensory testing were performed the following day.

Emulsion Gel Preparation

A series of 6 whey protein isolate (WPI) gels were processed to a final composition given in Table I. Protein suspensions were prepared by hydrating whey protein isolate (WPI)(Davisco International Inc., Le Sueur, MN) in salt buffers under constant stirring for 90 min. Salt treatments were chosen to produce gels of either stranded or particulate structure. The suspensions were degassed under vacuum for 1 hour to remove all gas bubbles produced during mixing. Sunflower oil and/or distilled water were added to each protein suspension to produce solutions of 12% (w/v) protein and 0 or 20% (v/v) lipid.

Each aqueous solution was mixed and homogenized using a single valve homogenizer for 3 min at a pressure of 3000 psi. The median lipid globule size in the 20% sunflower oil emulsions was determined using a Shimadzu centrifugal particle size analyzer (Shimadzu Scientific Instruments, Inc., Columbia, MD). The 20% (v/v) sunflower oil emulsion was diluted with the WPI suspension containing no sunflower oil to make a 2.5% (v/v) lipid solution for each gel structure type. Prior to gelation, diacetyl (butter flavor)(Aldrich Chemical, Co., Milwaukee, WI) or δ -decalactone (coconut flavor)(Aldrich, Chemical Co., Milwaukee, WI) was added to each emulsion solution at a fixed concentration of 50 ppm and 100 ppm, respectively. To induce gelation, solutions were heated in stoppered glass tubes (19 mm in diameter) for 30 min in an 80°C water bath. Gels were stored overnight at 4°C and sensory testing was performed the following day.

Table I. Physical Characteristics and Composition of Emulsion Gels

<i>Sample code</i>	<i>P/0</i>	<i>P/2.5</i>	<i>P/20</i>	<i>S/0</i>	<i>S/2.5</i>	<i>S/20</i>
Protein % (w/v)	12	12	12	12	12	12
NaCl (mM)	25	25	25	25	25	25
CaCl ₂ (mM)	10	10	10	0	0	0
Structure/appearance ¹	P, O	P, O	P, O	S, T	S, T	S, T
Sunflower oil % (v/v)	0	2.5	20	0	2.5	20
Fracture stress (kPa)	11.9	17.8	43.4	11.1	15.6	54.5
Fracture strain	0.97	1.15	1.08	2.87	2.82	2.01
Water held % (w/w)	59	60	80	99	99	96

¹ P = particulate, O = opaque, S = stranded, T = translucent

Physical Properties

Fracture Properties

Torsional analysis was used to determine the fracture properties of each gel at 20°C. Six samples were tested per gel type over three replications. For torsional fracture, gel samples were cut 28.7 mm in length. Samples were mounted onto notched styrene disks with cyanoacrylate glue and ground to a capstan shape, with a minimum diameter of 10 mm, using a specimen-grinding machine (Gel Consultants, Raleigh, NC). Samples were twisted to fracture at 2.5 rpm using a Torsion Gelometer (Gel Consultant, Raleigh, NC) as described by Kim *et al.* (13). The fracture stress (force/area), fracture strain (deformation/unit length), and fracture modulus (fracture stress/fracture strain) were calculated.

Held-Water

The water-holding properties of gels were measured using a microcentrifuge-based technique described by Kocher and Foegeding (14). Three samples were tested for each gel over three replications. Gels were cut into cylindrical samples of 10 mm in height and 4.4 mm in diameter using a metal cork borer. Samples were inserted into microcentrifuge filtration units (Lida Corporation, Kenosha, WI) and spun in a Beckman Microfuge[®] 11 horizontal rotor microcentrifuge (Beckman Instruments, Inc., Palo Alto, CA) at a relative centrifugal force of 153 g for 10 min.

For emulsion gels, the proportion of total moisture held in the sample was determined based on the amount of drained fluid and total moisture. Total moisture

was determined using a modification of the AOAC method (15). Samples were weighed into aluminum pans and dried in a 70°C vacuum oven (92kPa) for 4 h. Total moisture (% w/w) was used in the determination of held water (% total moisture held) for emulsion gels.

Sensory Protocol

Protein Gels

A computerized time-intensity (TI) method developed at North Carolina State University was used to evaluate cherry or grape flavor intensity. Twelve judges, staff and students from North Carolina State University, selected on the basis of their interest and ability to perceive flavors used in this study, participated on the TI panel. The entire panel of twelve completed the cherry study where only nine participated in the grape evaluations.

Prior to formal evaluations, each panelist participated in six training sessions to become familiar with the TI methodology. To evaluate samples, panelists placed the entire 3 g sample into their mouth at time zero and recorded cherry or grape flavor intensity as the sample was masticated. Samples were swallowed after 20 s and panelists continued to rate flavor intensity until extinction of the perceived sensation. Intensity was rated on an unstructured line scale labeled with "no flavor" (0) and "extreme flavor" (200). Data were collected every 0.5 s for 2 min. A non-flavored gel and a high intensity gel were provided at each session for reference. Following each evaluation, panelists rinsed their mouth with drinking water (Culligan, Raleigh, NC). For each flavor, panelists evaluated six samples in triplicate according to a completely randomized design. Six samples were evaluated per session.

Emulsion Gels

(TI) methodology was used to evaluate the release of diacetyl or δ -decalactone. Ten judges, staff and student from North Carolina State University, selected on the basis of their interest and ability to perceive the flavors in this study, participated on the panel. The entire panel of ten completed the butter flavor study where only eight participated in the coconut flavor evaluations.

Training and sample evaluations were performed in as described in for protein gels. For each flavor, panelists evaluated six samples in duplicate according to a completely randomized design. Three samples were evaluated per morning and afternoon session.

Data Analysis

Six parameters were extracted from each individual TI profile including time of onset (T_{onset}), time to maximum intensity (T_{max}), maximum intensity (I_{max}), plateau time (T_{plat}), total duration (T_{dur}), and rate of release (M_{release}). TI parameters were

analyzed by three-way analysis of variance to determine if significant sample differences existed and the Least Significant Difference (LSD) test was used to specify differences (16). Fracture and water-holding values were evaluated using one-way analysis of variance and differences were specified using the LSD test (16).

Gas Chromatography

Solvent extraction in combination with gas chromatography was utilized in order to determine that the concentration of flavorants were relatively equal in the finished gels. 2, 4-Dimethylbenzaldehyde was quantitatively extracted from each gel sample in duplicate. Samples (10 g) were placed into a 50 ml blender cup and mixed with 25 ml Optima grade hexane (Fisher Scientific, Fair Lawn, NJ). Extracts were filtered through Whatman 42 filter paper into a 125 ml side armed Erlenmeyer flask. Extraction procedure was repeated on filtrate. Hexane extracts were diluted to a constant volume of 50 ml. 2,4-dimethylbenzaldehyde concentration was determined using a Hewlett Packard (Model 5890-Series II) gas chromatography equipped with a flame ionization detector. A 1.0 μ l sample of each extract was injected directly onto a DB-5 fused silica capillary column (J & W Scientific, Folsom, CA). An oven temperature program of 40°C to 220°C at 6°C/min was used.

Sensory Texture Characteristics

Previously, the sensory texture characteristics of a series of 16 whey protein isolate gels varying in structure and lipid content were defined and quantified using modified descriptive analysis (16). Panelists developed a list of 18 terms to describe the complete texture profile of the emulsions gels including breakdown and chewing rate properties. The data, averaged across panelists and replications, were subjected to principal component analyses (PCA) using SAS[®] (17). Subsequently, a sub-set of six emulsion gels were evaluated for flavor release properties.

Results and Discussion

Characterization of Protein Gel Matrices

A series of whey protein gels that varied in structure, water-holding, and fracture properties were developed at a fixed protein concentration. The physical properties of each gel are summarized in Table IIA-B. Gels with particulate structure were characterized by low water-holding (3.8-4.9 g water/g protein) while stranded gels were high in water-holding (5.4-6.7 g water/g protein). This relationship has been demonstrated previously in whey protein isolate gels (18). Gels varied in fracture

stress (strength), fracture strain (deformability), and fracture modulus (rigidity) within each structure classification.

Table IIA. Physical Characteristics of Whey Protein Gels¹

<i>SAMPLE</i>	<i>A</i>	<i>B</i>	<i>C</i>
Salt	25mM NaCl/ 10mM CaCl ₂	50mM NaCl/ 10mM CaCl ₂	5 mMNaCl/ 10mM CaCl ₂
Structure Appearance	Particulate Opaque	Particulate Opaque	Particulate Opaque
Stress (kPa)	26.4 (24.1)	28.9 (30.7)	10.8 (10.4)
Strain	1.56 (1.41)	1.74 (1.75)	1.25 (1.18)
Gf (kPa)	17.0 (17.0)	16.5 (17.7)	8.42 (8.89)
Held-water (g/g prot.)	4.02 (4.03)	3.79 (4.13)	4.92 (4.48)

¹Values in parentheses reflect characterization from gels flavored with ethyl butyrate and those without parentheses reflect gels flavored with 2, 4-dimethylbenzaldehyde

Table IIB. Physical Characteristics of Whey Protein Gels¹

<i>SAMPLE</i>	<i>D</i>	<i>E</i>	<i>F</i>
Salt	40mM NaCl/ 5mM CaCl ₂	10mM NaCl/ 5mM CaCl ₂	25mM NaCl
Structure Appearance	Stranded Translucent	Stranded Translucent	Stranded Translucent
Stress (kPa)	33.9 (40.9)	30.9 (29.6)	22.6 (20.7)
Strain	1.37 (1.49)	2.55 (2.48)	3.08 (2.91)
Gf (kPa)	24.8 (29.1)	11.4 (11.9)	7.35 (7.14)
Held-water (g/g prot.)	5.46 (5.35)	6.47 (6.44)	6.69 (6.68)

¹ - Values in parentheses reflect characterization from gels flavored with ethyl butyrate and those without parentheses reflect gels flavored with 2, 4-dimethylbenzaldehyde

Flavor Release from Protein Gels

There were significant differences in T_{onset} , T_{max} , I_{max} , $M_{release}$, and T_{dur} , for both cherry (Table III) and grape flavor (Table IV), among the six gel samples. Because the aim of this study was to evaluate release of flavor, only I_{max} and $M_{release}$ will be discussed further.

Table III. Mean TI Parameters for Cherry Flavor in Whey Protein Isolate Gels

<i>Parameters</i>					
<i>Gel sample</i>	T_{onset} (s)	T_{max} (s)	I_{max}	$M_{release}$ (l/s)	T_{dur} (s)
A	2.1 ^a	19.3 ^{ab}	162 ^a	10.6 ^a	51.5 ^a
B	2.4 ^{ab}	18.2 ^a	122 ^b	11.6 ^a	46.0 ^{bc}
C	2.0 ^a	17.7 ^a	146 ^a	11.9 ^a	50.1 ^{ab}
D	2.7 ^{abc}	20.9 ^{ab}	96 ^c	6.0 ^b	44.6 ^{cd}
E	3.3 ^c	27.4 ^b	82 ^{cd}	5.6 ^b	40.5 ^d
F	3.2 ^{bc}	18.1 ^a	71 ^d	4.8 ^b	34.7 ^e

^{a-c} - Samples with the same subscript within a column are not significantly different ($p < 0.05$)

Table IV. Mean TI Parameters for Grape Flavor in Whey Protein Isolate Gels

<i>Parameters</i>					
<i>Gel sample</i>	T_{onset} (s)	T_{max} (s)	I_{max}	$M_{release}$ (l/s)	T_{dur} (s)
A	1.4 ^a	14.6 ^a	179 ^a	9.7 ^b	41.1 ^a
B	1.5 ^a	15.9 ^{ab}	164 ^a	12.5 ^a	40.9 ^{ab}
C	1.4 ^a	16.0 ^{ab}	176 ^a	8.8 ^b	42.3 ^a
D	2.8 ^b	19.2 ^c	122 ^b	7.6 ^b	37.4 ^{bc}
E	2.6 ^b	17.5 ^{bc}	117 ^b	2.4 ^c	35.8 ^c
F	3.0 ^b	18.6 ^c	95 ^c	8.6 ^b	34.3 ^c

^{a-c} - Samples with the same subscript within a column are not significantly different ($p < 0.05$)

There was no relationship between gel strength (fracture stress) or rigidity (fracture modulus) and the intensity and rate of cherry or grape flavor released. In contrast to this, Guinard and Marty (10) found that the maximum intensity of benzaldehyde, ethyl butyrate and d-limonene flavor was suppressed by increasing the strength of gelatin, carrageenan, and starch gels. Further, Wilson and Brown (11) demonstrated that the strength of gelatin gels had a significant effect on the I_{max} and T_{max} of perceived banana flavor. In each of these studies, gel strength was adjusted by increasing the concentration of gelling agent, thus the effect of flavor binding could not be distinguished from those of gel strength. Gels, which were characterized by low water-holding released cherry and grape flavor at a greater intensity (Figure 1) and faster (Figure 2) than those that held-water well. Although, 2,4-

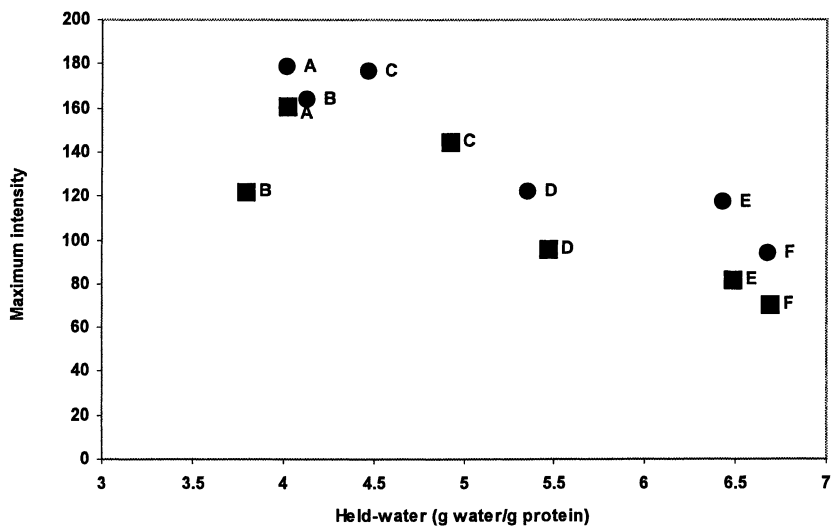


Figure 1. Maximum intensity as a function of held-water and microstructure:(■) cherry flavor; (●) grape flavor; (A-C) particulate structure; (D-F) stranded structure.

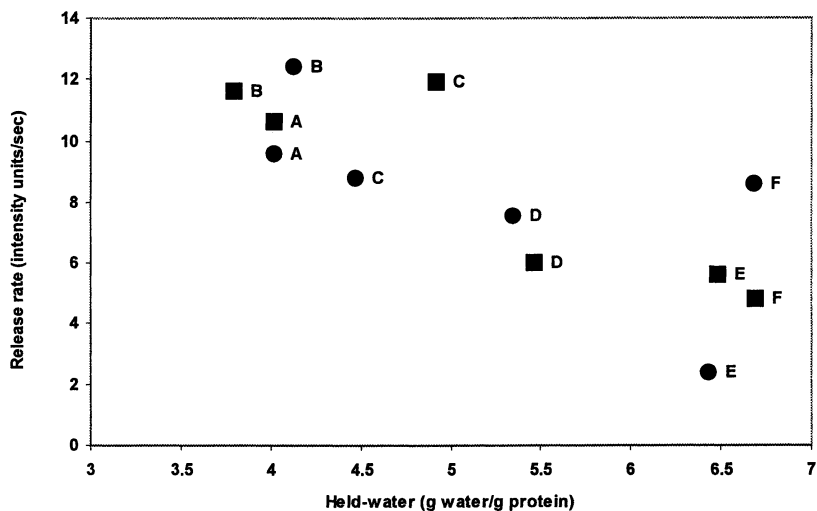


Figure 2. Rate of release as a function of held-water and microstructure:(■) cherry flavor; (●) grape flavor; (A-C) particulate structure; (D-F) stranded structure.

dimethylbenzaldehyde and ethyl butyrate are fairly non-polar compounds, it is assumed that any “free” flavor is associated with the water phase. In this gel system, any flavor which is not bound to the protein must exist in the water; possibly as a microemulsion. When a particulate gel is masticated, water is expressed quickly and therefore so is flavor. In contrast, very little water is released from gels with a stranded structure resulting in a low flavor intensity and release.

It was important to verify that TI differences were a result of physical properties of the gel and not of differences in flavorant concentration. To confirm equality of flavorant concentration in finished gels, 2,4-dimethylbenzaldehyde was extracted quantitatively from each gel sample. There was no difference in the quantity of extractable flavor compound in each gel ($p < 0.05$).

The effect and relative contribution of the oral breakdown process was not quantified in this study. However, the texture was described in informal bench testing. Particulate gels broke down quickly into many small distinct particles that created large amount of surface area for fast and intense release. Stranded samples were characterized by a geometric breakdown of the gel into smaller and smaller pieces that created increasing amounts of surface area at a much slower rate. These observations were confirmed in the next segment describing the sensory texture of the emulsion gels.

Physical and Sensory Texture Characterization of Emulsion Gels

The physical properties of each emulsion gel are summarized in Table I (24). Fracture stress increased as the volume of sunflower oil increased above 2.5% (v/v) in both the stranded and particulate gels. Further, in stranded gels, fracture strain decreased above a fat content of 2.5% and remained unchanged in particulate gels. Held-water represents the fraction of total moisture that is held by the protein network under a given force. Particulate gels held less water than stranded gels across all lipid levels.

A principal component analysis of the sensory texture data illustrates the relationship among 16 emulsion gel samples (Figure 3). Principal component one (PC1) represents 78% of the variance in the data set and shows a clear separation between stranded and particulate structured gels. Particulate gels are described by high values of cohesiveness of mass, crumbliness, adhesiveness, rate of breakdown, particle size distribution, and moisture release. In contrast, stranded gels were characterized by high values of surface smoothness, slipperiness, springiness, compressibility, particle size, irregular particle shape, smoothness, and moisture. Principal component two (PC2) represents 19% of the variance and separates samples according to lipid content. Gel samples that were high in sunflower oil were more firm and required more chews and longer times to prepare for swallowing.

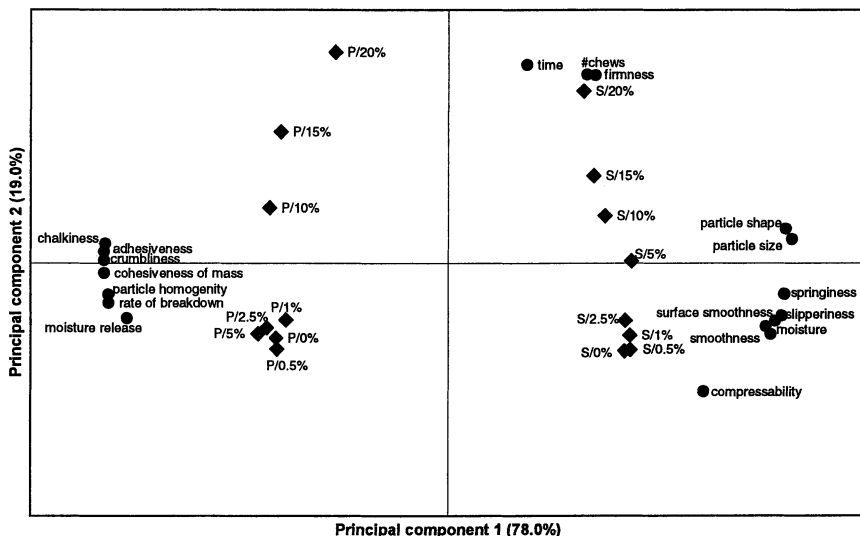


Figure 3. Principal component analysis of sensory texture data:(diamond) sample loadings; (circle) attribute loadings.

Flavor Release from Emulsion Gels

There were significant differences in T_{onset} , T_{max} , I_{max} , M_{release} , and T_{dur} , for both butter (Table V) and coconut (Table VI) flavor, among the six gel samples.

Table V. Mean TI Parameters for Diacetyl (butter) Flavor in Whey Protein Isolate Gels

<i>Parameters</i>					
<i>Gel sample</i>	T_{onset} (s)	T_{max} (s)	I_{max}	M_{release} (I/s)	T_{dur} (s)
S/0%	2.2 ^{ab}	15.8 ^{ab}	149.2 ^b	13.4 ^{ab}	53.6 ^{bc}
S/2.5%	2.8 ^a	19.4 ^{ab}	143.9 ^b	9.1 ^{bc}	54.5 ^b
S/20%	2.3 ^a	15.1 ^{ab}	97.0 ^c	6.8 ^c	50.0 ^{bc}
P/0%	1.1 ^c	14.4 ^b	187.5 ^a	16.4 ^a	57.5 ^{ab}
P/2.5%	1.2 ^c	14.0 ^b	188.5 ^a	16.0 ^a	63.3 ^a
P/20%	1.3 ^{bc}	24.2 ^a	86.4 ^c	6.0 ^c	47.0 ^c

^{a-c} Samples with the same subscript within a column are not significantly different ($p < 0.05$)

Table VI. Mean TI Parameters for δ -Decalactone (coconut) Flavor in Whey Protein Isolate Gels

<i>Parameters</i>					
<i>Gel sample</i>	<i>T_{onset} (s)</i>	<i>T_{max} (s)</i>	<i>I_{max}</i>	<i>M_{release} (l/s)</i>	<i>T_{dur} (s)</i>
S/0%	3.2 ^{ab}	23.8 ^a	129.7 ^{ab}	6.1 ^b	56.3 ^{ab}
S/2.5%	3.1 ^{ab}	23.0 ^a	117.5 ^b	5.9 ^b	66.1 ^a
S/20%	4.4 ^a	18.7 ^{ab}	55.6 ^c	4.2 ^b	37.9 ^c
P/0%	1.7 ^b	16.8 ^b	139.8 ^a	10.0 ^{ab}	63.1 ^a
P/2.5%	2.7 ^b	17.3 ^b	135.3 ^{ab}	14.4 ^a	66.3 ^a
P/20%	3.1 ^{ab}	19.1 ^{ab}	60.4 ^c	4.3 ^b	47.7 ^{bc}

^{a-c} - Samples with the same subscript within a column are not significantly different ($p < 0.05$)

At 0% and 2.5% (v/v) sunflower oil, gels that were particulate in structure released butter and coconut flavor faster (M_{release}) and with a greater intensity (I_{max}) than those that were stranded in structure. Further, the difference was more so for butter flavor. The particulate gels broke down quickly into small uniform particles creating large amounts of surface quickly for fast and intense release. Stranded gels were characterized by a slower breakdown into larger and irregular shaped particles that created increasing amounts of surface area at a much slower rate. Further, there was no relationship between gel strength (fracture stress) and the rate and intensity of flavor released. This is consistent with findings from protein gels that flavor release from WPI gels was not dependent on gel strength.

Particulate structured gels were distinguished by low water-holding or high moisture release and those that were stranded in structure by high water-holding or low moisture release (Table I). Diacetyl is a fairly polar compound and it is reasonable to assume that for a 0% (v/v) lipid system, any flavor that is not bound to protein is associated with the water phase. At 2.5% or 20% (v/v) lipid, diacetyl will partition between both the water and lipid. Although δ -decalactone is a non-polar compound it too must associate with the water phase in the 0% (v/v) lipid system. Interestingly, the flavor release properties of diacetyl or δ -decalactone were not affected by a lipid concentration of 2.5% (v/v). It is unclear why no differences were observed at low lipid levels. In this system, flavor was added after the emulsion was formed. One possibility is that, at low lipid levels, protein completely coated the surface of the oil droplets and therefore created a barrier to the flavor compound. Therefore, when the particulate gels were masticated, water was expressed quickly and therefore so was flavor. In contrast, very little water released from gels with stranded structure resulting in a low flavor intensity and release.

At 20% (v/v) sunflower oil, flavor release and intensity decreased and was independent of gel texture and flavor type. Both diacetyl, a polar compound, and δ -decalactone, a non-polar compound, associated with the lipid phase of the emulsion gels. Therefore, the mechanism of flavor release changed. In gels with little or no lipid, flavor release was dependent on water release and the generation of surface area. In gels with 20% (v/v) sunflower oil, flavor perception appeared to become a function of how flavor is released from lipid droplets.

Conclusion

By adjusting the amounts of NaCl and CaCl₂ in whey protein gels the effects of gel strength and water-holding could be evaluated at a fixed gel network concentration. The results show that flavor release in whey protein gels is dependent on structure and water-holding properties. Further, the dependence of flavor release on gel texture and lipid content was demonstrated. At low concentrations of lipid, flavor release in WPI gel systems was dependent on gel structure and independent of the flavorant properties. Particulate gels released large amounts of water and broke down quickly into small, spherical particles creating large amounts of surface area for fast and intense release. Stranded gels were characterized by no moisture release and a more geometric breakdown into larger and irregular shaped particles that created an increasing amount of surface area at a much slower rate. In contrast, when the composition of lipid was high, flavor release was independent of gel texture and the polarity of the flavor compound.

Literature Cited

1. Calorie Control Council (CCC). Fat replacers; Food Ingredients for healthy eating, 1996, pp 1-16.
2. Shamil, S.; Kilcast, D. *Nutrition Food Sci.* **1992**, *4*, 7-10.
3. Shamil, S.; Wyeth, L.J.; Kilcast, D. *Food Qual. Pref.* **1991/92**, *3*, 51-60.
4. Overbosch, P.; Afterof, W.G.M.; Haring, P.G.M. *Food Rev. Int.* **1991**, *7*, 137-184.
5. Bennett, C.J. *Cereal Foods World* **1992**, *37*, 429-432.
6. Pangborn, R.M.; Gibbs, Z.M.; Tassan, C. J. *Texture Studies* **1978**, *9*, 415-536.
7. Baines, Z.V.; Morris, E.R. *Food Hydrocolloids* **1987**, *1*, 197-205.
8. Chai, E., Oakenfull, D.G.; McBride, R.L.; Lane, A.G. *Food Australia* **1991**, *43* (6), 256-261.
9. Jaime, I.; Mela, D.J.; Bratchell, N. *J. Sensory Studies* **1993**, *8*, 177-188.
10. Guinard, J.X.; Marty, C. *J Food Sci.* **1995**, *60* (4), 727-730.
11. Wilson, C.E.; Brown, W.E. *J. Sensory Studies* **1997**, *21*, 69-86.
12. Kuhn, P.R.; Foegeding, E.A. *J. Agric. Food Chem.* **1991**, *39*, 1013-1016.
13. Kim, B.Y.; Hamann, D.D.; Lanier, T.C.; Wu, M.C. *J. Food Sci.* **1986**, *51* (4), 951-956, 1004.
14. Kochar, P.N.; Foegeding, E.A. *J. Food Sci.* **1993**, *58* (5), 1040-1046.
15. AOAC, *Official Methods of Analysis*, 16th ed. AOAC International, Gaithersburg, MD, 1995.
16. Gwartney, E.A. Ph.D. dissertation, North Carolina State University, Raleigh, NC, 1998.
17. SAS®, *SAS/STAT User's Guide*, Fourth edition, Volume 1, SAS Institute Inc., Cary, NC 1992.
18. Bowland, E.L.; Foegeding, E.A. *Food Hydrocolloids* **1995**, *9* (1), 47-56.

Chapter 30

The Relationship between Carvone Release and the Perception of Mintyness in Gelatine Gels

T. A. Hollowood, Rob S. T. Linforth, and Andrew J. Taylor

Samworth Flavour Laboratory, Division of Food Sciences,
University of Nottingham, Sutton Bonington Campus,
Loughborough, Leicestershire LE12 5RD, United Kingdom

A sensory panel rated the intensity of minty flavor in a 6% gelatine gel, containing varying concentrations of carvone. The flavor was assessed using Magnitude Estimation and Time Intensity Methods. In addition, the quantity of carvone released from the gel and reaching the assessor's nose was measured, breath by breath during eating, using the MS Nose™. The results showed that the quantity of volatile delivered to the nose was directly proportional to the concentration in the sample, however, the absolute quantity varied greatly between individuals. Furthermore, the relationship between perceived intensity and sample concentration was linear for both types of sensory data. Neither the speed of eating nor the concentration of volatile reached in-nose, affected an individuals ability to judge intensity. There was evidence to suggest, however, that the speed of eating affected the level of adaptation to the carvone stimulus.

Flavor can be defined as a complex pattern derived from the interaction of volatile, non-volatile, trigeminal and textural properties of food (1). Aroma delivery is arguably the most important aspect of flavor and, therefore, it is important to understand its impact on consumer perception.

The type of volatile compounds present, their concentrations, and their interactions with non volatile components are important factors. Historically, Stevens Law dictated that the relationship between perceived and actual intensity of a stimulus was governed by the power law $I=k(S-S^*)^n$ (2). This included terms for stimulus intensity (S) and perception threshold (S^*) but did not account for adaptation to a stimulus during prolonged exposure, nor the effect of varying the stimulus over time (3). Later derivations of the original equation included a term for the adapted perception threshold (4-5). Volatile components in food interact with non volatile components to produce a heightened response. For example, the perception of

mintyness has been found to correlate with the release of sugar from chewing gum rather than simply the release of menthone (6).

The means by which the components of a foodstuff become available to the sensory receptors is another controlling factor in perception. The breakdown of the food matrix during mastication coupled with the transport of gaseous volatiles to the olfactory epithelium, are governed by aspects of human physiology, behaviour, and anatomy; not to mention food structure, ingredients, and interactions. Early investigations of perception and adaptation used olfactometry and other orthonasal sniffing methods (7). Unfortunately sniffing a volatile compound cannot compare with the complexities of eating as described above, given that contact with the olfactory epithelium is greater for expired air than inspired air (8). Further work showed that sniffing and inhaling citral and vanillin solutions were consistent with Stevens Law, while sipping gave a very different response due to the influence of adaptation and trigeminal stimulation (9). It has been demonstrated using gels of varying gelatine concentration, flavored with furfuryl acetate, that the rate of volatile release has more influence on the intensity of perception than the absolute quantity released (10). The variation among individuals makes it difficult to provide more than general trend information about how volatile release will be affected by certain parameters. Variation observed during previous breath by breath analysis and release profile studies was probably due to differences in the rate of chewing, frequency of swallowing, saliva flow, rate of breathing, and anatomy (11-12). Detailed work looking at the effect of mastication patterns has shown that perception of flavor is linked to an individuals chewing style (13).

The following paper looks at the aspects of aroma delivery from a model foodstuff containing volatile, non volatile and textural properties. It seeks to find the differences that occur among individuals and how do these affect their perception.

Materials

Sensory Panel

A sensory panel consisting of 4 men and 10 women aged between 25 and 60 were selected on the basis of their ability to discriminate between samples of different intensity. Selection procedures included the ranking of citric acid solutions of differing concentrations and magnitude estimation (14) of orange flavor intensity using a cordial diluted to different strengths.

Training of the panel, during 8x 3hour sessions, and subsequent experience focused on Time Intensity (TI) as a means of continually assessing the intensity of specific attributes (e.g. mintyness or sweetness) during eating and thereafter.

Samples

The base gel mixture was prepared using 30% granulated sugar, 35% water, 40% glucose syrup, 6% gelatine (Type A – US mesh 20, 250 bloom), and 1% citric acid.

All quantities were on a w/w basis. The molten gel was mixed with quantities of carvone dispersed in propylene glycol to give final volatile concentrations of 125, 250, 500, 750 and 1000 ppm (mg/Kg).

Individual samples were cut to produce cubes of gel weighing 6g +/- 1g. Samples were stored at 4°C but allowed to equilibrate to room temperature (18-20°C) prior to eating. The selected concentration range fell between the individuals recognition and terminal thresholds.

Equipment

In-nose volatile concentration was monitored by the MS Nose™ (Micromass Manchester UK) using an Atmospheric Pressure Chemical Ionisation – Mass Spectrometry source (APCI-MS) Breath was sampled into the APCI-MS from a plastic nosepiece inserted into one nostril. Volatile compounds present were ionised and detected on the basis of their characteristic ion masses.

Flavor intensity was measured by means of a pivoting lever set against a 10-point scale. The positioning of the lever and the speed of measurement corresponded to the changing flavor intensity perceived in-mouth. The lever was attached to a 9-volt battery and performed as a potentiometer allowing more or less current to flow, dependent on its position. The output from the TI lever was interfaced to a computer and the electrical signal was converted into a trace showing perceived changes in flavor intensity in real time.

Procedure

Magnitude Estimation

Five samples containing different carvone concentrations were presented simultaneously to the panel. To reduce a sampling order effect, each assessor received the samples in a different random order. The panel was instructed to assess the first sample and attribute a score of 100 to its perceived minty flavor. All subsequent samples were scored for minty flavor relative to this sample. Mineral water and unsalted crackers were provided as palate cleansers.

Time Intensity and In-nose Volatile Release

TI and in-nose measurement of volatile release were performed simultaneously. Individual assessors were given time to relax and become accustomed to breathing through the plastic nosepiece. The pattern of acetone released on the breath was monitored to ensure that relaxed, regular breathing was achieved before a sample was introduced. The samples were presented to each assessor in a different random order. Individuals were instructed to chew the gel samples with their mouths closed, breathe

regularly, swallow as necessary, and record the perceived carvone concentration using the lever.

The assessment was complete when no more minty flavor was perceived. Assessors received a 15 min break between samples. The MS Nose™ was calibrated by direct comparison of the peak height for carvone released on each breath against the peak height for a known concentration of volatilised carvone injected directly.

Results and Discussion

The Effect of Increasing Carvone Concentration on Volatile Release

It is reasonable to assume that increasing the concentration of volatile in the sample results in a proportional increase in volatile delivered to the olfactory epithelium. Non linear behaviour would, however, occur if there were changes in the way in which the volatile was distributed in the food matrix (e.g. formation of droplets at high concentrations). The results in Figure 1 show the maximum quantity of carvone achieved in-nose ($I_{\max-ins}$) for each sample concentration, averaged across the panel. The clearly linear relationship is supported by an R^2 value of 0.9842

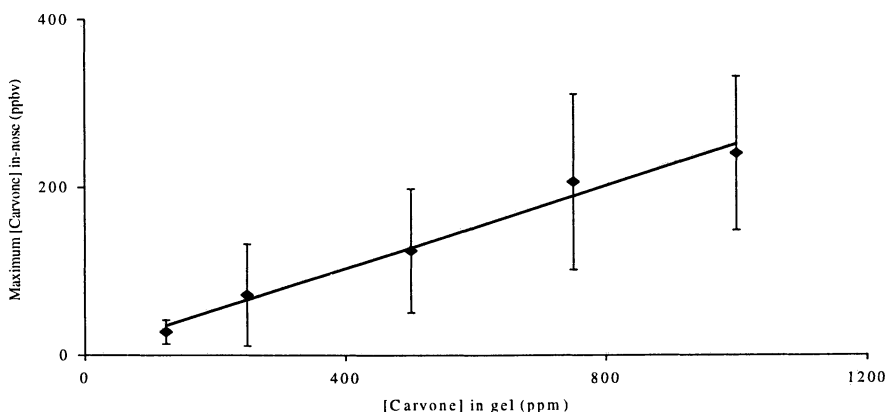


Figure 1. The relationship between carvone concentration in sample and the maximum volatile measured in-nose (average panel results)

The standard deviation, shown as error bars in Figure 1, highlights a significant variation in quantity of volatile delivered to the nose when comparing individual panellists.

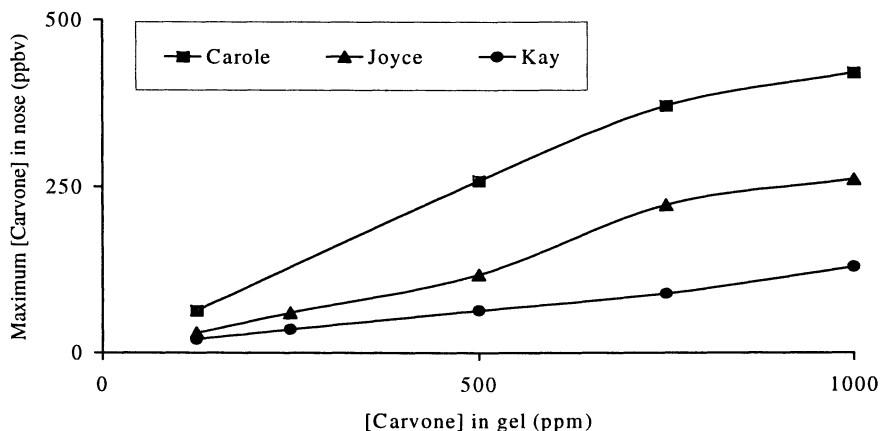


Figure 2. Relationship between carvone concentration in sample and the maximum volatile measured in-nose (individual panellists)

The quantities in-nose achieved by Carole were 3 times greater than those seen from Kay (Figure 2). This variation may have arisen from differences in their human physiology or may have been due to the mechanics of their eating, swallowing and breathing during eating. These differences were, however, consistent across the entire range of samples studied.

The Relationship Between Stimulus and Perception

The maximum perceived flavor intensity extracted from the TI data ($I_{\text{max-sen}}$) was averaged across the panel for each sample concentration. As long as all the data is gathered in the same way, the pooling of data from individual curves is a more robust measure of sensory effects from changes in stimuli (15). The relationship between perceived mintyness and sample carvone concentration was linear for the concentration range used giving an R^2 value of 0.972 (Figure 3). This linear relationship is most likely due to the exponents (0.2-0.9) for volatiles in Stevens Law, which tend to give linear relationships over limited concentration ranges. Magnitude Estimation data in the same way supported this relationship (Figure 4).

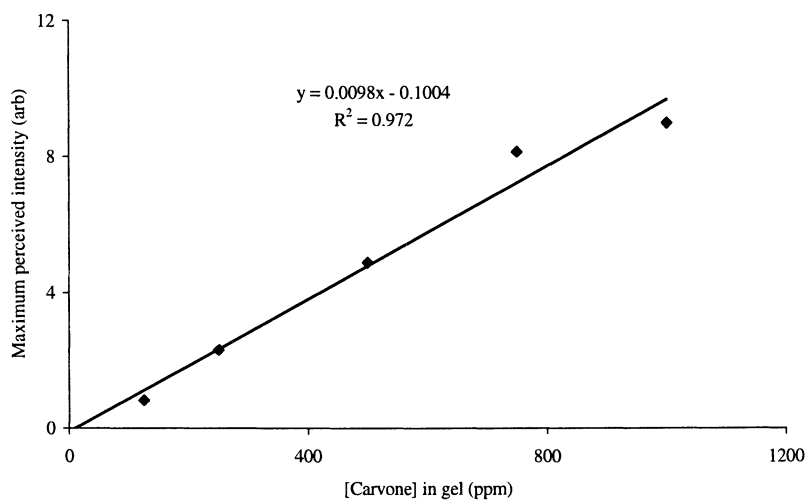


Figure 3. The relationship between maximum perceived mintyness determined by TI, and sample concentration.

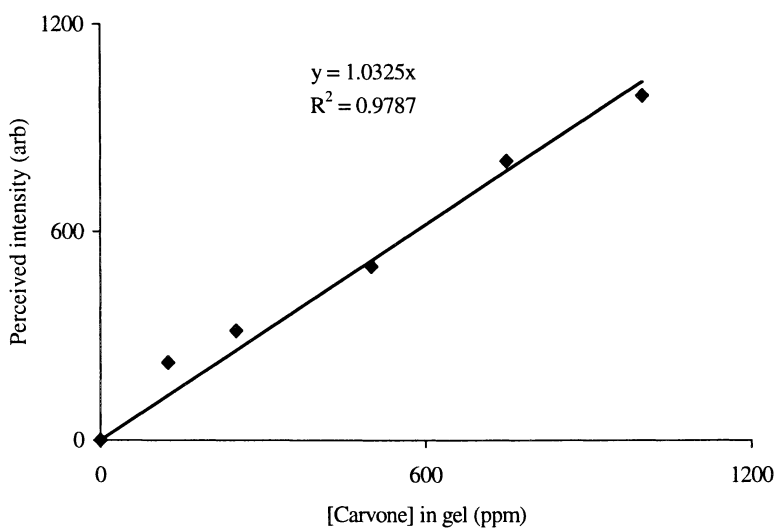


Figure 4. The relationship between perception of mintyness as determined by Magnitude Estimation, and sample concentration.

Differences Within the Panel

The results presented above utilise averaged data across the panel, however, some individuals did not exhibit a truly linear response for perception in relation to stimulus. Figure 5 illustrates the effect of increasing the in-nose concentration of carvone on the maximum perceived mintyness ($I_{\max\text{-sen}}$) for two assessors. Comparing the two individuals, Mike achieved a lower maximum concentration in-nose ($I_{\max\text{-ins}}$) and a poorer linear correlation between perception and stimulus ($R^2 = 0.821$) whereas the in-nose concentration and linear correlation for Sally was much higher ($R^2 = 0.942$).

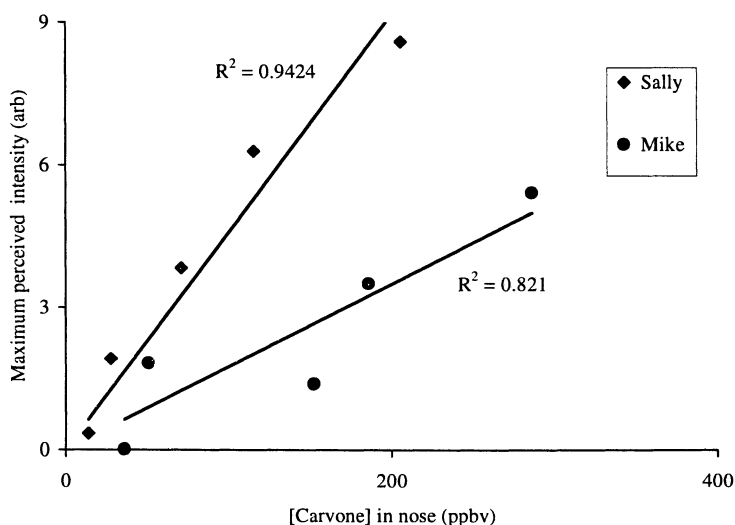


Figure 5. The effect of changing stimulus on perception – a comparison of two assessors.

Does this suggest that the speed of eating and/or the efficiency of volatile delivery to the nose affect the linearity of the response? To investigate this possibility further the R^2 values were calculated for each individual panellist as a measure of their ability to perceive changes in stimulus concentration.

The speed of eating was identified using the time to reach maximum carvone concentration in-nose ($T_{\max\text{-ins}}$). It is reasonable to assume that later T_{\max} values occur when food was kept in the mouth for longer. $T_{\max\text{-ins}}$ values were very similar for an individual regardless of the sample concentration. Therefore, values for all samples were averaged for each assessor giving a more robust measure of their eating speed.

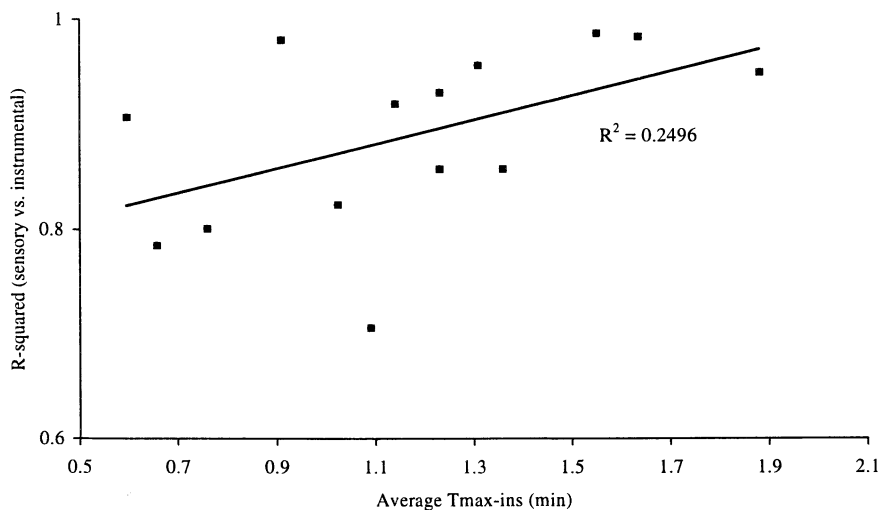


Figure 6. The effect of eating speed on the linear correlation of stimulus and perception.

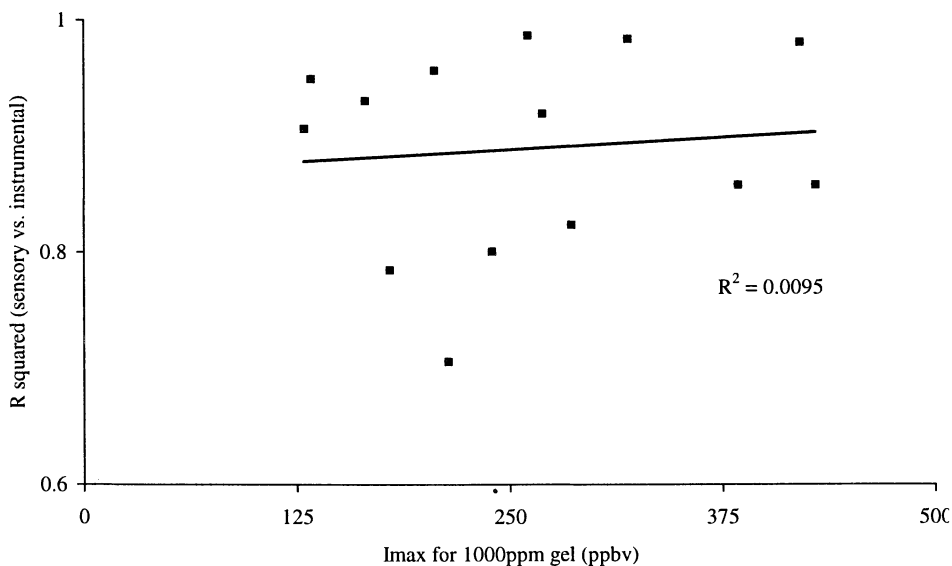


Figure 7. The effect of the maximum breath volatile concentration (1000ppm gels) on the linear correlation between stimulus and response.

Figures 6 and 7 showed there was clearly no effect of speed of eating or efficiency of volatile delivery on the R^2 values for the relationship between stimulus and perception. Therefore, panellists who ate quickly or who had greater breath I_{\max} values, performed no better or worse than the other panellists. Furthermore, Figure 8 showed that speed of eating and the delivery of volatile to the nose were independent variables. The maximum quantity achieved in nose for the 1000 ppm gel did not increase just because the food remained in the mouth for longer.

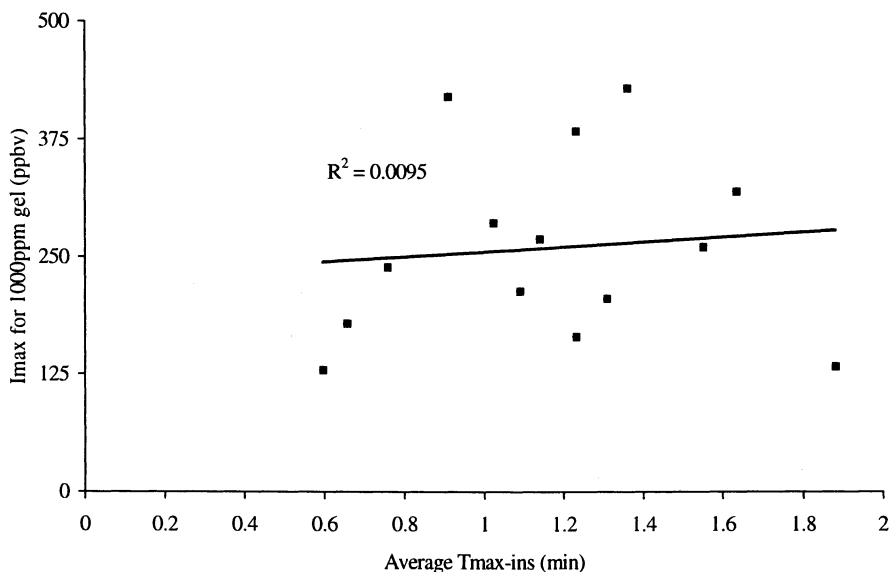


Figure 8. The effect of eating speed on the maximum [carvone] measured in-nose (1000ppm gel).

Adaptation

When comparing the time to maximum concentration in-nose (T_{\max} -ins) and the time to maximum perception (T_{\max} -sen) there appeared to be a difference in the timing of the two events. For several assessors, T_{\max} -sen occurred before T_{\max} -ins suggesting adaptation. Previous work has shown that for volatiles released slowly from a food system, the perceived maximum intensity occurs before the in-nose maximum due to adaptation to the stimulus. Conversely, volatiles released quickly from a food system tend to show a perceived maximum intensity after that measured in-nose (16). Could the adaptation effect observed for the carvone data be linked to the eating process?

The effect of adaptation was taken as the time difference between T_{50} -ins and T_{50} -sen, that is, the time to fall to 50% of the maximum intensity for stimulus and

perception (Figure 9). Figure 10 shows the effect of eating speed on the level of adaptation. There was evidence to suggest that the slower the eating event, the greater the adaptation to the stimulus. The relationship gave an R^2 value of 0.50 and the linear regression was significant at a 0.05 probability.

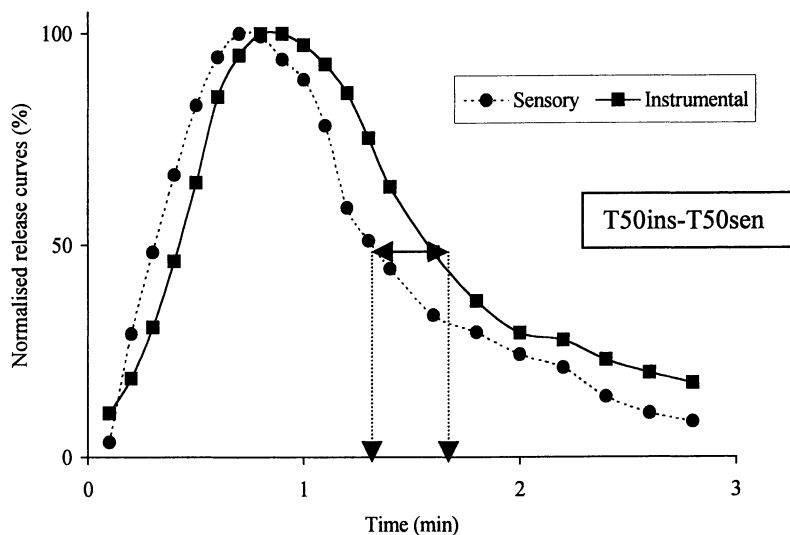


Figure 9. The use of T50 values from sensory and volatile release curves as a means of measuring adaptation.

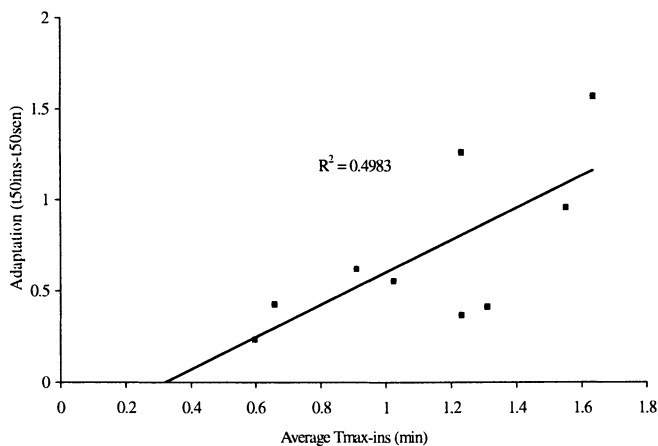


Figure 10. The effect of eating speed on adaptation.

Conclusion

The investigation into the effect of increasing the carvone concentration on the perception of minty flavor in a 6% gelatine gel revealed that, on average, the relationship between stimulus and perception was linear for the system used. Some individual assessors showed more linearity in this relationship than others. Further analysis of the data revealed that the speed of eating and the maximum quantity of volatile delivered to the nose had no effect on the linear correlation. However, there was some evidence that the speed of eating affected the level of adaptation to the stimulus.

Acknowledgements

This work was funded through a BBSRC Link Scheme which included Firnenich and Nestlé as industrial partners.

Literature Cited

1. Thomson, D. M. H. In *Development of Food Flavours*; Birch, G. G.; Lindley, M. G., Eds.; Elsevier: London, 1986; 1.
2. Stevens, S. S. *Am. Psychol.* **1962**, *17*, 29.
3. Overbosch, P.; Afterof, W. G. M.; Haring, P. G. M. *Food Reviews International.* **1991**, *7(2)*, 137-184.
4. Overbosch, P. *Chem. Senses.* **1986**, *11(3)*, 315-329.
5. Overbosch, P.; De Jong, S. *Physiol. Behav.* **1989**, *45*, 607-613.
6. Davidson, J. M.; Linforth, R. S. T.; Hollowood, T. A.; Taylor, A. J. *J. Agric. Food Chem.* In press.
7. Kosler, E. P.; Wijk, R. A. In *The Human Sense of Smell*; Laing, D. G.; Doty, R. L.; Breipohl, W., Eds.; Springer: Verlaa, 1991, pp 199-215.
8. Laing, D. G. *Physiol. Behav.* **1985**, *34*, 569.
9. Voirol, E.; Daget, N. *Lebensm. Wiss. Technol.* **1986**, *19*, 316-319.
10. Baek, I.; Linforth, R. S. T.; Blake, A.; Taylor, A. J. *J. Chem. Senses.* **1999**, *24*, 155-160.
11. Soeting, W. J.; Heidema, J. *J. Chem. Senses.* **1988**, *13*, 607.
12. Ingham, K. E.; Linforth, R. S. T.; Taylor, A. *Lebensm. Wiss. U-Technol.* **1995**, *28*, 105-110.
13. Wilson, C. E.; Brown, W. E. *J. Sensory Studies.* **1997**, *12(1)*, 69-86.
14. Moskowitz, H. R. *J. Food Qual.* **1977**, *1*, 195.
15. Overbosch, P.; Van den Eenden, J. C.; Keur, B. M. *Chem. Senses.* **1986**, *11(3)*, 331-338.
16. Linforth, R. S. T.; Baek, I.; Taylor, A. *J. Food Chemistry.* **1999**, *65*, 77-83.

Chapter 31

Flavor Release from Composite Dairy Gels: A Comparison between Model Predictions and Time–Intensity Experimental Studies

I. P. T. Moore¹, T. M. Dodds, R. P. Turnbull, and R. A. Crawford

New Zealand Dairy Research Institute, Palmerston North, New Zealand

We tested a spreadsheet-based model for flavor release from composite (fat, protein, water) gels in the mouth using a simplified gel system with single flavors added and a sensory panel trained in the use of time-intensity methods. Gel manufacture was adjusted to control the parameters used in the model. The model mimicked the shape of the experimental time-intensity plot only when it incorporated removal of flavor by breathing and swallowing. The predicted time-intensity curve depended on the exchange flow of air between the mouth and throat. Factors associated with the gel had a much smaller effect. The model predicted correctly that flavor diffusivity and fat particle size had a small effect on perceived maximum intensity of flavor (IMax) and time of maximum intensity (TMax). It also predicted that IMax would be proportional to flavor concentration in the gel, but the experimental increase in IMax was less than proportional to changes in concentration.

The balance of perceived flavors in a food material can be changed by changing the concentration of the flavor compounds in the food, for example by changing the ingredients. However, it is also possible to obtain different perceived flavors by changing the texture of the food, without altering the composition. This occurs because changing the texture affects the speed of release of the individual flavor compounds to different extents. Thus the balance of flavors as perceived in the mouth is also changed.

To avoid lengthy sensory trials during product development, a method is required which can be used to predict the perceived flavor. One part of this method is to be able to estimate the rate of flavor release from a knowledge of some simple physical properties of the flavor compound and the food. This chapter describes the development of a method to calculate the release rate of a flavor compound from a

¹Current address: Goodman Fielder Ingredients, 45–47, Green Street, Botany, New South Wales 2019, Australia.

composite gel (made up of an aqueous protein matrix plus discrete fat particles). It then compares the predictions, obtained by applying the methods to a real system, with experimental measurements of dynamic flavor perception using time-intensity techniques.

The particular focus of the study reported here was the effect of fat particle size on flavor release from a composite gel (similar to processed cheese). Most of the critical volatile flavor compounds in cheese and processed cheese are fat soluble (1). The release of volatile fat-soluble flavor compounds from liquid emulsions has been widely studied and modelled (2-10). Some of the studies indicated that the flavor release rate from emulsions depends on the fat droplet size in the emulsions (3, 6) and we expected to observe a similar effect in composite gels. As far as possible, we manufactured composite gels with similar firmness, to avoid the texture of the gels interfering with the measurement of the effects of fat particle size.

Model Development

The method adopted in developing our model was similar to that of Harrison & Hills (5). We differ in the method of realising the model, where we have chosen to implement a direct numerical simulation within an Excel spreadsheet and in some minor details of the stages in the release process. Harrison and Hills (5) identified rate-determining steps in the release process; we included all the steps we could identify in the model. The composite gel was assumed to contain two phases, an aqueous protein phase and a dispersed fat particle phase. The only mechanism for bringing the flavor compounds to the surface of a gel particle was assumed to be diffusion. Melting of the gel at the surface and direct transfer from the fat to saliva were neglected.

Typically, a real gel sample for sensory testing would be roughly cubic in shape. Inside the gel, the fat particles would be roughly uniformly dispersed. For composite gels, the fat particles are typically 1-50 μm in diameter and a variety of shapes (Figure 1). Within the sample, some fat particles will be very close to the sample surface, while others will be close to the sample center and so roughly at a distance of half the sample size from the surface. Thus flavor compounds dissolved in the fat will have different distances to diffuse to the sample surface, from almost zero to half the sample size.

To simplify the mathematical model, the fat particles were assumed to be all spherical, of identical size, and surrounded by a spherical shell of protein material. Flavor compounds diffused through the spherical shell to reach the surface, where they passed into a surrounding pool of aqueous liquid which represented the saliva in the mouth (Figure 2).

For spherical diffusion: $\frac{dc}{dt} = D \left\{ \frac{d^2c}{dr^2} + \frac{2}{r} \frac{dc}{dr} \right\}$ where c is the concentration

of the flavor compound in the gel, D is the diffusivity and r is the distance out from the center of the sphere.

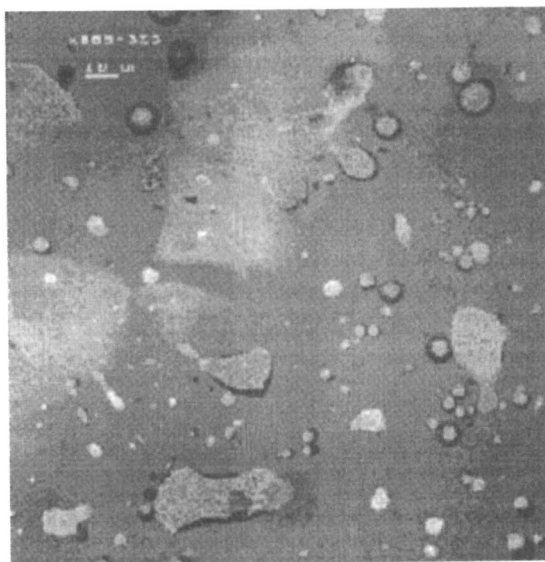


Figure 1. Confocal laser micrograph of a typical composite gel. Paler regions are the fat particles; darker regions are the protein matrix.

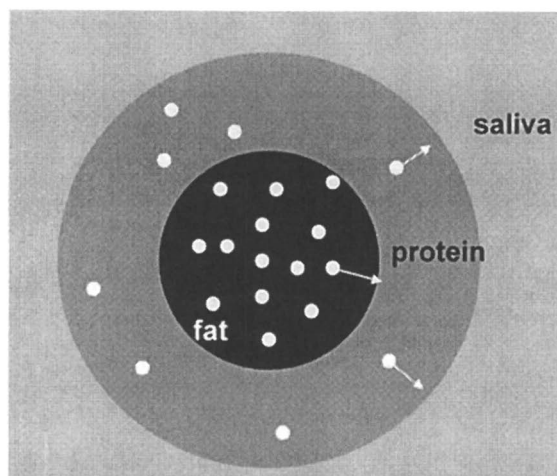


Figure 2. Conceptual model of the composite gel particle. White circles represent flavor molecules.

For a fat-soluble flavor compound, diffusion through the fat particle was also included. At the interface between the fat and the protein matrix, the flavor concentrations in the two phases were assumed to be in equilibrium. The concentration in the saliva was assumed to be equal to the concentration at the outer surface of the spherical shell of protein. At the interface between fat (A) and protein

$$(B), \text{ flux} = D_A \frac{\partial c_A}{\partial r_A} = D_B \frac{\partial c_B}{\partial r_B} = F(c_I, t) = F^*(c^*_I, t)$$

where $c^*_B = K c_A$ (K is the partition coefficient)

For the numerical solution, each particle was divided into 40 spherical shells at equal radial steps (20 through the fat, 20 through the protein). The model used Fickian diffusion through the spherical particles, with the rate of diffusion proportional to the concentration gradient.

Once the initial model was tested, the model was extended to include mechanisms for removing flavor compounds from the mouth. The first mechanism was to allow for swallowing of saliva, which simply resulted in a step decrease in the concentration of flavor in the saliva. It was assumed that the volume of saliva in the mouth remained constant - the swallowed saliva was replaced instantaneously by fresh saliva.

At the same time the model was adapted to allow for the effects of chewing, at least in a very simplified manner. It was assumed that chewing resulted in a step change in the particle size in the mouth, which occurred at the same time as the swallowing. The smaller particle size resulted in a shorter distance for the flavor to diffuse over to the particle surface, so increasing the rate of flavor release from each particle. The mathematical procedure for modelling the step change was not strictly accurate, since the concentration profile in the particles also changed, but the overall effect appeared to be consistent with the expected change in release rates. The increase in complexity required to include a mathematically exact description of the concentration profile after the particle size change was not expected to give a significant improvement in the predictions of the model.

The next step was to allow for evaporation of volatile flavors into the respired air at the back of the mouth. The absorption of volatile flavor compounds in the nose is a key part of flavor perception and it was expected that the concentration in the respired air would be a key predictor of flavor release. In addition, the evaporation of flavor compounds provides another mechanism for the loss of flavor from the mouth.

Modelling this process required the introduction of two further parameters, the interfacial area between the saliva and the air, and the mass transfer coefficient between the saliva and the air. At this stage no values were available for either and so estimated values were used. It was assumed that the evaporation occurred into a fixed volume of air at the back of the mouth and that the fixed volume was swept by a constant flow of respired air (Figure 3).

The mass transfer between the retronasal air (flowrate Q) and the saliva is described by the differential equation:

$$\frac{dc_G}{dt} = \frac{h_{SG} A_{SG}}{V_G} (c_S - K_w c_G) - \frac{Q}{V_G} c_G = (V_S + V_C) \frac{dc_{(S+C)}}{dt}$$

where h_{SG} = mass transfer coefficient between saliva and air, A_{SG} = interfacial area between saliva and air, K_W = equilibrium constant for partition of flavor between saliva and air, $c_{<S+C>}$ = the overall mean concentration in the saliva and composite gel. V_C , V_S , V_G refer to the volumes of the gel particle, the saliva and the air in the mouth respectively; c_S , c_G , are the concentrations of the flavor compound in the saliva and the air.

The differential equations for the diffusion were converted to a numerical format using the Crank-Nicolson method. The resulting set of 42 simultaneous equations (including the saliva and the gas) was solved using a matrix inversion method implemented in a Microsoft Excel Spreadsheet. This approach made it possible to make step changes in the parameters during the simulation, such as the changes due to chewing and swallowing. Once written, the spreadsheet ran the simulations reasonably quickly (about 4 minutes on a 133 MHz Pentium PC to simulate a 1 minute flavor release experiment).

Experimental Method

Panel Training

Time Intensity Methods

Time intensity (TI) is a sensory method that measures human response to a stimulus over a time period. TI has most commonly been used to measure attributes such as bitterness, sweetness, astringency and trigeminal sensations. TI has also been used effectively for evaluating textural attributes and flavor release in products which undergo changes of phase in the mouth.

Panel Training

A key part of the training for this trial was to establish a common evaluation procedure amongst the panelists. The sensory panel was made up of twelve members, who were selected for their sensory acuity and trained in the evaluation of natural cheese. As none of the panel members had experience in the evaluation of composite gels or the time intensity method, a training program was implemented to cover these two areas.

The training program aimed to

- allow panelists to become familiar with the composite gel product
- develop an evaluation procedure
- allow panelists to understand and practice the time intensity method
- identify and develop descriptors for the flavor compound

Twenty-eight training sessions were held. Approximately four sessions focused on developing a method for sample evaluation. Once the decision had been made to use ethyl butyrate as the flavor compound for this trial, training focused on the flavor and intensities associated with the chosen levels of ethyl butyrate (approximately seven sessions).

During initial training sessions panelists recorded their responses on a paper ballot at 5 s intervals. At more advanced training sessions and for the duration of this trial, CSA (Version 5.2.4) was used to record the data. The computerised system allows panelists to indicate their response by movement of a mouse cursor along an unstructured scale. Panelists were able to use the scale freely and were not forced to return the cursor to the zero position at the end of the time period.

Composite Gel Manufacture

We used composite gels manufactured from rennet casein, anhydrous milkfat, water and emulsifying salts (Trial 1) and from Mozzarella cheese, water and emulsifying salts (Trial 2) as shown in Table I.

Table I. Formulations used for Sample Production

	Levels – Trial 1	Levels – Trial 2
Mozzarella cheese	-	87.9% w/w
Water	48.0% w/w	9.8% w/w
Anhydrous milkfat	19.4% w/w	-
Rennet casein	29.2% w/w	-
Emulsifying salt	2.4% w/w	2.4% w/w
Hydrochloric acid (0.1M)	1.5% w/w	
Emulsifier type	None, Tween 60 (at 0.5% w/w)	None, Tween 60 (at 0.5% w/w)
Flavoring	Ethyl Butyrate Absent, 50ppm (low), 100ppm (high)	Absent, 50ppm Ethyl Butyrate
Mixer speed	120 rpm (slow), 180 rpm (fast)	1500 rpm (slow), 3000 rpm (fast)

In both trials we used Sodium Hexametaphosphate as the calcium scavenger to release casein to emulsify the fat particles. Sodium Hexametaphosphate gives a firm-textured product. The protein source was selected to minimise any flavors which would distract from the added flavor. In addition, the cheese-based gels proved to be significantly more palatable than the rennet casein-based gels.

We added ethyl butyrate to the gels in both trials to give a distinctive flavor at a controlled level. Ethyl butyrate is preferentially fat soluble, gives a fruity (pineapple) flavor and is often found in cheese.

The gels for trial 1 were manufactured in a 25 kg capacity Blentech twin-screw cooker. Those for trial 2 were made using a 25 kg capacity Stephan cooker-cutter. All the ingredients (including the flavor) were blended together in the cooker at ambient temperature and the mixture was then heated by steam injection to 85°C over 90 s. The mixture was then cooked for 3 minutes at 85°C and packed. During the cooking process, the cooker was kept closed, to prevent loss of the flavor compounds by evaporation.

We tested for flavor losses due to processing in a separate experiment in which we used direct and indirect heating. The level of flavor compound in the product was tested by solid phase microextraction followed by gas chromatography and we found that in both cases the levels of flavor compound after processing were similar to those in a sample which had been blended with the desired amount of the flavor compound after cooling.

For both trials, we manufactured 10 kg of each gel sample, and filled each sample into 500g pots. After taking 1 pot each for chemical analysis, microbiological testing, texture testing and confocal laser microscopy, the remaining samples were stored at 4°C until required by the sensory panel.

Experimental Design for Composite Gel Manufacture

The three factors used to produce the samples for each trial formed a randomised block design. Details of the levels are shown in Table I.

The design intended that replicate samples be produced in two blocks. Each block was to have consisted of two days of gel manufacture, with all ten samples within a block being produced in random order. However, difficulties during production meant that this schedule was not fully adhered to and the block effect was lost from the design.

Sensory Analysis

Samples were presented to panelists in four sessions, each session consisting of two sittings. Each session was held on a separate day. A total of six experimental samples were presented at each session, one of which was a duplicate (5 samples + 1 duplicate). Of these six samples, 3 were presented at a sitting, with the sample presentation order being randomised over the 2 sittings held each day.

The panel members were given a 1.5 cm cube of each gel. The panel were instructed to record the flavor intensity while chewing the gel. After 30s, the panel were allowed to swallow naturally, and after 60s they spat out any remaining cheese. There was a 2 minute interval between samples, during which panellists rinsed their palates with soda water, carrots, and water at 24°C.

A 'warm up' control sample was presented first at each sitting to allow panelists to orientate themselves with the base flavors of the gels.

The CSA software produces 7 parameters which we used to analyse differences among samples and among experimental variables. The parameters are shown in Table II.

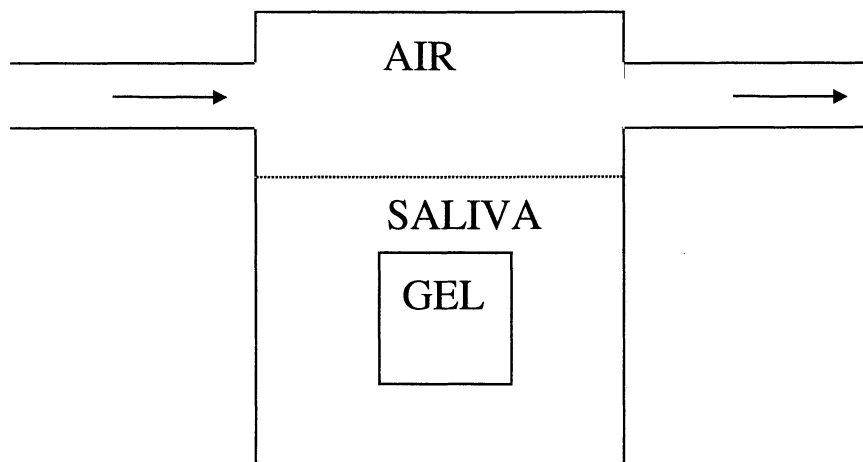


Figure 3. Conceptual model of the mouth.

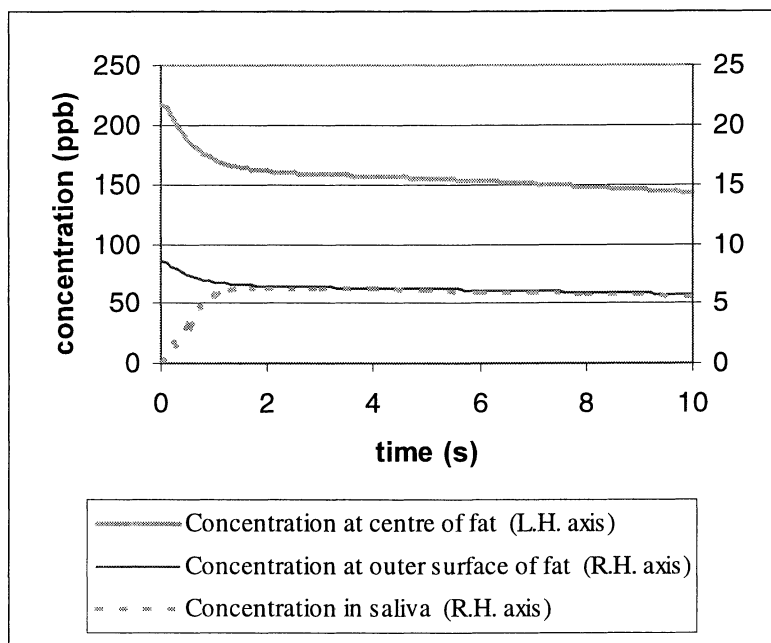


Figure 4. Initial development of flavor concentrations - simplified model. L.H. = left hand axis; R.H. = right hand axis.

Table II. Definition of TI Parameters

Parameter	CSA Version 5.2.4 Definition
Time at maximum intensity (TMAX)	The time required to reach maximum intensity
Maximum Intensity (IMAX))	The highest point on the curve
Duration (DURr)	The total time (seconds) from the time the attribute is first detected to the finish of the test
Area Under Curve (AUC)	The total area under the curve
Increase Angle (Inc Angle)	The angle (in degrees) of ascent from start to IMax.
Increase Area (Inc Area)	The area under the ascending portion of the curve from start to Imax
Decrease Angle (Dec Angle)	The angle (in degrees) of descent from IMax to the last recorded value
Decrease Area (Dec Area)	The area under the descending portion of the curve from IMax to the last recorded value

Results

Modelling

Figure 4 illustrates the typical changes in concentration of a flavor volatile in the gel particles and the saliva for the simplest case of the model, where there is no swallowing and no removal of flavor from the mouth by breathing. The curves are tending to an equilibrium (plateau) value because the mechanisms for removal of the flavor volatiles have been excluded. In practice, as Baek *et al* (11) have shown, the flavor concentration in the mouth rises to a peak and then falls during a flavor release test.

Figure 5 shows the effect of assuming that 50% of the saliva is removed by swallowing every 10 s. The model assumes all the solid gel remains in the mouth. The steps in concentration are very sharp, since it was also assumed that the total saliva volume was constant and that the swallowed saliva was instantly replaced by fresh saliva. By allowing the air in the mouth to also exchange with air in the throat, the effect of the sharp changes in the saliva concentration were considerably smoothed. The air in the mouth acts as a pool of flavor which only responds slowly to changes in the saliva.

The effect of changing the air flow rate through the mouth is shown in Figure 6. When the flow rate in the model was increased to near normal breathing rate, the concentration of flavor in the mouth followed the changes in saliva more closely. This suggested that an exchange process between air in the mouth and air in the throat would be a more realistic way to interpret this part of the model.

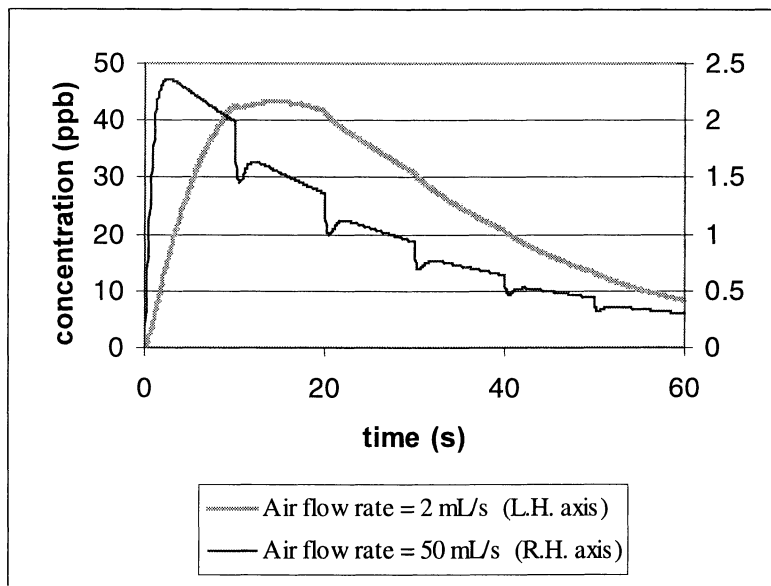


Figure 5. Effect of air flow rate on flavor concentration in air.

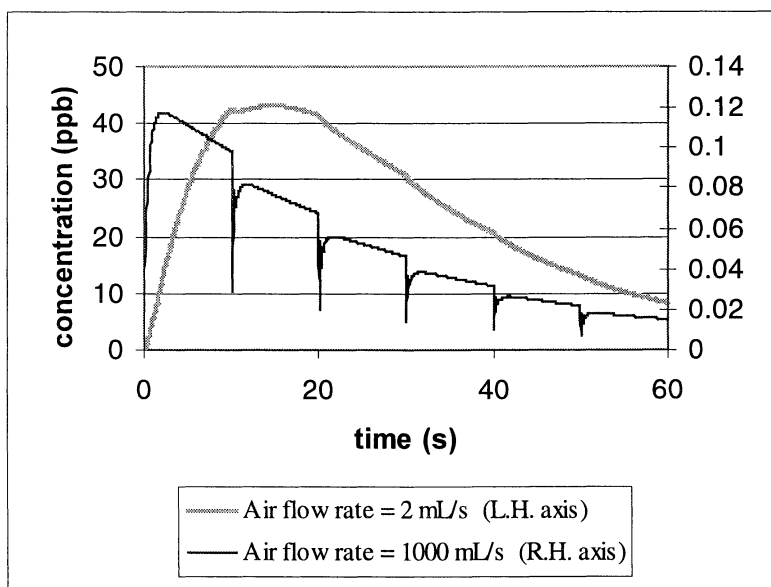


Figure 6. Effect of air flow rate on flavor concentrations in air.

Experimental Study

For each sample in the trial, we averaged the time intensity parameters over all the panel members. Figure 7 shows a typical experimental time-intensity curve. The comparable data from the model have also been shown. The two curves are very similar up to 30s. At this point, the panellist was allowed to swallow freely, and the model assumed that the panellist swallowed 50% of the saliva (and no solids) at 30s, again at 40s and again at 50s. The appearance of the experimental curve suggests that this panellist swallowed almost all the sample and saliva at 30s, so removing all the flavor from the mouth. Because we allowed free swallowing, the model could not be expected to perfectly match any single panel member.

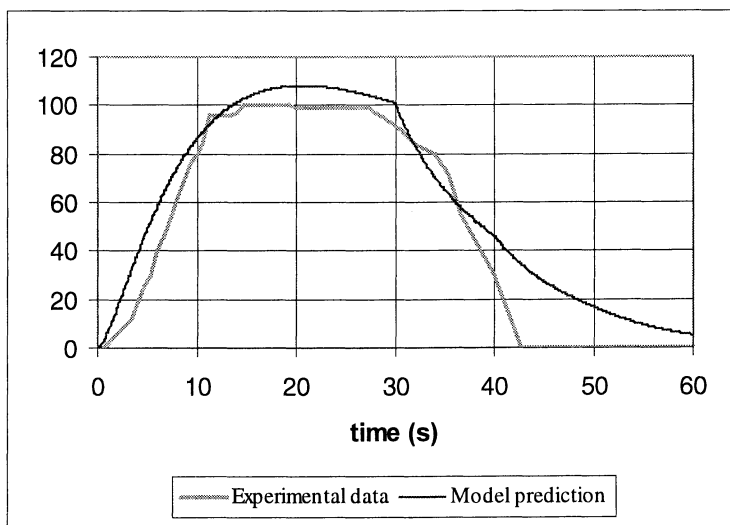


Figure 7. Experimental time-intensity curve of one panellist and model prediction

To compare the time intensity parameters against the model predictions, we required two key measurements. The first was the fat particle size, which we used to establish the gel particle size in the model. We measured fat particles using images from confocal laser microscopy (similar to Figure 1). By measuring and counting about 500 fat particles, we were able to obtain a representative mean size.

The second parameter in the model that changed with varying processing conditions was the diffusivity of the flavor in the protein part of the gel. We could not measure this directly, but we assumed that the diffusivity was inversely proportional to the firmness of the gel. These values were then used in the model to predict the time-intensity parameters for each sample.

For the experimental time-intensity parameters, we used the average values for all the panel members. This introduced some noise into the comparisons since the

physiological coefficients (saliva volume, air flow rate and mas transfer rates) would be different for each panel members and we had to assume a single value for the model.

Figure 8 and 9 show the comparison between the predicted and experimental parameters for the 50 ppm ethyl butyrate samples (trials 1 and 2). There is considerable scatter around the ideal match between experiment and model (shown as a solid line).

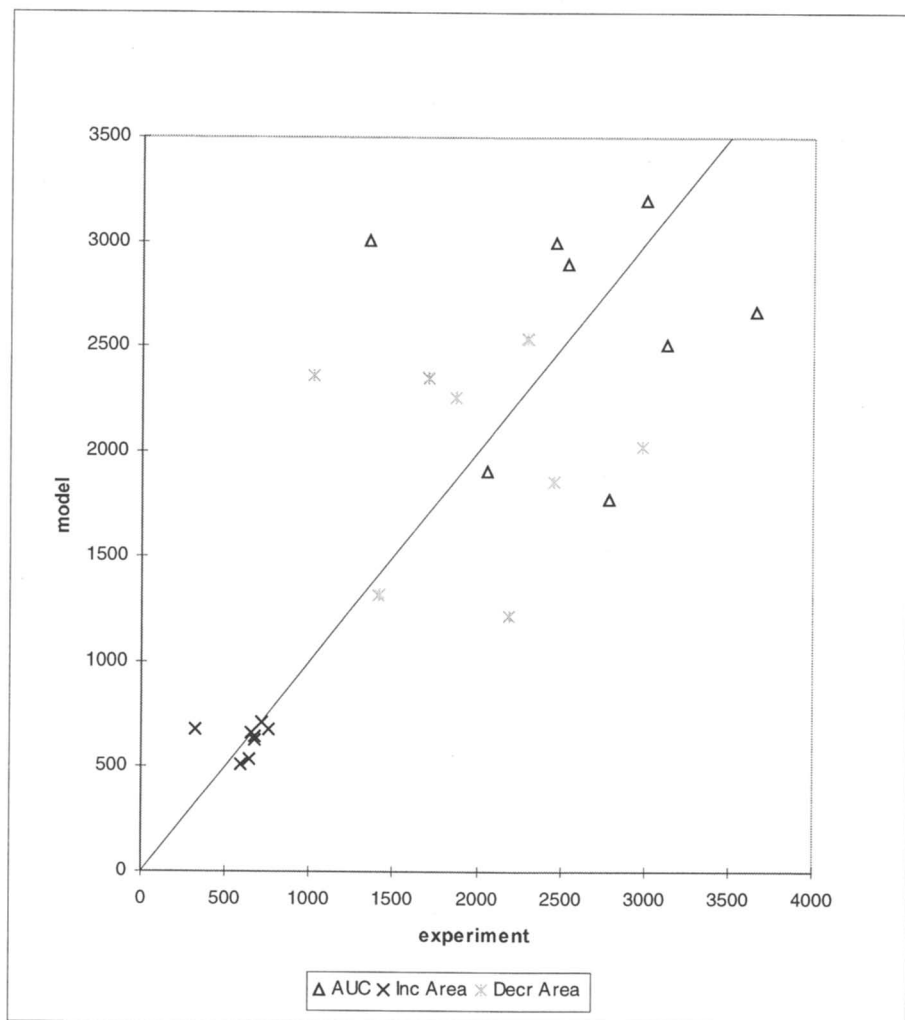


Figure 8. Comparison of experimental parameters and model predictions

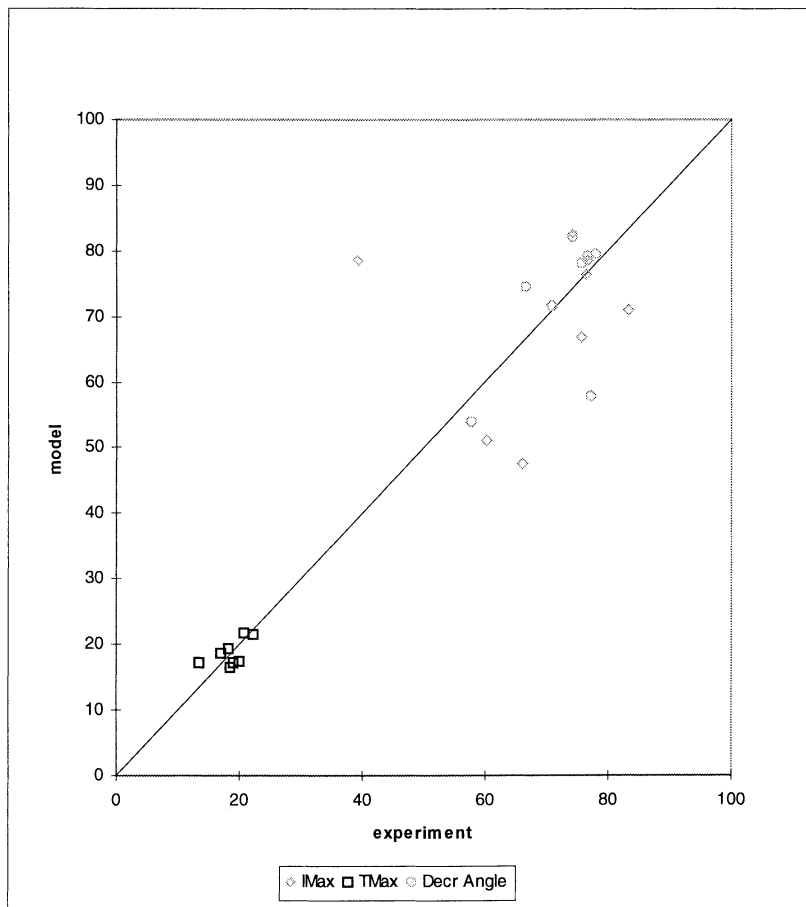


Figure 9. Comparison of experimental parameters and model predictions

The best match between model and experiment was for the area under the increasing part of the curve. As shown in Figure 8, the trends were correctly predicted apart from a single outlying point. We could not find any obvious explanation for this single point, but it does appear as an outlier in some of the other data too.

The initial part of the curve is most likely to be matched by the model. The simulation was less valid for the later part of each experimental trial because we had allowed free swallowing, which the model could not match.

Figure 9 shows a good match for both time to maximum intensity (TMAX) and maximum intensity (IMAX), although the outlier is clear again in this set. In particular, the trends of the experimental data were well matched by the model for TMAX. We also attempted to correlate the results for TMAX directly with the two measured properties of the gels, the hardness and the fat particle size. We found no direct correlation between these properties and any of the time-intensity parameters.

One of the problems which we encountered with this study was the difficulty in changing the experimental conditions sufficiently to see significant variations in the time-intensity parameters. Within a range of similar gels, the mean fat particle size could only be changed by a factor of about 10 times and both the experiments and the model showed that this had a relatively small effect on the flavor release. Similarly, for gels of similar gross texture (solids as opposed to liquids), we were limited to a hardness variation by a factor of approximately 5. This gave only a small variation in both experimental and predicted flavor release parameters.

In addition, we found that the experimental sensory parameters for the water-soluble flavor differed between replicate manufactures. TMAX varied by up to 2 times and IMAX by up to 1.5 times. We were unable to find any relationship between the variations and the instrumentally measured properties (firmness and fat particle size). We believe that the differences in the sensory parameters were caused by panel variability.

Conclusions

A mathematical model has been developed which can predict the release of flavor from a composite gel into saliva in the mouth or retronasal air. The model for flavor release predicted the variation in TMAX for fat soluble flavors. IMAX and AUC were less well predicted by the model. There was no evidence of a consistent difference between the predicted and the experimental values of IMAX and AUC; this may indicate that the differences were mainly caused by random noise in the measured parameters.

References

1. Urbach, G. *Int. J. Dairy Tech.*, **1997**, 50, 79-89
2. Brossard, C.; Rousseau, F.; Dumont, J. P. In *Flavor Science: Recent Developments*, Taylor, A. J.; Mottram, D. S., Eds.; Royal Society of Chemistry: London, 1996; pp 375-379
3. De Roos, K. B. *Food Tech.*, **1997**, 51, 60-62
4. Dickinson, E.; Evison, J.; Gramshaw, J. W.; Schwoppe, D. *Food Hydrocolloids*, **1994**, 8, 63-67
5. Harrison, M.; Hills, B. P. *Int. J. Food Sci. Tech.*, **1997**, 32, 1-9
6. Harrison, M.; Hills, B. P.; Bakker, J.; Clothier, T. *J. Food Sci.*, **1997**, 62, 653-664
7. McNulty, P. B.; Karel, M. *J. Food Tech.*, **1973**, 8, 309-318
8. McNulty, P. B.; Karel, M. *J. Food Tech.*, **1973**, 8, 319-331
9. Rousseau, F.; Castelain, C.; Dumont, J. P. *Food Qual. Pref.*, 1996, 7, 299-303
10. Salvador, D.; Bakker, J.; Langley, K. R.; Potjewijd, R.; Martin, A.; Elmore, J. S., *Food Qual. Pref.*, **1994**, 5, 103-107
11. Baek I; Linforth R S T; Blake A; Taylor A J, *Chemical Senses*, **1999**, 24, 155-160

Chapter 32

Sweetness and Salivary Sweetener Concentration: A Time–Intensity Study

G. G. Birch, R. Karim, and T. Raymond

The Department of Food Science and Technology, The University of Reading,
P.O. Box 226, Whiteknights, Reading, Berkshire RG6 6AP, United Kingdom

A time- intensity study of sweetness of glucose syrup solutions was conducted by the “SMURF” technique. Both intensity and persistence of sweetness declined with increasing chain length (DP) of glucose syrup solution but persistence lasted up to 79 s whereas all carbohydrates had declined to sub-recognition threshold concentrations in saliva by 20 s. This behavior is in sharp contrast to that of saccharin. Apparent specific volumes of oligosaccharides decline with increasing DP, indicating better hydration. This leads to better receptor recruitment and thus greater intensity and persistence of sweetness in longer chain molecules.

Relating the intensity of a gustatory stimulus to its physical concentration during tasting is a difficult task to undertake because of the genetic differences in taste acuity between individual assessors as well as their intrinsic differences in salivary flow-rate (*I*). Salivary flow-rate itself is further affected by the chemical nature of the stimulus (e.g. acids enhance salivary flow), and the taste quality, as well as intensity, of the stimulus is affected by the interaction with water (2, 3). Therefore any attempt to relate stimulus intensity to physical concentration of tastant may be affected by many variables.

A useful technique for attempting to study the relationship between sweetener concentration and the perceived sensation, under the constantly changing conditions of the buccal cavity, is time-intensity (TI) analysis (4). The so-called “SMURF” method allows a continuous recording of intensity to be obtained over the course of time for individual assessors and the resulting data are then available for comparison with physical concentrations of the stimulus which are separately determinable. In such an experiment, if the physical presence of the stimulus remains above the tasting threshold concentration in the saliva after the perception has disappeared, this indicates adaptation. If the sensation ceases at the point that the physical

concentration reaches the threshold concentration, there is a simple direct relationship. If, on the other hand, the sensation continues after the physical concentration has declined below the threshold concentration, this demands a more profound explanation. For example either a localised concentration of stimulus molecules might build up, deep in the lingual epithelium (close to the receptor) or, alternatively, second messenger (transduction) events might continue after the initial chemoreception events. The experiments described in this chapter help to distinguish between these possibilities.

Materials and Methods

Physical Concentrations of Carbohydrate and Saccharin in Saliva

All glucose syrups tested in this study consisted of typical mixtures of oligomers. No analyses of individual monomers or polymers were conducted and degrees of polymerization (DP) computed from dextrose equivalents (DE) are therefore average values. Solutions used were 10, 28, 30, 40 and 51% w/v solutions using five different DE materials. In one experiment, four panellists tasted and swallowed glucose syrup solutions at concentrations of 10 % (w/v) and 50 % (w/v). The dextrose equivalents (DEs) of these syrups were 12, 38 and 100. Twenty seconds after imbibing 5 mL of sample and, thereafter, every 20 seconds or longer, the panellists were required to spit into a weighing boat. The saliva collected was weighed and diluted to an appropriate concentration (10-100 µg/mL) with distilled water and the total carbohydrate content determined by the phenol-sulfuric acid method. (5) In a second experiment with 15 panellists tasting saccharin (5 mL, 0.05 % w/v), the same collection procedure was applied but the physical concentration was determined using a flame photometer to measure residual sodium. A third experiment repeated this procedure with 15 panellists tasting 5 mL of 5 % w/v sodium chloride solution and a fourth experiment involved the same 15 panellists tasting 5 mL of 10 % w/v D-glucose solution (AnalaR grade) and determining residual glucose by the phenol-sulfuric acid procedure.

Apparent Specific Volumes (ASVs) of Glucose Syrups.

ASVs were determined with an Anton Paar Density Sound Analyser (DSA 48) from Paar Scientific, Raynes Park, London, UK. Temperature was maintained at 20 ±0.1°C. The density of the sample was measured from the period of oscillation of a U-tube. The instrument was calibrated with air and distilled water. Density measurements were accurate to ±1×10⁻⁴ g cm⁻³. Apparent molar volumes (ϕ_v) and apparent specific volumes (ASV) were determined from equations (1) and (2)

$$\phi_v = 1000(d_0 - d) / m d d_0 + M_2 / d \quad (1)$$

$$ASV = \phi_v / M_2 \quad (2)$$

where d_0 = density of water (g cm^{-3}) at 20°C
 d = density of solution at 20°C
 m = molality of the solution (mol /kg water)
 M_2 = molecular weight of solute

Average molecular weights of glucose syrups were determined from average degrees of polymerization (DP) using the relationship:

$$\text{DP} = \frac{100}{\text{DE}}$$

Time Intensity Study of Sweetness of Carbohydrate and Saccharin Solutions

Fifteen to twenty four panellists were selected after an initial screening for sensitivity to sweet taste. Panelists were then instructed and trained in the use of the SMURF technique (6) for time-intensity analysis. In this procedure, each panellist imbibed the sweetener solution (5 mL) and immediately began to move a lever on a potentiometer box along a scale. The box was connected by cable to a moving chart recorder (removed from the panellist). The lever was pushed to a maximum position corresponding to the maximum perception of sweetness, then retracted toward the zero position as the perception declined. Analysis continued until zero perception. Full time-intensity plots were thus obtained for each panellist but only maximum intensity and total persistence are recorded in the tables.

In one experiment, 24 panellists tasted 5 mL of four glucose syrups and D-glucose at five different concentrations. In a second experiment, 15 panellists tasted 5 mL of D-glucose (10 % w/v), or sodium chloride (5 % w/v) or saccharin (0.05 % w/v) twice each. Only the times to 75%, 50% and 25% of the maximum intensity were recorded.

Results and Discussion

Figures 1 and 2 illustrate the results for 24 panellists tasting 5 mL of 30 % solutions of DE 38 glucose syrup. Only maximum intensity and total persistence are shown (experiment 1). Significant variations in individual maximum intensities are evident but variations in total persistence times are much more marked. One contribution to the latter observation might be the differences in individual salivary flow-rates (I) which were not measured in this experiment.

Tables I and II, list the average intensities and persistences respectively, for all four glucose syrups and D-glucose itself, used in experiment 1. As expected, in all cases, both sweetness intensity and persistence drop as DP increases. However, the decrease is not stoichiometrically proportional. For example, at almost every concentration, the intensity of sweetness at DP 8.3 (Table I) is greater than that at DP 1.0 divided by 8.3 and the same holds for the persistence data (Table II). This

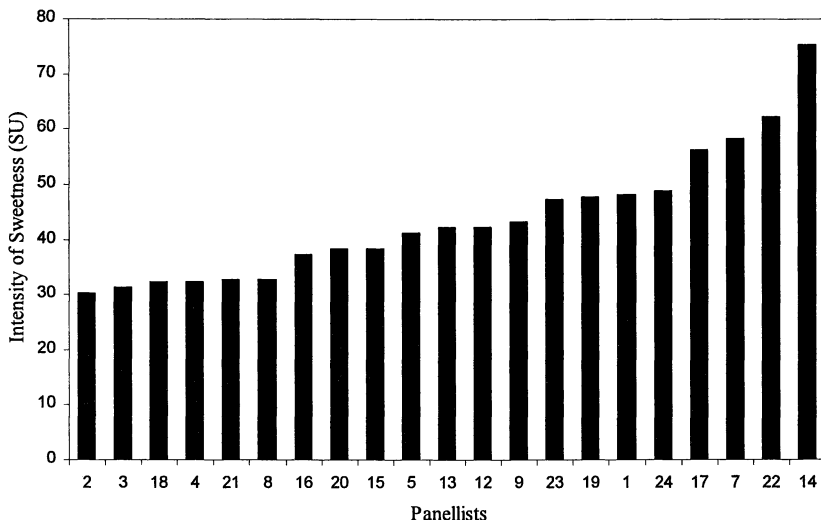


Figure 1. Variation in the Intensity of 30 % w/v DE 38 Sweetness Among Panellists (N=24)

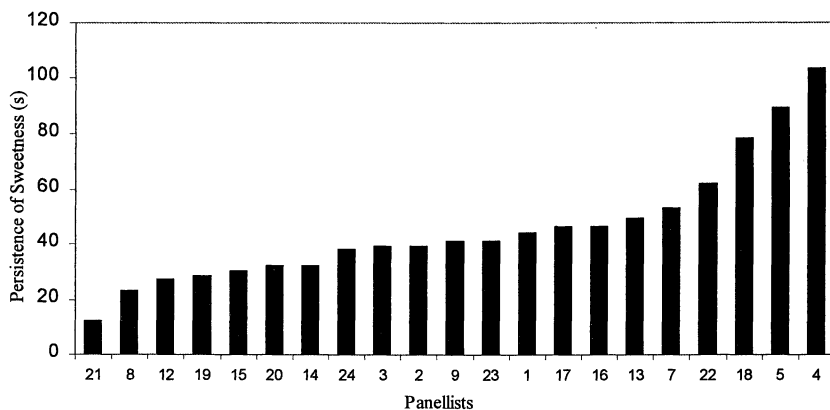


Figure 2. Variation in the Persistence of 30 % w/v DE38 Sweetness Among Panellists (N=24)

phenomenon probably results from the intrinsic solution differences between monomers and oligomers, which will be explained below.

Table III lists the average total carbohydrate concentration in saliva of 4 panellists at time intervals after imbibing and swallowing 5 mL samples of glucose syrups. Assuming that the taste threshold of D-glucose itself is around 1% w/v, it is clear that even at the first time interval after imbibing 10% or 50% w/v glucose syrup,

Table I. The Intensity of Sweetness for D-Glucose and Four Glucose Syrups at Different Concentrations (N=24)

<i>D.E.</i> [*]	<i>D.P.</i> [∂]	<i>Intensity of Sweetness (SMURF Units or S.U.)</i>				
		<i>Concentration (%w/v)</i>				
		10	20	30	40	50
12	8.3	3.2 (0.6)	7.7 (1.0)	15.1 (1.5)	22.3 (1.6)	22.2 (1.5)
21	4.8	5.7 (0.8)	13.7 (1.4)	22.1 (1.5)	29.5 (1.4)	37.1 (1.9)
38	2.6	12.3 (1.1)	24.5 (1.2)	42.0 (1.9)	53.9 (2.8)	60.2 (3.0)
62	1.6	16.3 (1.2)	34.5 (1.4)	52.2 (2.6)	66.3 (2.4)	75.0 (2.7)
100 [≠]	1.0	25.4 (1.9)	45.5 (1.8)	63.7 (2.2)	75.9 (2.4)	83.8 (2.3)

* Dextrose equivalent of glucose syrups.

∂ Degree of polymerization is equivalent to 100/D.E.

≠ D-Glucose AR.

() Values in parentheses are the standard errors of the means

Table II. The Persistence of Sweetness for D-Glucose and Four Syrups at Different Concentrations (N=24)

<i>D.E.</i> [*]	<i>D.P.</i> [∂]	<i>Persistence of Sweetness (s)</i>				
		<i>Concentration (%w/v)</i>				
		10	20	30	40	50
12	8.3	4.8 (0.9)	14.0 (1.6)	24.7 (2.4)	32.9 (3.4)	30.8 (2.7)
21	4.8	9.5 (1.7)	23.1 (3.3)	31.5 (3.5)	40.9 (4.1)	46.8 (4.2)
38	2.6	14.9 (1.8)	28.6 (2.9)	42.0 (3.5)	50.0 (3.5)	59.3 (4.4)
62	1.6	19.2 (2.1)	37.8 (4.2)	52.1 (4.6)	62.1 (4.9)	73.6 (5.4)
100 [≠]	1.0	29.7 (3.2)	48.8 (3.9)	61.9 (4.7)	73.8 (5.7)	79.2 (5.4)

See footnotes for Table I

i.e. 20s, the residual salivary carbohydrate is well below threshold concentration. However, the persistences listed in Table II, for 20 % - 50% w/v solutions and higher,

are almost all longer than 20s. Thus the panelists are tasting sweetness which is not physically possible, from the salivary concentration. The explanation may be a localised concentration of stimulus at or around the receptor site (6,7).

Table III. The Average Concentration of Salivary Total Carbohydrate at Different Time Intervals Determined by Phenol-Sulfuric Acid Method.

Time (s)	Glucose levels in the oral fluid (mg/100mL) ϕ				
	DE ζ 12		DE 38	DE 100 ψ	
	10%	50%	10%	10%	50%
0 γ	0.0174	0.00920	0.0190	0.0181	0.0181
20	2.81	18.2	2.24	2.66	6.79
40	1.73	9.09	1.68	1.833	4.57
60	1.17	6.14	1.15	1.545	3.01
90	0.833	4.39	0.846	1.19	2.03
120	0.542	3.30	0.737	0.950	1.43
180	0.327	2.20	0.468	0.796	0.865
300	0.182	0.882	0.261	0.373	0.466
420	0.0937	0.468	0.176	0.170	0.291

ϕ Average values of the four panelists.

ζ Dextrose equivalent.

γ Zero time is before tasting commenced.

ψ D-Glucose AR.

Table IV Disappearance of Stimulus and Taste (N=15) (Average of 2 tastings)

	Persistence (s)					
	Salivary Stimulus			Taste Sensation		
	(% of max-concn)			(% of max-intensity)		
	75%	50%	25%	75%	50%	25%
Glucose	7.7	16.4	45.3	8.3	12.3	16.8
NaCl	11.6	28.0	55.7	9.1	15.3	22.7
Na	21.0	53.4	>120	12.4	23.0	34.1
Saccharin						

The chief purpose of experiment 2, was to make a careful study of the disappearance of stimulus from saliva after tasting and swallowing D-glucose, sodium chloride or sodium saccharin solutions. The fifteen panellists who undertook this experiment (twice) also monitored the perception of taste by time-intensity analysis. However, only the times to 75%, 50% and 25% of the maximum intensities

are recorded in Table IV, and compared to the times 75%, 50% and 25% of the maximum salivary concentrations. It is clear that both physically and sensorially, the saccharin solution is slowest to disappear. The drop of concentration of stimulus in saliva is listed over 120s in Table V.

Table V. Drop in Concentrations* of Stimuli in Saliva

<i>Time (s)</i>	<i>Supra-Residual Salivary Stimulus Concentration (mg/100ml)</i>		
	<i>Glucose</i>	<i>NaCl</i>	<i>Na saccharin</i>
Residual	7.68	3.72	8.45
10	59.2	50.8	29.4
20	40.1	35.6	20.0
30	26.9	29.9	16.9
40	23.1	21.9	14.9
60	16.7	14.4	14.5
80	9.6	11.5	8.3
100	5.3	8.2	8.5
120	1.9	5.6	6.8

* Na salts are determined as Na – Values are the means of duplicate determination from 15 panelists

Assuming that the taste thresholds (7) for glucose and sodium chloride are 1000mg/100mL and 55mg/100mL, respectively, the concentrations in saliva were already below taste threshold at 10s (Table V). However, the taste threshold concentration of saccharin is 1mg/100mL. Therefore the level was above the threshold for this stimulus throughout the testing period (Table V). Why saccharin behaves differently from the other two sweeteners is open to question. However, its greater lipophilicity might enable it to bind to non-specific buccal membranes and to be released slowly during the course of the experiment. The more hydrophilic glucose and sodium chloride, on the other hand, bind only to the direct environs of the receptor.

Table VI lists the apparent specific volumes of D-glucose and four glucose syrups at 5-50% w/v. Although the apparent molar volumes of these solutes obviously increase with increase of molecular weight, it is interesting that the apparent specific volumes show the opposite trend. This is because of the greater number of hydration sites and degree of order in the larger molecules (9) and herein lies the possible explanation of their stoichiometrically greater sweetness intensities and persistences (Tables I & II).

Water acts as a transporting medium for the movement of stimulus molecules to saliva. Those molecules which interact strongly with water (e.g. salts) are transported to deep layers of the lingual epithelium to reach an appropriate receptor region. (It is now well accepted that salts act directly on ion-channels). Most sweet substances are less heavily hydrated than inorganic salts. Their receptors are therefore likely to be less deep in the epithelium and it is thought sweet receptors may be proteins protruding out of the apical membranes of taste cells. Apparent specific volume reflects the hydrostatic packing efficiency of stimulus molecules among water molecules and it has been shown that sweet molecules have ASV's within the range 0.51-0.71cm³g⁻¹. (2). For a molecule to taste sweet it must normally fit within this range and possess an appropriate glycochore (i.e. AH,B system) (10). Carbohydrates seem always to have ASV's within the range 0.60-0.64cm³g⁻¹, which is the central part of the ASV sweetness range. This could account for their pure sweet taste (11). Molecules with ASV's above or below the carbohydrate range are closer to the ASV ranges defining bitterness or sourness (2) and may be contaminated with these extraneous tastes though their main effect is still to elicit sweetness (2). Sodium saccharin, for example, has an ASV of 0.52 cm³g⁻¹ and gives a poor quality of sweetness compared to the carbohydrates (2, 11).

Table VI. The Apparent Specific Volumes of D-Glucose and Four Glucose Syrups at Different Concentrations

		<i>Apparent specific volumes, ϕ_v/mol wt (cm³/g)</i>					
		<i>Concentration (% w/w)</i>					
<i>DE^a</i>	<i>DP^b</i>	5	10	20	30	40	50
12	8.3	0.6062 (0.0007) ^c	0.6070 (0.0008)	0.6076 (0.0008)	0.6084 (0.0008)	0.6114 (0.0009)	0.6116 (0.0009)
21	4.8	0.6055 (0.0007)	0.6065 (0.0006)	0.6089 (0.0007)	0.6097 (0.0007)	0.6115 (0.0007)	0.6124 (0.0006)
38	2.6	0.6078 (0.0008)	0.6089 (0.0007)	0.6098 (0.0009)	0.6112 (0.0008)	0.6133 (0.0008)	0.6139 (0.0008)
62	1.6	0.6138 (0.0008)	0.6137 (0.0007)	0.6157 (0.0009)	0.6190 (0.0008)	0.6207 (0.0007)	0.6228 (0.0009)
100 ^d	1.0	0.6196 (0.0011)	0.6202 (0.0009)	0.6235 (0.0009)	0.6262 (0.0009)	0.6294 (0.0011)	0.6322 (0.0009)

^a Dextrose equivalent of glucose syrups.

^b Degree of polymerization is equivalent to 100/DE.

^c Values in parentheses are the standard errors of the means.

^d D-glucose.

SOURCE: Reproduced with permission from reference 9. Copyright 1992 Wiley.

The apparent specific volumes of glucose syrups (Table VI) decrease with increasing chain length. This implies a shift in depth of accessibility to receptor regions. It is possible that the decrease in apparent specific volume leads to greater receptor recruitment. Alternatively, the longer chain molecules may undergo a more orderly and extensive degree of hydration than the shorter molecules and this is sufficient to give them an advantage for receptor activation. In any case, the molar advantage in sweetness of the larger molecules, both in intensity and persistence (Tables I and II), may be related to their smaller apparent specific volumes.

Tables III, IV and V indicate that persistence of sweetness (of carbohydrates tested) continues after their physical concentrations in saliva drop to below tasting threshold concentrations. These results rule out any major role for adaptation of the panellists. Rather they suggest that either a localised concentration of stimulus molecules exists near the receptor (7) or that second messenger events continue to transduce the initial sweet chemoreception signal. The former possibility seems most likely because second messengers, such as inositol triphosphate (IP₃), peak within 1s and, at stimulus exposures greater than 10s, are not even detectable (12). If a localised concentration of stimulus molecules (7) is responsible for the persistence of sweetness, it is interesting that the larger molecules show the greatest sweetness advantage. Possibly the degree of order in the larger molecules is manifested as a corresponding degree of hydrogen bond co-operatively (13) and chains of stimulus molecules constitute the store of sweetness in the receptor environment

Saccharin contrasts sharply with the above behavior as the concentration in saliva remains above tasting threshold after the sweetness has ceased. The involvement of adaptation in the taste of saccharin cannot therefore be ruled out.

Conclusions

Panelists tasting sweet carbohydrate solutions continue to perceive sweet taste after salivary concentrations of sweetener decline to below taste threshold. This phenomenon is best explained by a localised store of stimulus molecules at or near the receptor. This is accompanied by a molecular advantage in sweetness potency of the larger oligomers which is related in turn to their lower apparent specific volumes. Sodium saccharin does not behave like carbohydrate sweeteners.

Literature Cited

1. Bonnans, S.R. and Noble, A.C. *Physiol. Behav.* **1995**, *57*, 569-574.
2. Shamil, S.; Birch, G.G.; Mathlouthi, M. and Clifford, M.N. *Chem. Senses.* **1987**, *12*, 397-409.
3. Birch, G.G.; Parke, S.; Siertsema, R. and Westwell, J.M. *Pure and Appl. Chem.* **1997**, *69*, 685-692.
4. Birch, G.G. and Munton, S.L. *Chem. Senses.* **1981**, *6*, 45-52.

5. Dubois, M.; Gilles, K.A.; Hamilton, J.K.; Rebers, P.A. and Smith, F. *Anal. Chem.* **1956**, 350-356.
6. Kemp, S.E. and Birch, G.G. *Chem. Senses*, **1992**, *17*, 151-168.
7. Birch, G.G.; Latymer, Z. and Holloway, M. *Chem. Senses*, **1980**, *5*, 63-78.
8. Moncrieff, R.W. *The Chemical Senses*, Leonard Hill, London, 1967.
9. Birch, G.G. and Karim, R. *J. Sci. Food Agric.* **1992**, *58*, 563-568.
10. Shallenberger, R.S. and Acree, T.E. *Nature*, **1967**, *216*, 480-482.
11. Parke, S.A. and Birch, G.G., *J. Agric. Fd. Chem.*, **1999**, *47*, 1378-1384.
12. Bernhardt, S.J., Naim, M., Zehavi, U. and Lindemann, B., *J. Physiol*, **1996**, *490*, 325-336.
13. Jeffery, G. *Food Chem.*, **1996**, *56*, 241-246.

Chapter 33

Volatile Compound Release during Consumption: A Proposed Aroma Stimulus Index

Conor M. Delahunty¹ and Brendan Guilfoyle²

¹Department of Food Science and Technology, Division of Nutrition,
University College Cork, Cork, Ireland

²Mathematics Department, IT Tralee, Tralee, Kerry, Ireland

The flavor of a food can be described as the generally expressed response by a number of consumers to the food's stimulus of their senses of smell, taste, and trigeminal mouthfeel that occurs during and immediately after consumption. To fully understand flavor it is necessary to understand the nature of the flavor stimulus, the mechanisms of sensory perception, and the psychology of the expressed response. Studies that had an objective to understand the nature of the aroma stimulus have resulted in quantitative data of volatile compounds released in the mouth of individual consumers during consumption of different food types. Differences in the release of total volatile compounds from food to food and differences in the release of total volatile compounds between individuals have been observed. However, in many cases, the total quantity of all volatile compounds released during consumption was similar in proportion from one consumer to another. When volatile release data were related in this regard it was found that an index, termed here the Aroma Stimulus Index (ASI), could be used to quantify this relationship. In this paper, we also postulate that this index is constant in time during consumption and we consider its potential shortfalls and applications.

The study of flavor release from foods has received much attention in recent years, recognized most recently by a European Union Concerted Action (1) and this dedicated Symposium (2). Volatile compounds released from food contribute much to perceived flavor quality, and therefore knowledge of the relative contribution to flavor of those found in a food, or produced during consumption of a food, is sought. In recent years apparatus and methodology to measure volatile compound release in the mouth have been developed to study food systems (3-6), and now there are data of the

total, and the dynamics, of volatile compounds released by different consumers eating the same food (3-17).

Aroma Stimulus Index Theory

The quantity and balance of volatile compounds, which are released from a food during consumption, and are available for perception, represent an aroma stimulus. An individual aroma stimulus is influenced by the composition and structure of the food and by the physiology of the consumer. In studies of volatile compounds released from cheese during consumption, O'Riordan et al. (10) and Delahunty et al. (11) found that although the total quantity of a compound released from any single cheese varied considerably from one consumer to another, there was a relationship between consumers of that cheese. This relationship was that the difference between any two consumers in the total quantity of any individual compound released during consumption of the cheese was a constant across all compounds and by scaling out this difference between the consumers, differences in volatile compounds released between cheeses could be determined. Ingham et al. (14) found a similar relationship

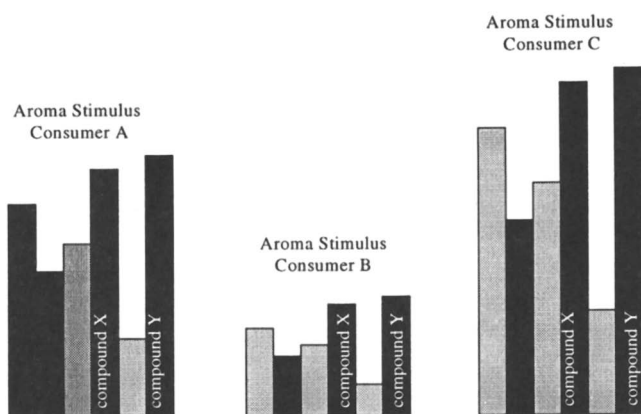


Figure 1. Representation of the relationship between three consumers (A, B and C) of a hypothetical food which released six compounds during consumption (including compound X and compound Y).

between volatile compounds released by consumers of mint sweets, regardless of whether they sucked or chewed the sweet. Van Ruth et al. (16) found this relationship between consumers of French beans, bell peppers, and leeks, and Linforth et al. (17) found this relationship between consumers of tomatoes. This finding can be illustrated as in Figure 1.

This common finding is interesting if one considers the relationship between the volatile compounds illustrated in Figure 1 (X and Y) released by two consumers (A and B) in the following terms:

$$\frac{\text{Concentration of X released by A}}{\text{Concentration of X released by B}} = \frac{\text{Concentration of Y released by A}}{\text{Concentration of Y released by B}} = \lambda$$

In addition, when you consider more than two consumers, and the many more volatile compounds which are released during consumption, it could be said that any individual consumer has a certain capacity to release volatile compounds from a food (for those which were tested). Then the ability of all consumers to release volatile compounds from a given food can be represented by an Aroma Stimulus Index (ASI), and the difference between any two consumers on the index can be denoted by λ .

The fact that λ is different from unity may arise from differences between consumers in physiological and habitual factors of consumption e.g. variations in saliva production (10,18), mastication behavior (10, 18, 19), time of swallow (13), and breathing volume and behavior (18). However, while these factors are extremely complex and inter-related, it is remarkable that the single constant λ appears to describe the final concentration released during consumption across different compounds.

The Aroma Stimulus Index and Dynamic Flavor Release

Up to now, this paper has not considered volatile release over time. However, release from the food begins as soon as the food is placed into the mouth and continues until just after the food is swallowed. In parallel, perception of aroma begins very soon after the food is placed in the mouth and continues until all released volatile compounds (the aroma stimulus) have disappeared from the buccal cavity some time after the food is swallowed (due to adsorption onto the buccal cavity tissues and regurgitation from the stomach). The quantity and the nature of the aroma stimulus will change during the time of consumption, as will the intensity and the quality of the aroma perception. Therefore, the temporal aspects of volatile compound release and subsequent perceptions by consumers are an important dimension of perceived flavor quality (13, 18)

Given the evidence presented to determine relationships between the total aroma stimulus of different consumers, we postulate that the ASI is also a constant in time during consumption (at least for the food types referenced above). This hypothesis was formed by giving consideration to the potential of any volatile compound to re-establish aroma stimulus proportionality (λ) with any other compound at the time of measured total release, if it had erred from this proportionality at any time during consumption. We believe that this could not be possible. Therefore, one could consider the dynamic relationship between any two consumers (A and B) as they release any volatile compound (X) during consumption as follows:

$$\frac{\text{Concentration for A of X at any time t}}{\text{Concentration for B of X at any time t}} = \frac{\text{Total concentration for A of X}}{\text{Total concentration for B of X}} = \lambda$$

To illustrate this relationship in an easy to understand way, assume initially that the accumulation of a volatile compound released over time of consumption, and trapped, is linear. Then, for compound X, Figure 2 would describe the release over time for consumers A and B and the ASI postulate would hold as:

$$\lambda = \frac{70}{50} = \frac{a}{b}$$

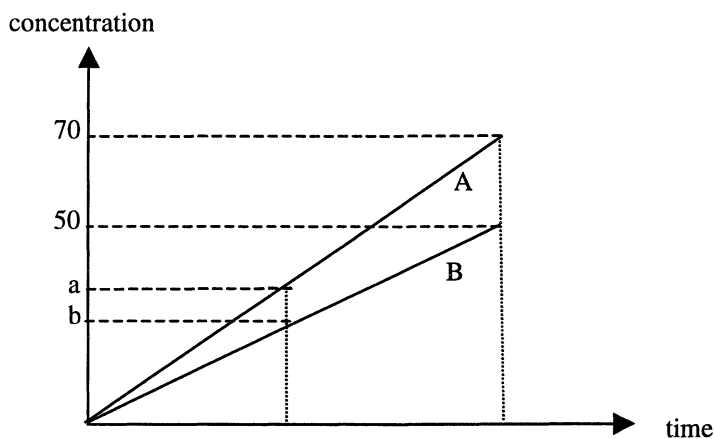


Figure 2. Linear cumulative release of a volatile compound (X) during consumption of a hypothetical food by two consumers (A and B). A measure of the quantity of X released at two time points during consumption is illustrated at the vertical cross-sections.

However, it is known that the accumulation of a trapped volatile compound released from a food over time of consumption will not be linear as the rate of its release will not be constant. This is because a volatile compound's affinity for a food's compositional components (e.g. fat, protein, carbohydrate, pH) differs according to the physical and chemical properties of the volatile compound. In addition, there are also well documented mechanisms of volatile release, namely partition between bulk phases (18) and mass transfer (20), either of which can have the greatest role in release depending on the food system. Yet, it is still possible for the reasons already provided, that regardless of the shape of a cumulative release curve of any individual compound, the ASI is constant in time. Figure 3 illustrates how this can be so, where again:

$$\lambda = 70 / 50 = a / b$$

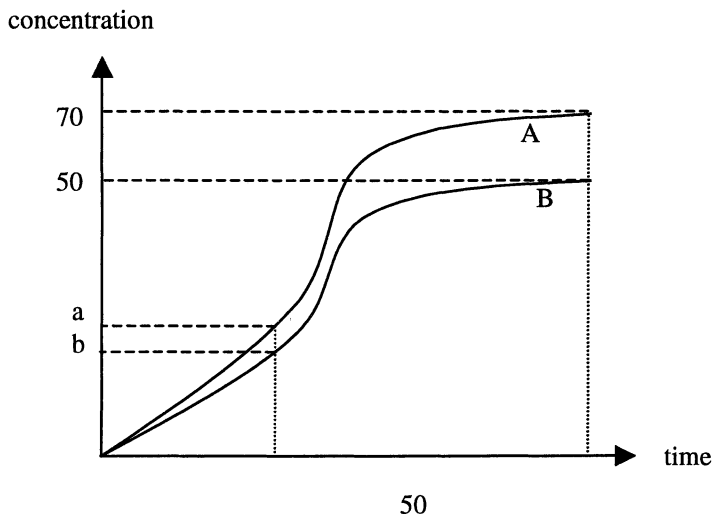


Figure 3. Non-linear cumulative release of a volatile compound (X) during consumption of a hypothetical food by two consumers (A and B). A measure of the quantity of X released at two time points during consumption is illustrated at the vertical cross-sections.

Determining the Validity of the ASI Theory

Is the ASI Constant Across a Wide Range of Compounds?

Data of many different volatile compounds released during consumption exists (although from a limited number of food types)(5,10,14,16,17). These compounds have different physical and chemical properties. However, it will be necessary to examine these data and data generated in the future more carefully to determine whether specific compound properties (e.g. degree of hydrophobicity) influence the validity of the ASI.

Is the ASI Constant for Compounds Generated During Consumption (e.g. by Enzymes) and for Compounds Already Present that are Released During Consumption?

Van Ruth et al. (16) found relationships, which could be described by the ASI, between twelve consumers of French beans, bell peppers and leeks. Volatile compounds will have been generated as these plant tissues were disrupted by

mastication. Linforth et al. (17) found that for tomatoes, when compounds were generated enzymatically during consumption, that three different consumers had closely related volatile release ratios. Data that supports the ASI has also been described by O'Riordan et al. (10) for cheese and by Ingham et al. (14) for mint sweets where compounds are not generated during consumption.

Is the ASI Constant Across Different Food Types?

In the study of Van Ruth et al. (16), the same twelve consumers consumed all the three food types. Where similar compounds were released from the foods, we have further analyzed the data by Friedman two-factor analysis of variance to observe ratios of release between consumers. No significant differences were found between consumers for the three foods, which would support the ASI theory. However, much more work with foods having greater differences should be carried out.

Is the ASI Constant During Time of Consumption as Postulated?

Ingham et al. (15) found that for mint sweets consumed over 300s, the relative release of compounds measured was similar for four consumers. We analyzed time-concentration data, generated by Legger and Roozen (5), to further test the time independence theory of the ASI. Although the difference in the aroma stimulus between two of the six consumers was a consistent proportion at each of the nine time intervals measured, variable differences were found between other pairs of consumers. However, as the coefficient of variation in measurement of total quantity released is often as great as 50% between samples for the same consumer (17), this finding is perhaps not surprising when the ASI is tested at numerous time intervals during consumption. More data, and more precise data, is required for analysis before any conclusion can be made.

What are the Physiological Determinants of the Value of the ASI for any Consumer?

This question may be ahead of its time. However, if the ASI is shown to have some validity then it will be a reasonable objective to categorize consumers by their ASI. One means of doing so may be to determine physiological determinants such as time of swallow, mastication rate, breathing behavior or saliva composition and production volume. Could there be differences between consumers by gender? Does a consumer's ASI change as they grow older? Are there differences between ethnic groups in the population, for example between Asian and Caucasian populations?

Why Might the ASI be Important and What are the Potential Applications of it?

If consistent differences exist between consumers in their aroma stimulus, and if such differences can be generalized to population groups by an ASI, then there may be a need to provide foods that have tailored differences in how they release their flavor. Also, for fundamental understanding of flavor, both instrumental and sensory methodology could be optimized using this knowledge. For example, a model mouth would have a much greater role in volatile release analyses, if it were calibrated to a particular point on the ASI. In sensory time-intensity methodology, where unaccountable differences in the data generated by assessors causes problems for data interpretation, pre-training and establishing individualized protocol for assessors using ASI information and knowledge of physiological determinants of the ASI would be advantageous and could improve the determination of instrumental / sensory relationships.

Conclusions

An Aroma Stimulus Index (ASI) that can be used to define a consumer's ability to release volatile compounds from a food has been postulated. Data we have analyzed supports this hypothesis. It is also postulated that the ASI is independent of time during consumption. However, the validity of this argument needs further investigation for general acceptance. If the ASI is shown to be a constant for consumers, it will be a very useful tool in both instrumental and sensory studies to understand flavor.

References

1. European Commission Cost Action 96. *Interactions of Food Matrix with Small Ligands Influencing Flavour and Texture*; European Commission: Brussels, 1997, 1998, 1999, Vol. 1-4.
2. Flavour Release Symposium. *Division of Agricultural and Food Chemistry, American Chemical Society National Meeting*; New Orleans, 1999.
3. Linforth, R.S.T.; Ingham, K.E.; Taylor, A.J. In *Flavour Science: Recent Developments*; Taylor, A.J.; Mottram, D.S., Eds.; Royal Society of Chemistry: Cambridge, 1997, pp 361 – 368.
4. Delahunty, C.M.; Piggott, J.R.; Conner, J.M.; Paterson, A. In *Trends in Flavour Research*; Maarse, H.; van der Heij, D.G., Eds.; Elsevier Applied Science: Amsterdam, 1994, pp 47-52.
5. Legger, A.; Roozen, J.P. In *Trends in Flavour Research*; Maarse, H.; van der Heij, D.G., Eds.; Elsevier Applied Science: Amsterdam, 1994, pp 287-291.
6. Linforth, R.S.T.; Taylor, A.J. *Food Chem.* **1993**, *48*(2), 115-120.

7. Baek, I.; Linforth, R.S.T.; Taylor, A.J. In *Interactions of Food Matrix and Small Ligands Influencing Flavour and Texture Volume 4*; Guichard, E. Ed.; European Communities: Brussels, 1999, pp 57-62.
8. Brauss, M.S.; Linforth, R.S.T.; Cayeux, I.; Harvey, B.; Taylor, A.J. In *Interactions of Food Matrix and Small Ligands Influencing Flavour and Texture Volume 4*; Guichard, E. Ed.; European Communities: Brussels, 1999, pp 117-122.
9. Grab, W. (1999). In *Interactions of Food Matrix and Small Ligands Influencing Flavour and Texture Volume 4*; Guichard, E. Ed.; European Communities: Brussels, 1999, pp 74-79.
10. O'Riordan, P.J.; Delahunty, C.M.; Sheehan, E.M.; Morrissey, P.A. *J. Sens. Stud.* **1998**, *13* (4), 435-459.
11. Delahunty, C.M.; Crowe, F.; Morrissey, P.A. In *Flavour Science: Recent Developments*; Taylor, A.J.; Mottram, D.S., Eds.; Royal Society of Chemistry: Cambridge, 1997, pp 339 - 343.
12. Linforth, R.S.T.; Taylor, A.J.; Brown, W.E. In *Interactions of Food Matrix and Small Ligands Influencing Flavour and Texture Volume 1*; Bakker, J. Ed.; European Communities: Brussels, 1997, pp 78-81.
13. Delahunty, C.M.; Piggott, J.R.; Conner, J.M.; Paterson, A. *J. Sci. Food Agric.* **1996**, *71*, 273-281.
14. Ingham, K.E.; Linforth, R.S.T.; Taylor, A.J. *Flav. Frag. J.* **1995**, *10*, 15-24.
15. Ingham, K.E.; Linforth, R.S.T.; Taylor, A.J. *Lebensm.-Wiss. u.-Technol.* **1995**, *28*, 105-110.
16. Van Ruth, S.M.; Roozen, J.P.; Cozijnsen, J.L. *Food Chem.* **1995**, *53*, 15-22.
17. Linforth, R.S.T.; Savary, I.; Pattenden, B.; Taylor, A.J. *J. Sci. Food Agric.* **1994**, *65*, 241-247.
18. Overbosch, P.; Afterof, W.G.M.; Haring, P.G.M. *Food Rev. Internat.* **1991**, *7*(2), 137-184.
19. Browne, W.E.; Dauchel, C.; Wakeling, I. *J. Tex. Stud.* **1996**, *25*, 455-468.
20. Hills, B.P.; Harrison, M. *Int. J. Food Sci. Tech.* **1997**, *30*, 425-436.

Chapter 34

Effect of Base and Processing on Flavor Release from Snacks

Bonnie M. King and C. A. A. Duineveld

Quest International Nederland BV,
P.O. Box 2, 1400 CA Bussum, the Netherlands

Tortilla chips, potato chips and corn-based snacks created by either direct or indirect expansion were evaluated by profiling and time-intensity (TI) evaluations made by a trained panel. In the TI tests both saltiness and a retronasal flavor (paprika, spicy/herbs) were measured for single as well as multiple ingestions. It was shown that processes such as direct expansion can weaken the distinctive base flavor of corn snacks, and that low bulk density snacks require a higher flavor dosage. For both single and multiple ingestions, the retronasal flavor was distinguished from saltiness by lower intensity-related TI parameters. Panelists took longer to swallow when making TI evaluations of retronasal flavor than when evaluating saltiness. The flavor on potato-based as opposed to corn-based snacks lasted longer and was more intense for both descriptors independent of the number of ingestions.

Flavor is applied to snacks either as an oil-based slurry sprayed onto the surface of the product or as a powder that can be dusted onto a product that already has a fatty surface. Potato chips, corn tortillas and numerous types of pasta (corn, potato, wheat or rice based pellets) that obtain their final volume after being fried in vegetable oil are examples of products flavored by dusting. The latter are often referred to as snacks having undergone *indirect expansion* as opposed to the *direct expansion* that occurs in the extruder. Directly expanded snacks are usually flavored by slurry. Given that both slurry application and dusting are surface treatments, there might not be chemical evidence for flavor-base interactions in the classical sense. On the other hand, perceptual differences during eating can be attributed to the combined sensation of added flavor and base. Corn bases distort the balance of many savory flavorings.

The purpose of the present investigation was to determine which sensory characteristics were most influenced by specific changes in snack base or processing. Flavor formulation and blending are key to producing optimal eating enjoyment,

which is determined to a large extent by flavor release in the mouth. Flavor must not appear immediately and then disappear, leaving a tasteless, chewy mass to be swallowed.

Materials and Methods

Samples

All samples used in these experiments were prepared by the Quest Snack Department. Samples can be classified according to the scheme given in Figure 1. Samples used in Experiment 1 (D1, D2, D3, I1, I2, I3) were all flavored with the same cheese/ham/bacon flavor. For Experiment 2 there were 18 samples prepared according to a full-factorial design: 3 bases (R, F, T), two cheese/onion flavors and 3 flavor dosages (5%, 6%, 7%). Only samples of type R were used in Experiment 3. The paprika flavor used in this experiment was dosed at 4% and 8%. For Experiments 4 and 5 the samples (flavor dosages) were C (8%), R (6%) and T (6%). The paprika flavor used in these experiments was different from the flavor used in Experiment 3.

Samples were presented in plastic cups coded with 3-digit numbers. Larger samples (R, F, T) were broken into pieces in order to provide a more homogeneous distribution of flavor. Panelists consumed *ad libitum* for profiling tests. TI tests, on the other hand, were conducted with weighed portions taken in their entirety as a single ingestion: 2.5 g for Experiment 3 and 1.0 g (respectively 4 times 1.0 g) for Experiments 4 and 5.

Sensory Measurements

The Quest Sensory Research paid professional panel (20 women) was used in all experiments. Profiling was done by the audio method previously described (1). Thirteen descriptors were used in Experiment 1 and 18 descriptors in Experiment 2. Profiling tests were replicated twice with an interval of at least 24 h between replications. No more than 4 products were evaluated in the same session. Statistical designs were used to balance serving order, carry-over and session effects.

TI measurements were made by using a special transducer system: a squeezable handgrip that transmits hand force via a strain gauge to an amplifier. The device, the method for using it, and panel training in this technique have been described previously (2). For Experiments 3-5 panelists were instructed to empty the contents of the cup into their mouths, click the squeezer on and begin evaluating the descriptor indicated while chewing the sample according to their normal eating habits. Panelists indicated swallowing by pressing the space bar. For the repeated ingestions in

Flavor Application

Slurry

Direct expansion

- D1, D2, D3 (corn base)
- C (corn curls)

Popcorn

Cakes

- (rice, corn)

Dust

Potato chips

- R (rippled)
- F (flat)

Corn chips

- T (tortilla)

Indirect expansion pellets

- I1, I2, I3 (corn base)

Peanuts / coated nuts

1. *Classification of samples used in Experiments 1 – 5.*

Experiment 5, panelists were prompted on the screen every 30 s. Recording was stopped after 101 s for single ingestion experiments and after 161 s for the repeated ingestion test. Different descriptors for the same product were evaluated in different sessions, usually separated by 2 days. TI tests were replicated three times with an interval of at least 48 h between replications. Statistical designs were used to balance serving order, carry-over and session effects.

Data Processing

Genstat 5 (1998 PC/Windows 95, release 4.1 Fourth Edition: Lawes Agricultural Trust, IACR Rothamsted, UK) was used to perform all calculations and statistical analyses.

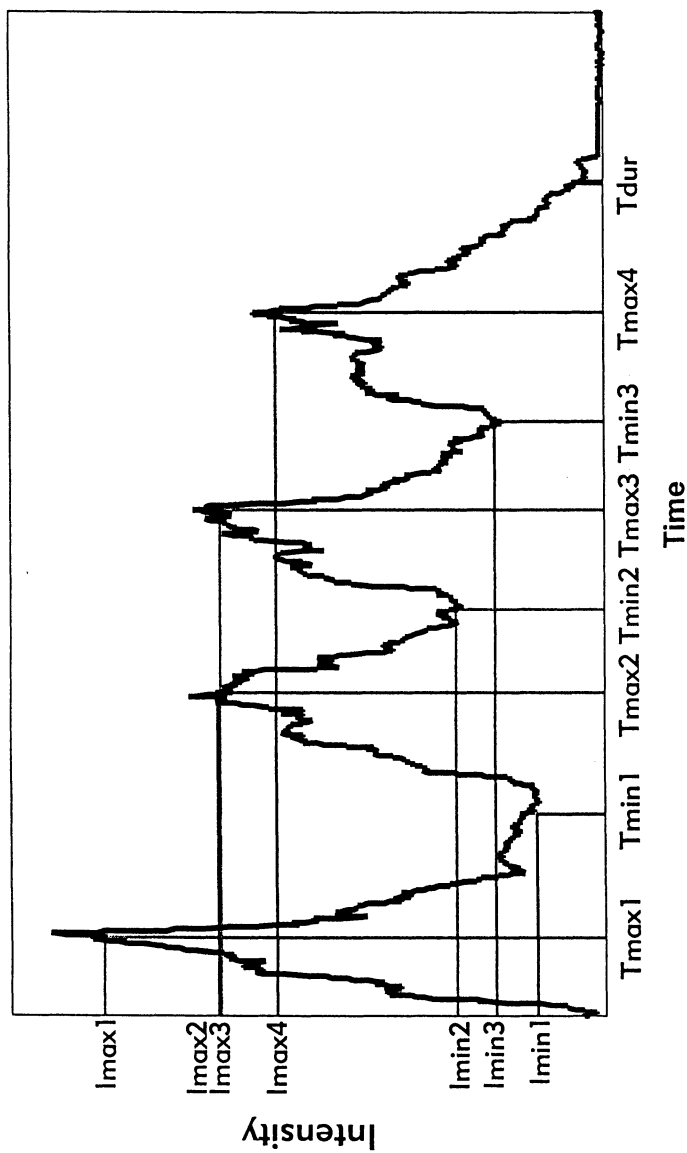
Profiling tests

Profiling descriptors were fitted by variance components models using Restricted Maximum Likelihood (REML). The REML model for a given descriptor comprised the sum of terms for the following effects: Score = product + panelist + panelist.product + session(panelist) + error, where panelist.product is the interaction between panelist and product, and session(panelist) is sessions nested in panelists. Random effects were: panelist $\sim N(0, \sigma_{\text{panelist}}^2)$, panelist.product $\sim N(0, \sigma_{\text{panelist.product}}^2)$ and session(panelist) $\sim N(0, \sigma_{\text{session(panelist)}}^2)$

TI tests

Raw data from TI tests were filtered in order to remove digitation noise while keeping all other features intact. A nine point Epanechnikov kernel smoother was used as filter (3). Seven parameters were abstracted from single-ingestion TI filtered curves: **area** under the curve, **Imax** (highest intensity over complete curve), **Tmax** (average time where intensity is 95% of maximum), **durmax** (duration of intensity >90% of maximum), **Tdur** (earliest time after maximum at which intensity equals only 5% of Imax), **Iswal** (intensity at swallowing), **Tswal** (time at swallowing). Figure 2 shows additional parameters extracted from the multiple-ingestion curves to give a total of 26 parameters used for Experiment 5. In order to stabilize the variance, logarithmic transformations of the parameters were used in all calculations. The REML model for a given TI parameter comprised the sum of terms for the following effects: TI parameter = product + panelist + panelist.product + session(panelist) + error, with random effects panelist $\sim N(0, \sigma_{\text{panelist}}^2)$, panelist.product $\sim N(0, \sigma_{\text{panelist.product}}^2)$ and session(panelist) $\sim N(0, \sigma_{\text{session(panelist)}}^2)$.

When comparing descriptors, the REML model comprised the sum of terms for the following effects: TI parameter = product + descriptor + product.descriptor + panelist + panelist.product + session(panelist) + panelist.descriptor + error, with random effects panelist $\sim N(0, \sigma_{\text{panelist}}^2)$, panelist.product $\sim N(0, \sigma_{\text{panelist.product}}^2)$, session(panelist) $\sim N(0, \sigma_{\text{session(panelist)}}^2)$ and panelist.descriptor $\sim N(0, \sigma_{\text{panelist.descriptor}}^2)$. Non-significant effects were removed from the analysis.



2. Typical TI curve and parameters for multiple ingestion, Experiment 5.

Data from Experiments 4 and 5 were combined so that both descriptors and ingestion methods (variable indicated by “type”) could be compared. The REML model comprised the sum of terms for the following effects: TI parameter = product + descriptor + type + product.descriptor + product.type + type.descriptor + panelist + panelist.product + session(panelist) + panelist.descriptor + panelist.type + error, with random effects $\text{panelist} \sim N(0, \sigma_{\text{panelist}}^2)$, $\text{panelist.product} \sim N(0, \sigma_{\text{panelist.product}}^2)$, $\text{session(panelist)} \sim N(0, \sigma_{\text{session(panelist)}}^2)$, $\text{panelist.descriptor} \sim N(0, \sigma_{\text{panelist.descriptor}}^2)$ and $\text{panelist.type} \sim N(0, \sigma_{\text{panelist.type}}^2)$. Non significant terms were eliminated from the model.

TI curve averaging

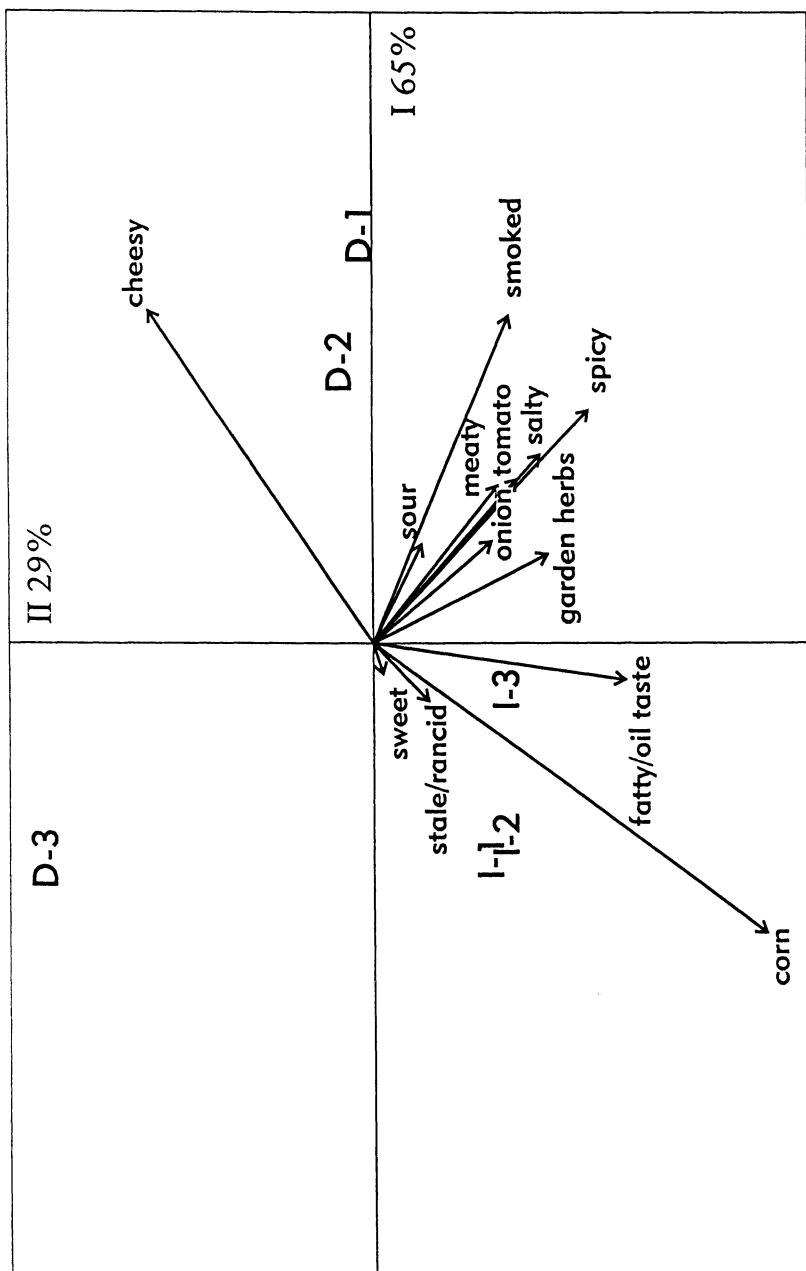
The following procedure was used to produce TI curves averaged over sessions and panelists in the figures. The raw data (TI curve) were integrated to create monotonic increasing curves. The integrated curves were divided into (unequal) time segments using increments equal to 2% of the maximum found for this curve. (This procedure is similar to one proposed by Overbosch (4); however, problems related to double peaks and plateaus are avoided by using the integrated curves.) An average value of log (time) per segment was determined according to the following REML model: Time = product + panelist + panelist.product + session(panelist) + error, with random effects $\text{panelist} \sim N(0, \sigma_{\text{panelist}}^2)$, $\text{panelist.product} \sim N(0, \sigma_{\text{panelist.product}}^2)$ and $\text{session(panelist)} \sim N(0, \sigma_{\text{session(panelist)}}^2)$.

The series of points thus obtained form an average *integrated* TI curve. The normal representation of a TI curve is the first derivative of this curve. In order to carry out numeric differentiation, the integrated TI curve was first fitted by M-splines. (The spline and fitting method were chosen to ensure a monotonic increasing curve.) The area under each differentiated TI curve (which equals 1) was multiplied by the antilog of the average log (area) determined by the REML analysis.

Results and Discussion

Experiment 1

The PCA biplot in Figure 3 shows the effect of processing on the different corn bases in terms of flavor perception. Samples I1, I2, I3 are made from pasta-type corn pellets that expand when fried in hot vegetable oil. They retain the corn flavor associated with their base, and they pick up a fatty, oily taste during processing. Direct expansion in the extruder acts as a steam distillation that weakens the taste of the corn base. The directly-expanded samples (D1, D2, D3) therefore have more of the cheesy flavor and less of the corn flavor than the indirectly-expanded corn pellets (samples I1, I2, I3). Low bulk density snacks require a much higher flavor dosage in order to be perceived in the same way as their higher bulk density counterparts. The



3. PCA of panel profiling REML scores from Experiment 1.

isolation of sample D3 in this figure can be explained by the fact that, as a low bulk density product, it scored very low on all of the flavor attributes.

Experiment 2

When a biplot for PCA results from Experiment 2 was produced based on all the descriptors used to evaluate the samples, the first dimension accounted for 95% of the variation in the data; the second dimension accounted for 3%. This one-dimensional separation of the samples was explained by base flavor. Eliminating the base-related descriptors (corn, corn aftertaste, potato, potato aftertaste) produced the biplot shown in Figure 4. There is still a very large distinction between corn-based products on the right and potato-based products on the left along the first dimension. Interestingly, the choice of flavor, independent of base, creates the same order of difference in the samples as varying the flavor dosages between 5% and 7%. A closer examination of products R and F showed no support for modifying flavor type or dosage to compensate for the higher fatty-taste associated with the F structure.

In both Figures 3 and 4 the descriptors *spicy* (a retronasal sensation) and *salty* (one of the basic tastes) are orthogonal to the descriptors responsible for major product separation. For this reason it was possible to conduct TI experiments on all samples using both of these descriptors.

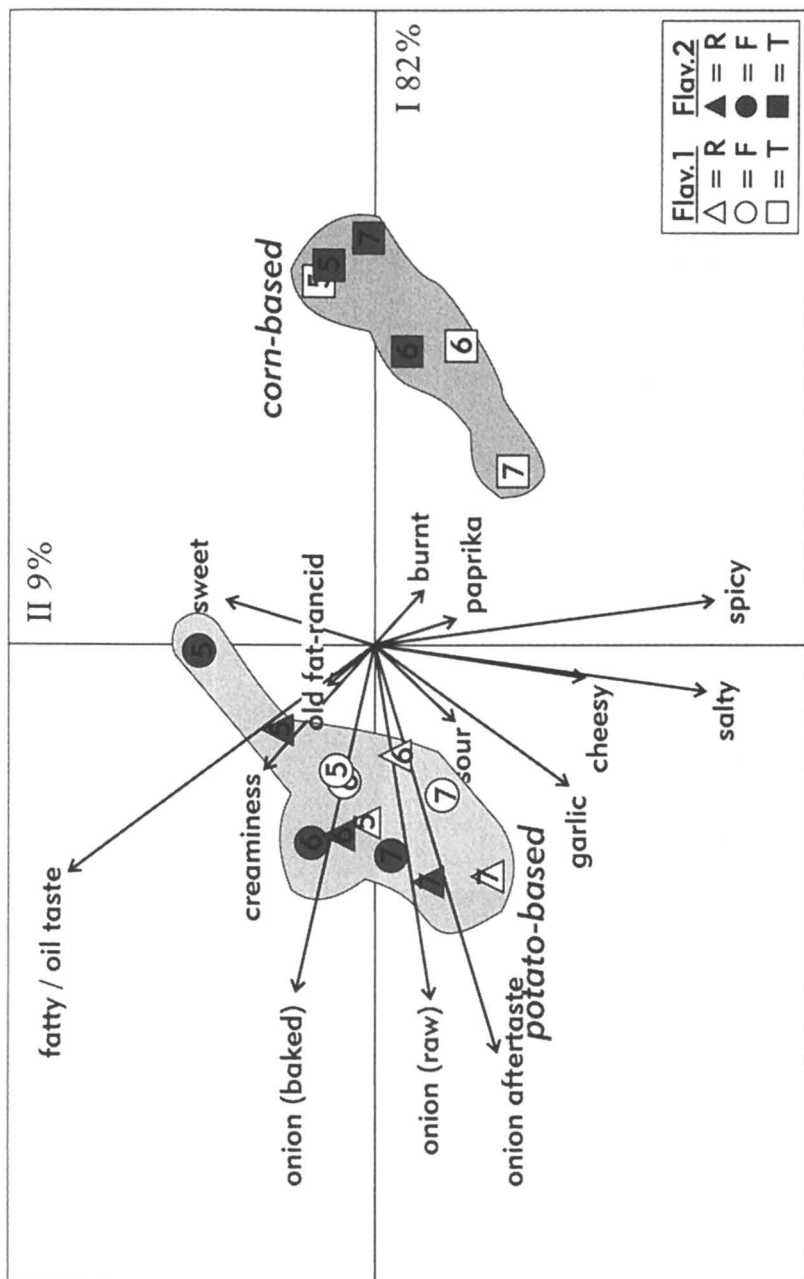
Experiment 3

As a rule of thumb, snack flavors are usually prepared so that there is 1.8% salt on the finished product. Experiment 3 was designed to investigate by TI the effect of flavor dosage *without* such a correction. The average TI curves shown in Figure 5 indicate that all the intensity-related parameters for both descriptors are indeed directly proportional to the dosage. The REML analysis per descriptor indicated that the 8% dosage was significantly greater than the 4% dosage for log (area), log (Imax) and log (Iswal) obtained on both descriptors. For *salty* the higher dosage also had a significantly larger log (Tdur). There was no significant dosage-related difference in log (durmax), log (Tmax) or log (Tswal).

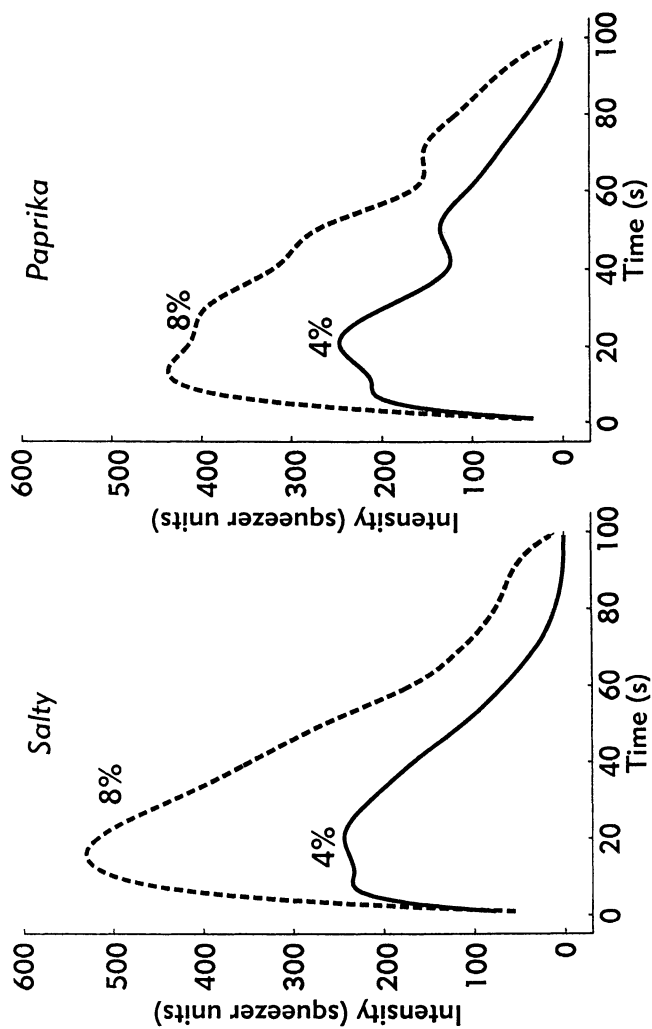
Conducting the REML analysis per TI parameter over the two descriptors and two products showed that panelists swallowed later when evaluating the retronasal descriptor *paprika* than when evaluating saltiness. This difference was larger at lower dosage, as shown in the biplot for this experiment (Figure 6).

Experiments 4 and 5

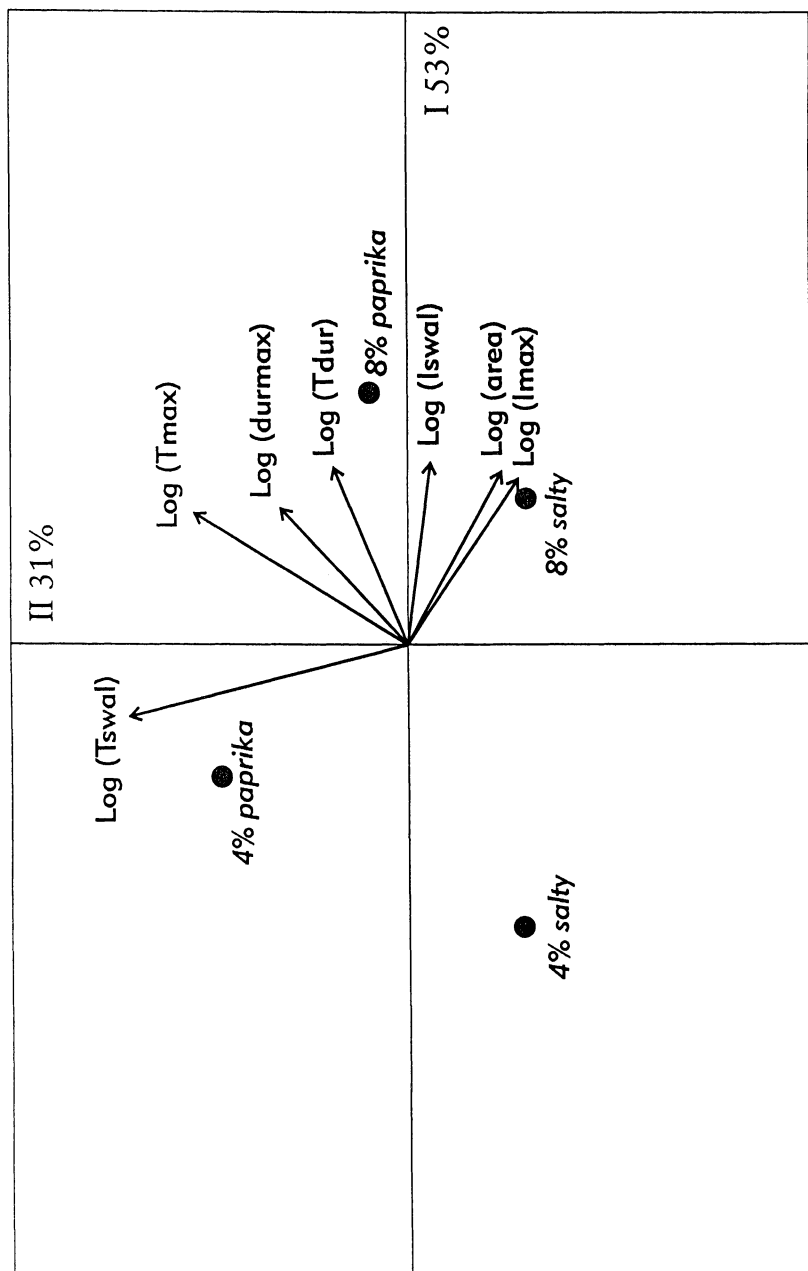
In both single and multiple ingestion TI tests using the products C, T and R, flavor perception was most intense and longest lasting on the potato base, product R. The average TI curves for Experiment 4 (Figure 7) show an increase in intensity-



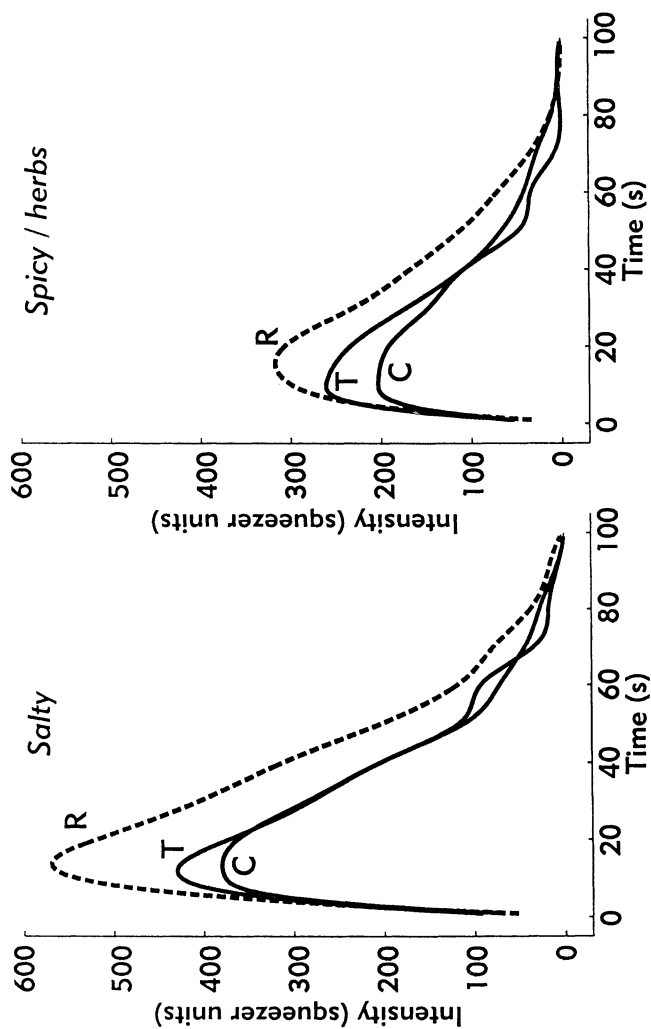
4. PCA of panel profiling REML scores from Experiment 2 without 4 base descriptors (*corn*, *corn aftertaste*, *potato*, *potato aftertaste*). Flavor dosage (5%, 6%, 7%) is indicated within the sample symbol.



5. Average TI curves from Experiment 3.



6. PCA of panel TI parameters (REML) from Experiment 3.



7. Average TI curves from Experiment 4.

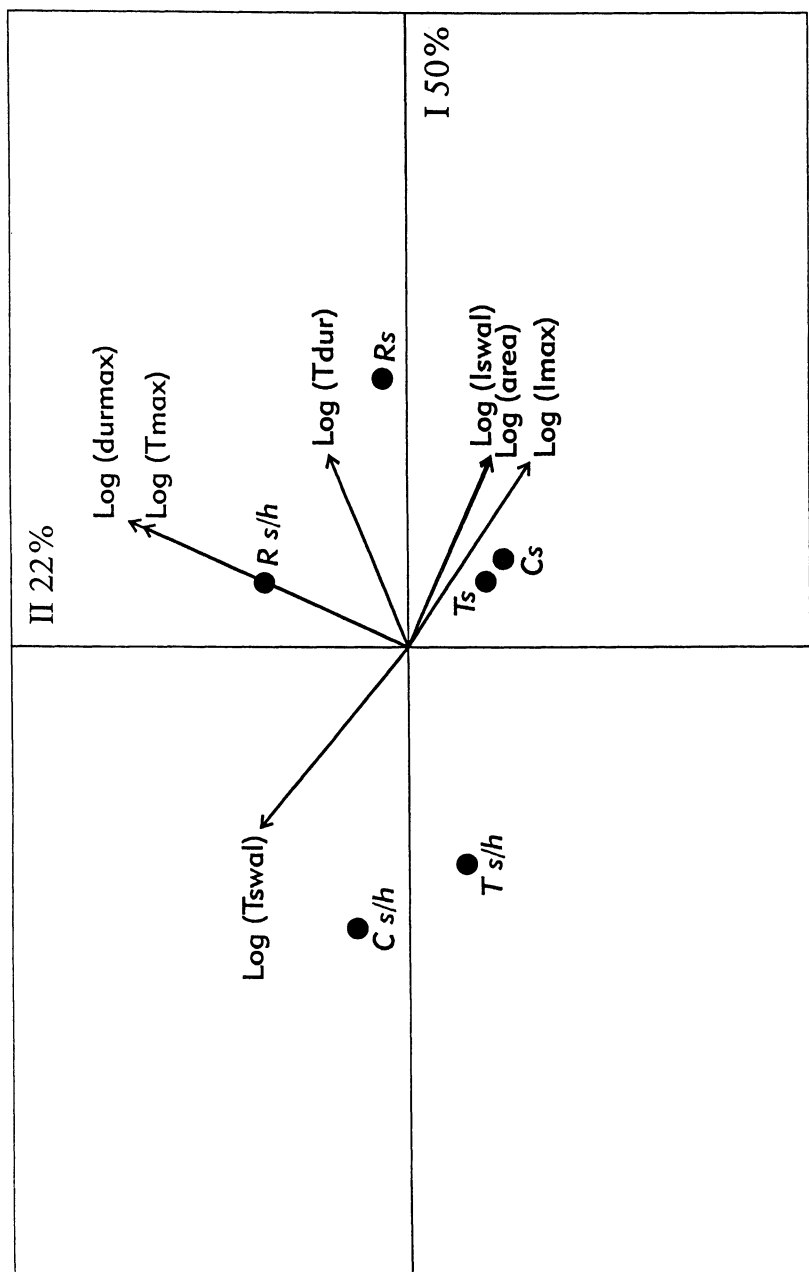
related TI parameters going from C to T to R for both descriptors. The REML analysis per descriptor indicated no significant differences between C and T for any parameter on either *spicy/herbs* or *salty*. R was significantly larger than C for log (area) and log (Imax) on *spicy/herbs*, and R was significantly larger than both C and T for these parameters when *salty* was evaluated. The only significant time-related TI parameter was log (Tdur): R lasted longer than C for the retronasal *spicy/herbs*.

When the REML analysis was conducted per TI parameter over the two descriptors and three products it was evident that the *salty* curves had a larger area, a larger maximum intensity, and they lasted longer than the *spicy/herbs* curves. *Salty* curves also had a larger intensity at swallowing, but swallowing occurred faster, as was seen in Experiment 3. These differences in descriptors and products are summarized in the biplot shown in Figure 8.

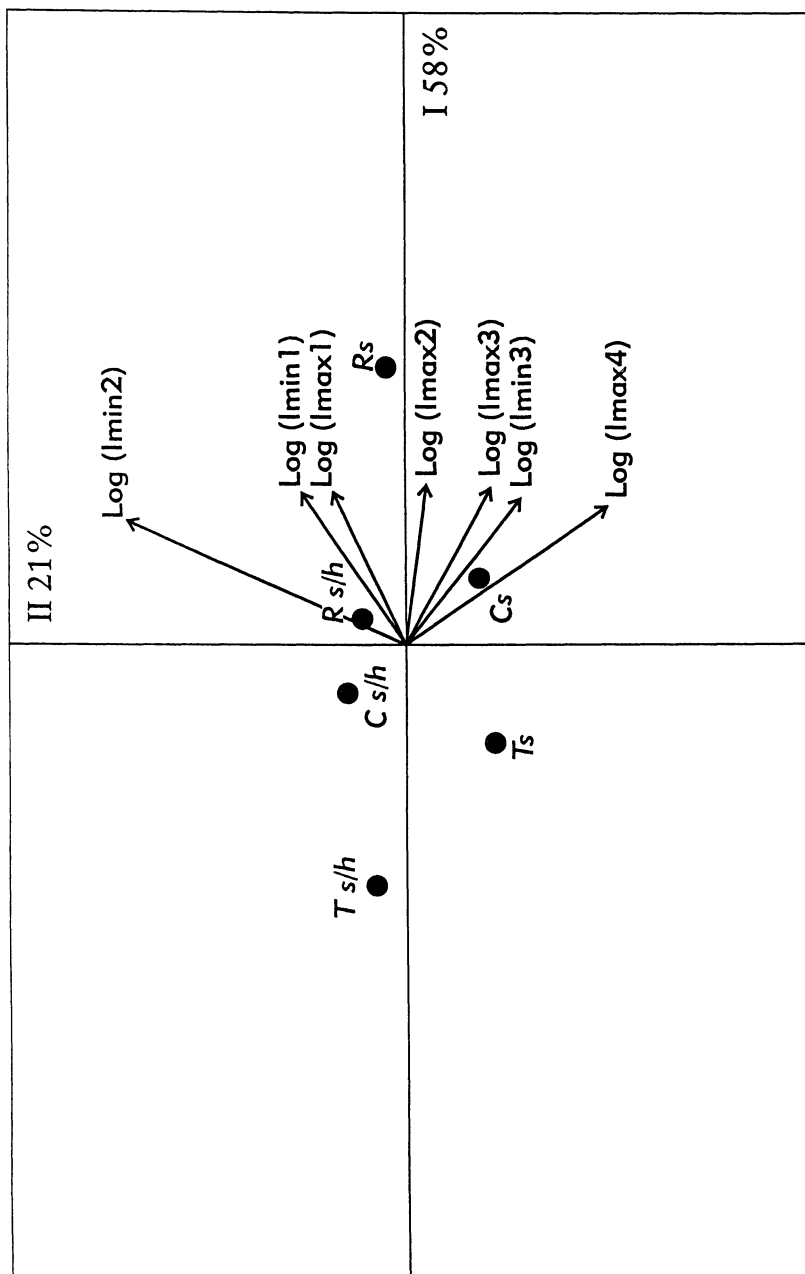
Repeated ingestion of the same products (R, T, C : Experiment 5) reversed the order of increasing intensity parameters for the two corn-based samples, i.e., T was perceived as less intense than C. There was insufficient evidence from these tests to prove a faster build-up of flavor in the mouth for the low bulk density C because none of the TI parameters was able to show significant differences between the four ingestions. The biplot for intensity-related TI parameters (Figure 9) shows product separation along the first dimension with T, C, R positioned in order of increasing intensity. The second dimension separates the two descriptors. These descriptors are no longer clearly separated in the biplot for time-related TI parameters shown in Figure 10, although product separation does follow along a diagonal from the 3rd to 1st quadrant.

In a REML analysis for log (Imax) over all data collected in Experiments 4 and 5 it was shown that R > (C, T) with no significant difference between the two corn-based products. Imax for a single ingestion was greater than for any of the multiple ingestions, the latter being not significantly different going from first ingestion to fourth. The *salty* evaluations were always more intense than the *spicy/herbs* evaluations. The corresponding REML analysis for log (Tmax) in which only the first of the multiple ingestion maxima was used, showed that T products reached their maximum intensity faster than R products. The fact that the first maximum of the multiple ingestions occurred sooner than for the single ingestion might be an artifact of the test if panelists felt rushed or stressed by the multiple ingestion procedure

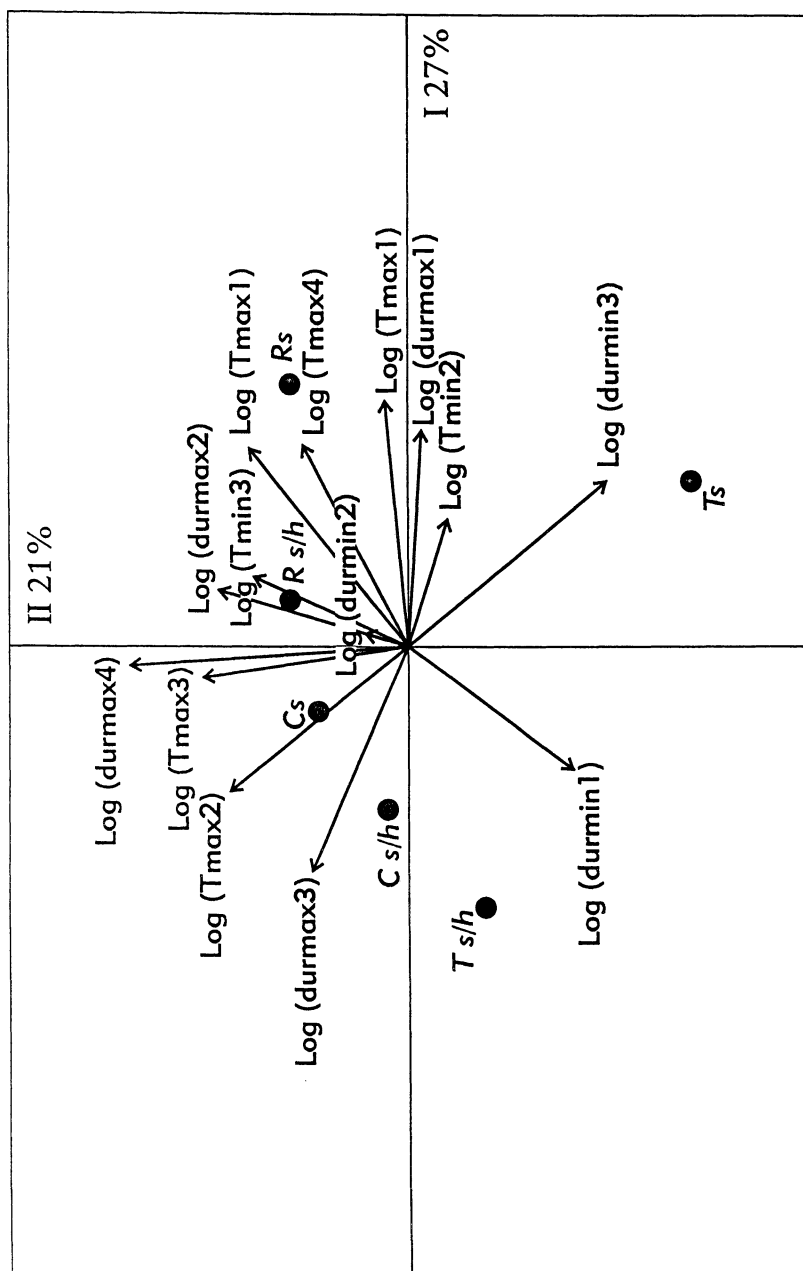
The REML analysis for log (Tmax) on these combined data also showed a significant difference between the two descriptors: the retronasal sensation reached its maximum 1.7 s *before* the basic salty taste. (This difference was not significant in either of the single ingestion tests.) Cliff and Noble (5), reporting TI measurements of sweetness (basic taste) and fruitiness (retronasal) in model solutions of glucose/peach essence, found that Tmax for sweetness was 3.8 s *shorter* than Tmax for fruitiness. They speculated that retronasal perception was aided by the convection and turbulence that occurred during expectoration since sweetness was perceived before expectoration and fruitiness afterward. The same order of perception was found in a later study (6) for binary and tertiary mixtures using sweeteners, although it was only significant for binary systems.



8. PCA of panel TI parameters (REML) from Experiment 4.



9. PCA of panel intensity TI parameters (REML) from Experiment 5.



10. PCA of panel TI time parameters (REML) from Experiment 5.

If the difference between Tmax for retronasal as opposed to basic tastes is not simply an artifact of peak size, procedural differences may explain why Noble's group found longer times to reach a retronasal maximum. Panelists in the current study were free to swallow whenever they chose. The fact that panelists swallowed later when evaluating the retronasal flavor might indicate that they required more time to recognize this flavor. No expectoration was allowed in the current study. Other experimental differences in these studies are the nature of the samples (liquid as opposed to solid), and the nature of the basic taste (sweetness versus saltiness). Additional testing of various flavors and products is necessary in order to understand the temporal perception of retronasal as opposed to basic tastes.

Acknowledgements

Appreciation is expressed to Laith Wahbi, Rob Walraven and Walter van Damme from Quest Snacks. Paul Arents, Susanne Schroff and Seeta Soekhai are thanked for their help in collecting and processing these data.

References

1. King, B.M. *Lebensm.-Wiss. u.-Technol.* **1994**, *27*, 450-456.
2. King, B.M.; Moreau, N. *J. Inst. Brew.* **1996**, *102*, 419-425.
3. Härdle, W. *Applied Nonparametric Regression*; Econometric Society Monographs No. 19; Cambridge University Press: Cambridge, 1991; pp 24-36.
4. Overbosch P.; van den Enden J.C. and Keur B.M. *Chem. Senses.* **1986**, *11*, 331-338.
5. Cliff, M.; Noble, A.C. *J. Food Sci.* **1990**, *55*, 450-454.
6. Matysiak, N.L.; Noble, A.C. *J. Food Sci.* **1991**, *56*, 823-826.

Chapter 35

Release of Odorants from Roasted Coffee

W. Grosch and F. Mayer

Deutsche Forschungsanstalt für Lebensmittelchemie,
Lichtenbergstraße 4, D-85748 Garching, Germany

An apparatus designed for quantitative headspace analysis was used for the determination of the release of 22 potent odorants from roasted Arabica coffee. Within 5 min of grinding, 32 % of methanethiol present in the coffee sample as well as 15-20 % of acetaldehyde, methylpropanal, 2- and 3-methylbutanal were lost by volatilization. Within 30 min 20-30 % of 2-furfurylthiol, methional, vanillin and 2-isobutyl-3-methoxypyrazine, approximately 10 % of four alkylpyrazines and only 1 % of three furanones were lost from ground coffee. In contrast, after a storage period of 15 min, the losses of these odorants amounted only to 2-12 % in whole beans. The different evaporation rates of the odorants caused changes in the odor profile of the coffee sample. A synthetic mixture of 21 odorants in the concentrations found in the headspace was prepared. Sensory assessment of the aroma from this mixture compared well with that of the authentic coffee sample.

One goal of flavor research is the identification and quantification of volatile compounds which are perceived by the human nose in the air above a food. Two techniques, static and dynamic headspace sampling, have been proposed to solve this problem (1-3). The static method accurately provides the odorant composition, but the samples are too small to quantify odorants that are present at low concentrations. A dynamic method in which volatile compounds are swept by an inert gas into a trap containing a porous polymer which, more or less adsorbs the organic constituents, might be an alternative. However, the disadvantages of this technique are the strong dependence of the yields of the odorants on the velocity of the carrier gas (4) and on the selectivity of the adsorption and desorption processes (5, 6). As it is difficult to control these parameters accurately, the results of quantitative measurement may be inaccurate.

As shown in a study on the flavor of French bread (baguette) the results of quantification are independent of the conditions of dynamic headspace sampling when stable isotopomers of the odorants are used as internal standards (7). After

injection of known amounts of these compounds into the headspace, they were collected by the dynamic procedure together with the odorants to be analyzed.

In the present study, the new method was applied to medium roasted Arabica coffee from Colombia. The headspace concentrations of the volatiles which contribute significantly to the aroma of roasted coffee (reviewed in references 8-10) were quantified. As the aroma of freshly ground coffee changed rapidly when the sample was stored in the presence of air, the effect of this condition on the release of odorants was measured. Furthermore, the aroma of roasted coffee was reproduced on the basis of the results of headspace analysis and assessed sensorially.

Experimental Section

Coffee. Coffee beans (*Coffea arabica*) that originated in Colombia were medium roasted, stored under vacuum at -35°C and ground just before analysis (9).

Chemicals. Pure samples of the compounds in the tables and of the labeled internal standards were obtained as previously reported (9, 10).

Headspace Sampling and Quantification. The apparatus used for headspace sampling (Figure 1) was made of glass as detailed by Zehentbauer and Grosch (7). The inside surface was deactivated by treatment with dichlorosilane (7).

The coffee sample (0.1-10 g) was placed into tube no. 8 which was then sealed. Valves nos. 3 and 4 were opened and a solution containing known amounts of the odorants in diethyl ether was injected onto the glass finger no. 10 which was heated up to 80°C. These odorants were labeled with stable isotopes to differentiate them from the analytes. The release of odorants was determined for a period of 15 min or 30 min (see Tables for details) during which time the coffee sample remained in the apparatus. To equilibrate the odorants and the labeled internal standards in the apparatus (volume 6.84 L), the piston (no. 5) was pushed and pulled during this period. Subsequently, the valves nos. 3 and 4 were closed and nos. 1 and 2 were opened. After opening valve no. 1, the gaseous nitrogen pressed the headspace collected in tube no. 6 into the Tenax trap no. 7 by moving the piston. For analysis of the highly volatile odorants 1-7 (Table I) the Tenax trap no. 7 (Figure 1) was put in the desorption heating block of a gas chromatograph (7). The analytes and their labeled internal standards were desorbed and then analyzed by mass chromatography (10). The less volatile odorants 8-22 (Table I) were extracted from the Tenax trap no. 7 using diethyl ether and then quantified by multidimensional gas chromatography (10, 11).

Analysis of the Coffee Sample. The odorant content of samples was quantified by stable isotope dilution assays (10).

Odor Profile Analysis. After removal of the Tenax trap (no. 7 in Figure 1) the apparatus for headspace sampling was used as an olfactometer (7). With the exception of 2-ethenyl-3-ethyl-5-methylpyrazine, 21 odorants in the headspace concentrations listed in Table I were dissolved in pentane. To compensate for the lack of 2-ethenyl-3-ethyl-5-methylpyrazine, the amount of pyrazine no.15 (Table I) was

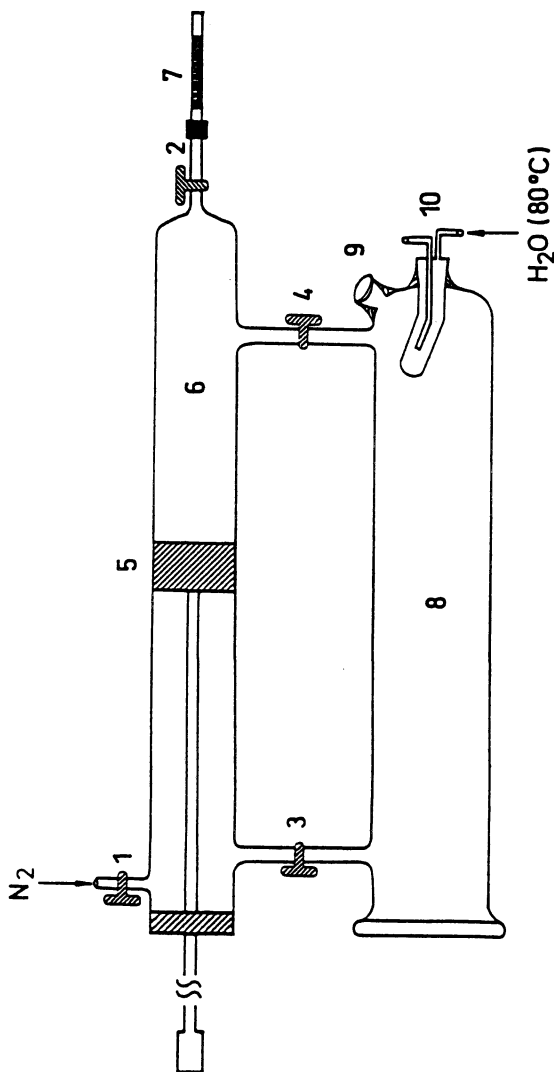


Figure 1. Apparatus for quantitative headspace analysis (7)
1-4, Valves; 5, piston; 6, tube; 7, Tenax trap; 8, tube containing the coffee sample; 9, septum; 10, glass finger

Table I. Concentrations ($\mu\text{g/g}$) of Odorants in the Ground Coffee Sample and in the Headspace after 30 min Equilibration.^a

No.	Odorant	Concentration		
		in coffee		Release
		$\mu\text{g/g}$	$\mu\text{g/g}$	%
1	Methanethiol	4.4	2.9	66
2	Acetaldehyde	118	54	45
3	Methylpropanal	24.2	6.0	25
4	2-Methylbutanal	25.8	8.2	32
5	3-Methylbutanal	16.5	4.4	27
6	2,3-Butanedione	48.8	9.1	19
7	2,3-Pentanedione	35.3	9.0	25
8	(E)- β -Damascenone	0.26	0.030	12
9	2-Furfurylthiol	1.65	0.38	23
10	Methional	0.25	0.070	29
11	Guaiacol	3.42	0.60	18
12	4-Ethylguaiacol	1.78	0.15	8.4
13	4-Vinylguaiacol	45.1	2.2	4.9
14	Vanillin	4.05	0.79	20
15	2-Ethyl-3,5-dimethylpyrazine	0.4	0.050	12
16	2,3-Diethyl-5-methylpyrazine	0.1	0.013	13
17	2-Ethenyl-3,5-dimethylpyrazine	0.053	0.0035	6.6
18	2-Ethenyl-3-ethyl-5-methylpyrazine	0.015	0.0020	13
19	2-Isobutyl-3-methoxypyrazine	0.117	0.024	21
20	4-Hydroxy-2,5-dimethyl-3(2H)-furanone	144	2.0	1.4
21	2-Ethyl-4-hydroxy-5-methyl-3(2H)-furanone	15.9	0.20	1.3
22	3-Hydroxy-4,5-dimethyl-2(5H)-furanone	1.85	0.020	1.1

^a Ground coffee (0.1-10 g) was placed into the apparatus (Figure 1).

correspondingly increased. The pentane solution was injected onto the glass finger no. 10 which had been heated up to 80°C. To distribute the odorants evenly in the apparatus, the piston (no. 5) was pushed and pulled for 10 min. Valves nos. 3 and 4 were closed and no. 2 was opened. The piston was pushed slowly to produce a constant stream of odorants which were smelled by an assessor at the outlet of valve no. 2. As the solvent pentane was odorless, it did not disturb the sensory evaluation of the odorants. To prepare the reference sample, the coffee sample (2.5 g) was placed into the apparatus and after 30 min the assessor at the outlet of valve no. 2 smelled the headspace. Altogether, six assessors compared the synthetic mixture of the odorants with the original coffee sample.

Results and Discussion

Detection of Odorants

Of the 28 volatiles screened in dilution experiments as potent odorants of roasted coffee (see review 8), the compounds listed in Table I were detected by gas chromatography/mass spectrometry. In this experiment headspace samples were drawn from 10 g of ground coffee which was placed into the apparatus (Figure 1) for 30 min. Only 2-methyl-3-furanthiol, 3-mercapto-3-methylbutyl formate, 3-methyl-2-butenthioi and 5-ethyl-3-hydroxy-4-methyl-2(5H)-furanone were not detected in the headspace by instrumental analysis. Furthermore, propanal and dimethyltrisulfide were not analyzed.

Release of Odorants

In Table I the release of 22 odorants during a period of 30 min is contrasted with their total concentrations in the coffee sample. Methanethiol and acetaldehyde showed the greatest reductions in concentration with 66 % of the former and 45 % of the latter lost in 30 min. The losses of 2-furfurylthiol, methional, vanillin and 2-isobutyl-3-methoxypyrazine (20 % to 30 % in 30 min) were comparable with that of the malty smelling *Strecker* aldehydes methylpropanal, 2- and 3-methylbutanal. The four alkylpyrazines were liberated at a slower rate; approximately 10 % of the amounts present in the coffee sample were lost in 30 min. The lowest evaporation rates were found for the three furanones of which only 1 % disappeared.

Sensory Experiment

A sensory experiment was performed to examine whether it was possible to imitate the aroma of roasted coffee on the basis of headspace data. The odorants in concentrations equal to those shown in Table I were dissolved in pentane. As not enough 2-ethenyl-3-ethyl-5-methylpyrazine was available, the concentration of 2-ethyl-3,5-dimethylpyrazine was correspondingly increased in the aroma model, as both compounds have very similar aroma quality and odor thresholds (12).

The results in Table II indicate that the aroma profile of the synthetic mixture matched the aroma profile of the coffee sample very closely. The highest differences in intensity which amounted only to 0.2 points for the sweetish/caramel and the roasty, sulfurous notes, were not significant. The good agreement in the aromas was underlined by the high score of 2.6 given by the assessors for the similarity of the overall odor of the imitate with that of the real coffee sample.

In a previous sensory experiment, the odorants found in medium roasted coffee (provenance Colombia) were dissolved in an oil/water mixture (1:20 w/w). In contrast to the headspace imitate M this model only reached a score of 2.3 (9). The lower score is mainly caused by the base, which differs from the solid coffee matrix in the binding of the odorants. This conclusion is supported here by the experiment with the headspace aroma model. The higher similarity of this model with the aroma of ground roasted coffee was achieved by elimination of the matrix. Furthermore, the

Table II. Odor Profiles of Ground Coffee and of the Corresponding Headspace Aroma Model M. Values for odor intensity and similarity range from 0 (absent or no similarity) to 3 (strong or identical).

Attribute	Coffee ^a	M ^b
	Intensity	
Sweetish/caramel-like	2.2	2.4
Earthy	1.5	1.4
Roasty/sulfurous	2.5	2.3
Smoky	1.2	1.3
Similarity		2.6

^a The coffee was equilibrated for 30 min in the apparatus and then smelled.

^b Mixture of the 21 odorants which were found in the headspace (cf. Table I).

Table III. Sensory Changes in the Odor Profile of Roasted Coffee with Storage Time. Values (0 no odor; 3 strong odor) are the mean of six assessors.

Attribute	Storage time in air ^a (h)			
	0	0.25	1	3
	Intensity			
Sweetish/caramel-like	1.5	0.8	0.6	0.3
Earthy	1.5	1.7	1.7	2.1
Roasty/sulfurous	2.4	2.3	2.3	2.2
Smoky	1.2	1.6	1.8	2.1

^a After grinding the coffee sample (2.5 g) was stored in air for the times given in the table. Then it was placed into the apparatus (Figure 1). After equilibration (15 min) the odor profile was evaluated by the assessors.

concentrations of the odorants in the headspace are much lower than in the matrix. Hence, chemical reactions of the odorants are very unlikely.

Change in the Odor Profile

As detailed in Table III the odor profile of the roasted coffee sample changed rapidly after grinding. The intensity of the sweetish/caramel-like odor quality decreased distinctly within 15 min and continuously during the next 3 h. The earthy and the smoky notes increased slowly whereas the roasty/sulfurous note remained nearly constant.

To get an insight into the changes in the concentrations of the odorants during storage of roasted coffee in the presence of air, the following experiment was undertaken. The ground coffee sample was stored at room temperature and, after different periods of time, the sample was placed into the apparatus (Figure 1) and then the highly volatile odorants which were released within 15 min were determined.

Table IV. Headspace Concentrations ($\mu\text{g/g}$) of Highly Volatile Odorants after Storage of Coffee at Room Temperature

Odorant	Storage time (h) in air after grinding			
	0	0.25	1	3
Methanethiol	1.9	1.9	n.d.	n.d.
Acetaldehyde	45.7	40.0	n.d.	n.d.
2,3-Butanedione	7.5	3.5	2.6	2.1
2,3-Pentanedione	7.4	3.7	3.7	3.3
Methylpropanal	4.9	1.7	1.2	1.0
2-Methylbutanal	7.0	2.3	1.8	1.6
3-Methylbutanal	3.6	1.4	1.1	1.0

n.d.: not determined

The results in Table IV. indicate that the release of methanethiol was not affected by a storage period of 15 min and also the relatively high amount, which evaporated from acetaldehyde, remained nearly constant. This was in contrast to the diones and to the malty smelling *Strecker* aldehydes methylpropanal, 2- and 3-methylbutanal. The release of the latter compounds decreased to one third and that of butanedione and pentanedione by 50 %. In the case of the diones and *Strecker* aldehydes, the release within 15 min was determined in coffee samples which had been stored for up to 3 h. The results in Table IV indicate that the amounts liberated decreased further, although the differences become much smaller with respect to the amounts found after the first 15 min of storage.

In the experiments listed in Table V the release of 7 highly volatile odorants was determined at different times and related to their total concentrations in the coffee sample. According to the results in Table V, methanethiol was the most volatile odorant of which 32 % evaporated during the first 5 min. Acetaldehyde evaporated somewhat slower, but after 1 h its loss (64 %) was nearly as high as that of methanethiol (70 %). The released amounts of the two diones agreed although their concentrations in the coffee sample were different. During the first 5 min, 15 % to 19 % of the *Strecker* aldehydes were lost. Then, as also found for the other odorants, the rate of loss slowed down. After 1 h the concentration of the *Strecker* aldehydes had decreased to one third.

Whole versus Ground Beans

In the final experiment (Table VI), the release of the highly volatile odorants from whole beans as well as from ground beans during a period of 15 min was compared. As expected the increase in surface area, caused by the grinding process, strongly enhanced the amount of odorants, which were lost from the coffee sample. The largest increase was found for 2,3-butanedione. The amount released in the gas phase was 8-times higher in ground beans than in whole beans. The smallest

Table V. Concentration ($\mu\text{g/g}$) of the Highly Volatile Odorants in the Headspace above Ground Roasted Coffee with Time at Room Temperature. Percentage Figures are the Amounts Expressed as a Percentage of the Original Sample Content

<i>Odorant</i>	<i>Amount of volatile in headspace with time</i>							
	<i>5 min</i>		<i>15 min</i>		<i>30 min</i>		<i>60 min</i>	
	$\mu\text{g/g}$	%	$\mu\text{g/g}$	%	$\mu\text{g/g}$	%	$\mu\text{g/g}$	%
Methanethiol	1.4	32	1.9	43	2.9	66	3.1	70
Acetaldehyde	23.8	20	45.7	39	53.5	45	75.1	64
2,3-Butanedione	4.6	9.4	7.5	15	9.1	19	10.2	21
2,3-Pentanedione	4.7	13	7.4	21	9.0	25	9.8	28
Methylpropanal	3.6	15	4.9	20	6.0	25	6.6	27
2-Methylbutanal	5.0	19	7.0	27	8.2	32	9.4	36
3-Methylbutanal	2.7	16	3.6	22	4.4	27	5.2	32

Table VI. Headspace Concentrations of Highly Volatile Odorants after 15 minutes for Roasted Whole and Ground Beans. Figures represent the actual headspace concentration ($\mu\text{g/g}$) and the Percentage Figures are the Amounts Expressed as a Percentage of the Original Sample Content

<i>Odorant</i>	<i>Whole beans</i>		<i>Ground beans</i>	
	$\mu\text{g/g}$	%	$\mu\text{g/g}$	%
Methanethiol	0.5	11	1.9	43
Acetaldehyde	14.1	12	45.7	39
2,3-Butanedione	0.9	1.8	7.5	15
2,3-Pentanedione	1.1	3.1	7.4	21
Methylpropanal	0.9	3.7	4.9	20
2-Methylbutanal	1.1	4.3	7.0	27
3-Methylbutanal	0.6	3.6	3.6	22

difference was found for acetaldehyde, as the amount was only 3-times higher than in ground beans.

Conclusions

The results confirm that the new analytical method is sufficient for an accurate quantification of the odorants occurring in the headspace of foods. The rapid change in the odor profile of ground roasted coffee is caused by large differences in the evaporation rates of potent odorants. The aroma of roasted coffee can be reproduced on the basis of the results of headspace analysis.

References

1. Schaefer, J. In: *Isolation, Separation and Identification of Volatile Compounds in Aroma Research*; Maarse, H.; Belz, R.; Eds.; Akademie-Verlag, Berlin, **1981**, pp. 37-49.
2. Parliment, T.H. In: *Biogenesis of Aromas*; Parliment, T.H.; Croteau, R.; Eds.; ACS Symposium Series 317, American Chemical Society, Washington, DC, **1987**, pp. 34-52.
3. Risch, S.J.; Reineccius, G.A. In: *Thermal Generation of Aromas*; Parliment, T.H.; McGorin, R.J.; Ho, C.-T.; Eds.; ACS Symposium Series 409, American Chemical Society, Washington, DC, pp. 42-50.
4. Werkhoff, P.; Bretschneider, W.; Herrmann, H.-J.; Schreiber, K. *Lab. Prax.* **1989**, 426-430.
5. Jennings, W.; Filsoof, M. *J. Agric. Food Chem.* **1977**, 25, 440-445.
6. Schaefer, J. In: *Flavour '81*; Schreier, P.; Ed.; de Gruyter, Berlin, **1981**, pp. 301-313.
7. Zehentbauer, G.; Grosch, W. *Z. Lebensm. Unters. Forsch.* **1997**, 25, 262-267.
8. Grosch, W. *Nahrung* **1998**, 42, 344-349.
9. Czerny, M.; Mayer, F.; Grosch, W. *J. Agric. Food Chem.* **1999**, 47, 695-699.
10. Mayer, F.; Czerny, M.; Grosch, W. *Euro Food Res. Technol.* **1999**, 209, 242-250.
11. Reiners, J.; Grosch, W. *J. Agric. Food Chem.* **1998**, 46, 2754-2763.
12. Wagner, R.; Czerny, M.; Bielohradsky, J.; Grosch, W. *Z. Lebensm. Unters. Forsch.* **1999**, 208, 308-316.

Author Index

- Acree, T. E., 333
Antipova, Anna S., 260, 293
Appelqvist, Ingrid A. M., 212
Baek, I., 153
Belyakova, Larisa E., 260
Birch, G. G., 395
Boukobza, F., 44
Brauss, M. S., 22
Brevard, H., 58, 112
Brondeur, Phillipe, 342
Buettner, A., 87
Charles, Marielle, 342
Chengappa, S., 44
Conde-Petit, B., 230
Courthaudon, Jean-Luc, 342
Crawford, R. A., 381
Davidson, J. M., 99
de Roos, Kris B., 126
Deibler, K. D., 333
Delahunty, Conor M., 405
Dodds, T. M., 381
Druaux, C., 142
Duineveld, C. A. A., 413
Dunphy, P., 44
Escher, F. E., 230
Espinoso Diaz, M. A., 142
Foegeding, E. Allen, 355
Friel, E. N., 166
Gfeller, Hans, 33
Goff, Terry C., 212
Golovnya, Rimma V., 260, 293
Goubet, Isabelle, 246
Grab, Willi, 33
Grosch, W., 430
Guichard, Elisabeth, 282, 342
Guilfoyle, Brendan, 405
Gwartney, Elizabeth A., 355
Harrison, Marcus, 179
Harvey, B. A., 22
Hollowood, T. A., 99, 370
Homan, Jenny E., 212
Jordan, A., 58, 112
Karim, R., 395
King, Bonnie M., 413
Labows, John N. Jr., 73
Lambert, Sandrine, 342
Landy, P., 142
Lanot, A., 44
Larick, Duane K., 355
Le Quééré, Jean-Luc, 246, 282
Lian, Guoping, 201
Lindinger, W., 58, 112
Linforth, Rob S. T., 8, 22, 99, 166, 370
Liu, Xiaoyan, 73
Lübke, Markus, 282
Malone, Mark E., 212
Marin, Michèle, 153, 192
Mayer, F., 430
Misharina, Tamara A., 260, 293
Moore, I. T. P., 381
Mottram, Donald S., 274
Nobrega, Ian C. C., 274
Nuessli, J., 230
Parker, Alan, 192
Payne, Richard K., 73
Polikarpov, Yurii N., 260
Pollien, Phillipe, 321
Raymond, T., 395
Roberts, Deborah D., 1, 321
Roozen, Jacques P., 309
Schieberle, P., 87
Semenova, Maria G., 260, 293
Sémon, E., 246
Seuvre, A. -M., 246
Taylor, Andrew J., 1, 8, 22, 99, 153, 166, 370
Terenina, Margarita B., 260, 293
Turnbull, R. P., 381
van Ruth, Saskia M., 309
Voilley, A., 142, 246
Wilkins, J., 44
Wilkins, John P. G., 212
Yeretzian, C., 58, 112

Subject Index

- A**
- Acesulfame potassium**
effect on odorants in beverages, 337, 338*t*
range in experiments, 335*t*
See also Beverages
- Acetaldehyde**
aqueous solution study, 157*t*
decrease in model solutions during mastication, 93
kinetic properties in water, 158–160
partition coefficient in aqueous solution, 157–158
release curve, 159*f*
See also Aldehydes; Coffee, roasted; Dynamic headspace dilution method
- Acetates**
major factors and interactions affecting volatility from beverages, 339, 340*t*
See also Beverages
- d₆-Acetone**
flavor release from standard and microstructured emulsions, 220*f*
measured flavor release rate constant, 216*t*
See also Lipophilic flavor release in low fat foods
- Acid-base equilibrium, effect on phase partitioning, 128**
- Adaptation**
definition, 395
interaction of non-volatile and volatile compounds, 99
panelists for menthone with time, 105–106
- Affinity chromatography, interaction measurement between proteins and aroma, 345**
- AFFIRM. *See* Analysis of flavor and fragrances in real time (AFFIRM)**
- Air sampling during eating, relationship between volatiles and sensory perception, 10–11**
- Air-water equilibrium constant**
aroma compounds, 195
effect on interfacial flux, 197
See also Gas-liquid interfacial mass transfer (GLIM) cell
- Alcohols**
amounts formed in oils and emulsions, 316*t*
chemical assignment of proton transfer reaction–mass spectrometry (PTR–MS) profile of green coffee beans, 118*t*
predicted volatile release curves for ethanol, dodecanol, decanol, and hexanol, 175, 176*f*, 177
relative release of odor active compounds in model mouth system, 316*f*
relative static headspace concentrations of reference odor active compounds added to sunflower oil (SFO) and its emulsion, 317*f*
volatility and aroma release experiments, 311
- Aldehydes**
amounts formed in oils and emulsions, 316*t*
chemical assignment of proton transfer reaction–mass spectrometry (PTR–MS) profile of green coffee beans, 118*t*
comparing esters and aldehydes in masticated model solutions, 93, 94*f*
comparison of recovery after mastication of orange juice and model solutions, 96, 97*f*
gas chromatogram of beverage headspace in dynamic and static

conditions, 336, 337*f*
 influence of duration of mastication, 94, 95*f*
 major factors and interactions affecting volatility from beverages, 339, 340*r*
 model experiments using aqueous solutions of reference odorants, 91
 relative release of odor active compounds in model mouth system, 316*f*
 relative static headspace concentrations of reference odor active compounds added to sunflower oil (SFO) and its emulsion, 317*f*
 volatility and aroma release experiments, 311
See also Beverages; Mastication
 Alkanes, chemical assignment of proton transfer reaction–mass spectrometry (PTR–MS) profile of green coffee beans, 118*t*
 Alk(en)yl cysteine sulfoxide wound response of garlic, 51
See also Garlic
 Alkyl acetates binding differing in length of hydrocarbon chain, 298–301
 binding isotherms from their equimolar mixtures with native legumin, 303*f*
 binding isotherms with native legumin, 299*f*
 binding parameters with native legumin from equimolar mixture, 305*t*
 comparison of binding extent for alkyl acetates alone and from equimolar mixtures for same concentration of free ligands in system, 306*t*
 effect on thermodynamic parameters of legumin heat denaturation process, 301*f*
 Scatchard plots showing binding to native legumin, 300*f*, 304*f*
See also Legumin binding with aroma esters

Allium
 alk(en)yl cysteine sulfoxide pathway, 45
 materials, 46
See also Garlic
 Allyl isothiocyanate effect of droplet size on flavor release from emulsions, 350*f*
 effect of nature of proteins as emulsifier on flavor release from oil/water emulsions, 347*f*
 global affinity with proteins, 347*f*
 physicochemical and sensory characteristics, 343*t*
 Amylopectin complexation with flavor compounds, 241
 starch constituent, 231
 Amylose appearance, rheological properties, and structure of dispersions, 239
 characteristics of potato starch dispersions without and with addition of ligands, 240*t*
 complexation of flavor compounds in diluted starch dispersions, 239–241
 complexation of flavor compounds in diluted starch solutions, 238
 formation of inclusion complexes, 237
 modeling starch polymorphs A and B, 232*f*
 molecular structure of complexes, 240–241
 representative model for unit cell, 242*f*
 schematic presentation of possible arrangement of helices complexed with thymol, 242*f*
 starch constituent, 231
 terminology for complexation with flavor compounds, 237–238
See also Starch
 Analysis of flavor and fragrances in real time (AFFIRM)
 development of flavors and fragrances, 15
 flavor quality deterioration following homogenization, 28
 main advantages, 23

- time dependence of release of enzymatically generated volatiles, 30
See also Real time flavor release
- Anethole, release rates of flavor compound from yogurts, 29, 30*f*
- Apparent specific volumes equations, 396–397
 glucose syrups and D-glucose, 401, 402*t*, 403
See also Sweetness and salivary sweetener concentration
- Aqueous and lipid phase, phase partitioning between, 128–129
- Aqueous phase composition, effect on phase partitioning, 128
- Arabica coffee. *See* Coffee, roasted; Coffee roasting
- Aroma compounds
 determining diffusivity, 144
 effect of matrix breakage on flavor release, 149–150
 interaction with non-volatile ingredients, 293
 mass balance, 196
 mass transfer, 148–149
 method for retention capacity, 248
 molar volume and diffusivity, 148*t*
 physicochemical characteristics, 143*t*
 physicochemical properties, 247*t*
 vapor-liquid partition coefficients in water, 146*t*
 volatility, 146–147
See also Aroma release models; β -Cyclodextrins binding aroma compounds; Flavor release from emulsions and complex media; Gas-liquid interfacial mass-transfer (GLIM) cell; Legumin binding with aroma esters
- Aroma esters
 determination of binding with protein, 295
 determination of concentration in solutions, 295
 role of legumin structure in binding with, 296–298
- role of structure in competitive binding of alkyl acetates from equimolar mixtures with native legumin, 302–306
See also Legumin binding with aroma esters
- Aroma release models
 breath volatile composition analysis by MS-Nose™, 168
 contour plot of predicted maximum volatile concentration (I_{\max}) values for aroma compounds from eaten gelatin gels, 170*f*
 contour plot of predicted T_{25} (time to decline to 25% max) values for aroma compounds from eaten gelatin gels, 174*f*
 correlation between predicted and observed $\log I_{\max}$ values, 171*f*
 effect of Hartree energy on $\log I_{\max}$, 173*f*
 gelatin gels preparation, 167–168
 materials and methods, 167–168
 model for temporal parameters, 171–174
 modeling breath I_{\max} , 168–171
 modeling entire release profile, 175
 observed and predicted volatile release curves for ethyl butyrate from gelatin gel, 175*f*
 observed and predicted volatile release curves for pyrazine from gelatin gel, 176*f*
 physicochemical parameters for compounds and their predicted and observed I_{\max} values, 172*t*
 predicted volatile release curves for ethanol, dodecanol, decanol, and hexanol, 176*f*
 prediction of volatile release for homologous series, 175, 177
 quantitative structure property relationships (QSPR), 167
 relationship between absolute value for Hartree Energy of compound and its molecular weight, 169*f*
 three-dimensional model, 169–170

- Aroma stimulus index (ASI)
 ASI and dynamic flavor release, 407–409
 compounds already present released during consumption, 409–410
 compounds generated during consumption, 409–410
 determining validity of theory, 409–411
 different food types, 410
 hypothesis of ASI constant in time, 407–409
 importance, 411
 linear cumulative release of volatile compound during consumption of hypothetical food by two consumers, 408*f*
 non-linear cumulative release of volatile compound during consumption of hypothetical food by two consumers, 409*f*
 physiological determinants for value of ASI, 410
 potential applications, 411
 range of compounds, 409
 representation of relationship between three consumers of hypothetical food releasing six compounds during consumption, 406*f*
 theory, 406–407
 time of consumption, 410
 volatile release over time, 407
- Aspartame
 effect on odorants in beverages, 337, 338*t*
 range in experiments, 335*t*
See also Beverages
- Atmospheric pressure chemical ionization–mass spectrometry (APCI–MS)
 banana headspace analysis, 17*f*
 breath analysis method, 213–214
 monitoring in vivo temporal changes of volatile flavors, 100
 potential for gas phase analysis in real time, 23
 quantification, 23
 reaction with protonated water, 45
 real time release of aroma molecules, 55
 specially developed interface, 22
See also Analysis of flavors and fragrances in real time (AFFIRM); FLAVORSPACE method; Wound response in plants
- Atmospheric pressure ionization–mass spectrometry (API–MS)
 applications, 15
 compounds with characteristic isotopic ratios, 14–15
 differences between proton transfer reaction and API, 15
 early literature, 13–14
 identification of compounds by mass resolution, 14
 interface for breath by breath analysis, 14*f*
 real-time measurement of volatile release at low concentration, 154–155
 sensitivity, 13
 soft ionization method, 13
See also Dynamic headspace dilution method
- B**
- Banana, headspace analysis, 16, 17*f*
 Beans, coffee. *See* Coffee, roasted
 Benzyl alcohol
 physicochemical properties, 247*t*
 retention of volatiles after dehydration of mixtures initially containing excess aroma, 250*t*
See also β -Cyclodextrins binding aroma compounds
- Beverages
 acesulfame potassium effects, 338*t*
 aspartame effects, 338*t*
 compounds for ethanol based stock solutions, 334*t*
 effect of sweeteners and acids on ionic environment, 333
 evaluating volatiles from sample in simulated mouth, 336

- experimental factors, 335*t*
 gas chromatogram of beverage
 headspace for dynamic and static
 equilibrium conditions, 337*f*
 interactions between factors, 338–339
 justification for sampling from
 retronasal aroma simulator (RAS),
 335
 major factors and interactions
 affecting volatility, 339, 340*t*
 model beverage, 335–336
 selecting effects producing significant
 sensory differences, 337
 simulated mouth system for aroma
 analysis, 334
 stock solution, 334
 sucralose effects, 338*t*
 system resembling situation in real
 products, 154
 test conditions, 335
 Weber ratio, 337
 Binding capacity. *See* Hexyl acetate and
 legumin interactions
 Blends, oils. *See* Volatile oxidation
 products
 Breath
 approaches to sampling, 73–74
 See also Malodors
 Breath by breath analysis
 atmospheric pressure ionization mass
 spectrometry (API–MS), 14*f*, 15
 difficult for proton transfer reaction–
 MS (PTR–MS), 18
 real time flavor release, 12
 volatile flavor release during eating of
 strawberry, 36–37
 Breath maximum volatile concentration
 (I_{\max})
 correlation between predicted and
 observed log I_{\max} values, 171*f*
 effect of Hartree energy on log I_{\max} ,
 173*f*
 modeling, 168–171
 physicochemical parameters for
 compounds and their predicted and
 observed I_{\max} values, 172*t*
 See also Aroma release models
 2,3-Butanedione. *See* Coffee, roasted
 1-Butanol
 effect of droplet size on flavor release
 from emulsions, 351*f*
 effect of nature of proteins as
 emulsifier on flavor release from
 oil/water emulsions, 347*f*
 global affinity with proteins, 347*f*
 physicochemical and sensory
 characteristics, 343*t*
 Butanone
 flavor release profile as function of fat
 content, 216*f*
 log-log plot of flavor intensity (FI_{\max})
 for microstructured and standard
 emulsions as function of oil content,
 223*f*
 measured flavor release rate constant,
 216*t*
 See also Lipophilic flavor release in
 low fat foods
 Butter flavor, mean time-intensity
 parameters for flavor in whey protein
 isolate gels, 365*t*
- ## C
- Calcium, in-mouth concentration from
 cheddar cheese by one panelist using
 ribbon saliva collecting technique,
 108*f*
 Carbohydrates
 ability to complex with aroma
 compounds, 322
 apparent specific volumes, 402*t*
 time intensity study of sweetness, 396
 total concentration in saliva of four
 panelists, 400*t*
 See also Sweetness and salivary
 sweetener concentration
 Carbon dioxide, release during coffee
 roasting, 121
 CarboxenTM/polydimethylsiloxane
 (CAR/PDMS) fiber, analysis of
 volatile sulfur compounds, 77
 Carvone release

- adaptation to stimulus, 378–379
- differences within panel, 376, 378
- effect of changing stimulus on perception—comparison of two assessors, 376*f*
- effect of eating speed on adaptation, 379*f*
- effect of eating speed on linear correlation of stimulus and perception, 377*f*
- effect of eating speed on maximum measured in-nose, 378*f*
- effect of increasing carvone concentration on volatile release, 373–374
- effect of maximum breath volatile concentration on linear correlation between stimulus and response, 377*f*
- experimental equipment, 372
- gelatin gel samples, 371–372
- magnitude estimation for carvone concentrations, 372
- relationship between carvone concentration in sample and maximum volatile measured in-nose (average and individual results), 373*f*, 374*f*
- relationship between maximum perceived mintyness determined by TI and sample concentration, 375*f*
- relationship between perception of mintyness as determined by magnitude estimation and sample concentration, 375*f*
- relationship between stimulus and perception, 374
- sensory panel, 371
- Stevens Law, 371, 374
- time intensity and in-nose volatile release measurements, 372–373
- use of T_{50} values for sensory and volatile release curves as means of measuring adaptation, 379*f*
- Charge transfer process, ionization, 13
- Cheddar cheese
- in-mouth sodium, calcium, and potassium concentration using ribbon saliva collecting technique, 108*f*
 - release of different salts, 107
- Cheeses
- preparation of processed cheese, 144
 - release of 2-nonanone from model, 150–151
- Chemical engineering approach seeking physical parameters controlling flavor release, 154
- See also* Dynamic headspace dilution method
- Chemical ionization (CI)
- bracketing proton affinities by selective, 65, 66*f*
 - ionization of volatiles, 13
 - proton transfer reaction mass spectrometry (PTR–MS), 59
- See also* Ionization
- Chemical ionization–mass spectrometry (CI–MS)
- identification and quantitation of mixtures of volatile organics, 45
 - real time monitoring, 45
 - time-resolved headspace analysis, 59, 60*f*
- See also* Proton transfer reaction–mass spectrometry (PTR–MS)
- Cherry flavor
- maximum intensity as function of held-water and microstructure, 363*f*
 - rate of release as function of held-water and microstructure, 363*f*
 - time-intensity (TI) parameters for release in whey protein isolate gels, 362*t*
- See also* Whey protein isolate gels
- Chewing. *See* Mastication
- Chewing gum
- chewing movements like bellows, 183
 - computer simulation algorithm, 186–187
 - demonstrating and comparing release of volatiles, 23
 - differences between gums and panelists, 106–107
 - differences in time to achieve maximum concentration, 107

- dilution of volatiles by saliva flow into oral cavity, 183
- effect of chewing efficiency on flavor release, 138*f*
- effect of encapsulation in Flexarome® matrices on release of amyl valerate in-nose from tutti-frutti flavored bubble gum, 26*f*
- effect of encapsulation on flavor release, 139*f*
- effect of varying partition coefficient on times and rates volatiles arrive at olfactory epithelium, 190
- encapsulation of liquid flavors for release profile modification, 24–27
- equilibrium saliva-gum partition coefficient, 182–183
- flavor bursts, 24
- flavor volatiles release depending on volatiles partition and mass transfer coefficients, 187, 188*f*
- Flexarome® flavor delivery systems, 24
- independence of chewing frequency on flavor release, 188
- influence of airways on transport processes, 188
- influence of breathing and chewing on nose-space heptanone and pentanone concentrations, 190*f*
- mass balance of flavor volatiles per unit cross-sectional area, 184
- mathematical representation of breathing velocity during inhalation and exhalation separated by finite pause, 183*f*
- measuring perceived sweetness and flavor of chewing gum using Dual-Attribute Time-Intensity, 100
- menthol release from peppermint chewing gum sticks, 25*f*
- modeling flavor release, 182–185
- new tutti frutti flavor with strong initial impact, 26
- non-equilibrium partitioning model for extraction of flavor compounds, 181
- non-volatile release, 5
- relationship between sucrose and menthone concentration and perceived mint flavor, 104–107
- release of mint volatiles, 15
- schematic of oral and nasal cavities, 182*f*
- schematic showing diffusion, convection, and absorption processes acting on flavor volatiles in airways, 184*f*
- stagnant-layer theory of interfacial mass transfer, 182–183
- sucrose release, menthone release, and perceived intensity of overall mint flavor from stick and tablet type chewing gums, 105*f*, 106*f*
- time-dependent heptanone release, 189
- See also* Cotton bud technique; Flavor release and transport from mouth to olfactory epithelium
- Chips**
- in-mouth sodium concentration using ribbon saliva collecting technique, 108*f*
- sodium concentration, 107
- See also* Snacks
- Citric acid**
- in-mouth concentration from fresh orange segments using ribbon saliva collecting technique, 109*f*
- in-mouth concentration from gelatin gel using ribbon saliva collecting technique, 110*f*
- Clean air, proton affinities of constituents, 62*t***
- Coconut flavor, mean time-intensity (TI) parameters for flavor in whey protein isolate gels, 366*t***
- Coffee**
- abundant compounds in headspace of green coffee, 116
- bracketing proton affinities by selective chemical ionization, 65, 66*f*
- chemical assignment of proton transfer reaction–mass spectrometry (PTR–MS) spectra, 65

headspace analysis, 68–70
 Henry's law calculation, 67–68
 ion-intensity profiles of selected masses upon reconstitution of soluble coffee with water, 70*f*
 profiles plotted on linear and logarithmic intensity scales, 69*f*
 selective ionization using lasers, 18
 two distinct types of information by PTR-MS, 64*f*
See also Proton transfer reaction-mass spectrometry (PTR-MS)

Coffee, roasted

analysis of coffee sample, 431
 apparatus for quantitative headspace analysis, 432*f*
 change in odor profile, 435–436
 chemicals, 431
 coffee beans, 431
 concentration of highly volatile odorants in headspace above ground roasted coffee with time at room temperature, 437*t*
 concentrations of odorants in ground coffee sample and in headspace after 30 minutes equilibration, 433*t*
 detection of odorants, 434
 experimental section, 431–433
 headspace concentrations of highly volatile odorants after 15 minutes for roasted whole and ground beans, 437*t*
 headspace concentrations of highly volatile odorants after storage at room temperature, 436*t*
 headspace sampling and quantification method, 431
 odor profile analysis, 431, 433
 odor profiles of ground coffee and corresponding headspace aroma model M, 435*t*
 release of odorants, 434
 sensory changes in odor profile of roasted coffee with storage time, 435*t*
 sensory experiment, 434–435
 whole versus ground beans, 436–437

Coffee roasting

Arabica (Columbia) coffee, 117, 119*f*
 batch roasting procedure, 115
 effect of roast-gas temperature on roasting process, 119
 emissions during roasting, 117–121
 emissions from green coffee beans, 116
 ion-intensity profiles for seven masses monitored during roasting of Arabica coffee beans at 190°C, 119*f*
 ion-intensity profiles for volatile compounds during roasting of Arabica coffee beans at 180°C and 190°C, 120*f*
 ion-intensity profiles for volatile compounds during roasting of six Arabica beans at 185°C (single beans), 121*f*
 method for determining emissions from green coffee beans, 114
 method for determining emissions of volatiles during roasting, 114–115
 monitoring batch and single bean roasting, 120–121
 objective to monitor on-line time-intensity profiles, 113
 phases, 117
 proton transfer reaction-mass spectrometry (PTR-MS) method, 113
 PTR-MS headspace profile of Robusta (Indonesia) green beans, 116, 117*f*
 quality assessment, 112
 schematic representation of PTR-MS, 114*f*
 setup for on-line analysis of coffee roast gas, 115*f*
 single bean roasting procedure, 115
 tentative chemical assignment of PTR-MS headspace profile of Robusta green coffee beans, 118*t*
 time-temperature-dependent process, 112–113
 Complex media. *See* Flavor release from emulsions and complex media
 Complexation

- appearance, rheological properties, and structure of dispersions, 239
- characteristics of potato starch dispersions without and with addition of ligands, 240*t*
- definition, 238
- effect on phase partitioning, 128
- flavor compounds in diluted starch dispersions, 239–241
- flavor compounds in diluted starch solutions, 238
- flavor compounds with amylopectin, 241
- flavor retention and release in systems with starch flavor complexes, 241, 243
- inclusion complexes with amylose, 237
- molecular structure of amylose complexes, 240–241
- possible arrangement of helices of amylose complexed with thymol, 242*f*
- terminology for flavor compounds with amylose, 237–238
- Composite dairy gels**
- allowing for effect of chewing, 384
- allowing for evaporation of volatile flavors into respired air, 384
- comparison between predicted and experimental parameters for 50 ppm ethyl butyrate samples, 392*f*, 393*f*
- composite gel manufacture, 386–387
- conceptual model of composite gel particle, 383*f*
- conceptual model of mouth, 388*f*
- confocal laser micrograph of typical composite gel, 383*f*
- Crank–Nicolson method for**
- converting differential equations to numerical format, 385
- definition of TI parameters, 389*t*
- developing method for calculating flavor release rate, 381–382
- difficulty in changing conditions for significant variations in time-intensity parameters, 394
- diffusion of fat-soluble flavor compound through fat particle, 384
- diffusivity of flavor in protein part of gel, 391
- effect of assuming 50% saliva removal by swallowing every 10 seconds, 389, 390*f*
- effect of changing air flow rate through mouth, 389, 390*f*
- experimental design for manufacture, 387
- experimental study, 391–394
- experimental time-intensity curve of one panelist and model prediction, 391*f*
- extending model to include swallowing saliva, 384
- fat particle size, 391
- focus of study, 382
- formulations for sample production, 386*t*
- good match for time to maximum intensity (T_{\max}) and maximum intensity (I_{\max}), 393
- initial development of flavor concentrations in simplified model, 388*f*
- mass transfer between retronasal air and saliva, 384–385
- model development, 382–385
- modeling results, 389
- panel training, 385–386
- sensory analysis, 387
- spherical diffusion, 382
- time intensity methods, 385
- Composite foods, peanut butter and jelly sandwiches, 27–29**
- Computer program, calculating matrix interaction factors, 34**
- Concentration methods, prior to GC–MS analysis, 11–12**
- Consumers**
- value of aroma stimulus index (ASI), 410
- See also* Aroma stimulus index (ASI)
- Consumption of food. *See* Aroma stimulus index (ASI); Volatile release in vivo during food consumption**

- Continuous sampling technique
 different profiles for different types of foods, 109
 in-mouth sodium, calcium, and potassium concentration from cheddar cheese by one panelist using ribbon saliva collecting technique, 108*f*
 in-mouth sodium concentration from crisps by one panelist using ribbon saliva collecting technique, 108*f*
 in-mouth sucrose, glucose, and citric acid concentration from gelatin gel by one panelist using ribbon saliva collecting technique, 110*f*
 in-mouth sucrose, glucose and fructose, citric acid, and malic acid concentration from fresh orange segments using ribbon saliva collecting technique, 109*f*
 novel technique, 107
- Controlled flavor release. *See*
 Lipophilic flavor release in low fat foods
- Corn-based snacks. *See* Snacks
- Corn syrup solids, encapsulation, 235
- Cotton bud technique
 adaptation of panelists to menthone with time, 105–106
 differences between gum and panelists, 106–107
 differences in time to achieve maximum concentration for gum, 107
 effect of swabbing location on measured sucrose concentration, 104
 materials, 100
 measurement of breath's menthone concentration, 101–102
 panel ascribing more flavor intensity to sweeter samples, 105
 relationship between sucrose and menthone concentration and perceived mint flavor, 104–107
 saliva sampling method, 100–101
 sensory analysis method, 102
 sucrose analysis method, 101
 sucrose release, menthone release, and perceived intensity of overall mint flavor from stick type chewing gum, 105*f*
 sucrose release, menthone release, and perceived intensity of overall mint flavor from tablet type chewing gum, 106*f*
See also Chewing gum
- Crackers
 commercial corn cracker sample, 38
 flavor release, 37–42
 flavor release from corn crackers by water addition using FLAVORSPACE measurement, 42*f*
 FLAVORSPACE, 40*f*
 FLAVORSPACE total mass spectrum of one breath, 41*f*
 GC of corn cracker solvent extract, 38, 39*f*
 headspace of corn crackers after 5% water addition using direct thermal desorption of volatiles, 39, 40*f*
 headspace of dry corn crackers using direct thermal desorption of volatiles, 38, 39*f*
 multistage mass spectrometry, 41
See also FLAVORSPACE method
- Crank model
 considering diffusion in particle, 210
 dimensionless flavor release rate for sphere predictions, 205*f*
 flavor release from heterogeneous media, 204–205
- Crank–Nicholson method, differential equations to numerical format, 385
- Cream, correction factors for same flavor perception in cream as in soft drink, 136*t*
- p-Cresol
 binding to β -lactoglobulin, 290–291
 differential spectra of changes in amide I region of β -lactoglobulin spectra at pH 2.0 and 7.5, 288*f*
See also β -Lactoglobulin interactions with flavor compounds
- Crystallization, effect on phase partitioning, 129

- β -Cyclodextrins binding aroma compounds
- aroma encapsulation method, 248
 - carbonyl and ethyl groups of esters interacting similarly with β -cyclodextrins, 256
 - competition between aroma and paramagnetic probe by electronic paramagnetic spectroscopy (EPR), 249
 - competition between ethyl propionate and ethyl hexanoate, 252–253
 - competition between volatiles and 4-oxo-2,2,6,6-tetramethylpiperidine-1-oxyl (4-oxo-Tempo) paramagnetic probe, 253–254
 - competition experiments, 248
 - determination of interaction parameters by Hummel and Dreyer method, 248–249
 - determination of spatial conformation by ^{13}C and ^1H NMR, 249
 - differences by chemical function of volatile in competition with paramagnetic probe, 254–255
 - effect of chemical function of aroma compounds on retention by β -cyclodextrins, 251–252
 - EPR spectrum of 4-oxo-Tempo in aqueous solution alone and with β -cyclodextrin, 254f
 - experimental materials, 247–248
 - Fourier transform infrared (FTIR) spectroscopy method, 249
 - ^1H NMR spectra indicating hydrogen bonding between hexanoic acid and β -cyclodextrin, 257–258
 - hydrogen bonding between ethyl hexanoate and β -cyclodextrins, 258
 - hydrophobic contribution for binding of ethyl hexanoate, 256
 - hypothesis for folded conformation in hexanol complex, 257
 - interaction parameters of ethyl propionate and ethyl hexanoate with β -cyclodextrin (Hummel and Dreyer), 253t
 - maximal retention after dehydration, 250–251
 - mean rotational correlation time of 4-oxo-Tempo in aqueous solution and in presence of β -cyclodextrin or complexes, 254t
 - physicochemical properties of aroma compounds, 247t
 - possible spatial conformation for ethyl hexanoate and ethyl propionate complexes, 255f, 256
 - retention capacity determination method, 248
 - retention of benzyl alcohol, 250
 - retention of volatiles after dehydration of mixtures initially composed of water, β -cyclodextrin, and increasing amount of four aroma compounds, 251f
 - retention of volatiles after dehydration of mixtures initially containing an excess of aroma (4 mole aroma/mole β -cyclodextrin), 250t
 - sample aroma compounds, 247
 - steric hindrance between aliphatic and aromatic compounds, 251
 - studying binding at molecular scale using paramagnetic probe 4-oxo-Tempo, 253–254
 - studying spatial conformation of complexes with hexanal, hexanoic acid, and hexanol, 256–257
 - variation in resonance frequency of ethyl hexanoate and ethyl propionate ^{13}C nuclei after encapsulation, 255t
 - variation of resonance frequency of hexanal, hexanoic acid, and hexanol ^{13}C nuclei after encapsulation by β -cyclodextrin, 257t
 - variations observed for ethyl propionate and ethyl hexanoate, 255t, 256

Cysteine-ribose reaction mixtures,
effect of protein on sulfur
compounds from, 276–277

D

Dairy. *See* Composite dairy gels

β -Damascenone

comparison between whole and skim
milk, 330, 331*f*

influence of milk components, 324*t*,
326, 329*f*

δ -Decalactone

flavor release from emulsion gels,
365–366

mean time-intensity (TI) parameters
for flavor in whey protein isolate
gels, 366*t*

γ -Decalactone

binding to β -lactoglobulin, 290–291
differential spectra of changes in
amide I region of β -lactoglobulin
spectra at pH 2.0 and 7.5, 288*f*

See also β -Lactoglobulin interactions
with flavor compounds

Decanal. *See* Aldehydes

Decanol, predicted volatile release
curves, 175, 176*f*, 177

Dextrose equivalent (DE)

concentrations of glucose syrups in
saliva, 396

See also Hexyl acetate and legumin
interactions

Diacetyl

aqueous solution study, 157*t*

comparison between experimental data
and models based on diffusion
coefficient and mass transfer
coefficient in liquid phase, 162*f*
comparison between whole and skim
milk, 330, 331*f*

effect of droplet size on flavor release
from emulsions, 351*f*

effect of polysaccharides on flavor
release from oil/water emulsions
and aqueous solution, 349*f*

flavor release from emulsion gels,
365–366

influence of milk components, 324*t*,
326, 327*f*

kinetic properties in water, 158–160

mean time-intensity parameters for
flavor in whey protein isolate gels,
365*t*

molar volume and diffusivity, 148*t*

partition coefficient in aqueous
solution, 157–158

physicochemical and sensory
characteristics, 343*t*

physicochemical characteristics, 143*t*

relative diffusion coefficient in
aqueous solution with variable
concentration of sucrose as function
of liquid viscosity, 160*f*

relative profile in different sugar
solutions, 160*f*

release curve, 159*f*

vapor-liquid partition coefficients in
water, 146*t*

See also Aroma compounds; Dynamic
headspace dilution method

Diffusion

determining flavor

volatilization/retention, 236

effective, 203–204

equation, 201–202

fat-soluble flavor compound through
fat particles, 384

Fick's first law, 203

mechanisms, 130–131

spherical, 382

See also Dynamic headspace dilution
method; Mass transfer; Oil
containing gel particles

Diffusivity

aroma compounds, 148

determining for aroma compounds,
144

parameter of experimental study of
composite gels, 391–394

Dimethyl disulfide, salivary headspace
by static headspace–solid phase
microextraction (HS–SPME), 78*f*,
81*t*

- 2,5-Dimethylpyrazine
 air-water equilibrium coefficient, 195
 aqueous solution study, 157*t*
 effect of air flow rate on release, 199–200
 effect of water flow rate on release, 199
 kinetic properties in water, 158–160
 partition coefficient in aqueous solution, 157–158
 release curve, 159*f*
 typical raw data from atmospheric pressure ionization–mass spectrometry (API–MS), 198
See also Dynamic headspace dilution method; Gas-liquid interfacial mass-transfer (GLIM) cell
- Dimethyl sulfide
 aqueous solution study, 157*t*
 calculated energy of absorption, 81*t*
 kinetic properties in water, 158–160
 oral active compound, 77
 partition coefficient in aqueous solution, 157–158
 relative diffusion coefficient in aqueous solution with variable concentration of sucrose as function of liquid viscosity, 160*f*
 release curve, 159*f*
 salivary headspace by static headspace–solid phase microextraction (HS–SPME), 78*f*, 81*t*
See also Dynamic headspace dilution method
- Dimethyl trisulfide, salivary headspace by static headspace–solid phase microextraction (HS–SPME), 78*f*, 81*t*
- Direct expansion
 classification of snacks, 415*f*
 effect of processing on flavor perception, 418, 419*f*, 420
 snack preparation, 413
See also Snacks
- Direct inlet mass spectrometry, time-resolved headspace analysis, 59
- Dissolution, mechanism for flavor release from solid products, 137
- Disulfides
 components of flavorings, 274
 interactions between proteins and, 279–280
 odor threshold values, 280
 quantities recovered from aqueous systems containing protein or carbohydrate substrates, 276*t*
 recovery from aqueous solutions containing proteins, 275–276
 recovery from cooked meat systems, 278–279
 recovery from cooked meat systems containing added disulfides, 279*t*
See also Sulfur-containing flavor compounds and proteins in foods
- Dodecanol, predicted volatile release curves, 175, 176*f*, 177
- Drinking, flavor release, 192
- Droplet size
 effect on flavor release from emulsions, 348, 353
 effect on flavor release of allyl isothiocyanate and ethyl hexanoate from emulsion, 350*f*
 effect on flavor release of diacetyl and butan-1-ol from emulsion, 351*f*
See also Oil/water emulsions
- Dual-Attribute Time-Intensity, measuring perceived sweetness and flavor of chewing gum, 100
- Dusting application of flavor. *See* Snacks
- Dynamic changes of flavor release. *See* FLAVORSPEACE method
- Dynamic flavor release
 aroma stimulus index (ASI), 407–409
 current research, 3
- Dynamic headspace analysis
 flavor of French bread, 430–431
 odorant composition and disadvantages, 430
See also Coffee, roasted
- Dynamic headspace dilution method
 asymptotic value of concentration at steady-state, 161–164
 atmospheric pressure ionization–mass

spectrometry (API-MS) for real-time measurement of volatile release, 154

comparison between experimental data and models based on diffusion coefficient and mass transfer coefficient in liquid phase, 162*f*

complex real situations, 164–165

concentration of volatile in gas phase as function of time, 155

diffusion of volatile from bulk of sample to interface, 155–156

experimental release curve, 155*f*

extrapolation, 164–165

factors characterizing flavor release, 157

initial operating conditions, 164

initial slope of flavor release, 161

kinetic properties of aqueous flavor solutions, 158–160

mass transfer of flavor compounds, 155–157

molecules studied in aqueous solutions, 157*t*

partition coefficients of flavor compounds diluted in aqueous solutions, 157–158

partition of molecule at interface, 156

relative concentration in gas phase as function of dimensionless number, 163*f*

relative diffusion coefficient obeying well-known Stokes–Einstein equation, 159–160

relative diffusion coefficient of diacetyl, menthone, and dimethyl sulfide, in aqueous solutions with variable concentration in sucrose, as function of liquid viscosity, 160*f*

release curves for volatiles in study, 159*f*

release profile of diacetyl in different sugar solutions, 160*f*

schematic view of cell, 155*f*

simplification of model and derivation

of dimensionless parameters, 161–164

theoretical approach, 154–155

thermodynamic and kinetics of flavor compounds, 157–160

transport of molecule in gas phase, 156–157

types of behavior defined by approach, 163–164

E

Eating, model mouth system, 310

Eating speed, effect on adaptation, 378–379

Electric conduction theory, Maxwell model, 202

Electromyography (EMG) mastication, perceived flavor of food, 179

Electronic nose (EN), time-resolved headspace analysis, 59, 60*f*

Electronic paramagnetic spectroscopy (EPR)

- competition between aroma and paramagnetic probe, 249
- See also* β -Cyclodextrins binding aroma compounds

Electron impact mass spectrometry (EI-MS), time-resolved headspace analysis, 59, 60*f*

Emulsification, effect on release of odor active secondary lipid oxidation products, 318

Emulsion gels. *See* Whey protein isolate gels

Emulsions

- accounting for formulation and structure for flavoring, 353
- amounts of odor active compounds formed in oils and emulsions, 316*t*
- effect of emulsification on release of odor active oxidation products, 318
- formation of volatile secondary lipid oxidation products in emulsions versus bulk oils, 314, 317

- isolating volatile compounds of sunflower oil, an oil blend, and their emulsions, 313–314
- model based on mass balance and partition coefficients of aroma compounds, 143
- relative release of odor active compounds in model mouth system, 316*f*
- studying release aspect by addition of reference compounds to oils and emulsions, 317–318
- volatile lipid oxidation products, 310–311
- See also* Flavor release from emulsions and complex media; Lipophilic flavor release in low fat foods; Oil/water emulsions; Volatile oxidation products
- Encapsulation**
- competition experiments for binding aroma compounds to β -cyclodextrin, 248
- main drawback, 246
- method for retention of single aroma compounds, 248
- types of starch and processes, 235
- See also* β -Cyclodextrins binding aroma compounds; Gelatin gels
- Entrapment**
- starch-flavor interactions in extrusion cooking, 235–237
- volatiles in starch matrices, 234–235
- Esters**
- comparing esters and aldehydes in masticated model solutions, 93, 94*f*
- comparison of recovery after mastication of orange juice and model solutions, 96, 97*f*
- experiments using reference esters important in orange juice aroma, 92
- influence of duration of mastication, 94, 95*f*
- See also* Mastication
- Ethanol**
- chemical assignment of proton transfer reaction–mass spectrometry (PTR–MS) profile of green coffee beans, 118*t*
- green coffee, 116
- predicted volatile release curves, 175, 176*f*, 177
- Ethyl 3-hydroxyhexanoate. *See* Esters
- Ethyl butanoate. *See* Esters
- Ethyl butyrate
- comparison between predicted and experimental, 392*f*, 393*f*
- composite gel manufacture, 386–387
- observed and predicted volatile release curves from gelatin gel, 175
- See also* Composite dairy gels
- Ethyl esters**
- major factors and interactions affecting volatility from beverages, 339, 340*t*
- molar volume and diffusivity, 148*t*
- physicochemical characteristics, 143*t*
- transfer through miglyol layer, 149*t*
- vapor-liquid partition coefficients in water, 146*t*
- See also* Aroma compounds; Beverages
- Ethylguaiaicol**
- comparison between whole and skim milk, 330, 331*f*
- influence of milk components, 324*t*, 326, 328*f*
- Ethyl hexanoate**
- competition with ethyl propionate, 252–253
- effect of droplet size on flavor release from emulsions, 350*f*
- effect of nature of proteins as emulsifier on flavor release from oil/water emulsions, 347*f*
- effect of polysaccharides, 352
- effect of polysaccharides on flavor release from oil/water emulsions and aqueous solution, 349*f*
- flavor release from standard and microstructured emulsions, 220*f*
- flavor release profile as function of fat content, 216*f*
- global affinity with proteins, 347*f*

hydrogen bonding with β -cyclodextrins, 258

interaction of carbonyl and ethyl groups with β -cyclodextrins, 256

interaction parameters (Hummel and Dreyer method), 253*t*

measured flavor release rate constant, 216*t*

physicochemical and sensory characteristics, 343*t*

physicochemical properties, 247*t*

possible spatial conformation for complex with β -cyclodextrin, 255*f*

release from microstructured and standard oil/water emulsions showing contribution from aqueous and oil phases, 221*f*

retention of volatiles after dehydration of mixtures initially composed of water, β -cyclodextrin, and increasing amount of aroma, 251*f*

retention of volatiles after dehydration of mixtures initially containing excess aroma, 250*t*

variation in resonance frequency of ^{13}C after encapsulation, 255*t*

See also β -Cyclodextrins binding aroma compounds; Esters; Lipophilic flavor release in low fat foods

Ethyl propionate

competition with ethyl hexanoate, 252–253

interaction of carbonyl and ethyl groups with β -cyclodextrins, 256

interaction parameters (Hummel and Dreyer method), 253*t*

physicochemical properties, 247*t*

possible spatial conformation for complex with β -cyclodextrin, 255*f*

retention of volatiles after dehydration of mixtures initially containing excess aroma, 250*t*

variation in resonance frequency of ^{13}C after encapsulation, 255*t*

See also β -Cyclodextrins binding aroma compounds

Eugenol

binding to β -lactoglobulin, 290–291

differential spectra of changes in amide I region of β -lactoglobulin spectra at pH 2.0 and 7.5, 288*f*

See also β -Lactoglobulin interactions with flavor compounds

European Union, attention to study of flavor release, 405

Experimental design

composite gel manufacture, 387

milk components, 322–323

Extraction, mechanism for flavor release from solid products, 137

Extrusion cooking

formation of inclusion complexes with amylose, 237

phase equilibria, volatility and diffusivity of flavors in starch, 236

sorption and formation of Staudinger complexes, 237

starch-flavor interactions, 235–237

See also Entrapment

F

Fat

effect of particle size on flavor release from composite gel, 382, 391

influencing flavor attributes, 212

levels in yogurt, 29, 30*f*

modifying flavor perception, 310

role as flavor reservoir, 29

See also Lipophilic flavor release in low fat foods; Milk components; Whey protein isolate gels

Fick's first law, diffusion, 203–204

Flavor

definition, 370

quality and acceptance of product, 179

Flavor application. *See* Snacks

Flavor binding, effect on phase partitioning, 128

Flavor chemists, linking with sensory scientists, 4

Flavor compounds

thermodynamics and kinetics, 157–160

- See also* β -Lactoglobulin interactions with flavor compounds; Sulfur-containing flavor compounds and proteins in foods
- Flavor encapsulation, protecting flavors from deterioration, 2
- Flavor industry
 imitating natural food properties with manufactured food, 38
 mimicking flavor of natural foods, 33
- Flavor perception, effect with time, 99
- Flavor profile, pattern of release, 8
- Flavor release
 aroma stimulus index and dynamic, 407–409
 asymptotic value of concentration at steady-state, 161–164
 Crank model, 204–205
 creating desired sensory property at consumption, 234
 description of study, 1
 diffusion through heterogeneous media in oil-containing gel particles, 201–202
 direct measurement of profiles, 356
 dynamic release, 355–356
 encapsulated flavors, 9
 equilibrium systems, 1
 extrapolation of model to other situations, 164–165
 factors characterizing, 157
 factors controlling release in mouth, 241
 fat levels in yogurt, 29, 30*f*
 flavor profile with time, 8
 influence of food texture, 356
 initial slope of release curves, 161
 integrity of components in composite foods, 27–29
 interfacial mass transfer, 207
 liquid products in mouth, 135–136
 mechanically damaged plant tissues, 45, 55
 membrane interfaces for measuring, 12
 methods for measuring in vivo, 3
 perception by sniff, 134–135
 previous modeling studies, 192–193
 real time breath-by-breath analysis, 12
 role of taste-active substances, 5
 Sherwood correlation, 206
 solid products in mouth, 136–139
 speed of analysis, 10
 systems with starch flavor complexes, 241, 243
 texture-structure influences, 4–5
 volatile and non-volatile flavor compounds, 1–2
See also Beverages; Composite dairy gels; Gas-liquid interfacial mass-transfer (GLIM) cell; Oil containing gel particles; Physicochemical models for flavor release
- Flavor release and transport from mouth to olfactory epithelium
 assumptions for predictions of how airways affect flavor release, 184
 breath-by-breath time-release profile by atmospheric pressure chemical ionization–mass spectrometry (APCI–MS), 180
 chewing movements acting like bellows, 183
 computer simulation algorithm, 186–187
 dependence of flavor release on volatiles partition and mass transfer coefficients, 187
 dilution of volatiles by saliva flow into oral cavity, 183
 effect of varying partition coefficient on times and rates of arrival at olfactory, 190
 equilibrium saliva-gum partition coefficient, 182–183
 factor by which flavor mass is lost from mouth, 186
 general theoretical model, 180–182
 influence of airways on transport processes, 188
 influence of breathing and chewing on nose-space heptanone and pentanone concentrations, 190*f*
 initialization of chewing in algorithm, 186
 ketone concentrations emerging from nasal cavity over period of one

minute, 189*f*
 main simulation loop, 186–187
 mass balance of flavor volatiles per unit cross-sectional area, 184
 mathematical representation of breathing velocity during inhalation and exhalation separated by finite pause, 183*f*
 mechanism of release, volatile extraction from food matrix by mastication, 181
 mechanisms governing mass transfer across solid-saliva and liquid-gas interfaces, 180–181
 method of validation, 181–182
 modeling flavor release from chewing gum, 182–185
 models focusing on whole foods or liquids, 181
 release independent of chewing frequency, 188
 schematic diagram showing diffusion, convection, and absorption processes acting on flavor volatiles in airways, 184*f*
 schematic of oral and nasal cavities, 182*f*
 simultaneous release by dissolution of sugar matrix or from gelled sweet, 181
 solubility of flavor in mucus determining rate of flavor transport, 190
 stagnant-layer theory of interfacial mass transfer, 182
 symbols and corresponding descriptions, 185*t*
 theoretical analysis, 187–190
 time-dependent flavor concentrations in gum as function of saliva-gum partition coefficient, 188*f*
 time-dependent flavor concentrations in saliva as function of saliva-gum partition coefficient, 187*f*
 time-dependent release of heptanone from chewing gum, 189*f*
 ultimate goal of mathematical models, 180

Flavor release from emulsions and complex media
 affinity of odorants for food product, 142
 determining diffusivity of aroma compounds, 144
 effect of matrix breakage on flavor release, 149–150
 experimental device measuring flavor release from model food matrix, 145*f*
 features influencing transfer and release, 143
 flavor release from different media versus time, 150
 flux of aroma compound, 148
 gas-liquid chromatography (GLC) method, 146
 mass transfer of aroma compounds, 148–149
 materials and methods, 143–146
 mathematical models, 143
 molar volume and diffusivity of aroma compounds, 148*t*
 physicochemical characteristics of aroma compounds, 143*t*
 predicting vapor-liquid partition coefficients, 147
 preparation of processed cheese, 144
 release of 2-nonanone from model cheeses, 150–151
 resistance of solute diffusing from one aqueous phase to another, 144–145
 rotating diffusion cell technique for mass transfer measurement, 144
 thickness of stagnant aqueous layers, 144
 transfer of ethyl esters through miglyol layer, 149*t*
 vapor-liquid partition coefficients of aroma compounds in water, 146*t*
 volatility of 2-nonanone in different media, 147*t*
 volatility of aroma compounds, 146–147
 Flavor research, historical development, 2–3
 Flavor retention

- food processing and preparation, 233
- formation of inclusion complexes with amylose, 237
- mechanisms controlling physical entrapment in low moisture systems, 234–235
- phase equilibria, volatility, and diffusivity of flavors in starch, 236
- physical entrapment in starch matrices, 234–235
- sorption and formation of Staudinger complexes, 237
- sorption of volatiles to native starch, 234
- starch-flavor interactions in extrusion cooking, 235–237
- systems with starch flavor complexes, 241, 243
- types of starch and processes used for encapsulation, 235
- Flavorings
- sensory response in different media, 126
 - See also* Physiochemical models of flavor research
- Flavors, analysis of flavor and fragrances in real time (AFFIRM), 15
- FLAVORSPACE method
- breath-by-breath analysis of volatile flavor release during eating of strawberry, 36–37
 - breath by breath release of volatiles during eating of strawberry, 37f
 - commercial corn cracker as sample, 38
 - experiments with Virtual Aroma Synthesizer, 35
 - flavor release from corn crackers by water addition using FLAVORSPACE measurement, 42f
 - flavor release from strawberry, 35–37
 - flavor release of unstable compounds from crackers, 37–42
 - FLAVORSPACE of corn crackers, 40f
 - gas chromatography of corn cracker solvent extract, 38, 39f
 - headspace measurements of fresh strawberries in vessel, 35
 - headspace of corn crackers after 5% water addition using direct thermal desorption of volatiles, 39, 40f
 - headspace of dry corn crackers using direct thermal desorption of volatiles, 38, 39f
 - measuring fast dynamic changes of flavor release during eating, 34, 42–43
 - purpose of measurements, 35
 - release of volatiles from strawberry, 36f
 - schematic of atmospheric pressure chemical ionization–mass spectrometry (APCI–MS) for breath monitoring, 34f
 - sensory perception correlating with analytical data for strawberry, 37
 - understanding time-intensity flavor profiles, 42–43
 - using multistage MS, 41f
- Flexarome®, encapsulation product for initial flavor impact, 24–27
- Food
- breakdown of matrix during mastication, 371
 - consequences of starch flavor interactions, 243
 - headspace gas of products, 58–59
 - overall flavor, 9
 - perceived flavor, 99
- Food components, interactions of starch, 233–234
- Food consumption. *See* Aroma stimulus index (ASI); Volatile release in vivo during food consumption
- Food-flavor interactions
- molecular level, 4
 - role of matrix, 282
- Food processing. *See* Starch
- Food quality, perceived, flavor release, 8
- Fourier transform infrared (FTIR) spectroscopy
- examining hydrogen bonds between aroma compounds and β -

cyclodextrins, 249
 hydrogen bonding between hexanoic acid and hydroxyl functions of β -cyclodextrins, 257–258
See also β -Lactoglobulin interactions with flavor compounds

Fracture properties

characteristics of whey protein gels, 361*t*

methods for determining, 358

See also Whey protein isolate gels

Fragrances, analysis of flavor and fragrances in real time (AFFIRM), 15

Fructose, in-mouth concentration from fresh orange segments using ribbon saliva collecting technique, 109*f*

Fruit odorants. *See* Mastication; Oranges; Strawberries

Future research

instrumental-sensory correlation, 3–4

in vivo analysis, 4

molecular level of food-flavor interactions, 4

non-volatile release, 5

texture-structure influences on flavor release, 4–5

G

Garlic

characteristic aroma, 51

extraction and volatile analysis procedure, 47

headspace analysis by solid phase microextraction (SPME–GC–MS) on freshly chopped clove, 51–52

interrelationship between compounds, 54

rapid analysis of freshly cut clove by atmospheric pressure chemical ionization–mass spectrometry (APCI–MS), 52, 53*f*

SIM–APCI–MS of volatiles released from needle damaged clove, 54*f*

See also Wound response in plants

Gas chromatography–mass spectrometry, trapping/pre-concentration methods, 11–12

Gas chromatography/sniffing port analysis

method, 312–313

sniffing chromatogram of emulsion of blend of sunflower and linseed oils, 313, 314*f*

See also Volatile oxidation products

Gas-liquid interfacial mass-transfer (GLIM) cell

air-water equilibrium constant for aroma compound, 195

cell design, 193–194

control of liquid level, 194–195

effect of air flow rate, 199–200

effect of air-water equilibrium constant on interfacial flux, 197

effect of co-current and counter current flow on release of octanal, 199*t*

effect of water flow rate, 199

experimental, 193–195

gas-phase or liquid-phase limited release depending on volatility of aroma compound, 196

GLIM cell as kind of liquid-gas contactor, 195

main observations, 198–199

mass balance of aroma compound, 196

octanal and 2,5-dimethylpyrazine

(DMP) as aroma compounds, 195

operating modes, 194

overall mass transfer coefficient, 195–196

relationships between Reynolds' number and flow rate for liquid and gas, 197

Reynolds' number determining type of flow, 197

schematic of GLIM cell, 193*f*

theory, 195–197

typical raw data for 2,5-DMP from atmospheric pressure ionization–mass spectrometry, 198

Gelatin gels

- adaptation to stimulus, 378–379
 correlation between initial gradient of nonspace release profile and maximum perceived intensity, 24–26
 differences within panel, 376, 378
 effect of eating speed, 378–379
 effect of increasing carvone concentration on volatile release, 373–374
 influence of intensity of perception, 371
 in-mouth sucrose, glucose, and citric acid concentration using ribbon saliva collecting technique, 110*f*
 magnitude estimation procedure for carvone concentration, 372
 relationship between stimulus and perception, 374
 relationships between perceived mintyness and sample concentration, 375*f*
 release profiles for glucose, sucrose, and citric acid, 109
 samples containing carvone, 371–372
 time intensity and in-nose volatile release method, 372–373
See also Aroma release models; Carvone release
- Gel particles. *See* Oil containing gel particles
- Gels. *See* Composite dairy gels
- GLIM. *See* Gas-liquid interfacial mass-transfer (GLIM) cell
- Glucose
 apparent specific volumes (ASVs) of syrups, 396–397
 disappearance of stimulus and taste, 400*t*
 drop in concentrations of stimuli in saliva, 401*t*
 in-mouth concentration from fresh orange segments using ribbon saliva collecting technique, 109*f*
 in-mouth concentration from gelatin gel using ribbon saliva collecting technique, 110*f*
 intensity and persistence of sweetness for syrups at different concentrations, 399*t*
 physical concentrations in saliva, 396
See also Sweetness and salivary sweetener concentration
- Grape flavor
 maximum intensity as function of held-water and microstructure, 363*f*
 rate of release as function of held-water and microstructure, 363*f*
 time-intensity parameters for release in whey protein isolate gels, 362*t*
See also Whey protein isolate gels
- Grape jelly
 reduced intensity of signal when blended with peanut butter, 29
See also Peanut butter and jelly sandwiches
- Green coffee beans. *See* Coffee roasting
- Ground coffee. *See* Coffee, roasted
- Guaiacol
 comparison between whole and skim milk, 330, 331*f*
 influence of milk components, 324*t*, 326, 328*f*
- Gum. *See* Chewing gum
- ## H
- Hartree energy
 effect on log I_{\max} (breath maximum volatile concentration), 173*f*
 modeling aroma release, 168–171
See also Aroma release models
- Headspace, definition, 310
- Headspace analysis
 bananas, 16, 17*f*
 methods for measuring, 4
 quantitative method for coffee, 431, 432*f*
 real time, 46–47
 static and dynamic sampling, 430
See also Coffee, roasted; Dynamic headspace dilution method; Headspace analysis, time-resolved;

Wound response in plants

Headspace analysis, time-resolved
 added value of time-intensity profiles, 59
 analytical techniques, 60*f*
 applications on coffee, 68–70
 capacity of proton transfer reaction–mass spectrometry (PTR–MS) to monitor time-dependent variations of headspace (HS) profiles, 69–70
 direct inlet mass spectrometry, 59
 electronic nose (EN), 59
 HS profiles of coffee brew plotted on linear and logarithmic intensity scales, 69*f*
 ion-intensity profiles of selected masses upon reconstitution of soluble coffee with water, 70*f*
 linear response of PTR–MS over four orders of magnitude, 62, 63*f*
 linking mass peaks to chemical compounds, 65–68
 potential difficulties of PTR–MS, 63–64
 proton affinities of constituents of clean air and various volatile organic compounds (VOCs), 62*t*
 PTR–MS, 60–65
 relation between measured PTR–MS intensities and actual concentrations of neutral compounds in headspace, 62
 rich source of information for foods, 58–59
 schematic of PTR–MS apparatus, 61*f*
 two distinct types of information by PTR–MS, 64*f*
 typical experiment, 64–65
See also Proton transfer reaction–mass spectrometry (PTR–MS)

Held-water properties
 characteristics of whey protein gels, 361*t*
 measurement, 358–359
See also Whey protein isolate gels

Henry's law, constant calculation, 67–68

Heptan-2-one
 flavor release profile as function of fat content, 216*f*
 log-log plot of flavor intensity (FI_{\max}) for microstructured and standard emulsions as function of oil content, 223*f*
 measured flavor release rate constant, 216*t*
 time-intensity flavor analysis of release from model iso-viscous emulsions with varying oil content, 218*f*
See also Lipophilic flavor release in low fat foods

Heptanone
 influence of breathing and chewing on nose-space concentration, 190*f*
 time-dependent concentration in nasal cavity during one minute, 189*f*

Heterogeneous media
 flavor release, 201–202
See also Oil containing gel particles

Hexanal
 physicochemical properties, 247*t*
 retention of volatiles after dehydration of mixtures initially composed of water, β -cyclodextrin, and increasing amount of aroma, 251*f*
 retention of volatiles after dehydration of mixtures initially containing excess aroma, 250*t*
 spatial conformation of complexes with β -cyclodextrin, 256–257
See also Aldehydes; β -Cyclodextrins binding aroma compounds

Hexanoic acid
 hydrogen bonding of carboxyl group with hydroxyl functions of β -cyclodextrins, 257–258
 physicochemical properties, 247*t*
 retention of volatiles after dehydration of mixtures initially composed of water, β -cyclodextrin, and increasing amount of aroma, 251*f*
 retention of volatiles after dehydration

- of mixtures initially containing excess aroma, 250*t*
- spatial conformation of complexes with β -cyclodextrin, 256–257
- See also* β -Cyclodextrins binding aroma compounds
- Hexanol
 - hypothesis for conformation when complexed, 257
 - physicochemical properties, 247*t*
 - predicted volatile release curves, 175, 176*f*, 177
 - retention of volatiles after dehydration of mixtures initially composed of water, β -cyclodextrin, and increasing amount of aroma, 251*f*
 - retention of volatiles after dehydration of mixtures initially containing excess aroma, 250*t*
 - spatial conformation of complexes with β -cyclodextrin, 256–257
 - See also* β -Cyclodextrins binding aroma compounds
- Hexenal, time dependence of release from tomatoes, 30, 31*f*
- Hexenol, time dependence of release from tomatoes, 30, 31*f*
- Hexyl acetate and legumin interactions
 - binding of hexyl acetate (HxAc) with biopolymers in aqueous medium, 264*f*
 - binding of HxAc with conjugate of legumin and maltodextrin SA-6, 269–270
 - binding of HxAc with conjugate of legumin with maltodextrin SA-2, 270–272
 - binding of HxAc with legumin alone and in conjugate with maltodextrin SA-6 in aqueous medium, 269*f*
 - binding of HxAc with legumin alone and in presence of maltodextrin SA-2 in aqueous medium, 266*f*
 - binding of HxAc with legumin alone and with simple mixture of legumin and maltodextrin SA-6, 268*f*
 - binding of HxAc with legumin in simple mixture with maltodextrin SA-6, 267–268
 - binding of HxAc with maltodextrins with different dextrose equivalents (DE); comparison with binding of HxAc with legumin, 263–265
 - characteristic parameters of binding of HxAc with legumin in conjugates with maltodextrins and alone, 270*t*
 - data on binding of HxAc with maltodextrin SA-2 alone and with conjugate of maltodextrin SA-2 with legumin in aqueous medium, 271*f*
 - determination of HxAc concentration in solutions, 261
 - determination of HxAc binding to maltodextrins in single protein + maltodextrin mixtures and in the protein + maltodextrin conjugates, 262–263
 - effect of conjugate formation between legumin and maltodextrin on binding capacity of legumin in reference to HxAc, 268–272
 - effect of HxAc with legumin in simple mixture with maltodextrin SA-2, 265–267
 - effect of maltodextrin on binding of HxAc with legumin in simple equimass mixed solutions: maltodextrin + legumin + water, 265–268
 - experimental materials, 261
 - experimental methods, 261–263
 - legumin competitor with maltodextrin SA-6 for HxAc, 272
 - maltodextrins forming inclusion complex with HxAc, 264–265
 - preparation of conjugate of legumin with maltodextrin, 262
 - preparation of conjugate solutions, 262
 - preparation of maltodextrin and mixed

legumin-maltodextrin solutions, 261–262

Scatchard's plot equation, 263

thermodynamic parameters of interaction between legumin and maltodextrins in aqueous medium, 267*t*

See also Legumin binding with aroma esters

Hill plot, equation, 297

History, flavor release research, 2–3

Human interface, physiological factors and influence on analyses, 10*t*

Human nose, odor thresholds, 9

Human perception, relating analytical results, 3

Humans

processes in mouth, 87

See also Mastication

Hydrocolloid-aroma interactions, sensory approach to studying, 2

Hydrocolloids, influencing flavor release, 322

Hydrogen bonding. *See* β -Cyclodextrins binding aroma compounds

Hydrogen sulfide

absence in chromatographic profiles, 77, 80

calculated energy of absorption, 81*t*

modeling experiments, 80

oral active compound, 77

I

Inclusion complexes

definition, 238

formation with amylose, 237

maltodextrins with hexyl acetate, 264–265

Indirect expansion

classification of snacks, 415*f*

effect of processing on flavor perception, 418, 419*f*, 420

snack preparation, 413

See also Snacks

Indone

presence in saliva, 80

salivary headspace by static headspace–solid phase microextraction, 78*f*, 81*t*

Infrared spectroscopy

tool to study protein secondary structures, 283

See also β -Lactoglobulin interactions with flavor compounds

Instrumental–sensory correlation, future areas of research, 3–4

Integrity, components in composite foods, 27–29

Interactions

determining parameters by high performance liquid chromatography, 248–249

methods to quantitatively study, 282–283

See also β -Cyclodextrins binding aroma compounds; Hexyl acetate and legumin interactions; β -Lactoglobulin interactions with flavor compounds; Starch; Sulfur-containing flavor compounds and proteins in foods

Interface, jet separators, 13

Interfacial mass transfer. *See* Mass transfer

Interfacial mass transfer theory, flavor release from heterogeneous media, 207

In vivo analysis

current research, 3

future research, 4

real time, 1

See also Non-volatile flavor compounds; Volatile release in vivo during food consumption

Ionization

atmospheric pressure ionization mass spectrometry (API–MS), 13–15

charge transfer mechanism, 13

proton transfer reaction–MS (PTR–MS), 15–18

selective using lasers, 18

α - and β -Ionone
 differential spectra for interaction with
 β -lactoglobulin, 290*f*
 differential spectra of changes in
 amide I region of β -lactoglobulin
 spectra at pH 2.0 and 7.5, 288*f*
 patterns for β -ionone, 289
See also β -Lactoglobulin interactions
 with flavor compounds
 Isobutylthiazole, time dependence of
 release from tomatoes, 30, 31*f*

J

Jelly. *See* Peanut butter and jelly
 sandwiches
 Jet separators
 interfacing GC columns to mass
 spectrometers, 13
 principle and practice, 13

K

Ketones, concentrations emerging from
 nasal cavity during one minute, 189*f*
 Kinetics
 flavor compounds, 158–160
See also Dynamic headspace dilution
 method

L

α -Lactalbumin. *See* Proteins
 β -Lactoglobulin
 effect of binding to compounds, 322
See also Proteins
 β -Lactoglobulin interactions with flavor
 compounds
 amide I region of β -lg in 50 mM
 phosphate buffer, 286*f*

assuming flavor compounds behaving
 like hydrophobic ligands, 283–284
 bands composing amide I envelope of
 β -lg and relative intensities, 286*t*
 binding of ligands p-cresol, eugenol,
 2-nonanone, and γ -decalactone,
 290–291
 central calyx-shaped cavity as binding
 site for fatty acids, 283
 conditions for β -lg solubilization, 285
 curve fitting of differential spectra to
 analyze relative change in
 individual bands, 289
 curve fitting of results for retinol,
 tetradecanoic acid, α -ionone, and β -
 ionone, 290*f*
 differential spectra at pH 2.0, 286–
 287, 288*f*
 differential spectra at pH 7.5, 288–289
 infrared spectroscopy studying protein
 secondary structures, 283
 ligands in study and association
 constants, 285–286, 287*t*
 materials and methods, 284–285
 patterns for β -ionone, 289
 results of pH 2.0 and 7.5 further
 supporting retinol and fatty acids
 binding to same site, 289–290
 solutions preparation, 284
 spectral changes by ionone isomers,
 287
 Tanford transition, 283, 288
 Laser ionization mass spectrometry,
 time-resolved headspace analysis,
 59, 60*f*
 Lasers, selective ionization, 18
 Legumin binding with aroma esters
 binding isotherms for alkyl acetates
 from their equimolar mixtures with
 native legumin, 303*f*
 binding isotherms for alkyl acetates
 with native legumin in aqueous
 medium, 299*f*
 binding isotherms for methameric
 esters differing in the position of the
 ester group in hydrocarbon chain
 with native legumin, 302*f*

- binding of alkyl acetates differing in length of hydrocarbon chain, 298–301
- binding of methameric esters differing in position of ester group in hydrocarbon chain, 302
- binding parameters for alkyl acetates with native legumin from equimolar mixture in aqueous medium, 305*t*
- binding parameters for butyl acetate (BuAc) and hexyl acetate (HxAc) with native legumin in aqueous medium at pH 7.2, 299*t*
- binding parameters for HxAc with legumin in aqueous medium at pH 7.2, 297*t*
- comparison of binding extent for alkyl acetates alone and from equimolar mixtures at same concentration of free ligands in system, 306*t*
- data on binding of HxAc with 11S globulin in aqueous medium, 296*f*
- determination of binding of aroma esters with protein, 295
- determination of concentration of aroma esters in solutions, 295
- determination of protein concentration in solutions, 294
- differential scanning calorimetry (DSC) method, 295–296
- effect of alkyl acetates on thermodynamic parameters of legumin heat denaturation process, 301*f*
- experimental materials, 294
- experimental methods, 294–296
- role of legumin structure in binding, 296–298
- role of structure of aroma esters in binding with native legumin, 298–306
- role of structure of aroma esters in competitive binding of alkyl acetates from their equimolar mixtures with native legumin, 302–306
- Scatchard plot and Hill plot, 297
- Scatchard plots showing binding of alkyl acetates to native legumin in aqueous medium, 300*f*, 304*f*
See also Hexyl acetate and legumin interactions
- Ligands
- binding by complexation in diluted starch solutions, 238
- characteristics of potato starch dispersions without and with addition of ligands, 240*t*
- complexation in diluted starch dispersions, 239–241
- definition, 237
- Limonene, decrease in model solutions during mastication, 93
- Lipid oxidation products. *See* Volatile oxidation products
- Lipids, absorbing and solubilizing lipophilic flavor compounds, 322
- Lipophilic flavor release in low fat foods
- air-product partitioning, 216–217
- aqueous flavor component primary contributor to initial flavor release from microstructured emulsions, 222
- atmospheric pressure chemical ionization–mass spectrometry for breath analysis, 213–214
- comparing perceived intensity and analytical responses, 218*f*
- diffusion coefficients, 224–226
- effect of oil concentration, 215
- effect of particle size on ethyl hexanoate release from microstructured emulsions, 225*f*
- ethyl hexanoate release from microstructured and standard oil/water (o/w) emulsions showing contributions from aqueous and oil phases, 221*f*
- flavor release control dependent on oil water partition coefficient (K_{ow}), and oil content, 223–224
- flavor release from standard and microstructured emulsions, 220*f*

- flavor release profiles of butanone, heptane-2-one, and ethyl hexanoate as function of fat content, 216*f*
- formation of o/w emulsions, 214
- gas/product partition coefficient, 217
- half-life by Crank approximation for diffusion from spherical particle, 222
- log-log plot of flavor intensity (FI_{\max}) for microstructured and standard emulsions as function of oil content, 223*f*
- Mackie–Meares equation estimating reduction of solute's diffusion coefficient as function of polymer concentration, 226
- mastication triggering release by breaking initial flavor equilibrium between phases, 220–221
- Maxwell equation, 225
- means of selectively controlling release of lipophilic flavors, 220
- measured flavor release rate constants b , 216*t*
- microstructured emulsions, 219–222
- microstructured emulsions preparation, 214–215
- oil content and K_{ow} , 222–224
- particle size for controlling release rate, 224
- percentage of flavor in oil phase, 222–223
- plot of FI_{\max} versus particle diameter, 225*f*
- schematic representation of microstructured emulsions and standard o/w emulsions, 219*f*
- slower rate of diffusional transport for decrease in flavor release, 220–221
- time-intensity analysis, 217–218
- time-intensity assessment method for flavor release from emulsion systems, 214
- time-intensity flavor analysis of heptan-2-one release from model iso-viscous emulsions varying in oil content from 0% to 30%, 218*f*
- Liquid products
- correction factors for same flavor perception in cream as in soft drink, 136*t*
- models for flavor release in mouth, 135–136
- practical consequences of differences in flavor release, 136
- Low fat foods
- market, 355
- See also* Lipophilic flavor release in low fat foods
- ## M
- Mackie–Meares model
- equation estimating reduction of solute's diffusion coefficient as function of polymer concentration, 226
- stochastic obstruction theory, 202
- Malic acid, in-mouth concentration
- from fresh orange segments using ribbon saliva collecting technique, 109*f*
- Malodors
- absence of hydrogen sulfide from chromatographic profiles, 77, 80
- approaches to sampling, 73–74
- calculated energies of absorption for hydrogen sulfide, methyl mercaptan, and dimethyl sulfide, 81*t*
- chromatographic profile of incubated saliva, 78*f*, 79*f*
- compounds in salivary headspace (HS) by dynamic HS–SPME (solid phase microextraction), 84*t*
- compounds in salivary HS by static HS–SPME, 81*t*
- determination of equilibrium profile, 75
- dynamic HS sampling tube, 76*f*
- dynamic HS–SPME, 75
- dynamic HS–SPME of oral, 82, 83*f*
- gas chromatography–mass spectrometry (GC–MS) method, 75, 77
- HS–SPME methods, 74–75

- ideas to improve efficiency of dynamic HS-SPME, 82
- methyl(methylthio)methyl disulfide in saliva, 80
- modeling experiments, 80
- phenol and indole, 80
- salivary malodors, 77, 80
- static headspace SPME, 74
- sulfur compounds in saliva, 77, 80
- threshold data for *S*-methyl thioesters, 80
- Maltodextrins**
- binding of hexyl acetate with maltodextrins with different dextrose equivalents (DE), 263–265
- determination of hexyl acetate binding to, 262–263
- effect on binding of hexyl acetate with legumin, 265–268
- effect of conjugate formation between legumin and maltodextrin on binding capacity of legumin in reference to hexyl acetate, 268–272
- encapsulation, 235
- inclusion complex with hexyl acetate, 264–265
- preparation, 261–262
- preparation of conjugate of legumin with maltodextrin, 262
- thermodynamic parameters of interaction between legumin and maltodextrins, 267*t*
- See also* Hexyl acetate and legumin interactions
- Mass spectrometry (MS)**
- analytical technique of choice, 10
- linking mass peaks to chemical compounds, 65–68
- See also* Atmospheric pressure ionization mass spectrometry (API-MS); Proton transfer reaction-mass spectrometry (PTR-MS)
- Mass transfer**
- aroma compounds, 148–149
- basic models of interfacial, 132–134
- between retronasal air and saliva, 384–385
- diffusion of volatile from bulk of sample to interface, 155–156
- effective diffusion, 203–204
- effect of resistance to mass transfer on flavor release from aqueous media, 131–132
- factor in aroma release, 318
- flavor compounds, 155–157
- interfacial, 130–132
- mechanism across solid-saliva and liquid-gas interfaces, 180–181
- mechanisms of diffusion, 130–131
- molecular diffusion, 143
- non-equilibrium partition model, 133
- partition of molecule at interface, 156
- penetration theory, 132
- rate of unidirectional diffusion from product to vapor phase, 130
- rotating diffusion cell technique, 144
- schematic of flavor concentrations at liquid-gas interface during release from liquid phase, 130*f*
- stagnant-film model, 132
- transport of molecule in gas phase, 156–157
- See also* Dynamic headspace dilution method; Gas-liquid interfacial mass-transfer (GLIM) cell
- Mass transport**
- driving force, 127
- factor affecting flavor release, 127–128
- rate to achieve equilibrium, 128
- Mastication**
- breakdown of food matrix during, 371
- comparing esters and aldehydes in masticated model solutions, 93, 94*f*
- comparing recovery of esters and aldehydes after mastication of fresh orange juice and model solutions, 96, 97*f*
- determination of odorants by static headspace analysis, 89
- determination of odorants in solvent extracts, 89
- experimental materials, 89
- experiments using aqueous model solutions of reference odorants, 91

- experiments using reference esters
 important in orange juice aroma, 92
- flavor dilution factors of important
 odorants of fresh, hand-squeezed
 orange juice, 88*t*
- influence of duration of mastication on
 remaining quantity of aldehydes and
 esters, 95*f*
- influences of time of mastication, 94,
 95*f*
- interactions of matrix compounds in
 real food systems, 96
- method for quantification of flavor
 compounds, 89
- model experiments, 91–96
- orange juice by SOOM-concept (spit-
 off odorant measurement), 90
- orange juice odorants limonene and
 acetaldehyde in model solutions, 93
- remaining quantity of acetaldehyde
 and limonene in spit-off aqueous
 solutions after mastication, 93*f*
- remaining quantity of aldehydes in
 spitted off aqueous solutions after
 mastication, 91*f*
- remaining quantity of esters in spitted
 off aqueous solutions after
 mastication, 92*f*
- remaining quantity of selected
 odorants in spit-off orange juice
 after mastication, 90*f*
- respiration and processes in mouth,
 87–88
- retronasal transfer of odorants, 88
- SOOM-concept, 88
- trigger for controlled release by
 breaking initial flavor equilibrium
 between oil and water phases, 220–
 221
- See also* Flavor release and transport
 from mouth to olfactory epithelium
- Maxwell model
 diffusion coefficients, 225
 electric conduction theory, 202
- Mechanical damage in plants
 release of aroma compounds, 45
See also Wound response in plants
- Mechanism
 charge transfer, 13
- controlling physical entrapment in low
 moisture systems, 234–235
- diffusion, 130–131
- mass transfer across solid-saliva and
 liquid-gas interfaces, 180–181
- modeling physical of flavor release,
 153–154
- product dissolution and product
 extraction mechanisms of flavors
 from solid food to saliva, 136–137
- volatile extraction from food matrix by
 mastication, 181
- See also* Dynamic headspace dilution
 method
- Membrane interfaces
 mass spectrometry (MS), 12
 measuring flavor release from foods,
 12
- Menthone
 aqueous solution study, 157*t*
 kinetic properties in water, 158–160
 measurement of breath's concentration,
 101–102
- partition coefficient in aqueous
 solution, 157–158
- relationship between sucrose and
 menthone concentration and
 perceived mint flavor, 104–107
- relative diffusion coefficient in
 aqueous solution with variable
 concentration of sucrose as function
 of liquid viscosity, 160*f*
- release curve, 159*f*
- release from chewing gum, 25*f*, 27*f*
- See also* Chewing gum; Cotton bud
 technique; Dynamic headspace
 dilution method
- Methameric esters
 binding differing in position of ester
 group in hydrocarbon chain, 302
 binding isotherms, 302*f*
- Methanethiol. *See* Coffee, roasted
- Methanol
 change in ion-intensity with roasting
 of coffee, 118–119
 chemical assignment of proton transfer
 reaction–mass spectrometry profile
 of green coffee beans, 118*t*
 green coffee, 116

- 2-Methyl-3-butenal, comparison between whole and skim milk, 330, 331*f*
- 2-Methylbutan-1-ol
effect of polysaccharides on flavor release from oil/water emulsions and aqueous solution, 349*f*
physicochemical and sensory characteristics, 343*t*
- 2-Methyl butyric acid
physicochemical properties, 247*t*
retention of volatiles after dehydration of mixtures initially containing excess aroma, 250*t*
See also β -Cyclodextrins binding aroma compounds
- 3-Methyl-2-butenal, influence of milk components, 324*t*, 326, 329*f*
- 2-Methylbutanal. *See* Coffee, roasted
- 3-Methylbutanal
comparison between whole and skim milk, 330, 331*f*
influence of milk components, 324*t*, 326, 328*f*
See also Coffee, roasted
- Methyl mercaptan
calculated energy of absorption, 81*t*
oral active compound, 77
salivary headspace by static headspace–solid phase microextraction, 78*f*, 81*t*
- Methylpropanal. *See* Coffee, roasted
- 2-Methylpropanal
comparison between whole and skim milk, 330, 331*f*
influence of milk components, 324*t*, 326, 328*f*
- S-Methyl thioesters, threshold data, 80
- Microcapsules, uses, 246
- Microstructured emulsions
preparation, 214–215
schematic representation, 219*f*
See also Lipophilic flavor release in low fat foods
- Miglyol layer, transfer of ethyl esters through, 148–149
- Milk components
aroma compound lipophilicity measurement, 325
comparison of flavor compound retention between whole and skim milk, 331*f*
compounds showing no effect, 326, 327*f*
design for samples showing fat and milk-solids-non-fat (MSNF) levels, 323*f*
effect of milk fat on headspace concentrations of compounds, 330
experimental design, 322–323
flavor compounds in study, 324*t*
headspace analysis method by SPME GC–FID (solid phase microextraction gas chromatography/flame ionization detector), 325
large reduction in volatility due to fat and protein/carbohydrate effect only at no fat, 326, 329*f*
protein-flavor versus oil-flavor interactions, 322
recipes for milk preparations representing experimental design points, 324*t*
reduction in volatility due to fat without effect of protein/carbohydrates, 326, 328*f*, 329*f*
relationship between compound lipophilicity and relative headspace amount in whole milk, 330*f*
sample preparation, 323–324
theory behind flavor compound interactions with milk, 325, 326*f*
values for mid- and high-fat levels, 330
- Mintyness
perception of, 370–371
See also Carvone release
- Models
Crank model, 204–205
current research, 3
development for flavor release from composite gels, 382–385

- flavor release, 2–3
 general theoretical for transport of
 flavors from mouth to olfactory,
 180–182
 interfacial mass transfer theory, 207
 mathematical for flavor release from
 emulsions, 143
 modeling physical mechanisms of
 flavor release, 153–154
 model mouth system, 310
 mouth, 388*f*
 Sherwood correlation, 206
See also Aroma release models;
 Composite dairy gels; Dynamic
 headspace dilution method; Flavor
 release and transport from mouth to
 olfactory epithelium; Mastication;
 Oil containing gel particles;
 Physicochemical models for flavor
 release; Volatile oxidation products
- Molar volume, aroma compounds, 148
- Mouth
 balance of flavors, 381
 conceptual model, 388*f*
 determining aroma concentrations in
 actual eating situations, 310
 factors controlling flavor release, 241
 model system, 310
 retronasal aroma simulator, 335
- Mouth to nasal cavities. *See* Flavor
 release and transport from mouth to
 olfactory epithelium
- MS-Nose[™]
 commercially available, 14
 monitoring expired air from nose,
 166–167
- N**
- Nasal cavities. *See* Flavor release and
 transport from mouth to olfactory
 epithelium
- 2-Nonanone
 binding to β -lactoglobulin, 290–291
 differential spectra of changes in
 amide I region of β -lactoglobulin
 spectra at pH 2.0 and 7.5, 288*f*
 log-log plot of flavor intensity (FI_{\max})
 for microstructured and standard
 emulsions as function of oil content,
 223*f*
 measured flavor release rate constant,
 216*t*
 physicochemical characteristics, 143*t*
 release from different media versus
 time, 149–150
 release from model cheeses, 150–151
 vapor-liquid partition coefficients in
 water, 146*t*
 volatility in different media, 147*t*
See also Flavor release from emulsions
 and complex media; β -
 Lactoglobulin interactions with
 flavor compounds; Lipophilic flavor
 release in low fat foods
- Non-equilibrium partition model,
 interfacial mass transfer, 133
- Non-volatile flavor compounds
 adaptation of panelists to menthone
 with time, 105–106
 character to foods, 1–2
 continuous sampling technique, 102–
 103
 cotton bud technique, 100–102
 differences between gum and
 panelists, 106–107
 differences in time to achieve
 maximum concentration for gum,
 107
 different profiles for different types of
 foods, 109
 effect of swabbing location on
 measured sucrose concentration,
 104
 in-mouth sodium, calcium, and
 potassium concentration from
 cheddar cheese when consumed by
 one panelist using ribbon saliva
 collecting technique, 108*f*
 in-mouth sodium concentration from
 crisps when consumed by one
 panelist using ribbon saliva
 collecting technique, 108*f*

in-mouth sucrose, glucose, and citric acid concentration from gelatin gel when consumed by one panelist using ribbon saliva collecting technique, 110*f*

in-mouth sucrose, glucose and fructose, citric acid, and malic acid concentration from fresh orange segments using ribbon saliva collecting technique, 109*f*

interactions with volatile components, 370

materials for continuous sampling technique, 102

materials for cotton bud technique, 100

measurement of breath's menthone concentration, 101–102

monitoring in vivo temporal changes of volatile flavors, 100

perceived flavor of food, 99

relationship between sucrose and menthone concentration and perceived mint flavor, 104–107

release, 5

ribbon technique setup for sampling liquid phase from mouth during eating, 103*f*

saliva sampling method for continuous sampling technique, 102–103

saliva sampling method for cotton bud technique, 100–101

sensory analysis for cotton bud technique, 102

sucrose analysis for cotton bud technique, 101

sucrose release, menthone release, and perceived intensity of overall mint flavor from stick type chewing gum, 105*f*

sucrose release, menthone release, and perceived intensity of overall mint flavor from tablet type chewing gum, 106*f*

O

Octanal

air-water equilibrium coefficient, 195

effect of co-current and counter current flow on release, 199*t*
See also Aldehydes; Gas-liquid interfacial mass-transfer (GLIM) cell

1-Octen-3-one

comparison between whole and skim milk, 330, 331*f*
 influence of milk components, 324*t*, 326, 329*f*

Odor, flavor of food, 9

Odorant release from roasted coffee.

See Coffee, roasted

Oil containing gel particles

basic model describing flavor release to liquid, 207–208

Crank model, 204–205

diffusion equation, 201

dimensionless flavor release rate for sphere predicted by Crank solution, early time, and first order approximations, 205*f*

effective diffusion, 203–204

effective diffusion in two-phase materials, 202

equation for system equilibrium, 208

flavor molecules diffusing through heterogeneous media, 201–202

flavor release, 204–207

interfacial mass transfer theory, 207

Mackie–Meares model based on stochastic obstruction theory, 202

mass transfer from solid to fluid phase 202

Maxwell model based on electric conduction theory, 202

predicted half-life time, 208, 210

predicted half-life time as function of partition coefficient, 209*f*

predicted half-life time as function of volume fraction of oil, 209*f*

Reynolds and Schmidt numbers, 206

Sherwood correlation, 206

Sherwood number, 206

Oil and blends

volatile lipid oxidation products, 310–311

See also Volatile oxidation products

Oil/water emulsions

aroma compounds, 343
 differing in droplet size, 344
 effect of droplet size on flavor release
 of allyl isothiocyanate and ethyl
 hexanoate, 350*f*
 effect of droplet size on flavor release
 of diacetyl and butan-1-ol, 351*f*
 effect of nature of proteins as
 emulsifier on flavor release, 347*f*
 effect of polysaccharides on flavor
 release from oil/water emulsions
 and aqueous solution, 349*f*
 emulsion characterization methods,
 344
 formation, 214
 global affinity of aroma compounds
 with proteins, 347*f*
 headspace analysis, 345
 influence of fat droplet size, 348, 353
 influence of polysaccharides, 346, 348,
 352
 influence of proteins, 346, 348, 352
 measurement of interactions between
 proteins and aroma by affinity
 chromatography, 345
 model emulsions, 343–344
 physicochemical and sensory
 characteristics of aromas, 343*t*
 polysaccharides as thickeners, 344
 polysaccharide solutions preparation,
 344
 protein concentrates as emulsifiers,
 343–344
 protein content determination method,
 344–345
 salad dressings, 342–343
 statistical analysis, 345
 structural characteristic of emulsions
 with or without polysaccharides,
 346*t*
See also Emulsions; Lipophilic flavor
 release in low fat foods
 Olfactory epithelium. *See* Flavor release
 and transport from mouth to
 olfactory epithelium
 Onion
 extraction and volatile analysis

 procedure, 47
 See also Wound response in plants
 On-line monitoring. *See* Coffee roasting
 Oral malodors
 direct analysis by dynamic headspace–
 solid phase microextraction, 82, 85
 See also Malodors
 Oranges
 comparing recovery of esters and
 aldehydes after mastication of fresh
 orange juice and model solutions,
 96, 97*f*
 continuous sampling technique, 102–
 103
 flavor dilution factors of important
 odorants of fresh, hand-squeezed
 orange juice, 88*t*
 in-mouth sucrose, glucose and
 fructose, citric acid, and malic acid
 concentration from fresh orange
 segments using ribbon saliva
 collecting technique, 109*f*
 interactions of matrix compounds in
 real food systems, 96
 Oxidation products. *See* Volatile
 oxidation products

P

Pain, flavor of food, 9
 Panel. *See* Sensory panels
 Paprika descriptor, snacks, 420
 Paramagnetic probe. *See* β -
 Cyclodextrins binding aroma
 compounds
 Particle size
 controlling release rate from
 microstructured emulsions, 224,
 225*f*
 effect of fat particle size on flavor
 release from composite gel, 382,
 391
 Particulate structure. *See* Structure
 Partition coefficients
 air-product partitioning, 216–217
 flavor compounds in aqueous

- solutions, 157–158
 influence of emulsification, 318
See also Dynamic headspace dilution method; Lipophilic flavor release in low fat foods
- Partitioning. *See* Phase partitioning
- Peanut butter and jelly sandwiches
 deterioration in flavor quality upon homogenization, 28
 integrity of components in composite foods, 27–29
- Penetration theory
 accounting for boundary layers not being completely stagnant, 143
 interfacial mass transfer, 132
 mass transfer from solid to fluid phase, 202
- 2,3-Pentanedione
 comparison between whole and skim milk, 330, 331*f*
 influence of milk components, 324*t*, 326, 327*f*
See also Coffee, roasted
- Pentanone, influence of breathing and chewing on nose-space concentration, 190*f*
- Perceived food quality, flavor release, 8
- Persistence. *See* Sweetness and salivary sweetener concentration
- Phase partitioning
 acid-base equilibria, 128
 between aqueous and lipid phase, 128–129
 composition of aqueous phase, 128
 crystallization, 129
 effect of pH on vapor pressure of *n*-alkanoic acids in 5% oil-in-water emulsion, 129*f*
 factor affecting flavor release, 127–128
 flavor binding/complex formation, 128
 flavors in starch, 236
 sorption to suspended particles, 129
 temperature, 128
- Phenol
 presence in saliva, 80
 salivary headspace by static headspace–solid phase microextraction, 78*f*, 81*t*
- Physicochemical models for flavor release
 basic models of interfacial mass transfer, 132–134
 correction factors for same flavor perception in cream as in soft drink, 136*t*
 effect of chewing efficiency on flavor release from chewing gum, 138*f*
 effect of encapsulation on flavor release from chewing gum, 139*f*
 effect of pH on vapor pressure of *n*-alkanoic acids in 5% oil-in-water emulsion, 129*f*
 factors affecting flavor release and perception, 127–134
 factors complicating development of mathematical models for flavor release from solid products, 138
 flavor release during perception by sniff, 134–135
 flavor release in mouth-liquid products, 135–136
 flavor release in mouth-solid products, 136–139
 flavor release under equilibrium and dynamic conditions from aqueous solutions at 37°C, 131*f*
 interfacial mass transfer, 130–132
 non-equilibrium partition model, 133
 penetration theory, 132
 phase partitioning, 128–129
 practical consequences of differences in flavor release, 136
 principal symbols, 127
 product dissolution and product extraction mechanisms of flavors from solid food to saliva, 136–137
 schematic diagram of flavor concentrations at liquid-gas interface during release from liquid phase, 130*f*
 schematic of flavor release from static and dynamic fluid phase at constant airflow rate over surface, 134*f*
 stagnant-film model, 132
- Physicochemical parameters. *See* Aroma release models
- Plants

- managing repair of tissue, 44
See also Wound response in plants
- Polysaccharides
 effect on flavor release from aqueous solution, 349*f*
 effect on flavor release from emulsions with different droplet sizes, 349*f*
 inclusion complexes with aroma compounds, 260
 influence on flavor release from emulsions, 346, 348, 352
 thickeners for emulsions, 344
See also Oil/water emulsions
- Potassium, in-mouth concentration from cheddar cheese by one panelist using ribbon saliva collecting technique, 108*f*
- Potato-based snacks. *See* Snacks
- Pre-concentration, prior to GC-MS analysis, 11-12
- Processed cheese. *See* Cheeses
- Protein-flavor binding
 hydrophobic interactions for binding aroma compounds, 260
 protecting flavors from deterioration, 2
See also Hexyl acetate and legumin interactions; Legumin binding with aroma esters
- Proteins
 binding capacity of flavor compound, 293
 content determination, 344-345
 emulsifiers in model emulsions, 343-344
 influence on flavor release from emulsions, 346, 348, 352
 interaction measurement with aroma by affinity chromatography, 345
 reversible and non-reversible binding, 321-322
See also Disulfides; Milk components; Oil/water emulsions; Sulfur-containing flavor compounds and proteins in foods; Thiols; Whey protein isolate gels
- Proton transfer reaction-mass spectrometry (PTR-MS)
 allyl sulfide analysis, 16
 applications of coffee, 68-70
 banana headspace (HS) analysis, 16, 17*f*
 bracketing proton affinities by selective chemical ionization, 65, 66*f*
 capacity to monitor time-dependent variations of HS profiles, 69-70
 collision-induced break-up patterns, 65, 66*f*
 description, 60-61
 differences between PTR and atmospheric pressure ionization (API), 15
 difficult for breath by breath analysis, 18
 Henry's law calculation, 67-68
 HS profiles of coffee brew plotted on linear and logarithmic intensity scales, 69*f*
 introduction and applications, 60
 ion-intensity profiles of selected masses upon reconstitution of soluble coffee with water, 70*f*
 key elements, 16*f*
 key features, 113
 linking mass peaks to chemical compounds, 65-68
 liquid-gas partitioning of volatile compounds, 67-68
 partition coefficient calculation, 67
 potential difficulties, 63-64
 reaction with protonated water, 45
 relation between measured PTR-MS intensities and actual concentrations of neutral compounds in headspace, 62
 schematic, 61*f*, 114*f*
 selected ion flow tube (SIFT-MS) method, 15
 sensitivity, 15
 studying ion chemistry, 15
 time-resolved headspace analysis, 59, 60*f*
 two distinct types of information by PTR-MS, 64*f*
 valuable complement to gas chromatography, 63
See also Coffee roasting; Headspace analysis, time-resolved

Putrefied saliva, *in vitro* sampling, 74
 Pyrazine, observed and predicted
 volatile release curves from gelatin
 gel, 175, 176*f*

Q

Quality assessment
 coffee, 112
 off-flavors of coffee drive research,
 116
 Quality of food, perceived, flavor
 release, 8
 Quantitative headspace analysis. *See*
 Coffee, roasted
 Quantitative Structure Property
 Relationships (QSPR)
 relating behavior of compound to
 physicochemical parameters, 167
See also Aroma release models

R

Real situations, extrapolation of
 dynamic headspace dilution method,
 164–165
 Real time flavor release
 breath by breath analysis, 12
 chewing gum for demonstrating and
 comparing release of volatiles, 23
 effect of encapsulation in Flexarome®
 matrices on release of amyl valerate
 in-nose from tutti-frutti flavored
 bubble gum, 26*f*
 encapsulation of liquid flavors, 24
 fat levels in yogurt, 29
 integrity of components in composite
 foods, 27–29
 menthol release from market
 peppermint chewing gum sticks, 25*f*
 modifying flavor release profiles, 24–
 27
 peanut butter and concord grape jelly
 sandwiches, 28–29
 perceptual deterioration, 27–28
 release in-nose of menthone

encapsulated in two matrices, 27*f*
 release in-nose of preformed and
 enzymatically generated volatiles
 from plum tomatoes, 31*f*
 release in-nose of volatiles from
 flavored gelatin/pectin gels, 25*f*
 release of marker volatiles in-nose
 from sandwiches containing peanut
 butter and grape jelly as discrete
 layers and after homogenization, 28*f*
 strong initial impact using
 Flexarome® products, 26
 time dependence of release of
 enzymatically generated volatiles,
 30
 variation between times to maximum
 intensity, 24
 varying release profiles between
 individuals, 24
 volatile release in-nose of anethole
 from yogurts of different fat
 content, 30*f*
See also Analysis of flavor and
 fragrances in real time (AFFIRM);
 FLAVORSAPCE method
 Research, future
 instrumental-sensory correlation, 3–4
in vivo analysis, 4
 molecular level of food-flavor
 interactions, 4
 non-volatile release, 5
 texture-structure influences on flavor
 release, 4–5
 Resonance enhanced multiple photon
 ionization (REMPI), selective
 ionization, 18
 Retinol
 differential spectra for interaction with
 β -lactoglobulin, 290*f*
 differential spectra of changes in
 amide I region of β -lactoglobulin
 spectra at pH 2.0 and 7.5, 288*f*
See also β -Lactoglobulin interactions
 with flavor compounds
 Retronasal air, mass transfer between
 retronasal air and saliva, 384–385
 Retronasal aroma simulator (RAS)
 justification for sampling, 335

- model beverage, 335–336
See also Beverages
- Reynolds' number
 definition, 206
 determining type of flow, 197
 relationship to flow rate for liquid and gas, 197
- Ribbon saliva collecting technique
 different profiles for different types of foods, 109
 efficiency, 110
 in-mouth sodium, calcium, and potassium concentration from cheddar cheese by one panelist, 108f
 in-mouth sodium concentration from crisps when consumed by one panelist, 108f
 in-mouth sucrose, glucose, and citric acid concentration from gelatin gel by one panelist, 110f
 in-mouth sucrose, glucose and fructose, citric acid, and malic acid concentration from fresh orange segments, 109f
- Ribose-cysteine reaction mixtures, effect of protein on sulfur compounds from, 276–277
- Roasting. *See* Coffee roasting
- Robusta coffee. *See* Coffee roasting
- Rotating diffusion cell, measuring mass transfer of solutes, 144

S

- Saccharin. *See* Sodium saccharin
- Salad dressings, factors affecting flavor release, 342
- Saliva
 approaches to sampling, 73–74
 continuous sampling technique, 102–103
 cotton bud sampling technique, 100–102
 dilution of flavor by saliva flowing into oral cavity, 181, 183
 mass transfer between retronasal air and saliva, 384–385
 samples, 74

- See also* Composite dairy gels;
 Continuous sampling technique;
 Cotton bud technique; Malodors;
 Non-volatile flavor compounds
- Salivary flow rate, influences, 395
- Salivary sweetener. *See* Sweetness and salivary sweetener concentration
- Salty descriptor, snacks, 420, 425
- Sampling air during eating, relationship between volatiles and sensory perception, 10–11
- Scatchard's plot
 equation, 263, 297
 ratio of binding extent to free ligand concentration versus binding extent, 264f, 266f, 268f, 269f, 271f
See also Hexyl acetate and legumin interactions; Legumin binding with aroma esters
- Schmidt number, defined, 206
- Selected ion flow tube (SIFT), mass spectrometry method, 15
- Selected ion recording mode, atmospheric pressure ionization–mass spectrometry (API–MS), 14
- Selective ionization, lasers, 18
- Sensitivity
 atmospheric pressure ionization mass spectrometry (API–MS), 13
 physiological factors and influence on analyses, 10r
 proton transfer reaction MS (PTR–MS), 15
- Sensory analysis
 flavor of beverage, 333
 method for cotton bud technique, 102
See also Analysis of flavors and fragrances in real time (AFFIRM)
- Sensory evaluation, methods for measuring, 4
- Sensory panels
 adaptation to stimulus, 378–379
 assessing attributes, 371
 perception differences within panel, 376, 378
 time-intensity (TI) characteristics of food during eating, 179
 training for composite gel study, 385–386

- Sensory properties, relating to flavor compounds, 3–4
- Sensory scientists, linking with flavor chemists, 4
- Sherwood correlation
 flavor release from heterogeneous media, 206
 mass transfer from particle suspended in infinite fluid, 210
- Slurry application of flavor. *See* Snacks
- SMURF technique of time-intensity (TI) analysis
 description, 395–396
See also Sweetness and salivary sweetener concentration
- Snacks
 average time-intensity (TI) curves with intensity-related TI parameters from corn to potato, 420, 424*f*, 425
 biplot for intensity-related TI parameters, 427*f*
 biplot for time-related TI parameters, 428*f*
 classifications of samples, 415*f*
 data processing, 416, 418
 differences in descriptors and products, 426*f*
 differences in reaching retronasal T_{\max} , 429
 directly versus indirectly expanded corn samples, 418, 420
 distinction between potato- and corn-based products, 420, 421*f*
 flavor application, 413
 flavor formulation and blending for optimal eating enjoyment, 413–414
 investigating effect of flavor dosage, 420, 422*f*, 423*f*
 parameters from single-ingestion TI filtered curves, 416
 PCA biplot showing effect of processing on different corn bases in terms of flavor perception, 419*f*
 profiling tests using restricted maximum likelihood (REML), 416
 REML analysis for log (I_{\max}) data, 425
 REML analysis for log (T_{\max}) data, 425
 repeated ingestion of same products, 425
 salty versus spicy/herbs evaluations, 425
 samples, 414, 415*f*
 sensory measurements, 414, 416
 TI curve averaging, 418
 TI tests, 416, 418
- Sniffing
 first flavor impression, 9
 flavor release during perception by, 134–135
- Sodium
 in-mouth concentration from cheddar cheese by one panelist using ribbon saliva collecting technique, 108*f*
 in-mouth concentration from crisps by one panelist using ribbon saliva collecting technique, 108*f*
- Sodium chloride
 disappearance of stimulus and taste, 400*t*
 drop in concentrations of stimuli in saliva, 401*t*
- Sodium saccharin
 disappearance of stimulus and taste, 400*t*
 drop in concentrations of stimuli in saliva, 401*t*
 physical concentration in saliva, 396
 time intensity study of sweetness, 396
See also Sweetness and salivary sweetener concentration
- Soft drink, correction factors for same flavor perception in cream as in soft drink, 136*t*
- Solanaecae* family
 brushing of leaf and stem trichomes, 48
See also Tomato; Wound response in plants
- Solid phase microextraction (SPME)
 advantages of technique, 73
 dynamic headspace (HS) SPME method, 75
 glass sampling apparatus for dynamic HS–SPME, 76*f*
 static HS SPME method, 74

- See also* Malodors
- Solid products
 effect of chewing efficiency on flavor release from chewing gum, 138*f*
 effect of encapsulation on flavor release from chewing gum, 139*f*
 factors complicating development of mathematical models for flavor release, 138–139
 models for flavor release in mouth, 136–139
 product dissolution mechanism, 137
 product extraction mechanism, 137
- SOOM concept (spit-off odorant measurement)
 orange juice, 90
 quantification of flavor changes during mastication, 88, 96
See also Mastication
- Sorption, volatiles to native starch, 234
 Sorption to suspended particles, effect on phase partitioning, 129
- Spatial conformation
 determination by ^{13}C and ^1H NMR, 249
See also β -Cyclodextrins binding aroma compounds
- Speed, physiological factors and influence on analyses, 10*t*
- Spherical particles
 release of diffusive material, 210
See also Oil containing gel particles
- Spicy descriptor, snacks, 420, 425
- Stagnant-film model
 flavor release, 203
 interfacial mass transfer, 132
- Starch
 appearance, rheological properties, and structure of dispersions, 239
 characteristics of potato starch dispersions without and with addition of ligands, 240*t*
 complexation of flavor compounds in diluted starch dispersions, 239–241
 complexation of flavor compounds in diluted starch solutions, 238
 complexation of flavor compounds with amylopectin, 241
 consequences of starch flavor interaction for real food systems, 243
 constituents of many foods, 230
 extrinsic and intrinsic factors affecting extent of transformation, 233
 flavor retention and release in systems with starch flavor complexes, 241, 243
 formation of inclusion complexes with amylose, 237
 interactions with other food components, 233–234
 mechanisms controlling physical entrapment in low moisture systems, 234–235
 models for starch polymorphs A and B, 232*f*
 molecular structure of amylose complexes, 240–241
 native structure, 231
 phase equilibria, volatility, and diffusivity of flavors in starch, 236
 physical entrapment in starch matrices, 234–235
 representative model for unit cell of V_h amylose, 242*f*
 schematic presentation of possible arrangement of helices of V amylose complexed with thymol, 242*f*
 sorption and formation of Staudinger complexes, 237
 sorption of volatiles to native starch, 234
 starch-flavor interactions in extrusion cooking, 235–237
 terminology for complexation of flavor compounds with amylose, 237–238
 transformation rendering accessible to digestion, 231, 233
 types of starch and processes used for encapsulation, 235
- Starch, modified. *See* Polysaccharides
- Static equilibrium, partitioning in systems, 1
- Static headspace analysis, odorant

- composition, 430
- Staudinger complexes, sorbation and formation, 237
- Steven's Law
including effect of adaptation, 2
power law, 370
sniffing and inhaling, 371
- Stochastic obstruction theory, Mackie–Meares model, 202
- Storage time
headspace concentrations of highly volatile odorants after storage of coffee at room temperature, 436*t*
sensory changes in odor profile of roasted coffee, 435–436
See also Coffee, roasted
- Stranded structure. *See* Structure
- Strawberries
breath-by-breath analysis of volatile flavor release during eating, 36–37
flavor release, 35–37
headspace measurements of fresh, in vessel, 35
release of volatiles, 36*f*
See also FLAVORSPACE method
- Structure
characteristics of whey protein gels, 361*t*
flavor release from protein gels, 363*f*
particulate and stranded whey proteins gels, 361
particulate structured gels, 366
See also Whey protein isolate gels
- Sucralose
effect on odorants in beverages, 337, 338*t*
range in experiments, 335*t*
See also Beverages
- Sucrose
analysis method for cotton bud technique, 101
effect of swabbing location on measured concentration, 104
in-mouth concentration from fresh orange segments using ribbon saliva collecting technique, 109*f*
in-mouth concentration from gelatin gel using ribbon saliva collecting technique, 110*f*
relationship between sucrose and menthone concentration and perceived mint flavor, 104–107
See also Cotton bud technique
- Sulfur. *See* Volatile sulfur compounds (VSC)
- Sulfur-containing flavor compounds and proteins in foods
approximate quantities of volatile sulfur compounds recovered by simultaneous steam distillation and solvent extraction (SDE) from cysteine and ribose model systems in absence or presence of egg albumin, 277*t*
effect of protein on sulfur compounds from ribose-cysteine reaction system, 276–277
interactions between proteins and disulfides and thiols, 279–280
low odor threshold values, 274
quantities of disulfides and thiols recovered from aqueous systems containing protein or carbohydrate substrates, 276*t*
recovery of disulfides from aqueous solutions containing proteins, 275–276
recovery of disulfides from cooked meat systems, 278–279
recovery of thiols and disulfides from cooked meat systems containing added disulfides, 279*t*
volatile extraction using SDE, 280
- Sunflower oil
experimental samples of SFO and a blend (VEGO) of SFO and linseed oil, 311
See also Volatile oxidation products
- Surface area, relationships among textural properties and flavor release profiles, 356
- Swallowing
retronasal transfer of odorants during eating, 88
See also Mastication
- Sweeteners
ionic environment in beverages, 333
See also Beverages

Sweetness and salivary sweetener concentration
 apparent specific volumes (ASVs) of glucose syrups, 396–397
 apparent specific volumes of D-glucose and four glucose syrups, 401, 402*t*, 403
 average intensities and persistence for four glucose syrups and D-glucose, 397, 399*t*
 average total carbohydrate concentration in saliva of four panelists, 398, 400*t*
 disappearance of stimulus from saliva after tasting and swallowing, 400–401
 drop in concentrations of stimuli in saliva, 401*t*
 materials and methods, 396–397
 persistence of sweetness, 403
 physical concentrations of carbohydrates and saccharin in saliva, 396
 SMURF method of time-intensity (TI) analysis, 395–396
 TI study of sweetness of carbohydrate and saccharin solutions, 397
 variations in intensity and persistence of 30% w/v/ DE38 sweetness among panelists, 398*f*
 water as transporting medium for movement of stimulus molecules to saliva, 402

T

Tanford transition
 pH-driven structural change, 283
See also β -Lactoglobulin interactions with flavor compounds
 Taste, flavor of food, 9
 Taste sensations, perceived flavor, 99
 Temperature, effect on phase partitioning, 128
 Tetradecanoic acid
 differential spectra for interaction with β -lactoglobulin, 290*f*

differential spectra of changes in amide I region of β -lactoglobulin spectra at pH 2.0 and 7.5, 288*f*
See also β -Lactoglobulin interactions with flavor compounds
 Texture
 determining sensory characteristics, 360
 influences on flavor release, 4–5, 356
 obtaining different perceived flavors by changing, 381
 physical and sensory texture characterization of emulsion gels, 364
See also Whey protein isolate gels
 Thermodynamics
 flavor compounds, 157–160
See also Dynamic headspace dilution method
 Thickening agents. *See* Polysaccharides
 Thiols
 components of flavorings, 274
 interactions between proteins and, 279–280
 odor threshold values, 280
 quantities recovered from aqueous systems containing protein or carbohydrate substrates, 276*t*
 recovery from cooked meat systems containing added disulfides, 279*t*
See also Sulfur-containing flavor compounds and proteins in foods
 Time-Intensity, Dual-Attribute, measuring perceived sweetness and flavor of chewing gum, 100
 Time-intensity (TI) methods
 data analysis, 359–360
 definition of TI parameters, 389*t*
 experimental study of composite gel, 391–394
 flavor release profiles, 356
 panel training, 385–386
 perceived intensity during eating, 9
 sensory protocol for protein and emulsion gels, 359
See also Composite dairy gels; Sweetness and salivary sweetener concentration

Time-resolved headspace analysis. *See* Headspace analysis, time-resolved

Tomato

atmospheric pressure chemical ionization–mass spectrometry analysis of volatiles released from mechanically damaged leaf, 50

brushing and crushing of leaves, 48–51

leaf and stem analysis by solid phase micro extraction (SPME), 47–48

materials, 46

scanning electron microscopy (SEM) method, 48

SPME–GC–EI–MS of aroma compounds of stem and leaf trichomes, 49*f*

time dependence of release of volatiles, 30, 31*f*

See also Wound response in plants

Tortilla chips. *See* Snacks

Transport. *See* Flavor release and transport from mouth to olfactory epithelium

Trapping, prior to GC–MS analysis, 11–12

V

Valencia oranges. *See* Oranges

Vapor-liquid partition coefficients, aroma compounds in water, 146*t*

Volatile compounds, interactions with non-volatile components, 370

Volatile flavor compounds

character to foods, 1–2

factors affecting partitioning between product and vapor phase, 310

factors affecting rate of volatilization, 309

liquid-gas partitioning, 67–68

perception of volatile, 179

physical entrapment in starch matrices, 234–235

physicochemical study, 2

retention by β -cyclodextrins, 246–247

sorption to native starch, 234

See also Aroma stimulus index (ASI);

Volatile oxidation products

Volatile organic compounds (VOCs)

proton affinities of constituents, 62*t*

See also Coffee roasting

Volatile oxidation products

amounts of odor active compounds

formed in oils and emulsions, 316*t*

defining headspace, 310

determining concentrations in actual eating situations, 310

effect of emulsification, 318

experimental samples of sunflower oil (SFO) and a blend (VEGO) of SFO

and linseed oil and their emulsions (SFO-E and VEGO-E), 311

factors affecting rate of volatilization, 309

formation in emulsions versus bulk oils, 314, 317

gas chromatography/mass spectrometry (GC/MS) method, 313

gas chromatography/sniffing port analysis method (GC/SP), 312–313

important for aroma of oils and emulsions, 310–311

isolating volatile compounds of SFO, VEGO and emulsions, 313–314

method for isolation of volatile compounds, 312

odor descriptors and numbers of assessors perceiving odor active compounds, 315*t*

orientation of lipid molecules in interfacial region for lipid oxidation in emulsions, 317

relative release of odor active compounds in model mouth system from SFO, VEGO, and emulsions, 316*f*

relative static headspace

concentrations of reference odor active compounds added to SFO and SFO-E, 317*f*

sniffing chromatogram of VEGO-E, 314*f*

static headspace analysis, 311–312

statistical analysis, 313

studying formation of compounds for release, 314, 317

studying release aspect by addition of reference compounds to oils and emulsions, 317–318

volatility and aroma release experiments, 311

Volatile release in vivo during food consumption

atmospheric pressure ionization mass spectrometry (API–MS), 13–15

collection and analysis of expired air by Tenax trapping and GC–MS, 11*f*

headspace volatiles from banana using PTR–MS and API–MS, 17*f*

interface (API–MS) for breath-by-breath analysis, 14*f*

jet separator interface, 13

key elements of proton transfer reaction–MS (PTR–MS), 16*f*

membrane interfaces for MS, 12

MS–Nose™, 14

physiological, compositional, and analytical considerations, 9–10

physiological factors and influences on analyses, 10*t*

PTR–MS, 15–18

sampling air during eating, 10–11

selected ion flow tube (SIFT–MS) method, 15

selective ionization using lasers, 18

trapping and pre-concentration methods, 11–12

Volatile sulfur compounds (VSC)

approaches to sampling saliva, 73–74

approximate quantities of VSC recovered by simultaneous steam distillation and solvent extraction (SDE) from cysteine and ribose model systems in absence or presence of egg albumin, 277*t*

saliva samples, 74

See also Oral malodors; Sulfur-containing flavor compounds and proteins in foods

Volatility

aroma compounds, 146–147

flavors in starch, 236

influence of emulsification, 318

2-nonanone in different media, 147*t*

See also Milk components

W

Water

content in starch transformation, 233

mechanisms controlling physical entrapment in low moisture systems, 234–235

transporting medium for moving stimulus molecules to saliva, 402

Water tolerant, physiological factors and influence on analyses, 10*t*

Weber ratio

differences of sensory significance, 337, 338*t*

See also Beverages

Whey protein isolate gels

characterization of protein gel matrices, 360–361

data analysis, 359–360

determining physical properties, 358–359

emulsion gel preparation, 357

flavor release from emulsion gels, 365–366

flavor release from protein gels, 362, 364

gas chromatography (GC) method, 360

goal of research, 356–357

held-water measurement, 358–359

influence of food texture on flavor release, 356

maximum intensity as function of held-water and microstructure, 363*f*

mean TI parameters for cherry and grape flavors, 362*t*

mean TI parameters for δ -decalactone (coconut) flavor, 366*t*

mean TI parameters for diacetyl (butter) flavor, 365*t*

- methods for fracture properties, 358
 physical and sensory texture
 characterization of emulsion gels, 364
 physical characteristics and
 composition of emulsion gels, 358*t*
 physical characteristics of whey
 protein gels, 361*t*
 principal component analysis of
 sensory texture data, 365*f*
 protein gel preparation, 357
 rate of release as function of held-
 water and microstructure, 363*f*
 sensory protocol for protein and
 emulsion gels, 359
 sensory texture characteristics by
 descriptive analysis, 360
 time-intensity (TI) methodology, 359
- Whey proteins**
 emulsifiers, 346
 See also Oil/water emulsions
- Wound response in plants**
 ability to maintain 'milieu interieur', 44
 APCI-MS (atmospheric pressure
 chemical ionization-mass
 spectrometry) analysis of volatiles
 from tomato leaf, 50
 APCI-MS method, 46-47
 APCI-MS-MS method, 47
 brushing and crushing of tomato
 leaves, 48-51
 chemical ionization-mass
 spectrometry (CI-MS) for real time
 monitoring, 45
 contributing to aroma signature, 45
 defense initiatives, 44
 experimental materials, 46
 extraction and analysis of volatiles,
 47-48
 garlic and onion analyses, 47
 headspace analysis by solid phase
 microextraction (SPME) GC-MS of
 freshly cut garlic cloves, 51-52
 interrelationship between compounds
 in garlic, 54
 MS-MS analysis of garlic, 54-55
 rapid analysis of freshly cut garlic
 clove using APCI-MS, 52, 53*f*
 real time headspace analysis, 46-47
 real time responses of volatiles
 released from mechanically
 damaged tomato leaf, 50*f*
 scanning electron microscopy (SEM)
 method, 48
 SIM-APCI-MS of volatiles released
 from needle damaged garlic clove,
 54*f*
 SPME-GC-EI-MS of aroma
 compounds of tomato stem and leaf
 trichomes, 49*f*
 strategy for intercellular segregation of
 responses, 45-46
 tomato leaf and stem analysis by
 SPME, 47-48
- X**
- Xanthan. *See* Polysaccharides
- Y**
- Yogurt, fat levels and flavor release, 29,
 30*f*